

JOURNAL OF THE MYANMAR ACADEMY OF ARTS AND SCIENCE



Geology

Vol. XVIII, No.5A, July, 2020

Myanmar Academy of Arts and Science

Journal of the Myanmar Academy of Arts and Science

Vol. XVIII, No.5A

Contents

Geology

<u>Sr. No.</u>	<u>Title</u>	<u>Page</u>
1	Ye Kyaw Thu , *Metamorphic Conditions of High-Grade Marbles from Mogok-Kyatpyin Area of the Middle Segment of the Mogok Metamorphic Belt, Central Myanmar	1
2	Teza Kyaw , Petrology of Igneous Rocks Exposed in Khuntha-Mindaw Area, Salingyi Township	11
3	Khine Zar Wai , Petrochemistry and Tectonic Implication of High K-Calc-Alkaline Series, Peraluminous S-Type Granitoids of Kyaing Tong, Shan State (East), Myanmar	29
4	Yu Yu San , Petrology and Structures of Volcanoclastic Sedimentary Rocks and Igneous Rocks in Shinmataung Area, Pakokku Township, Magawe Region	41
5	Myo Ma Ma Htwe , Comparative Study on Geochemistry and Tectonic Implication in Two Volcanic Environments: Singu Area and Kyaukphyu-Webaung Area, Mandalay Region	53
6	Mya Moe Khaing , Petrochemical Characteristics and Geochronology of the Igneous Rocks in Bilin and its Environs, Bilin Township, Mon State	63
7	Min Min Khaing , Geology and Heavy Mineral Analysis of Loose Sand from Aukzeik Area, the Kalekok Island, Laming Sub-Township, Mon State	73
8	Wathon Chit , Petrographical and Petrochemical Analyses of Igneous Rocks of Laungzin Area, Mogok Township, Mandalay Region	85
9	Myo Thiri Sandar Aung , Geochemistry of Subduction Related Lamprophyres from Mokpalin-Kanni Area, Mon State, Myanmar	97
10	Thet Paing Kyaw Win , Petrography and Petrochemical Characteristics of Skarn around Monbinzon Village and Minbon Taung Area, Thazi Township, Mandalay Region	105
11	Wai Yan Lai Aung , Morphology of Pyrite and Its Significances from Bawlonelay Area, Mogok	117
12	Lai Lai Min , Geological, Ore Mineralogy and Ore Processing of Copper Deposits, Monywa, Salingyi Township, Sagaing Region	127
13	Tin Aung Myint , Origin of Iron Ore Deposits in Maymyo Formation exposed around Baw Village, Pyin Oo Lwin Township, Mandalay Region, Myanmar	139
14	Tun Naing Zaw , Structural Controls on Lead Mineralization at Linwe Area, Yengan Township, Shan State (South)	149

<u>Sr. No.</u>	<u>Title</u>	<u>Page</u>
15	Kyaw Thu Oo , Ore Mineralogy and Geochemical Investigation of Lead Mineralization in Kyauktap Area, Kalaw Township, Shan State (South)	167
16	Aye Khaing , Geology and Ore Genesis of Lead-Zinc-Copper Mineralization in Myinhe Taung -Yasagyi Area, Ywangan Township, Shan State (South)	183
17	Aung Ye Ko , Preliminary Study of Lead Mineralization at Taung Gaung Area, Madaya Township, Mandalay Region, Myanmar	199
18	Win Khan , Sphalerites Composition and Sulphidation State of Polymetallic Epithermal Quartz Veins at Soripesa Prospect Area, Sumbawa Island, Indonesia	219
19	Hnin Min Soe , Chromite Mineralization at Saisaquine Worksite, Thabeikkyin Township, Mandalay Region	229
20	Than Htoo Aung , Wall-rock Alterations and Associated Hydrothermal Quartz Textures in Antimony Deposits of Thabyu Area, Kya-in-seikkyi Township, Kayin State	247
21	Zaw Win , Granodiorite-hosted Gold deposit in the Magyibin-Kaba Area, Pinlebu Township, Sagaing Region	257
22	Cho Cho Lwin , Sequence Stratigraphic Implication of the Napeng Formation Exposed at Napeng – Namon Area, Kyaukme Township, Northern Shan State	269
23	Nandar Myint Maung , Sedimentology of Moulmein Limestone in Kawkalut-Hnidon Area, Kyaikmaraw Township, Mon State	279
24	Ko Yi Hla , Occurrence of Glauconite and Phosphate in the Sediments from Ayeyarwady Continental Shelf	293
25	Moe Moe Lwin , Sequence Stragraphy of Taungnyo Formation in the Southern part of Mawlamyine Area, Mon State	305
26	Yin Min Htwe , Interplay of Cementation, Mechanical and Chemical Compaction in Early Silurian Phacoidal (Nodular) Limestones of the Pindaya Range, Southern Shan State	317
27	Mi Mi Ko , Sequence Stratigraphy of the Oligocene Limestones exposed at Htondaung Area, Thayet Township, Magway Region, Myanmar	325
28	Khaing Khaing San , Discovery of the Middle Devonian (Givetian) Rugose Corals from the Maymyo Formation, Pyinoolwin and Hsipaw Townships	335
29	Win Win Myint , Facies Analysis of the Kyaukkok Formation in the Sin the Chaung near Milepost 240 between Nay Pyi Taw- Mandalay High-Way	351
30	Naw Chel Phaw , Application of Markov Chain and Entropy Function for Cyclicity Analysis of Oligocene Formations of Ngape-Yenama Area, Southern Part of Minbu Basin, Myanmar	361
31	Kyaw Khaing , Geochemical Analysis of Sandstone of Laungshe Formation in the Ale Ban Area, Tilin Township, Magway Region	373

<u>Sr. No.</u>	<u>Title</u>	<u>Page</u>
32	Wai Wai Lwin , Sedimentary Facies Analysis of the Kalaw Formation in the Tigyit Area, Southern Shan State, Myanmar	381
33	Tun Tun Win , Correlation of Shear Wave Velocity (Vs) and SPT-N Value of Various Soil Deposits for Chanayetharzan Township in Mandalay District	393
34	Zin Mar Kyaw , Environmental Geochemistry of Solid Mine Wastes from Kyitaukpauk – Chaunggyi Area, Singu and Thabeikkyin Townships, Mandalay Region	401
35	Aung Kyaw Myat , A Study on Landslide Potentials and Slope Stability of the Road at Zwekabin Range near Khalauknos Village, Hpa-an Township	413
36	Khin Soe Moe , Estimation of Ground Settlement by Earthquake Induced Liquefaction in Downtown Area, Yangon	429
37	Thant Sin , Analysis of Natural Environmental Changes Using Remote Sensing and Geographic Information System (GIS): Case Area of Moeyungyi Wetland Wildlife Sanctuary and its Environment, Bago Region in Myanmar	441
38	Win Khine Tun , Hydrochemical Analysis and Evaluation of Groundwater Quality in Pyawbwe-Nyaungyan-Payangazu Area, Thazi and Pyawbwe Townships	453

Edition

2020, July, 700 Copies

Copyright

Ministry of Education

Published by

Dr Aung Min (00322) Chairman, Journal Publication Committee,
Myanmar Academy of Arts and Science

ISSN 2520-0186

LCCN 2003-323143

Printed by

U Win Aung (00171), Manager,
Universities Press, Yangon, Myanmar

METAMORPHIC CONDITIONS OF HIGH-GRADE MARBLES FROM MOGOK-KYATPYIN AREA OF THE MIDDLE SEGMENT OF THE MOGOK METAMORPHIC BELT, CENTRAL MYANMAR*

Ye Kyaw Thu¹, Khin San², Yin Kay Thwe Tun³, Hay Mar Tun⁴

Abstract

The Mogok-Kyatpyin area forming a mountainous region with two distinct valleys of Mogok valley and Kyatpyin valley is well known for its gem minerals. A variety of marbles, calc-silicate rocks, gneisses, migmatites and locally granulites are well exposed with the emplacement of various types of granitoid rocks. The high-grade assemblages of marble samples are characterized by calcite + dolomite + diopside + spinel + graphite with forsterite and clinohumite in some samples. Based on the mineral assemblages and textural relationship, temperature and fluid (T - X_{CO_2}) diagrams indicate temperature and X_{CO_2} conditions of $> 800\text{ }^{\circ}\text{C}$ and > 0.5 at an isobaric pressure of 0.8 GPa for the clinohumite-bearing and forsterite-bearing marble samples for the peak stage. Re-equilibrium texture of clinohumite + tremolite + dolomite indicates a decrease in temperature and X_{CO_2} condition, and yields $< 540\text{ }^{\circ}\text{C}$ and < 0.02 at an isobaric pressure of 0.4 GPa. The present study combining with other high-grade areas along the Mogok metamorphic belt suggest widespread distribution of upper amphibolite to granulite facies metamorphism in the middle segment including Mogok-Kyatpyin area. During peak metamorphic stages, the fluid conditions had higher X_{CO_2} value. In contrast, decreasing X_{CO_2} values with decreasing temperature and pressure might indicate that infiltration of H_2O -rich fluid occurred during retrograde metamorphism.

Keywords: clinohumite, granulite, metamorphic fluid, retrograde

Introduction

The Cenozoic Mogok metamorphic belt, extending for about 1500 km, is exposed at the western margin of the Shan-Thai Block, and forms a prominent part for understanding the continental evolution of Southeast Asia. It consists of meta-igneous rocks and meta-sedimentary rocks with subduction-related granitoid intrusions. Geochronological studies indicate that an assemblage of the Mogok high-grade metamorphic rocks formed during the Paleogene to early Neogene in association with the India-Eurasia continental collision (Bertrand et al., 1999; 2001; Barley et al., 2003; Searle et al., 2007).

Peak metamorphic conditions appear to vary between different parts of the elongated belt, such as the amphibolite facies in the Kyanigan and Kyauske areas (e.g., Searle et al., 2007) and the granulite facies in the northern Mogok region (Yonemura et al., 2013) and the Sagaing ridge (Maw Maw Win et al., 2016). Ye Kyaw Thu et al. (2016) reported a paragneiss with a spinel + quartz assemblage coexisting with Ti-rich biotite (up to 6.9 wt% TiO_2) that formed under granulite facies conditions. These results imply that high-grade metamorphic rocks occur extensively in the western Shan-Thai Block.

However, mineralogical and petrological characteristics of the Mogok metamorphic rocks and their conditions including pressure, temperature and metamorphic fluid have been poorly

¹ Dr, Assistant Lecturer, Department of Geology, Taungoo University

² Professor and Head, Department of Geology, Magway University

³ Associate Professor, Department of Geology, Pakkoku University

⁴ M.Sc, Department of Geology, Magway University

* Best Paper Award Winning Paper in Geology (2019)

constrained. The present study combining with other reported areas attempts to deduce the metamorphic conditions during the peak and retrograde stages of the marbles rocks, which may provide understanding the metamorphism of the Mogok metamorphic belt.

Geological Setting

The Mogok metamorphic belt occurs along the western margin of the Shan Plateau extending up to about 1500 km from the Gulf of Mantaban through Mogok to eastern Himalayan Syntaxis (Mitchell et al., 2007; Searle et al., 2007). This belt consists of schist, gneiss, quartzite, marble, calc-silicate rock, locally granulite and migmatite with various granitoid intrusions. These metamorphic rocks were regionally metamorphosed under medium- to high-grade amphibolite facies and localized granulite facies conditions (e.g., Barley et al., 2003; Mitchell et al., 2007; Searle et al., 2007; Yonemura et al., 2013; Ye Kyaw Thu et al., 2016; 2017).

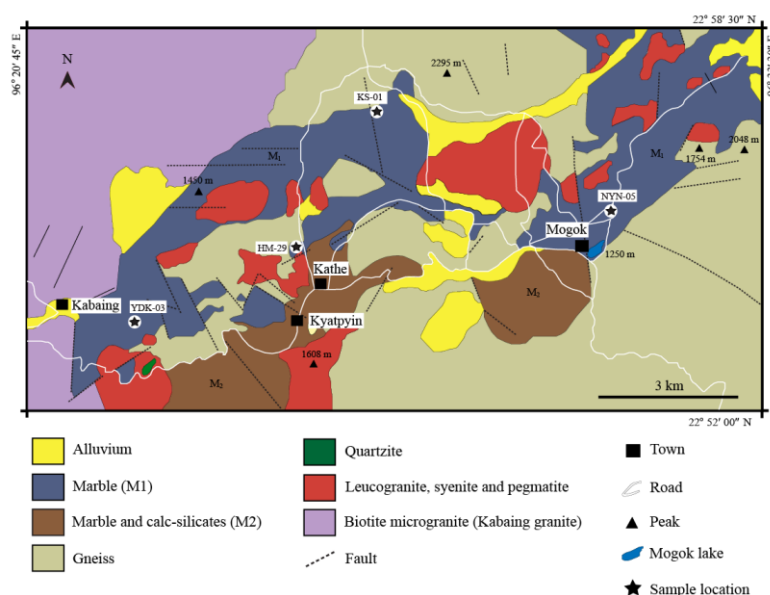


Figure 1 Geological map of the Mogok-Kyatpyin area (simplified from geological maps of Kyaw Thu, 2007; and Themelis, 2008).

A wide variety of marbles are divided into two groups; M1 marbles (gem-bearing marbles) and M2 marbles (non-gem bearing marbles) based on composition, texture and mode of occurrence (Themelis, 2008). The marbles form massive or commonly interbedded with calc-silicate rocks, and show fine to coarse-grained granoblastic texture. Both M1 and M2 marble units are widespread in the Mogok-Kyatpyin area and its environs without distinctive configuration.

Diopside marbles are fine to medium grained and frequently associated with calc-silicate rocks. Forsterite-bearing marbles occur as thick-bedded to massive and show medium- to coarse-grained granoblastic texture. Clinohumite-bearing marbles are exposed locally and form in massive cliffs and show medium grained granoblastic texture. Among the collected samples clinohumite-bearing marble (KS01 sample), forsterite-bearing marbles (HM29 and NYN05 samples) and diopside-bearing marble (YDK03 sample) are made for detailed studies, and the common constituent minerals of the analyzed marble samples are listed in table 1.

Table 1 Constituent mineral assemblage of marble samples from the Mogok-Kyatpyin area.

Sample	Cal	Dol	Chu	Fo	Spl	Di	Amp	Qz	Phl	Other
KS01	+, i	+	+	+, i	+		r			Gr
HM 29	+, i	+, sym		+			r	+	+	Gr, Pl
NYN05	+, i	+, sym		+	+					Gr, Srp
YDK03	+	+			+	+	r	+		Gr, Ttn

+, present as a primary phase; i, inclusion phase; sym, symplectitic phase; r, retrograde phase.

Petrography of Marble Samples (KS01, HM29, NYN05 and YDK03) Clinohumite-bearing marble (KS01 sample)

The sample is collected from Kyauksin village (latitude 22° 57' 25" N and longitude 96° 25' 36" E), and is characterized by the assemblages of Cal + Dol + Chu + Fo + Spl + Gr.

Calcite grains occur as subhedral to anhedral grains in matrix and as elongated and irregular inclusions in forsterite, spinel and clinohumite grains (Figs. 2a – d). The calcite inclusions range in size from 0.2 to 1 mm in diameter. Dolomite grains occur as subhedral grains in matrix and intergrown phase with calcite inclusion. The intergrowth phase is rarely observed in matrix dolomite. Forsterite grains occur as irregular or rounded-grains ranging from 0.5 – 1.5 mm in diameter (Fig. 2b). Some forsterite grains occur as inclusion (0.2 mm in diameter) in clinohumite grains. Spinel forms as prismatic porphyroblast or smaller grains (about 0.2 – 2.5 mm in diameter) (Figs. 2a and b). Clinohumite occurs as granular to irregular grains and range in size from 1 – 3 mm in diameters (Figs. 2a – d). Some grains contain inclusions of rounded calcite and granular forsterite grains, which is considered to form at a retrograde stage after forsterite. Some grains also form as a corona around dolomite and forsterite (Fig. 2b). The rims of the clinohumite grains are mostly replaced by symplectitic amphibole and dolomite (Figs. 2c and d). Amphibole occurs as elongated grain intergrowing with dolomite around clinohumite grains (Figs. 2c and d). Graphite occurs as minor amount.

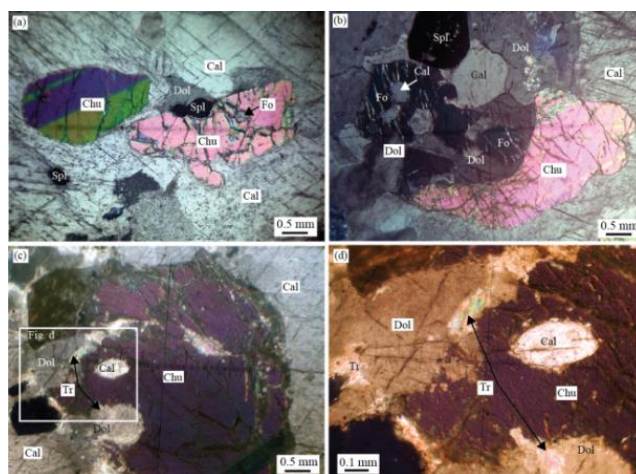


Figure 2 Photomicrographs of clinohumite-bearing marble (KS01 sample) showing (a) subhedral and irregular clinohumite grains (b) granular forsterite grain coexisting with dolomite, and clinohumite which forms corona around forsterite and dolomite (c) intergrowth of tremolite with dolomite around clinohumite grain boundary, (d) enlarged view of the intergrowth of tremolite with dolomite. All photomicrographs are under cross-polarized light.

Forsterite-bearing and diopside-bearing marbles (HM29, NYN05 and YDK03 samples)

Forsterite-bearing samples of HM29 and NYN05 are collected near Kathe (latitude $22^{\circ} 54' 33''$ N and longitude $96^{\circ} 24' 55''$ E) and from Ngayantinn (latitude $22^{\circ} 56' 00''$ N and longitude $96^{\circ} 30' 29''$ E), and diopside-bearing sample (YDK03) is from (latitude $22^{\circ} 54' 23''$ N and longitude $96^{\circ} 22' 34''$ E), respectively. These sample are characterized by Cal + Dol + Fo + Spl + Gr in NYN05 sample (Figs. 3a and b), Cal + Dol + Fo + Phl + Gr in HM29 sample (Figs. 3c and d), and Cal + Dol + Di + Spl + Gr in YDK03 sample (Figs. 3e and f).

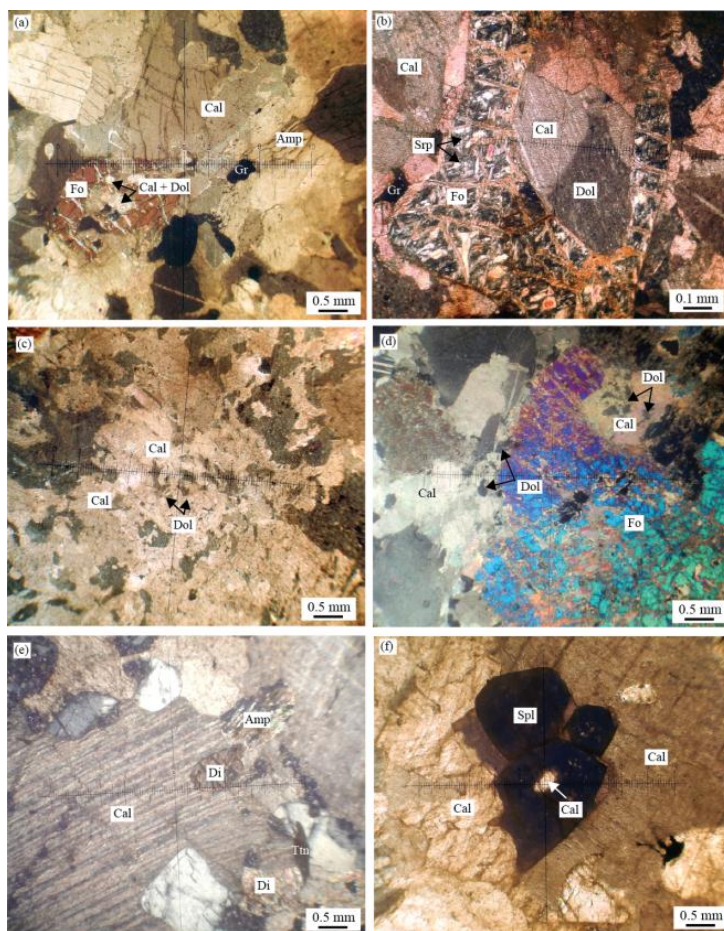


Figure 3 Photomicrographs of forsterite-bearing marble (NYN05 and HM29 samples) and diopside-bearing marble (YDK03) showing (a) granular forsterite grain with calcite inclusion which is intergrown with dolomite (b) enlarged view of the forsterite with inclusion grain of subhedral calcite grain intergrown with dolomite, (c) exsolution blebs of dolomite with different size and shape in matrix, (d) subrounded forsterite grain with calcite and dolomite intergrowths, (e) subhedral diopside grain coexisting with matrix phases and (f) prismatic spinel grain. All photomicrographs are under cross-polarized light.

Calcite grains occur as isolated grain in matrix and inclusions in forsterite and spinel grains (Figs. 3a–d and f). They form subhedral to anhedral in matrix and elliptical or irregular grains (0.5 – 1.5 mm) as inclusion. Dolomite grains occur as subhedral grains, and commonly occur as intergrown phase with calcite both in matrix and in inclusions (Figs. 3a – d). Dolomite grains intergrown with calcite are about 0.5 mm or smaller in size, and tend to form blebs of various shapes. Forsterite grains occur as irregular porphyroblastic grains ranging from 0.5 –

3 mm in diameter in NYN05 sample (Figs. 3 a and b) and up to 5 mm in HM29 sample (Fig. 3d). Some forsterite grains are commonly fractured and partly replaced by serpentine (Fig. 3b). Diopside grains occur as major phase in YDK03 sample. They form subhedral to rounded grains, and range in size from 0.4 – 0.7 mm in diameter, and some grains are replaced by secondary amphibole (Fig. 3e). Spinel forms as smaller prismatic grains with an average size of 0.5 mm in diameter (Fig. 3f). Amphibole grains occur as elongated or prismatic grain in NYN05 and HM29 samples, and as secondary pseudomorph on diopside in YDK03 sample. Phlogopite occurs as a tabular grain in sample HM29. Graphite occurs as minor amount, and serpentine only occurs as pseudomorph or replacement phase on forsterite grains.

T - X_{CO_2} Estimates for Clinohumite-Bearing Sample and Forsterite-Bearing Samples

Although the chemical data of mineral are not available for the present study, based on similar mineral assemblages in metacarbonate rocks and textural relationships, T - X_{CO_2} diagrams for collected metacarbonate samples were calculated using the analyzed mineral chemical data of marble samples from Onzon, Zayetkwin and Thabeikkyin areas reported by Ye Kyaw Thu and Enami (2018). THERMOCALC software (Powell and Holland, 1988) with an internally consistent thermodynamic data set (Holland and Powell, 1998) has been used to construct the temperature and X_{CO_2} relations. The average peak pressure of 0.8 GPa, which was obtained from the reported gneisses from Mogok area (Yonemura et al., 2013) and those from Onzon and Thabeikkyin areas (Ye Kyaw Thu et al., 2016, 2017) was assumed here as an isobaric pressure for the present study. Based on the observed mineral assemblages and textural relationships, T - X_{CO_2} grids have been constructed for the system $\text{CaO-MgO-SiO}_2\text{-H}_2\text{O-CO}_2$ with clinohumite, forsterite, diopside, tremolite, calcite, dolomite and magnesite for marble samples (Fig. 4) at isobaric pressure of 0.8 GPa to determine their relations, temperature conditions, fluid composition and retrogression of marble samples.

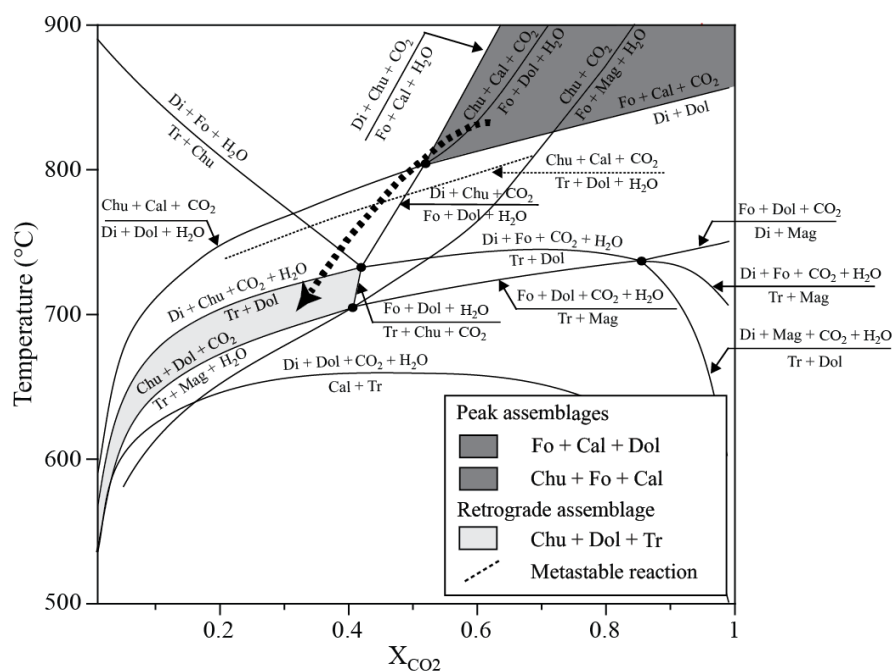
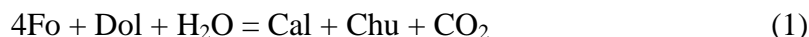


Figure 4 T - X_{CO_2} diagram employed for the clinohumite-bearing sample (KS01) and forsterite-bearing samples (HM29 and NYN05) in the system $\text{CaO-MgO-SiO}_2\text{-H}_2\text{O-CO}_2$ at an isobaric pressure of 0.8 GPa. Dashed arrow shows possible retrogression.

The high-grade assemblage of studied marbles comprises forsterite, clinohumite, calcite and dolomite. Clinohumite grains form corona around forsterite + dolomite grains (Fig. 2b) or some grains contain minute forsterite inclusions (Fig. 2a). The textural relations indicate that forsterite, calcite and dolomite coexist before and during the formation of clinohumite grains, and clinohumite was formed from the following reaction:

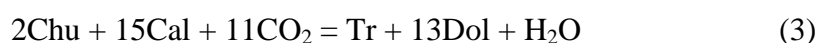


Its stability field displays positive slope in T - X_{CO_2} diagram, and a decrease in

X_{CO_2} require forming clinohumite from forsterite. The stable assemblage of Chu + Fo + Cal and Fo + Cal + Dol at isobaric pressure of 0.8 GPa yields temperature of $> 800^\circ\text{C}$ and X_{CO_2} value of >0.52 (Fig. 4). A further decrease in X_{CO_2} results in diopside and clinohumite formation.

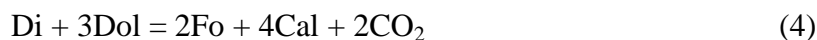


Although diopside occurs as a stable phase in associated marble outcrops, it is rare in sample KS01 sample. Instead, tremolite and dolomite occur between calcite and clinohumite grains as symplectite-like intergrowths observed in KS01 sample (Figs. 2c and d), forming the decarbonation reaction



Based on the textural relationship and T - X_{CO_2} diagram, the retrograde assemblage occurs in association with decrease in pressure, and this overstepped reaction 3 begins to be stable at isobaric pressure of < 0.7 GPa in association with the decrease in temperature and X_{CO_2} (Figs. 4 and 5). The temperature and fluid condition of this retrograde assemblage indicate 530°C and 0.02 at isobaric pressure of 0.4 GPa with decreasing pressure condition (Fig. 5). The reaction 3 continues under lower X_{CO_2} conditions with infiltration of hydrous fluid during retrograde stage.

In HM29 and NYN05 samples, the peak mineral assemblage is forsterite, calcite and dolomite (Figs. 3a – d), and the stability of this assemblage is described by the combination of reaction 1 and the following reaction.



The stable assemblage of Fo + Cal + Dol assemblage at isobaric pressure of 0.8 GPa also yields minimum temperature and X_{CO_2} value of 800°C and higher X_{CO_2} value compared with clinohumite-bearing sample for the same compositional conditions (Fig. 4). In addition, based on the inferred assemblages of KS01, NYN05 and HM29 samples Di + Cal + Dol assemblage in YDK03 (Figs. 3e and f) is stable under high temperature and X_{CO_2} condition.

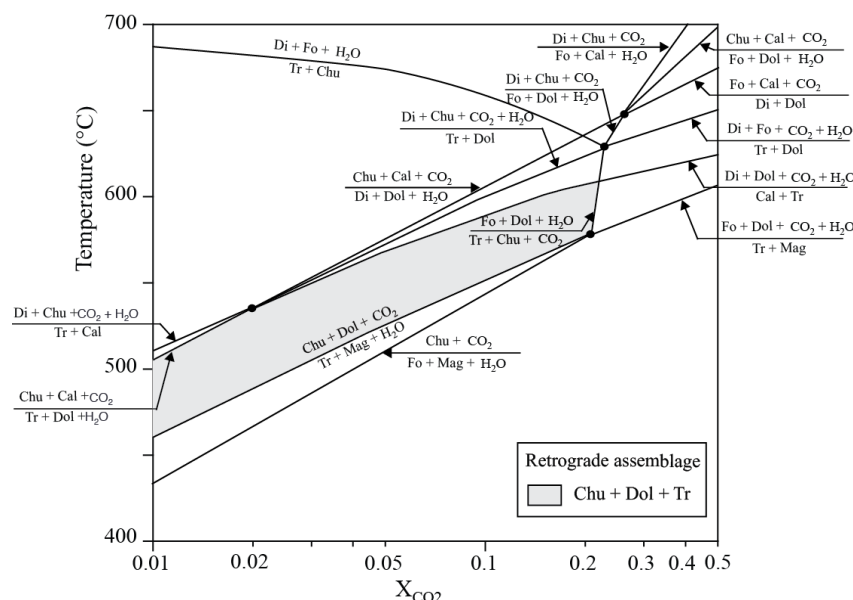


Figure 5 T - X_{CO_2} diagram calculated for the retrograde assemblage in the system $\text{CaO-MgO-SiO}_2\text{-H}_2\text{O-CO}_2$ at isobaric pressure of 0.4 GPa.

Discussion and Conclusion

The high-grade assemblages of marble samples are characterized by $\text{Cal} + \text{Dol} + \text{Chu} + \text{Fo} + \text{Spl} + \text{Gr}$, $\text{Cal} + \text{Dol} + \text{Fo} + \text{Phl} + \text{Gr}$, $\text{Cal} + \text{Dol} + \text{Fo} + \text{Spl} + \text{Amp} + \text{Gr}$ and $\text{Cal} + \text{Dol} + \text{Di} + \text{Spl} + \text{Ttn} + \text{Gr}$. The minimum temperature and X_{CO_2} values suggest 800 °C and 0.52 for the stable assemblage of $\text{Chu} + \text{Fo} + \text{Cal} + \text{Dol}$ and 800 °C and higher X_{CO_2} value for the stable assemblage of $\text{Fo} + \text{Cal} + \text{Dol}$ assemblage at isobaric pressure of 0.8 GPa. The pressure and temperature condition of 0.60–0.82 GPa/700–860 °C using the conventional geothermobarometers were reported from cordierite-bearing paragneisses and associated garnet-biotite paragneisses of Onzon and Thabeikkyin areas. From the same areas the temperature and X_{CO_2} condition of > 780–800 °C and > 0.2 – 0.6 were reported from metacarbonate rock samples (Ye Kyaw Thu and Enami, 2018). Yonemura et al., 2013 reported pressure and temperature of 0.65–0.87 GPa/800–950 °C for garnet–orthopyroxene granulite in the Mogok area. Wai Yan Lai Aung (2016) also reported high-temperature granulite facies metamorphism with the P - T conditions of 0.62–0.93 GPa/740–810 °C for spinel and pyroxene-bearing gneiss and garnet-sillimanite gneiss from the Mount Loi-Sau and Pain Pyit areas. These pressure and temperature estimates of paragneiss and metacarbonate rocks are consistent with the present study.

During peak metamorphic stages, the fluid of the analyzed marbles samples had distinctly higher X_{CO_2} value (> 0.5) in the fluid, compared with paragneisses which were free of carbonate phases. The migration of fluid phases were limited between carbonate mineral-bearing rocks and paragneisses. Homogenization of composition of metamorphic fluid has not extensively occurred during prograde metamorphic stage. In contrast, low-grade assemblages of tremolite + dolomite intergrowths at the boundary between clinohumite and calcite, and tremolite after diopside indicate significant drop in X_{CO_2} (<0.02) at lower temperature. This decrease in X_{CO_2} value of carbonate mineral-bearing rocks with decreasing temperature and pressure probably suggest that infiltration of H_2O -rich fluid extensively occurred beyond the lithologic boundaries during retrograde metamorphism.

These homogeneous nature of fluid composition during retrogression suggests hydrous fluid might have been liberated externally from crystallization of accompanied granitic magma. Although one potential source could be related by dehydration reaction of associated paragneisses, that might be unlikely due to homogeneous hydrous fluid composition attended during retrogression, and most of the dehydration reaction might have occurred during prograde stage. In the study area, syn- and post-tectonic granitoid rocks are commonly associated with metacarbonate rocks, and the potential fluid source might be related with the release of crystallization of syn- and post-peak granitoid rocks (late Paleogene to Neogene in age) (Searle et al., 2007; Kyaw Thu, 2007).

Acknowledgments

We would like to express our gratitude to Myanmar Gem Enterprise in Mogok Township and staff of Bawmar mine for their kind assistance during the fieldwork. We would like to thank to Kyaw Thu and Ted Themelis for allowing us to cite their field data of Mogok and Kyatpyin areas. Our appreciations also go to colleagues at the Department of Geology, Magway University and Taungoo University for their valuable suggestions, and third year honours students at the Department of Geology, Magway University for valuable assistance during the field trip.

References

- Barley, M.E., Pickard, A.L., Khin Zaw, Rak, P. and Doyle, M.G. (2003) "Jurassic to Miocene magmatism and metamorphism in the Mogok metamorphic belt and the India-Eurasia collision in Myanmar." *Tectonics*, vol. 22, doi:10.1029/2002TC001398.
- Bertrand, G., Rangen, C., Maluski, H. and Bellon, H. (2001) "Diachronous cooling along the Mogok metamorphic belt (Shan Scarp, Myanmar); the trace of the northward migration of the Indian syntaxis." *Journal of Asian Earth Sciences*, vol. 19, pp. 649-659.
- Bertrand, G., Rangen, C., Maluski, H., Tin Aung Han, Ohn Myint, Win Maw and San Lwin. (1999) "Cenozoic metamorphism along the Shan Scarp (Myanmar); evidences for ductile shear along the Sagaing Fault or the northward migration of the eastern Himalayan syntaxis?" *Geophysical Research Letters*, vol. 26, pp. 915-918.
- Enami, M., Nagaya, T. and Maw Maw Win. (2017) "An integrated EPMA-EBSD study of metamorphic histories recorded in garnet." *American Mineralogist*, doi: 10.2138/am-2017-5666.
- Holland, T.J.B. and Powell, R. (1998) An internally consistent thermodynamic data set for phases of petrological interest. *Journal of Metamorphic Geology*, vol. 16, pp. 309-343.
- Kyaw Thu (2007) *The igneous rocks of the Mogok Stone Tract: their distribution, petrography, petrochemistry, sequence, geochronology and economic geology*. Ph.D Thesis Geology Department, Yangon University (Unpublished).
- Maw Maw Win, Enami, M. and Kato, T. (2016) "Metamorphic conditions and CHIME monazite ages of Late Eocene to Late Oligocene high-temperature Mogok metamorphic rocks in central Myanmar." *Journal of Asian Earth Sciences*, vol. 117, pp. 304-316.
- Mitchell, A.H.G., Myint Thein Htay, Htun, K.M., Myint Naing Win, Thura Oo and Tin Hlaing. (2007) "Rock relationships in the Mogok metamorphic belt, Tatkon to Mandalay, central Myanmar." *Journal of Asian Earth Sciences*, vol. 29, pp. 891-910.
- Powell, R. and Holland, T.J.B. (1988) "An internally consistent dataset with uncertainties and correlations: 3. Applications to geobarometry, worked examples and a computer program." *Journal of Metamorphic Geology*, vol. 9, pp. 173-204.
- Searle, M.P., Noble, S.R., Cottle, J.M., Waters, D.J., Mitchell, A.H.G., Tin Hlaing and Horstwood, M.S.A. (2007) "Tectonic evolution of the Mogok metamorphic belt, Burma (Myanmar) constrained by U-T/Pb dating of metamorphic and magmatic rocks." *Tectonics*, vol. 26, TC3014.
- Themelis T. (2008) *Gems & mines of Mogok*. A & T, Bangkok.

- Wai Yan Lai Aung (2016) *Mineralogy and Petrology of the Igneous and Metamorphic Rocks of the Mount Loi-Sau and its environs, Momeik Township, Shan State (North)*. Ph.D Thesis Geology Department, Yangon University (Unpublished).
- Whitney, D.L. and Evans, B.W. (2010) "Abbreviations for names of rock-forming minerals." *American Mineralogist*, vol. 95, pp. 185-187.
- Ye Kyaw Thu and Enami, M. (2018) "Evolution of metamorphic fluid recorded in granulite facies metacarbonate rocks from the middle segment of the Mogok metamorphic belt in central Myanmar." *Journal of Metamorphic Petrology*, doi: 10.1111/jmg.12419.
- Ye Kyaw Thu, Enami, M., Kato, T. and Tsuboi, M. (2017) "Granulite facies paragneisses from the middle segment of the Mogok metamorphic belt, central Myanmar." *Journal of Mineralogical and Petrological Sciences*, vol. 112, pp. 1-19.
- Ye Kyaw Thu, Maw Maw Win, Enami, M. and Tsuboi, M. (2016) "Ti-rich biotite in spinel and quartz-bearing paragneiss and related rocks from the Mogok metamorphic belt, central Myanmar." *Journal of Mineralogical and Petrological Sciences*, vol. 111, pp. 270-282.
- Yonemura, K., Osanai, Y., Nakano, N., Adachi, T., Charusiri, P. and Tun Naing Zaw. (2013) "EPMA U-Th-Pb monazite dating of metamorphic rocks from the Mogok Metamorphic Belt, central Myanmar." *Journal of Mineralogical and Petrological Sciences*, vol. 108, pp. 184-188

PETROLOGY OF IGNEOUS ROCKS EXPOSED IN KHUNTHA-MINDAW AREA, SALINGYI TOWNSHIP

Teza Kyaw¹, Pyae Phyo Han², Htay Maung³, Zaw Win⁴

Abstract

The Khuntha-Mindaw area is situated in part of the 45-km long Monywa-Salingyi segment of Western Myanmar magmatic arc (WMA). Lithologically, the area comprises diorite, granite, gabbro, and pegmatite of intrusive and basalt, andesite, dacite and rhyolite of extrusive rocks which are formed during Cretaceous. These igneous rocks are overlain by Oligocene to Pliocene clastic sedimentary units with locally Upper Oligocene-Lower Miocene limestone. The mineral composition and textures of diverse rock units are analyzed and interpreted by binocular polarizing microscope and chemical composition by XRF from Department of Chemistry, Monywa University. Mineralogically, the volcanic rocks contain more than 20% phenocrysts of plagioclase feldspar, pyroxene, hornblende, biotite and quartz embedded in microlites to crystallites groundmass. The zoning, cumulophyric and resorbed textures indicate the fractional crystallization and magma mixing igneous activity in long-lived evolving magma. The multiple twinned plagioclase with interstitial quartz and orthoclase in granites suggest the calc-alkaline plutonic rocks. Petrochemically, the plutonic and volcanic rocks in the study area belong to the subalkaline series and falls within the calc-alkaline suite. Moreover, the major chemical compositions of the plutonic rocks fall within I-type and S-type granitoid field. Thus all igneous rocks exposed in the present area may be erupted from subduction related calc-alkaline magmatic volcanic-arc of convergent plate margins.

Keywords: Monywa-Salingyi segment, calc-alkaline, convergent plate margin

Introduction

Myanmar, located in the eastern margin of the India-Asia collision zone (Lee et al., 2016) that is characterized by the exposures of (1) Cretaceous–Paleogene granitoids correlating northward to the Gangdese batholith (Barley and Pickard, 2003; Gardiner et al., 2015; United Nations, 1979; Mitchell et al., 2012), and (2) a series of Miocene–Quaternary volcanoes extending to those in the Andaman–Sunda (Sumatra)–Banda subduction system in southeast Asia (Hutchison, 1989).

The present area is situated within the Central Volcanic Line (Chhibber, 1934) and southern part of the Wuntho-Popa or Western Myanmar magmatic arc (WMA) (Mitchell et al., 2012) (Fig. 1 and 2). The WMA, located in the central part of the Burma terrane, is a N-S trending magmatic belt delineated by the Banmauk-Wuntho Batholith in the north, and the Monywa and Popa Volcanics in the south (Mitchell et al., 2012). In the Salingyi segment of the arc, amphibolites, gabbros, diabases, and pillow basalts (Barber, 1936; United Nations, 1979) are interpreted as part of an ophiolite, overlying mica-schists, gneisses and pegmatites occurring in small inliers beneath conglomerates of similar materials (Mitchell, 1993).

The Chindwin Basin including study area lies west of the WMA, and is regarded as the forearc basin of the WMA (Wandrey, 2006 in Wang et al., 2014). The 22° N uplift area separates the Central Basin from the Chindwin Basin that was filled by the upper Cretaceous-Eocene

¹ Dr, Lecturer, Department of Geology, Monywa University

² Assistant Lecturer, Department of Geology, Monywa University

³ Assistant Lecturer, Department of Geology, Monywa University

⁴ Dr, Associate Professor, Department of Geology, Pinlon University

shallow marine or deltatic clastic rocks and carbonates, and the unconformably overlying Neogene fluvial sediments (Bender, 1983).

This paper documents petrographical data and geochemical data for igneous rocks in the area, and all results can examine the petrogenesis and tectonic implications to better understand the magmatic evolution of the part of WMA.

Method of Investigation

Detailed field work was carried out in order to perform the geologic mapping at 1: 50,000 scale of UTM map, and geological map of United Nations (1979). The field observations were carried out along car-road, cart-tracts, food-paths, mountain ridges and quarries where good exposures are appeared. 60 samples were collected for petrography and 16 representative samples of different plutonic and volcanic units were selected for geochemical analysis of major elements.

The 60 thin sections are examined by using polarizing microscope for mineral identification according to Kerr (1959), for mineral composition according to William et al., (1982) and for textural analysis according to Winter (2014).

The whole rock geochemical analyses were performed at Defense Service Academy, Pyin Oo Lwin and Department of Chemistry, Monywa University by using XRF (X-ray Fluorescence). From these major oxides, the classification of rocks according to Le Bas et al., (1986) for volcanic rocks and Cox et al., (1979) for plutonic rocks; identification of magma series according to Irvine and Bragar (1971), Peccerillo and Taylor (1976), Chappel and White (2001), Frost et al. (2001); and then possible tectonic settings are interpreted.

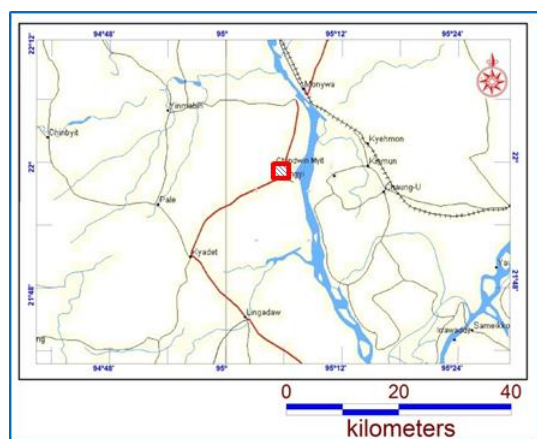


Figure 1 Location map of the study area

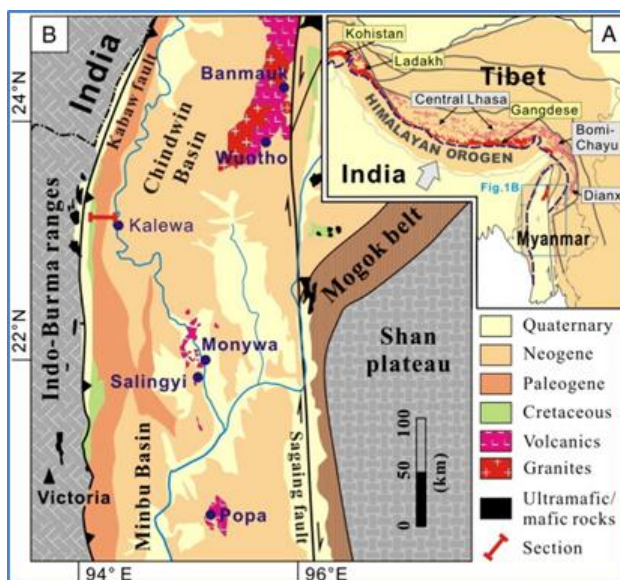


Figure 2 A Simplified tectonic map of the Tibetan plateau and adjacent regions, B: Geological Map of northern Myanmar. Western Myanmar Arc is delineated by the Banmauk - Wuntho - Monywa - Poma magmatic belt (Wang *et al.*, 2014)

Lithologic Units

The Salingyi Uplands consist of a complex of igneous and metamorphic rocks mostly and probably entirely of pre-Tertiary age. Moreover, the Tertiary sediments are also exposed in this area. The geological map of the study area is shown in Fig. (3)

Metamorphic Rock Unit

Hornblende schist

Hornblende schists are well exposed near the Magyikyin of the Kuntha village. The schists are black or dark grey, compact, strongly cleavage and showing compositional banding (Fig. 4). In hand specimens, it consists entirely of hornblende laths or prisms, micas and plagioclase. This hornblende schist is intruded by granite at east of Salingyi (Fig. 5). Thus, the age of this unit may be regarded as pre-Cretaceous.

Igneous Rocks Units

Diorite

Diorite are abundantly exposed in west of Saga village, Shwe-taung-oo taung and Nyaungbinaing monastery. It is medium- to coarse-grained, highly jointed showing dark grey on weathered surface and greyish green on fresh surface (Fig. 6). Diorites are mainly composed of quartz, feldspar and hornblende. In some places, diorite displays faint foliation. The age of diorite at Salingyi has a zircon U-Pb age of 105.3 ± 1.7 Ma (Mitchell, 2012), K/Ar determinations from hornblende ages on diorites of 106 ± 7 Ma (United Nation, 1979).

Granite

Granites are well exposed near at the northern part of the complex, western part of the Kuntha village, southern part of Shwe-own-pin monastery and east of Salingyi. The color of granite is white to grey with the varying proportion of biotite. It is medium- to coarse-grained, pale greenish-grey, highly jointed and fairly exfoliation (Fig. 7). The predominant minerals are quartz, feldspar and biotite with minor hornblende. In some places, hornblende schist and gabbroic dykes are intruded by granite. The age of granite on the basis of a biotite may be 103 ± 1 Ma (United Nation, 1978).

Gabbro

The gabbro bodies form as a small isolated body within the dioritic masses along stream section near the Nyaungbinaing monastery and the quarry at the south of Taung-paw-kyaung monastery. It is a coarse-grained, dark-green on fresh surface and dark-grey on weathered surface (Fig. 8). It is a hard and compact rock, and composed mainly of hornblende, feldspar and pyroxene minerals.

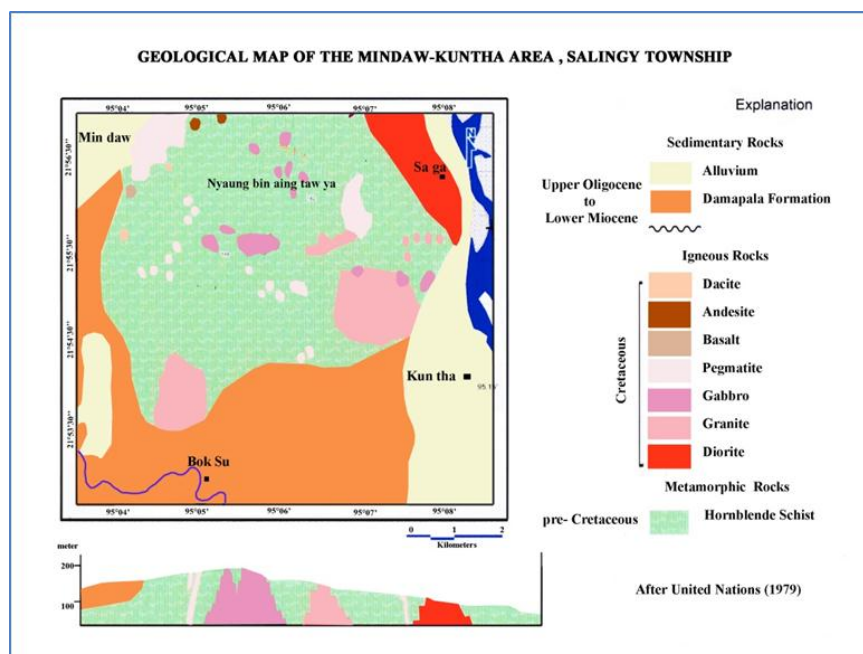


Figure 3 Geological Map of the study area

A K/Ar radiometric age determination on hornblende from a coarse-grained mafic body yielded an age of 91 ± 8 Ma.

Basalt

The basalts are locally crop out in the stream section near the Nyaungbinaing Monastery. They are dark green on fresh surface, fine-grained and massive type (Fig. 9). In this rock type, fine-to medium grained diorite or gabbro are locally found. These appear to be irregular bodies, presumably intrusive into the basalt. This basalt may be regarded as pre-Upper Cretaceous in age (United Nations, 1978).

Andesite

The andesites are exposed at the quarry in the southern part of the study area. This rock is dark grey to greenish grey on fresh and reddish brown color on weathered surface. It usually occurs as massive, and bedding like joints often in these bodies (Fig. 10). The andesites have mostly plagioclase, hornblende phenocrysts that vary in size from 0.5mm to 4mm.

Dacite

Dacite outcrop is exposed at quarry near the Taung-paw-kyaung monastery. It shows a dark brown color on the weather surface and whitish pink and whitish blue on the fresh surface (Fig. 11). It is composed essentially of phenocrysts of quartz, feldspar, and biotite embedded in very fine-grained matrix.

Pegmatite

Pegmatite dykes are exposed NE-SW trending at south of the Taung-paw-kyaung monastery and NW-SE trending at Shwe-taung-oo Taung (Fig. 12). These pegmatite dykes are 5 to 10 feet in wide and nearly half-mile long that intrude in the diorite intrusive. The constituent minerals are very coarse-grained mostly quartz and minor feldspar. Mitchell (2012) mentioned in his map as silicic dykes. These pegmatite dykes may be younger than the diorite in age.



Figure 4 Highly weathered, and foliated hornblende schist exposed at east of Salingyi (21°58'02" N, 95°06'35"E)



Figure 5 Dyke like granite intrude in the schist exposed at east of Salingyi (21°58'02"N, 95°06' 35"E)



Figure 6 Greyish green, highly jointed diorite exposed at near Saga village (21°55'55.8"N, 95°07' 11.5"E)



Figure 7 Granite with fairly exfoliation exposed at east of Mindaw village (21°58' 07" N, 95°06' 33"E)



Figure 8 Coarse-grained, dark-green gabbro exposed along the stream section near the Nyaungbinaing monastery (21°56'50.2"N,95°05'36.1"E)



Figure 9 Dark green colored basalt exposed at Taugpawkyang (21°57'37" N, 95°04' 57"E)



Figure 10 Greyish green, highly jointed, porphyritic andesite exposed at Taungpaw Kyaung (21°57'31.8" N, 95°05'04.5"E)



Figure 11 Dark brown colored on weather surface of dacite (21°55'47" N, 95°04' 18"E)



Figure 12 NW-SE trending Pegmatite dykes that is 5 -10 feet wide and ½ mile long at ½ mile NE of Shwe-taung-oo Taung (21°55'20.4" N, 95°07'0.1"E)

Damapala Formation

This formation was proposed for the rocks of thin- to thick-bedded, pale green to buff colored sandstones with concretion in the lower member and alternation of clay, silt and sandstone layers in Salingyi Township (Min Aung, 1994). Moreover, Damapala Formation is subdivided into two Members, Lower Member and Upper Member.

In the study area, the rocks of Damapala Formation are mainly exposed at the northwestern part. This unit consists of tuffaceous sandstone, limestone, gritty sandstone, medium-grained sandstone, clay and siltstone.

Lower Member

The tuffaceous sandstone are exposed at southwest of Mindaw village. They are whitish, massive, tuffaceous, medium-grained sandstones that are intercalated with buff-colored, medium- to coarse-grained, cross-stratification sandstones (Fig. 13). Moreover, buff-colored, coarse-grained, medium bedded gritty sandstones are found north of the Shwe-taung-oo Taung (Fig. 14).



Figure 13 Buff colored, medium-to coarse-grained sandstone intercalated with the whitish, medium-grained, tuffaceous sandstone (21°55'52.0" N, 95°02'53.0"E)N, 95°07'0.1"E)



Figure 14 Buff colored, coarse-grained, medium bedded gritty sandstone (21°56'57.4" N, 95°03' 58.1"E)

Upper Member

The Upper Member is observed along the Boksu Chaung that is mainly composed of the ripple cross-laminated sandstone-mudstone alternations, thin parallel-bedded sandstones and concretionary thick sandstones, and minor amounts of limestone beds.

In the ripple cross-laminated sandstone-mudstone alternation, the sandstones are greenish grey, medium-grained and thinly laminated interbedded with the mudstone. The ripple marks are current ripple marks that show the way-up indicator of the beds (Fig. 15).

The thin parallel-bedded sandstones are buff-colored, coarse-to fine-grained (Fig. 16). The sandstone beds show graded bedding and the thickness of beds are thinning upward as the grain size decrease. The concretionary thick sandstones are dark grey, coarse-grained, thick bedded sandstone with 10 to 50 cm size concretions (Fig. 17). At 1.5 kilometer south of Mindaw village, fossiliferous limestone are well exposed that strike NNW-SSE direction (Fig. 18). The limestones are light grey, compact and thick bedded that contain abundant gastropod, pelecypod, coral and algae fossils (Fig. 19).

From the assemblage of fossils, the age of Damapala Formation may be regarded as Upper Oligocene to Lower Miocene.



Figure 15 Ripple cross-laminated sandstone-mudstone alternations exposed along the Boku Chaung (21°52'41.06" N, 95°04'55.53"E)



Figure 16 Buff-colored, coarse- to fine-grained thin parallel bedded sandstone exposed along the Boku Chaung (21°52'41.06"N,95°04'55.53"E)



Figure 17 Dark-grey, coarse-grained, thick bedded sandstone with concretions exposed along the Boku Chaung (21°52'41.06"N, 95°04'55.53" E)



Figure 18 Light grey, hard and thick bedded fossiliferous limestone (21°55'27.6" N, 95°03'18.4"E)



Figure 19 Pelecypod fossils found on the surface of limestone (21°55'48.0" N, 95° 03'27.7"E)

Petrography

Basalt

The rock is composed of phenocrysts of pyroxene and hornblende and randomly oriented feldspar laths as groundmass (Fig. 20). Moreover, the opaque minerals are disseminated throughout the rocks. Pyroxene phenocrysts are subhedral with a few alterations and hornblende minerals are also present. The groundmass mostly feldspar laths may be more calcic according to the albite twinning.

Andesite

Andesite displays porphyritic texture that is composed essentially of plagioclase feldspar, and hornblende phenocrysts (Fig. 21). Some plagioclase phenocrysts show compositional zoning (Fig. 22) that are formed when a mineral change in composition as it grows during cooling (Gill, 2010). Moreover, this irregular compositional change may indicate magma mixing, unstable crystallization or both (Aslan, 2005).

Dacite

It contains phenocrysts of quartz, plagioclase and biotite embedded in the groundmass of quartz, alkali feldspar, biotite and plagioclase. The groundmass is holocrystalline and felsic minerals.

Quartz occurs as phenocrysts and groundmass and mostly anhedral. Quartz phenocrysts are corroded and embayed (Fig. 23). A drop in pressure or P_{H_2O} is suddenly to 50 MPa, the same melt composition will lie within the alkali feldspar field, making quartz unstable and prone to resorption (Whitney, 1988; Blundy and Cashman, 2001 in Gill, 2010).

Some dacite show spherulitic texture in which needle of quartz and alkali-feldspar grow radially from center (Fig. 24). Spherulites in rhyolitic lavas are spherical to ellipsoidal bodies of radiating, intergrown crystals, typically feldspar and quartz, that form by rapid crystallization of lava in response to significant cooling (Lofgren, 1971a, 1971b; Fenn, 1977; Swanson, 1977 in Befus *et al.*, 2015).

Diorite

The rock is essentially composed of medium- to coarse-grained plagioclase, biotite and hornblende with orthoclase and quartz in subordinate amounts showing hypidiomorphic to allotriomorphic (Fig. 25).

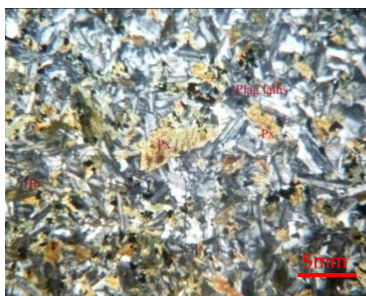


Figure 20 Subhedral phenocryst pyroxene with minor hornblende minerals, plagioclase laths and opaque minerals in basalt (X.N)



Figure 21 Andesite composed of Hornblende and Plagioclase phenocrysts (X.N)

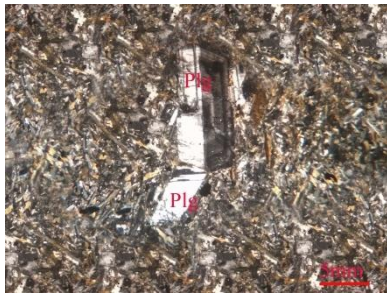


Figure 22 Andesite composed of zoning plagioclase and hornblende phenocrysts embedded in groundmass (X.N)

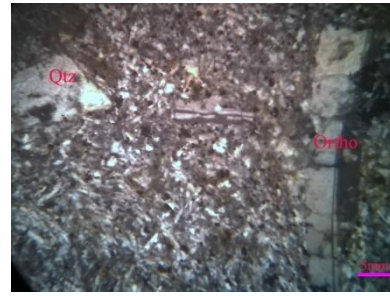


Figure 23 Dacite composed of orthoclase and embayed quartz phenocrysts embedded in groundmass (X.N)

The feldspars are subhedral plagioclase showing polysynthetic twins that are more common than the orthoclase. Hornblende is the most abundant of ferromagnesian mineral, forming a prismatic or irregular form.

Granite

It is constituted mainly of quartz, alkali feldspar and plagioclase. The accessory minerals are biotite and opaque minerals. Quartz minerals are the subhedral to anhedral forms that fill interstitial spaces between other minerals. Orthoclase minerals are subhedral to anhedral forms that range from 0.8-2 mm in size. The contact between orthoclase and plagioclase is highly irregular and show small myrmekitic textures (Fig. 26). Myrmekites appear to have grown from the plagioclase/K-feldspar boundary into the K-feldspar. As the plagioclase replaces the K-feldspar, SiO_2 released, thereby producing the quartz. Myrmekite commonly forms during cooling of granitic rocks (Winter, 2001; Collins and Collins, 2013).

Biotite minerals are the most ferromagnesian minerals that form in flakes. It is strongly paleochroic variety; vary from brown to deep brown. It shows any degree of alteration to chlorite or ore minerals.

Gabbro

The rocks consist approximately 60 % of plagioclase feldspar and 40 % of pyroxene and small amounts of hornblende (Fig. 27). The pyroxene minerals are coarse-grained and subhedral to euhedral with a few alteration fibrous amphibole. The plagioclase feldspars may be more calcic because they show albite and pericline twinning.

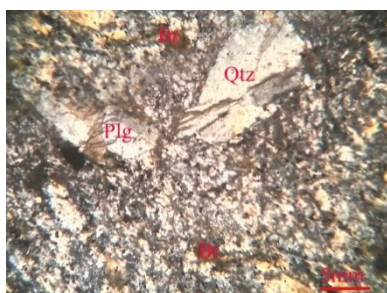


Figure 24 Dacite showing the spherulitic texture that composed of Quartz and Orthoclase spherules (X.N)



Figure 25 Quartz (Qtz), Plagioclase (Plg), Orthoclase (Ortho), Hornblende (Hb) in diorite showing allotriomorphic-granular texture (X.N)

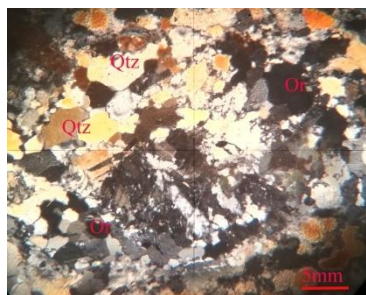


Figure 26 Quartz (Qtz), Orthoclase (Ortho), Biotite (Bt) in granite showing myrmekitic texture (X.N)

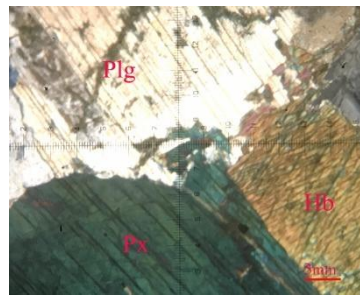


Figure 27 Gabbro composed of Pyroxene, Hornblende and Plagioclase (X.N)

Petrochemistry

Major oxides and minor oxides of igneous rocks in the study area are used to discuss the petrochemical characters. The volcanic rocks are mainly basalt, basaltic andesite, and dacite, and the plutonic rocks mainly consist of the diorite, and granite. The results of the geochemical analysis of whole-rock major oxides data are presented in table (1) and (2).

Petrochemical Character of Volcanic Rocks

According to the chemical classification based on total alkalis and silica content, the volcanic rocks of the study area belongs to the basalt, basaltic andesite, dacite, and rhyolite clan (Fig. 28) (Le Bas *et al.*, 1986). Moreover, these rock samples fall within the subalkaline field.

The subalkaline series of volcanic rocks can be further subdivided into tholeiitic and calc-alkaline type. In the AFM diagram of the ($\text{Na}_2\text{O} + \text{K}_2\text{O}$), FeO and MgO, most of the subalkaline series volcanic rocks falls within the calc-alkaline suite except three sample in tholeiite suite (Fig. 29) (Irvine and Baragar, 1971 in Rollinson, 1993). The calc-alkaline series is essentially restricted to convergent boundaries and is generally the dominant series (Winter, 2014). Moreover, tholeiitic rocks have been found to coexist with calc-alkalic rocks in a single volcanic system in some mature arcs (Tatsumi & Suzuki, 2009).

Shand (1927) grouped igneous rocks based on the total *molar* alkali versus alumina content as either **peralkaline** [$\text{Al}_2\text{O}_3 < (\text{Na}_2\text{O} + \text{K}_2\text{O})$], **peraluminous** [$\text{Al}_2\text{O}_3 > (\text{CaO} + \text{Na}_2\text{O} + \text{K}_2\text{O})$], or **metaluminous** [$\text{Al}_2\text{O}_3 < (\text{CaO} + \text{Na}_2\text{O} + \text{K}_2\text{O})$]. All volcanic rocks exposed in the study area falls peraluminous series.

The volcanic samples of calc-alkaline series have a wide range in SiO_2 ranging from 49 wt% to 75 wt% and potassium content is low-K tholeiite, calc-alkaline series (Fig. 30). All three series (low-, medium- and high-K) are well represented in subduction-related magma suites (Winter, 2014). Arc-related volcanic rocks vary widely in their K_2O contents, which often correlate with the stage of arc development and with geographical location relative to the arc axis (Gill, 2010). Moreover, some spatial and temporal patterns in K_2O contents in the distribution of magma series are found in several island arcs (Winter, 2014).

Petrochemical Character of Plutonic Rocks

According to the chemical classification based on total alkalis and silica content, the plutonic rocks of the study area belongs to the gabbroic diorite, diorite and granite clan of subalkaline series (Fig. 31) (Cox *et al.*, 1979). In the AFM diagram of the ($\text{Na}_2\text{O} + \text{K}_2\text{O}$), FeO and

MgO, subalkaline series of all plutonic rocks fall within the calc-alkaline suite (Fig. 32) (Irvine and Baragar, 1971 in Rollinson, 1993). Although the three magma series (tholeiitic, alkaline and calc-alkaline series) are represented at subduction zones, the calc-alkaline series is essentially restricted to convergent boundaries and is generally the dominant series (Winter, 2014).

To classify the I-type and S-type granitoid, when plotted on the ACF ($\text{Al}_2\text{O}_3\text{-Na}_2\text{O}+\text{K}_2\text{O}$, CaO, and $\text{FeO}+\text{MgO}$) diagram on the basis of major oxides, it is found that the studied samples fall in the I-type as well as S-type field (Fig. 33) (Chappell and White, 1992).

Table 1 Major oxides composition (in weight %) of the volcanic rocks in the study area

Sample No	L3	L32	L20	L18	L9	L5	L6
Rock Units	Basalt	Basalt	Basalt	Basalt	<u>Dacite</u>	Rhyolite	Rhyolite
SiO ₂	50.502	52.01	50.06	49.12	63.861	75.099	71.788
TiO ₂	1.365	1.57	1.33	1.11	0.459	0.172	0.303
Al ₂ O ₃	17.653	16.5	17.01	15.67	17.629	13.498	13.586
Fe ₂ O ₃	10.349	9.51	10.4	10.58	5.538	3.003	5.033
<u>MnO</u>	0.202	0.115	0.185	0.171	0.104	0.013	0.034
<u>MgO</u>	8.04	5.23	5.26	6.63	1.466	0.107	0.434
<u>CaO</u>	7.804	9.55	9.81	11.35	5.735	0.85	2.684
Na ₂ O	2.881	3.65	2.95	2.34	4.091	6.969	5.551
K ₂ O	0.064	0.53	0.452	0.366	0.417	0.019	0.081
P ₂ O ₅	0.338	0.24	0.375	0.12	0.297	0.017	0.123

Table 2 Major oxides composition (in weight %) of the plutonic rocks in the study area

Sample No	L8	L10	L11	L15	L4	L31	L35	L38	L41
Rock Units	Diorite	Diorite	Diorite	Diorite	Granite	Granite	Granite	Granite	Granite
SiO ₂	50.502	57.851	53.516	52.404	71.42	74.48	72.44	69.45	70.55
TiO ₂	0.692	0.383	0.259	0.452	0.476	0.0703	0.095	0.05	0.08
Al ₂ O ₃	18.948	16.016	26.975	17.884	12.837	14.74	14.51	13.68	14.11
Fe ₂ O ₃	8.731	7.57	2.419	8.371	5.115	1.113	1.36	0.78	1.41
<u>MnO</u>	0.178	0.16	0.046	0.218	0.041	0.018	0.045	0.02	0.033
<u>MgO</u>	5.747	4.973	1.231	5.908	1.389	0.274	0.0369	1.2	0.34
<u>CaO</u>	10.415	9.234	12.538	11.065	4.728	1.41	2.43	2.13	3.65
Na ₂ O	2.942	2.708	2.251	2.448	3.203	5.26	4.3	3.69	4.01
K ₂ O	0.166	0.337	0.414	0.469	0.06	2.57	4.43	5.01	4.21
P ₂ O ₅	0.273	0.188	0.132	0.149	0.359	0.191	0.45	0.36	0.41

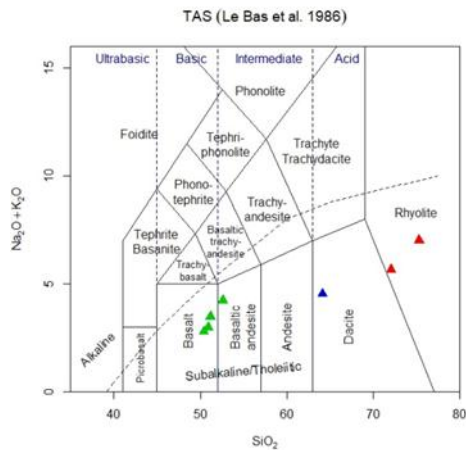


Figure 28 The chemical classification of volcanic rocks based on total alkalis ($\text{Na}_2\text{O} + \text{K}_2\text{O}$) and silica (SiO_2) (Le Bas et al., 1986) (GCDkit 5)

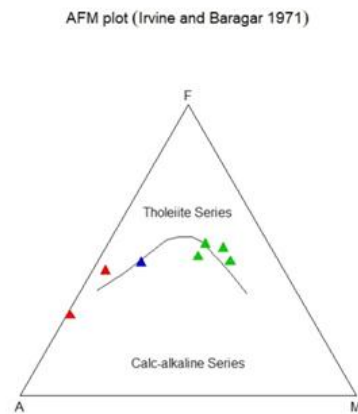


Figure 29 AFM diagram for volcanic rocks of the study area showing the discrimination between tholeiitic and calc-alkaline suite (Irvine and Bragar, 1971) (GCDkit 5)

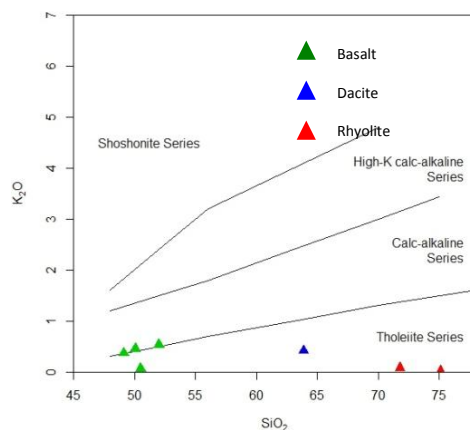


Figure 30 The chemical classification of the volcanic rocks based on K_2O - SiO_2 (Peccerillo and Taylor, 1976) (GCDkit 5)

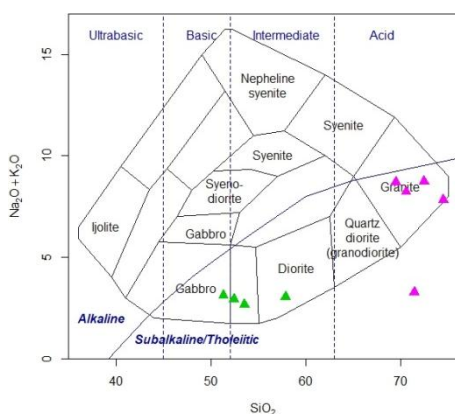


Figure 31 The chemical classification of plutonic rocks based on total alkalis ($\text{Na}_2\text{O} + \text{K}_2\text{O}$) and silica (SiO_2) (Cox et al., 1979) (GCDkit 5)

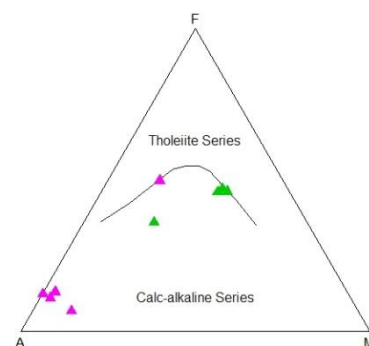


Figure 32: AFM diagram for plutonic rocks of the study area showing the discrimination between tholeiitic and calc-alkaline suite (Irvine and Bragar, 1971) (GCDkit 5)

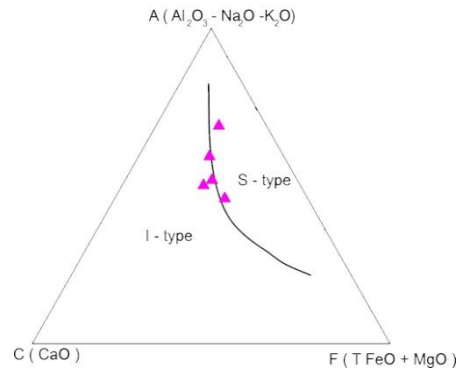


Figure 33 ACF diagram for the granite rock of the study area compared with the typical I- type and S-type (Chappel and White, 1992)

Tectonic Discrimination of Igneous Rocks

Basalt

According to eight major element discrimination diagram, the three samples of basalt falls calc-alkali basalt and island arc tholeiite field whereas only one sample falls within the MORB (Fig. 34). Moreover, the three samples fall within volcanic-arc and active continental margin (orogenic) field but one sample falls within the MORB based on $\text{MgO-FeO}^{\text{T}}\text{-Al}_2\text{O}_3$ (Fig. 35). Most of these basalts are island-arc tholeiite whereas one is the ocean-island tholeiite based on $\text{MnO-TiO}_2\text{-P}_2\text{O}_5$ (Fig. 36).

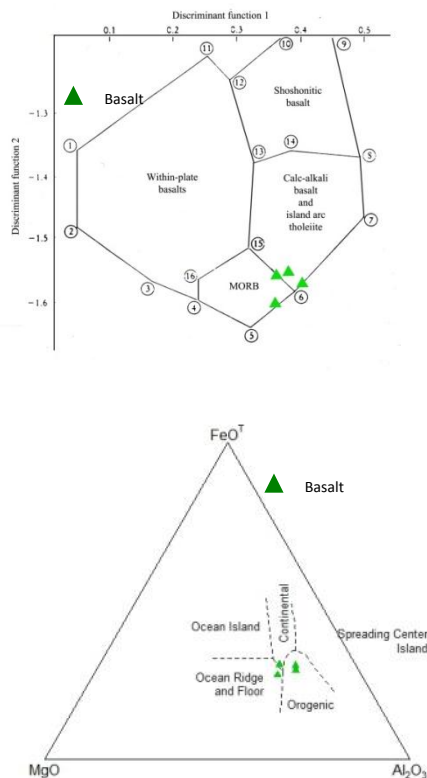


Figure 34 Major element discrimination diagrams for basalts (after Pearce, 1976 in Rollinson, 1993), showing the fields of within-plate basalts, MORB, calc-alkali basalts, island-arc tholeiites and shoshonitic basalts.

$$F1 = + 0.0088\text{SiO}_2 - 0.0774\text{TiO}_2 + 0.0102\text{Al}_2\text{O}_3 + 0.0066\text{FeO} - 0.0017\text{MgO} - 0.0143\text{CaO} - 0.0155\text{Na}_2\text{O} - 0.0007\text{K}_2\text{O}$$

$$F2 = - 0.0130\text{SiO}_2 - 0.0185\text{TiO}_2 - 0.0129\text{Al}_2\text{O}_3 - 0.0134\text{FeO} - 0.0300\text{MgO} - 0.0204\text{CaO} - 0.0481\text{Na}_2\text{O} - 0.0715\text{K}_2\text{O}$$

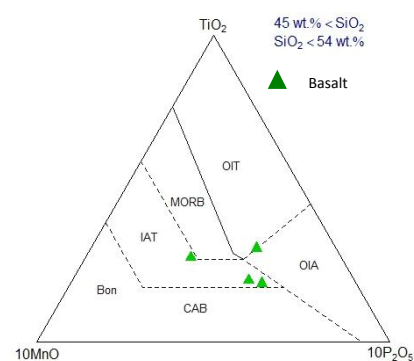


Figure 35 $\text{MgO-FeO}^{\text{T}}\text{-Al}_2\text{O}_3$ diagram for basalt (after Pearce, 1976 in Rollinson, 1993), showing MORB, ocean-island basalt, continental basalt, volcanic-arc and active continental margin (orogenic), and spreading center island basalts. (GCDkit 5)

Figure 36 $\text{MnO-TiO}_2\text{-P}_2\text{O}_5$ discrimination diagram for basalt and basaltic andesite (45-54 wt% SiO_2) (Mullen, 1983 in Rollinson, 1993), showing MORB, OIT- ocean-island tholeiite, OIA-ocean-island alkali basalt, CAB- calc-alkaline basalt, IAT- island-arc tholeiite, Bon- boninite (GCDkit 5)

Granite

According to Frost *et al.* (2001), the geochemical classification for granitoids was determined based on Fe-number [$\text{FeO}/(\text{FeO} + \text{MgO})$] ratio of the rock to classify the ‘ferroan’ (Tholeiitic) and ‘magnesian’ (Calc-alkaline); based on modified alkali-lime index (MALI) (SiO_2 vs $\text{Na}_2\text{O} + \text{K}_2\text{O} - \text{CaO}$); and is based on aluminum saturation index (ASI). The samples fall within the magnesian field except one sample; within calcic to alkali-calcic field; and within metaluminous field except one sample (Fig. 37).

The granites of the study area fall within the syn-collision field based on the R_1 - R_2 binary multicationic parameter (Batchelor and Bowden, 1985) (Fig. 38).

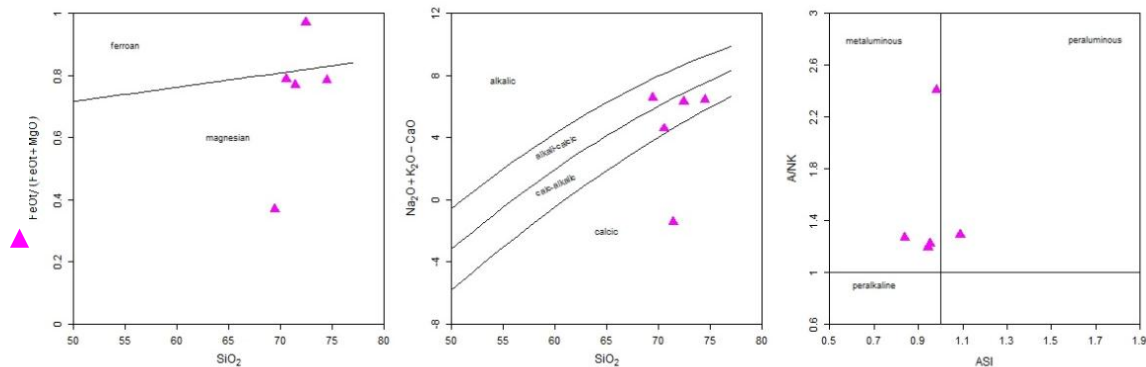


Figure 37 Granite tectonic discrimination (Frost *et al.*, 2001) (GCDkit 5)

(a) Fe-number [$\text{FeO}/(\text{FeO} + \text{MgO})$]

(b) modified alkali-lime index (MALI) (SiO_2 vs $\text{Na}_2\text{O} + \text{K}_2\text{O} - \text{CaO}$)

(c) aluminum saturation index (ASI)

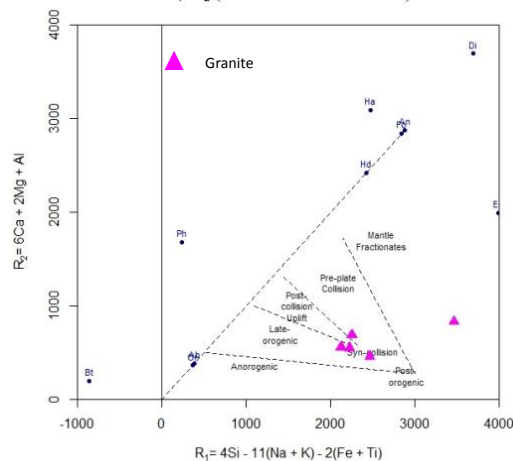


Figure 38 Multicationic discrimination diagram of granites (Batchelor and Bowden, 1985)

(GCDkit 5) $R_1 = 4\text{Si} - 11(\text{Na} + \text{K}) - 2(\text{Fe} + \text{Ti})$ $R_2 = 6\text{Ca} + 2\text{Mg} + \text{Al}$

Discussion

The present area, part of Salingyi Upland of the Western Myanmar Magmatic arc, consists of diverse igneous rocks from felsic to mafic in composition during pre-Tertiary age.

Most of the volcanic rocks in the area display porphyritic texture that exceeds more than 20% of the total volume of rocks. The phenocrysts are mostly pyroxene in basalts, plagioclase in andesites, and quartz and biotite in dacite. The phenocrysts are used to determine rock origins and transformations, as when and whether crystals form depends on pressure and on temperature. Island arc volcanic rocks are generally phyric (>20%), although tholeiitic rocks may be less so (Winter, 2001).

These phenocrysts show some characteristics of magmatic processes during cooling. The compositional zonings in andesites and dacites point out magma mixing, unstable crystallization. When phenocrysts exhibit zoning, it is a sign that the plutonic stage of crystallization has been sufficiently prolonged for significant evolution in melt composition to take place (Gill, 2010). The embayed quartz phenocrysts in dacite indicate the drop of pressure in the same melt composition. In plutonic rocks, some plagioclase show zoned textures in diorite whereas myrmekitic textures in granites. In addition to that the multiple twinned plagioclase with interstitial quartz and orthoclase is the characteristic feature of calc-alkaline granodioritic plutonic rock (Wilson, 2007).

The orderly sequence in which phenocrysts appear and change their relative proportions in a series of intermediate to acid lavas or pyroclastics is treatment to advancing fractional crystallization (Gill, 2010). Moreover, the various disequilibrium features in igneous rocks suggest that magma mixing is common (Eichlberger, 1978) but may also reflect complex convection effects (plus recharge) in shallow magma chambers (Singer, 1995 in Winter, 2001). Thus the igneous processes acting on the rocks exposed in the area may be the combination of fractional crystallization and magma mixing.

The chemical composition of the volcanic and plutonic rocks falls within the subalkaline based on total alkalis ($\text{Na}_2\text{O} + \text{K}_2\text{O}$) and silica (SiO_2). These subalkaline igneous rocks are further classified as calc-alkaline and tholeiite based on ($\text{Na}_2\text{O} + \text{K}_2\text{O}$), FeO and MgO in which most rocks fall within the calc-alkaline except two basalts and one rhyolite in tholeiite. The volcanic rocks contribute the tholeiite and calc-alkaline series according to SiO_2 - K_2O content. The granites in the study area belong to I-type and S-type granitoid according to A (Al_2O_3 - Na_2O - K_2O), C (CaO), F (FeO+MgO) data. Considering the I-type granitoid, White and Chappell (1983 in Chappell and White, 2001) concluded that S-type granites probably were formed near continental margin environment from anatexis of sediments at the base of a thickened crust during continental collision, whereas the I-type granites probably assumed as products of Cordilleran subduction post orogenic uplift regimes (Pitcher, 1983 in Ibrahim *et al.*, 2000).

The major and minor chemical composition of basalts and granites are further discriminated to infer possible tectonic environment. The basalts belongs to the calc-alkali basalt and island arc tholeiite field based on the eight major elements discrimination, volcanic-arc and active continental margin (orogenic) field based on MgO - FeO^T - Al_2O_3 , island-arc tholeiite based on MnO - TiO_2 - P_2O_5 . Moreover, most of the granites fall within the magnesian (calc-alkaline) field based on Fe-number [$\text{FeO}/(\text{FeO} + \text{MgO})$] ratio; within calc-alkalic field based on modified alkali-lime index (MALI); and within metaluminous field based on aluminum saturation index

(ASI). In addition to that the granites belong to the syn-collision field based on the R_1 - R_2 binary multicationic parameter.

In conclusion from the above facts, all igneous rocks exposed in the present area may be erupted from subduction related calc-alkaline magmatic volcanic-arc of convergent plate margins.

Acknowledgements

We are grateful to Rector Dr Thura Oo, Pro-Rectors Dr Thet Naing Oo and Dr Khin San San Win, Monywa University for their permission. We are greatly indebted to Dr. Zaw Myint Ni, Professor and Head, and Dr. Myat Khaing, Professor, Department of Geology, Monywa University, for their permission to conduct this research and valuable suggestions. Finally, we also thanks to our colleague in the Department of Geology, Monywa University, for their supporting everything in this research.

References

- Aslan, Z., (2005). Petrography and Petrology of the Calc-Alkaline Sarihan Granitoid (NE Turkey): An Example of Magma Mingling and Mixing, *Turkish J. Earth Sci.*, vol.14, pp.185-207.
- Barber, C. T., (1936). The Intrusive and Extrusive Rocks of the Salingyi Uplands and Linzagyat, *Memoir of the Geological Survey of India*.
- Barley, M. E., Pickard, A. L., Khin Zaw, Rak, P., Doyle, M. G., (2003). Jurassic to Miocene magmatism and metamorphism in the Mogok metamorphic belt and the India-Eurassia collision in Myanmar, *Tectonics*, vol. 22, No. 3, 1019, TC001398.
- Batchelor, R.A. and Bowden, P., (1985). Petrogenetic Interpretation of Granitoid Rock Series Using Multicationic Parameters, *Chemical Geology*, 48, 43-55.
- Befus, K.S., (2016). Crystallization kinetics of rhyolitic melts using oxygen isotope ratio, *Geophysics Research Letter*, 43, 592-599, doi:10.1002/2015GL067288.
- Bender, F., (1983). *Geology of Burma*, Gebruder Brontraeger, Berlin.
- Chappell, B.W. and White, A.J.R., (1992). I and S-type granites in the Lachlan Fold Belt. Transactions of the Royal Society of Edinburgh: *Earth Sciences* 83, 1-26.
- Chappell, B.W., and White, A.J.R., (2001). Two Contrasting Granite Types: 25 years later, *Australian Journal of Earth Sciences*, vol. 48, pp. 489-499.
- Chhibber, H. L., (1934). *Geology of Burma*, Macmillan, London.
- Collins, L. G. and Collins, B. J., (2013). Origin of myrmekite as it relates to K-, Na-, and Ca-metasomatism and the metasomatic origin of some granite masses where myrmekite occurs, www.csun.edu/~vcgeo005/Nr56Metaso.pdf.
- Cox, K. G., Bell, J. D. and Pankhurst, R. J. (1979). *The interpretation of igneous rocks*. Boston, George Allen and Unwin London.
- Frost, B.R., Barnes, C.G., Collins, W.J., Arculus, R.J., Ellis, D.J., Frost, C.D., (2001). A Geochemical Classification for Granitic Rocks, *Journal of Petrology*, V.42, No.11, p.2033-2048.
- Gardiner, N., Robb, L.J., Morley, C.K., Searle, M.P., Cawood, P.A., Whitehous, M., Kirkland, C.L., Roberts, N.M.W., Tin Aung Myint, (2016). The Tectonic and Metallogenic Framework of Myanmar: A Tethyan mineral system, *Ore Geology Reviews*, 79, 26-45.
- Gill, R., (2010). *Igneous Rocks and Process: A Practical Guide*, Wiley-Blackwell, A John Wiley & Sons, Ltd., Publication, U. K.

- Hutchison., C. S., (1989). *Geological Evolution of South-East Asia*, 2nd ed., Art Printing Works Sdm. Bhd., Malaysia.
- Irvine, T. N., and Baragar, W. R. A., (1971). A guide to the chemical classification of the volcanic rocks, *Canada Journal of Earth Science*, Vol. 8, pp 523-548.
- Kerr, P.F., (1959). *Optical Mineralogy*, 3rd Edition, McGraw-Hill Book Company Inc., New York.
- Le Bas, M. J., Lemaitre, R. W., Streckeisen, A. L. and Zanettin, B., (1986). A chemical classification of volcanic rocks based on the total alkali-silica diagram, *Journal of Petrology*, Vol. 27, pp 745-750.
- Lee, H.Y., Chung, S.L., Yang, H.M., (2016). Late Cenozoic volcanism in central Myanmar: Geochemical characteristics and geodynamic significance, *Lithos*, 245, pp. 174-190.
- Min Aung, (1994). Geology of the Powintaung-Silaung area, Yinmabin Township, *M. Sc. Thesis*, University of Mandalay, unpub.
- Mitchell, A. H. G., (1993). Cretaceous-Cenozoic tectonic events in the western Myanmar (Burma) – Assam region in *Journal of the Geological Society of London*, vol. 150, p. 1089-1102.
- Mitchell, A., Chung, S. L., Thura Oo, Lin, T. S., Hung, C. H., (2012). Zircon U-Pb ages in Myanmar: Magmatic-metamorphic events and the closure of a neo-Tethys ocean?, *Journal of Asian Earth Sciences*.
- Peccerillo, A., Taylor, S.R., (1976). Geochemistry of Eocene calc-alkaline volcanic rocks from Kastamonu area, Northern Turkey, *Mineralogy and Petrology*, 58, 63–81.
- Rollinson, H. R., (1993). *Using Geochemical Data: Evaluation, Presentation, Interpretation*, Longman, P. 352.
- Tatsumic, Y. and Suzuki, T., (2009). Tholeiitic vs Calc-alkali Differentiation and Evolution of Arc Crust: Constraints from Melting Experiments on a Basalt from the Izu-Bonin-Mariana Arc, *Journal of Petrology*, vol. 50, p. 1575-1603.
- United Nations, (1979). Geology and Exploration Geochemistry of the Salingyi-Shinmataung Area, Central Burma, *Technical report 5*, New York.
- Williams, H., Turner, F. J., Gilbert, C. M., (1982). *An Introduction to the Study of Rocks in Thin Sections*, 2nd Edition, W. H. Freeman and Company, New York.
- Winter, J. D., (2014). *An Introduction to Igneous and Metamorphic Petrology*, Prentice-Hall Inc., Upper Saddle River, New Jersey.

PETROCHEMISTRY AND TECTONIC IMPLICATION OF HIGH K-CALC-ALKALINE SERIES, PERALUMINOUS S-TYPE GRANITOIDS OF KYAING TONG, SHAN STATE (EAST), MYANMAR

Khine Zar Wai¹, Min Aung², Zin Maung Maung Thein³

Abstract

The study area is situated about 8 km north of Kyaing Tong. It covers a part of UTM map sheet No.2199/11. Areal coverage is about 130 square kilometers. Regionally, the study area comprises the Eastern High Lands Province, located in the western part of the Shan-Thai Block. The present area lies within the Eastern Granitoid belt of Myanmar, comprise in mostly igneous units in the area. Representative samples from the study area were used to analyze the geochemical study of the granitoid rocks. Although Kyaing Tong batholith mainly consists of biotite granite, porphyritic biotite granite, foliated granite, hornblende granite, granodiorite and leucogranite, this study will focus on geochemistry and tectonic setting of Kyaing Tong S-type granite. A total of 7 representative samples have been selected and analysed for this study. The whole rock major oxides and trace element compositions were analyzed by XRF (X-ray fluorescence) spectrometer using standard calibration method at Economic Geology Lab., Department of Earth Resources Engineering, Kyushu University, Japan. Fresh rock specimens of about 0.5-1kg were crushed for XRF sample preparation method. Major oxides analysis was carried out on fusion discs and trace elements were pressed powered pills. Aims of this research which are: to study geochemical characteristics and to interpret the tectonic setting of the study area, tectonic discrimination diagrams were illustrated by using PetroGraph 2Beta software and GCD kits software. All analyzed samples fall in in acid group, recognized in subalkaline/tholeiitic series. Kyaing Tong granitoid rocks are the high abundance of Cr, Rb Ba, S, Zr and Sr. Based on the geochemical data, most granitoid rocks belong to the peraluminous field. Kyaing Tong S-type Granitoids of subduction related rocks due to the collision effects of Sibumasu and Indochina Block during Late Triassic closure of paleotethys, later Indosinian orogeny event.

Keywords: *Kyaing Tong Area, S-Type Granitoids, geochemical study, tectonic setting*

Introduction

Kyaing Tong is comprised in Eastern Granitoid Belt of Myanmar. The study area is located in Eastern most part of Myanmar, which is bounded by North Latitudes 21° 23' 47" to 21° 28' 15" and East Longitudes 99° 34' 45" and 99° 42' 35". It is bordered nearby Northern Thailand, Lao and Southwestern Yunan. The location map of the study area is shown in (Figure 1).

Regional Geologic Setting

The study area in the easternmost province of Myanmar, comprising high lands and plateaus, east of the Sagaing fault, referred to as the Eastern High Lands Province (EHP) covers the entire eastern half of the country. Regional geologic setting around the study area is shown in (Figure 2) and geological map of the study area is shown in (Figure 3).

The present area lies within the Eastern Granitoid belt of Myanmar (Khin Zaw, 1990). The eastern belt granitoids are characterized by medium to coarse porphyritic textures and country rocks of regionally metamorphosed, turbiditic sediments of Chaung Magyi Group (Upper Precambrian). This eastern granitoid belt lies immediately to the north of mostly Triassic

¹ Assistant Lecturer, Department of Geology, University of Yangon

² Pro-rector, MaUbin University

³ Lecturer, Department of Geology, Magway University

granitoids in northern Thailand, and the Sn-W bearing, mesozonal, Permo-Triassic, Main Range granitoids in the western part of the Malay Peninsula.

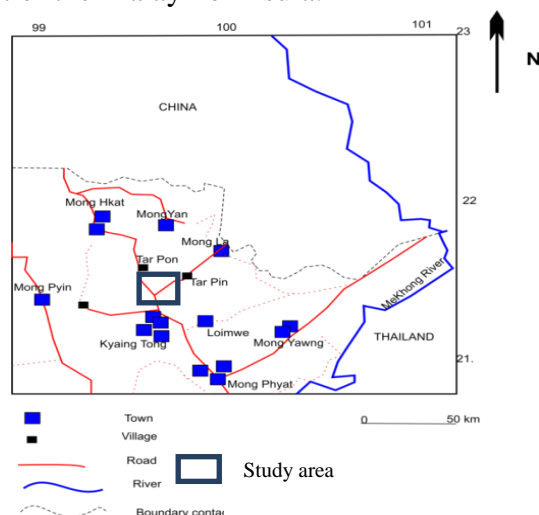


Figure 1 Location map of the study area.

Method of Study

Field methods and laboratory methods have been carried out for the present work. Modern analytical methods such as XRD and XRF were used to get geochemical data for this research work. The major and trace elements data were illustrated in variation diagrams, ternary diagrams, binary diagrams and triangular plots by using Petro Graph 2Beta software and GCD kits 4.1 software. Thornton and Tuttle Index (TTID or D.I, Differentiation Index) were calculated from standard CIPW norms which can be used as an indicator of bulk composition. To interpret the tectonic setting of the study area, tectonic discrimination diagrams were illustrated by using PetroGraph 2Beta software and GCD kits software.

Petrography

Leucogranite

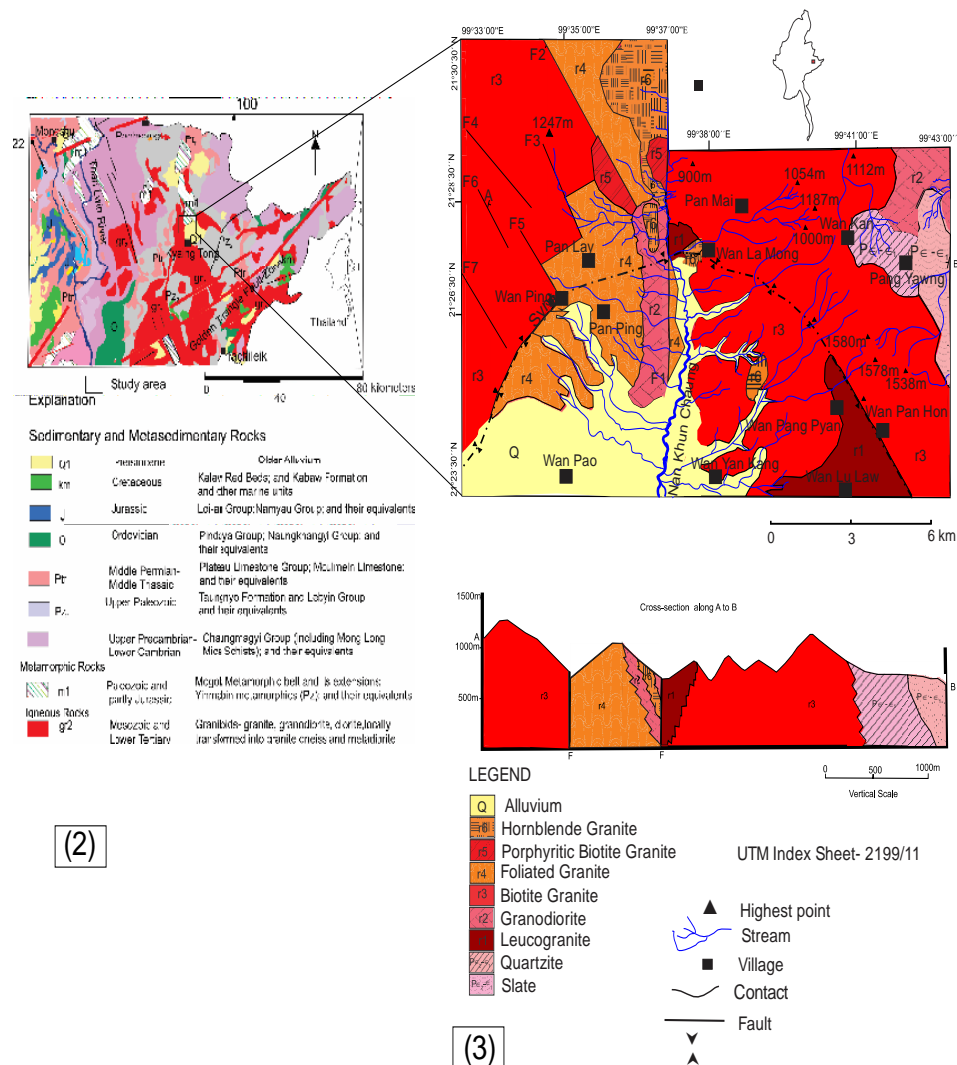
Leucogranite in the area shows distinct kaolinization developed on most outcrops(see Figure 4 a). It develops in highly weathered zone near metamorphic terrane. Petrographically, it shows holocrystalline, hypidiomorphic granular texture (Figure 4 b). It is characterized by sub equal proportions of quartz, alkali feldspar and plagioclase with a few amounts of muscovite. Accessory minerals are apatite, zircon and sphene. The main alkali feldspars are perthitic orthoclase, microperthite and orthoclase which shows Carlsbad twin. It contains about 40 % by volume of rock.

Granodiorite

Granodiorite is poorly exposed in the study area. It is observed at the northeastern part and core of the area with nearly north-south trend. In some exposures, it is also exposed in the form of boulder due to the exfoliation weathering of very large different joint sets (Figure 5 a). Microscopically, granodiorite shows holocrystalline, medium-grained hypidiomorphic granular texture (Figure 5 b). It is mainly composed of feldspar, quartz and biotite. Feldspars make up the greater part of granite, a potshand soda-bearing feldspar in equal amount. Accessory minerals are apatite, zircon and sphene.

Biotite Granite

Biotite granite is one of the major intrusive igneous rocks of the study area (Figure 6 a & b). Exfoliation nature is occasionally found in this unit. The occurrences of xenoliths size are 0.5 inch to 5 inches wide and 1.0 inch to 11 inches long. Petrographically, Biotite granite shows holocrystalline, coarse-grained hypidiomorphic granular texture (Figure 6 c & d). Biotite is significantly present compared to other granites of the study area, comprising about 10 percent of the total volume of the constituent minerals. Apatite, sphene, chromite, zircon and magnetite occur as accessory minerals as inclusions in biotite flakes.



(Source: Myanmar Geoscience Society (2014)).

Figure 2 Regional geological map of the Kyaing Tong area, Eastern Granitoid Belt of Myanmar

Figure 3 Geological map of the study area (Khine ZarWai, 2018).

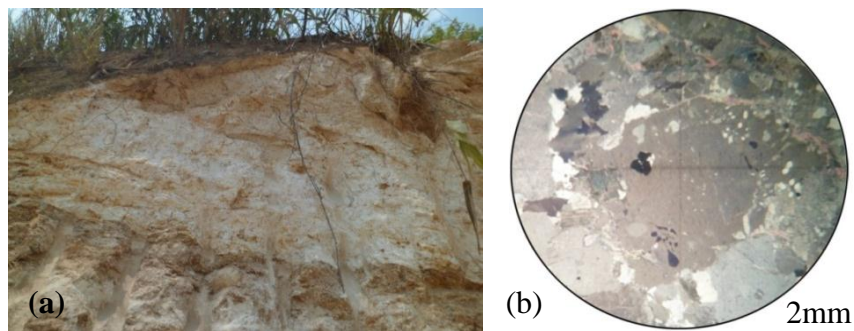


Figure 4 (a) Massive outcrop nature but highly weathered of leucogranite. (b) Holocrystalline texture in leucogranite, under XN.



Figure 5 (a) Outcrop of granodiorite boulder (Loc 21° 27' 30" N & 99° 37' 00"E). (b) Medium-grained, holocrystalline, hypidiomorphic granular texture of under X.N view of granodiorite.

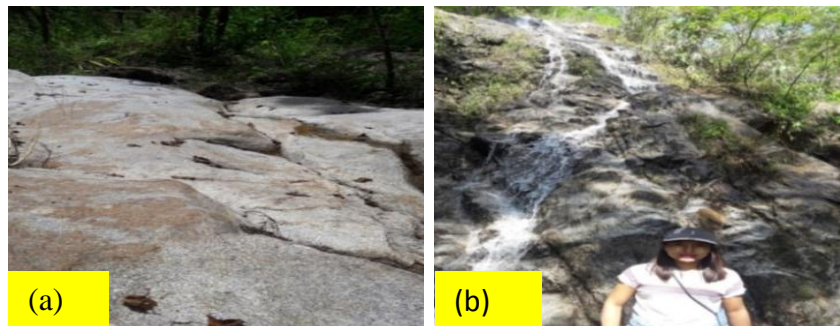


Figure 6 (a) Highly exfoliated character of biotite granite outcrop (Loc. 21° 27' 07.54" N & 99° 36' 54.31" E) (b) Very massive outcrop of biotite granite (Loc. 21° 27' 15.562" N & 99° 37' 43.293" E).

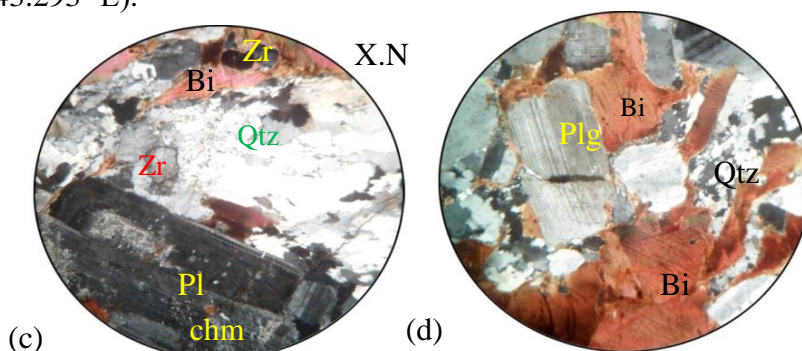


Figure 6 (c) Photomicrograph showing sericitization, zoning and simple twin in euhedral large orthoclase, under XN. (d) Automorph plagioclase surrounded by recrystallization of biotite, under XN.

Petrochemistry

Geochemical Characteristics of Granitoid Rocks

Major oxides and trace elements compositions of 7 representative samples from the study area have been selected and analyzed. The major oxide and trace element compositions of the representative granitoid rocks from the study area are shown in (Table (1) & (2)). Standard CIPW norms and CIPW norm with biotite and hornblende are calculated following to the rules of Hutchison (1975) by using the aid of computer (Table 3).

SiO₂ contents of biotite granite samples are in the range (65.83- 70.69%), granodiorite(66.80- 68.22%) and leucogranite(73.23-74.73%) respectively. Al₂O₃ contents are (13.6%-15.25%) in biotite granite, (15.11%-15.46%) in granodiorite and (13.8%-14.06%) in leucogranite. K₂O contents are (3.64%-3.95%) in biotite granite, (2.99%-3.96%) in granodiorite and (4.01%-6.31%) in leucogranite. CaO contents are (1.92%-3.06%) in biotite granite, (0.61%-2.57%) in granodiorite and (0.31%-0.52%) in leucogranite each other. A/CNK (molecular Al₂O₃/ (CaO+Na₂O+ K₂O) content in all analyzed samples show >1.1 values. According to Chappell & White (2001), I-type and S-type of granitoid rocks are distinguished by the 1.1 limited values based on molecular Al₂O₃/ (CaO+Na₂O+ K₂O) content. CIPW normative corundum content in all granitoid rocks show >1%.

Differentiation Index (D.I) of granitoid rocks in the study area varies from 73.8 to 92.7. CIPW norms with hypersthene contents range from 2.50 % to 13.10%. Magnetite contents (0.52-2.54%), ilmenite contents (0.04-1.69%) and zircon content (0.03-0.06%) are noted. Total alkali content (Na₂O+ K₂O) ranges from 4.48% to 7.71% while (Na₂O+ K₂O+CaO) contents are (6.68%-9.27%) and (Al₂O₃+Na₂O+ K₂O) contents are (19.32%-21.72%). Kyaing Tong granitoid rocks show high abundance of Cr, Rb, Sr, Ba, and Zr.

According to White (1979), the two types of granite come from source rocks of fundamentally different origin, one formed by deposition on the crust, S-type (Sedimentary or Supracrustal source) and the other by accretion beneath the crust, I-type (Igneous or Infracrustal source). Based on the geochemical data, the weight percent of alumina is higher in all granitoids (13.6-15.46 wt %), indicating that all analyzed granitoid rocks in the study area belong to the peraluminous field and some to metaluminous field.

In AFM diagrams (after Irvine and Barragar, 1971) (Figure 7), all granitoid samples fall in calc-alkaline field. According to K₂O Vs SiO₂ diagram by Peccerillo and Taylor (1976), most granitoid samples fall in high- K calc-alkaline series and one leucogranite sample falls in shoshonite series (Figure 8). Na₂O-Al₂O₃-K₂O diagram (Figure 9) shows all granitoid rocks of the study area fall in the metaluminous+peraluminous field clan with more potassic feldspar than sodic proportions.

Table 1 Major oxide weight (%) compositions of the S-type granitoid rocks from the study area.

Sample NO.	KZW-8	KZW-19	KZW-3	KZW-12	KZW-18	S-1	K-2
SiO ₂	66.80	68.22	74.73	73.23	65.83	68.7	70.69
TiO ₂	0.88	0.79	0.02	0.23	0.89	0.83	0.47
Al ₂ O ₃	15.11	15.46	14.06	13.8	13.96	13.6	15.25
Fe ₂ O ₃	6.02	5.23	1.19	2.01	5.54	4.87	2.35
MnO	0.09	0.08	0.31	0.02	0.09	0.07	0.03
MgO	3.76	3.24	0.36	0.76	3.51	2.47	1.27
CaO	2.57	0.61	0.52	0.31	3.06	1.92	2.81
Na ₂ O	1.49	2.11	3.65	1.4	1.81	1.77	3.07
K ₂ O	2.99	3.96	4.01	6.31	3.64	3.95	3.39
P ₂ O ₅	0.29	0.29	0.06	0.2	0.31	0.19	0.13
Total	100.00	99.99	98.91	98.27	98.64	98.4	99.46

In A/Nk (molecular $\text{Al}_2\text{O}_3 / (\text{Na}_2\text{O} + \text{K}_2\text{O})$ versus A/CNK (molecular $\text{Al}_2\text{O}_3 / (\text{CaO} + \text{Na}_2\text{O} + \text{K}_2\text{O})$) diagram by Shand(1943), all granitoid samples fall in peraluminous field (Figure10). Various plots are used to distinguish the genetic type of granitoids rocks of the study area. All variation diagrams indicate that S-type signature.

S-type granites are always oversaturated in Al, or peraluminous, and that is the case also for the more felsic I-type granites. Chappell and White (1974) recognized this in drawing their boundary between the I- and S-types, with a limiting value for the Aluminium Saturation Index (ASI;Zen 1986) of 1.1, or 1% normative corundum with respect to the above geochemical signatures. The magmatic differentiation trend of S-type granitoid rocks of the study area are in accordance with of molecular (A/CNK) Vs SiO_2 diagram (Figure 11).

Table 2 Trace elements (ppm) compositions of the S-type granitoid rocks from the study area.

Sample NO.	KZW-8	KZW-19	KZW-3	KZW-12	KZW-18	S-1	K-2
As	0	4	0	0	3	2	0
Ba	1501	783	28	488	918	913	1536
Co	43	25	53	34	30	38	38
Cr	122	103	0	0	110	70	5
Cu	24	2	2	2	19	26	5
Mo	8	8	0	7	11	8	16
Nb	18	18	26	17	17	17	7
Ni	37	47	7	11	31	39	10
Pb	38	33	29	56	32	43	62
Rb	152	255	352	414	218	208	111
S	181	180	98	559	491	1837	343
Sr	305	142	10	34	203	143	1089
V	142	113	5	10	122	123	44
Y	33	40	35	36	47	35	16
Zn	75	69	0	15	65	68	44
Zr	312	268	24	125	306	293	225

Table 3 Standard CIPW norms and CIPW norm with biotite and hornblende weight (%) compositions of the S-type granitoid rocks from the study area.

Sample No.	KZW-8	KZW-19	KZW-3	KZW-12	KZW-18	S-1	K-2
Quartz	32.58	32.59	35.92	38.83	28.28	34.32	30.72
Orthoclase	18.37	23.52	23.70	37.65	15.32	24.07	21.27
Albite	12.19	17.52	30.89	11.85	13.21	14.98	25.98
Anorthite	10.63	1.20	2.19	0.23	22.24	8.34	13.44
Corundum	5.02	6.97	2.91	4.52	2.07	3.22	1.38
Hypersthene	13.10	11.37	2.50	3.26	12.36	8.88	4.51
Magnetite	2.54	2.23	0.52	0.87	2.41	2.07	1.03
Ilmenite	1.61	1.46	0.04	0.44	1.69	1.58	0.89
Apatite	0.65	0.65	0.14	-	0.72	0.44	0.30
Zircon	0.60	0.06	-	0.03	0.06	0.06	0.04
Chromite	0.03	0.03	-	-	0.03	0.01	-
Pyrite	0.04	0.04	0.02	0.13	0.11	0.38	0.06
D.I	73.8	74.8	92.7	88.6	79.0	81.7	91.4
Total	96.82	97.64	98.84	98.27	98.49	98.34	99.62

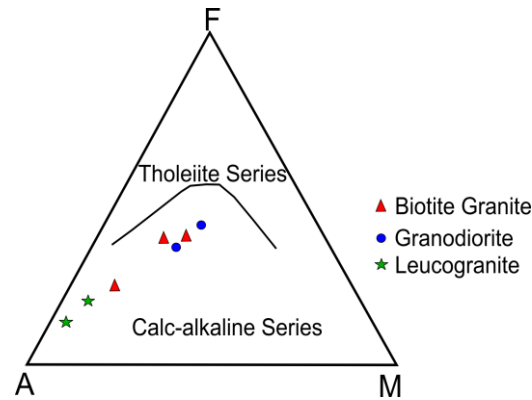


Figure 7 AFM diagram (after Irvine and Barragar, 1971) shows the Calc-alkaline magma series of granitoids of Kyaing Tong.

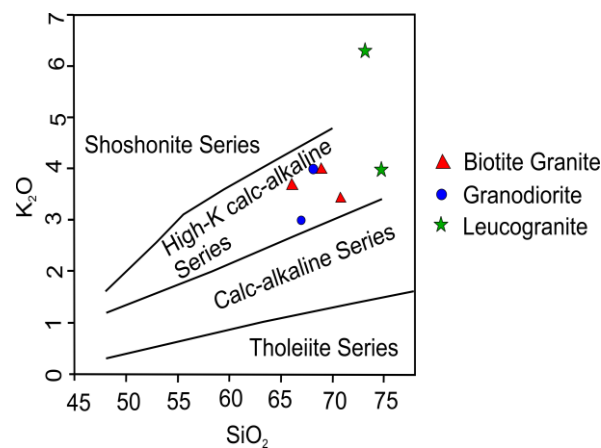


Figure 8 K₂O Vs SiO₂ diagram by Peccerillo and Taylor (1976) shows most granitoid samples fall in high- K calc-alkaline series and one leucogranite sample falls in shoshonite series.

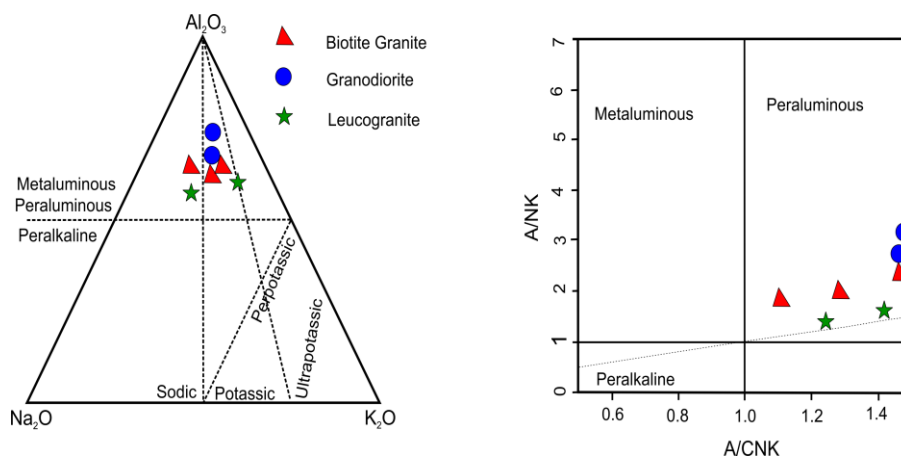


Figure 9 Na₂O-Al₂O₃-K₂O diagram shows all granitoid rocks of the study area fall in the metaluminous+peraluminous field

Figure 10 A/Nk versus A/CNK diagram by Shand (1943) shows all granitoid samples fall in peraluminous field.

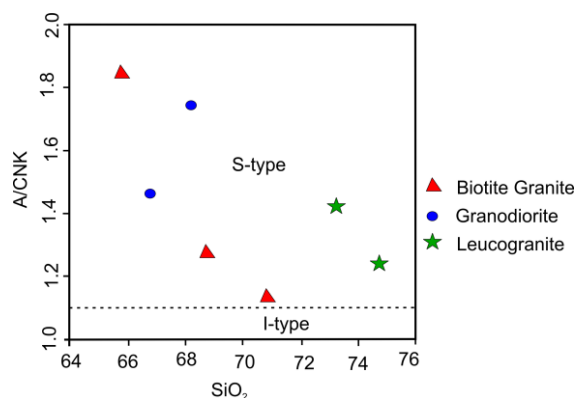


Figure 11 Molecular (A/CNK) Vs SiO₂ diagram shows S-type granitoid rocks of the study area.

Geotectonic Setting of Granitoids

When trace element data plotted by (Pearce et al, 1984), one biotite granite sample falls in VAG + syn-COLG setting and the others are WPG setting (Figure 12 a & b).

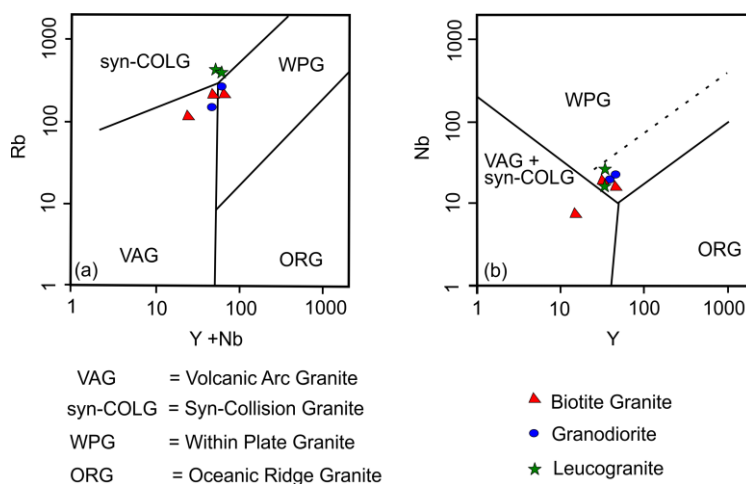


Figure 12 (a) (Y+ Nb) vs Rb diagram and (b) Y vs Nb diagram show tectonic setting of granitoids rocks of the study area. (after Pearce et al, 1984)

Regional Tectonic Setting

Plate tectonic interpretations of geological events within the Burmese region have been made by many workers in recent years (Mitchell, 1973, 1977, 1979, 1981, Mitchell and Garson 1972, 1976, Goossens 1978, Curray *et al.* 1979, 1982, Hla Maung 1987, Win Swe 1981a, b, Maung Thein 1983, Bender 1983, Khin Zaw 1986, 1987a, 1989). Kyaing Tong granitoid batholith is the most important part of eastern granitoids belt of Myanmar (Khin Zaw, 1990). Eastern granitoid belt of Myanmar lies in important mineralized granitoid province in the Southeast Asian region. It is geographically considered as a part of the Shan-Thai Block, tectonically defined as a part of Sibumasu Block, especially considered as a northern continuation of Inthanon Zone of central granitoid belt of Thailand.

Eastern Granitoid Belt of Myanmar

KhinZaw (1990) reported that there are three granitoid belts of Burma which are namely Eastern Granitoid Belt, Central Granitoid Belt and Western Granitoid Belt from east to west (Figure 13 (a)). Mitchell (1977) suggested the Eastern Granitoid Belt of Myanmar as being the result of continental collision and similar to the Malay Peninsula Granitoids. Bender (1983) commented on large granite complexes found east of the Salween River. He presumed a Early Triassic age on these based on their apparent correlation with the granites in the Fang District in northern Thailand as dated by Von Braun et al. (1976), and now inferred to be a part of the Main Range Province. More recently, the Department of Geological Survey and Exploration of Myanmar (DGSE) has undertaken mapping within the Eastern Shan State, and they have assigned a Mesozoic age to the Tachileik granite (MyintKo et al., 2007; U Nyunt Htay, Personal communication). Than Htun et al. (2014) reported a Late Triassic age from a biotite granite within the Mong Ton – Mong Hsat tin district, on the Myanmar - Thailand border.

Kyaing Tong Granitoids

Kyaing Tong granitoid batholiths (including the present study area) appear to intrude the preexisting Chaung Magyi sediments. During the final collisional consolidation of these terranes, Late Triassic to Early Jurassic collisional tin-bearing Main Range granitoids were formed in Southeast Asia. However, the study area is mainly concerned with the subduction zone related to the Inthanon Zone, especially Central granitoid belt of Thailand.

Possible Tectonic Setting

Sibumasublock was eastward dipping underneath the Indochina Block forming the subduction zone during Late Triassic which might induce the intrusion of the Kyaing Tong Granitoids. S-type granitoids are believed to be derived from the partial melting of continental crust at the edge of Sibumasu (WPG, within Plate) due to the evidences: magmatic differentiation in Rb,Ba and Sr correlation. Kyaing Tong Basin is considered as the back-arc basin type behind the subduction suture. Southern portion of the study area entirely belongs to the northern marginal segment of Kyaing Tong Basin. It took place in Late Indonesian orogeny event, the closure of Palaeo-Tethys time. Possible tectonic setting of Kyaing Tong granitoids is shown in (Figure 13(b)).

Possible Tectonic Setting of Eastern Granitoid Belt of Myanmar

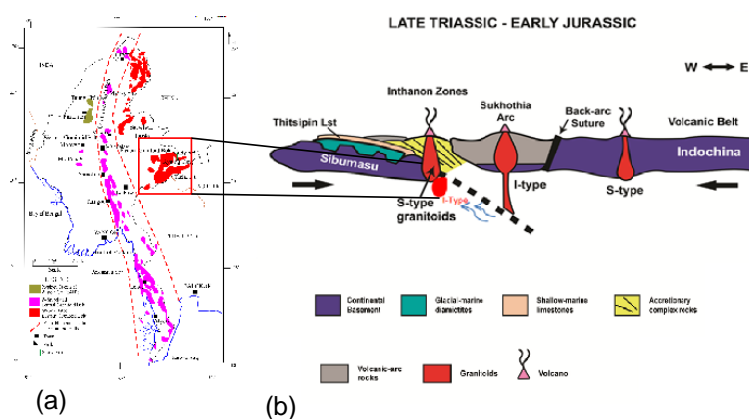


Figure 13 (a) Granitoid Belt of Myanmar (Eastern, Central & Western) (KhinZaw, 1990). (b) Possible tectonic setting of Kyaing Tong granitoids (Modified after Metcalfe et al., 2011).

Conclusion

The granitoid rocks in the study area are mostly in peraluminous field. It indicates that the distinct crustal sources and high peraluminosity of the granites also prefer more pelitic sediments may contribute in the magma. Main body of eastern granitoid belt of Myanmar, the Kyaing Tong granitoids also has the same kind of geological characteristics of the Taung Peng Granites and Central granitoid belt of Thailand. Moreover, these entirely differ from Tak Batholiths of Eastern granitoid belt of Thailand. It is tectonically defined as a part of Sibumasu Block, especially considered as a northern continuation of Inthanon Zone of Central Thailand.

According to the geochemical signatures of trace elements data interpretations, Kyaing Tong granitoids is very complicated marked by syn-collision, volcanic arc granites and within plate granite. These are closely similar to the Inthanon Zone of Central Granitoid Belt of Thailand. Granitoid rocks of the study area (S-type) originated as a result of partial melting of thick continental crust. It may have been directly related to the collision of Shan-Thai (Sibumasu Block) and Indochina block. These produced voluminous S-type granitoids occurring as highly mountain chains generally as a NW-SE trending. Emplacements of granitoids are formed when collision related granites were generated late in the Triassic, the collision was already completed. The Sibumasu Block may have been continued eastward dipping subduction beneath Indochina block and that consequently the margin of Sibumasu Block overthrust the margin of Indochina causing the subduction zone.

Acknowledgements

We wish to express my special thanks to Professor Dr Day Wa Aung, Professor Dr Htay Lwin, Department of Geology, and University of Yangon for their advice, comment and great encouragement to this goal. This paper could not be completed without the helpful hands and willing help from all staff members from Geology Department, University of Yangon.

References

- Bender, F., (1983). *Geology of Burma*; Gebrüder Borntraeger, Berlin. 293p.
- Braun, V.E., Besang, C., Eberle, W., Harre, W., Kreuzer, H., Lenz, H., Muller, D., Wendt, I., (1976). Radiometric age determinations of granites in Northern Thailand. *Geologisches Jahrbuch* 21, 171–204.
- Gardiner, N. J., Searle, M. P., Morley, C. K., Whitehouse, M. P., Spencer, C. J., Robb, L.J. 2016. The Closure of Palaeo-Tethys in Eastern Myanmar and Northern Thailand: New Insights from Zircon U-Pb and Hf Isotope Data. *Gondwana Research*, 39, 401–422.
- Chappell B. W. & White A. J. R., (1974). Two Contrasting Granite Types: Pacific Geology. 173–4.
- Chappell B. W. & White A. J. R., (2001). Two Contrasting Granite Types: 25 years later. *Australian Journal of Earth Sciences* (2001) 48, 489–499.
- Curry, J.R., Moore, D.G., Lawver, L.A., Emmel, F. J., Riatt, E.W., Henry, M. & Kiekhefer, R., (1979). Tectonic of the Andaman Sea and Burma. In: Khin Zaw, 1990. Geological, petrological and geochemical characteristics of granitoid rocks in Burma: with special reference to the associated W-Sn mineralization and their tectonic setting. *Jour. SE Asian Earth Sciences* 4 (4), p.293–335.
- Goossens, P., (1978). The metallogenic provinces of Burma: their definitions, geological relationships and extension into China, India and Thailand. Third Regional Conference on Geology and Mineral Resources of Southeast Asia, P.431. In: Khin Zaw, 1990. Geological, petrological and geochemical characteristics of granitoid rocks in Burma: with special reference to the associated W-Sn mineralization and their tectonic setting. *Jour. SE Asian Earth Sciences* 4 (4), p.293–335.
- Hla Maung, (1987). Transcurrent movements in the Burma-Andaman Sea region. In: Khin Zaw, 1990. Geological, petrological and geochemical characteristics of granitoid rocks in Burma: with special reference to the associated W-Sn mineralization and their tectonic setting. *Jour. SE Asian Earth Sciences* 4 (4), p.293–335.
- Irvine, T.N., & Baragar, W.R.A., (1971). A Guide to the chemical classification of the Common Volcanic Rocks. *Can. Jour.*

- Khin Zaw, (1990). Geological, petrological and geochemical characteristics of granitoid rocks in Burma: with special reference to the associated W-Sn mineralization and their tectonic setting. *Jour. SE Asian Earth Sciences* 4 (4), p.293-335
- Khin Zaw. (1986). Geological, petrological and geochemical characteristics of granitoid rocks in Burma: with special reference to the emplacement of W-Sn mineralization. In: KhinZaw ,1990. Geological, petrological and geochemical characteristics of granitoid rocks in Burma: with special reference to the associated W-Sn mineralization and their tectonic setting. *Jour. SE Asian Earth Sciences* 4 (4), p.293-335
- Khin Zaw. (1987a.) Tectonic settings for the emplacement of granitoid rocks in Burma. In: KhinZaw ,1990. Geological, petrological and geochemical characteristics of granitoid rocks in Burma: with special reference to the associated W-Sn mineralization and their tectonic setting. *Jour. SE Asian Earth Sciences* 4 (4), p.293-335
- Khin Zaw. (1989). Comment on Transcurrent movements in the Burma-Andaman Sea region. In: KhinZaw ,1990. Geological, petrological and geochemical characteristics of granitoid rocks in Burma: with special reference to the associated W-Sn mineralization and their tectonic setting. *Jour. SE Asian Earth Sciences* 4 (4), p.293-335
- Maung Thein, (1983). The geological evolution of Burma. Dept. of Geology, Mandalay University, Mandalay, Burma (unpublished). In: KhinZaw, 1990. Geological, petrological and geochemical characteristics of granitoid rocks in Burma: with special reference to the associated W-Sn mineralization and their tectonic setting. *Jour. SE Asian Earth Sciences* 4 (4), p.293-335.
- MaungThein,(2014). Geological Map of Myanmar.Myanmar Geosciences Society.pp.1-32.
- Metcalf, I., (2006). Palaeozoic and Mesozoic tectonic evolution and palaeogeography of East Asian crustal fragments: the Korean Peninsula in context. *Gondwana Research* 9, 24–46. Gardiner, N. J., Searle, M. P., Morley, C. K., Whitehouse, M. P., Spencer, C. J., Robb, L.J. 2016. The Closure of Palaeo-Tethys in Eastern Myanmar and Northern Thailand: New Insights from Zircon U-Pb and Hf Isotope Data. *Gondwana Research*, 39, 401-422.
- Michael F. Ridd, Anthony J. Barber & Michael J. Crow, (2011). *Geology of Thailand*. Geological Society, London. pp. 629.
- Mitchell, A.H.G., &Garson,M.S. (1976). Mineralization at plate boundaries. In: KhinZaw ,1990. Geological, petrological and geochemical characteristics of granitoid rocks in Burma: with special reference to the associated W-Sn mineralization and their tectonic setting. *Jour. SE Asian Earth Sciences* 4 (4), p.293-335.
- Mitchell, A.H.G., (1977). Tectonic settings for emplacement of Southeast Asian tin granites. *Bulletin of the Geological Society of Malaysia* 9, pp. 123-140.
- Myint Ko, Aung Than Myint, NyuntHtay, (2007). Regional geological map of Paliao-Keng Lap Area, Tachileik Township, Eastern Shan State, Block Nos. 400, 401, 426.
- Myanmar Ministry of Mines, Department of Geological Survey and Mineral Exploration.
- Gardiner, N. J., Searle, M. P., Morley, C. K., Whitehouse, M. P., Spencer, C. J., Robb, L.J. (2016). The Closure of Palaeo-Tethys in Eastern Myanmar and NorthernThailand: New Insights from Zircon U-Pb and Hf Isotope Data.*Gondwana Research*, 39, 401-422.
- Pearce, J.A. Pearce, J. A., Harris, N. B. W., and Tindle, A. G., (1984). Trace elements discrimination diagrams for tectonic interpretation of granitic rocks. *Jour. petrology*, vol. 25, p. 956-983.
- Pececrillo, A., & Taylor, S.R., (1976).Geochemistry of Eocene calc alkaline rocks from the Kastamonu area, Northern Turkey.*Contriburion to Mineralogy and Petrology*. 58, p. 68-81.
- Shand, S.J., (1943). *Eruptive Rocks*. T. Murby and Co., London, 444pp.
- Sial. A.N., Bettencourt, J.S, De Campos, C.P and Ferreira, V.P, 2011. *Granite – Related Ore Deposits*.
- Than Htun, Somboon, K., Manaka, T., (2014). Preliminary Investigation of New Tin Deposits in Mong Ton-MongHsat Area, Shan State (East), Myanmar. In: Win Swe, SoeThuraTun, Myo Thant, KhinZaw (Eds.), Thirteenth Regional Congress on Geology. Mineral and Energy Resources of Southeast Asia GEOSEA 2014 Abstracts, p. 8. Gardiner, N. J., Searle, M. P., Morley, C. K., Whitehouse, M. P., Spencer, C. J., Robb, L.J. 2016. The Closure of Palaeo-Tethys in Eastern Myanmar and NorthernThailand: New Insights from Zircon U-Pb and Hf Isotope Data.*Gondwana Research*, 39, 401-422.
- Thornton, C.P., & Tuttle, O. F, (1960). Chemistry of igneous rock; I. Differentiation Index, *Am. J. Sci.*, vol. 258, p.664-684.

- Win Swe. (1981a). Tectonic evolution of the Western Ranges of Burma. *Contrib. Burmese Geol.* 1, 45-56. In: Khin Zaw, 1990. Geological, petrological and geochemical characteristics of granitoid rocks in Burma: with special reference to the associated W-Sn mineralization and their tectonic setting. *Jour. SE Asian Earth Sciences* 4 (4), p.293-335.
- Win Swe. (1981 b). A major strike-slip fault in Burma. *Contrib. Burmese Geol.* 1, 63-74. In: Khin Zaw, 1990. Geological, petrological and geochemical characteristics of granitoid rocks in Burma: with special reference to the associated W-Sn mineralization and their tectonic setting. *Jour. SE Asian Earth Sciences* 4 (4), p.293-335.
- Zen, E., (1986). Aluminum enrichment in silicate melts by fractional crystallization: some mineralogic and petrographic constraints. *J. Petrol.* 27, 1095-1117.

PETROLOGY AND STRUCTURES OF VOLCANOCLASTIC SEDIMENTARY ROCKS AND IGNEOUS ROCKS IN SHINMATAUNG AREA, PAKOKKU TOWNSHIP, MAGAWE REGION

Yu Yu San¹, Tun Naing Zaw²

Abstract

The study Shinmataung area situated between latitudes (21° 33' to 21° 37') N and longitude (95° 4' to 95° 10') E. Volcanic eruption might occur during and after the time of deposition of Irrawaddy Formation. Bender (1983) stated that west zone of "Pegu - Mt. Popa Line" begins south of Kabauk Village in the Shinmataung area and runs for about 100km with width of up to 18km via Salingyi, Silaungtaung and Twintaung to Natyintaung in the N. The lower Chindwin volcanic including Shinmataung area is situated north of Mt-popo and NNW striking section of the Central Volcanic Arc. The rocks are Tertiary in age except the igneous rocks of Salingyi area. Igneous rocks of the study area are rhyolitic agglomerate, breccia, diorite, olivine basalt, andesitic tuff and altered andesite. During the Miocene to sub-recent time, episodes of intermittent volcanic activity have been firstly recognized in the present area. The first phase was the extrusion of andesites. This activity appears to have been followed by the violent activity going rise to andesitic tuff-cones associated with rhyolitic agglomerate and breccia. Igneous rock units are also occurred in the western part of the present study area. These rock units are occurred isolated cone shaped hill half miles east of Kabauk village and Thardon- U hill about one mile south east of Kabauk. Moreover, dacite, fine-grained igneous rock also occurred in the valley between Taungnigyi and Shinmataung hill. Igneous rock units hill, lying nearly parallel to the Shinmataung hill, The study area (Shinmataung) is located in the Central Cenozoic Belt of Myanmar. Geologically, it is situated on the northeastern most edge of the Minbu Basin. This basin is a kind of gradually subsiding geosyncline related to subduction of India Plate beneath the Burma Plate in which tremendous thickness of clastic sediments were deposited during Oligocene to Pliocene?. The Shinmataung area is located in Yesagyo Township, Pakokku District, situated between are separated by a fault valley. Contact between igneous and sedimentary rocks can be noted beside Taunggya-Kabauk cart tract. In the Shinmataung area is the contemporaneous volcanic intercalations towards the base of the Oligocene and towards the upper limit of the composed strata. These volcanic rocks have been recorded as Miocene age in the present study area.

Keywords: andesite, rhyolitic agglomerate, breccia, diorite, olivine basalt, andesitic tuff, Pegu-Mt. Popa Line

Introduction

Location and size

The study Shinmataung area is located in Yesagyo Township, Pakokku District, situated between latitudes (21° 33' to 21° 37') N and longitude (95° 4' to 95° 10') E. It. The study area, 5.1miles long and 6.2 miles wide, covers 31.68 square miles.

The highest peak of Shinmataung is about 1723 ft about sea level. Shinmataung is a north plunging anticline ridge which is trending nearly NNW - SSE direction. It is located about 6 miles west of Yesagyo.

It is readily accessible through the year because is bounded by vertical grids 42 to 53 and horizontal grids 16 to 25 in one inch topographic map 84 O/2. It is bounded on the north by Mongywa-Yesagyo motor-car-road and on the east by Yesagyo-Pakokku road. (Fig.1.1) shows the location and aerial extent of the study area.

¹ Assistant Lecturer, Department of Geology, University of Yangon,

² Lecturer, Department of Geology, University of Yangon

Previous study

The Tertiary geology of Myanmar had been given much attention since 1854. Much progress has been made since the appearance of Theobald's memoir (1873), on the Geology of Pegu. During the intervening years up to the Second World War the investigators from the Geological Survey of India made some important contributions towards the subject.

Edwin Pascoe's reference to the vents of Shinmataung in (1908) appears to be the first published reference to the igneous rocks of the study area. In this reference, he mentioned that some of the volcanic rocks of the Shinmataung area are later age, but some at least are contemporaneous with the Pegu rocks. The volcanic occurrences and associated rocks further south of Shinmataung were studied by Dr. E Vredenburg in (1921). As a result of his investigation, he stated:

“Of particular interest, in the Shinmataung area is the contemporaneous volcanic intercalations towards the base of the Oligocene and towards the upper limit of the composed strata.”

Dr. C. T Berber of the Geological Survey of India continued the work of the work of the letter four authors in Pakokku in 1925, 26. He described the regional geology of the area and studied the petrography of andesites, basalts, and pyroclastics of the area.

Bender (1983) stated that west zone of “Pegu - Mt. Popa Line” begins south of Kabauk Village in the Shinmataung area and runs for about 100km with width of up to 18km via Salingyi, Silaungtaung and Twintaung to Natyintaung in the N.

General Statements

The area investigated is situated in the lower Chindwin Area, lying NNW striking section of the Central volcanic arc which coincides with the axis of the central Cenozoic Sedimentary Basin, dividing it into Western and Eastern Troughs. The occurrences of igneous rocks are here bound to two structural zones. The western zone is the continuation of the “Pegu- Mt. Popa” line. It begins at the Kabauk of the Shinmataung and Twintaung to Natyin Taung in the north. The second line runs parallel to the first, east of Monywa and can be followed for a distance of about 40km.

The present study area occurring at Minbu basin in the Central Lowland is composed of Cenozoic Rock Units. The Cenozoic sequence of the study area contains sedimentary rocks and igneous rocks. From the petrographic characteristics and reasonable evidences, the greater part of the source area was formed by the granitic plutons and low to high grade metamorphic rocks. The area might have been the Salingyi upland area and Kawlin-Wuntho area. During the period of Miocene to sub-recent time, episodes of intermittent volcanic activity have been firstly recognized in the present area. The first phase was the extrusion of andesites. This activity appears to have been followed by the violent activity going rise to andesitic tuff-cones associated with rhyolitic agglomerate and breccia.

Almost all of the andesites in the study area have been affected by alteration. The dominant processes alteration found in these rocks are porphyllization, kaolinization, albitization and chloritization. The probable sequences of rock units mapped in the paper are recognized. The sedimentary rock units are classified according to the distinctive lithological characteristic of the each formation. They are described namely Shwezettaw Formation, Padaung Formation and Irrawaddy Formation. The Igneous rock units are given on the basis of petrographic characteristics.

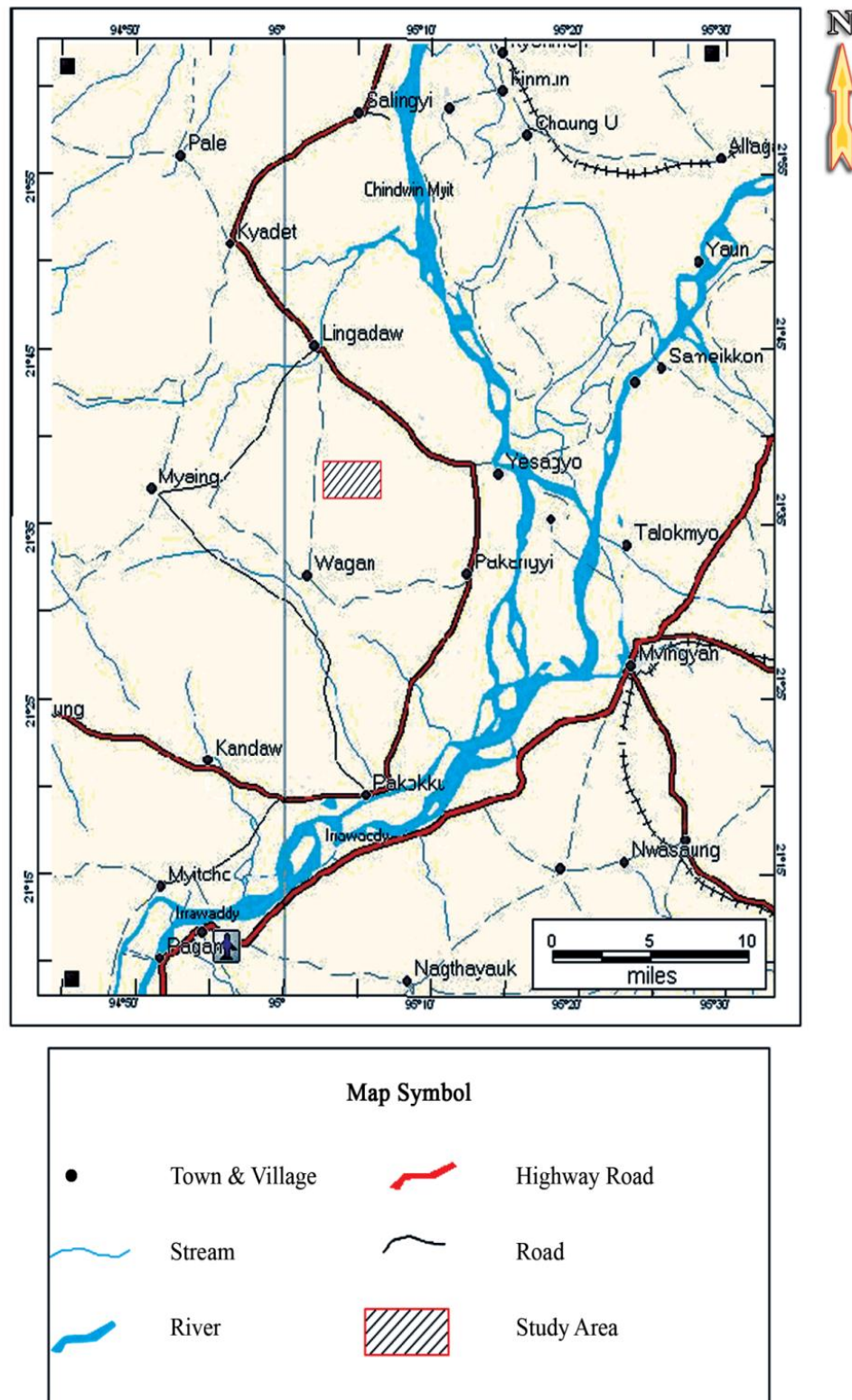


Figure 1 Location Map of the Study Area

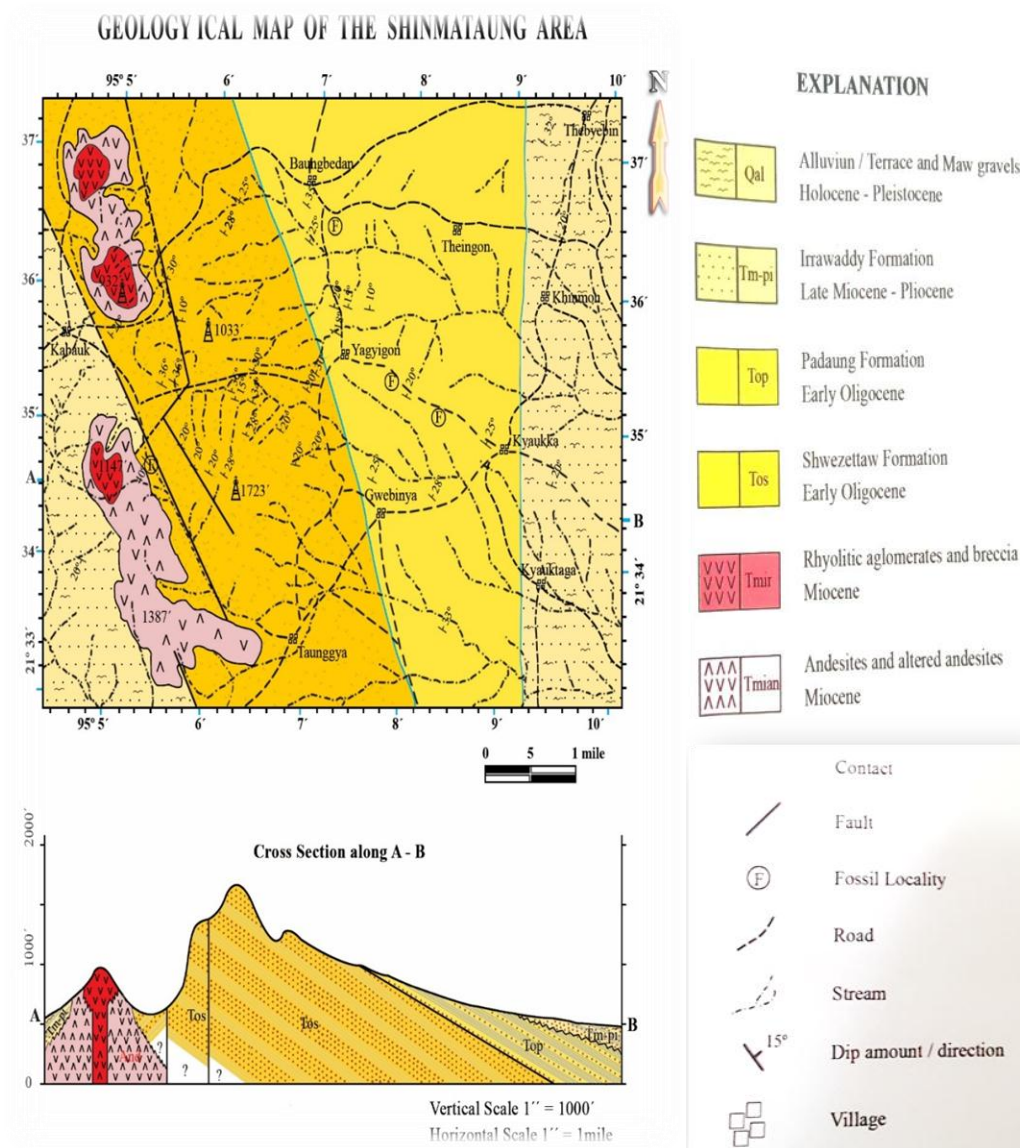


Figure 2 Geology Map of the Shinmataung Area

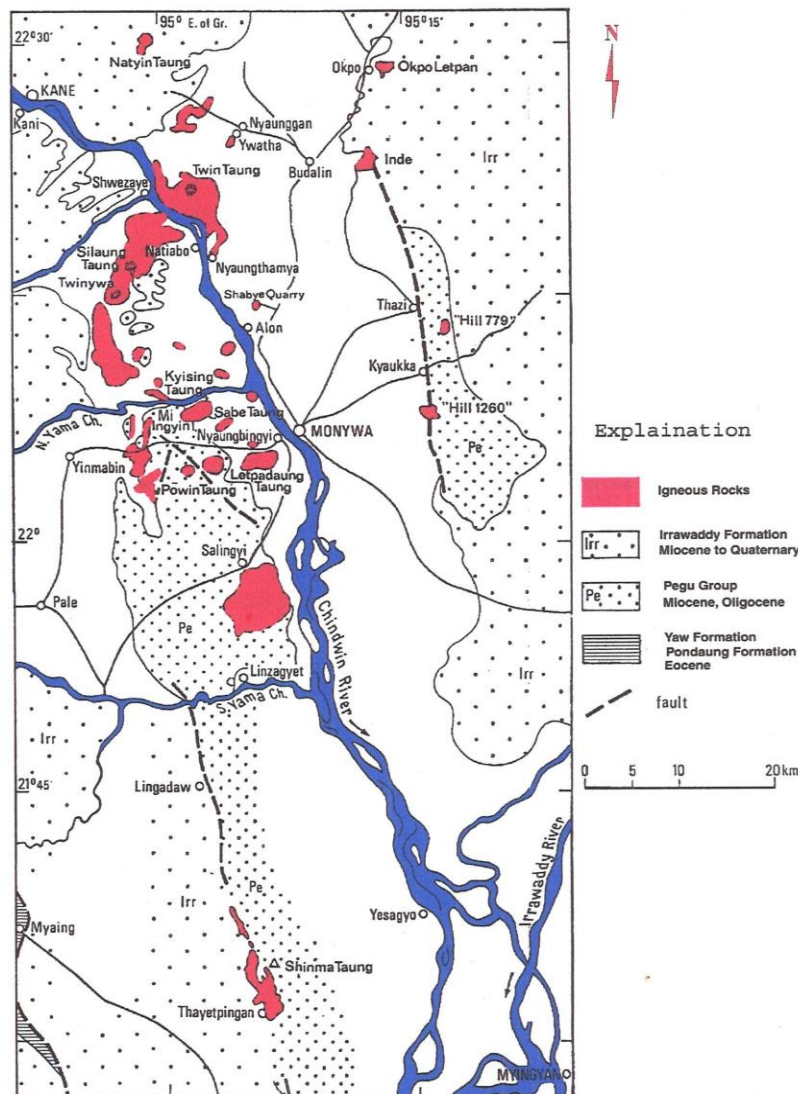


Figure 3 The occurrences of igneous rocks of lower Chindwin area (base on Bender 1983)

Structures of Volcanoclastic Sedimentary Rocks and Igneous Rocks

Shinmataung Valley Fault (F_1) between the main Shinmataung hill and volcanic units, and steep scarps on the western side of the Shinmataung are good indicators for this fault. Kabauk Fault (F_2) is developed in the east of Kabauk village. The Irrawaddy Formation is faulted against Shwezettaw Formation. In the northern part of this fault, the contact of volcanic rocks and Irrawaddy Formation along the fault can be noted. Taungwataung Fault (F_3) is developed in the western base of Taungwataung ridge half mile east of Kabauk. This fault is between Taungwataung and volcanic unit. The volcanic rocks extruded along the fault zone. The volcanic structures in the area are mesa-like structure, pyroclastic cones, and flow structures ropy and blocky structures, vesicular and fragmental top and pyroclastic structures.

Petrography of Volcanoclastic Sedimentary Rocks and Igneous Rocks

The hard-sandstone bands contain then tuffaceous sandstone and hard sandstone of Shwezettaw Formation commonly contain many fossils in this section. In some thin section of Shwezettaw sandstone, (mainly the place where close to the volcanic eruption), volcanic fragment comprise 50 percent of total rock volume.

Igneous rock units are also occurred in the western part of the present study area. These rock units are occurred isolated cone shaped hill, half miles east of Kabauk village and Thardon-U hill about one mile south east of Kabauk. Moreover, dacite, fine-grained igneous rock also occurred in the valley between Taungnigyi and Shinmataung hill. Igneous rock units hill are lying nearly parallel to the Shinmataung hill, which is separated by a fault valley. Contact between igneous and sedimentary rocks can be noted beside Taunggya-Kabauk cart tract.

Some of the igneous rocks are later age, but some sedimentary rocks are contemporaneous exposed on the surface of the Shinmataung area. These volcanic rocks have been recorded as Miocene age in the present study area. Igneous rocks of the study area are rhyolitic agglomerate, breccia, andesitic tuff and altered andesite.

Diorite

Diorites occur as bomb and vine type in Sonetaung .They are usually found together with andesite and basalt. Diorite has a coarse grained, hypidiomorphic granular texture. It is composed mainly of plagioclase and hornblende. It can be said to be oversaturated due to the presence of quartz. Besides, biotite occurs in subordinate amounts.

Rhyolitic Agglomerate and Breccia

In the present study area, the hill tops above half mile east of Kabauk and west of Shinmataung are covered by rhyolitic agglomerates and breccias. They are composed of block of igneous, metamorphic and sedimentary rocks. These blocks are welded by tuff. Both rounded and angular igneous rocks ranging in size from 1 inch to 2 ft in diameter are more predominant than sedimentary rocks.

On the slope of the western foot of these hill, fragments of metamorphosed rock are scattered among the rhyolitic agglomerates and breccias.



Figure 4 Breccia in handspecimen



Figure 5 Breccia in West Shinmataung
(21° 37' N Longitude (95° 08' E))



Figure 6 Rhyolitic agglomerates in handspecimen

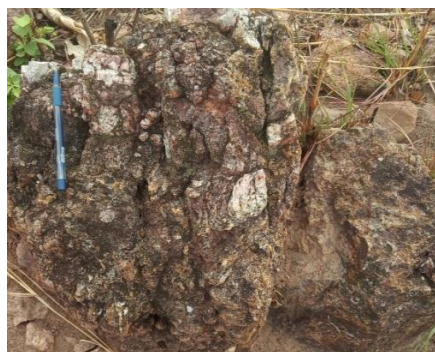


Figure 7 Rhyolitic Agglomerates in West of Shinmataung latitudes (21° 36' N Longitude (95° 08' E))

Andesitic Tuff and altered Andesite

In the vicinity of Thardon-U hill, about one mile south east of Kabauk, it is occupied by altered andesites and andesitic tuffs. Some andesites are weathered to red clays. The dark gray to bluish gray fresh andesite are not occurred and associated with agglomerates and breccias. The andesites of the study area show porphyritic texture in which the phenocrysts are attributed to early crystallization.

Altered andesite is occupied on the Taungle and west of Taunglungyi, Taungshe and Taungbed. The isolated nature of these hill and appearance of volcanic plugs may suggest that each have the separate focus of eruption.

Taungnigyi, eastern most part of these volcanic hills is also occupied by the altered andesites. A small dolerite intrusion is found in the valley the relationship of the dolerite with the adjacent rocks is not easy to identity because of thick capping of soil and dense vegetative cover.

At the lower part of these hills, andesitic tuffs are occurred. By the study of the isolated nature of these hill and scattered of various igneous rock, the igneous rocks from the area may be fracture eruption. In the present study area, dark grey to bluish grey dacite can be found in the valley between Taungnigyi and Shinmataung hills.



Figure 8 Diorite Vein in Basalt in handspecimen



Figure 9 Augite Andesite in handspecimen



Figure 10 Basalt in handspecimen

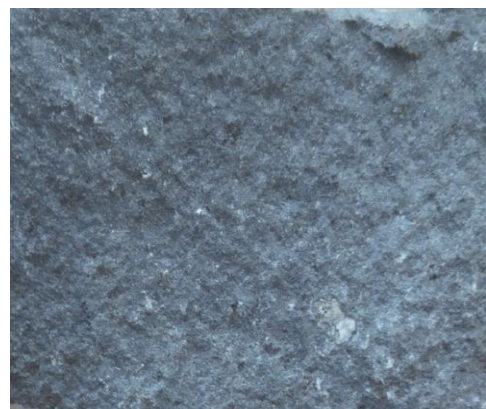


Figure 11 Andesite Tuff in handspecimen

Table 1 Terms for mixed pyroclastic-epiclastic rocks

Phyoclastic	Tuffites (mixed phyoclastic- epiclastic)	Epiclastic (volcanic and/or nonvolcanic)	Avg Clast size (mm)
Agglomerate, agglutinate, phyoclastic breccia	Tuffaceous conglomerate, tuffaceous breccia	Conglomerate, breccia	64
Lapilli tuff			2
(Ash)tuff	Tuffaceous sandstone	Sandstone	1/16
Coarse	Tuffaceous siltstone	Siltstone	1/125
Fine	Tuffaceous mudstone, shale	Mudstone, shale	
75		25	%by volume
<div style="display: flex; align-items: center; justify-content: center;"> <div style="margin-right: 10px;"> \longleftarrow \longrightarrow </div> <div> Phyoclastic Volcanic+ nonvolcanic epiclastic (minor amounts of biogenic, chemical sedimentary and authigenic constituents) </div> </div>			

Microscopic Study of Volcanoclastic Sedimentary Rocks and Igneous Rocks

Diorite

Diorite occur in Songtaung near Taunggar Village. They are usually found together with andesite and basalt. Diorite has a coarse-grained, hypidiomorphic granular texture. It is mainly composed of plagioclase and hornblende and biotite. Plagioclase is 1.3 to 2.7 mm in grain size. It is subhedral in shape. Twin bands are well developed. Fractures are commonly found due to tightly forces. Some plagioclase crystals show oscillatory normal zoning. Hornblende is 1.7 to 2.7 mm in grain size. It is subhedral to anhedral in shape. Cleavages of hornblende are sometime bent. Biotite occurs in subordinate amounts. Biotite is 0.4 mm in grain size. Some biotites have bent cleavage. It is subhedral in shape. Some diorites are found to be totally altered rocks. The rocks are greenish in colour due to chloritization.

Andesitic Tuff

The andesitic tuff consists of the fragments of andesite, quartz-sericite-schist and feldspar crystals. The diameter of pyroclasts varies from 0.3mm to 1mm in length. Some fragments of quartz sericite schist are as large as 8mm in length and 1.5mm in width. Small needles of green tourmaline are also present in it. Due to feldspar determination method of Michel Levees, the average content ranges from 35 to 40 per cent which falls in andesite composition. Some feldspar crystal were slightly zoning with the care of more acid in composition. Some feldspar crystals are mostly altered to kaolinite that is somewhat strained by limited.

Tuff

Tuff consists of crystals, rock fragments and glass. Tuffs are feldspar (plagioclase), hornblende and quartz. Feldspar and hornblende are juvenile pyroclasts. They have been produced by disruption of magma. Quartz is accidental pyroclast. It has been derived from the country rocks (Irrawaddy Formation). Identifiable crystals in thin section are 0.1 to 0.2 mm in

size. The other constituents are minute rock fragments, dust and glass. Any clast in tuff having less than 0.25 mm in size is known as dust.

Olivine Basalt

The basalts in this area are olivine basalt. The basalt has a porphyritic texture with phonocrysts of olivine and plagioclase embedded in fine grained groundmass composed of plagioclase microlites, augites granules, magnetite grains and glass. The vesicle size varies from 0.2mm to 3mm. Subhedral to anhedral minerals of the groundmass are sometimes protruding into the visicles. Olivine phenocrysts occur as subhedral to anhedral crystals. Olivine boundaries are dark brown due to irripient rimming by iddingside and magnetite. Olivine is also found in groundmass. Plagioclase is euhedral and subhedral in shape. Plagioclase phenocryst is 1.3mm in average grain size. Plagioclase phenocrysts show zoning. Plagioclase microlites in groundmass are lath shaped. They are 0.5mm to 1mm in grain size. Plagioclase microlites are randomly oriented and sparsely unique. But when closer to the phenocrysts, presences of microlites are considerable. They bear abundant and some weakly and roughly aligned in groundmass trends to produce flow structure.

Agglomerate

It is composed mainly of andesite blocks. Some bombs of andesite and other igneous rocks are found. The other igneous blocks are rarely found. The size blocks in agglomerate are usually more than 20 cm in diameter.

Rock fragments

Dark brown volcanic glass is also present in this rock. Some fragments of andesite have rounded out lines whereas the metamorphic fragments are subangular in shape.

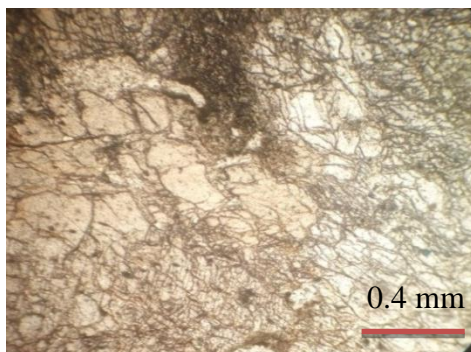


Figure 12 Microscopic Study of Diorite. Under PPL

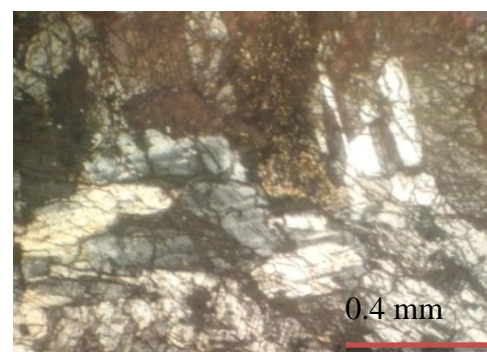


Figure 13 Microscopic Study of Diorite. Between XN

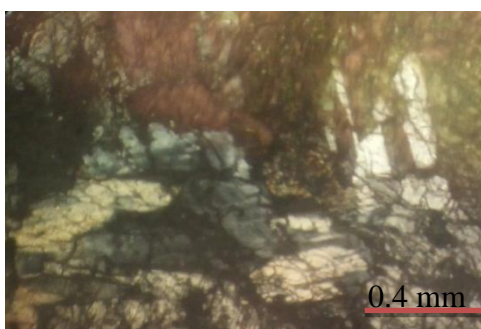


Figure 14 Microscopic Study of Diorite. Between XN



Figure 15 Plagioclase showing oscillatory normal zoning in diorite

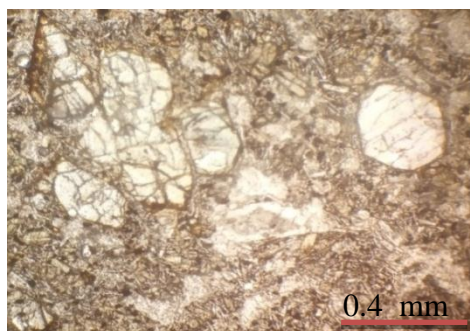


Figure 16 Micrograph showing plagioclase microphenocryst in Olivine Basalt. Under PPL.

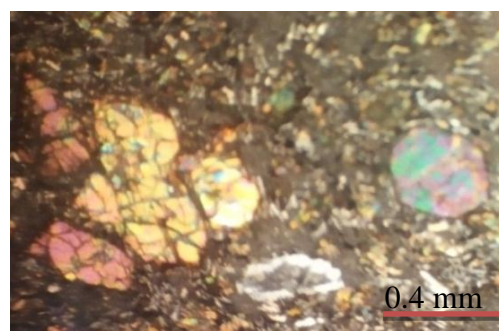


Figure 17 Micrograph showing plagioclase microphenocryst in Olivine Basalt. Between XN.

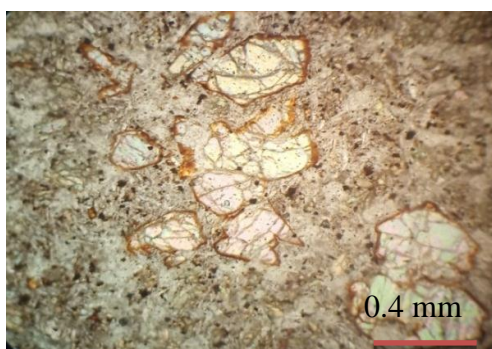


Figure 18 Micrograph showing of Olivine Basalt. Between XN.



Figure 19 Micrograph showing of Olivine Basalt. Between XN.

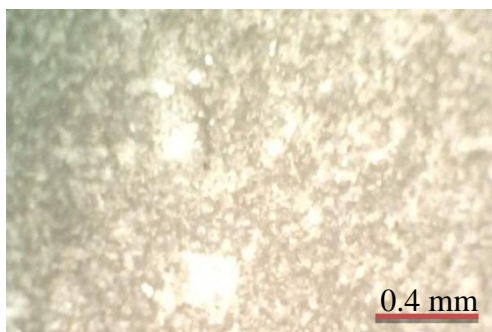


Figure 20 Microphotograph showing tuff.

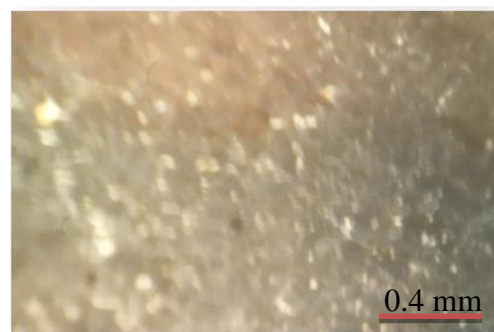


Figure 21 Microphotograph showing tuff. Between XN

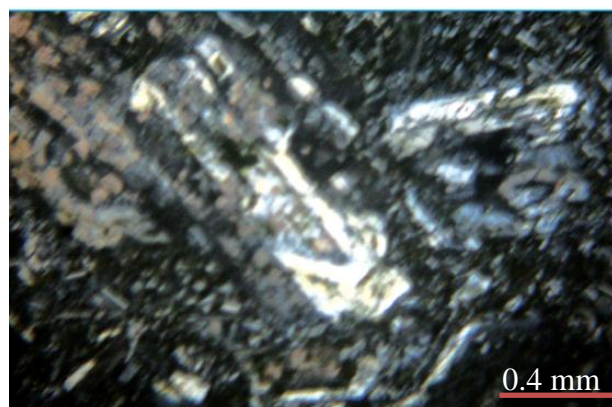


Figure 22 Microphotograph showing andesite tuff. Between XN

Summary and Conclusions

The Shinmataung area between lat ($21^{\circ} 33' - 21^{\circ} 37'$) N & Lon ($95^{\circ} 4' - 95^{\circ} 10'$) E, is located by vertical grids 42 to 53 and horizontal grids 16 to 25 in one-inch topographic map 84 O/2. It is situated about 6 miles west of Yesagyo Township, Magwe Division, covering a surface area of 31.68 square miles. The study area, a small segment of central igneous line is located at the north eastern part of Minbu Basin in the Central lowland. It is composed of Cenozoic sedimentary and volcanic rocks. The lithostratigraphic units older than Oligocene age are not encountered. The lithologic units of formation rank are ascending over are: Shwezettaw Formation, Padaung Formation and Irrawaddy Formation.

Igneous rocks of the present area are mapped and they are rhyolitic agglomerate and breccia, olivine basalt, andesitic tuff; and altered andsite. From the petrographic characteristics and reasonable evidences, the greater part of the source area was formed by the granitic plutons and low to high grade metamorphic rocks. The area might have been the Salingyi upland area and Kawlin-Wuntho area. During the period of Miocene to sub-recent time, episodes of intermittent volcanic activity have been firstly recognized in the present area. The first phase was the extrusion of andesites. This activity appears to have been followed by the violent activity going rise to andesitic tuff-cones associated with rhyolitic agglomerate and breccia.

Almost all of the andesites in the study area have been affected by alteration. The dominant processes alteration found in these rocks are porphyllization, kaolinization, albitization and chloritization. In the study area, the strata of lower Pegu Group & Irrawaddy Formation are exposed and the volcanic rocks extruded along the fault zone. This condition may indicate that the reservoir rock and the channel way for the migration of oil and gas were probably not occurred in the study area.

Acknowledgements

I am especially thankful to Professor and Head Dr. Day Wa Aung, Department of Geology, University of Yangon for permission to carry out the research and his advice on the research works. I am indebted to Dr. Ko Ko Gyi, Pro-Rector (Retd), Department of Geology, Pakokku University for guided my research work. I would like to express my thanks to Dr. Toe Toe Yi, Associate Professor, Department of Geology, Kalay University for his close supervision and guidance throughout the research works.

References

- Barber C. T., (1936), The Extrusive and Intrusive rocks of the Shinmataung area. Mem. Geol. surv. India. V.E.S, Pt.2, p.159-160.
- Bender F., (1983), Geology of Burma: Gerbrüder Borntraeger, Berlin Stuttgart, p. 49-70.
- Khin Maung Tun, (1993), Petrology of the Shinmataung Area, Yesagyo Township, Magway Division, M.Sc. Thesis, unpub. paper, M.U., Geol. Dept., 122p.
- Ko Ko Gyi, (2008), A Study on the Sedimentation and Volcanic Activities in the Shinmataung-Sonetaung Area, Pakokku District., *Ph.D Prelim Paper*. Geol. Dept. M.U., 95p.
- Neotling F., (1894), Note on the Geology of Wuntho in Upper Burma. Rec. Geol. Surv. India, V.27, 4: p.115-124.
- Williams. H., F.J. Turner & C.M. Gilbert, (1953), PETROGRAPHY, An Introduction to the Study of Rocks in Thin Sections. 2nd Edn.
- Win Swe, (1972), Tectonic Evolution of the Western Ranges of Burma. VII. Burma Res. Congr. Rangoon, 49p.

COMPARATIVE STUDY ON GEOCHEMISTRY AND TECTONIC IMPLICATION IN TWO VOLCANIC ENVIRONMENTS: SINGU AREA AND KYAUKPHYU-WEBAUNG AREA, MANDALAY REGION

Myo Ma Ma Htwe¹, Myo Swe Ei², Zar Oo Sann³

Abstract

The objective of this paper is to present the main results of a comparative study of geochemistry and tectonic implication on Singu Area and Kyaukphyu-Webaung Area. The Singu area is composed mainly of the basaltic rocks from the younger lava of Singu Plateau. Singu Lava Plateau is made up of a thick pile of very fluid basaltic flows displaying segregation structure. They form a 100 km² plateau which overlies Mio-Pliocene sandstones as well as the upper part of the Irrawaddy Formation. Most basaltic rocks of Singu area are aphanitic, glassy, and pyroclastic rocks in which plagioclase and pyroxene are major constituents with subordinate amounts of olivine and Fe-Ti oxides. Basaltic rocks often show porphyritic, vesicular and trachytic texture. Major element data suggest that the Singu lava are predominantly of basaltic trachyandesite and show the alkaline nature. According to the immobile trace element concentrations, the basaltic rocks are dominated by alkali basalt. The trace element geochemistry suggests geochemical characteristic of Within-Plate Basalt. Lavas from the Singu area show a clear intraplate character with no subduction signal.

In Kyaukphyu-Webaung area, the basaltic rocks are mainly composed of olivine, plagioclase and pyroxene and minor amount of chrome spinel and opaque minerals. They show porphyritic, trachytic texture and reaction rims. According to the major element data, the volcanic rocks fall in tephrite, trachy basalt, basalt and basaltic andesite. They show tholeiitic and calc-alkaline character. The spider diagram of the basaltic rocks confirm that the basaltic lavas are originated from variable partial melting degrees of subduction-related mantle source and island arc nature. The trace element analyses of the basaltic rock samples indicate that these are having characteristics of either IAT or transitional between MORB and IAT and they have formed in supra-subduction zone tectonic setting. This suggests that there may be significant tectonic differences between Singu Area and Kyaukphyu-Webaung Area.

Keywords: alkaline nature, within-plate basalt, subduction related mantle, MORB and IAT

Introduction

The study area is situated between Singu and Kabwet in Mandalay division and Kyaukphyu-Webaung area in Thabeikkyin and Mongmit Township. This area lies within latitudes 22° 32' N to 23° 15' N and longitudes 95° 56' E to 96° 17' E. It covers part of 93-B/2, 84-N/14, 93-A/4 and 93-A/8 one inch topographic maps (Fig. 1). In the investigated area, tholeiitic, calc-alkaline and alkaline basaltic lavas display contrasted geochemical signatures. These are usually thought to reflect the contributions of variable partial melting degrees of subduction-related mantle source and island arc nature, or that of deep sub-oceanic or subcontinental intraplate mantle, respectively. The setting and origin of the Singu alkalic volcanics are also rather unusual. The case of Singu volcanics located along the Sagaing Fault is not of subduction related affinity, but is more likely to have derived from the melting of deep enriched mantle. The volcanic rocks of the Kyaukphyu-Webaung area can be due to modification of the depleted

¹ Dr, Lecturer, Department of Geology, Yadanabon University

² Dr, Lecturer, Department of Geology, Yadanabon University

³ Dr, Lecturer, Department of Engineering Geology, Defense Service Technological Academy

mantle by a subduction slab component or may be due to variable degree of mobilization during the alteration processes.

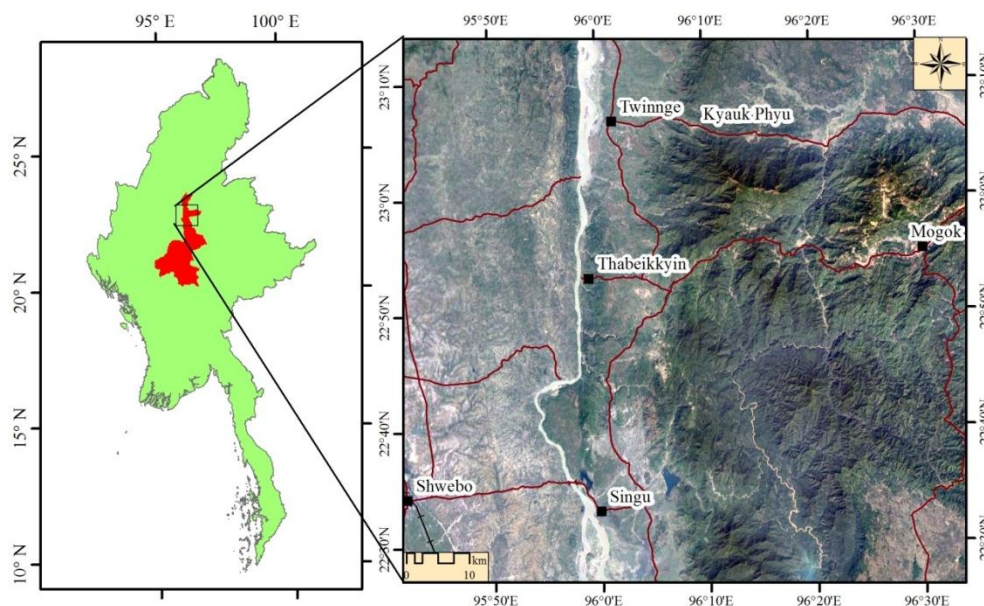


Figure 1 Location map of the Singu Area and Kyaukphyu-Webaung Area

Method of Study

Due to the lack of detailed geological map of the study area, mapping is carried out during the field season and the representative samples of rocks units were collected. The sample localities, lithologic boundaries and distinctive structural positions are located by using GPS.

The major oxides and trace elements of representative samples with reference to the X-ray fluorescence spectroscopy (XRF) data were tested at Geochemistry Laboratory, Applied Geology Department, Yangon University and Physics Department, Mandalay University.

Geochemical Studies

Singu Plateau is made of a thick pile of very fluid basaltic flows displaying segregation structures (Caroff *et al.*, 2000). They form a 100 km² plateau which overlies Mio-Pliocene sandstones as well as the upper part of the Irrawaddy formation (Chhibber, 1934; Bender, 1983). It has been offset by the Sagaing fault. These observations suggest a lack of very recent volcanic activity in the plateau, a feature in agreement with the 0.25 to 0.31 Ma ⁴⁰K-⁴⁰Ar ages of five basaltic samples (Bertrand *et al.*, 1998).

The volcanic rocks in Kyaukphyu-Webaung Area are dacite, andesite, basaltic andesite, basalt, trachy basalt, tephrite and foidite. These rocks are well exposed at the western flank of Dokhta Taung, Ayo-O Taung and Shar Taung, Subok Taung, Nansein Taung, No.1 Taung, Thandaung and along the Nansein Chaung, Pyaunggyauk Chaung and Pinhet Chaung. The basalts in Kyaukphyu-Webaung Ophiolite fall in Tagaung-Myitkyina Belt. The ophiolite rocks from near Myitkyina indicate early Middle Jurassic zircon U-Pb ages of 171±173 Ma. (Liu *et al.*, 2016).

Rock Classification

In the study area, the fresh samples with L.O.I (Loss on Ignition) values lower than 2 wt. % are chosen. Most of the lavas from Singu and Kyaukphyu-Webaung are mafic lava and display rather low content in compatible trace elements (Cr, Co, Ni). In Le Bas *et al.* (1986) diagram (Fig. 2), the Singu lava plot within the fields of phonotephrite, basaltic trachyandesite and trachybasalt and it shows alkaline nature. However, the analyzed lava from Kyaukphyu-Webaung area plot within the field of foidite, tephrite, basanite and trachybasalt which are alkaline in nature and in basalt, basaltic andesite, andesite and dacite which display subalkaline/tholeiitic nature according to Le Bas *et al.* (1986) diagram (TAS).

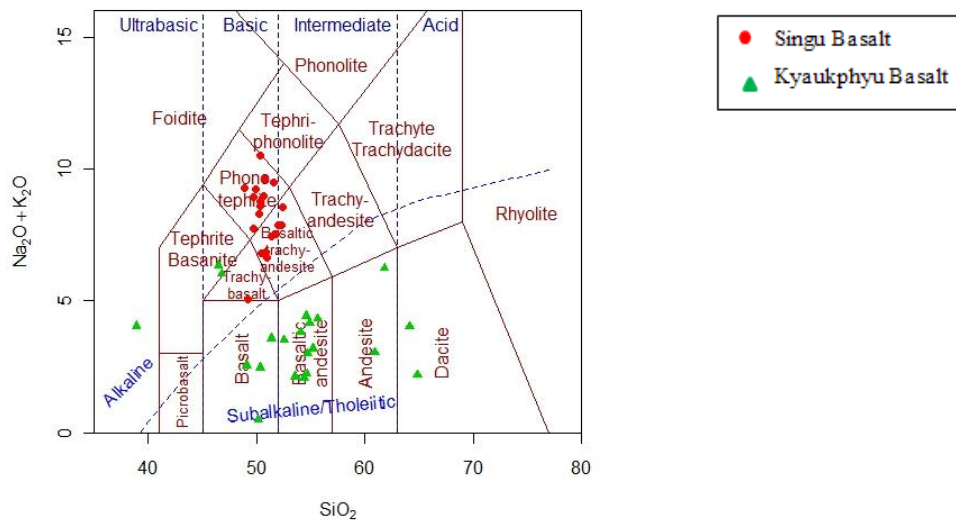


Figure 2 The total alkali versus silica (TAS) diagram of Le Bas *et al.* (1986)

In K_2O - SiO_2 diagram (Peccerillo and Taylor, 1976) (Fig. 3), the Singu lava plot within the field of Shoshonite Series and Kyaukphyu-Webaung lava plot within the field of Calc-alkaline Series and Tholeiitic Series. In Na_2O - K_2O - CaO diagram (Fig. 4) the two lavas plot within the field of Sodic. The Singu lavas which display an “anorogenic” trace element signature, has been categorized as basaltic trachyandesite following their position in $(Na_2O + K_2O)$ vs. SiO_2 diagram.

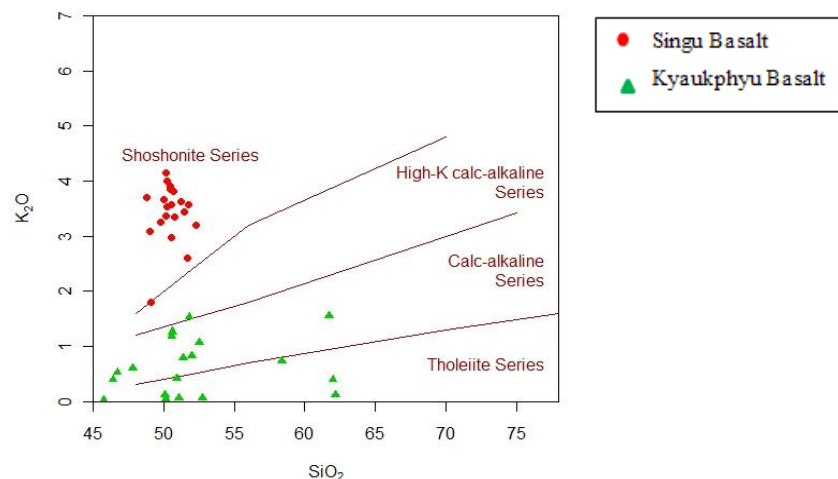


Figure 3 SiO_2 vs. K_2O plot showing the various series of basaltic rocks (Peccerillo and Taylor, 1976)

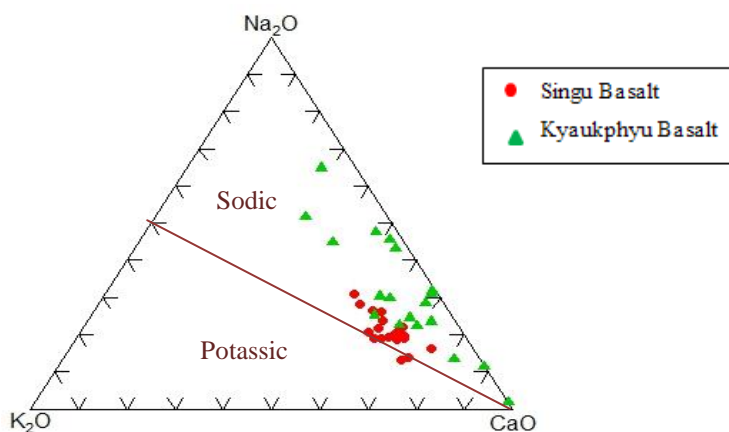


Figure 4 K₂O-Na₂O-CaO showing the alkali series of basaltic rocks (Green & Poldervaort, 1958)

Petrographic Notes

Singu basaltic trachyandesites display hypocrystalline, intergranular, intersertal, trachytic texture and subaphyric microlitic texture with less than 5% phenocryst of olivine and microphenocrysts of plagioclase (labradorite-andesine). Plagioclase microlites are long prismatic and they often show penetrated twin. Augite phenocrysts are surrounded by sub-parallel alignment of plagioclase microlites which show trachytic texture. Their groundmass is generally vesicular and contain olivine, plagioclase, augite and titanomagnetite.

The basaltic rocks in Kyaukphyu-Webaung area have highly porphyritic microlites texture with up to 25% of millimetric to centimetric phenocrysts. Some plagioclase often shows glomeroporphyritic texture and trachytic texture. These are, by order of decreasing abundance, Olivine often converted to serpentine and chlorite, plagioclase often converted to saussurite, sericite, augite and scarce chrome spinel. Some olivine crystals show quenched texture. Their groundmass contains augite granules, plagioclase microlites, opaque minerals and small amount of Cr-spinel. Oscillatory zoning occurs in some tabular phenocryst of plagioclase.

Major Element Characteristics

The major and trace elements of the studied lavas allow to distinguish two different groups, the first one comprising Singu lavas and the second one comprising Kyaukphyu-Webaung basaltic rocks. For instance, TiO₂ contents are close to 3% for Singu lavas and lower than 1.44% for the second group, a feature usually considered as typical of orogenic magmas. The former value fall within the range commonly observed for intraplate alkali basalts. The normative nepheline contents of Singu basaltic trachyandesites (less than 5%) allow to consider them as mildly alkalic lavas. Most of the Kyaukphyu-Webaung volcanic rocks are silica-saturated, with normative quartz contents increasing regularly from basalts to dacite (Table 1). Kyaukphyu-Webaung lava compositions define an almost continuous calc-alkaline series ranging from basalts to dacites through basaltic andesites and andesites.

Tectonic Implication

The geochemical signatures of the studied lavas document two contrasted tectonic environments for Singu lava and Kyaukphyu-Webaung basaltic rocks respectively. This is mainly based on the trace element characteristic of basaltic rocks (Table 2).

On a triangular plot of $Zr/4$, $2 \times Nb$ and Y (Fig. 5), Meschede (1986) showed that four main basalt fields can be identified. Within-plate alkali basalts plot in field A; within-plate tholeiites plot in fields AII and C. E- type MORB plots in field B whilst N- type MORB plots in field D. Volcanic-arc basalts also plot in fields C and D. The several areas of overlap mean that only within-plate alkali basalts and E- type MORB can be identified without ambiguity. According to this diagram, the basaltic rocks from the Singu area fall in within-plate alkali basalts (field A) and the basaltic rocks from the Kyaukphyu-Webaung area plot within N- type MORB and volcanic-arc basalts (field D).

Table 1 Major Oxides of the Basaltic Rocks of Singu Area and Kyaukphyu-Webaung Area

	Sample	SiO ₂	TiO ₂	Al ₂ O ₃	Fe ₂ O ₃	FeO	MnO	MgO	CaO	Na ₂ O	K ₂ O	P ₂ O ₅	H ₂ O	LOI	Total
SINGU AREA	B8	51.64	2.82	12.48	7.85	-	0.15	2.47	14.79	4.92	2.61	0.03	-	0.05	99.81
	C1	50.54	1.85	11.58	7.05	-	0.12	1.99	15.96	4.65	2.98	0.02	-	0.11	96.85
	I1	52.25	2.31	11.44	10.48	-	0.32	2.45	11.89	5.30	3.20	0.02	-	0.18	99.84
	I2	51.45	2.85	12.90	10.95	-	0.22	1.81	10.05	6.00	3.44	0.04	-	0.05	99.76
	J3	51.21	2.85	14.02	10.65	-	0.15	2.32	11.07	3.82	3.62	0.04	-	0.06	99.81
	J7	50.57	2.11	12.58	9.01	-	0.12	2.55	13.13	6.03	3.57	0.03	-	0.07	99.77
	J9	50.25	2.04	12.32	8.63	-	0.11	2.62	16.95	3.25	3.54	0.03	-	0.02	99.76
	J12	50.44	2.14	13.50	8.37	-	0.12	1.97	14.17	5.04	3.91	0.04	-	0.12	99.82
	J16	50.79	2.54	15.00	11.67	-	0.14	2.26	10.66	3.28	3.35	0.03	-	0.11	99.83
	K1	49.74	2.17	12.30	9.61	-	0.14	2.80	13.70	5.95	3.25	0.02	-	0.07	99.75
	K2	50.44	2.17	14.93	5.31	-	0.11	2.38	17.06	5.21	3.86	0.03	-	0.12	101.62
	K3	49.06	0.57	17.93	4.31	-	0.46	7.38	15.06	3.23	1.81	0.01	-	0.14	99.96
	K5	49.04	1.04	11.62	10.07	-	0.16	2.84	16.28	4.58	3.08	0.02	-	0.10	98.83
	L2	50.18	2.13	12.33	9.79	-	0.13	2.63	13.76	5.37	3.37	0.02	-	0.17	99.88
	L4	48.77	2.04	11.89	7.88	-	0.11	2.11	17.62	5.55	3.70	0.03	-	0.28	99.98
	L5	50.20	2.29	13.43	8.67	-	0.12	2.13	12.33	6.46	4.01	0.04	-	0.06	99.74
	L7	51.76	2.13	12.82	8.47	-	0.11	2.20	14.29	4.28	3.57	0.03	-	0.11	99.77
	L10	50.00	2.06	12.44	8.14	-	0.11	2.13	16.47	4.62	3.66	0.03	-	0.12	99.78
KYAUKPHYU- WEBANG AREA	L13	50.66	2.14	13.74	8.14	-	0.11	2.00	16.07	3.02	3.81	0.04	-	0.24	99.97
	SG	50.13	2.21	13.10	8.49	-	0.11	2.39	14.65	4.40	4.15	0.04	-	0.04	99.71
	3152	62.16	0.69	13.75	-	9.16	0.20	5.46	2.26	1.98	0.12	0.09	4.04	-	99.91
	25026	61.98	1.09	13.77	-	8.79	0.19	5.24	1.51	3.49	0.39	0.24	3.22	-	99.90
	2804	61.70	0.40	19.00	2.76	2.64	0.15	2.56	4.19	4.67	1.55	0.24	0.00	-	99.86
	2606	58.38	1.44	15.19	4.31	4.69	0.38	6.67	1.33	2.19	0.73	0.54	4.10	-	99.96
	2608	52.76	1.39	14.57	5.83	7.45	0.30	8.40	4.17	1.96	0.06	0.13	2.80	-	99.82
	27 (A)	52.50	0.86	16.86	-	8.84	0.19	4.87	6.02	3.00	1.07	0.13	5.33	-	99.67
	28 (A)	51.98	1.02	15.73	-	11.57	0.30	4.49	5.88	2.17	0.82	0.15	5.76	-	99.87
	2806	51.80	0.76	17.30	-	9.73	0.29	4.82	5.59	2.39	1.53	0.19	5.48	-	99.88
	28(B)	51.38	1.04	15.65	-	11.69	0.31	4.71	6.24	2.02	0.79	0.16	5.89	-	99.87
	2607 L	51.05	1.22	13.95	-	12.76	0.26	7.70	4.30	2.01	0.06	0.12	6.41	-	99.85
	2605	50.89	1.31	13.74	-	14.99	0.31	4.98	7.10	2.97	0.41	0.14	2.62	-	99.46
	2802	50.59	0.71	16.17	4.04	5.60	0.26	5.87	6.67	2.30	1.26	0.10	0.17	-	93.74
	616	50.57	0.86	16.46	-	9.16	0.26	5.64	5.48	2.90	1.19	0.20	7.17	-	99.88
	2607 R	50.12	1.25	14.29	-	13.41	0.28	8.04	4.16	1.93	0.05	0.12	6.17	-	99.82
	2607	50.10	1.15	17.10	6.44	8.86	0.27	8.00	5.12	2.33	0.12	0.12	0.00	-	99.61
	2801	47.79	1.27	14.26	4.69	7.07	0.32	5.76	8.32	2.72	0.60	0.21	6.84	-	99.85
	2606 a	46.70	0.46	21.40	4.69	7.31	0.41	7.25	5.52	5.47	0.53	0.15	0.00	-	99.89
	2606 b	46.40	0.54	20.90	4.14	6.46	0.38	7.20	7.44	5.94	0.39	0.13	0.00	-	99.92
	2902 a	45.75	0.57	9.64	2.64	4.15	0.14	2.39	25.41	0.43	0.01	0.09	8.62	-	99.84
	27 B	43.74	0.60	14.88	-	9.09	0.22	8.45	9.77	1.62	0.65	0.06	10.80	-	99.89
	2902 b	38.80	0.63	12.50	2.88	5.81	0.30	4.11	30.50	3.90	0.13	0.25	0.00	-	99.81

Table 2 Minor and Trace Elements of the Basaltic Rocks of Singu Area and Kyaukphyu-Webaung Area

Sample	Ni	Co	Cr	Cu	Zn	V	La	Rb	Ba	Sr	Pb	Zr	Nb	Ta	Y	S	As	Mo	Cl
B8	34.6	10.9	35.9	56.1	172	202	<2.0	65.7	855	833.8	6.3	330.8	37.8	-	28.5	330.6	<0.	<1.0	-
C1	25.6	7.8	45.7	36.1	149.1	114	<2.0	86.2	1162	971	14.3	383.6	54.4	-	22.9	202.4	<0.	<1.0	-
I1	36.6	736	38.5	44.8	169.5	123	<2.0	87.4	1308	1201	10.4	376.3	61.3	-	36.2	237	<0.	<1.0	-
I2	41.5	8	30.3	48.7	157	191	<2.0	87.4	1308	1201	10.7	376.3	61.3	-	36.2	266.9	<0.	<1.0	-
J3	36.2	9.4	31.3	56.3	158.8	230	131	92.1	1199	1015	11.2	384.9	62.5	-	30.7	302.3	<0.	<1.0	-
J7	40.6	8.1	46.8	36.5	160.2	628.	<2.0	113.	1560	1050	8.2	443.8	68	-	29.6	245.3	<0.	<1.0	-
J9	32.6	11.6	35.3	35.8	131.1	164	<2.0	96	1151	938.1	6.5	383.6	57.6	-	24.4	243.8	<0.	<1.0	-
J12	30.6	8.2	33.1	37.4	138.7	115	139	117.	1673	1103	11.5	439.6	64.3	-	26.6	285.7	<0.	<1.0	-
J16	39.2	13.7	42.8	45	165.9	153	<2.0	83.7	1479	929.7	5.2	417.2	65.1	-	27.8	39.8	<0.	<1.0	-
K1	41.3	7.9	35.3	39.7	159.4	119	70	94.1	1285	1008	17.9	462.8	76.2	-	25	274.6	<0.	<1.0	-
K2	30.9	7.1	31.1	38.9	130	175	<2.0	108.	1247	990.2	-	430.8	63.8	-	24.4	18.8	<0.	<1.0	-
K3	23	<3.0	65.4	16.4	84.2	109	155	85.3	646	542.6	-	276.4	13.1	-	30.3	<2.0	<0.	<1.0	-
K5	33.8	13	37.5	35.5	154.1	110	<2.0	87.3	1181	954.2	-	393.3	53.8	-	23.3	273.8	<0.	<1.0	-
L2	33.9	11.5	53.5	38.7	152.4	143	<2.0	102.	1197	975.2	-	392.7	63.8	-	25.5	260.8	<0.	<1.0	-
L4	28.1	9.9	25.9	39.1	131.2	148	<2.0	107.	1329	1192	-	414.6	61.1	-	27.7	242.1	<0.	<1.0	-
L5	35.5	10.9	33.9	40	146	305	<2.0	115.	1618	1224	-	472.5	78.3	-	25.8	271.5	<0.	<1.0	-
L7	27.7	10.1	29.5	36.6	136.2	133	<2.0	94.6	1753	1161	-	397.5	57.2	-	27.3	261.7	<0.	<1.0	-
L10	28.9	13	29.6	31.4	133.1	266	90	99.2	1760	1287	-	404	58.8	-	21.7	243.9	<0.	<1.0	-
L13	26.4	8	42	35	126.3	167	109	104	1168	974.2	-	402.3	62.4	-	23.1	283.2	<0.	<1.0	-
SG	31.5	11.7	34.3	38.6	137.3	140	<2.0	120.	1445	1096	-	477.4	73.2	-	24.5	251.5	<0.	<1.0	-
3152	6	16	9	48	182	125	-	1	0	142	0	173	5	0	54	145	4	0	6
25026	3	11	0	67	99	276	-	1	56	104	2	79	1	0	39	285	0	1	-
2804	-	-	-	-	99	99	-	-	-	91	-	137	1	-	38	98	-	-	182
2606	2	40	0	3	137	92	-	8	146	48	0	110	1	0	44	203	0	0	-
2608	8	37	8	168	143	542	-	1	44	129	0	79	1	0	37	639	0	0	-
27(A)	12	38	8	12	83	274	-	18	438	243	0	67	3	0	30	2043	0	0	-
28(A)	1	63	1	181	116	353	-	10	116	211	0	70	2	0	31	177	0	0	-
2806	2	32	0	72	79	233	-	16	178	331	0	58	2	0	23	168	2	0	2
28(B)	2	46	0	184	118	357	-	9	73	217	3	71	3	0	32	190	0	0	-
2607L	6	33	9	188	128	461	-	0	38	118	1	67	1	0	32	404	0	0	-
2605	2	41	13	413	131	619	-	6	152	287	5	67	1	0	35	3466	2	0	-
2802	11	53	11	159	87	351	-	14	305	385	0	36	2	0	22	246	0	0	-
616	31	64	82	23	77	263	-	20	67	184	0	78	3	0	27	180	0	0	-
2607R	7	42	17	158	136	487	-	0	32	125	1	70	3	0	35	670	0	0	-
2607	-	-	-	232	179	600	-	-	-	153	-	101	1	0	56	300	-	-	124
2801	0	62	0	32	99	394	-	5	243	203	3	57	1	0	36	457	0	0	-
2606a	-	-	-	-	200	314	-	-	-	292	-	-	-	-	-	66	-	-	-
2606b	-	-	15	-	216	-	-	-	-	399	-	-	-	-	-	211	-	-	137
2902a	62	47	365	593	27	275	-	3	0	27	1	37	1	0	16	161	0	0	-
27B	65	64	74	100	81	290	-	13	81	183	2	49	1	0	18	124	0	0	-

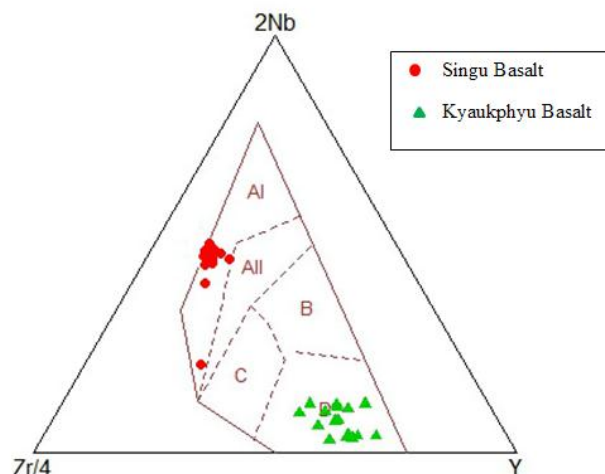


Figure 5 The ternary plot of Zr/4-2Nb-Y of Meschede (1986) showing tectonic setting of basaltic rocks

In the Cr versus Y diagram (Pearce, 1996), Cr is compatible in the mineral olivine, orthopyroxene and clinopyroxene and the spinels in a basaltic melt. The low levels of Cr in volcanic-arc rocks therefore are either a function of a different amount of mantle melting from MORB and/ or a difference in the fractionation history. The precise cause is difficult to define. Y is also depleted in island – arc basalts relative to other basalt types, for a given degree of fractionation. Thus a Cr vs. Y plot (Figure 6) discriminates effectively between MORB and volcanic arc basalts, with only a small amount of overlap between the two fields. Within-plate basalts, on the other hand, overlap the fields of MORB and volcanic- arc basalts. The wide range of Cr values in the volcanic-arc basalt field is most efficiently obtained through crystal fractionation, indicating that Cr is a useful fractionation index in these rocks. According to this discrimination diagram, the Singu volcanics belong to within-plate basalts (WPB) and the Kyaukphyu-Webaung volcanics fall in volcanic-arc basalts (VAB) and midoceanic ridge basalts (MORB).

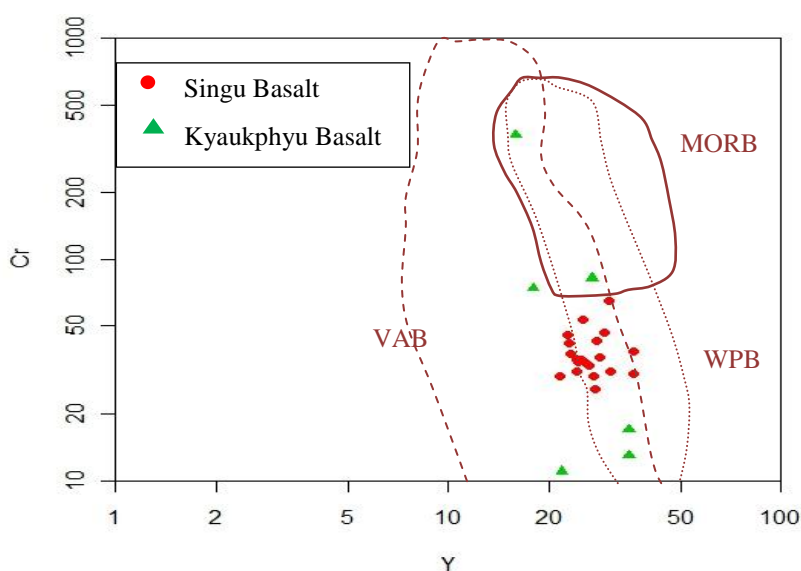


Figure 6 Tectonic discrimination Cr vs. Y diagram of the basaltic rocks (Pearce, 1982)

The Zr/Y versus Zr diagram (Figure 7) successfully separates the Within-Plate Basalts group from Mid-Oceanic Ridge Basalts and Island Arc Basalts. Within-Plate Basalts have higher Zr/Y and higher Zr than the other types of basalt, suggesting the enriched mantle source relative to the source of Mid-Oceanic Ridge Basalts and Island Arc Basalts (Rollinson, 1996). On this tectonic discrimination diagram, the Singu Volcanics have trace element characteristic of within-plate setting and the Kyaukphyu-Webaung volcanics belong to Island Arc and Mid-Oceanic Ridge settings.

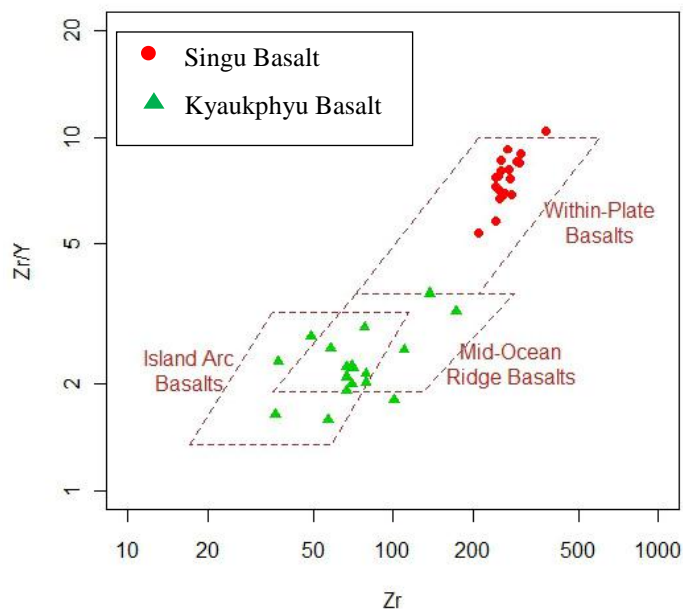


Figure 7 Zr-Zr/Y binary diagram showing tectonic setting of basaltic rocks (Pearce and Norry, 1979)

According to these diagrams the two volcanic areas have rather different tectonic environments. The Singu basaltic rocks form in within plate environment and the basaltic rocks from Kyaukphyu-Webaung area form in an oceanic environment and within either Island Arc or Mid-Oceanic Ridge.

Discussion

Evidence for contrasted mantle sources

The petrologic and geochemical signatures of the studied lavas document two contrasted magmatic affinities for Singu lava and for Kyaukphyu-Webaung basaltic rocks, respectively. The former group displays the features typical of deep enriched intraplate-type mantle source. Volcanism in the Singu area did not seem to have directly related to the subduction. In this area pre-existing crustal structures would serve pathways for the ascent of mafic alkaline melts. Lavas under investigation suggest intraplate character with no clear subduction signal. On the other hand, the geochronologic data presented in this study, indicate that the mafic alkaline pulse occurred at 0.25-0.31 Ma suggesting that a common regional mechanism served to trigger melting at the mantle. In this region, the volcanic pulse was short and of limited volume. This is consistent with a thermal origin for enriched mantle melting because this region was underlain by a dry mantle unaffected by subduction. In this work the Singu plateau is considered as a surface reflection of a mantle hot spot on a moving lithospheric plate.

The geochemical signature of the Singu alkaline mafic basaltic trachyandesites which are offset by the Sagaing Fault suggests that they derive from the melting of deep enriched intraplate-type mantle, similar to the source of common Plio-Quaternary alkali basalts and related rocks from the Sundaland. Rapid uprise of high temperature alkaline magmas derived from the melting of enriched Sundaland-type mantle and channelled by Neogene fault planes parallel to the Sagaing Fault led to the emplacement of the Singu lavas. More rarely, it has been proposed that alkaline magmas could be emplaced along major transcurrent lithospheric faults, e.g. the Trans-Alboran lineament [Hernandez et al., 1987; de Larouziere et al., 1988], which would channel towards the surface magmas derived from distinct mantle sources (Maury et al., 2004).

The Kyaukphyu Webaung basaltic lava displays the features typical of "orogenic" magmas derived from the partial melting of metasomatised mantle carrying a subduction imprint. These basalts are generally considered as part of paleoceanic crust formed through magma derived from depleted mantle (DM) (Dey et.al., 2018). The enrichment in LIL elements in the volcanic rocks of the study area can be due to modification of the depleted mantle by a subducted slab component or may be due to variable degree of mobilization during the alteration processes. However, the enrichment of Ba and depletion of Nb relative to other incompatible elements are considered to represent the addition of subduction zone component (in Kakar, 2012).

Acknowledgements

We are greatly indebted to Rector Dr. Maung Maung Naing, Pro-rectors Dr. Si Si Khin and Dr. Tint Moe Thuzar, Yadanabon University, for their permission to carry out this research and for paying attention to this work. We wish to express our sincere gratitude to Dr. Htay Win, Professor and Head, Dr. Khine Khine San, Professor and Dr. Min Nyo Oo Associate Professor of Geology Department, Yadanabon University for allowing to do this research.

References

- Bender, F., (1983). Geology of Burma. Beitrage zur regionalen Geologie der Erd n 16. Berlin, Stuttgart, 293p.
- Bertrand et al., (1998). The Singu basalts (Myanmar): new constraints for the amount of recent offset on the Sagaing Fault. *Earth and Planetary Sciences*, Vol. 327, pp.479-484.
- Caroff, M., Maury, R. C., Cotton, J. & Clement, J. P., (2000). Segregation Structures in vapor-differentiated basaltic flows. *Bull. Volcanol.*, Vol. 62, pp. 171. 187.
- Chhibber, H. L., (1934). *The geology of Burma*. MacMillan & Co., London, 538p.
- Cole, R. B. & Basu, A., (1992). Middle Tertiary volcanism during ridge trench interactions in western California. *Science*, Vol. 258, pp.793-796.
- Dey, A., Hussain, M.F., Barman, M.N., (2018) Geochemical characteristics of mafic and ultramafic rocks from the Naga Hills Ophiolite, India: Implications for petrogenesis. *Geoscience Frontiers* 9, 517-529.
- Hernandez, J., Larouziere, F. D. De, Bloze, J. & Bordet, P., (1987). Le magmatisme neogene betico-rifain et le couloir de décrochement trans-Alboran. *Bull. Soc. geol. Fr.*, (8), III, (2): pp.257-267.
- Kakar, M.I., Mahmood, K., Kerr, A.C., Collins, A.S., Khan, M., Kasi, A.K., (2012) Geochemistry and petrogenesis of the volcanic rocks from Bagh complex, northern Balochistan, Pakistan, *Journal of Himalayan Earth Science* 45 (1), 17-29.
- Larouziere, F. D. De, Bolze, J., Bordet, P., Hernandez, J., Montenat, C. & Ott D'Estevou, P., (1988). The Betic segment of the lithospheric Trans- Alboran shear zone during the late Miocene: *Tectonophysics*, Vol. 152, pp. 41-52.

- Le Bas, M. J., Le Maitre, R. W., Streckeisen, A. & Zanettin, B., (1986). A chemical classification of volcanic rocks based on the total alkali silica diagram. *J. Petrol.*, Vol. 27, pp. 745-750.
- Liu. C. Z., C. Zhang, Yang Xu, J. G Wang, Yi Chen, Shun Guo, Fu-Yuan Wu, Kyaing Sein (2016) Petrology and geochemistry of mantle peridotites from the Kalaymyo and Myitkyina ophiolites (Myanmar): Implications for tectonic settings, *Jour. of Elsevier*, www.elsevier.com/locate/lithos. *Lithos* (2016) 495-508.
- Maury, R. C., Pubellier, M., Rangin, C., Wulput, L., Cotton, J., Socquet, A., Bellon, H., Guillaud, J. P. & Htun, H. M., (2004). Quaternary calc-alkaline and alkaline volcanism in a hyper-oblique convergence setting, central Myanmar and western Yunan. *Bull. Soc. geol. Fr.*,
- Peccerillo, A., & Taylor, S.R., (1976). Geochemistry of Eocene calc-alkaline volcanic rocks from the Kastamonu area, northern Turkey. *Contrib. Mineral. Petrol.*, 58, pp. 63-81.
- Meschede, M., (1986). A method of discriminating between different types of mid oceanic ridge basalts and continental tholeiites with the Nb2-Y diagram, *Chamice- Geology*, Vol. 56, pp. 207-218.
- Pearce, J. A. (1996). A user's guide basalt discrimination diagrams. In Wvman, D.A (ed) Trace element geochemistry of volcanic rocks. Applications for massive sulphide exploration Vol. 12. *Geological Association of Canada short Course Notes*, pp. 79-113.
- Rollinson, R.H. (1996). Using Geochemical Data: Evaluation, Presentation, Interpretation, *Longman Scientific & Technical*, 392p.

PETROCHEMICAL CHARACTERISTICS AND GEOCHRONOLOGY OF THE IGNEOUS ROCKS IN BILIN AND ITS ENVIRONS, BILIN TOWNSHIP, MON STATE

Mya Moe Khaing¹, Hla Kyi², Thein Win³

Abstract

The research area is located in Bilin Township and its vicinity, Mon State. It lies between Latitude 17°12'45"N to 17°21'45"N and Longitude 97°09'00"E to 97°14'45"E. The total area coverage is about 116.5 km². Four samples were sent to ALS laboratory of Geological Survey of Japan and analysed by XRF and LA-ICPMS. Eight samples were analyzed at DSSTRC (Defence Service Science and Technology Research Centre) in Pyin-Oo-Lwin Township and seven samples were sent to Geology Department, Mandalay University for XRF analysis. Geochemically, biotite granite, biotite-muscovite granite and biotite microgranite show chemical composition (weight percent) of SiO₂ (69.4 - 75.96), Al₂O₃ (13.34-16.8), TiO₂ (0.154-0.284), Na₂O+K₂O (7.765-10.31), Fe₂O₃+MgO (1.149-2.64), MnO (0.039-0.151), CaO (0.897-3.14) and P₂O₅ (0.027-0.159), suggesting calc-alkaline series and are predominantly peraluminous. Diorites and microdiorite exhibit SiO₂ (52.3-55.95), Al₂O₃ (17.69-22.3), TiO₂ (0.738-0.973), Na₂O+K₂O (4.95-6.364), Fe₂O₃+MgO (9.211-13.35), MnO (0.121-0.359), CaO (5.435-7.51) and P₂O₅ (0.285-0.602); proposing calc-alkaline series and are metaluminous. According to Harker's variation diagrams, TiO₂, Al₂O₃, Fe₂O₃, MnO, CaO, MgO and P₂O₅ are negatively correlated with SiO₂ and then Na₂O, K₂O are positively correlated with SiO₂. Result from geochemical analysis, biotite-muscovite granite and some biotite granites have high sodium content, normative corundum ranges from 0.831 to 0.974 and biotite microgranite is low in sodium content, Na₂O Vs K₂O diagram shows that the granitic rocks involve both I and S-types, Chappell and White (1994). Based on the tectonic discrimination diagram of Maniar and Piccoli (1989), the granitic rocks fall within the IAG+CAG+CCG field. In Y Vs Nb diagram; all the granitic rocks fall in the field of Syn-COLG and VAG. Y+Nb Vs Rb diagram indicates that all granites fall in the VAG field. U-Pb zircon dating of the biotite granite from the northern part of Lakhin pagoda gives the age of 51.9±0.7 Ma and suggests that the biotite granite was emplaced in Eocene.

Keywords; calc-alkaline, peraluminous, I-type, S-type, COLG, VAG, fractional crystallization

Introduction

The study area is chiefly covered by igneous and metasedimentary rocks, Fig (1). Igneous rocks are well exposed in the northern, north-western and south-eastern parts and metasedimentary rocks are cropped out in the central and western parts of the study area. Best exposure is observed along the stream sections and along the crest of the ridges.

¹ Dr, Associate Professor (Head), Department of Geology, Sittway University

² Part- Time Professor, Applied Geology Department, University of Yangon

³ Professor, Pro-Rector (Retired), West Yangon University

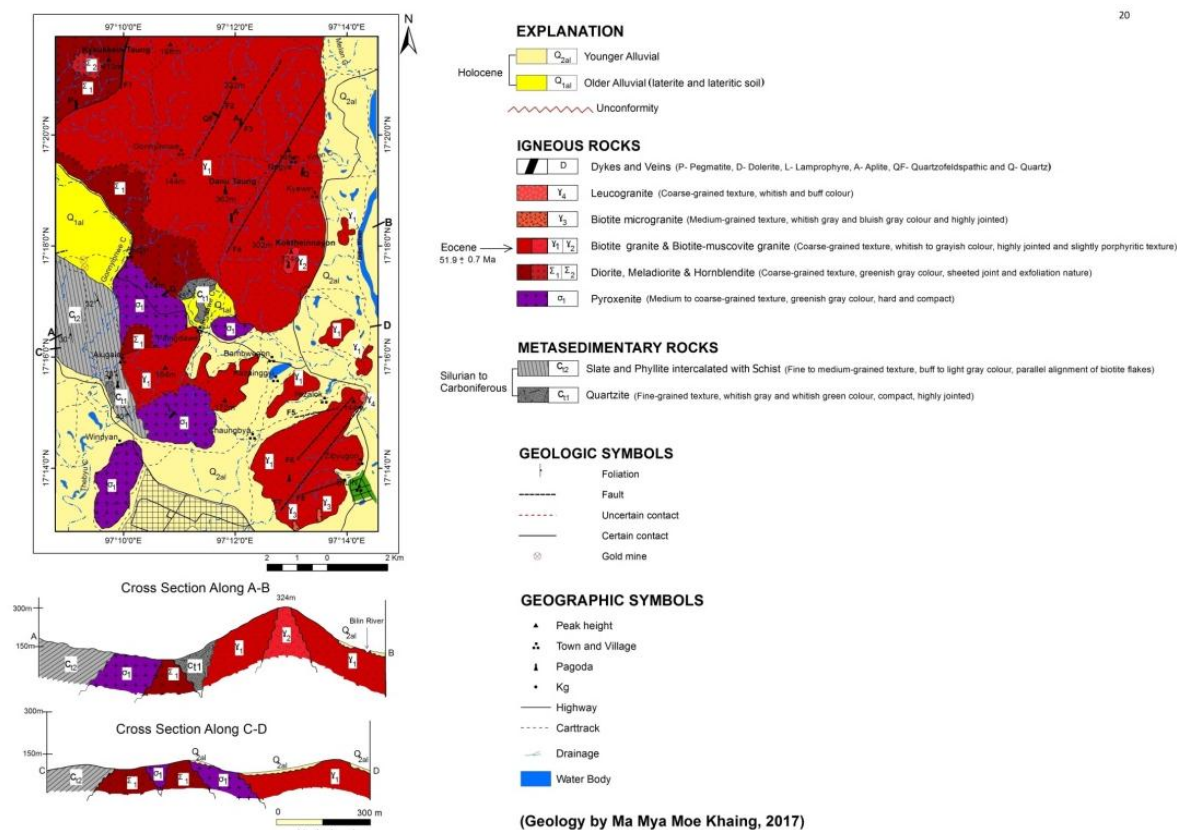


Figure 1 Geological Map of Bilin and its environment, Bilin Township, Mon State

Materials and Methods

The representative igneous rock samples including 6 biotite granites (sample no. KK-11, NG-23, mmk-1, mmk-5, mmk-11, mmk-13), 1 biotite-muscovite granite, (sample no. KK-04), 1 biotite microgranite, (sample no.15-26), 2 diorites, (sample no. R-01, KS-13), 1 microdiorite, (sample no. KS-04), 5 pyroxenites, (sample no. R-02, R-03, R-04, R-05, R-06), 1 hornblendite, (sample no. R-07), 2 lamprophyres (spessartite), (sample no.B-04, R-08) from the study area were selected for analysis. Four samples were sent to ALS laboratory of Geological Survey of Japan and analysed by XRF and LA-ICPMS. Eight igneous rock samples from the study area were analysed at DSSTRC (Defence Service Science and Technology Research Centre) in Pyin-Oo-Lwin Township and seven igneous rock samples were analysed at the Department of Geology, Mandalay University. The major oxide and trace elements abundance were determined by X-ray fluorescence spectrometry.

Results and Findings

The igneous rocks of the study area are biotite granites, biotite-muscovite granite, biotite microgranite, diorites, microdiorite, pyroxenites and hornblendite. The biotite granites, biotite-muscovite granite and biotite microgranite show chemical composition (weight percent) of SiO₂ (69.4 - 75.96), Al₂O₃ (13.34-16.8), TiO₂ (0.154-0.284), Na₂O+K₂O (7.765- 10.31), Fe₂O₃+MgO (1.149-2.64), MnO (0.039-0.151), CaO (0.897-3.14) and P₂O₅ (0.027-0.159). The chemical composition (weight percent) of diorites and microdiorite exhibit SiO₂ (52.3-55.95), Al₂O₃ (17.69-22.3), TiO₂ (0.738-0.973), Na₂O+K₂O (4.95-6.364), Fe₂O₃+MgO (9.211-13.35), MnO

(0.121-0.359), CaO (5.435-7.51) and P_2O_5 (0.285-0.602). Pyroxenites indicate SiO_2 (43.38-47.91), Al_2O_3 (13.10-25.56), TiO_2 (0.443-1.11), Na_2O+K_2O (2.005-4.74), Fe_2O_3+MgO (10.98-21.86), MnO (0.074-0.251), CaO (8.696-13.27) and P_2O_5 (0.060-0.421). Hornblendite illustrates the chemical composition (weight percent) of SiO_2 (43.81), Al_2O_3 (20.57), TiO_2 (1.07), Na_2O+K_2O (3.246), Fe_2O_3+MgO (16.96), MnO (0.127), CaO (11.89) and P_2O_5 (0.11). SiO_2 - Na_2O+K_2O - FeO_t+MgO diagram, (Fig. 2) shows the rise of SiO_2 and depletion of $FeO_t + MgO$ during the entire process of magmatic differentiation. In Harker's variation diagram, Al_2O_3 , TiO_2 , Fe_2O_3 , CaO, MgO, MnO and P_2O_5 are negatively correlated with SiO_2 . Na_2O and K_2O are positively correlated with SiO_2 . Plots of Harker's variation diagrams, selected trace elements of Ba, Sn, Nb, Zn, Rb, Zr, Y and Mo are positively correlated with SiO_2 . Plots of trace elements Sr, Ni, Ce versus SiO_2 show decreasing of those elements with increasing of SiO_2 contents, Fig (3). The normative anorthite content against the Thornton and Tuttle Differentiation Index (TTDI) diagram show the degree of differentiation, the hornblendite and diorite contain proportionately more normative anorthite in plagioclase than the biotite granite, shown in Fig (4). Na_2O+K_2O/Al_2O_3 Vs SiO_2 variation diagram, Fig (5) and K_2O Vs SiO_2 , Fig (6) show the trend of magmatic differentiation. Plot of alkali ($Na_2O + K_2O$) versus silica (SiO_2) diagram, Fig (7) exhibits the granitic rocks in the study area fall in the subalkaline series. K_2O Vs Na_2O diagram, Fig (8) shows that the granitic rocks of the study area involve both I-type and S-type. TAS diagram after Cox et. al. (1979), Fig (9) indicates four groups of igneous and the dividing line between alkaline and subalkaline magma series. The igneous rocks from the study area generally range from acid to ultrabasic group and belong to the subalkaline affinity. The granites are predominantly peraluminous with high Aluminum Saturation Indexes (ASI) of A/NK (Molecular $Al_2O_3/(Na_2O+K_2O)$) and A/CNK (Molecular $Al_2O_3/(CaO + Na_2O+K_2O)$) ranging from 1.384 to 1.879 and from 1.054 to 1.524, respectively. In the $Na_2O - Al_2O_3 - K_2O$ diagram, the granitic rocks in the study area fall in the peraluminous field. Diorite and microdiorite fall in the metaluminous field.

Genetic Type of Granitoid Rocks

Geochemical analysis data, Table (1) have been plotted on a various diagram to distinguish I and S type granitic rocks. K_2O Vs Na_2O diagram show that the granitic rocks of the study area involve both I-type and S-type. Some biotite granites are relatively high in sodium, Na_2O normally $> 3.2\%$ in the range of (3.57%-3.93%) with approximately 5% K_2O and one biotite granite and one biotite-muscovite granite from Koktheinnayon pagoda are low in sodium, Na_2O normally $< 3.2\%$, their content are 2.72% and 3.072%. The normative corundum ranges from 0.757 - 0.974. Only biotite microgranite is sodium low, Na_2O (2.86%), it is generally $< 3.2\%$. Lack of normative magnetite is characteristic of S-type. Above these facts, the granitic rocks in the study area are I and S-types granite according to Chappell and White (1974). The relatively high quartz content, up to 35.24 wt% of this S type granite can be considered that this granite was derived from the quartz rich sedimentary rocks. It may be formed from the supracrustal origin (Chappell and White, 2001).

Table 1 Major oxide and trace elements abundances of the igneous rocks from the study area

Sample No	KK-11	15-16	NG-23	KK-04	mmh-1	mmh-5	mmh-11	mmh-13	B-04	R-08
SiO ₂	71.9	69.7	69.4	70.5	75.96	72.5	75.72	74.2	68.8	51.92
TiO ₂	0.199	0.284	0.213	0.202	0.154	0.266	0.161	0.204	0.67	0.627
Al ₂ O ₃	15.2	12.9	16.8	16	12.65	14.59	12.24	14.42	19.4	14.5
Fe ₂ O ₃	1.12	2.29	0.855	1.19	0.972	2.076	1.057	1.525	10.5	9.694
MnO	0.029	0.078	0.068	0.151	0.029	0.065	0.06	0.048	0.227	0.155
MgO	0.226	0.256	0.294	0.223	0.273	0.56	0.309	0.456	4.39	7.059
CaO	1.54	2.14	1.59	1.29	1.01	1.809	0.897	1.618	7.49	7.548
Na ₂ O	2.72	2.86	2.78	2.072	2.577	2.923	2.695	2.745	4.29	2.02
K ₂ O	6.79	7.18	6.52	6.27	6.55	3.822	4.58	4.235	2.56	2.91
F ₂ O ₃	0.106	0.159	0.161	0.129	0.027	0.064	0.021	0.052	0.266	0.222
Total	99.92	99.94	99.67	99.88	100	99.7	99.87	100.5	99.7	97.98
ΔCNK	1.275	1.054	1.411	1.405	1.472	1.524	1.455	1.504	1.264	1.075
ΔNK	1.598	1.284	1.829	1.585	1.855	1.879	1.612	1.809	2.471	2.661
Sn	15.51	8.884	15.97	-	6.969	15.48	-	11.54	-	-
Cd	42.89	29.22	50.24	22.18	20.05	20.27	8.246	25.17	2.814	1.286
Ag	22.2	11.62	24.88	12.4	-	22.68	-	18.24	2.871	2.294
Pd	66.89	28.21	59.18	20.87	29.84	24.9	14.24	28.99	2.894	2.687
Rh	40.64	20	28.66	27.66	15.12	28.48	5.189	22.7	1.267	-
Ru	6.644	4.26	6.907	4.164	2.281	5.912	-	4.249	-	-
Mo	6.025	4.79	5.884	2.768	5.154	5.006	2.767	4.894	0.062	0.067
Nb	8.426	8.066	12.21	8.24	5.92	4.762	2.691	4.217	0.051	0.049
Pb	19.19	19.71	20.11	26.49	64.15	8.618	9.714	9.245	6.625	2.252
Ga	8.812	8.855	7.864	8.026	-	4.621	2.46	2.027	-	0.01
Zn	6.667	6.102	6.294	10.1	17.45	9.104	15.94	6.849	6.278	11.08
Cu	-	-	6.051	2.929	6.224	4.052	5.859	2.208	5.742	2.882
Co	-	4.79	-	11.68	5.474	0	7.087	5.25	10.29	9.587
Fe	714.4	789.9	650.9	764.5	774.5	771.4	868	797.2	919	897
Mn	26.61	20.82	61.8	55.47	24.67	20.91	22.1	25.64	17.55	21.7
Ti	-	-	-	-	-	-	-	-	14.14	19.82
Nd	0.224	0.492	0.214	0.215	0.288	0.245	0.642	0.292	0.722	0.84
Fr	0.222	0.249	0.226	0.2	-	0.185	0.299	0.194	0.51	0.524
Ce	16.68	26.42	17.1	14.25	16.55	12.45	24.19	17.1	29.8	27.2
La	0.176	0.267	0.128	0.106	-	0.142	0.206	0.217	0.295	0.211
Ba	214.8	228.2	178.2	169.9	542.6	767.6	611.7	666.2	0.298	0.211
Sr	-	0.022	0.028	0.088	2.012	0.144	0.594	0.422	0.075	0.212
Zr	44.22	28.24	22.57	69.11	59.92	99.15	108.2	105.21	26.96	62.69
Y	1.84	-	2.08	5.87	2.04	2.66	1.86	-	1.72	2.15
Sr	42.28	72.06	26.21	49.22	88.88	176.9	162.2	177.1	206.7	475.4
Rb	86.18	90.21	128.9	90.87	57.4	48.08	48.27	66.02	28.18	27.22
Ca	4.664	6.628	2.801	7.126	12.95	9.529	10.86	9.765	28.12	28.51
K	20.48	22.15	21.64	20.27	22.28	20.66	20.22	17.22	11.66	11.67
Al	1.2	1.839	1.801	1.328	2.022	1.854	1.927	1.55	19.22	22.14
Si	24.06	25.21	21.26	22.7	24.26	26.15	20.72	28.24	18.21	19.11
Cl	1.67	1.424	1.605	1.666	0.889	1.148	1.121	0.957	29.15	25.29
S	0.718	0.594	0.712	0.609	12.84	2.929	7.202	7.272	7.08	14.2

Sample No	KS-04	R-01	KS-12	R-02	R-03	R-04	R-05	R-06	R-07
SiO ₂	52.2	55.82	52.1	45.84	46.28	42.48	42.28	47.91	42.81
TiO ₂	0.972	0.75	0.728	0.56	0.506	1.11	0.725	0.642	1.07
Al ₂ O ₃	22.2	17.69	18	12.1	22.26	18.08	25.56	16.5	20.57
Fe ₂ O ₃	8.25	6.24	9.4	12.06	6.097	12.61	7.45	8.884	10.67
MnO	0.229	0.121	0.21	0.251	0.086	0.144	0.074	0.196	0.127
MgO	2.92	2.971	2.85	8.8	6.262	7.411	2.42	7.761	6.297
CaO	7.29	5.425	7.51	9.694	11.24	11.22	12.27	8.696	11.89
Na ₂ O	2.69	4.024	1.98	2.26	2.01	1.6	1.79	2.62	2.65
K ₂ O	2.26	2.22	4.27	1.48	0.221	0.405	0.291	1.15	0.596
F ₂ O ₃	0.247	0.285	0.402	0.421	0.087	0.062	0.06	0.222	0.11
Total	99.79	95.81	99.76	96.47	97.26	97.22	98.14	94.27	97.79
ΔCNK	1.807	1.499	1.208	0.907	1.584	1.255	1.665	1.222	1.259
ΔNK	4.505	2.779	2.88	2.762	6.961	9.017	12.28	4.265	6.227
Sn	-	-	0.896	-	1.572	-	-	0.864	0.695
Cd	2.002	4.639	2.778	2.764	6.216	2.199	1.51	2.458	2.072
Ag	2.827	5.752	5.492	4.549	5.976	2.625	2.469	4.526	2.691
Pd	4.698	5.987	4.474	4.299	7.221	2.228	2.766	4.177	2.254
Rh	0.908	2.992	1.972	1.24	4.708	0.821	-	1.852	0.506
Ru	0.26	0.7	0.651	0.29	0.966	0.207	-	0.299	-
Mo	0.784	0.881	0.628	0.524	2.092	0.649	0.298	0.779	0.664
Nb	0.718	0.472	0.471	0.45	1.878	0.499	0.229	0.742	0.661
Pb	4.022	5.975	1.898	2.422	2.654	1.424	0.805	1.647	0.827
Ga	1.575	1.985	1.412	1.295	2.241	0.685	-	0.809	1.286
Zn	10.29	4.856	4.454	5.657	6.572	6.765	5.218	2.682	5.621
Cu	2.471	2.439	12.7	5.817	8.012	2.069	4.894	1.97	1.841
Ni	-	-	-	2.712	4.089	2.521	2.088	2.487	2.028
Co	10.95	8.202	5.854	9.459	7.994	7.57	6.839	7.97	6.599
Fe	899.6	922	912.7	917.7	899.8	929.1	927.4	920.4	917.9
Mn	27.62	12.87	9.272	20.24	17.12	15.22	14.81	12.66	11.12
Ti	27.24	12.21	24.86	14.5	17.69	19.24	15.25	17.69	28.82
Nd	0.76	0.756	0.774	0.707	0.656	0.826	0.892	0.829	0.847
Fr	0.507	0.42	0.48	0.427	0.441	0.602	0.616	0.292	0.599
Ce	21.42	22.92	22.46	22.66	22.22	25.61	29.92	26.91	22.01
La	0.208	0.212	0.242	0.274	0.222	0.246	0.222	0.242	0.242
Ba	494	257.6	218.7	228.2	274.6	682.8	275.7	642.6	288.8
Sr	0.028	0.122	-	0.051	0.055	0.040	-	-	-
Zr	69.62	16.12	28.8	25.72	102.9	27.56	-	25.99	26.21
Y	2.18	-	-	-	2.2	2.17	2.22	1.91	2.67
Sr	222.9	448.2	565.9	405.58	524.6	567.2	562.2	429.4	512.5
Rb	22.62	4.64	2.5	9.84	25.62	22.81	7.47	21.25	0
Ca	27.24	68.01	74.82	49.19	28.4	28.26	75.82	28.78	61.19
K	8.405	1.962	2.505	6.255	15.18	16.46	2.616	20.05	2.597
Al	2.522	2.827	4.55	2.201	1.606	2.228	2.14	2.16	4.052
Si	25.21	27.11	26.08	24.77	18.85	15.95	21.24	29.02	22.72
Cl	1.642	2.812	2.062	2.026	1.291	1.647	1.762	2.28	2.942
S	0.609	0.828	0.969	0.996	1.227	0.425	0.742	0.612	1.162

Condition during Crystallization of the Granitic Rocks

Normative data plot of Quartz - Albite - Orthoclase diagram after Tuttle and Bowen (1985), H₂O saturated liquidus field boundaries in the system for various water pressures. This diagram, Fig (10) indicates the granitic rocks in the study area lie within 2kb and 10 kb during crystallization. It can be suggested that the granitic rocks from the study area were consolidated under the low pressure condition. If the igneous rocks were assumed as crystallization at minimum pressure of 2kb, their liquid temperature can be estimated from the diagram showing the relationship between differentiation index and temperature at 2 kb water pressure.

Depth of the crystallization of the igneous rocks can be expressed from the schematic depth-temperature diagram (after Marmo, 1969), Fig (11). From this diagram, the liquidus temperatures are 680°C to 712°C, 690°C, 700°C for biotite granites, biotite-muscovite granite, biotite microgranite. Diorites and microdiorite crystallized at 750°C to 760°C, 760°C and then pyroxenites at 870°C to 940°C. Generally, it may be suggested that biotite granites, biotite-muscovite granite and biotite microgranite may crystallized at the depth of 22km to 24km, 24km, 22km. Diorites and microdiorite may differentiated at 25km and pyroxenites may be at the depth between 30 km to 33 km.

Tectonic Discrimination of the Granitoid Rocks

The configurations of tectonic environments for the granitic rocks of the study area were made by using Maniar and Piccoli (1989) classification schemes. SiO₂ versus K₂O diagram are shown to classify the tectonic environment into IAG+CAG+CCG+CEUG+POG +RRG and OP field. The granitic rocks of the study area fall within the IAG+CAG+CCG +CEUG+POG field. In plots of M/AFM (MgO/Al₂O₃ +FeO +MgO) versus F/AFM (FeO /Al₂O₃ +FeO +MgO) variation diagram and plots of C/ACF (CaO /Al₂O₃ +CaO + FeO) versus F/ACF (FeO/Al₂O₃+CaO+FeO) variation diagram show the granitoid rocks of the study area fall within the IAG+CAG+CCG field. Again in the Shand's Index diagram, plots of the granitic rocks fall in the CAG and CCG field, Fig (12, A). According the above mentioned data, it can be safely considered that the granitoid rocks of the study area are orogenic granitoids. Therefore, the granitic rocks of the biotite granites, biotite-muscovite granite and biotite microgranite were formed on the continent relation to the subduction of an oceanic plate beneath the continent. Pearce et al (1984) postulated that the discrimination diagram to integrate granite geochemistry into the plate tectonic framework. In the Y versus Nb diagram; all granites in the study area fall in the field of Syn-COLG and VAG and Y+Nb versus Rb diagram indicates that all granite rocks are fitted in the VAG field. According to the above data, the syn-collision granites support mantle of crustal sources augmented by melt and fluids from subducted continental crust. The volcanic arc granite is generally depleted mantle sources enriched by a subduction fluid ± interaction with continental crust. Batchelor and Bowden (1985) used to discriminate the tectonic setting of granite according to R₁-R₂ binary (mellication) diagram; Fig (12, B) indicates the granitoid rocks of the study area correspond to syn-collision zone.

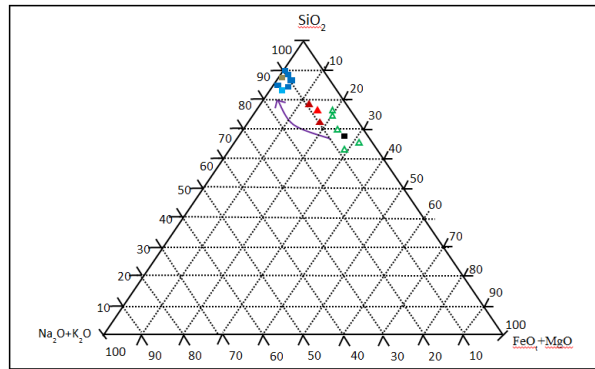


Figure 2 $\text{SiO}_2 - (\text{Na}_2\text{O} + \text{K}_2\text{O}) - (\text{FeO} + \text{MgO})$ diagram showing the evolutionary trend of the igneous rocks (after Le Meitre, 1989)

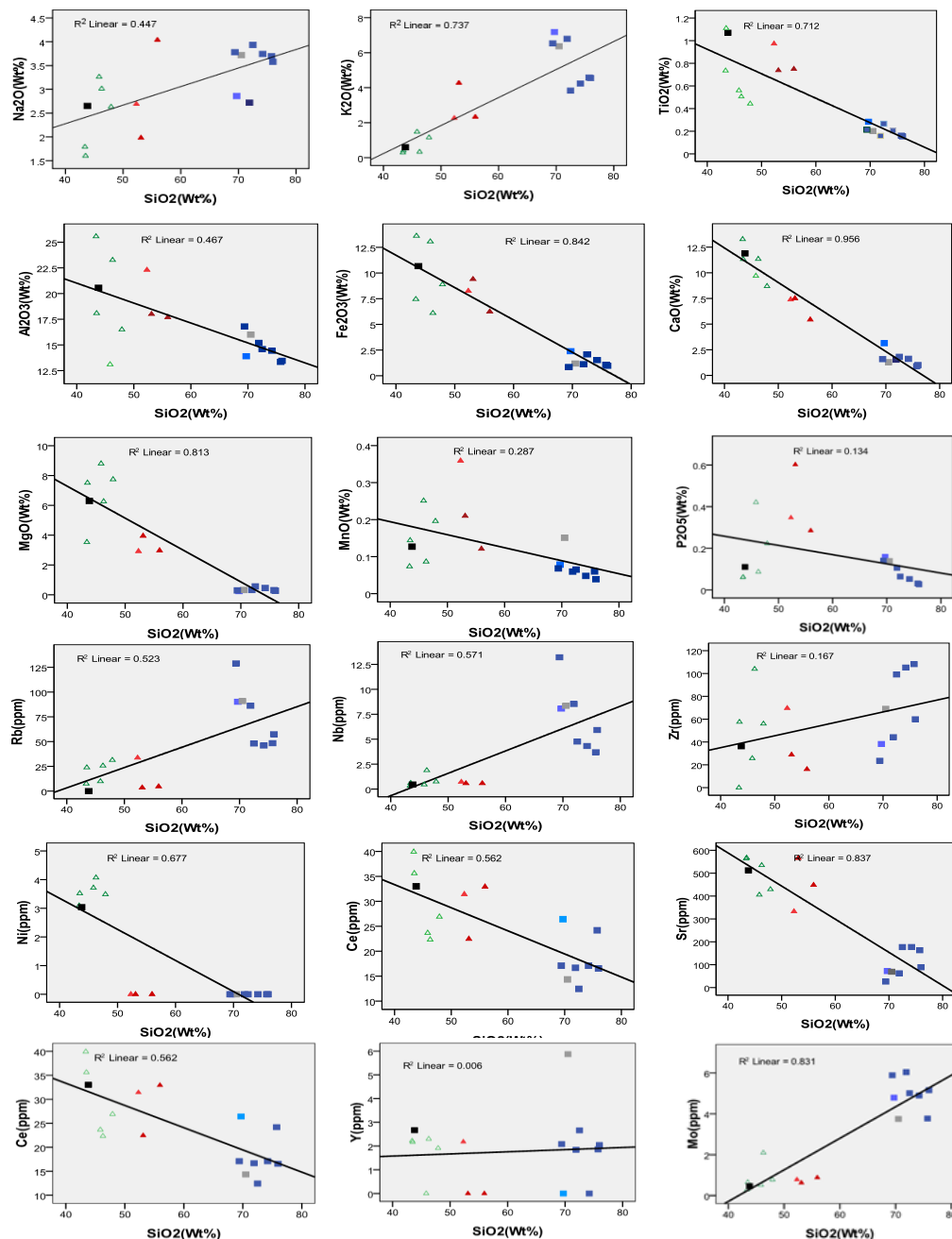


Figure 3 Harker's variation diagrams showing the correlation between major oxides and trace elements Vs SiO_2 of the igneous rocks from the study area, Symbols as in Table (1)

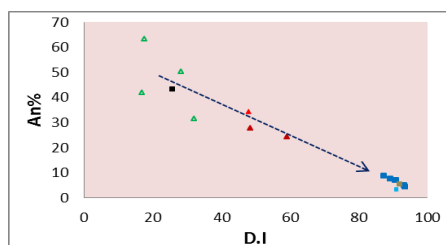


Figure 4 Anorthite percent (An%) in normative plagioclase plotted against Differentiation Index (D.I) of Thornton and Tuttle (1960). Symbols as in Table (1)

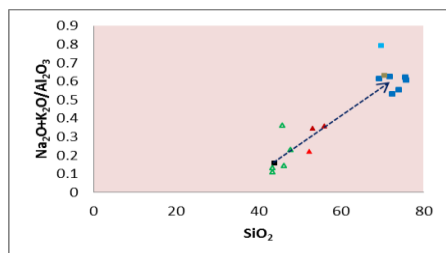


Figure 5 $\text{Na}_2\text{O}+\text{K}_2\text{O}/\text{Al}_2\text{O}_3$ Vs SiO_2 variation diagram, showing the trend of differentiation (after Chappell and White, 1974), Symbols as in Table (1)

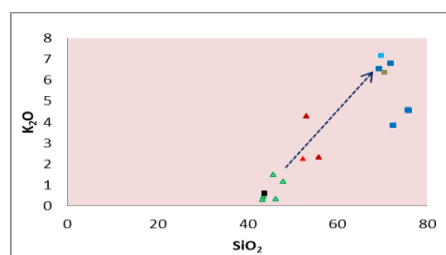


Figure 6 K_2O Vs SiO_2 variation diagram, showing the trend of differentiation (after Le Maitre, 2001), Symbols as in Table (1)

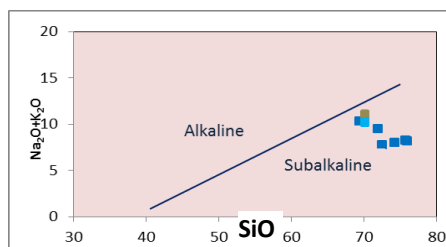


Figure 7 $\text{Na}_2\text{O}+\text{K}_2\text{O}$ Vs SiO_2 diagram distinguishing between alkaline and subalkaline series, (after MacDonald, 1968). The granitic rocks in the study area fall in the subalkaline series of the study area, Symbols as in Table (1).

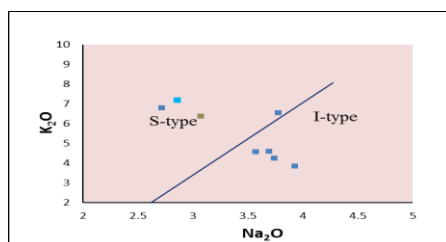


Figure 8 K_2O Vs Na_2O diagram for the granitic rocks of the study area, (after Chappell and White, 1983)

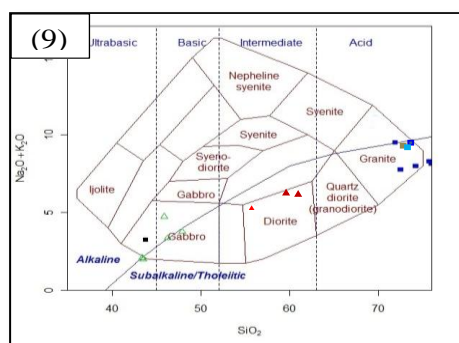


Figure 9 TAS diagram of Cox et. al. (1979) showing subalkaline series of the study area, Symbols as in Table (1)

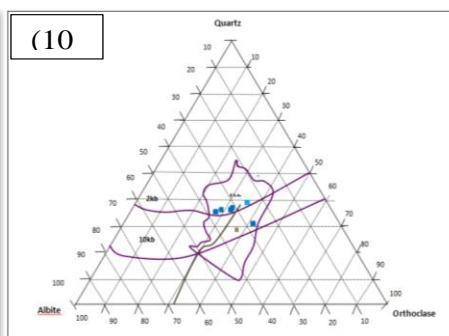


Figure 10 Normative data plot of Quartz - Albite - Orthoclase ratio exhibits the granitic rocks in the study area have water pressure within 2 kb and 10 kb (after Tuttle and Bowen, 1985), Symbols as in Table (1)

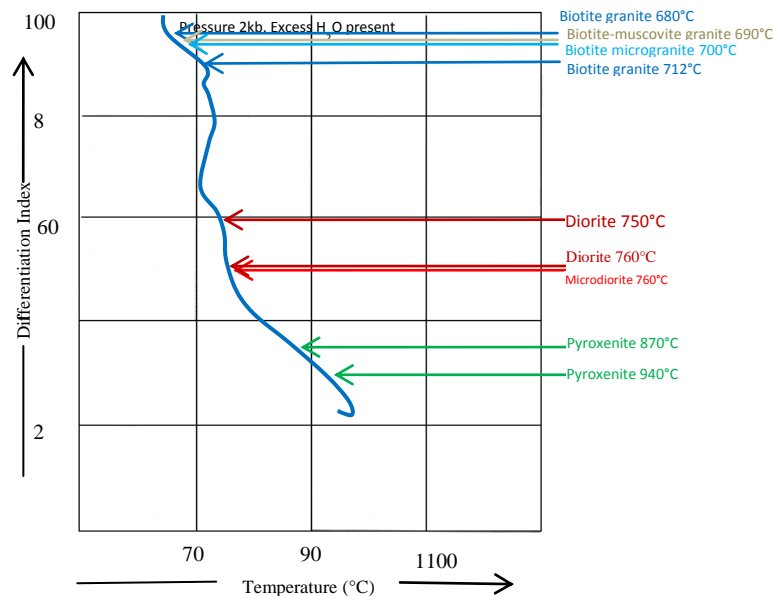


Figure 11 Temperature-differentiation index diagram for the igneous rocks of the study area, at 2 kb water pressure (after Piwinski and Wyllie, 1970)

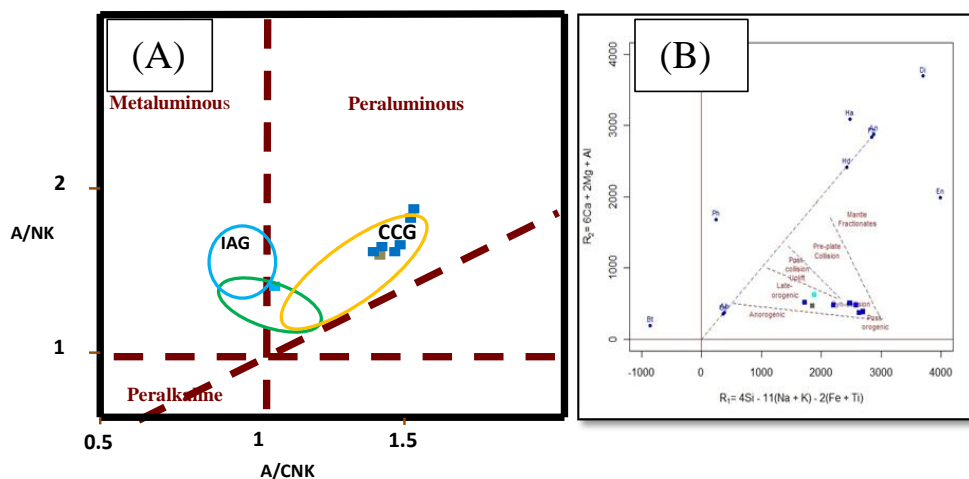


Figure 12 (A) Shand's Index diagram for granitic rocks of study area, which fall within the CAG and CCG field, Symbols as in Table (1) (B) R_1 - R_2 binary (millication) diagram indicates the granitoid rocks of the study area correspond to syn-collision zone

Geochronology of the igneous rock of the study area

Biotite granite (MMK-5) cropped out at the northern part of Lakhin pogoda, Latitude N $17^{\circ}14'16''$, Longitude E $97^{\circ}12'46''$ was sent to the geochemical and isotope laboratory at the ALS laboratory of Geological Survey of Japan for LA-ICPMS. Biotite granite gives the zircons age of 51.9 ± 0.7 Ma, Fig (13). The result from zircon crystallization suggests that the biotite granite was emplaced in Eocene.

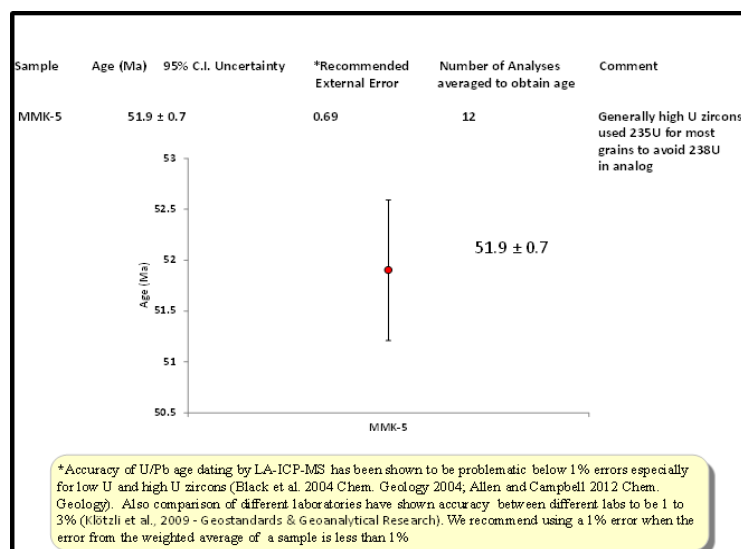


Figure 13 Result of biotite granite at Latitude N 17° 14' 16", Longitude E 97° 12' 46", Accuracy of U/Pb age dating by using LA-ICPMS technique

Conclusion

Geologically, the study area is chiefly covered by igneous and metasedimentary rocks. Geochemically, plots of Harker's variation diagrams selected on major oxides and trace elements, Al_2O_3 , TiO_2 , Fe_2O_3 , CaO , MgO , MnO and P_2O_5 are negatively correlated with SiO_2 . Na_2O and K_2O are positively correlated with SiO_2 . Ba, Sn, Nb, Zn, Rb, Zr, Y and Mo are positively correlated with SiO_2 . Sr, Ni, Ce versus SiO_2 show decreasing of those elements with increasing of SiO_2 contents. The normative anorthite content against the Thornton and Tuttle Differentiation Index (TTDI) diagram, hornblende and diorite contain proportionately more normative anorthite in plagioclase than the biotite granite. If the igneous rocks were assumed as crystallization at 2 kb water pressure, the liquidus temperatures are 680°C to 712°C, 690°C, 700°C for biotite granites, biotite-muscovite granite, biotite microgranite. Diorites and microdiorite crystallized at 750°C to 760°C, 760°C and then pyroxenites at 870°C to 940°C. Depth of the crystallization of the igneous rocks can be expressed from the schematic depth-temperature diagram (after Marmo, 1969), biotite granites, biotite-muscovite granite and biotite microgranite may crystallized at the depth of 22km to 24km, 24km and 22km. Diorites and microdiorite may differentiated at 25km and pyroxenites may be at the depth of 30 km to 33 km. According to Maniar and Piccoli (1989) diagrams; the granitic rocks of the study area fall in the IAG + CAG + CCG field. It can be safely considered that the granitoid rocks of the study area are Orogenic granitoids. Therefore, the granitic rocks of the biotite granites, biotite-muscovite granite and biotite microgranite were formed on the continent relation to the subduction of an oceanic plate beneath the continent. The tectonic setting of granite according to R_1 - R_2 binary (millication) diagram indicates the granitoid rocks of the study area correspond to syn-collision zone. Radiometric dating by zircon U-Pb method indicates that the age of biotite granite gives the zircons age of 51.9 ± 0.7 Ma. The result from zircon crystallization suggests that the biotite granite was emplaced in Eocene. According to Chappell and White (1974), the genetic types of granitic rocks of the study area are regarded as both I-type and S-type. S-type granites probably originated from the remelting of metasediments and I-type granites derived from the remelting of deep-seated igneous materials. Biotite granite contain two mica are considered as sedimentary protolith of S-type and some biotite granite are I-type. Harker's variation diagrams are not only

linear but also irregular or scatter. Binary plots of Na₂O Vs K₂O diagram of Chappell and White (1983) shows that the granitic rocks of the study area involve both I-type and S-type.

Acknowledgements

My deepest thanks to U Aung Kyaw Htoon, Part-Time Lecturer, Geology Department, Dagon University for providing collected data for my research.

References

- Chappell, B.W., White, A.J.R., (2001). Two contracting granite types : 25 years later, *Australian Journal of Earth Science* (2001) 48. 489-499
- Chhibber, H.L., (1934). *The Geology of Burma*, Macmillan & Co.Ltd., London.
- Fryer, B.J., Jackson, S.E., Longerich, H.P. (1993). *The application of Laser Ablation Microprobe-Inductively Coupled Plasma-Mass Spectrometry (LAM-ICP-MS) to insitu U-Pb Geochronology*, *Chemical Geology*, 109, p.1-8.
- Khin Zaw, (1990). Geological, Petrological, and Geochemical characteristics of granitoid rocks in Burma, with special reference to the associated of W-Sn mineralization and their tectonic setting, *Journal of Southeast Asian Earth Sciences*. Vol.4.
- Le Maitre, R. W. (2001). *Igneous rocks; A classification and Glossary of Term*. 2nded., Recommendation of the International Union of Geological Science Subcommittee on the systematic of igneous rocks. Cambridge University Press.
- Maniar, P.D, Piccoli, P.M. (1989). *Tectonic discrimination of Granitoids*. G.A.S. Bull., volume.101, p.635-643
- Marmo, V., (1956). *On the emplacement of Granites*. Am. Journal of Science. volume-254. p.479- 492
- Middlemost, E.A., (1994). *Naming material in the magma/igneous rock system*. *Earth Science reviews*, 37(3), p.215-244
- Pearce. J. A., Harris, N.W., Tindle, A.G., (1984). Trace element discrimination diagrams for the tectonic interpretation of granitic rocks. *Journal of Petrology* 25.p. 956-983.
- Rollinson, H.R., (1993), *Using Geochemical data: evaluation, presentation, interpretation*, Longman Group UK Ltd. P.48-80
- Rollinson, H.R., (1994), *Using Geochemical data: evaluation, presentation, interpretation*, Longman Group UK Ltd. P.352.
- Thornton, C.P., and Tuttle, O.F., (1960). Chemistry of Igneous Rocks. Differentiation index. *Am. Journal of Science*, volume 258, p.664-684.

GEOLOGY AND HEAVY MINERAL ANALYSIS OF LOOSE SAND FROM AUKZEIK AREA, THE KALEKOK ISLAND, LAMING SUB-TOWNSHIP, MON STATE

Min Min Khaing¹, Win Win Myint², Thant Sin³, Aye Aye Aung⁴

Abstract

Heavy mineral analysis was systematically carried out mainly focus on the beach sand of the Kalekok island. It is situated about 144km south of Mawlamyine and about 35 km north of Ye township, Mon State. It lies between latitude N 15°29'00" to 15°32' 30" and longitude E 97° 38'30.00" to 97° 40' 15.00" in one inch Topographic Map no.95 E/10. The topographic features of the whole area are generally mountainous and the drainage pattern show medium to coarse texture, subparallel pattern. The igneous rocks are microdiorite, hornblende biotite granodiorite with microdiorite xenoliths, biotite granite and leucogranite. The probable age of the igneous rocks may be emplaced in Early Cretaceous. The study area falls in tropical monsoonal climate and the annual rain fall is 99.83". The maximum temperature is 36.2°C and the minimum temperature is 20.14°C. The wind speed lies between 6 to 25 mph and most of wind direction is SW, E and SE directions. The XRF assay results and average heavy mineral data of the research area related to the silicic igneous origin, related to high rank metamorphism and the deposition through Triassic to Miocene. Titanium, zirconium, ilmenite, monazite, magnetite, REEs and radioactive elements are commonly occurred. These minerals are very important for industrial purposes and economical point of view. This research is supporting for the genesis of heavy minerals and related rocks, to get foreign income of the country, to explore the ore mineral resources, to development of industrial zone, to get the opportunities of employment for the local people, to maintain and reduce the damage of the coastal's natural environment.

Keywords: Heavy Minerals Analysis, Drainage Pattern, REEs, Radioactive Elements

Introduction

Heavy minerals are volumetrically minor constituents in terrigenous rocks. They are characterized as having a specific gravity greater than 2.85. Heavy minerals are now studied as guide to source rock lithologies and dispersal patterns. They are also useful in evaluating diagenetic history as well as the pre- erosional weathering and tectonic history of the source area. The various heavy mineral species present in sediments or rock comprise the heavy minerals assemblage. Rock units in a vertical succession containing different assemblages are called heavy mineral zones. Lateral variation within a lithologic unit, the various assemblages are known as heavy mineral associations. The research area is situated about 144km south of Mawlamyine and about 35 km north of Ye township, Mon State. It lies in one inch Topographic Map no.95 E/10. The study area falls in tropical monsoonal climate alternating mostly heavy rain and dry spell. The drainage pattern is fairly poor, medium to coarse texture and displays sub parallel pattern, as shown in Fig. 2.

¹ Lecturer, Department of Geology, Dagon University

² Lecturer, Department of Geology, Dagon University

³ Dr, Lecturer, Department of Geology, Dagon University

⁴ Dr, Professor, Department of Geology, Dagon University

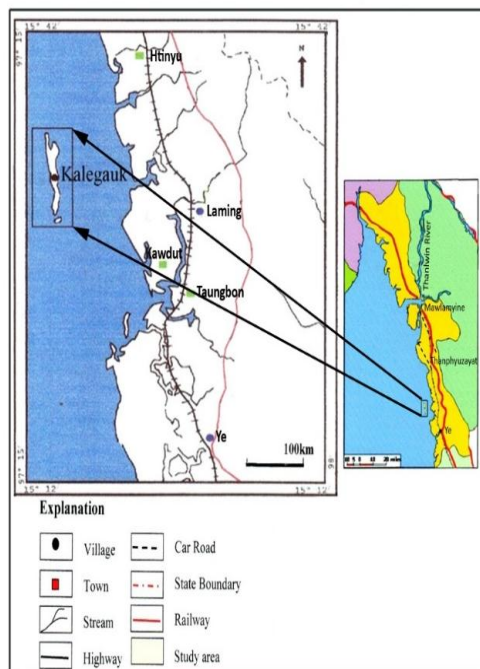


Figure 1 Location map of the research area

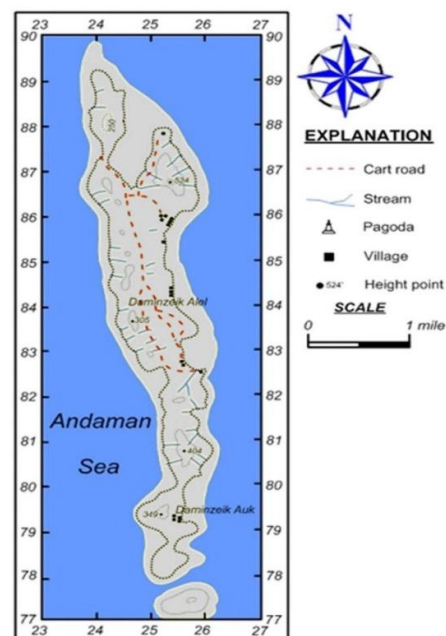


Figure 2 Drainage pattern of the research area

Purpose of Research

- The principal objectives of the research area as follows:
- To prepare a detailed geological map
- To study petrology, to understand the sampling, processing and content of heavy minerals, radioactive elements and REEs from loose sand.
- To provide detail economic exploration from underground beach sand development of industrial zone.
- To support foreign income of our country and the opportunities of the employments for local people.

Methods of Study

Field investigation

Before conducting the field works, literature collection and studies of previous works have been performed. Based on the available data and information, the field programme was planned. Field works including systematic sampling, measurement of the geological structures and geological mapping have been carried out by using tape and compass traverse method and GPS. After the ground checking, detail geological mapping was carried out and to make regional geological survey, see Fig. 3. The heavy minerals bearing beach sand are collected by making 2"Ø pile analyzed and to collect geochemical sampling for the petrochemical analysis. At each station, sand sample weighting 250g were collected.

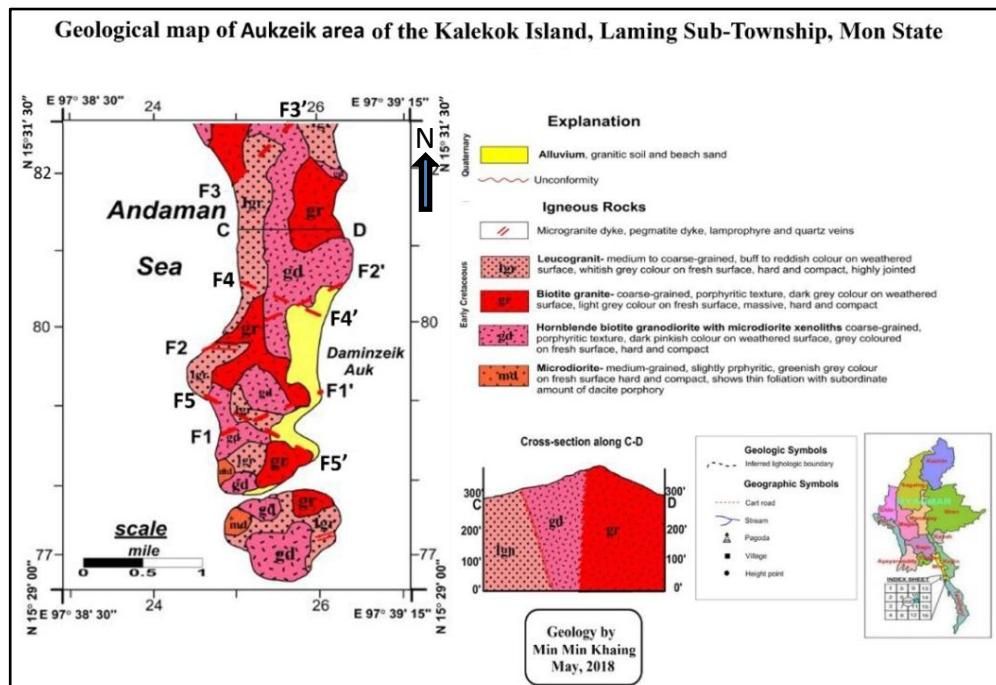


Figure 3 Geological Map of the Research Area

Distribution of rock units and field description

The study area is mainly composed of igneous rocks of microdiorite, hornblende biotite granodiorite with microdiorite xenoliths, biotite granite locally porphyritic and foliated texture, leucogranite. Igneous rocks are well exposed in the southern part of the Kalekok island and lamprophyre, pegmatite, microgranite, aplite dykes and quartz veins are intruded into it. Good exposures are found as boulder, as domes and as small bodies at the coastlines in the study area. Igneous rocks are highly weathered and are developed as different types, shapes and sizes of the igneous landforms. Microdiorite are commonly occurred at the southern part of the Kalekok island. Hornblende biotite granodiorite with microdiorite xenoliths are mostly occurs at outboard portion of the island and the southern part of Aukzeik area. Biotite granite locally with porphyritic and foliated texture are mostly occurred as large domes and batholiths and they are sometimes gradationally contacted with hornblende biotite granodiorite with microdiorite xenoliths especially occurred at the eastern part of Aukzeik beach. Biotite granite is sharply contact with hornblende biotite granodiorite with microdiorite xenoliths and leucogranite mainly encounter at the Aukzeik pagoda hill and western part of Warsho hill. Leucogranite are mainly exposed at southern part of the study area and good exposure are found at the beach of Cavendish island and Aukzeik area. It is generally hard, compact and highly jointed. They intruded hornblende biotite granodiorite with microdiorite xenoliths and biotite granite. Lamprophyre dykes are intruding hornblende biotite granodiorite with microdiorite xenoliths, biotite granite and leucogranite. Lamprophyre dykes are mainly intruded into leucogranite as dyke swams at Cavendish island and Aukzeik area. Pegmatite dykes intruded hornblende biotite granodiorite with microdiorite xenoliths and biotite granite. Pegmatite dykes and veins are mainly occurred at Warsho hill. Aplite dykes mainly intruded into hornblende biotite granodiorite with microdiorite xenoliths and biotite granite. They are mainly found at southern part of Aukzeik area. Microgranite (biotite microgranite) dykes are mainly intruded into hornblende biotite granodiorite with microdiorite xenoliths and biotite granite, especially occurred at Aukzeik area. Quartz veins are intruding in all the granitoid rocks and they are widely distributed.

Geological Structures

There are five minor normal fault in the research area. F_1 - F_1' , F_2 - F_2' and F_3 - F_3' are trending NE-SW. F_4 - F_4' and F_5 - F_5' are trending NW-SE.



Figure 4 Loose sand samples location map of the research area

Laboratory investigation

The laboratory investigation of the representative samples include the following; thin section study of different rock units exposed in the research area and modal analysis were analyzed by means of polarizing microscope. Quantitative and qualitative elements analyses of various rock types and unknown minerals have been carried out using XRF and XRD analyses. The collected the loose sand samples are dried and weighted. Grain size differentiation by sieving and after sieving, the samples are weighted. Magnetic fraction by hand magnet and weighted. Heavy minerals are removed from more abundant light minerals by gravity separation by using a high density heavy liquid of Bromoform, Acetylene tetrabromite, Methlene iodide.

Previous Works

Brown and others (1951), Hutchison (1973) (1978), Bender (1983), Nyan Thin (1984) and Khin Zaw (1990) studied the regional geological study of the neighbouring area. Min Min Khaing (2013) studied petrological and petrochemical analysis on granitic rocks of the Kalekok Island and its environs.

The research area is part of the Shan-Tanintharyi Block and the northern continuation of Thanintharyi Ranges. The area can be regarded as a southern continuation of SE-Asia Tin-Tungsten Belt. It lays the Western Granite Province of SE-Asia and also within the Central Granitoid Belt of Myanmar, as shown in Fig.4

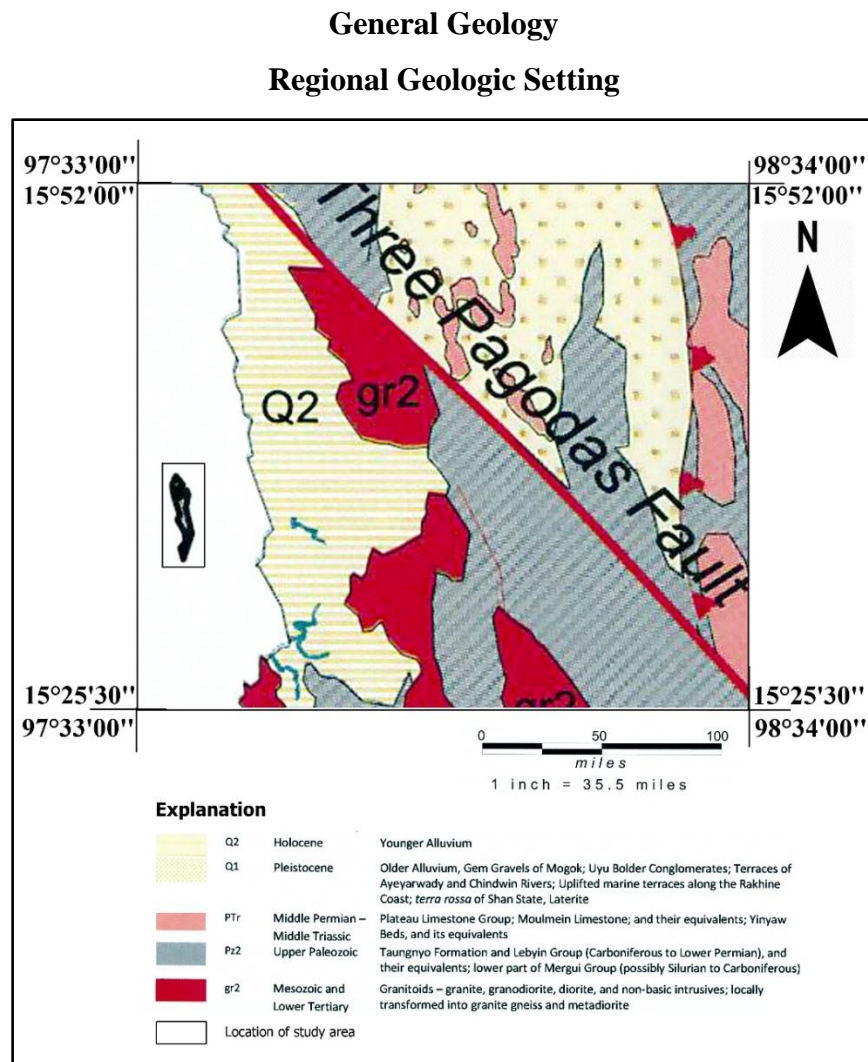


Figure 5 Regional Geological Map (After 1 million scale Geological Map of Burma, 2014)

Minerals Description

Most of the heavy minerals of the research area are anisotropic minerals but spinel and garnet are isotropic. Opaque grains are ilmenite and hematite, these minerals are very similar physical characteristics but different streak and crystal form. Ilmenite is also known as manaccanite, primary titanium ore and mostly connected with igneous deposits. Ilmenite is reddish brown colour and commonly altered to leucoxene. Quartz, apatite, amphibole monazite, tourmaline, epidote, rutile, zircon and sphene are also observed, See Fig. 5, Fig. 6. According to the mineral distribution map of the study area, Chromite, Leucoxene and Zircon are mostly distributed at the northern part and Geothite, Ilmenite and Sphene are distributed in southern part of the research area.

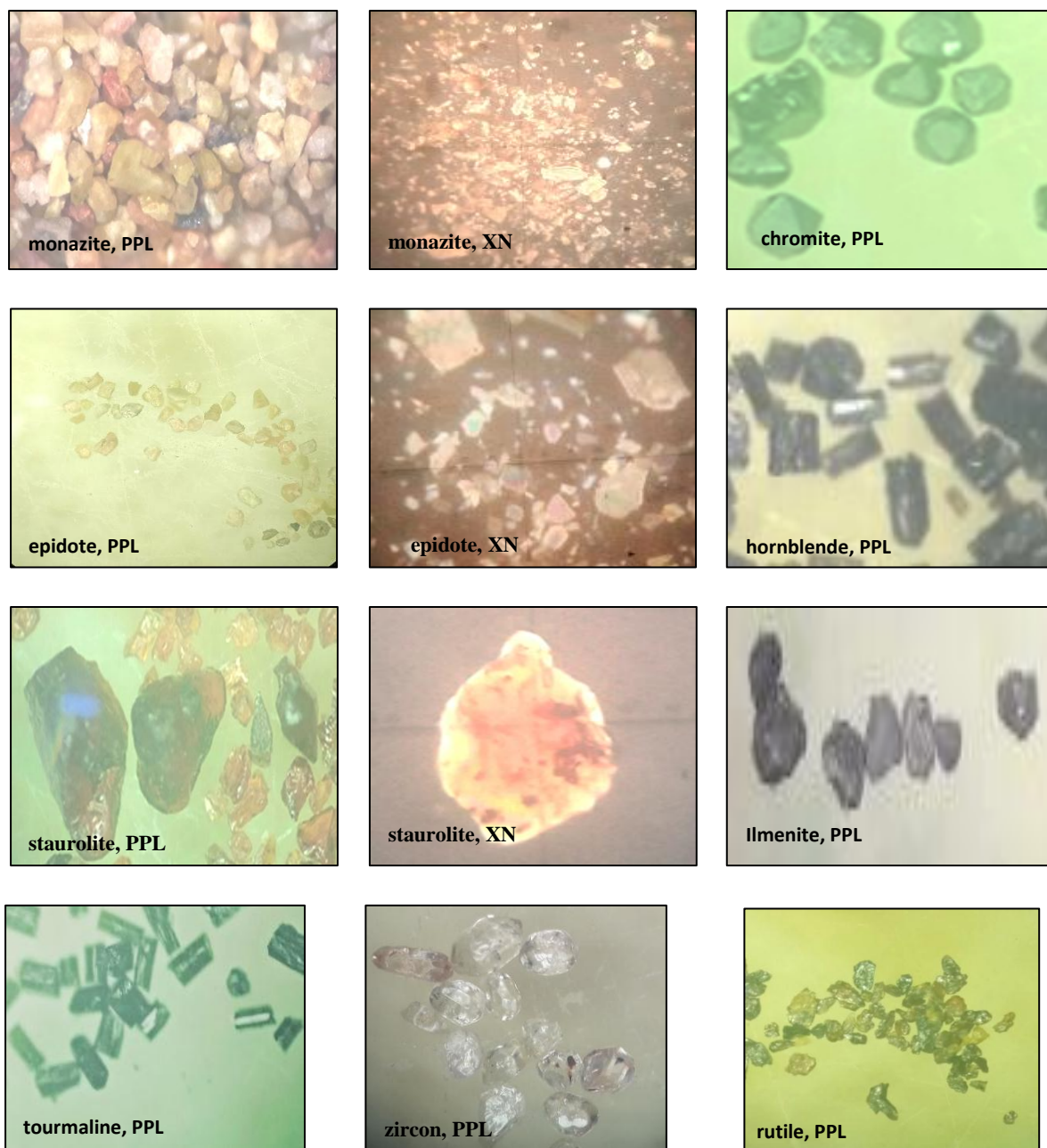


Figure 6 Microscopic study of heavy minerals

Results and Finding

At the beach of the research area, heavy minerals bearing sand are commonly occurred as layer by layer about 2cm to 6cm thick. Generally, the surface ground radiation is (100) CPM to (1000) CPM are widely distributed on beach sand flats. In some place, locally surface ground radiation is mostly occurred as (20) CPM to (100) CPM and strong radiation (300) CPM to (1000) CPM are found, Table. 1, Table. 2, Table. 3, Table. 4. REE minerals of Y, La, Ce, Pr, Nd and Th are observed. Y is up to 0.088 ppm, La is up to 0.235 ppm, Ce is up to 4.7 ppm, Pr is up to 0.206 ppm, Nd is up to 0.167 ppm and Th is up to 0.113 ppm respectively.

Table 1 List of heavy mineral analysis data from Aukzeik area (2015-16)

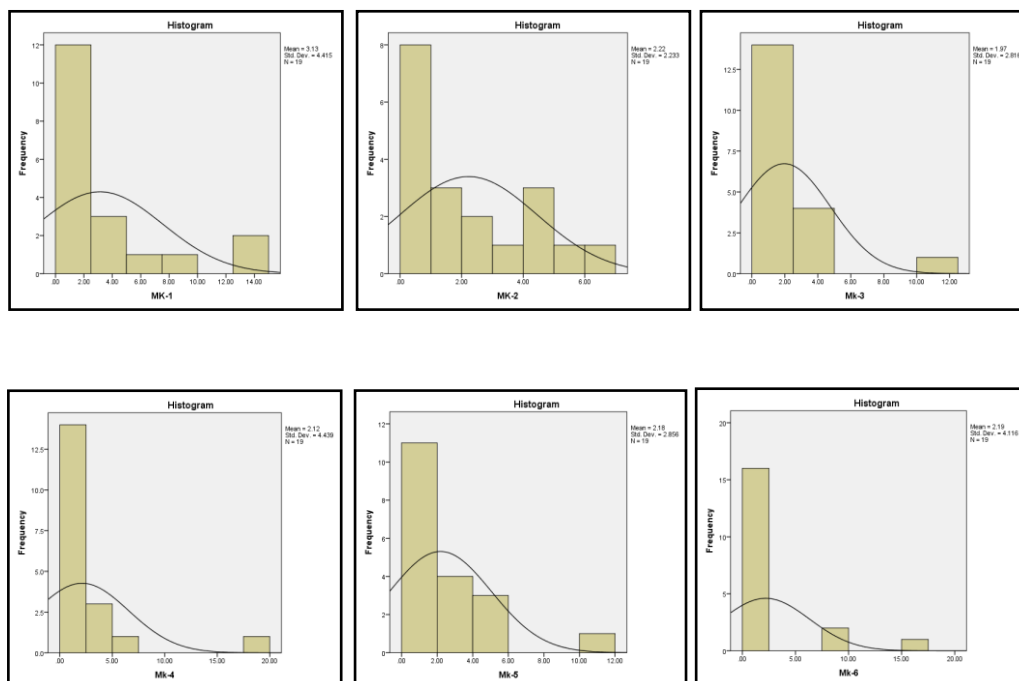
Sample No	mm 1 Aukzeik-S		mm 2 Aukzeik-S		mm 3 Aukzeik		mm 4 Aukzeik-N		mm 5 Aukzeik-N	
Magnetic fraction %	0.88		Trace		0.10		10.13		73.02	
Light Mineral %	88.70	65.30	92.04	56.05	93.80	55.30	3.35	2.50	18.62	-
Quartz		22.40		35.99		26.50		0.84		-
Feldspar		1.00		-		12.00		0.01		-
Mica										
Heavy Mineral (%)										
Zircon		3.40		2.30		1.90		3.63		1.08
Monazite		0.50		1.45		0.10		0.13		0.18
Ilmenite		3.60		1.27		2.70		79.87		4.53
Tourmaline		2.10		1.86		0.70		0.62		0.05
Garnet		0.06		0.43		0.10		0.99		0.09
Epidote		0.30		Trace		0.40		-		0.07
Xenotime		-		-		-		0.01		0.33
Rutile		0.43		0.65		0.10		1.27		0.34
Diopside		-		-		-		-		-
Cassiterite		0.03		-		0.10		-		0.20
Anatase		-		-		-		-		-
Uraninite		-		-		-		-		-
Sphene										0.31
Hematite										0.11
Amphibole										0.08
Andalusite										0.05
Geothite & Limonite										0.53
Leucoxene										0.41

Table 2 List of heavy mineral analysis data from Aukzeik area (2018)

Heavy Minerals	MK-1	MK-2	MK-3	MK-4	MK-5	MK_6
Magnetic fraction Wt%	33.25	34.63	48.42	47.39	50.92	55.24
Light fraction Wt %	7.25	23.18	14.23	12.42	7.56	3.16
Heavy fraction Wt %	59.5	42.19	37.35	40.19	41.51	41.6
Ilmenite	12.81	6.86	3.67	2.97	3.72	2.43
Epidote	1.51	3.86	3.46	2.77	4.15	0.79
Garnet	2.99	0.45	1.28	0.35	0.22	0.2
Leucoxene	3.22	2.71	1.5	2.16	4.45	1.63
Amphibole	8.54	1.81	3.85	0.21	2.56	0.01
Geothite	2.45	1.58	1.22	0.94	2.08	1.17
Staurolite	14.62	5.68	12.12	19.54	11.51	7.94
Kyanite	2.12	1.72	1.14	1.05	0.45	0.34
Tourmaline	0.9	4.82	0.36	0.71	1.36	0.72
Rutile	4.88	4.43	2.03	5.09	2.46	8.03
Zircon	5.46	4.87	4.02	2.61	5.64	15.99
Anatase	0.01	0.07	0.11	0	0	0.09
Sphene	0	2.34	0.81	1.09	1.64	0.99
Monazite	0	0.99	0.3	0	0.65	0.25
Sillimanite	0	0.01	0.64	0.4	0.49	0.01
Chromite	0.01	0.01	0.84	0.19	0.08	0.75
Rock clasts	0	0	0	0.11	0.05	0.28
Spinel	0	0	0	0	0	0.01
Xenotime	0	0	0	0	0	0

Table 3 Comparison of heavy mineral analysis datas from Aukzeik area (2015– 2016–2018)

Heavy Minerals	2015-16	2018
Ilmenite	1.27-79.84	2.97-12.81
Epidote	Trace-0.40	0.79-4.15
Garnet	0.06-0.99	0.20-2.99
Leucoxene	0-0.41	1.5-4.45
Amphibole	0-0.08	0.01-8.54
Geothite	0-0.53	0.94-2.45
Staurolite	-	5.68-19.54
Kyanite	-	0.34-2.12
Tourmaline	0.05-2.1	0.36-4.82
Rutile	0.1-1.27	2.03-8.03
Zircon	0.08-3.63	2.61-15.99
Anatase	-	0-0.11
Sphene	0-0.31	0-2.34
Monazite	0.1-1.45	0-0.99
Sillimanite	-	0-0.64
Chromite	-	0.01-0.84
Rock clasts	-	0-0.28
Spinel	-	0-0.01
Xenotime	0.01-0.33	-
Cassiterite	0.03-0.1	-
Hematite	0-0.8	-
Andalusite	0-0.05	-

**Figure 7** Histogram of heavy minerals from the research area. Data used in Table. 4.

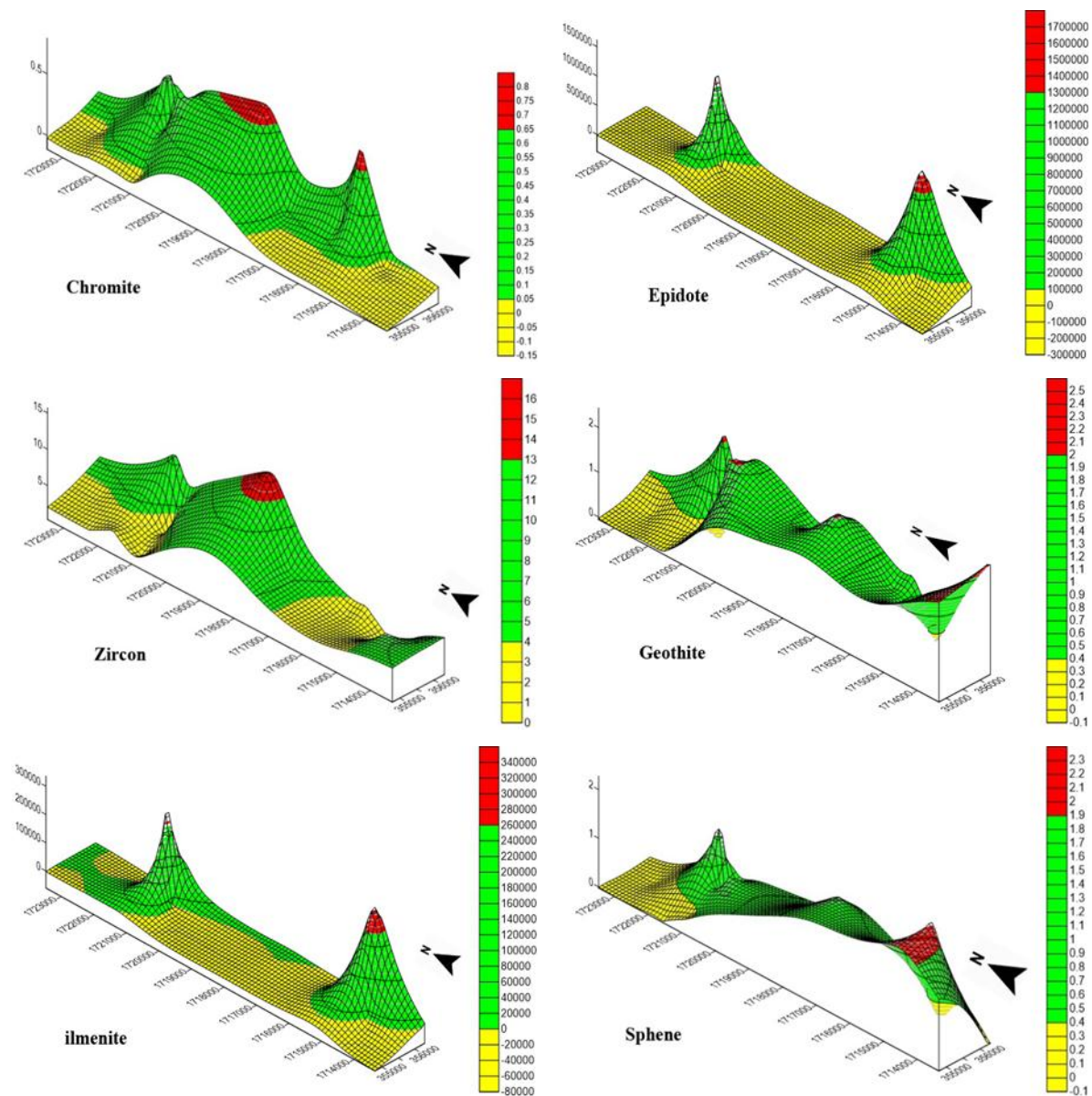


Figure 8 Minerals distribution map of the research area

Discussion and Conclusion

The research area is mainly composed of igneous rocks (Early Cretaceous) and they are intruded by lamprophyre, pegmatite, microgranite, aplite and quartz vein. Heavy mineral assemblages in marine deposits are strongly influenced by major rivers, on adjacent land masses, with drainage basins of different lithologic make up. The origin of many heavy mineral species are limited to rather specific rock types. In the research area, rutile, tourmaline and zircon are commonly occurred. According to detrital heavy mineral suites characteristic of source rock types (modified from Pettijohn, 1970) this fact indicated that it is reworked sediments. Andalusite, epidote, garnet, hornblende are found, so it is related to high rank metamorphism. Also apatite, amphibole, monazite, sphene, tourmaline and zircon are occurred it is the origin of silicic igneous origin. Some mineral species (e.g zircon and rutile) are minor constituents in source rock. Other more abundant mineral species (e.g hornblende) are relatively unstable and most are destroyed during weathering in source area.

Table 4 XRF analysis data of heavy minerals from loose sand of Aukzeik area

	mk 1	mk 1a	mk 2	mk 2a	mk 2b	mk 3	mk 3b	mk 3c	mk 3d	mk 4	mk 4a	mk 4b	mk 4c	mk 4d	mk 5	mk 5a	mk 5c	mk 6	mk 6c
Ti	1.3	5.29	0.2	0.2	0.35	0.33	8.334	10.51	2.07	8.358	7.874	8.355	4.199	2.98	14	14.1	2.909	0.3	0
V	-	0.02	-	-	-	-	0.035	0.043	-	0.039	0.04	0.036	0.018	-	0.04	0.03	-	-	-
Cr	0.1	0.38	-	0	-	0.015	0.731	1.12	0.123	0.875	0.763	0.855	0.37	0.194	0.59	0.7	0.141	-	-
Mm	0.1	0.35	0.1	0	0.06	0.028	0.562	0.708	0.167	0.582	0.533	0.575	0.292	0.205	1.21	1.2	0.231	0	0
Fe	2.8	10.3	2.2	2.4	2.95	0.014	13.59	16.64	5.896	14.36	13.54	14.01	8.23	7.402	17.2	17.1	3.871	0.8	3
Co	0	-	0	-	0	0.005	0.011	0.011	0.0061	-	0.0112	-	0.006	0.002	-	0.01	0.002	0	0
Zn	-	0.02	0	-	0.01	-	0.03	0.034	0.0408	0.034	0.0272	0.027	0.0175	0.016	0.03	0.03	0.017	-	-
Se	0	-	-	-	-	-	-	-	-	-	-	-	-	-	-	-	-	0	-
Rb	0	-	0	0	0.02	0.005	-	-	0.005	-	-	-	-	-	-	-	-	0	0
Sr	-	0.02	0	0	0.05	-	0.018	0.012	0.0092	0.01	0.0123	0.011	0.0112	0.014	-	-	-	0	-
Y	0	0.05	-	-	-	-	0.088	0.136	0.0175	0.115	0.102	0.108	0.0488	0.022	0.07	0.09	0.0167	-	-
r	0.8	1.19	0	0.1	0.03	0.138	2.824	4.884	0.4194	4.377	3.723	3.886	1.544	0.408	6	7.09	1.237	0.1	0
Nb	0	0.02	-	-	-	-	0.02	0.021	0.0062	0.015	0.164	0.016	0.0096	0.01	0.03	0.03	0.0083	-	-
Ba	-	-	-	-	0.08	-	-	-	-	-	-	-	-	-	-	-	-	-	-
La	-	0.08	-	-	-	-	0.169	0.235	-	0.186	0.19	0.196	-	-	-	0.11	-	-	-
Ce	-	0.15	-	-	-	-	0.293	0.47	-	0.398	0.369	0.379	0.157	0.074	0.17	0.2	-	-	-
Pr	-	-	-	-	-	-	-	0.206	-	-	-	-	-	-	-	-	-	-	-
Nd	-	-	-	-	-	-	0.138	-	-	0.16	0.167	0.166	-	-	-	-	-	-	-
Hf	-	-	-	-	-	-	0.067	0.1	-	0.1	0.082	0.083	-	-	0.13	0.18	0.021	-	-
W	0.1	-	0.1	-	0.04	0.114	-	-	0.049	-	-	-	-	-	-	-	-	0.1	0
Th	-	0.03	-	-	-	-	0.067	0.113	-	0.102	0.0879	0.096	0.04	-	0.06	0.08	-	-	-

During the time, when a sedimentary sequence is being deposited the character of the source area will be likely change. Such changes may be reflected in the succession of heavy mineral zones. According to heavy mineral zone (modified from Pettijohn 1974, based on data from Anderson 1948); the heavy mineral zone of rutile, zircon, tourmaline, garnet minerals fall in Triassic zone, rutile, zircon, tourmaline, garnet and epidote minerals fall in Upper Cretaceous zone, rutile, zircon, tourmaline, garnet, epidote and amphibole minerals fall in Miocene zone. The trend most cited is an upward increase in the complexity of the assemblages. Minerals present in the younger beds but absent in the older ones are commonly less stable species. According to the heavy mineral zones, the heavy mineral situation involves the deposition through Triassic to Miocene, especially fall in Cretaceous. The XRF assay results, average heavy minerals data, the heavy minerals relation of histogram and mineral distribution map of the research area, in Fig. 7, Fig. 8, ilmenite mineral commonly occurred in the southern part and suggest that related to the silicic igneous origin. Ilmenite is a major ore of titanium, a minor ore of iron, so used as a metal need make a variety of high- performance alloys, used to manufacture of titanium dioxide, pigment, whiting and polishing abrasive. The occurrences of heavy minerals and REEs are important for military and industrial purposes.

Acknowledgements

The author would like to express their most heartfelt thanks and offer our deepest homage to Dr. U Win Naing (Rector), Dr. Daw Nu Nu Yi (Pro-Rector) and Dr. Daw Nay Thwe Kyi (Pro-Rector), Dagon University for their encouragement and permission. Special thanks are due to their gratitude with respects to Dr. Daw Kyi Kyi Maw (Professor and Head, Department of Geology, Dagon University) and Dr. Daw Aye Aye Aung (Professor, Department of Geology, Dagon University) for their kind permission and manuscript. The author also thanks to Dr. U Day Wa Aung (Professor and Head, Department of Geology, Yagon University), U Hla Kyi (part-time Professor, Applied Geology Department) and U Thein Win (Pro- Rector, Retd., West Yangon University) for valuable advices and valuable suggestions. The authors wish to express their sincere thanks to Department of Higher Education (Lower Myanmar) and Myanmar Academy of Arts and Science for providing financial aid to carry out this research. Finally, the author deepest thanks are due to my family for their encouragement and supporting in carrying out my research.

References

- Bender, F. (1983). *Geology of Burma*. Gebruder Borntraeger Berlin, Stuttgart, 293pp.
- Brown, J.C. (1924). A geographical classification of the mineral deposits of Burma. *Records of the Geological Survey of India*, 56, 65- 108.
- Chhibber, H.L. (1934b). *The Geology of Burma*. Macmillan, London.
- Cobbing, E.J, P.E.J. Pitified, D.P.E. Darbyshire and D.J.J. Mallik, (1992). The granite of south- East Asia tin belt.
- Hutchison, C.S., (1973). Tectonic Evolution of Sundaland. *Bulletin of the Geological Society of Malaysia*, p. 61-86.
- Hutchison, C.S., (1978). Southeast Asia Tin Granitoid of contrasting Tectonic Setting. *Jour. Phys.Earth*.vol.26, p.211-273.
- Khin Zaw, (1990). Geological, petrological and geochemical characteristics of granitoid rocks in Burma: with special reference to the associated W-Sn mineralization and their tectonic setting. *Jour. Southeast Asian Earth Sci.* vol.4. p. 293-335.
- Maung Thein, (1983). *The Geological Evolution of Burma*, Geological Association, Mandalay University.
- Min Min Khaing, (2013). *Geology of the Kalegauk Island, Ye Township, Mon State*. (Unpublished), Department of Geology, Mawlamyine University.
- Nyan Thin, (1984). *Some aspects of granitic rocks of Tenasserim Division*. (Unpublished), Department of Geology, University of Yangon.
- Nyi Nyi Win Swe, (2016). *Petrological and petrochemical analysis on granitic rocks of the kalegauk island, Ye Township, Mon State*. (Unpublished) Department of Geology, Mawlamyine University.
- Pettijohn, (1974). *A practical approach to sedimentology*, p.164- 234.
- Roylindholm, (1978). *A Practical Approach to Sedimentology*, p.208- 230.

PETROGRAPHICAL AND PETROCHEMICAL ANALYSES OF IGNEOUS ROCKS OF LAUNGZIN AREA, MOGOK TOWNSHIP, MANDALAY REGION

Wathon Chit¹, Mi Paik², Min Min Khaing³

Abstract

The study area is situated in Mogok Township, Mandalay Region. It is bounded by latitude 22°42'00"N to 22°54'00"N and longitude 96°19'00"E to 96°27'00"E. The igneous rocks exposed in the study area consist of pegmatite and granite. The 16 granitoid samples were analyzed for major and trace elements by XRF method. Most of the peraluminous granitoids are plotted in felsic peraluminous field, one biotite microgranite falls in high-peraluminous field, one biotite microgranite and one tourmaline granite fall in moderate-peraluminous field and one hornblende granite fall in low-peraluminous field. According to the major and trace elements composition granitoids of the study area are both of S-type granite and I-type granite. Major elements analysis indicates that most of granitoids belong to the field of IAG, CAG and CCG and they correspond to syn-collision and late orogenic zone. Moreover, trace elements composition shows these granitoids belong to the field of VAG and syn-collision granite and they are tectonically located in the active continental margin. Economically important rare earth elements are discovered in the study area in granitoids and pegmatites.

Introduction

The study area is situated in Mogok Township, Mandalay Region. The study area lies between horizontal grids 300 to 400 and vertical grids 110 to 240 in one inch topographic map No. 93-B/5. The location map of the study area is shown in Fig. (1).

Purpose of Research

The study area has been investigated on the following objectives;

1. To describe the detailed petrography of igneous rock units observed in the study area
2. To study the petrochemical characteristics of the rocks of the study area
3. To investigate the economic possibility encountered in the study area

Methods of Investigation

The reconnaissance study included the topographic map analysis which was combined with satellite image to interpret the topography and drainage pattern. Landsat TM image was studied for possible distribution of rock unit by mean of band analysis and structure such as folds, faults and joints.

Field study was carried out for drawing detailed geological map. The Brunton Compass and GPS were using along the traverse. Representative samples were collected for references and investigation of mineralogical and petrological characteristics of rocks with the aid of GPS location. Measuring dip and strike of bedding, foliation, joints, structural information and major trends of dykes and veins were made by mean of Brunton Compass.

¹ Assistant lecturer, Department of Geology, Dagon University

² Lecturer, Department of Geology, Dagon University.

³ Lecturer, Department of Geology, Dagon University.

As laboratory works, detailed petrographic study of representative samples of various rock units were studied with the aid of transmitted light polarizing microscope. Major oxides, minor and trace elements were determined by applying XRF. The major oxides data were studied to calculate standard C.I.P.W norms and C.I.P.W norms with biotite and hornblende by using GCD kit 3.0 and microsoft excel. Moreover, rock classification, construction of variation diagram and comparison of rock composition with experimentally determined phase boundary for melt of similar composition were made by major oxides and trace elements composition. Trace elements such as Rb, Zr, Y, Nb, Ta, Yb, Th, Hf, Ce were used to determine the tectonic setting of granitoid rocks.

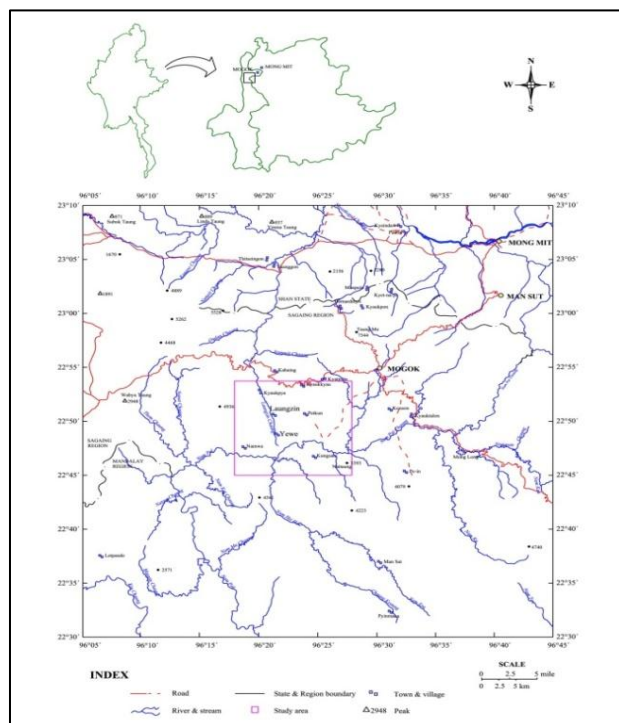


Figure 1 Location map of the study area.

Rock Sequence of the Research Area

Rock sequence of the research area is as shown in Table 1. Geological map of the research area is described in Fig. (2). The absolute age of igneous rocks is according to Kyaw Thu (2007).

Table 1 Rock Sequence of Laungzin Area, Mogoke Township, Mandalay Region (Age of igneous rocks after Kyaw Thu, 2007)

Rock Type	Age
Alluvium	Quaternary
Igneous Rocks	
Pegmatite	Middle Miocene(15 Ma)
Tourmaline granite	Middle Miocene(15 Ma)
Biotite microgranite	Early Miocene(15.8±1.1 Ma)
Leucogranite	Early Oligocene(32±1 Ma)
Hornblende granite	Jurassic ?

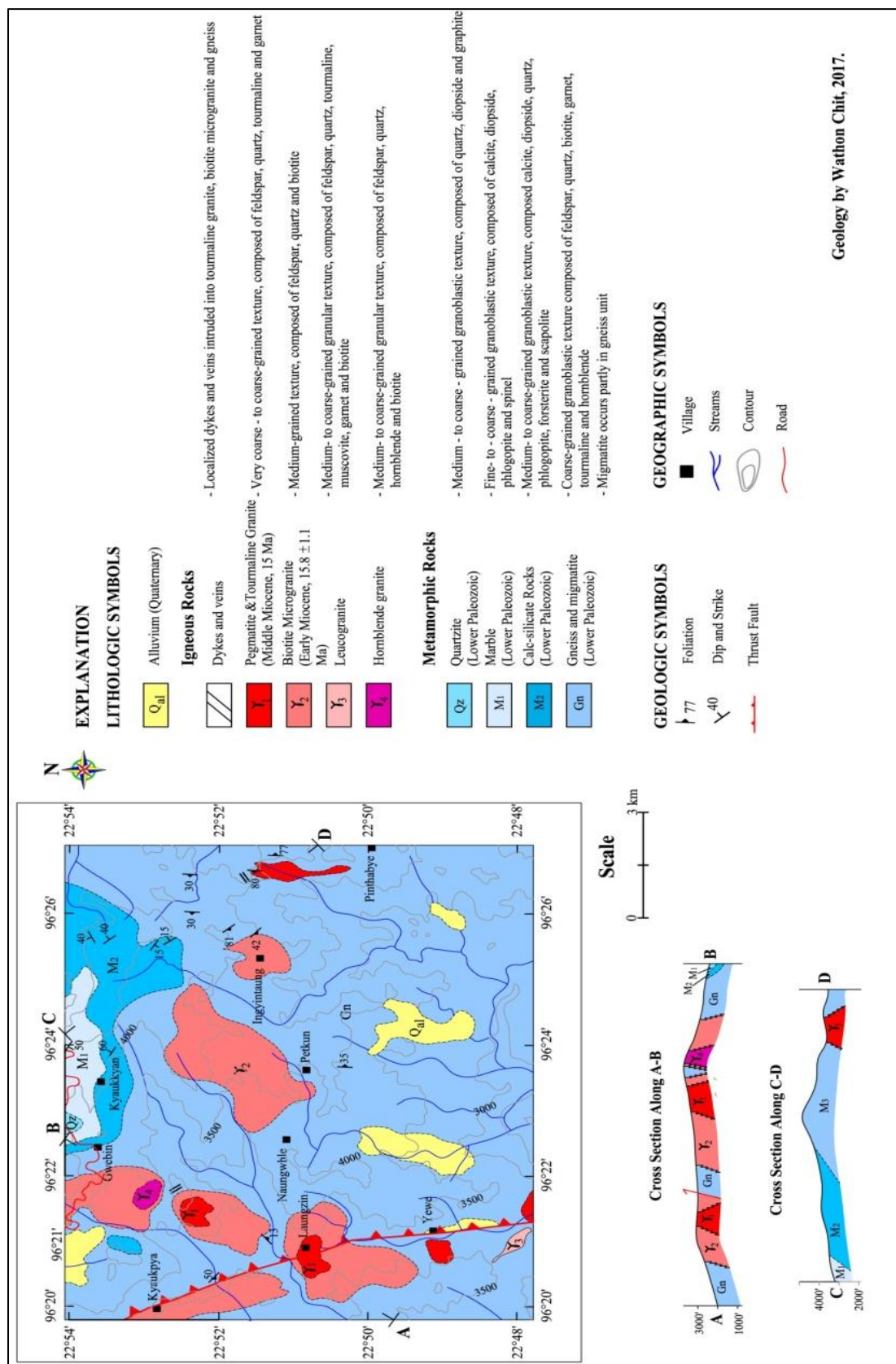


Figure 2 Geological Map of the Research Area

Petrography of Igneous Rocks

(i) Pegmatite

Megascopic study- Pegmatites are very prominent in the study area. Huge pegmatite bodies intruded into biotite microgranite and garnet-biotite gneiss at the vicinity of Laungzin Village and Pinthabye Village. Very coarse-grained quartz upto (1 inch diameter) is crystallized in pegmatite bodies. Weathered surface shows buff or dark grey colour and fresh colour is white. Kaolinization occurs on feldspars and chloritization occurs on biotite and garnet.

(ii) Tourmaline granite

Megascopic study- Tourmaline granite forms as a series of intrusions into the Mogok gneiss. The rock intruded into the country gneisses near Laungzin Village, Shwedwingyi, Yewe Village and Ingyin Taung. It is mainly composed of feldspar and quartz. The composition of tourmaline and garnet are variable Fig. (4).

Microscopic study- It shows coarse-grained hypidiomorphic granular texture and mainly composed of orthoclase, quartz, tourmaline and plagioclase with garnet, sphene, minute apatite and zircon Fig. (3). Tourmaline shows idiomorphic porphyritic texture and strongly pleochroic from bluish grey to green.

(iii) Biotite microgranite

Megascopic study- Biotite microgranite mainly distributes at the northwestern and in the middle of the study area and intruded into gneiss unit. The rock shows medium-grained granular texture. The composition of this rock contains feldspar, quartz, biotite and graphite

Microscopic study- The rock exhibits medium-grained hypidiomorphic granular texture and is mainly composed of orthoclase, quartz, plagioclase and biotite with small amount of hornblende Fig. (4). Accessory minerals are sphene, zircon, apatite, graphite and magnetite.

(iv) Leucogranite

Megascopic study- Small body of medium- to coarse-grained leucogranite intruded into leucogneiss between Kyaukpya and Laungzin Village. This unit is poorly exposed and some exposures show exfoliation nature due to weathering. This unit composed of medium- to coarse-grained feldspar and quartz essentially. Grain size varies from place to place from <1 mm up to 2 cm. Minor amount of mafic minerals such as biotite, garnet and graphite are also present.

Microscopic study- It shows medium- to coarse-grained allotriomorphic to hypidiomorphic granular texture. It is mainly composed of orthoclase, plagioclase and quartz Fig. (5). Accessory minerals include biotite, garnet, sphene, apatite, zircon and graphite.

(v) Hornblende granite

Megascopic study- It is locally distributed rock unit and the intrusion of hornblende granite is found in the east of Kyaukpya Village. It also intruded into hornblende-biotite gneiss near Yewe Village. The rock shows coarse-grained granular texture with the composition of feldspar, quartz, hornblende and minor biotite. Some of them show faintly foliated nature.

Microscopic study- They show medium- to coarse-grained hypidiomorphic granular texture and foliated nature is observed in some section. It is dominated by orthoclase, plagioclase, quartz and hornblende Fig. (6) with minor biotite, sphene, zircon and apatite.

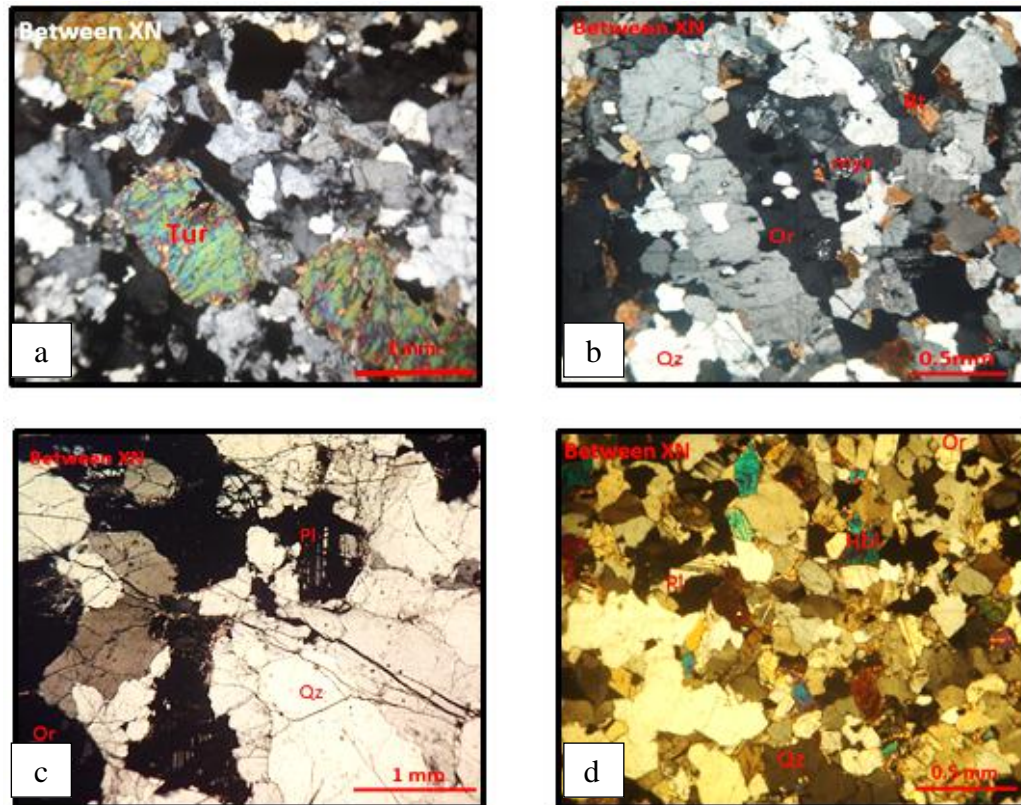












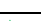
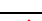




Figure 3 (a) Photomicrographs showing tourmaline phenocrysts in groundmass of alkali feldspar, quartz in tourmaline granite (sample- 29/17), (b) Photomicrographs showing mineral assemblages of orthoclase, quartz, biotite and plagioclase in biotite microgranite (sample- S-63), (c) Photomicrographs showing mineral assemblages of alkali feldspar, quartz and plagioclase in leucogranite (sample- S-50), (d) Photomicrographs showing mineral composition of hornblende granite from Yewe Village (sample- S-76)

Petrochemistry of Igneous Rocks of the Research area

The representative igneous rock samples (including 2 tourmaline granite, 6 biotite microgranites, 3 hornblende granites, 3 leucogranites and 2 pegmatites) from the study area were selected for analysis. All these samples were analysed by XRF method. The rock types and symbol used in diagrams of the selected samples are stated in Table 2. The weight percent oxide method, molar-percent and cation-percent methods in some diagrams were drawn by using GCD kit 3.0 software for the present study.

Table 2 Analysed samples, symbols and rock types of igneous rocks of the study area

Sample	Symbol	Rock Type	Sample	Symbol	Rock Type
wc-4		Tourmaline Granite	JGs-5		Biotite Microgranite
wc-5		Tourmaline Granite	JGs-69		Biotite Microgranite
GS-55		Hornblende Granite	JGs-81-a		Biotite Microgranite
JGs-6		Biotite Microgranite	JLgs-32		Leucogranite
JGs-50		Biotite Microgranite	JLgs-43		Leucogranite
JGs-87		Biotite Microgranite	JLgs-55		Leucogranite
JGs-76		Hornblende Granite	JPs-28-a		Pegmatite
JGs-109		Hornblende Granite	JPs-81-b		Pegmatite

According to the QAPF diagram (Si oversaturated), the igneous rocks of the study area are plotted in quartz-rich granitoids, Fig. (7). The SiO_2 vs $\text{Na}_2\text{O}+\text{K}_2\text{O}$ diagram of Middlemost (1985) indicates that the igneous rocks of the study area fall in granite field, Fig. (8). According to Irvine and Baragar (1971), the samples are classified in magmatic series of subalkaline and belong to calc-alkaline magmatic series, plotted in Fig. (9). Based on the SiO_2 vs K_2O diagram for classification of magmatic series proposed by Peccerillo and Taylor (1976), most of granites belong to high potassium calc-alkaline series Fig. (10).

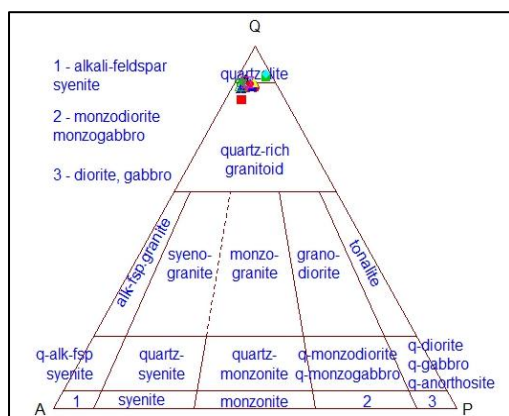


Figure 7 The QAPF diagram with plotted data of igneous rocks of the study area (Source: IUGS classification, 2006).

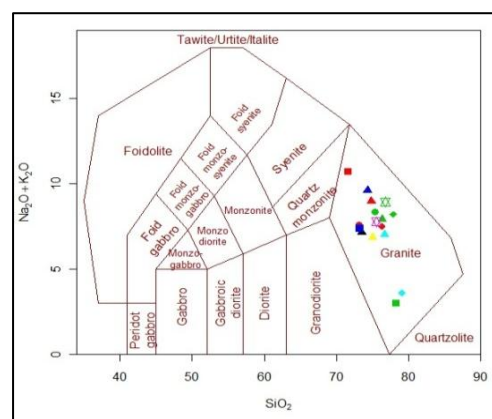


Figure 8 Classification of igneous rocks by Middlemost(1985) showing igneous rocks of the study area.

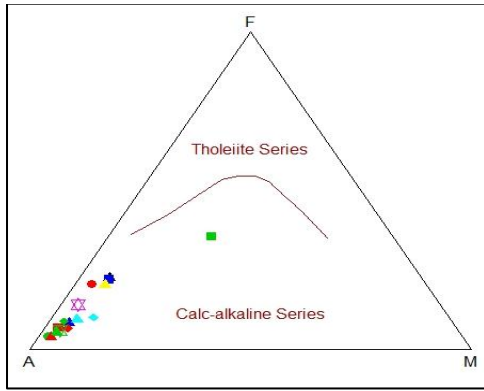


Figure 9 ($\text{Na}_2\text{O} + \text{K}_2\text{O}$)- FeO_t - MgO (AFM) diagram distinguishing tholeiite series and calc-alkaline series (Irvine and Baragar, 1971).

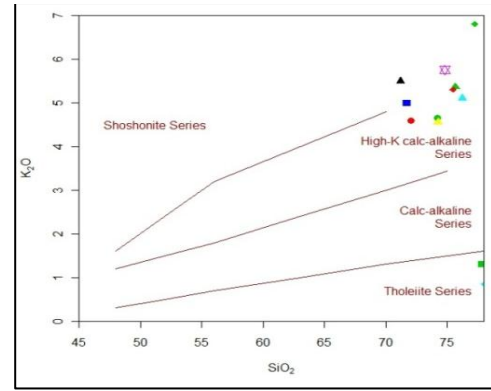


Figure 10 SiO_2 vs K_2O diagram distinguishing the tholeiite, calc-alkaline, high-K calc-alkaline and shoshonite series (Peccerillo and Taylor, 1976)

According to CaO - Al_2O_3 - ($\text{Na}_2\text{O}+\text{K}_2\text{O}$) ternary diagram Fig. (11), igneous rocks of the study area fall in the peraluminous field. According to ASI (aluminum saturation index) vs A/NK ($\text{Al}_2\text{O}_3/(\text{Na}_2\text{O}+\text{K}_2\text{O})$ mol) plot by Frost et al.(2001) Fig. (12), the tourmaline granites, leucogranites and biotite microgranites are predominantly peraluminous with high aluminum saturation indexes. Hornblende granites display a low alumina saturation index belonging to metaluminous field. Granite types discrimination is also plotted in Fig. (12). The most granitoids of the study are S-types granite and some are I-type granite according to Chappell and White, (2001). By means of Villaseca et al. (1998) outlined in B-A ((Fe+ Mg+ Ti) vs Al- (K+ Na+ 2Ca)) binary diagram, most of the peraluminous granitoids are plotted in felsic peraluminous, one biotite microgranite falls in high-peraluminous, one biotite microgranite and one tourmaline fall in moderate-peraluminous and one hornblende granite fall in low-peraluminous Fig. (13).

The ternary diagram Ba-Rb-Sr, Fig. (14) shows that one tourmaline granite and one biotite microgranite fitted in strongly differentiated granite. Two biotite microgranites, one tourmaline granite and one leucogranite fitted in high calcium granite. One hornblende granite and one leucogranite fitted in granodiorite and the rest samples fall in the normal granite with low calcium composition (Bouseily and Sokkary, 1975).

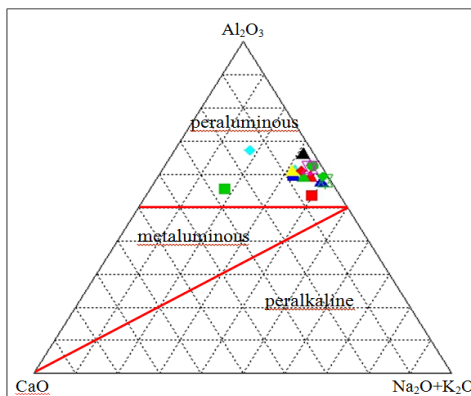


Figure 11 CaO - Al_2O_3 - ($\text{Na}_2\text{O}+\text{K}_2\text{O}$) diagram distinguishing peraluminous from metaluminous and peralkaline igneous rocks of the study area.

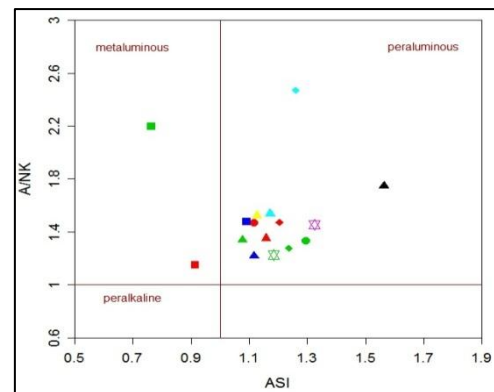


Figure 12 Binary diagram of aluminium saturation index and A/CNK to discriminate metaluminous/ peraluminous rocks from peralkaline rocks (Frost et al., 2001)

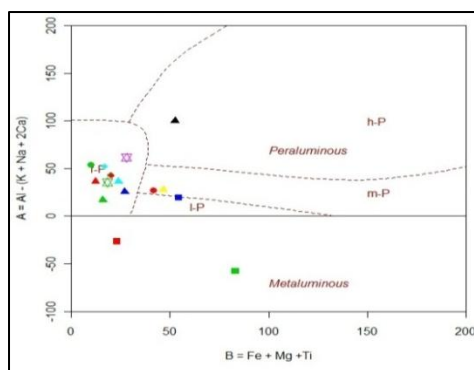


Figure 13 B-A plot of Al-saturation index todistinguish felsic, low, moderate and high peraluminous divisions of peraluminous rocks (using millications, after Villaseca et al., 1998).

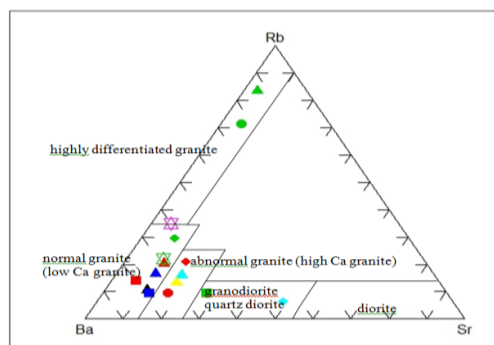


Figure 14 Ba- Rb- Sr ternary diagram used fordistinguishing different fields of granitoids (Bouseily and Sokkary, 1975)

Normative quartz, albite and orthoclase ratios are plotted in the Ab-Q-Or ternary diagram with water pressure of 2 kbar to 10 kbar, after Tuttle and Bowen, 1958, Fig. (15). Two biotite microgranites, two leucogranites and one hornblende granite lies below P_{H_2O} 2 kb, two biotite microgranites lie between P_{H_2O} 2 kb to 10 kb and one hornblende granite lies above 10 kb. All tourmaline granites, one hornblende granite and the other biotite microgranites lie in the 5kb curve of Wiebe (1974).

According to anorthite- quartz- orthoclase ternary diagram Fig. (16), most of the granitoids were formed below 0.5kb, two biotite microgranites were formed between 0.5 kb to 5 kb and one hornblende granite was formed above 5 kb of water vapour pressure, after Tuttle and Bowen (1958).

If the rocks have crystallized at minimum pressure of 2kb, their liquids temperatures can be estimated from the diagram showing the relationship between differentiation index and temperature at 2kb water pressure, Fig. (17). According to the diagram, biotite microgranites were formed at the liquidus temperature between 660° C and 700° C, and hornblende granite was formed at the liquidus temperature between (690° C and 710° C).

Depth of the crystallization of the igneous rocks can be stated from the schematic depth-temperature diagram after Marmo (1956), Fig. (18). According to the diagram, leucogranites probably crystallized at the depth of 21 km, tourmaline granites crystallized at 22 km, biotite microgranite at 23 km and hornblende granite at 24 km.

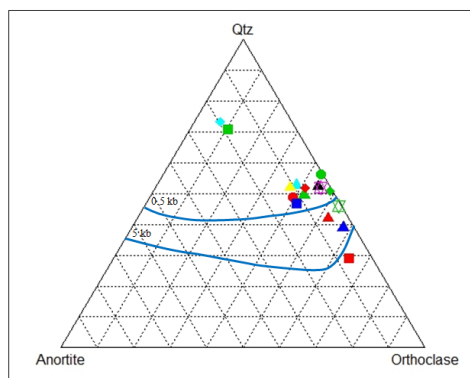


Figure 15 Albite- Quartz- Orthoclase ternary diagram showing water saturated liquidus field boundaries and isobaric temperature inthe system (after Tuttle and Bowen, 1958).

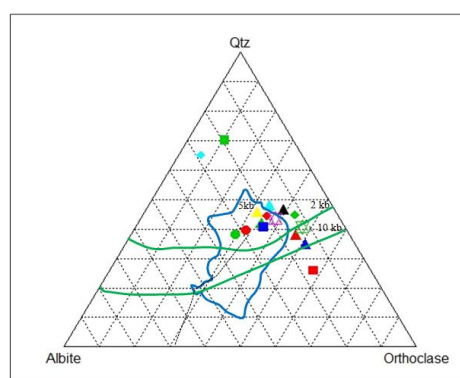


Figure 16 Normative ternary plot of anorthite-quartz- orthoclase diagram with dividing curves of water vapour pressure in the formation of igneous rocks (after Tuttle and Bowen, 1958).

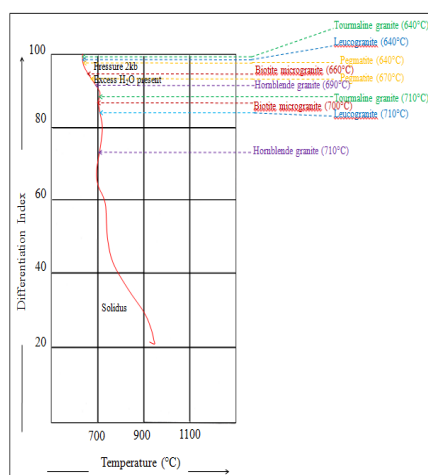


Figure 17 Temperature- differentiation index diagram for the igneous rocks of the study area at 2 kb water pressure (after Piwinski and Wyllie, 1970).

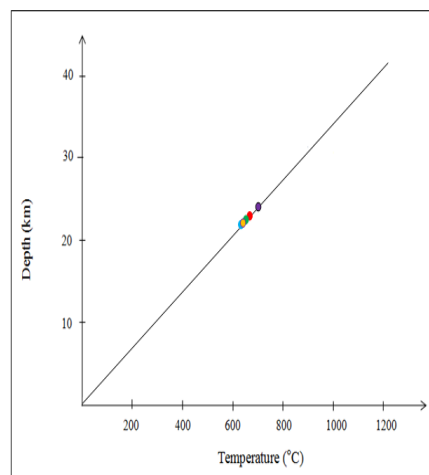


Figure 18 Schematic depth- temperature relation diagram for igneous rocks of the study area (after Marmo, 1956).

Tectonic Discrimination of Granitoid Rocks

Discrimination of a possible tectonic setting of the study area is particularly important for the purpose of characterization of granitoids. According to major elements analysis by C/ACF ($\text{CaO}/\text{Al}_2\text{O}_3 + \text{CaO} + \text{FeO}$) vs F/ACF ($\text{FeO}/\text{Al}_2\text{O}_3 + \text{CaO} + \text{FeO}$) variation diagram Fig. (19), all granitoids in the study area are mostly confined to the IAG, CAG and CCG field. It can be considered that the granitoids were formed on the continent owing to the subduction of an oceanic plate beneath the continent.

According to Ta/Hf- Th/Hf binary plots of Schandl and Gorton (2002), tourmaline granite of the study area is tectonically located in the active continental margin Fig. (20). By using (Y+Nb)- Rb, Y- Nb, (Ta+ Yb)- Rb and Yb- Ta binary diagrams proposed by Pearce et.al, the tourmaline granites are plotted in VAG (Volcanic Arc Granite) and syn-collision granite Fig. (21). Therefore, according to trace elements analysis, the tourmaline granites of the study area fall in the field of syn-COLG and VAG.

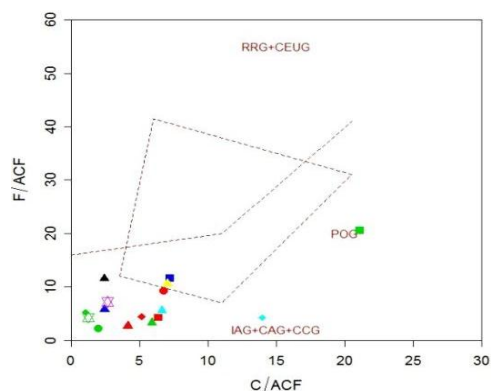


Figure 19 C/ACF vs F/ACF binary diagram showing the tectonic discrimination of granitoids of the study area (Maniar and Piccoli, 1989).

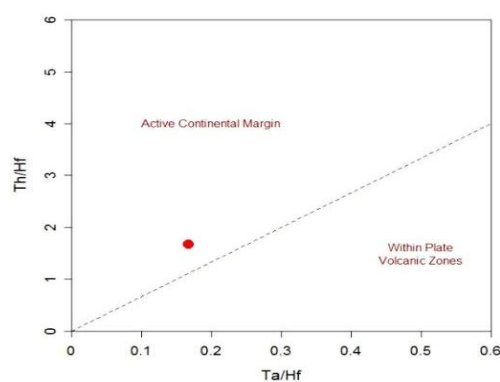


Figure 20 Ta/Hf- Th/Hf binary diagram classifying geotectonic environment of felsic rocks (after Schandl and Gorton, 2002).

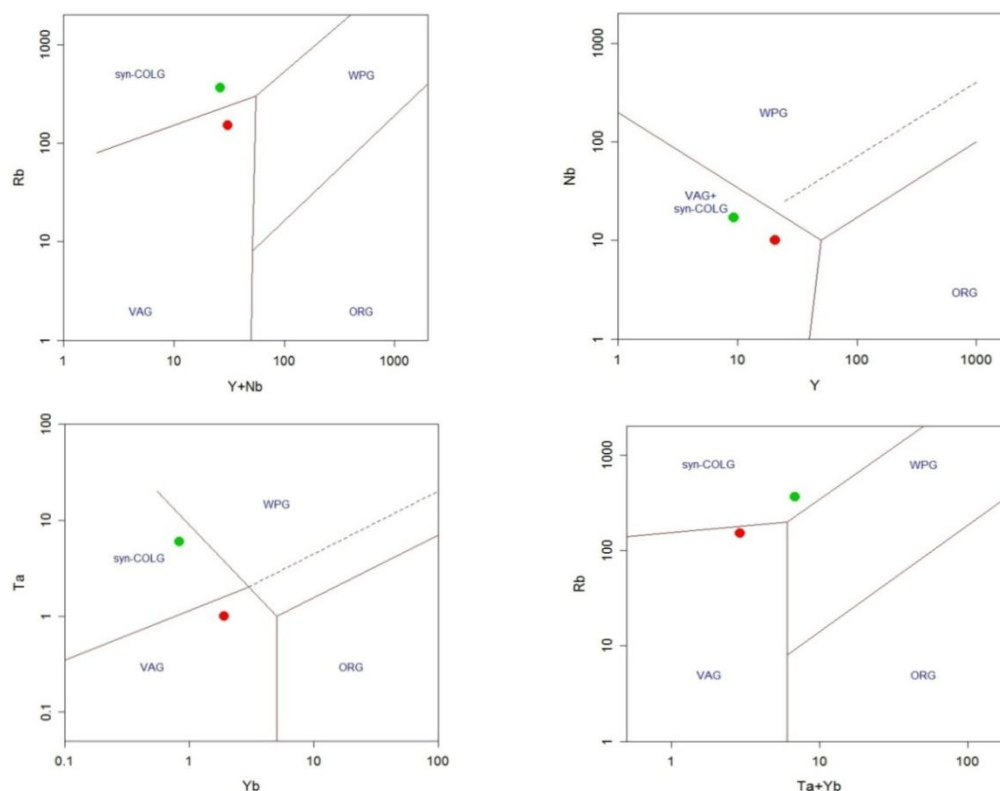


Figure 21 Granite tectonic discrimination diagram using trace elements by Pearce et al. (1984).

According to cations analysis, Batchelor and Bowden (1985) used to discriminate the tectonic setting of granites according to R1-R2 binary (using millications) diagram. By means of major element ratios of granitoids, the granites of the study area correspond to syn-collision and late orogenic zone Fig. (22).

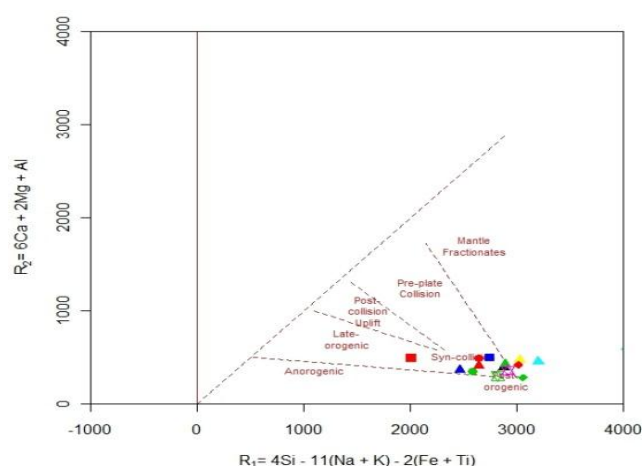


Figure 22 R1-R2 binary (in millications) diagram showing tectonic setting of granitoids correspond to syn-collision to late orogenic zone (after Batchelor and Bowden, 1985).

Economic Possibility of the Research Area

According to the investigation with XRF analysis, the granitoids and pegmatites of the study area associated with rare earth elements and actinides (uranium and thorium). Therefore, the study area can be expected for rare earth elements production in the future, although there has not been economically mined for rare earth elements.

Summary and Conclusions

The igneous rocks exposed in the study area consist of pegmatite and granite. 16 granitoid samples were analyzed for content of major and trace elements by XRF method. According to the QAPF diagram (Si oversaturated), the igneous rocks of the study area are plotted in quartz-rich granitoids. The SiO_2 vs $\text{Na}_2\text{O}+\text{K}_2\text{O}$ diagram by Middlemost (1985) indicates that the igneous rocks of the study area fall in granite field. According to Irvine and Baragar (1971), the samples are classified in calc-alkaline magmatic series. The SiO_2 vs K_2O diagram proposed by Peccerillo and Taylor (1976), most of granites belong to high potassium calc-alkaline series. According to $\text{CaO}-\text{Al}_2\text{O}_3-(\text{Na}_2\text{O}+\text{K}_2\text{O})$ ternary diagram, igneous rocks of the study area fall in the peraluminous field. According to B-A binary diagram outlined by Villaseca et al. (1998), most of the peraluminous granitoids are plotted in felsic peraluminous, one biotite microgranite falls in high-peraluminous, one biotite microgranite and one tourmaline fall in moderate-peraluminous and one hornblende granite fall in low-peraluminous. According to granite types discrimination diagrams of ASI vs A/NK described the most granitoids of the study are S-types granite and some are I-type granite. By using major elements, all granitoids in the study area are mostly confined to the IAG, CAG and CCG field. By using trace elements, tourmaline granite of the study area is tectonically located in the active continental margin in the field of syn-COLG and VAG granite. By using cations of major element ratios of granitoids, the granites of the research area correspond to syn-collision and late orogenic zone. The study area can be expected for rare earth elements production in the future, although there has not been economically mined for them.

Acknowledgements

The authors would like to express the most heartfelt thanks and offer the deepest homage to Dr. U Win Naing (Rector), Dr. Daw Nu Nu Yi (Pro-Rector) and Dr. Daw Nay Thwe Kyi (Pro-Rector), Dagon University for their permission and encouragement. Special thanks are due to their gratitude with respects to Dr. Daw Kyi Kyi Maw (Professor and Head, Department of Geology, Dagon University) and Dr. Daw Aye Aye Aung (Professor, Department of Geology, Dagon University) for their kind permission. The authors wish to express their sincere thanks to Department of Higher Education (Lower Myanmar) for providing financial aid to carry out this research. Finally, the authors deepest thanks are due to my family and my colleagues for their encouragement and supporting in carrying out this research.

References

- Batchelor, R. A. and Bowden, P., (1985). Petrogenetic interpretation of granitoid rock series using multicationic parameters. *Chemical Geology*, vol. 48, p. 43-55.
- Bouseilly, A. N., and Sokkary, A. A., (1975). The relation between Rb, Sr and Ba in granitic rocks. *Chemical Geology*, vol. 16, p. 207-219.
- Chappell, B.W. and J. J. R. White, (2001). Two constrasting granite types; 25 years later, *Australian Journal of Earth Science (2001)* vol. 48, p. 489-499.
- Frost, B. R., Barnes, C. G., Collins, W. J., Arculus, R. J., Ellis, D. J. and Frost, C. D., (2001). A geochemical classification for granitic rocks. *Journal of Petrology*, vol. 42, p. 2033-2048.
- Irvine, T.N. and W.R. A. Barager, (1971). A guide to the chemical classification of the common volcanic rocks. *Canadian Journal of Earth Sciences*, vol.8, p.523-548.
- Maniar, P. D. and Piccoli, P. M., (1989). Tectonic discriminations of granitoids. *Geological Society of America Bulletin*, vol. 101, p.635-643.
- Marmo, V., (1956). On the emplacement of Granites. *American Journal of Science* vol. 254, p. 479-492.
- Middlemost, E. A. K. (1985). *Magmas and Magmatic Rocks*. London: Longman.
- Pearce, J. A., Harris, N. W. and Tindle, A. G., (1984). Trace element discrimination diagrams for the tectonic interpretation of granitic rocks. *Journal of Petrology*, vol. 25, p. 956-983.
- Peccerillo, A and Taylor, S. R. (1976). Geochemistry of Eocene calc-alkaline volcanic rocks from the Kastamonu area, Northern Turkey. *Contributions to Mineralogy and Petrology* 58, p.63-81.
- Piwinskii, and Wyllie, P.J., (1970). Experimental studies of igneous rock series: felsic body suite from the Neddle point pluton, Wallowa Batholith, Oregon. *Journal of Geology*, vol.78, p.52-76.
- Schandl, E. S. and Gorton, M. P., (2002). Application of high field strength elements to discriminate tectonic settings in VMS environments. *Economic Geology*, vol. 97, p. 629-642.
- Shand, S. J., (1943). *Eruptive Rocks, Their Genesis, Composition, Classification, and Their Relation to Ore-Deposits with a Chapter on Meteorite*. New York: John Wiley & Sons.
- Tuttle, O.F., and N.L. Bowen, (1958). Origin of granite in the light of experimental studies in the system NaAlSi₃O₈-SiO₂-H₂O. *Geol. Soc. America Mem.*74. p.153.
- Villaseca, C., Barbero, L. and Herreros, V., (1998). A re-examination of the typology of peraluminous granite types in intracontinental orogenic belts. *Transactions of the Royal Society of Edinburgh, Earth Sciences*, vol. 89, p. 113-119.

GEOCHEMISTRY OF SUBDUCTION RELATED LAMPROPHYRES FROM MOKPALIN-KANNI AREA, MON STATE, MYANMAR

Myo Thiri Sandar Aung*

Abstract

The study area is located within southern part of the Mogok Metamorphic Belt and Slate belt, Kyaukse Township of Mon State, Myanmar. It is consisting of meladiorite, diorite and granitic rocks intruded by a variety of lamprophyre dykes. Most of lamprophyres are fine-grained, porphyritic in nature, with phenocrysts of hornblende, feldspar and sometimes biotite. Occasionally, medium-grained textures of spessartite are observed and their strikes are trending NE direction. There are three types of lamprophyre encountered in the study area, which are camptonite, minette and spessartite. The whole rock chemical compositions are wide span range of SiO₂ (52.47-60.06), CaO (4.28-6.8), MgO (2.5-5.1) and Fe₂O₃ (5.6-9.6) consisting mainly of calc-alkaline to high-K calc-alkaline. Lamprophyres fall within the basaltic andesite-basaltic andesite, and trachy-andesite field. Enrichments in Cs, Rb, Ba and Th while depletion in Nb, and Ti were generated from the partial melting of the subducted related shallower mantle lithosphere. Trace element ratios, the pattern of the LREE to HREE show that the rocks were come from spinel lherzolite mantle (< 50 km depth) rather than garnet lherzolite mantle source. Calc-alkaline of lamprophyre related to the eastward late-subduction of Tethys II of the ancestral Indian Ocean.

Keywords: Lamprophyres; geochemistry; calc-alkaline; late-subduction; Myanmar

Introduction

The presence of interchangeability between tholeiite and calc-alkaline magma mixing related to three types of lamprophyres studies on a regional scale including the assigned area and its environs Stamp (1926), Chhibber (1926), Chhibber (1934), and Khin Zaw (1990). Tin Mar Win (2006, unpublished) studied the manual description of lamprophyres. Lamprophyres are very rare, alkaline, silica-undersaturated, small volume igneous rocks that commonly occur as dikes or small intrusions. They are melanocratic hypabyssal igneous rocks characterized by porphyritic with mafic phenocrysts (Rock, 1987). Lamprophyres are characteristically rich in porphyritic mafic minerals, typically biotite, amphibole and pyroxene, feldspar being confined to the groundmass (Le Maitre, 1989). Chemically, they are of intermediate to ultrabasic composition, they show rather high alkali contents for their silica, and in many varieties, they have high modal alkali feldspar for their color index (Rock, 1991). In the present work, we accounted for petrological and geochemical data of lamprophyres and related rock with laser ablation ICP-MS trace element microanalysis in order to recognize the genesis of lamprophyres and petrochemical evidence.

Regional Geology of the study area

The general regional geologic setting southern part of Mogok Metamorphic belt and within Slate belt (Fig.1). It consists of rhyolitic tuff, meta-sedimentary rocks, probably of Carboniferous age close to the Mesozoic granite of Chhibber (1926). The Western granite belt of South East Asia and this belt are associated with eastward subduction of the Oceanic Indian plate (Pitcher, 1962). The study area lies in the northern part of western Tin Belt of South East Asia Tin province (Mitchell, 1977 and Nyan Thin, 1984) and lies within part of the Mogok Belt (Searle and Haq, 1964). Maung Thein (1983), regarded the central granitoid belt of Burma were

* Dr, Associate Professor, Department of Geology, Myeik University

developed in the tectonic setting of subduction related magmatic arc. The area belongs to the central granitoid belts of Myanmar (Khin Zaw, 1990). The area is structurally bounded by two major faults which are the Papun Fault system in the north and the Three Pagoda Fault in the south. The Sagaing fault was 1000Km to south and lies west of Mogok Metamorphic belt.

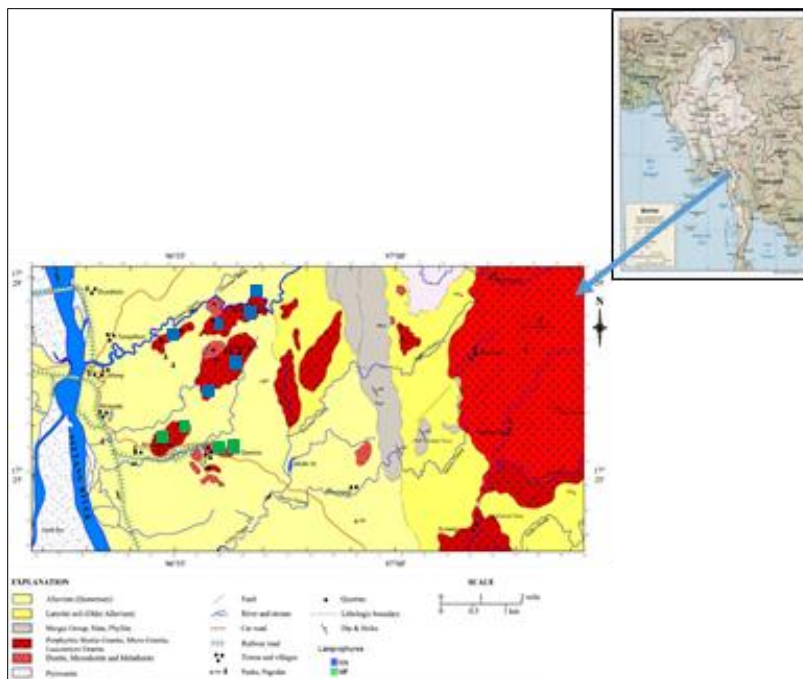


Figure 1 A geological map of the study area (modified after Zaw Naing Oo, 1998 unpublished).

Materials and Methods

Ten representative samples were sent to ALS laboratory of Geological Survey of Japan, AIST and the Acme analytical laboratories of Vancouver-Canada. In this study, most relevant methods available to determine contents of major, trace, and rare earth elements of the lamprophyres were applied for major and trace elements analysis were carried out using techniques of X-ray fluorescence spectrometry (XRF), inductively coupled plasma-mass spectrometry and inductively coupled plasma-atomic emission spectrometry.

Field study and Petrography of lamprophyres

Representative samples were collected from several locations throughout the Mokpalin and Kanni quarries. In the study area, twenty-five dikes of varying widths and orientations, exposed along the walls of the quarries. They strike is roughly trending N30°E and dip vertically and nearly parallel and tabular-shaped nature. Most of lamprophyres are acting a sharp contact with host rocks.

Sometimes horizontal joints are remarked and also small amount of quartzofeldspathic veins are intruded in it. The exposed portions of the dikes are approximately 45 m long and are found intruded into diorites and granitic country rocks (Fig 2). The widths of the dikes vary from 0.15 to 8 m Lamprophyres are mostly fine grained, dark and grey in color. Some dikes exhibit chilled margins and sometimes observed granite xenoliths (Fig.3). The typical camptonite exhibits a beautiful grey color with shining black elongated crystals of hornblende and occasionally with a few crystals of feldspar. It is found intruded into the dioritic rocks. Minette

show sharp contact with granitic rocks at Mokpalin Quarry No.2 and Kanni Quarries. Spessartites are found that intruded into the dioritic and granitic rocks at Mokpalin Quarries and Kanni and Kyauk-Tan-Lay Quarries. Occasionally, they show irregular, pitch and swell possibly indicating limited mobility of the granite after dike intrusion. Camptonites are observed throughout the study area.

Lamprophyres are mesocratic to melanocratic igneous rocks, usually hypabyssal, with a panidiomorphic texture. Porphy of hornblende are euhedral to subhedral (0.1-1.9mm) and most are simple twined (Fig.5), sometimes occur sieve, hollow, and skeletal character. According to the model composition, most are camptonite, spessartite, and minette. Biotite of lamprophyre shows euhedral- subhedral showing strong pleochroism of greenish-brown to reddish brown colored (Fig.4 a) occurred in minette. Most of hornblendes showed simple contact twined (Fig.4 b). Feldspar phenocrysts and matrix show a larger range of compositions and albite to labradorite (An_{24-66}). Plagioclase feldspar is the dominant feldspar as megacrysts or as matrix (Fig.5) and orthoclase is present in minor proportions.



Figure 2 Dike of lamprophyre intruded into granite at Kanni quarry area.

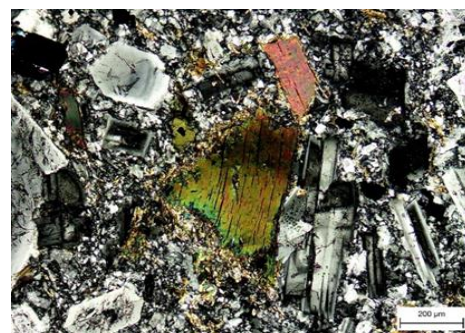


Figure 3 (a) Biotite granite xenolith in close-up view of camptonite lamprophyre (b) Showing strong pleochroism of subhedral biotite collected from Mokpalin and Kanni Quarries.

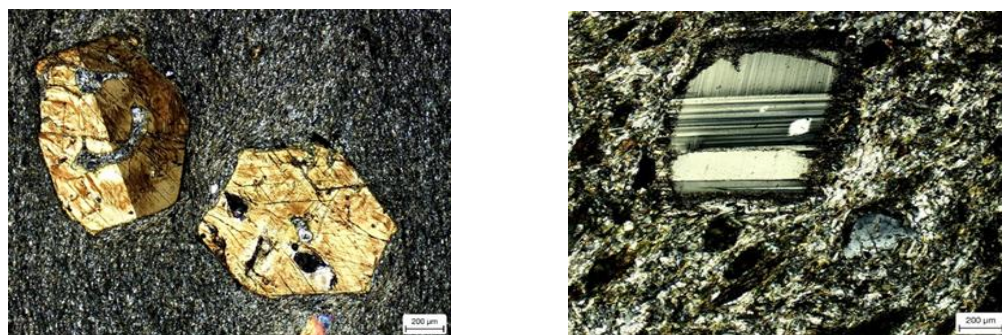


Figure 4 (a) Showing simple-contact twinned of hornblende between X.N (b) Ragged megacryst of feldspars in lamprophyres.

Geochemistry of Lamprophyres

The SiO₂ content of the ten representative samples are in the range of 52.47–60.06 wt. %. most probably derived from silica saturated magma. They have contents of alkalis, with K₂O ranging from 1.4–2.56 wt. % and Na₂O 4.04–5.0 wt. %. All of lamprophyres are sodic and (K₂O/Na₂O <1) ratios (0.28–0.59). The high values of Na₂O (4.3 to 5.0) indicates the presence of a sodic phase in the source region (amphibole-bearing source) and so amphiboles are observed in phenocrysts and matrix. Aluminum contents are high in lamprophyres within the ranges of Al₂O₃ 17.3–18.58 wt. %. Total FeO, 5.60–8.38 wt.%, and MnO, 0.0–0.1 wt.%, MgO, 2.55–5.12 wt.%, TiO₂ 0.5–1.3 wt.%, and P₂O₅ = 0.2–0.56 wt.% (Table 1) and notable that Al₂O₃ is higher than CaO, FeO_t and MgO. In Nb/Y-Zr/TiO₂ plot diagram (Winchester and Floyd 1977), all the lamprophyres included in the entire area fall andesite basaltic andesite and trachy-andesite group (Fig.6a). In FeO_t / MgO vs. SiO₂ diagram (Fig.5 b) notably two representative samples lie in the tholeiitic magma series and the rest in the calc-alkaline series (After Miyashiro, 1974). Fairly a flat and anomaly values are below <1 of HREEs and depletion of Nb, and Ti spikes in the N-MORB normalized multi-element diagrams are assume of arc magmatism and subduction related metasomatism (Fig.6 a). In chondrite-normalized diagram, negative slope of enrich REE relative to HREE values sign of moderate degree of partial melting (Fig.6 b). Slightly occur of negative Eu anomaly (Eu/Eu* = 0.87–1.03) may be few plagioclase fractionations the parent magmas. The sum of the REE data show arrange from (87.5 to 261.7) and suggesting a variable degree of REE fractionation. Most of the compatible elements (Ni, Sc, and Co) are no content and of Cr and V are low that seem to be depleted in the partial melting and highly fractionally from primary magma. The low mg# and low content of transition element show not from the primitive lamprophyres.

In Ba/Rb - Rb/Sr diagram (Furman & Graham, 1999), the values Ba/Rb show >20 and Rb/Sr vales < 0.1 and above are imply an amphibole bearing and a biotite or phlogopite bearing source (Fig.7 a). Plotted of lamprophyres in Nb - Nb/U diagram (after Ma et al., 2013) the amount of Nb/U between 0.22–20 observed that components the subducted sediments of upper crust and slab zone hydrous fluids (Fig.7 b). A quartz diorite dyke from one of the Mokpalin quarries gave a zircon U-Pb age of 90.8 ± 0.8 Ma and suggested that arc magmatism was related to the eastward subduction of Tethys II, the ancestral Indian Ocean (Mitchell et al., 2012). With references to the Th-Hf-Ta-Zr-Nb discrimination diagram (Fig 8), their tectonic setting indicates that all the representative samples of lamprophyres belong to the calc-alkaline basalt field.

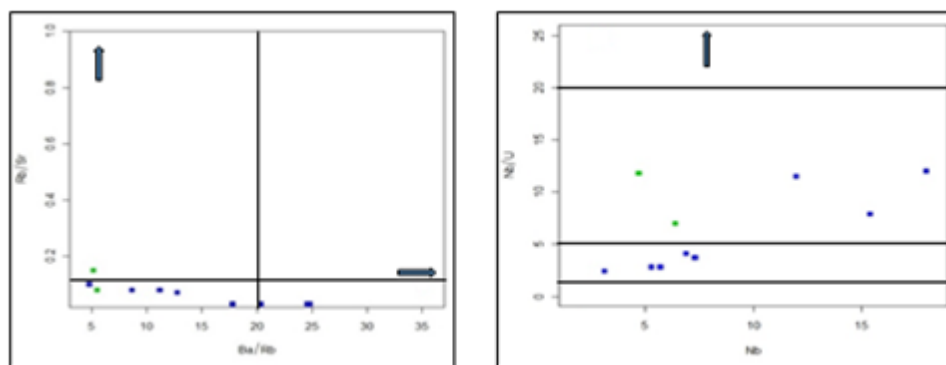


Figure 7 (a) Diagram plotted of lamprophyres Ba/Rb - Rb/Sr (Furman & Graham, 1999) and (b) Diagram plotted of lamprophyres Nb-Nb/U (redrawn after Ma et al., 2013).

Table 1 Representative selected whole-rock analysis for major and trace elements from lamprophyres

Rock type	Calc-alkaline				Tholeiitic		Calc-alkaline			
Sample	TKN-2	MKN-L	L3	5Q	Q-L	CHO	L7	L8	L9	L10
SiO ₂	53.23	59.87	60.06	57.78	52.47	59.3	58.1	58.5	58.8	56
TiO ₂	1.2	0.72	0.91	0.88	1.1	0.59	0.84	0.74	0.54	1.04
Al ₂ O ₃	17.3	17.44	17.56	17.56	19.01	17.89	17.41	17.8	18.56	17.48
Fe ₂ O ₃	8.38	5.77	5.69	6.85	9.67	5.61	6.5	8.26	6.27	7.07
MnO	0.19	0.09	0.07	0.09	0.15	0.09	0.09	0.15	0.13	0.12
MgO	5.12	2.81	2.45	3.15	3.41	2.89	3.16	2.55	2.57	3.5
CaO	6.81	5.27	4.57	5.41	6.79	5.3	5.44	4.28	5.2	5.08
Na ₂ O	4.04	4.66	4.72	5.01	4.13	4.65	5.01	4.59	4.57	4.32
K ₂ O	2.19	2.02	2.39	1.4	1.87	1.94	1.53	2.13	1.7	2.56
P ₂ O ₅	0.39	0.3	0.49	0.38	0.31	0.24	0.36	0.34	0.27	0.56
LOI	0.71	0.52	0.56	0.41	0.44	0.58	0.97	0.86	1.31	2.16
Total	99.57	99.47	100.0	98.94	99.36	99.09	99.41	100.	101.2	99.89
K ₂ O/Na ₂	0.54	0.4	0.51	0.28	0.45	0.42	0.31	0.46	0.37	0.59
Mg#	55.17	48.94	46.2	47.56	41.1	50.44	49.1	44.5	52.3	47.1
Eu	1.48	1.22	1.69	1.47	1.37	1	1.4	1.13	1.1	1.72
Cr	130	60	50	30	10	20	-	-	-	-
Zr	148	182	273	128	131	108	117	145	101	233
La/Yb	8.72	17.11	32.62	20.41	5.32	9.24	25.03	14.5	17.81	15.5
Eu/Eu*	0.97	0.98	0.93	0.94	1	1.02	0.96	0.78	1.04	0.87
Th/Ta	4	18	12	34	6	29	6	28	9	29
(Ta/Yb)	0.5	0.4	0.4	0.2	0.14	0.14	0.3	0.2	0.2	0.5
Rb/Sr	0.14	0.08	0.08	0.03	0.08	0.03	0.03	0.03	0.07	0.15
(La/Sm)	2.87	4.27	5.75	4.28	2.39	3.67	4.6	1.8	5.5	4.7
ΣREE	124.5	138.1	261.7	178.4	97.8	93.1	172	128.	221.3	87.5

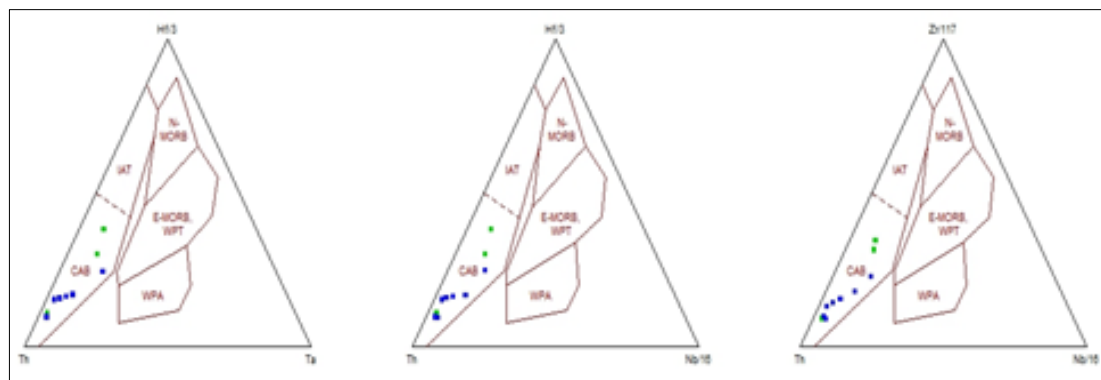


Figure 8 Triangular diagrams of the Th-Hf-Ta-Zr-Nb system showing lamprophyres fall in the field of calc- alkaline basalts, (After Wood 1980).

Acknowledgements

The author thanks to the Journal of Myanmar Academy of Arts and Science for editing on my research. She would like to acknowledge Dr. Ni Ni Oo, Acting Rector of the Myeik University, for his permission to carry out this research. She also would like to express her gratitude to Dr. Khin Zaw, University of Tasmania, Australia who provided valuable helps XRF data during the preparation of this manuscript.

References

- Chhibber, H.L., (1926) Hornblende lamprophyres and associated rocks of Mokpalin Quarries, Thaton District: Jour. Burma. Soc. V.xvi,p. 167-168.
- Chhibber, H.L., (1934). Geology of Burma: Macmillan and Co.Ltd, London, 538pp.
- De LaRoche, H., Leterrier, J., Grandclaude, P., and Marchal, M., (1980), A classification of volcanic and plutonic rocks using R1-R2 diagram and major-element-analyses. Its relationship with current nomenclature: Chemical Geology, v.29, p. 183-210
- Furman,T., & D. Graham., (1999). Erosion of lithospheric mantle beneath the East African Rift system: evidence from the Kivu volcanic province. Lithos. V 48. pp 237 to 262.
- Hyndman, D.W. (1985): Petrology of Igneous and Metamorphic rocks, second edition, McGraw-Hill, New York.
- Khin Zaw, (1990). Geological, petrological and geochemical characteristics of granitoid rocks in Burma with special reference to the associated W-Sn mineralization and their tectonic setting. Jour. Of Southeast Asian Earth Sciences, v.4. no.4. p.293-335.
- Ma L., Jiang S. Y., Hou M. L., Dai B. Z., Jiang Y. H., Yang T., Zhao K. D., Pu W., Zhu Z.Y. and Xu B. (2013b) Geochemistry of Early Cretaceous calc-alkaline lamprophyres in the Jiaodong Peninsula: Implication for lithospheric evolution of the eastern North China Craton. Gondwana Res.,<http://dx.doi.org/10.1016/j.gr.2013.05.012>.
- Maung Thein, (1983). The geological evolution of Burma, Department of Geology, Mandalay University, Mandalay, Burma, (Unpublish), 89p.
- Mitchell, A.H.G., Sun-Lin Chung, Thura Oo, Te-Hsien Lin, Chien-Hui Hung (2012). Zircon U-Pb ages in Myanmar: Magmatic-metamorphic events and the closure of a neo-Tethys ocean? Journal of Asian Earth Sciences 56, 1-23.
- Miyashiro, A. (1974). Volcanic rock series in island arcs and active continental margins. Am. Sci. 274, 321-55.
- Nakamura, N., (1974), Determination of REE, Ba, Fe, Mg, Na and K in carbonaceous and ordinary chondrites, Geochimica et Cosmochimica Acta, vol. 38, no.5, p.757-775.

- Nyan Thin, (1984). Some aspects of granitic rocks of Tenasserian Division, Department of Geology, Rangoon University, Rangoon, Burma (Unpublished), 125p.
- Pitcher, W.S., (1962). Granite type and Tectonic Environment, Mountain Building Process, p- 19-37.
- Rock, N.M.S., (1987). Nature and origin of calc-alkaline lamprophyres: a review. In:51.
- Searle, D.L., and Haq, B.T., (1964). The Mogok Belt of Burma and its relation to the Himalayan Orogeny. 22nd. Intern. Geol. Congress. India (in press).
- Stamp, L.D., (1926). The igneous complex of Green Island and the Amherst Coast, Lower Burma. Geol. Mag Vol. XIII, 399-410.
- Sun S.S. and Mc Donugh W.F., (1989), Chemical and isotopic systematics of oceanic basalts: implications for mantle composition and processes. In: Saunders A.D. and Norry M.J. (eds.), Magmatism in ocean basins. Geol.Soc. London. Spec. Pub. 42, pp. 313-345.
- Tin Mar Win (2006). Geological and Petrological of Mokpalin quarry, Mokpalin Area, Kyaikhto Township, Mon State. (Thesis) University of Dagon. Unpub: 103p.
- Winchester, J. A. and Floyd, P.A., (1977). Geochemical discrimination of different magma series and their differentiation products using immobile elements. Chemical Geology, 20: 325-343.
- Wood D.A., (1980). The application of a Th-Hf-Ta diagram to problems of tectonomagmatic classification and to establishing the nature of crustal contamination of basaltic lavas of the British Tertiary volcanic province. Earth Planet. Sci. Lett., 50, 11-30.
- Zaw Naing Oo, (1998). Mineralogical and Geological Studies of the Mokpalin East Area, Mon State. M.Sc (Thesis) University of Yangon. Unpub: 118p.

PETROGRAPHY AND PETROCHEMICAL CHARACTERISTICS OF SKARN AROUND MONBINZON VILLAGE AND MINBON TAUNG AREA, THAZI TOWNSHIP, MANDALAY REGION

Thet Paing Kyaw Win¹ and Kyaw Linn Zaw²

Abstract

The study area falls 24.3 km southeast of Thazi at Mandalay Region that covers two types of rocks; igneous and metasedimentary rocks. Meta-sedimentary rocks consist calc-silicate rocks and skarn. Calc-silicate rock occurred as roof-pendant, visible ridges and furrows nature. Skarn are exoskarn that subdivided into garnet skarn and garnet-clinopyroxene skarn. It contains garnet, diopside, plagioclase, quartz and tremolite. According to petrochemical study, the massive garnet-clinopyroxene skarn exhibit much flatter profiles in Chondrite-normalized REE patterns that indicating the garnet may preferentially concentrate HREE. In Harker variation diagrams, SiO₂, TiO₂ and K₂O show a systematic decrease from diorite to skarn and FeO_T display general increase to skarn rocks due to mass transfer during metasomatism. Cu, Zn and Y enrichment in skarn is relative to granite. Sr exhibits a perceptible decline in the direction of exoskarn.

Keywords: exoskarn, garnet skarn, garnet-clinopyroxene skarn

Introduction

The study area is situated about at the Monbinzon village and Minbon Taung in Thazi Township, Mandalay Region. It is about 24.3 km southeast of Thazi, situated along the Thazi-Taunggyi motor road. It is lying between latitude 20° 41' 30" N & 20° 45' 0" N and longitude 96° 14' 0" E & 96° 17' 0" E as shown in Figure 1. Physiographic feature of the area is typically expressed by roughly parallel ridges with relatively relief, especially in the southern part of the area. The general trend of the area is running in a northeast - southwest direction with respect to the regional strike trend.

The area is located in the eastern part of the Thazi-Pyawbwe plain which lies in the western part of the Shan Plateau which had become a stable block since the close of the Mesozoic. Granitic and metamorphic rocks within the study area are located within the Mogok Metamorphic Belt (Searle and Ba Than Haq, 1964). The area consists of igneous complex which was emplaced into a belt of low to medium grade metamorphism (of originally lower Paleozoic age) in the western part and sedimentary (Mesozoic age) in the eastern part. The granitic rock of the study area belongs to Payangazu granitoids and in central granitoids belt.

The study area can roughly be divided into mountainous region in the eastern part and the lowland region in the northwestern part. The highest-peak is Minbon Taung (704 m). The area is located at the western marginal part of the Shan-Plateau. Kyawme Chaung and Kywegya Chaung are main drainage of this area. They are flowing from east-west direction. In the whole area, drainage pattern is coarse dendritic pattern. All rocks can be traced along the mountain ranges but the mountain ranges are covered with highly weathered outcrops and spare vegetation. Thus most of the rocks units can be observed along the stream channels.

¹ Dr, Lecturer, Department of Geology, Dagon University

² Dr, Lecturer, Department of Geology, West Yangon University

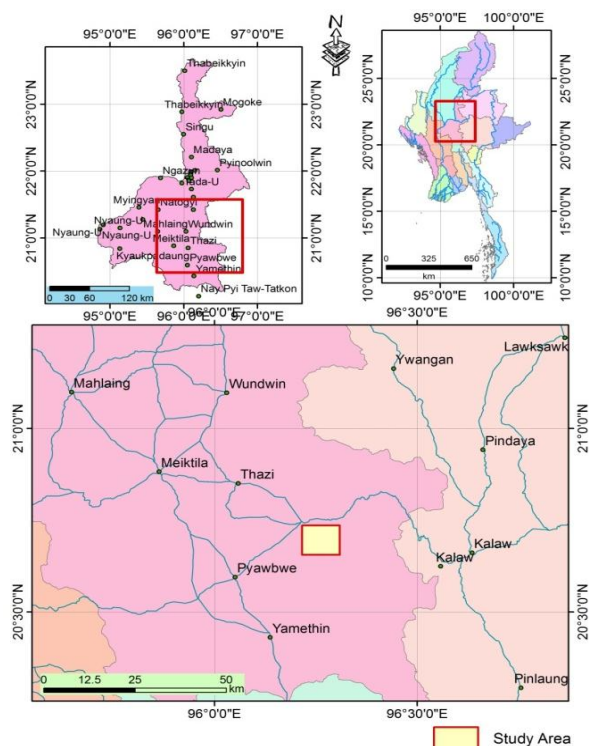


Figure 1 Location map of the area

Good exposures are noticed along Monbinzon at the northern part and Minbon Taung and Imagyi village at the southern part of the area. The study area is mainly composed of the igneous rocks and meta-sedimentary rocks. Igneous rocks are namely diorite, hornblendite, meladiorite, microdiorite, biotite granite, rhyolite, and dykes and veins (leucogranite, microgranite, pegmatite, aplite, quartz and quartzofeldspartic veins). Metasedimentary rocks mainly consists calc-silicate rock and skarn as shown in Figure 2.

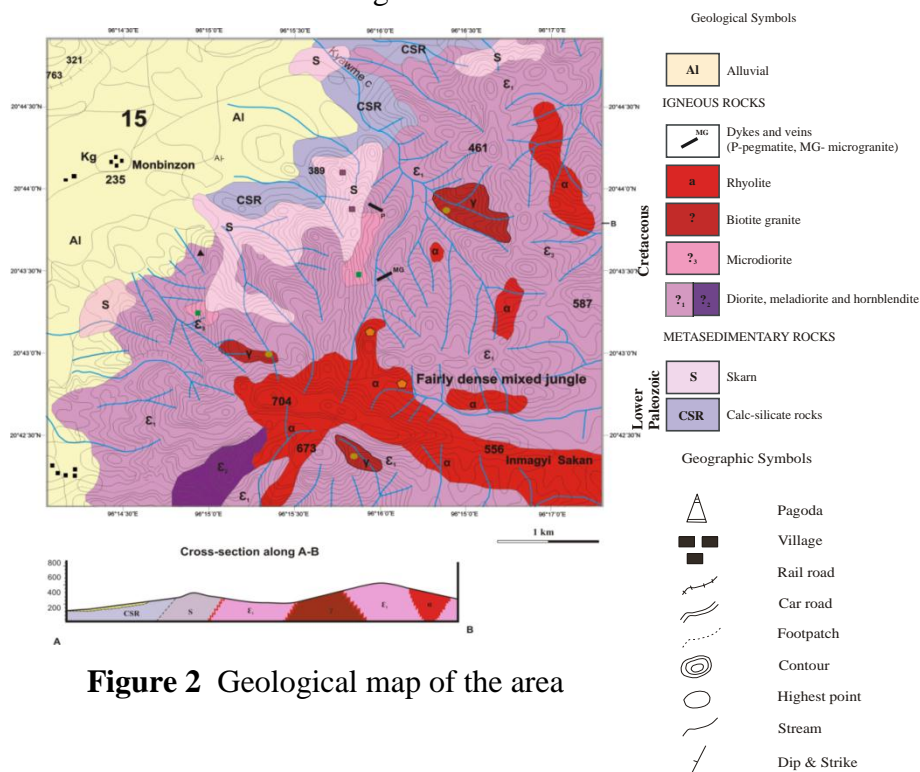


Figure 2 Geological map of the area

Nature of Skarn

The intrusion of diorite into impure limestone has recrystallized, part of the limestone to form a marble and the introduction of elements from the pluton has formed a skarn. Due to the effect of contact metamorphism to calcareous rocks, skarn have been observed on the southern part of Monbinzon village and south of Kywedatson car road. It occurs at the contact between diorite bodies and calc-silicate rocks and well exposed as a massive body.

As a result of contact metamorphism, the calc-silicate rocks become coarse-grained and show colour banding of greenish and reddish brown, the width of these colour bands vary. Skarn contain grossularite, tremolite and diopside. This rock is knotted, due to differential weathering of grossularite and calcite. The dominant constituent minerals are diopside, tremolite, grossularite, epidote, calcite and quartz.

It is generally consider that the existing geological structures are some related to the movement of the tectonically significant Sagaing fault. The granitoid rocks and meta-sedimentary rocks are most widespread study area. The metasedimentary unit so far encountered is in the form of roof pendent in Figure 3(a).

Skarn is medium grained texture, fresh color dark green and weather color dark grey. It contains garnet, diopside and tremolite. These rocks are coarse-grained and occasionally associated with quartzite bands as shown in Figure 3(b). This skarns is exoskarn and present adjacent to the diorite emplaced into skarn. Garnet-clinopyroxene skarn is dark green in clinopyroxene-rich and purplish brown in garnet-rich skarn occurred southern part of Monbinzon village.



(a)



(b)

Figure 3(a) Roof pendant at southeastern part of Monbinzon village
(b) Skarn at south eastern part of Monbinzon village

Garnet skarn

The contact between the diorite and garnet skarn, where observed, is sharp and garnet skarn generally grades outwards into garnet-pyroxene skarn away from the pluton. Pea sized and larger brown or dark reddish brown euhedral garnet crystals are very common in areain Figure 4(a). Coexisting garnet and vesuvianite are common near the contact see in Figure 4(b) and far from diorite intrusion, medium to coarse-grained pale brown garnet with or without brown coloured vesuvianite.

Garnet skarn is a coarse- to medium-grained, honey yellow to brown rock with a crude granoblastic to poikiloblastic texture in Figure 5(a). Epidote grains occur as inclusions in garnet and euhedral garnet with pyroxene and zoisite mineral in skarn as shown in Figure 5(b). Minor variable amounts of calcite, quartz, biotite, amphibole, chlorite, and magnetite are present.

Vesuvianite is present as columnar aggregates. It occurs as crystals and has neutral colour under P.P.L. It gives straight extinction, has a high relief and anhedral crystals. Quartz shows strain effect. Accessories are apatite and large euhedral sphene which has acute rhombic shape.



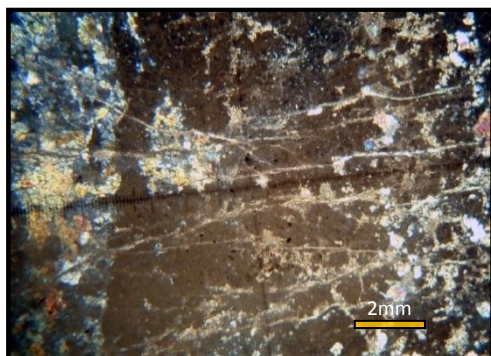
(a)



(b)

Figure 4 (a) Garnet knots on skarn at south eastern part of Monbinzon village

(b) Outcrop nature of skarn (garnet with vesuvianite) at southern part of Monbinzon village



(a)



(b)

Figure 5(a) Poikiloblastic form of garnet with calcite and clinopyroxene

(b) Zoisite and garnet in skarn under XN

Garnet-clinopyroxene skarn

Garnet-clinopyroxene skarn is mainly composed of quartz, plagioclase, diopside, garnet, and tremolite and characterized by the absence of hornblende and biotite in Figure 6(a). Accessory minerals are apatite, and magnetite. Clinopyroxene is commonly associated with garnet in garnet-clinopyroxene skarn. These two minerals are generally approximately equal or pyroxene is slightly greater in proportion to garnet in Figure 6(b).

Hypidiomorphic granular texture of garnet-pyroxene skarn is composed mainly of quartz, plagioclase (An 40-45), and poikiloblastic orthoclase enclosing euhedral-subhedral pale green clinopyroxene (diopside) seen in Figure 7.

Clinopyroxene (diopside) is subhedral and basal section shows two sets of pyroxene cleavage. It is colourless or pale green and non-pleochroic. Grossularite garnet is anhedral and it contains inclusions.

Magnetite occurs mostly interstitially to pyroxene, although inclusions of this phase are observed in both clinopyroxene, and rarely garnet. Additionally, magnetite occurs along fractures and in veinlets.



(a)



(b)

Figure 6(a) Garnet-clinopyroxene skarn at southern part of Monbinzon village

(b) Clinopyroxene mineral in skarn at south eastern part of Monbinzon village

Tremolite has a columnar form and is colourless in Figure 8(a). Interstices between garnet and clinopyroxene contain calcite, quartz or both, with or without k-feldspar and rare plagioclase.

Epidote forms as anhedral aggregates, giving high relief and strong birefringence and occurs usually as inclusions in larger garnet grains. Epidote is present interstitially to clinopyroxene grains. Accessory minerals are apatite, and magnetite. Sericite, pyrite, chlorite and calcite are common alteration products in Figure 8(b).

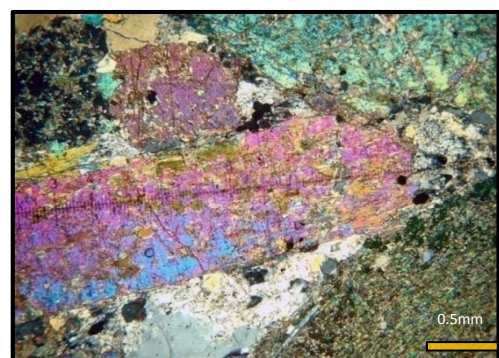
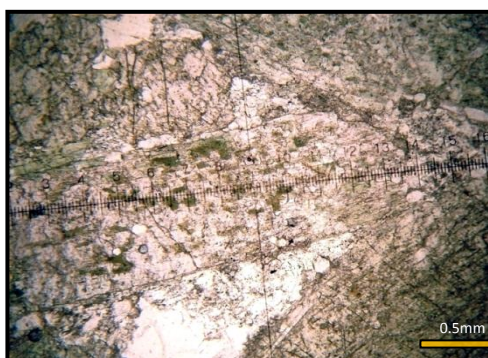


Figure 7 Clinopyroxene and garnet minerals in skarn under PPL and between XPL

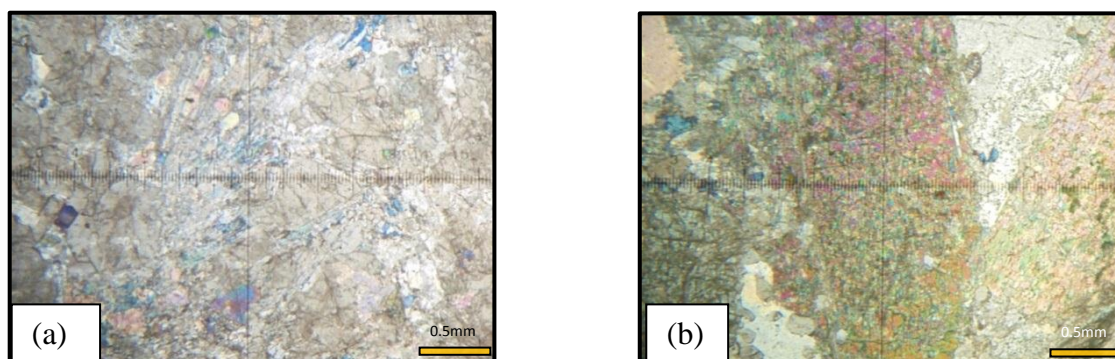


Figure 8 (a) Columnar aggregates of tremolite minerals in garnet-clinopyroxene skarn
(b) Clinopyroxene altered to chlorite in skarn

Distinguishing feature of garnet skarn and garnet-clinopyroxene skarn are shown in Table (1) and mineral assemblages are seen in Table (2).

Table 1 Distinguishing feature of garnet skarn and garnet-clinopyroxene

	Garnet Skarn	Garnet-clinopyroxene skarn
Grain size	Medium to coarse-grained	Medium to coarse-grained
Mineralogy	Garnet, Quartz, Plagioclase (An32-45), Hornblende, Biotite, Orthoclase, Magnetite	Pyroxene, Garnet, Quartz, Orthoclase(perthite), plagioclase (An20-34), Magnetite
Alteration	Sericite, epidote, chlorite, calcite	Sericite, chlorite, actinolite
SiO ₂	41.15	32.92
Na ₂ O	2.04	2.93
A/CNK	0.19	1.82
CaO	29.89	0.36
Sr	91	18

Coexisting garnet and clinopyroxene exhibit the following textural relationship:

- (i) Clinopyroxenes are xenoblastic and form granoblastic and vermicular aggregates with less abundant garnet grains.
- (ii) In garnet rich domains, massive garnet contains inclusions of calcite and clinopyroxene in poikiloblastic arrangement and
- (iii) Garnet-clinopyroxene domains with a crude granoblastic texture

Table 2 Mineral assemblages in recrystallized calc-silicate rocks, garnet skarn, garnet-clinopyroxene skarn and diorite.

Rock type	Mineral assemblage	Microstructure	Retrograde assemblages
CSR	Garnet + epidote + quartz ± k-feldspar ± plagioclase	Crude <u>granoblastic</u> , <u>anhedral</u> garnet in with minor <u>subhedral epidote</u> inclusions. <u>Anhedral-subhedral</u> K-feldspar and plagioclase.	
Garnet Skarn	Garnet + calcite + quartz ± magnetite	Crude <u>granoblastic</u> , <u>zoned-garnet</u> with minor <u>subhedral epidote</u> with minor plagioclase as cavity fillings or interstitial to garnet grains. <u>Subhedral-euhedral</u> magnetite normally associated with cavity fillings of amphibole prisms.	Some fine grained garnets replaced by calcite. Magnetite weathered to hematite.
Clinopyroxene Skarn	Clinopyroxene + garnet + calcite + quartz ± epidote ± K-feldspar ± plagioclase	Crude <u>granoblastic</u> , intergrowths of garnet and <u>clinopyroxene</u> . <u>Xenoblastic</u> calcite and quartz with minor K-feldspar and plagioclase. Some <u>subhedral</u> amphibole is long and normally aggregates. <u>Subhedral idioblastic</u> magnetite along <u>clinopyroxene</u> planes and with or without amphibole.	<u>Clinopyroxene</u> replaced by calcite plus magnetite and altered to amphibole. Isotropic garnet altered to calcite and magnetite.
Diorite	Hornblende + plagioclase + quartz + biotite + magnetite	<u>Hypidiomorphic</u> granular with <u>euhedral</u> quartz and <u>anhedral-subhedral</u> K-feldspar and plagioclase. <u>Subhedral-euhedral</u> epidote as inclusions large hornblende grains.	Hornblende altered <u>epidote</u>

Petrochemical Characteristic of Skarn

The analytical data of major and trace elements composition of skarn rocks are shown in Table (3). All of the samples were analyzed by XRF and ICP-MS analysis.

Table 3 Major oxide (wt %) and trace elements (ppm) abundances of the skarns

Type	Garnet skarn	Pyroxene skarn
SiO ₂	41.13	32.92
TiO ₂	0.33	0.2
Al ₂ O ₃	6.39	7.14
Fe ₂ O ₃	19.67	29.55
MnO	0.89	0.69
MgO	0.64	28.45
CaO	29.89	0.36
Na ₂ O	2.04	2.93
K ₂ O	0.85	0.62
P ₂ O ₅	0.13	0.12
Cr ₂ O ₃	2.04	2.93
LOI	0.51	1.08
Total	100.43	100.5

Type	Garnet skarn	Pyroxene skarn
Sr	91	18
Nb	n.d	6
Y	90	19
Zn	37	93
Ti	0.3	<0.1
Zr	103	53
Rb	20	16
Ni	3	3
La	57.1	27.4
Ta	0.5	0.4

Major Element Based Classification

The plots in Harker's variation diagrams as shown in Figure 9 indicate that SiO_2 , TiO_2 and K_2O show a systematic decrease from diorite to skarn in Figure 9(a). FeO_t display a similar distribution, general increase to skarn Figure 9(b). These distribution profiles are consistent with mass transfer during metasomatism.

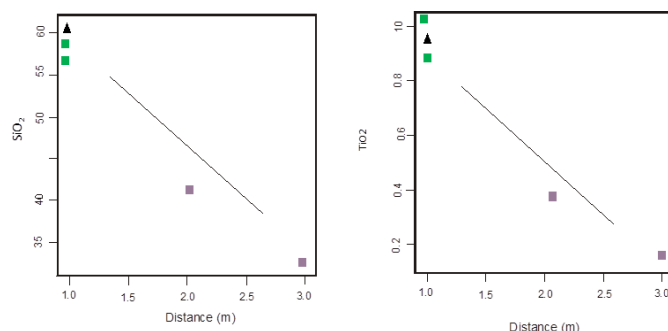


Figure 9(a) Harker's variation diagrams by using major element

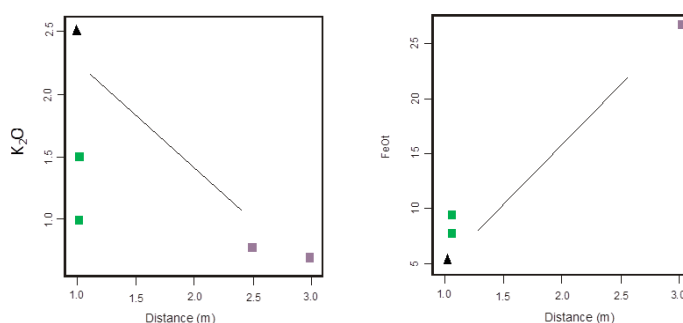


Figure 9(b) Harker's variation diagrams by using major element

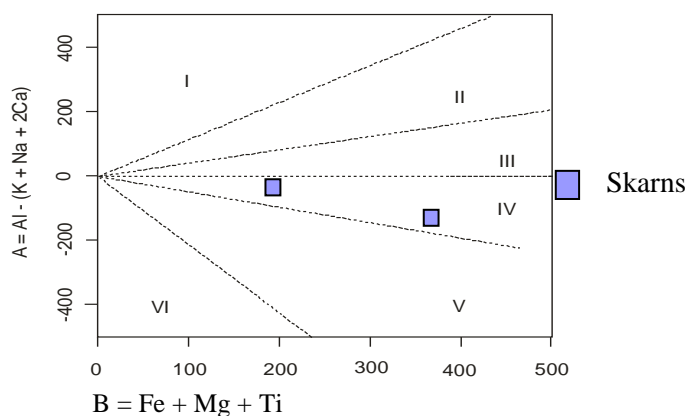


Figure 10 Mineral characteristic diagrams for the granitoid after Debon and Le Fort, 1983.

Sector I = Muscovite alone/muscovite biotite

Sector II = Biotite muscovite

Sector III = Biotite alone

Sector IV = Variety of characteristic minerals (biotite, hornblende, orthopyroxene, clinopyroxene, primary epidote and sphene)

Sector V = High proportion of clinopyroxene and/or primary epidote and/or sphene

Sector VI = only igneous rocks with very exceptional composition

Debon and Le Fort (1983) used a diagram based on two parameters. The character of skarns is analysed into sectors IV plot in Figure 10.

Type of Skarn

Cu, Zn and Y enrichment in skarn is relative to granite. Sr exhibits a perceptible decline in the direction of exoskarn. This decline again reflects geochemical decoupling is a reflection of crystal chemical controls on the ease of atomic substitution of Sr in garnet and pyroxene which form the exoskarn in this suite of samples. Zr concentration is much lower in adjacent exoskarn. Slightly enrichment in HREE (Y) is normally garnet rich. Strontium is decline in exoskarn due to forming of garnet and pyroxene because Sr can substitute in the lattice of garnet and pyroxene in Figure 11 (a). According to Thompson (1982) Chondrite normalized plots, the massive garnet-clinopyroxene skarn exhibit much flatter profiles in Figure 11 (b), suggesting that LREE/HREE enrichment is less pronounced, and indicating that garnet (see also Clark, 1984) may preferentially concentrate HREE.

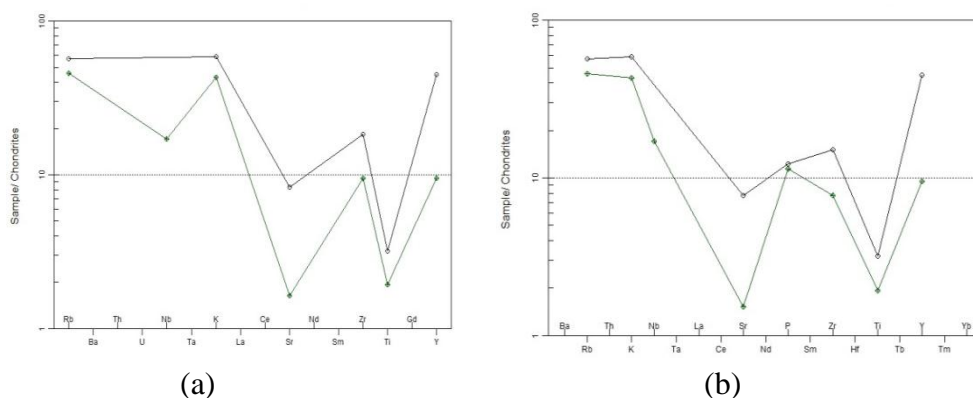


Figure 11(a) Chondrite-normalized REE patterns by Sun et al. (1980)

(b) Chondrite-normalized REE patterns by Thompson (1982)

Mass transfer studies conducted by other workers, during the evolution of skarn, numerous chemical components, including Si, Ti, Al, Fe, Mn, Mg, Zn, Nb, Cu and Zr are generally added and CaO, CO₂ and Sr are removed from the system. Of fundamental importance to an understanding of the process of skarn formation is how elements may be mobilized and finally incorporated in skarn.

Types of Metamorphism

The mineral assemblages indicated that the area had been subject to three types of metamorphism. They are regional metamorphism, localized contact metamorphism and cataclastic metamorphism.

Regional metamorphism is characterized by the formation of calc-silicate rocks. It is obvious that these rocks had low grade metamorphic minerals of chlorite reached up to Greenschist facies.

Regional metamorphism was superimposed by contact metamorphism by the emplacement of igneous intrusions, especially diorite intrusion. The skarn rocks are observed at the contact of diorite and adjacent metasedimentary rocks. Skarn rocks are the evidence of the existence of contact metamorphism. Contact metamorphism is indicated by the occurrence of

skarn containing grossularite, diopside, tremolite and vesuvianite; therefore, the study area had taken place under “Pyroxene hornfels facies”.

Cataclastic metamorphism is observed at or near the contact of igneous intrusion and adjacent metasedimentary rocks regarded by the occurrence of the bent twin bands of feldspar, the strain effect, cataclastic effect and highly brecciated nature of pegmatite.

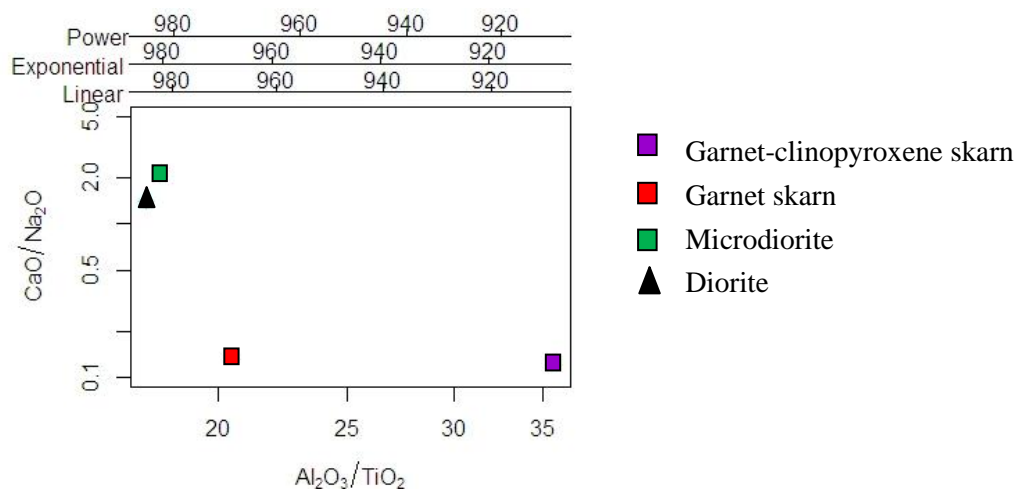


Figure 12 Temperature (°C) after Jung and Pfander (2007)

According to the CaO/Na₂O vs Al₂O₃/TiO₂ diagram after Jung and Pfander (2007), the temperature of diorite is slightly more than microdiorite and decrease to garnet skarn (~ 970°C) and garnet-clinopyroxene skarn (not more than 920°C) as shown in Figure 12.

Mechanism and Depth of Emplacement

The possible mechanism of emplacement of intrusion is considered to be of forceful injection that the foliations are generally parallel to the contact between the intrusion and the country rock.

According to Winter (2013), the probable depth of emplacement of granitic rocks based on the evidences, petrographic studies and petrochemical studies are as follow:

1. The igneous rocks may show partially concordant and discordant contacts.
2. The contacts with the country rocks are sharp.
3. Roof pendent of metasedimentary rocks are formed over the pluton.
4. The country rocks are medium to high grade regional metasedimentary rocks.
5. A contact metamorphic aureole is typically well developed. And there exists a skarn zone.
6. Achill zone is locally present along the contact.
7. Presence of contact migmatite.
8. Fibrous in the pluton are commonly foliated or lineated near the contact.
9. Pegmatite dykes and quartz veins are common.

The above mentioned evidence shows that the igneous rocks of the study area are emplaced at the upper level of mesozone to catazone to the metasedimentary rocks and forming skarns.

Summary and Conclusion

The study area is situated about 24.3 km southeast of Thazi Township, Mandalay Region. Physiographic feature of the area is typically expressed by roughly parallel ridges with relatively relief, especially in the southern part of the area. The western part is lowland and the eastern part is a mountainous region. The highest-peak of the area is Minbon Taung 704m which exposed the skarn.

The study area is located in the eastern part of the Thazi-Pyawbwe plain which lies in the western part of the Shan Plateau which had become a stable block since the close of the Mesozoic. Two major fault zones, the Sagaing Fault in the West and Shan scarp fault in the East.

The area composed of different lithologic units such as igneous rocks and meta-sedimentary rocks. The igneous rocks of are emplaced at the upper level of mesozone to catazone to the metasedimentary rocks and form as skarn.

In the area, skarn consist predominantly of garnet-rich skarn and garnet-clinopyroxene skarn, with respect to increasing distance from the pluton. Garnet-clinopyroxene skarn crops out as greenish brown coarse- to medium-grained rocks. On the side of calc-silicate rocks, it is clinopyroxene rich and becomes garnet rich along the pluton contact.

Skarn is medium to coarse grained. In garnet rich domains, massive garnet contains inclusions of calcite and pyroxene in poikiloblastic texture. In garnet-pyroxene domains, pyroxenes are xenoblastic and form granoblastic texture.

Geochemically, the distribution profiles of Harker's variation diagrams are consistent with mass transfer during metasomatism due to SiO_2 , TiO_2 and K_2O decrease from diorite to skarn and FeO_t increase to skarn.

Cu, Zn and Y enrichment in skarn and Sr exhibits a perceptible decline in the direction of exoskarn. This decline again reflects geochemical decoupling is a reflection of crystal chemical controls on the case of atomic substitution of Sr in garnet and pyroxene which form the exoskarn in this suite of samples. Zr concentration is much lower in adjacent exoskarn. Slightly enrichment in HREE (Y) is normally garnet rich. Strontium is decline in exoskarn due to forming of garnet and pyroxene. In Chondrite-normalized REE patterns, LREE/HREE enrichment is less pronounced, and indicating that garnet may preferentially concentrate HREE in skarns.

Acknowledgements

I wish to express grateful thanks to Dr. Kyi Kyi Maw (Professor and Head of the Department of Geology, Dagon University) for her permission to investigate the area and providing of necessary departmental facilities. I am deeply grateful to U Aung Kyaw Htun for his kind help during field and discussion, assistance and kind hospitality are much appreciated. I am grateful thanks to Professor Dr Graciano Yumul, University of Philippine for the geochemical analysis results which was carried out at Acme Labs, Canada.

References

- Debon, F. and Le Fort, P. (1983). A chemical-mineralogical classification of common plutonic rocks and associations. Earth Sciences Publication, pp. 73.135-149.
- Jung S., and Pfander, J. A., (2007). Source composition and melting temperatures of orogenic granitoids: constraints from CaO/Na₂O, Al₂O₃/TiO₂ and accessory mineral saturation thermometry. *European Journal of Mineralogy*. pp. 859-870. Vol.19, No. 6.
- Harker, A., (1909). *The National History of Igneous Rocks*. Methem, Landon.
- Serale, D.I., and Ba ThanHaq, (1964). The Mogok Belt of Burma, and its relation to the Himalayan Orogeny. *22nd Intern. Geol. Congress. India*.
- Sun et al., (1980). Lead isotopes study of young volcanics from mid-ocean ridges, ocean islands and island arcs. *Phil. Tran. R. Soc.*, A297, 409-445
- Thompson, R.N., (1982). British Tertiary volcanic provinces. *Scott.J.Geol.*, 18,49-107.
- Winter, J.D., (2013). *An introduction to Igneous and Metamorphic Petrology*, Prentice Hall, New Jersey.p.

MORPHOLOGY OF PYRITE AND ITS SIGNIFICANCES FROM BAWLONELAY AREA, MOGOK

Wai Yan Lai Aung¹, Thet Tin Nyunt², Htay Lwin³ and Day Wa Aung⁴

Abstract

In the marble of the Mogok Metamorphic Belt from Bawlonelay area, Mogok Township, pyrites crystals exhibit a wide range of different morphologies during regional metamorphism. The pyrite crystals are commonly found as cube, octahedra and cubo-octahedra, pyritohedra and cubo-pyritohedra habits in the research area. On the basis of pyrite crystal habits, they could form under the different temperature condition which controls the speed at which the crystal grew. Moreover, these pyrite crystals are found in association with ruby in the marble from Bawlonelay. Blue corundum (sapphire) is not associated with ruby in the primary gemstone-bearing bands indicates that available Ti may have been used up in forming sphene (titanite) which is a common associated mineral in these bands. There has no more Ti available to form blue sapphire. The present study would like to consider the hypothesis is that ruby in the marble from Bawlonelay together with pyrite indicate that the original limestone contain impurities of aluminous and iron rich materials. Although there has enough alumina from the intruded igneous rocks (i.e syenite), the element, Fe, that would be formed for the formation of sapphire were already used up as the crystallization of pyrite which is found in association with ruby in the marble of Bawlonelay and no more excess Fe for the formation of sapphire.

Keywords: Mogok, Mogok Metamorphic Belt, Bawlonelay, pyrite, ruby, sapphire

Introduction

The research area is situated in the Bawlonelay area, Mogok Township, Mandalay Region. Bawlonelay mine site is situated at the west of Pingu Taung, north of Kyat Pyin. It is about 16 miles west from Mogok and GPS location is 22° 54' 54.80" N and 96° 23' 56.50" E. The elevation of the area is 1536 meter above sea level. The Bawlonelay area is one of the noticeable gem mine sites of Mogok (Fig. 1).

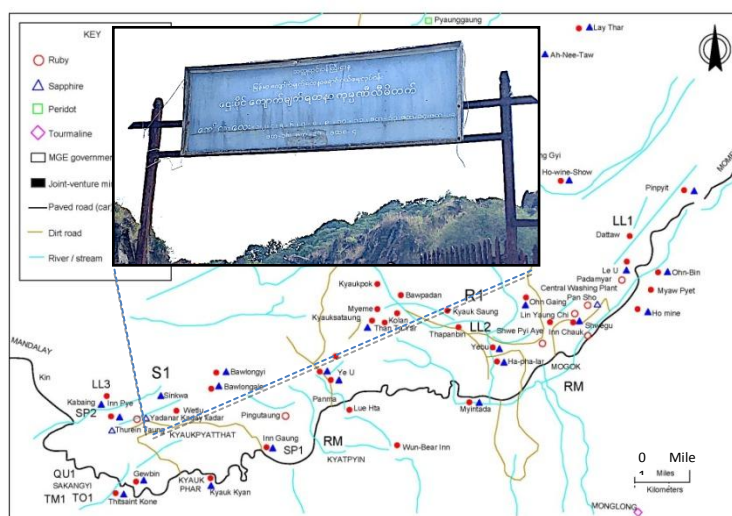


Figure 1 Location of gem mine sites from Mogok and its environs (redrawn after Kammerling *et. al.*, 1994)

¹ Dr, Demonstrator, Department of Geology, University of Yangon

² Dr, Director General, Department of Geological Survey and Mineral Exploration, Myanmar

³ Dr, Professor, Department of Geology, University of Yangon

⁴ Dr, Professor and Head, Department of Geology, University of Yangon

Pyrite is the most common iron sulphide mineral and the name come from the Greek for fire, as sparks may be struck from it (Liddell & Scott, 1940). Pyrite crystals observed Eighty-five forms (Dana, 1903) and they can exhibit a wide variety of habits; more than one hundred eighty forms (Goldschmidt, 1920). However, only three forms make up the majority of pyrite crystals; these are the cube $a \{100\}$, the octahedron $o \{111\}$, and the pentagonal dodecahedron (or pyritohedron) $e \{210\}$ (Sunagawa, 1957), (Fig. 2). Pyrite crystallized in cubic system and forms observed include cubes, pyritohedrons, octahedrons, conglomerates, framboids, and polyframboids (Dana, 1966). However, most of them are combination of cube and octahedron, and cube and pyritohedron habits in the research area.

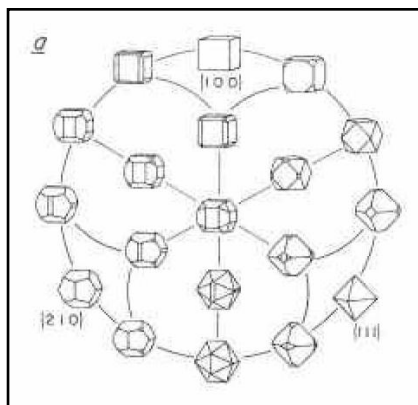


Figure 2 Common pyrite habits with forms $a \{100\}$, $o \{111\}$ and $e \{211\}$ (Sunagawa, 1957)

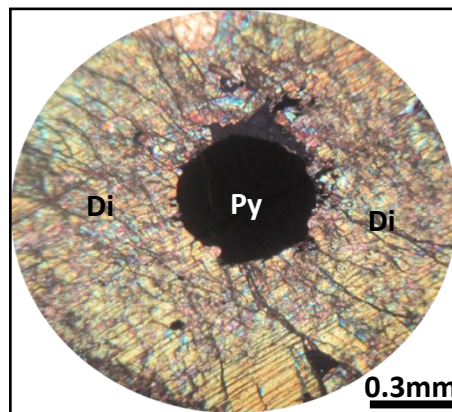


Figure 3 pyrite inclusion in diopside porphyblast in diopside marble at Bawlonelay mine (Photo Courtesy by Soe Ei Ei Myat).

The habit of pyrite varied with grain size (Sunagawa, 1957). In the range of 48 to 8 mesh (0.3 mm to 2.5 mm), the cube was dominant among the smallest grain sizes, the octahedron in the middle sizes, and the pyritohedron in the coarsest fraction. From his work at the Yanago mine, he concluded that pyrite grown with "abundant ore solution" shows a greater variety of habits within one grain-size fraction than crystals grown with a "poor supply of ore solution." Furthermore, highly altered host rock shows the greatest variety of habits and the strongest mineralization whereas the least-altered host rock contains only cubes. Amstutz and Ligasacchi (1958) and Amstutz (1963) noticed conspicuous, systematic changes in pyrite morphology from one ore zone or vein to another at Morococha, Peru. Bush *et al.* (1960) noticed the association of different pyrite habits with each of the stages of mineralization at Tintic, Utah. The lower-sulfide-content middle and late barren stages have cubic pyrite, and the sulfide-rich early productive stage has pyritohedra, implying corresponding degrees of supersaturation of the depositing solution. Amstutz (1963) showed a simple zoning pattern of pyrite from cubes to pyritohedra with increasing copper values at Cuajone, Peru. Amstutz noted that pyritohedra occurred in mineralized monzonite and limestone whereas barren granite hosted only cubes, suggesting that pyritohedra and cubes were indicative of ore-forming and non-ore-forming conditions, respectively at Antimina, Peru. Bitcher and Bouchard *et. al.*, (1968) experimentally studied the pyrite morphology. Large (5 mm) crystals of pyrite were grown by in a temperature gradient from 705 to 665°C over an unspecified distance using Cl_2 gas as the transport agent. Sunagawa (1957) and Endo's (1978) explained that larger temperature gradients produced wavy

rather than straight growth fronts and some twinned crystals. Yamada et al. (1979) used Bouchard's method with temperature gradients of 700 to 630°C and 700 to 400°C over an unspecified distance and the crystals were grown by vapor transport and may not accurately reflect growth from hydrothermal solutions. Murowchick and Barnes (1987) studied experimental synthesis of hydrothermal pyrite crystals shows that temperature and degree of supersaturation are important in determining pyrite morphology. But Alonso-Azcárate, J., *et. al.*, (1999a, 199b) said that there could not have been important differences in temperature between the pyrite morphologies. And In 2001, they studied the causes of variation in crystal morphology in metamorphogenic pyrite deposits of the Cameros Basin (N Spain). They said that temperature differences between pyrite deposits and As content are possible causes of the different pyrite morphologies in the deposits. They confirmed sulphur isotope data on the pyrites to investigate the degree of supersaturation.

Present work is, on the basis of pyrite crystals' morphologies, we hoped to study the effects of temperature, the degree of supersaturation and other significances of pyrite at Bawlonelay area.

Materials and Methods

To study the relation between pyrite and gem bearing rocks, some days were spent in the Bawlonelay area. Pyrite crystals were collected from the Bawlonelay mine site. Among the collected above 100 pyrite crystals, some are selected to realize the morphologies of pyrite crystals by using Gemmolite and chemical composition measured with the help of EDXRF.

Results

Connection between pyrite and gem bearing rocks

Bawlonelay mine site is one of the primary ruby mines. Ruby is extracted from marble that intruded by syenitic rocks. Pyrites are included into both ruby bearing marble and syenite. Moreover pyrite crystals are widely disseminated and can be seen easily around the outcrops (Fig. 3).

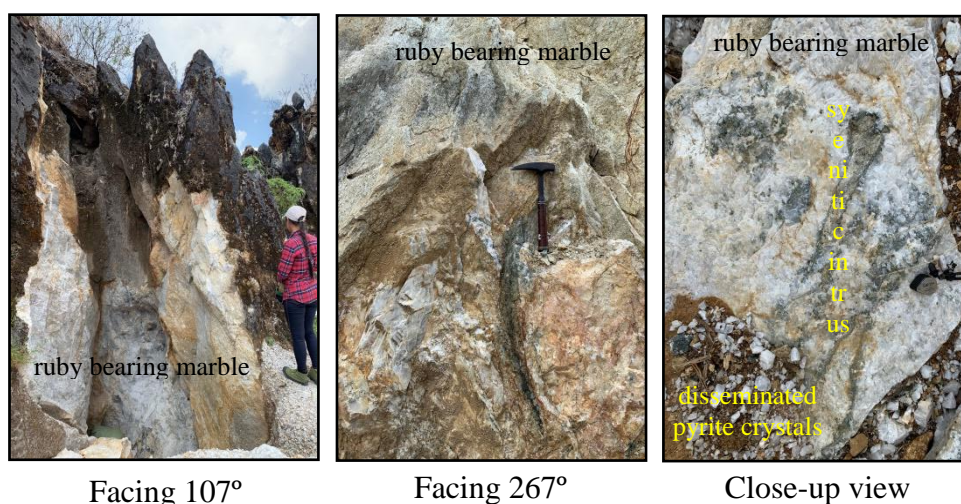


Figure 3 Nature of ruby bearing marble at Bawlonelay mine site (Loc. 182437)

These pyrite crystals are found in association with ruby in the marble from Bawlonelay. Blue corundum (sapphire) is not associated with ruby in the primary gemstone-bearing bands at there. Microscopically, pyrite inclusion is included in diopside porphyblast in the diopside skarn (diopside marble) from Bawlonelay, Htay Paing Mine, (Fig. 4, Photo Courtesy by Soe Ei Ei Myat).

Observed Morphologies of Pyrite

Pyrites crystals exhibit with a wide range of different morphologies during regional metamorphism. In the marble of the Mogok Metamorphic Belt from Bawlonelay area, Mogok Township, we observed 3 different habits of Isometric system and their combination forms in pyrite, generally. These are the cube ($\{100\}$), the octahedron ($\{111\}$), the pentagonal dodecahedron (or pyritohedron) ($\{210\}$) and their combination forms; cubo-octahedron and cubo-pyritohedron among common pyrite habits (Fig. 5). The colour is pale brass-yellow, tarnishes darker and iridescent. Pyrite is opaque and gives metallic lustre (Rutley, 2012).

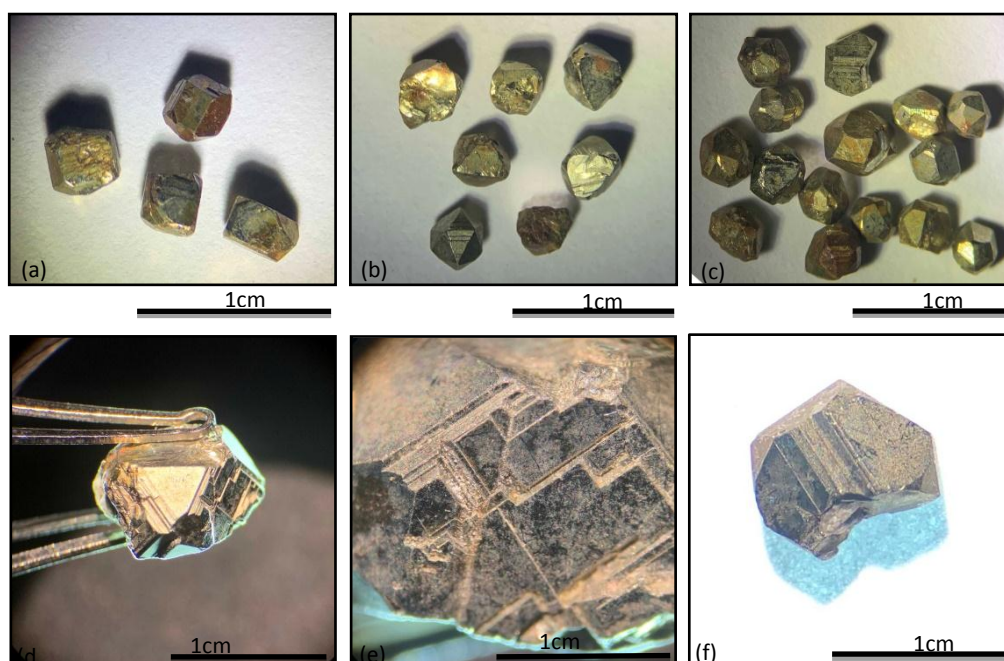


Figure 5 Characteristic pyrite habits in the Bawlonelay area.

- a) cube and cubo-octahedral crystals,
- b) octahedral crystals,
- c) pyritohedra and cubo-pyritohedral crystals,
- d) octahedral crystal with triangular facets,
- e) step facets on the surface of cubo-pyritohedral crystal and
- f) heavily strained twin crystal.

The cubic morphology (Fig. 5a) is frequent in nature but natural minerals are not perfectly cubic forms from the $\{100\}$ family. Some are equal lengths along the a_1 , a_2 , a_3 directions but some crystals are elongated along one axis. The average dimension of cubic crystal is $0.3 \text{ cm} \times 0.2 \text{ cm}$ and the rectangular face is $0.2 \text{ cm} \times 0.5 \text{ cm}$. Some cube has striations along the edge of the faces.

In the octahedral morphology (Fig. 5b) there are 8 facets from the {111} family. There are striations on plane triangles {111} (Fig. 5d), such as in the cubic case. Average size of octahedral crystal is 0.5 cm and some are distorted.

In the pyritohedral pyrite crystals (Fig. 5c) from the {210} family, some have striations on surface (Fig. 5d, 5e) and the crystals' sizes are around 0.5 cm.

Other forms of pyrite can be observed as combination forms of these facets with truncated corners (such as truncated cube, truncated octahedron, truncated dodecahedron) and twin crystals (Fig. 5f).

Analytical Data

The collected pyrite crystals were analysed to determine their composition by EDXRF and the results indicate that some are pyrite and other are arsenopyrite.

Table 1 Compositional variation of pyrite crystal from the study area

Sample	PY-1-Pellet		Sample	PY-1-Metal	
SO ₃	86.7		SO ₃	86.6	
Fe ₂ O ₃	6.54		Fe ₂ O ₃	6.72	
SiO ₂	3.5		SiO ₂	3.48	
Al ₂ O ₃	1.79		Al ₂ O ₃	1.72	
MgO	0.664		MgO	0.645	
CaO	0.233		CaO	0.25	
P ₂ O ₅	0.188		P ₂ O ₅	0.202	
Na ₂ O	0.167		Na ₂ O	0.182	
K ₂ O	0.0113		ZrO ₂	0.112	
K ₂ O	0.0113		K ₂ O	0.0133	
Cl	1100		ZnO	0.0005	
Zr	817		NiO	62.3	
As	37.6		As ₂ O ₃	50.1	
W	5.88		Co ₂ O ₃	47.9	
Zn	5.33		CuO	6.84	
Cu	3.54		SeO ₂	1.92	
Rn	1.14		Cl	1060	
Se	1.33		Ni	49	
			As	38	
			Co	34.1	
			Cu	5.47	
			Rn	2.21	
			Se	1.36	

Discussion

Pyrite morphology and growth mechanism

Possible controls of the habit of pyrite include mechanisms of its crystal growth (Sunagawa, 1957). According to Murowchick and Barnes (1987), morphological differences in pyrites are related to the differences in physiochemical conditions (mainly, supersaturation and/or temperature). They grew pyrite crystals under controlled conditions in the laboratory, in the temperature range between 250 and 500°C. Increasing growth temperature or supersaturation would lead to a change from surface-controlled growth to diffusion-controlled growth (Fig. 6). This change in the growth mechanism would be caused by different crystals morphologies. They found that temperatures around 250°C and low degrees of supersaturation produce needle-like pyrite crystals. An increase in the degree of supersaturation leads to the development of cubes with perfectly smooths *a* {100} and small *o* {111} faces. Higher temperatures (around 450°) and low degrees of supersaturation produce large striated cubes with small octahedral faces. The combination of high temperature and high supersaturation levels leads to the formation of heavily striated cubes with or without octahedral faces. Finally, crystals grown under the very high supersaturation levels achieved in quenching exhibit morphologies ranging from pyritohedral to

blocky crystals to skeletal octahedral and dendrites. Murowchick and Barnes (1987) considered that all the morphologies, except those relating to crystals formed during quenching, are the result of surface-controlled growth. Crystals formed during quenching show a sequence of morphologies (octahedral, skeletal octahedral, dendrites and fine-grained pyrite) that indicated the gradual transition from two-dimensional nucleation-controlled growth (surface-controlled growth) to continuous growth (diffusion-controlled growth).

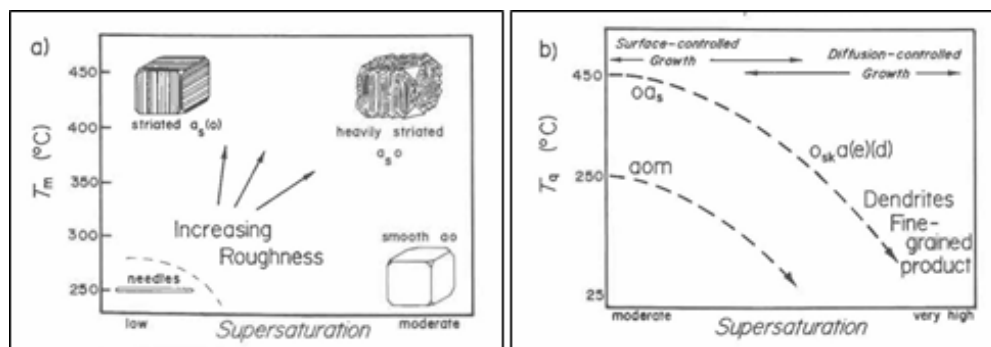


Figure 6 Morphologies of hydrothermally grown pyrite (after Murowchick and Barnes, 1987).

- Habits produced during steady-state conditions. T_m is the mean run temperature. The degree of supersaturation is known only approximately for this system.
- Typical temperature vs. supersaturation paths (heavy dashed lines) and habits produced during quenching. T_q is the temperature at the beginning of the quench. Crystal forms are given in decreasing order of development using the letters $a = \{100\}$, $o = \{111\}$, $e = \{210\}$, $m = \{311\}$, and $d = \{110\}$. Subscripts s and sk indicate the associated forms are striated or skeletal, respectively, and parentheses indicate minor development of the form or feature.

On the other hand, Alonso-Azcárate, J., *et. al.*, 2001 also showed the different pyrite habits and their possible relationship with crystal growth mechanism and degree of supersaturation (Fig. 7). They assumed that pyrite deposits originated during anchizone-epizone hydrothermal metamorphism. There is little variation in metamorphic conditions prevalent at the different deposits. Thus they concluded that temperature has not been an important factor in directly controlling the growth mechanism.

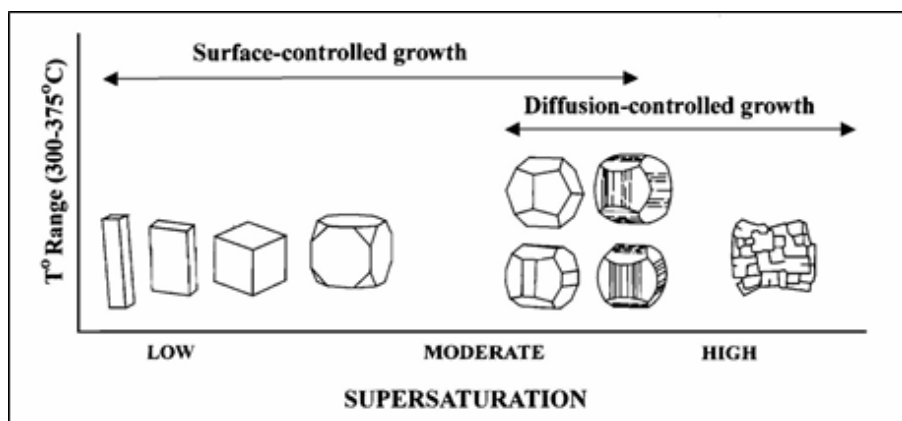


Figure 7 Relationships between pyrite habits, degree of supersaturation and crystal growth mechanism (Alonso-Azcárate, J., *et. al.*, 2001)

From the authors' point of view, the existence of a certain mineral is related to their environment. In the Bawlonelay area, Pyrite is associated with gem minerals, ruby. Ruby-bearing marbles formed in the amphibolite facies ($T=610$ to 790 °C and $P\sim 6$ kbar) (Winkler, 2013). Thus we considered the following conceptual model (Fig. 8) by using Murowchick and Barnes, 1987's experimental method with temperature gradients. These factors control the speed at which the crystals grew. At low temperature and slow growth rate, pyrite crystals are formed as the rod shaped and needle-like crystals. When the temperature is upper and/or supersaturation is increased, pyrite is formed as smooth cubes. The more cube striated, the greater supersaturation. If the temperature and/or supersaturation are higher, octahedrons and then pyritohedrons are formed. Larger temperature gradients produced wavy rather than straight growth fronts and some twinned crystals (Yamada *et al.* 1979). At the highest degrees of superstauration, crystal growth is very fast and odd dendritic clumps of pyrite.

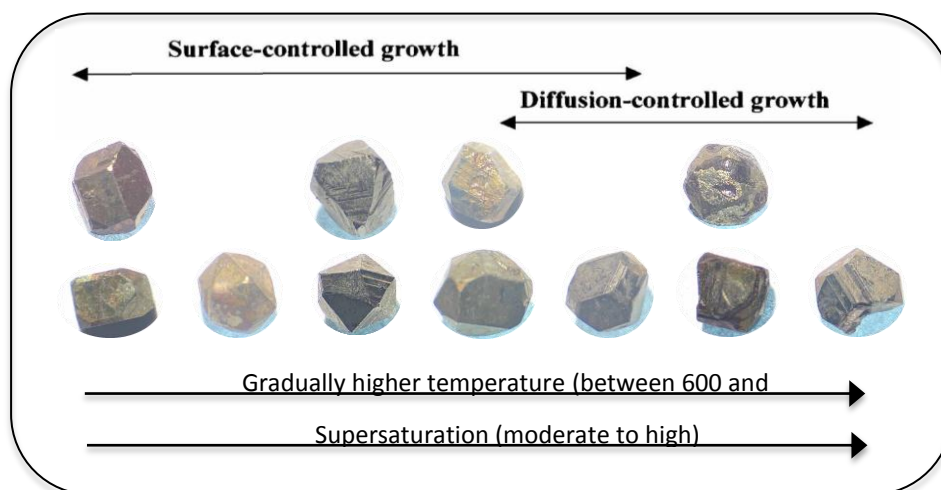


Figure 8 Relationships between pyrite habits and temperature variation at Bawlonelay area.

Possible conceptual factors on pyrite chemistry

Pyrite (FeS_2) is associated with corundum, especially ruby in Bawlonelay mine. Corundum is a crystalline form of aluminium oxide (Al_2O_3) typically containing traces of iron (Fe), titanium (Ti), vanadium (V) and chromium (Cr). The red (Cr-bearing) gem variety is called Ruby and the blue (Fe- and Ti-bearing) gem variety is called Sapphire (Anthony, 1997). These elements are special conditions and controlling factors of gemstones formation. Excess alumina from the syenitic intrusions may have formed ruby and sapphire in the skarns. Blue corundum (sapphire) is not associated with ruby in the primary gemstone-bearing marble bands indicates that available Ti may have been used up in forming sphene (titanite) which is a common associated mineral in these bands. There has no more Ti available to form blue sapphire (Maung Thein, 2008). In the Bawlonelay area, Pyrite is associated with gem minerals, ruby. This fact also indicates that the original limestone contain impurities of aluminous and iron rich materials. The element, Fe, is already used up in pyrite crystallization, so there is no more Fe and Ti to form sapphire in the research area.

Summary

Pyrite commonly forms cubes, octahedrons, pyritohedrons and some combinations of these forms in Bawlonelay area. All pyrite is FeS_2 with the same internal arrangement of iron and sulphur atoms. On the basis of pyrite crystal habits, they could form under the different temperature condition that controls the speed at which the crystal grew. The existence of a certain mineral is related to their environment. The present study would like to consider the hypothesis is that ruby in the marble from Bawlonelay together with pyrite indicate that the original limestone contain impurities of aluminous and iron rich materials. In addition, there has enough alumina from the intruded igneous rocks (i.e syenite), the element, Fe, that would be formed for the formation of sapphire were already used up as the crystallization of pyrite which is found in association with ruby in the marble of Bawlonelay. Further studies will focus on chemical analysis and hope to find detailed petrogenesis on individual different pyrite shapes.

Acknowledgements

We would like to express our sincere thanks to Rector, Yangon University for the permission to take this research. General Manager, MGE, Mogok office and Daw Cho Cho, MGE for their kind help during the field work are also acknowledged. Thanks are also extend to Authorities of Bawlonelay mine. Dr Soe Ei Ei Myat, Assistant Lecturer, East Yangon University is acknowledge for her courtesy of photomicrograph.

References

- Anthony, J.W., Bideaux, R.A., Bladh, K.W. and Nichols, M.C., (1997). Handbook of Mineralogy, *Mineralogical Society of America*.
- Amstutz, G. C. and Ligasacchi, A., (1958) Mineralization zoning based on habit changes of pyrite. *Geological Society of America Bulletin*, 69, pp.1529-1530.
- Amstutz, G. C., (1963) Accessories on pyrite, pyrite zoning and zoned pyrite. *Schweizerische Mineralogische and Petrographische Mitteilungen*, 33, 111-122.
- Alonso-Azcárate, J., Rodas, M., Fernández-Díaz, L., Bottrell, S.H., Mas, J.R. and López-Andrés, S., (2001) Causes of variation in crystal morphology in metamorphogenic pyrite deposits of the Cameros Basin (N Spain). *Geological Journal*, 36(2), pp.159-170.
- Bither, T. A., Bouchard, R. J., Cloud, W. H., Donohue, P. C. and Siemons, W. J., (1968) Transition metal pyrite dichalcogenides. High-pressure synthesis and correlation of properties. *Inorganic Chemistry*, 7(11), pp.2208-2220.
- Bush, J. B., Cook, D. R., Lovering, T.S., and Morns, H. T. (1960) The Chief Oxide-Burgin area discoveries, East Tintic district, Utah; A case history-Pt I, U.S.G.S studies and exploration. *Economic Geology*, 55, 1116-1147.
- Dana, E.S. (1903) *The system of Mineralogy of James Dwight Dana*, 6th edition, p. 84. Wiley, New York.
- Dana, J., Dana, E.S. and Frondel, C., (1966) *System of Mineralogy*: Vol. 3, Silicon Minerals [Russian translation].
- Goldschmidt V. (1920) *Atlas der Kristallformen*, Bd. 6. Markasit-Pyrit. Carl Winters University: Heidelberg; p.179-208, plates 101-144.
- Endo Y, Sunagawa I. (1973) Positive and negative striations in pyrite. *American Mineralogist* 58: 930-935.

- Kammerling, R.C., Scarratt, K., Bosshart, G., Jobbins, E.A., Kane, R.E., Gübelin, E.J. and Levinson, A.A., (1994) Myanmar and its gems—an update. *Journal of Gemmology*, 24(1), pp.3-40.
- Liddell, H.G. and Scott, R., (1940) *A Greek-English Lexicon*, revised and augmented by HS Jones.
- Maung Thein (2008) Modes of occurrence and origin of precious gemstone deposits of the Mogok Stone Tract, *Jour. of MGS*, vol. 1, No. 1, pp. 75-84.
- Martínez-Martínez, S., Acosta, J.A., Cano, A.F., Carmona, D.M., Zornoza, R. and Cerda, C., (2013) Assessment of the lead and zinc contents in natural soils and tailing ponds from the Cartagena-La Unión mining district, SE Spain. *Journal of Geochemical Exploration*, 124.
- Murowchick, J.B. and Barnes, H.L., (1987) Effects of temperature and degree of supersaturation on pyrite morphology. *American Mineralogist*, 72(11-12), pp.1241-1250.
- Palache, C., Berman, H. and Frondel, C., (1944) *Dana's System of Mineralogy*, 7th edit. Vol. I, 16.
- Rutley, F., (2012) *Rutley's elements of mineralogy*. Springer Science & Business Media.
- Sunagawa, I., (1957) Variation in crystal habit of pyrite. *Rep. Geol. Survey, Japan*.
- Winkler, H.G., (2013) *Petrogenesis of metamorphic rocks*. Springer Science & Business Media.
- Yamada, S., Nanjo, J., Nomura, S., and Hara, S. (1979) Morphology of iron pyrite crystals, *Journal of Crystal Growth*, 46, 10-14.

GEOLOGY, ORE OCCURRENCE AND ORE PROCESSING OF COPPER DEPOSITS, MONYWA, SALINGYI TOWNSHIP, SAGAING REGION

Lai Lai Min*

Abstract

In copper processing, many kinds of application methods are using in the world depend on the ore genesis, local environmental regulations and other factors. Among of these methods, in Monywa copper mine area, the electrowinning process is used for the concentrate of copper ore production. Processing of the copper ore involves three stages; Bio-Heap Leaching to dissolve the valuable copper from the ore, solvent extraction to purify and concentrate the copper solution generated by leaching and electrowinning to plate the copper metal into cathode sheet form. Mine reclamation is the process of restoring land that has been mined to a natural or economically usable state. Although the process of mine reclamation occurs once mining is completed, the planning of mine reclamation activities occurs prior to a mine being permitted or started. Electrowinning (EW) process is an environmental friendly way to economically produced high-grade copper from low-grade ore deposit. Kyisintaung and Sabetaung Mines adhere to a strict zero discharge operation and all solution flows are re-circulated to ensure that no effluence is discharged from the mine to outside of lease area. Letpadaung mine produces cathode copper that complies with Landon Market Exchange (LME) Grade-A rating and is more than 99.99% in purity. Therefore, using of Electrowinning (EW) method is slightly better than the other methods.

Introduction

The Monywa Copper District is located 115 km west of the township of Mandalay on the Western side of the Chindwin River Flood plain. Four major copper deposits (Letpadaung, Kyisintaung, Sabetaung and Sabetaung South) occur within an area of 20 square kilometers. Letpadaung and Kyisintaung mines are present production stage, but Sabetaung and Sabetaung South mines are already extracted. There are four major high sulfidation deposits of Miocene age.

Following exploration drilling which began in 1959, production of copper concentrates from a small open pit started at Sabetaung in 1983. Since 1997, when resources total 7 million tons contained copper in 2 billion tons ore. Using leach electro-winning operation, the project has produced over 400,000 t copper cathode from Sabetaung and Sabetaung South.

The district is on the northern margin of Myanmar's dry zone. Most mineralization is structurally-controlled with chalcocite in breccia dykes, in steeply dipping NE-trending sheeted veins, and the Cu grade pipe at Sabetaung is up to 30%.

The highest grade ore at the top of the supergene enrichment zone, within which copper grade, supergene kaolinite and cubic alunite decrease and pyrite increases with depth, in contrast, marcasite (use in jewelry) is mostly occur in shallow depth. Letpadaung and Kyisin hill rise to 322 m and 304 m respectively, Sabetaung was a 180 m hill prior to mining and Sabetaung South was a low rise.

Location

The research area is situated at the West of Chindwin River, Salingyi Township of Sagaing Region. It is about 115 km Northwest of Mandalay and about 30km Southwest of

* Dr, Associate Professor, Applied Geology Department

Monywa. It lies between North Latitude $22^{\circ}03' 1''$ to $22^{\circ}08' 57''$ and East Longitude $95^{\circ}02' 13''$ to $95^{\circ}07' 28''$. The research area refers to the one inch topographic map of 84 N/4.

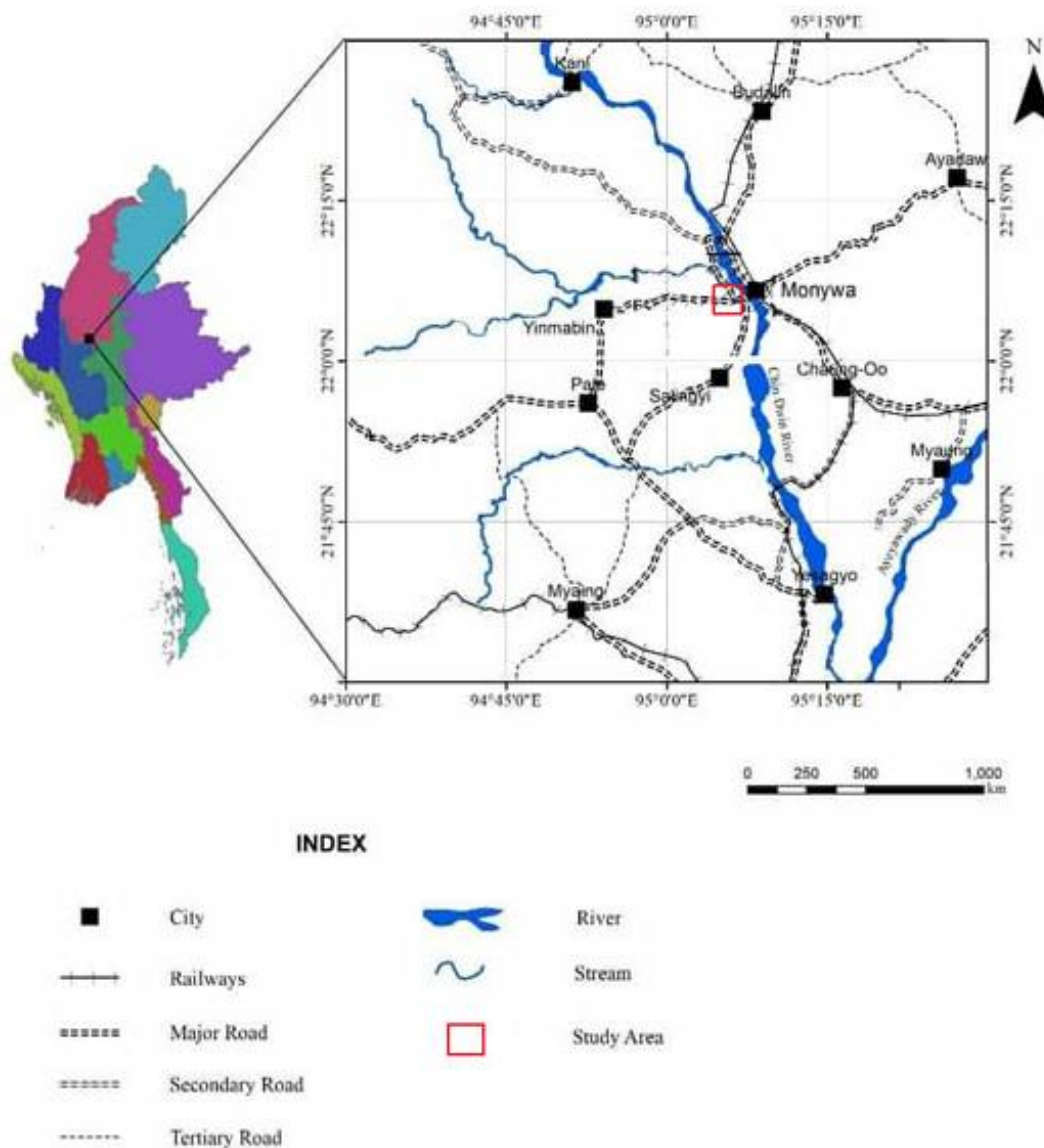


Figure 1 Location map of the study area

Topography and Drainage

The Research area lies within Monywa Copper district as a part in Salingyi Township, Sagaing Region. Sabetaung, Sabetaung South and Kyisintaung are continuous while Letpadaung lies 7 km far from the Southeast of Kyisintaung range. The highest mountains are Letpadaung (about 0.33km), Kyisintaung (about 0.31km) and Sabetaung (about 0.18km) are the dome shaped hills heaped up on the flat land. Elevation in the mine area reported as above sea level 500 m.

There is a Yama Chaung in the northern part of the research area. This stream is a major tributary to the Chindwin river and flows from West to East. The drainage density is generally coarse. The stream and their tributaries show mainly dendritic patterns. In some area radial pattern are noted.

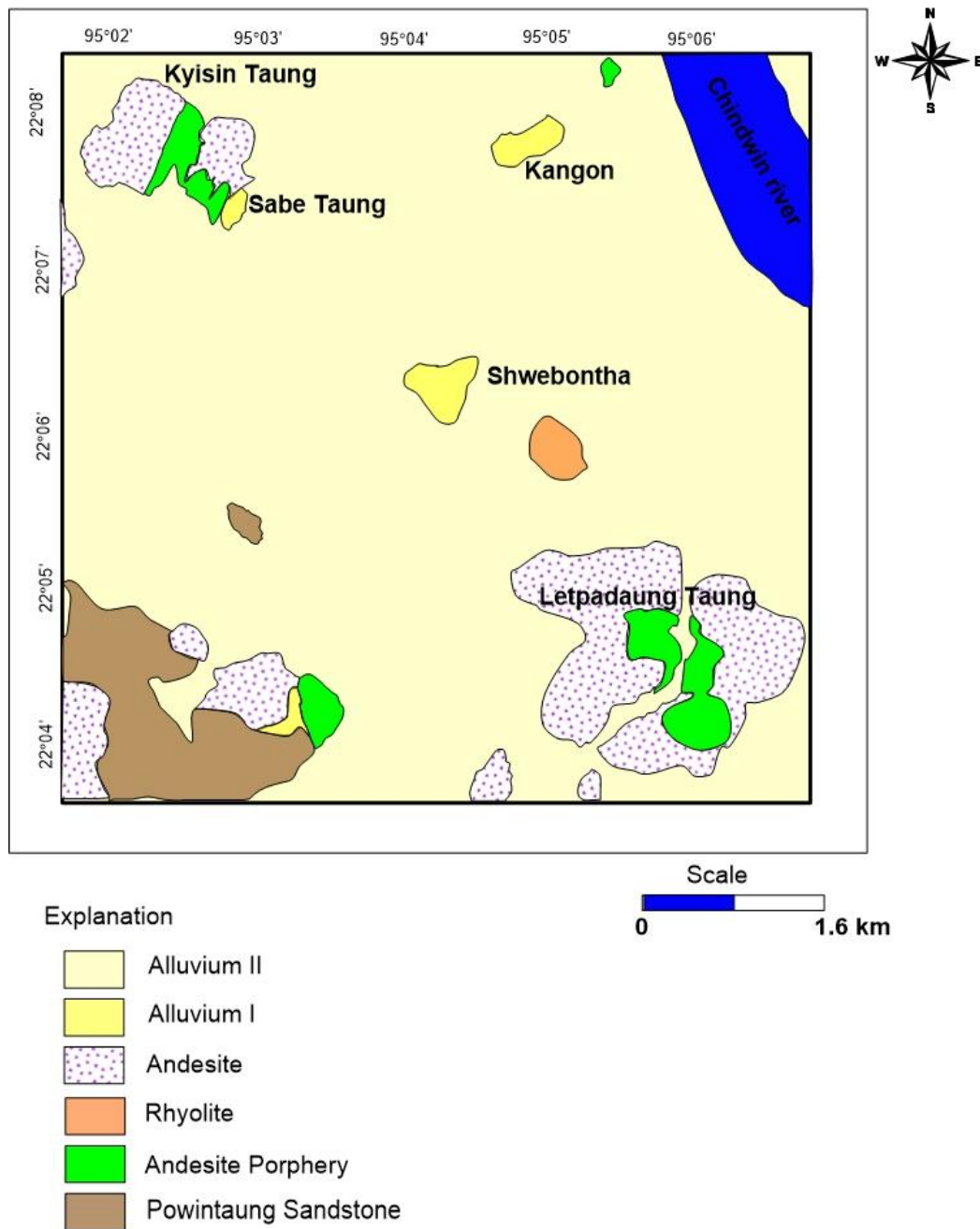


Figure 2 Geological map of Monywa Copper area

Rock Sequence of the Research Area

Monywa high sulphidation Copper deposit occurs in Magyigon Formation, unconformably rest on Salingyi basement complex of Cretaceous age and does not crop out in the mine area. In this area, sedimentary rocks are intruded by igneous rocks. The oldest rocks in the mine area are pillow basalts, basalts, flow breccias, granite, gabbros and granodiorite which are Mesozoic age.

The Miocene age of the Magyigone Formation and Powintaung Formation are intruded by andesite porphyries of both pre-mineralization and post-mineralization.

Rock sequence of the research area (After Mitchell, 2011)**Sedimentary Rock**

QUATERNARY	Alluvium
PLIOCENE	(Kangon Sands & Kanthit Gravels)
	Sandstone-Shale
	Cross Bedded and Massive Coarse Sandstone
MIDDLE MIOCENE	Magyigon Formation
	Powintaung SSTS
LOWER MIOCENE	Minzu East Conglomerate
	Igneous Rock
UPPER PLIOCENE	Basalt and Olivine Basalt
MIDDLE MIOCENE	Andesite Porphyry Pre-mineralization & Post Mineralization
MESOZOIC	Pillow Basalts, Basalts flow Breccia, Granite, Gabbros, Granodiorite

Distribution of Rock Unit**Sedimentary rock****Powintaung Formation**

The oldest rock in the mine area is chiefly sandstone of Eocene to Lower Miocene age. The Damapala Formation described in the Japanese report is considered to be the upper most member of this formation. The sandstone is composed chiefly of well-sorted sub-rounded to rounded, translucent to transparent quartz fragments, commonly cemented by clay and carbonate. Bedding nature is noted in many places. The thickness is 300m (Bender 1983).

Magyigon Formation

The Magyigon formation lies conformably over the Powintaung formation. It consists of sandstone, clasts of dacite, andesite porphyries, quartz and various pyroclastics units. The pyroclastic units are dominantly crystal-rich, lithic-tuffs of dacitic composition. The age of this formation is Upper Miocene to Pliocene.

Kangon Formation

The Pleistocene Quaternary rocks (Kangon Formation) can be divided into two members, the Lower member of poorly consolidated to essentially unconsolidated sands and gravels. The Upper is unconsolidated mud, which are cemented with porous calcium carbonated.

Igneous rock

Pre-mineral Andesite and Dacite Porphyry

It occurs as a stock forming the core of Kyisintaung hills and dykes of stocks at Letpadaung. The Andesite Porphyry has phenocryst population composed of 10-30 percent plagioclase feldspars, minor quartz and rare alkali feldspar. Where quartz phenocrysts and alkali feldspar content are visible, is called Dacite. This unit is the major host rock to hypogene and supergene copper mineralization.



Figure 3 Small dykes of Pre-Mineral andesite porphyry in Letpadaung

Post-mineral Andesite and Dacite Porphyry

It has a composition similar to the Pre-mineral Andesite Porphyry, more abundance of large fresh Biotite and Hornblende.



Figure 4 Whitish coloured Post-Mineral andesite porphyry in Letpadaung mine area

Pyroclastic rocks

They called Mine Pyroclastics units is the second most abundant rock types at Sabetaung and Kyinsintaung project area. These rocks are common next to andesite porphyry at the Monywa Copper District.

Hydrothermal breccia

It is the most important rock type for its association with copper mineralization. It occurs as dykes and cut the pre-mineral rocks. The breccia clasts are varied from angular to well-rounded mineralized andesite/dacite porphyry clasts. Among the northern corner of the Letpadaung, a number of phretomagmatic breccia zones occur.

Ore Mineralogy

Alunite ($\text{KAl}_3(\text{SO}_4)_2(\text{OH})_6$)

Alunite is occurred in Silica Alunite Zone that as pervasive replacement of the host rock groundmass by silica and complete alunitization of plagioclase feldspar. Alunite replacing the feldspars generally occurs as bright pink, translucent crystal. It widely occurs at Letpataung Taung mine area. Associated minerals are pyrite and gangue minerals. It widely occurs at LetpataungTaung mine area. Associated minerals are pyrite and gangue minerals.

Hematite (Fe_2O_3)

Hematite has variable color and lustre depending on its habit. It has a trigonal crystal system. It ranges from metallic lustre and steel or silvery grey to black color. All forms of hematite have a characteristic reddish-brown streak. Hematite is the most important ore of iron and is also a common alteration mineral.

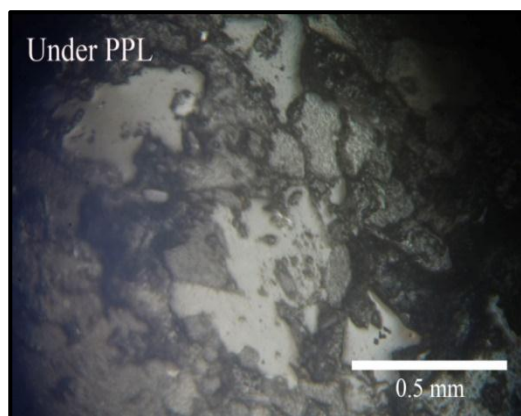


Figure 5 Photomicrograph showing alunite in andesites

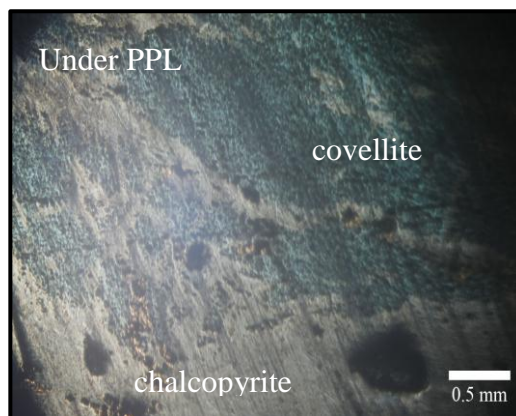


Figure 6 Photomicrograph showing covellite in andesites

Brochantite ($\text{Cu}_4\text{SO}_4\text{OH}_6$)

Brochantite has monoclinic system. It is associated with malachite, azurite and cuprite. It shows slight in shades of bluish green. It has vitreous lustre, sometime pearly. It can be prismatic or acicular needle-like crystals. Pleochroism of brochantite is weak. Commonly associated mineral is pyrite.

Covellite(Cu S)

Covellite has a characteristic deep indigo-blue color. It has a dark grey to black streak, a micaceous cleavage, and is very soft. covellite is a common supergene mineral associated with porphyry copper deposits.

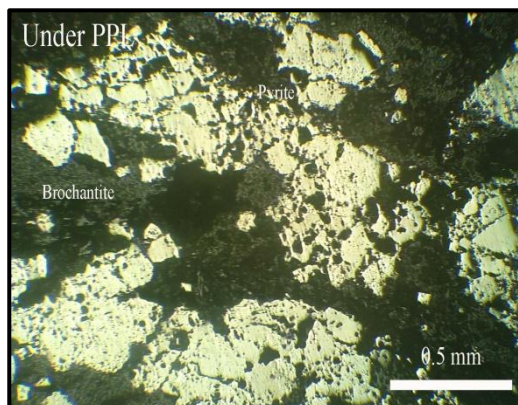


Figure 7 Photomicrograph showing brochantite in pyroclastic rock

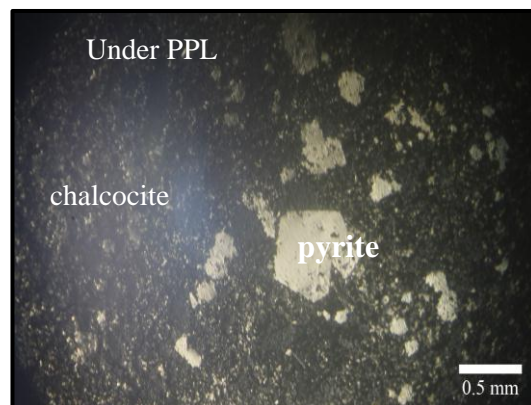


Figure 8 Photomicrograph showing chalcocite in andesite

Enargite($\text{Cu}_3 \text{As S}_4$)

Enargite is a copper arsenic sulfide mineral. It has grayish black to black colour. Enargites are intimately intergrowth with pyrite, chalcopyrite, and covellite.

Chalcocite ($\text{Cu}_2 \text{S}$)

Chalcocite is usually subhedral. It shows light grey colour, metallic lustre, indistinct cleavage and coarse grained. The high copper content makes chalcocite an important copper ore. (Primary) Hypogene of chalcocite has metallic lustre and massive in nature. Supergene chalcocite is fine grained and commonly appears sooty in polished section.

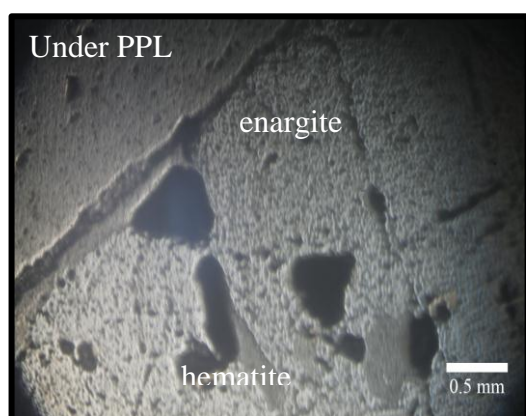


Figure 9 Photomicrograph showing enargite in andesite

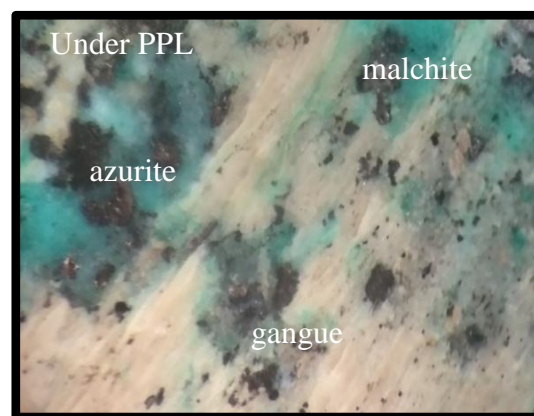


Figure 10 Photomicrograph showing azurite in andesite

Supergene High Grade Ore (Chalcocite)

Chalcocites are regarded as supergene high grade ore. It has two kinds of Primary (Hypogene) and Secondary (Supergene) zones. It is mainly occurred in Sabetaung mine area.

Azurite ($\text{Cu}_3 (\text{CO}_3)_3 (\text{OH})_2$)

The color of Azurite is blue and lighter blue streak are distinctive. The lustre is vitreous to dull depending on crystal habit. In polished section, it is grey and has strong anisotropism. Azurite occurs as less fibrous and thicker aggregates than malachite.

Malachite ($\text{Cu}_2 \text{CO}_3 (\text{OH})_2$)

The mineral occurs in association with one or many other copper minerals, such as native copper, chalcopyrite and azurite. Typically, it occurs as crystalline aggregates and commonly growth-zoned.

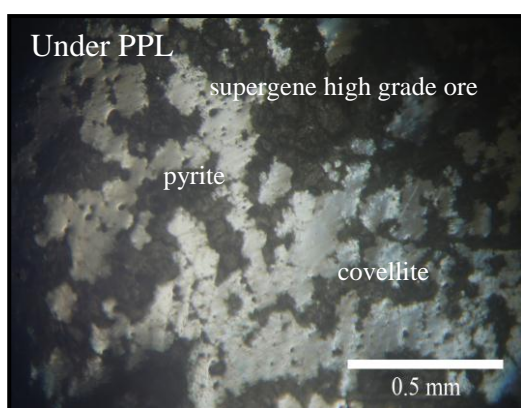


Figure 11 Photomicrograph showing Supergene high grade ore in andesite.

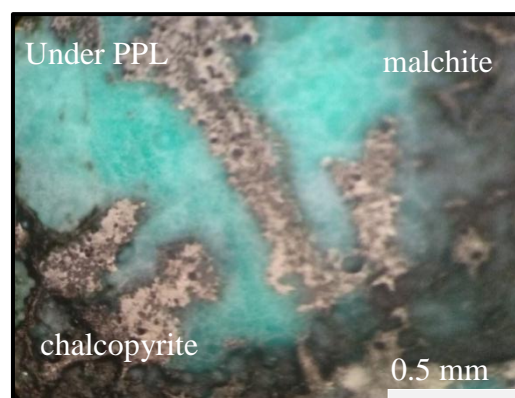


Figure 12 Photomicrograph showing malachite in andesite

Copper mineral processing of Monywa Cu Mine

Copper processing is a complicated process that begins with mining of the ore (less than 1% copper) and ends with sheets of 99.99% pure copper.

Crushing

In the research area, the processing of Letpadaungtaung mine is start to crushing. Primary crushers and the coarse ore bins may be located at the mine, where the mine and mill operation are separated. Primary crusher can crush 12000 tonnage per one hour. Secondary crushers and the fine ore bins are usually at the mill, along with blending or custom facilities where more than one kind of ore is mined or received. The fine ore is ground in ball or rod mills to a size small enough to liberate the ore minerals, then classified in various kinds of machines of machines to insure that the feed to the mill is uniform.

Heap leaching

The method is similar to the leaching method, except sulphuric acid is used to dissolve copper from its ores. The acid is recycled from the solvent extraction circuit and reused on the leach pad.

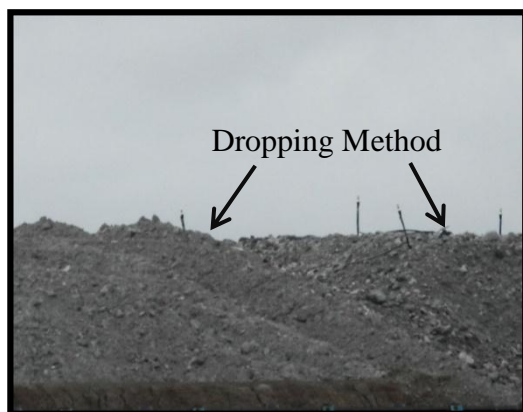


Figure 13 Heap is leaching by dropping methods

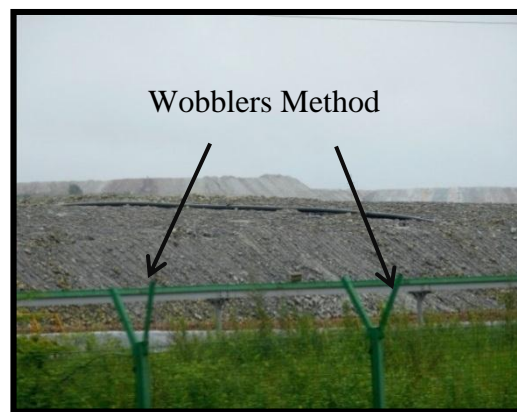


Figure 14 Heap is leaching by wobblers methods

Solvent extraction

The leach liquor is pumped from the leaching circuit through polishing filters into the extraction section of the solvent extraction plant. The extraction section of the solvent extraction plant consists of a number of mixer-settlers in series.

Electrowinning and final product

Electrowinning is the electrodeposition of metals from their ores that referred to as leaching. The electrowinning of copper is an electrolytic process that uses electricity to recover dissolved copper from solution as copper plate, also known as “cathode”. The process of electrorefining copper involves an impure copper anode and an inert cathode. An electric current is applied across the anode and cathode which causes the copper to dissolve from the anode to be then plated onto the cathode as pure copper metal.



Figure 15 Tank House for electro winning Process



Figure 16 Extracted copper plate from Tank House

Conclusions

The study area lies within Monywa Copper district as a part in Salingyi Township, Sagaing Region. Four major copper deposits (Letpadaung, Kyisintaung, Sabetaung and Sabetaung South) occur within an area of 20 square kilometers.

Letpadaung and Kyisintaung mines are present production stage, but Sabetaung and Sabetaung South mines are already extracted. Monywa copper deposits occur in Magyigon Formation with the age of Middle Miocene age. It is mainly composed of sandstone, rhyolite, dacite and andesite, pyroclastic rocks and hydrothermal breccia dykes. The ore mineral assemblages in the study area are alunite, hematite, brochantite, covellite, enargite, chalcocite and supergene high grade ore.

In copper processing, many kinds of applicable methods are using in the world depend on the ore genesis, relationship of host rock and morphology of ore occurrences, local environmental regulations and other factors. Among of these methods, the electrowinning process is used in Monywa copper mine area. Solvent Extraction to purify and concentrate the copper solution is generated by leaching and Electrowinning to plate the copper metal into cathode sheet form.

Electrowinning (EW) process is an environmentally friendly way to economically produce high-grade copper from low-grade ore deposits. Monywa Cu mine adheres to a strict zero discharge operation and all solution flows are

re-circulated to ensure that no effluence is discharged from the mine to outside of lease area. These mines produce cathode copper that complies with Landon Market Exchange (LME) Grade-A rating and is more than 99.99% in purity. Therefore, using of Electrowinning (EW) method is better than other methods for Cu mineral processing.

Acknowledgements

I am greatly indebted to Professor Dr. Day Wa Aung, Head of the Geology Department, University of Yangon, for his permissions to carry out present research area and for his encouragement, suggestions and valuable guidance. I also would like to express thanks to Dr. Myat Thuzar Soe, Professor/Director of Applied Geology Department for her constructive criticisms, discussions and suggestions of my research paper. I would like to thank Professors and Teachers who give patiently advises for my research Area.

I also would like to thank U Myo Htut Lwin (Coloss, Assistant General Manager) and U Win Pyae Phyto Paing (General Manager), and U Tun Thar Zan (Head of MoekyoSulphuric Acid Industry)

I also thank U Aung Zayra and U Myo Thet Paing (ISO officer), U Maung Oo (Head Field Geologist), U Soe Win (Mine Engineer, Disaster Safety Department) and U Nyi Naing Aung (Grade Control Geologist) from Myanmar-Yang Tse Company Limited at Sabetaung and Kyisintaung Mine in Monywa Copper District.

References

- Aye Khaing, (2018): "Geology and Lead Mineralization of Theingon Area, Ywangan Township, Shan State (South)" *Msc Thesis, Department of Geology, University of Yangon, Myanmar.*
- Andrew H.G. Mitchell (2010): "The Society of Resource Geology"
- Chhibber, H. L., (1934): "Geology of Burma. London, Macmillan"
- Dr. Mitchell, Win Myint, Kyi Lynn, MyintTheinHtay, Maw Oo & TheinZaw (2010): Geology of the High Sulfidation Copper Deposits, Monywa Mine, Myanmar.
- Feebrey, C. (2001): Geologic setting of the Monywa Copper District and characteristics of copper mineralization, Central Myanmar. Reported by Metal Mining Agency of Japan (MMAJ).
- Greenwood, P. G. & Tombs, I. H. (1975): "Geophysical surveys for copper deposits in the Monywa area"

Journal and Newspaper of Wanbao and Yang Tse Company LTD. (2010-2015).

Japanese Overseas Technical Cooperation Agency (1973), (1974): "Report on geological survey of the Monywa Area"

Khin Zaw, Ye Myint Swe, Tin Aung Myint & J. Knight (2017): "Copper deposits of Myanmar"

Knight, J & Khin Zaw (2015): "The geochemical and geochronological framework of the Monywa high sulfidation Cu and low sulfidation Au-epithermal deposits, Myanmar"

Kyaw Win & Kirwin, D (1998): Exploration, geology and mineralization of the Monywa copper deposits, central Myanmar.

Khin Khin Win (1974) : Distribution of some elements in Sabetaung copper deposit, Salingyi Township : Research paper, Geo.Sci.

Leach, T (1996): Report on Monywa Copper Deposits. Report for Ivanhoe Myanmar Holding Limited (IMHL) Company.

Mitchell (2010) : "Geology of the Monywa Copper District"

Manaka & Khin Zaw unpublished data (2012): Monywa Copper Deposits Area, Myanmar.

Mitchell (2011): "Regional geologic and tectonic setting of Monywa copper deposits"

Maung Maung Khin (1970): "Geology and Copper Deposit of Sabetaung in Monywa District"

Maung Maung Naing (2008): "Monywa Copper Deposits" Soe Win (2015): "Mineral Resources and Mines of Myanmar, Copper Unpublished Report"

ORIGIN OF IRON ORE DEPOSITS IN MAYMYO FORMATION EXPOSED AROUND BAW VILLAGE, PYIN OOLWIN TOWNSHIP, MANDALAY REGION, MYANMAR

Tin Aung Myint¹ & Mi Mi Ko²

Abstract

Iron ore deposits are located around Baw village (N Latitude 21° 53'96" and E Longitude 96° 32'08"), Mandalay region, Myanmar. It lies in the western margin of the Shan Plateau within Sibumasu Terrane. Rock units exposed in the area are Paleozoic rocks including Nyaungbaw Formation (Silurian age), Zebingyi Formation (early to middle Devonian age) and Maymyo Formation (middle Devonian to Permian age). Iron ores are mainly limonite and hematite with minor amounts of pyrite and magnetite. The deposit mainly forms in Maymyo Formation. Ore deposit entirely overlies on dolomite and sandstone of Maymyo Formation. Large ore boulders may reach about 15 cubic meters in size. Small nodular, concretionary iron ore and float ore also occur. In some places, these iron ores are embedded in reddish brown ferruginous sandy soil and sandy loam layers. Based on the result of borehole data, ore boulders decrease in size from south to north. This is because the fault that separates the two blocks, impounds oxidizing water and enriches iron in the hanging wall block (south), causing more concentration and thickening of the iron deposits. The occurrences of micro fossils (forams?) and ooids which are entirely or partially replaced by interlayered hematite indicate that the iron deposit is primarily of sedimentary origin probably formed at the end of Paleozoic time (Tin Aung Myint, 2002). The porous and soluble nature of Maymyo Formation is the favorable place for the formation of iron deposits on Shan Plateau. Besides, chemical weathering processes leached dolomite and calcite minerals from earlier formed iron deposit, causing the increasing of iron grade in the ore as well as removing of gangue minerals from the ore in order to form the ferric iron oxides as secondary residues that are found sporadically around Baw village. Jordan et al., (2017) dated the zircon U-Pb ages of 399 Ma, for a limestone near Pyinoolwin which suggests that the age is consistent with fossil ages of the Middle Devonian Maymyo Formation. The relativity plots of the zircons suggest that the provenance has a Gondwana affinity, as the peaks of the zircons confirm the affinity with the Sibumasu Terrane.

Keywords: iron ore deposits, Maymyo Formation, Gondwana affinity, Sibumasu Terrane

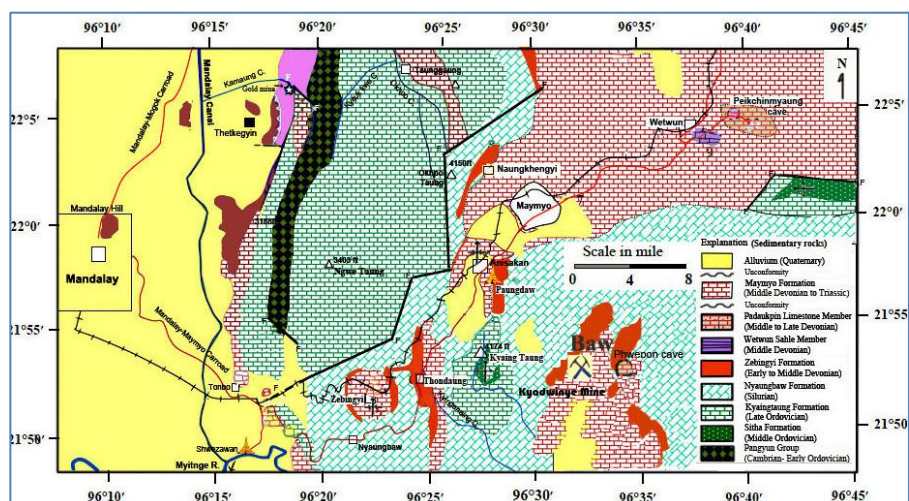
Introduction

Location

Iron is one of the most abundant elements in the earth's crust and few rocks are iron-free (Pettijohn, 1974). The study area is situated about 12.4 miles (20 km) south of the Pyinoolwin town. It falls in the one-inch topographic map 93C/9. The area is readily accessible in all weather.

¹ Dr, Associate Professor, Department of Geology, University of Mandalay

² Associate Professor, Department of Geology, Loikaw University



Source: Aye KoAung&Kyaw Min, 2011; Khaing Khaing San, 2005; Khin Maung Shwe, 1973; Myint Oo, 1997; Win WinKy; 1990, Tin AungMyint, 2002; 2013; &Zaw Min Thein, 1995)(*Compiled by Tin AungMyint, 2014*)

Figure 1 Location and regional geological map between Mandalay and Maymyo (PyinOoLwin) area.

Regional Geologic Setting

Iron ore deposits around Baw village lies in the western margin of the Shan Plateau (Shan-Thai Block) within Sibumasu Terrane. The Shan- Thai Block lies to the east of the west Myanmar Terrane (aks Myanmar Plate) separated by the well-known Sagaing Fault of Win Shwe (1971). These two blocks are also separated by the "Shan Scarp Fault" or "Boundary Fault". The Shan Scarp fault runs along the western margin of the Shan Plateau and the structural features in the study area are related to this regional fault. The basement of the plateau is composed of Chaung Magyi Group of Proterozoic age. On the west of the boundary fault, the metamorphic rocks of the Mogok Belt (Searle and Haq, 1964) and some granitic intrusions are exposed. The Paleozoic sediments are exposed repeatedly in the Zebingyi, Thondaung, Kyaing Taung, Aniskan and Baw villages (Fig. 1). The study area lies mostly in the Pyintha-Aniskan plain. The strata exposed in the present study area form a south-west-dipping homocline which itself is the eastern limb of the Kyaingtaung anticline.

Method of Study

Detailed geological study of the area, classification of rock units and the occurrences of the iron deposits were carried out during the course of field study. Detailed geological data on dip and strike of the lithologic units, attitude of joints and other structural elements were measured and recorded for structural interpretation. Tape-and-compass method and bore hole data are employed to determine the thickness of iron ore deposits, the nature of deposit types and the exposed rock units in the study area. The representative ore and rock samples were taken from each bore-hole and test-pit. The collected samples were analyzed by using PXRF. Photographs and sketches were taken for some significant features.

Result

In the study area, the regional strike generally runs north-south, parallel to the regional topographic trend. It represents the eastern limb of a major anticline (Kyaingtaung anticline see Fig. 1) whose anticlinal crest is located about six miles to the west of the study area. The detailed geological map of the study area is shown in Fig. (2). Rock units are as follows.

Lithostratigraphic Units	Geologic Age
Alluvium	Quaternary
<i>Unconformity</i>	
Maymyo Formation	Mid-Devonian to Permian
Zebingyi Formation	Early to Middle Devonian
Nyaungbaw Formation	Silurian

Iron Ore Deposits at Baw and Its Environs

At Baw and around it, iron ore occurs entirely in Maymyo Formation. At least 9 iron ore deposits of considerable sizes other than Kyadwinye deposit can be recognized in the study area. These iron ore deposits are Kyadwinye deposit, Kyaukphyagyaw (G.058534), Thegon (G.065519), Pongon(East) (G.099554), Nattawtaung (G.107558), Sintheka Taung (G.112564), Nattawlay Taung (G.124575), Pawpyin (NE) (G.106570), Baw(S) (G.091514), and Kyadwinye(S) (G.069529), respectively. Among them, Kyadwinye and Kyaukphyagyaw deposits contain high iron content (50%-60% Fe). Moreover, numerous small scale iron occurrences which are economically unfeasible are found throughout the area.

Iron Ore Deposit at Kyadwinye

Kyadwinye mine is located at latitude 21° 51'N and longitude 96° 32' 20"E. In Kyadwinye, the iron deposit occurs on the Main hill (Foot wall) (3498') and mine site in lower hill (Hanging Wall) separated by Kyadwinye fault. The area coverage is about 6725640 square feet (624811.9 sq.m.). Iron ore map (Fig. 3a), cross sections and bore hole profiles (Fig.3 b & c) are shown respectively.

The thickness of iron deposit on the Main hill is only 12.8' (4m) thick. However, at the mine, the iron ore deposit is much thicker, reaching up to 70' (22m) in thickness. Field investigation shows that the mine is situated on the down thrown side of the fault. This normal fault is thought to be formed before the deposit because ore body in lower hill is much thicker than the Main hill and there is no evidence that this fault separates the ore body.

In Kyadwinye, the iron ore deposit comprises limonite and hematite with minor amount of pyrite and magnetite found in dolomite and sandstone of Maymyo Formation. The bore-hole data indicates gradual increase of limonite content with depth. This is because limonite contains hydroxide and the nearer the water table, the more limonite content increases.

The surface of the ground shows scattered light brown ferruginous gravel and larger pieces of iron ores. Iron ore occurs in different forms: as boulders, nodular masses, gravels or floats Fig. (4 a-d). The sizes of the ore boulders decrease from south to north. The biggest one is reaching up to 15 cubic meters (530cubic feet). Iron ores are not cemented together nor very firmly embedded in the sandy loam which surrounds them; neither do they form a continuous layer. Some ore boulders show dendritic tubes filled with silt resembling worm burrow tubes Fig. (4b).

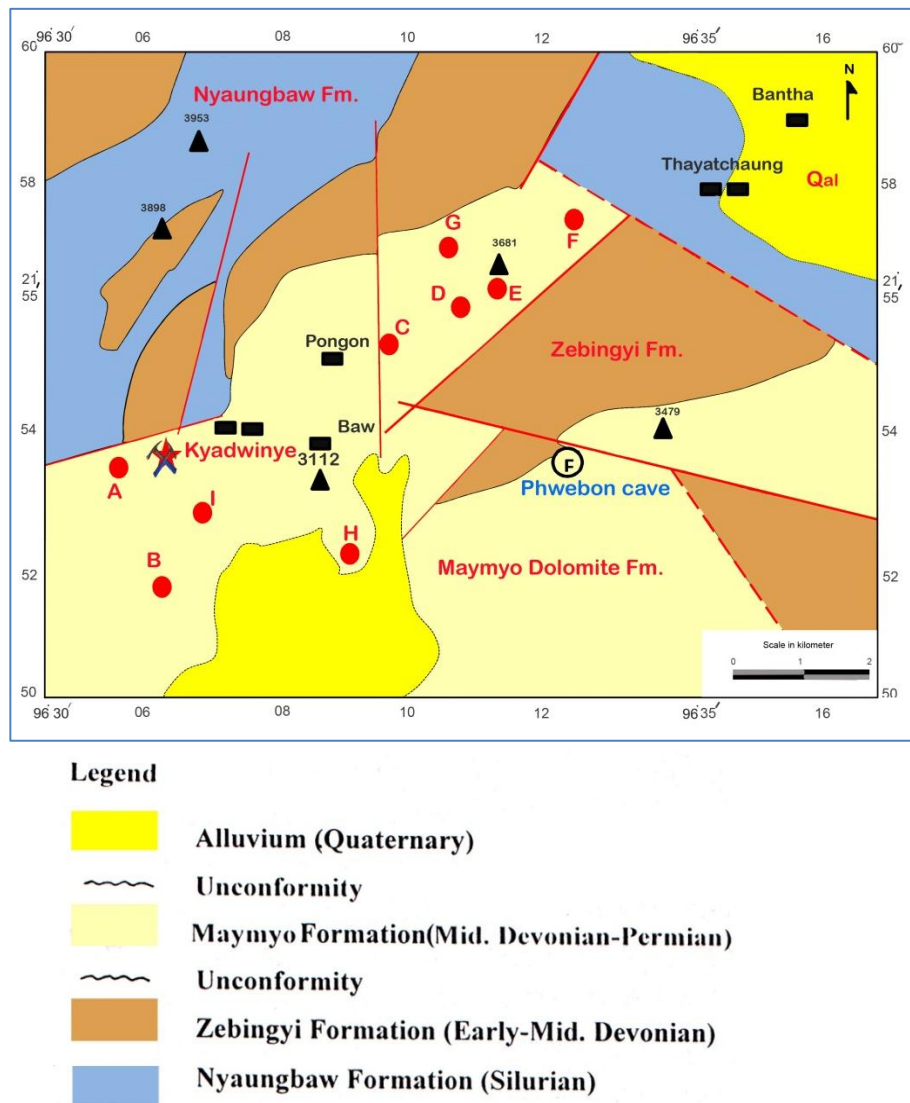


Figure 2 Geological map of the Baw area (Win WinKy, 1990 & Tin AungMyint, 2002)

Field investigation shows that the thickness of the ore body in the lower hill is from 1.6' (0.5m) to 70' (22m). Although the iron ore deposit is nearly parallel to the bedding planes of the underlying rocks, the iron ore in bedding is hardly noticeable. The boundary between the iron ore body and Maymyo Formation is undulatory mostly (Fig.4 d). Thus, the iron ore occurs as filling in the cavities and hollows in Maymyo Formation. This fact points out that iron ore deposit unconformably overlies on Maymyo Formation.

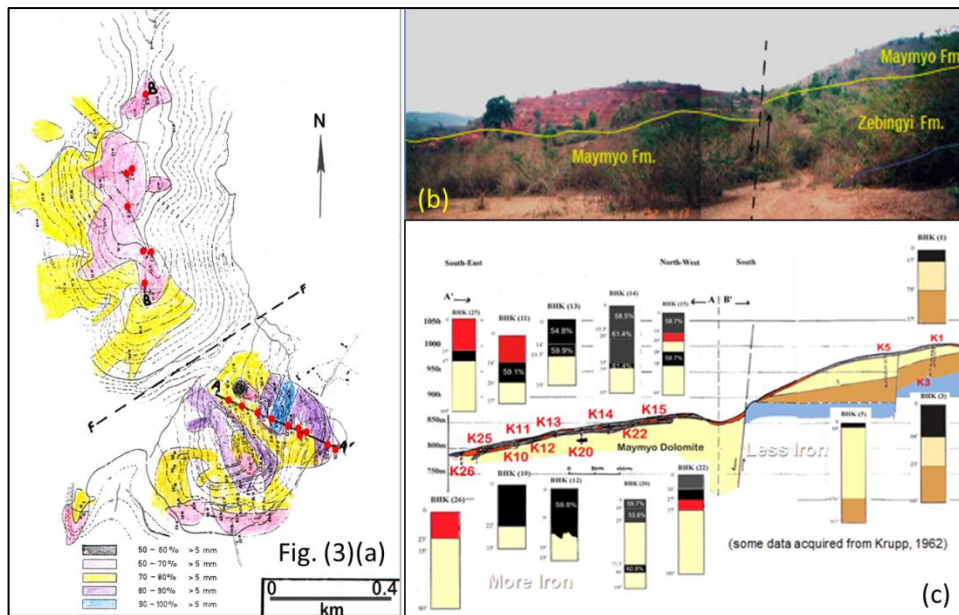


Figure 3 (a) Iron ore and bore hole location map, (b) Panoramic view of the mine area and (c) cross section passing through the Bore holes of (Fig. a) with their Fe content. (Tin Aung Myint, 2002) (some data acquired from Krupp, 1961-1962)

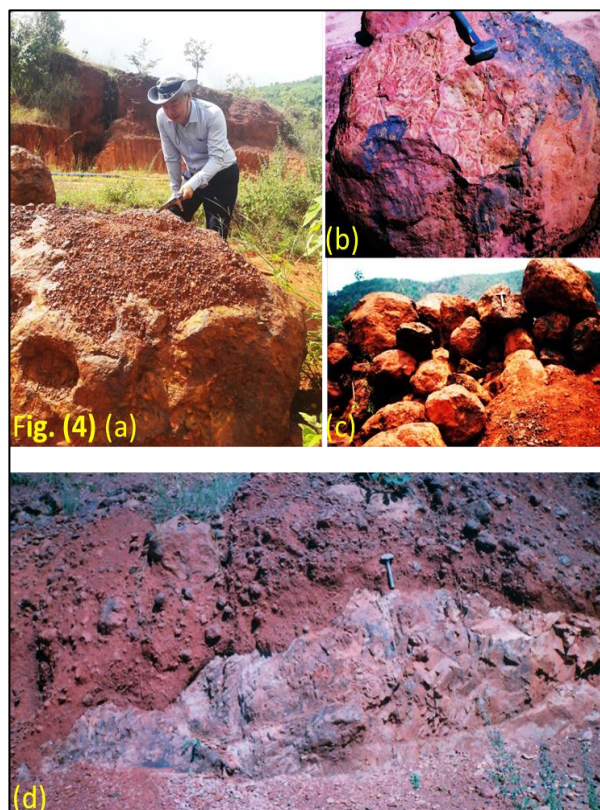


Figure 4 (a) Large ore boulder in mine, (b) Dendritic pattern like tubes filled with sandy silt in the area, (c) Various sizes of iron ores and (d) Iron gravels mixed with loam on Maymyo Formation.

The ore is trucked to the No.1 Iron and Steel Plant at Aniskan located about 16 km west of Pyinoolwin. The plant produces pig iron, steel billet, rounded bars and steel grinding balls (Soe Win, 1994). Although Krupp and BGD (1961-62) gave a reserve of 3 million tons, the estimated iron ore reserve is less than 2 million tons with average iron content of 58.5% (Tin Aung Myint & Mi Mi Ko, 2004).

Other Iron Ore occurrences around Baw

Around Baw, iron ore deposits unconformably overlies on the Maymyo Formation. These deposits are embedded in ferruginous sandy soil layer and sandy loam layer. The localities of iron occurrences and their detailed descriptions are shown in Fig (2) & Table (1).

There are altogether 9 occurrences that contain iron content of 21.33% to 61.38%. Thus, it can be correctly interpreted that Kyaukphyagyaw will be another alternative mining site of iron ore when the Kyadwinye Mine is exhausted.

Table 1 Ore Reserve and chemical analyses of small iron ore occurrences around Baw

No	Code	Work Site	Area (Sq.m)	Thickness (m)	Mineral Percent			Sp.Gr.	Category	Ore Reserve	
					FeO%	SiO ₂ %	Al ₂ O ₃ %			Total	>5mm
1	A	Kyaukphyagyaw (G.058534)	38100	0.9	61.38	1.27	8.66	4.18	P ₃	11000	9000
2	B	Thegon (G. 065519)	134112	1.2	39.03	26.51	12.72	3.12	P ₃	40800	34500
3	C	Pongon (East) (G.099554)	51816	1.8	26.10	45.71	12.43	3.47	P ₄	33800	26400
4	D	Nattawtaung (G.107558)	36576	2.7	32.33	37.98	11.03	3.66	P ₄	22400	19600
5	E	Sinthekataung (G.112564)	32004	1.7	26.25	45.27	10.09	3.29	P ₄	15800	12200
6	F	Nattawlaytaung (G. 124575)	45750	1.5	29.15	39.80	13.57	3.86	P ₄	24600	24400
7	G	Pawpyin (Northeast) (G.106570)	28956	2.3	24.49	46.78	5.63	3.82	P ₄	24300	20400
8	H	Baw (South) (G.091514)	41148	1.2	21.33	46.81	11.88	3.40	P ₄	15500	13700
9	I	Kyadwinye (South) (G.069529)	16764	1.0	27.28	31.71	18.81	3.25	P ₄	5300	4600

(Source: DGSE, 2000 & Tin Aung Myint, 2002)

Discussion

Origin

Mineral Paragenesis and Texture

Ore microscopic study reveals the most probable mineral paragenesis of iron ore at Baw. As shown in Fig (5) pyrite (white) is replaced by limonite (grey). Replacement is the result of a surface chemical reaction, hence, any channel between grains or through grain is a prime site for initiation of the replacement process (Craig and Vaughan, 1981). In the early stages of the process, replacement may be readily identified because much of the original phase (pyrite) remains and the original grain boundaries and fractures are still visible. Therefore, this appears to suggest that pyrite formed earlier than limonite and hence, limonite is thought to be considered as secondary replacement mineral. The resulting boundary between the replaced (pyrite) and the replacing mineral (limonite) is commonly sharp and irregular (corroded texture). The replacement features in which pyrite has been pseudomorphed by dense limonite (grey) and boxwork hematite (white). The open void 'boxwork' texture is essentially composed of cellular crisscross laths of hematite, showing the evidence of replacement. Judging upon these replacement textures, the most priority is pyrite, and second phase is not only hematite but also limonite. Therefore, it is also important to note that iron ore deposit in Kyadwinye may have more than ore paragenetic position.

Deposit Styles and Types

Field investigation shows that iron ore unconformable overlies on the Maymyo Formation and it is nearly parallel to the underlying beds. Peloids and some distorted oololiths occur in iron slide (see Fig. 5). Ooids and peloids are typically replaced by limonite and hematite. Some micro fossils (forams?) are also observed and partially replaced by hematite. It could be stated that iron ore in Baw was primarily sedimentary origin. Although the ores are found as sub-parallel to the bedding, they form rarely as layers. Despite them, the ores occur mostly as boulders and nodular masses. This is because the chemical weathering processes leached siliceous and carbonated minerals from the bedded iron deposit, resulting in an up grading of the iron content.

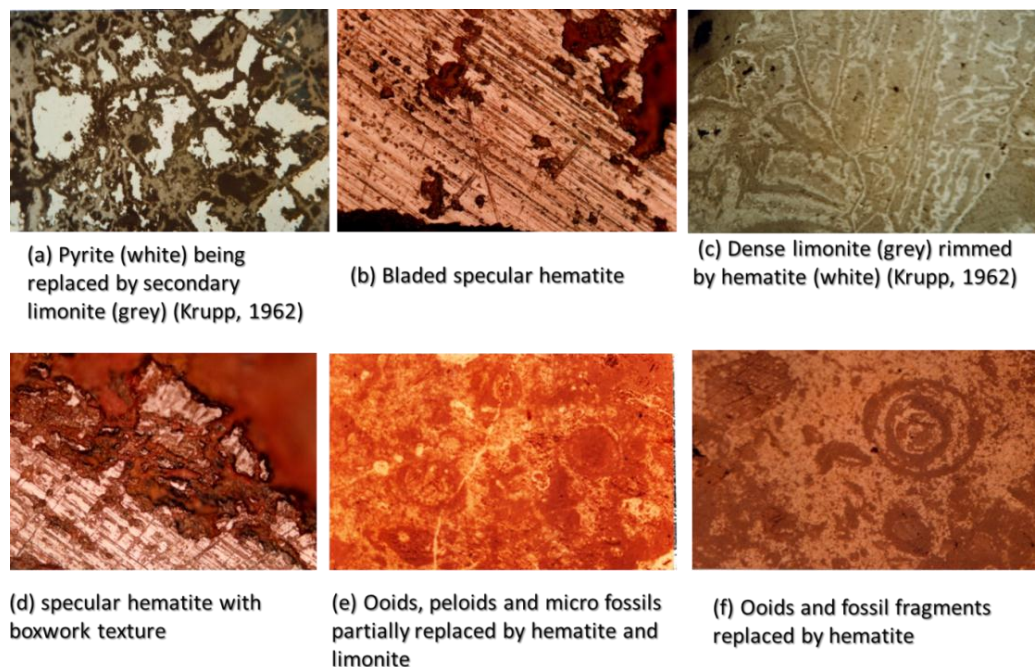


Figure 5 Some photomicrographs of iron ores in Maymyo Formation around Baw Village.

Geochronology

The Devonian is a period of Earth's history that went through radical change both physically and chemically. In this study, Laser Ablation Inductively Coupled Mass Spectrometry (LA-ICPMS) was used to determine detrital zircon ages within the black shales, sandy limestone and shaly limestone from the Lower Cambrian, Lower Ordovician and Middle Devonian and Middle to Upper Devonian in Myanmar together with scientists from Tasmania University, Australia. The zircon U-Pb ages for sample JS-18 which is a limestone, was aged at 399 Ma, which suggests that the age is consistent with fossil ages of the Middle Devonian Maymyo Formation. Sample JS – 22 is a sandstone from the Lower Ordovician Naungkhangyi group which was ages at $480.3 \text{ Ma} \pm 9.9 \text{ Ma}$. Sample JS-25 which is a black shale, is aged at $537 \text{ Ma} \pm 12 \text{ Ma}$ (Jordan Sheppard et al., 2017) (Fig. 6). This suggests the U-Pb zircon age of the rock to be from Lower Cambrian Ngwetaung Group. The relativity plots of the zircons suggest the provenance has a Gondwana affinity, as the peaks of the zircons confirm the affinity with the Sibumasu Terrane. This indicates both the source of the detrital zircons, and the source of the sediment

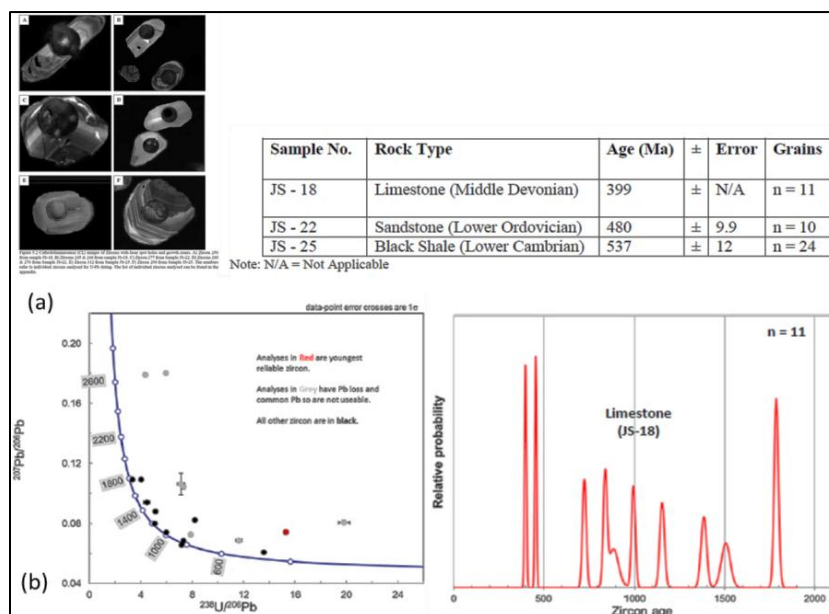


Figure 6: (a) Cathodoluminescence (CL) images of Zircons with laser spot holes and growth zones and (b) Concordia diagram and probability curves of ratios of $^{207}\text{Pb} / ^{206}\text{Pb}$ vs. $^{238}\text{U} / ^{206}\text{Pb}$ for sample A) JS-18 silty limestone from Middle Devonian Maymyo Formation. (Source: Jordan et al., 2017)

Summary and Conclusion

The study area is situated in Pyinoolwin Township, some 12.4 miles (20 km) south of the town. Baw is located at latitude $21^{\circ} 53'96''\text{N}$ and longitude $96^{\circ} 32'08''\text{E}$. It covers an area of approximately 40.8 sq. miles (106 sq. km). Actually, the present study area forms a south west dipping homocline which itself is the eastern limb of Kyaingtaung anticline located on the western margin of the Shan Plateau. Rock units exposed in the area are Paleozoic rocks including Nyaungbaw Formation (Silurian age), Zebingyi Formation (early to middle Devonian age) and Maymyo Formation (middle Devonian to Permian age).

Iron mineralization occurs mainly on dolomite and sandstone of Maymyo Formation. It is mainly composed of hematite and limonite with minor amounts of pyrite and magnetite. Iron ores occur in different forms as boulders, nodular masses, iron gravels and floats which are not cemented together or very firmly embedded in the sandy clay (loam) that surround them, neither do they form a continuous layer. The thickness of the iron deposit varies from 4 to 22 meters in mine site. Large ore boulders may reach about 529.7 cubic feet (15 cubic meters) in size. According to bore hole data, the size of the ore boulders decreases from south (lower hill) to north (Main hill). This is because the fault, that separates these two blocks, impounds oxidizing water and enriches iron in the hanging wall block, causing more concentration and thickening of the deposit. The deposit style is primarily of bedded sedimentary origin probably formed at the end of Paleozoic as the presence of micro fossils (forams?) and ooids which are entirely or partially replaced by interlayered hematite as the iron is essentially and completely precipitated as ferric oxide or may replace calcium carbonate shells or ooids. Moreover, readily soluble and porous natures of Maymyo Formation are the favorable site to concentrate the formerly formed bedded iron deposit. Therefore, the removal of soluble constituents and concentration of the insoluble ones must have been enormous. These conditions, limestone formation will be slowly

dissolved by chemical weathering, leaving the insoluble iron oxides as residue. As bed after bed of limestone disappears, the iron oxide of each bed persists. In this way, residual iron concentration was happened. The source was believed to be derived from the considerable iron ore in non-aluminous dolomite and ferruginous sandstone of the lower stratigraphic horizons of the plateau limestone. The origins of other iron occurrences around Baw are probably the same origin of Kyadwinye deposit.

Acknowledgements

We are deeply indebted to Rector, Dr Thida Win, University of Mandalay and Professor Dr Than Than Nu, Head of Geology Department, University of Mandalay for their kind permission and advice to publish in MAAS Journal. We wish to express our sincere gratitude to Professor Dr. Khin Maung Myint (Retired), Associate Professor Dr Than Zaw (who passed away many years but still in my mind) Department of Geology, University of Mandalay and Dr Soe Win, Professor emeritus (retired), Department of Geology, University of Yangon for their review, enthusiastic suggestions and helpful comments. This paper could not be completed without boundless helps from U Myint Kyi, Mine Manager, Kyadwinye Mine.

References

- Aye Ko Aung & Kyaw Min, (2011) Stratigraphy of the Lower Devonian sediments in the northwestern Shan Plateau, Myanmar, *Bulletin of the Geological Society of Malaysia* 57 (2011) 55 – 67, doi:10.7186/bgsm 2011008
- Craig, J. R. and Vaughan, D. J., (1981), *Ore Microscopy and Ore Petrography*. A Wiley_ Interscience Publication, New York.
- D. G. S. E. , (2000). *Report on Testing and Investigation of New Iron Ore Deposits around Kyadwinye, Pyin Oo Lwin Township, Mandalay Division*. D.G.S.E. Report (Unpublished) .
- Jordan Sheppard, KhinZaw, Charles Makoundi, Ross Large, Tin AungMyint, Sean Johnson,(2017), U-Pb Detrital Zircon and Pyrite Chemistry of Devonian Formations in Mandalay-Pyin Oo Lwin District, Myanmar: Implications for Ocean Chemistry, Gold Enrichment and Provenance of Sediments in Sibumasu Terrane. *MAESA, 2017 International Conference paper*, Novotel Hotel, Myanmar.p27
- Khaing Khaing San, (2005). *Middle Devonian Rugose Corals of the Padaukpin Limestone, Pyin Oo Lwin Township, Mandalay Division*, Ph D Thesis (unpublished) Geol. Dept., Mandalay University.
- Khin Maung Shwe, (1973). *Geology of the Sedaw-Taunggaung Area, Mandalay District*. M.Sc. Thesis (unpublished) University of Mandalay, 57 P.
- Krupp & B.G.D., (1961-62). *Iron Ore Deposit at Kyadwinye*. Unpublished report.
- Myint Oo, (1997). *Petrology and stratigraphy of the Zebingyi area, Pyin Oo Lwin Township* M.Sc thesis (unpublished), university of Mandalay.
- Myint Thein, (1983). *Geology of the Kywepnapa –Leppangon area, Patheingyi and Maymyo Townships*. M.Sc., Thesis (unpolished), Geol. Dept., Mandalay University.
- Pettijohn, F.J., (1974). *Sedimentary Rocks*, 3rd. Edition. India Press, CBS Publisher and Distributors, New Delhi.
- Searle, D.L and Haq, B.T., (1964). The Mogok Belt of Burma and its relationship to the Himalayan Orogeny. *Paper read at 22nd. International Geol., Congr.*, India 11, 133-161.
- Soe Win, (1994). *Iron Ore in Myanmar*. Unpublished Report.
- Tin Aung Myint, (2002). *A Genetic Study on the Iron Ore Deposits at Kyadwinye Mine and Its Environs, Pyin-Oo-Lwin Township, Myanmar*. Master of Research (Unpublished), Department of Geology, University of Mandalay

- Tin Aung Myint, (2013). Study on the mineral assemblages and zonation of the metamorphic rocks exposed at Zebyu-Thakhinma Taung area, Patheingyi Township, Mandalay Region, Myanmar. *Departmental research paper*.
- Tin Aung Myint & Mi Mi Ko, (2004). Occurrences of iron ores in Myanmar, research *paper read at 4th. Anniversary of Yandanabon University Opening*. Conference Hall, Yandanabon University, Mandalay City, Myanmar
- Win Swe, (1971). Strike –slip Faulting in Central Belt of Burma. Paper read at the Fifth Burma Research Congress. *Contributions to Burmese Geology*, Vol.1, No.1, pp. 63-72.
- Win Win Kyi, (1990). *Geology and Mineral Resources of Pathin-Kyadwinye Area, Pyin Oo Lwin Township*. M.Sc. Thesis (Unpublished), Geol. Dept. Mandalay University.
- Zaw Min Thein, (1995). *Geology and Stratigraphy of the Thanpyegin area, Pyin Oo Lwin Township*, M.Sc., Thesis (Unpolished), Geol. Dept., Mandalay University.

STRUCTURAL CONTROLS ON LEAD MINERALIZATION AT LINWE AREA, YENGAN TOWNSHIP, SHAN STATE (SOUTH)

Tun Naing Zaw¹, Day Wa Aung², & Swun Wunna Htet³

Abstract

The study area is located about 1.5km northeast of Ye-ngan Township, Shan State (South).It is also situated within Latitude 21° 12' 30" N to 21° 14' 30" N and longitude 96° 31' 30" E to 91° 34' 00" E. It covers about 4.6 kilometers. The area is covered by the Paleozoic units namely, Lokeyin Formation, Wunbye Formation, Nan-on Formation, and Tanshauk member of the Pindaya Group of Ordovician age, the Linwe Formation of the Mibayataung Group of Silurian age, the Thitsipin Formation of Permian age, and the Nwabangyi Dolomite Formation of Early Triassic age. Structurally, the area is significant due to the recognition of genesis of fault system which is previously not known from the area. The present study provides reevaluation of the structural geology of the research area. Recent study in the Linwe area, has significantly improved our knowledge of recognizing a lead mineralization in phacoidal limestone of Linwe Formation (Early Silurian) mainly occurred in nearly NW-SE trending fault zone. Linwe lead occurrence (latitude 21° 13' 16" N longitude 96° 32' 23" E) is situated at half mile northwest of Linwe monastery. The mineralization of the Linwe area is found to be definitely structurally controlled. The galena is observed to have mostly occurred in fault with brecciated zone. In the alteration map by ASTER data, many cyan tint pixels (alterations) are observed which the evidences of possible locations of mineralization area. The common wall rock alteration of Linwe lead mineralization may be dolomitization and the formation of sanded dolomite based on the alteration map by using aster and Landsat 8 images. Most of the Linwe ore bodies have been followed NW-SE trending faulted stream that is pre mineralization fault. On the surface, the mineralization can be followed the brecciated zone. Styles of mineralization occur as fracture filling and solution collapse breccia. Lead mineralization fill in cracks of deformed calcite crystals. Texture of lead sulphide minerals are mostly related to open-space filling of breccia's and fractures. This fault zone and lead mineralization were previously mapped and designated by Tun Naing Zaw et.al., (2017). Lead deposit in the Linwe Formation is hosted by sedimentary rock deposited during the later stage of at least two overprinting extensional events. Hydrothermal activity and alteration also acted as a heterogeneity focusing of dilational deformation and final stage of mineralization. Reactivated fault thereby accounting for the longevity of the hydrothermal system responsible for the alteration and mineralization at Linwe Formation. Analysis of the kinematic controls on lead mineralization in Linwe Formation is structurally controlled may enable other prospective structures in the near Linwe area to be identified. Need to seek possible means and ways for further exploration of Pb mineral deposits in the Linwe area.

Keywords: Phacoidal limestone, ASTER data, sanded dolomite, fracture filling, solution collapse breccia, brecciated zone

Introduction

For many years, no lead mineralization in Linwe Formation has been reported in Linwe-Pegin area, Ye-ngan Township, Shan State (South). Lead mineralization has been found in grey coloured nodular limestone which is exposed in southwestern part of Linwe village. This lead mineralization occurred in NW-SE trending fault zone. (Figure 1) This fault zone and lead mineralization were previously mapped and designated by Tun Naing Zaw et.al., (2017) as a possible structural control. The study aim to determine whether primary syntectonic mineralization or secondary tectonic mineralization are involved in the formation of economic mineralization.

¹ Dr, Lecturer, Department of Geology, University of Yangon

² Dr, Professor and Head. Department of Geology, University of Yangon

³ 3rd year Honours student, Department of Geology, University of Yangon

Location

The research area is situated in Ye-ngan Township, Shan State (South) and bounded between latitudes $21^{\circ} 12' 30''$ N - $21^{\circ} 14' 30''$ N and longitudes $96^{\circ} 31' 30''$ E - $96^{\circ} 34' 00''$ E. The area falls within the geographic limit of topographic map No. 93 C/2 on the scale of one-inch to one mile. It also covers about 4.6 square kilometers. Figure (1).

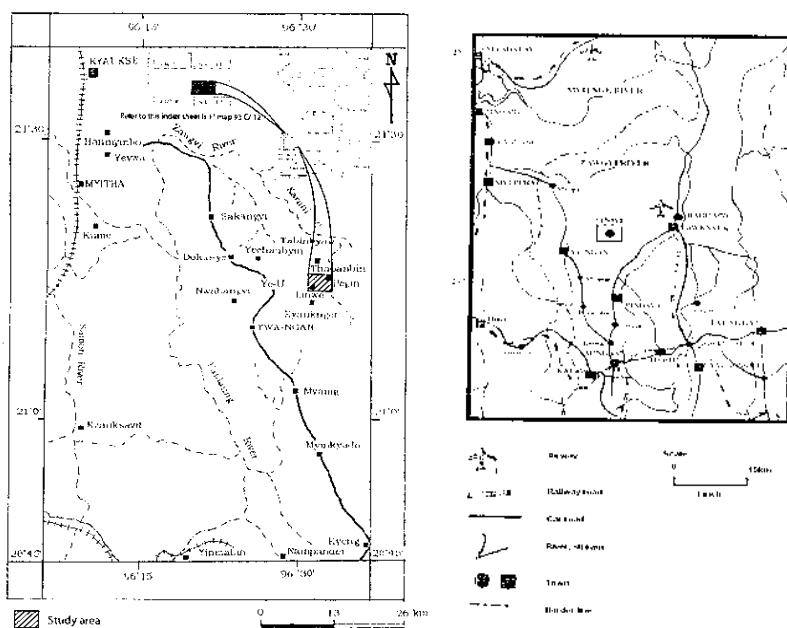


Figure 1 Location map of the study Area

Previous Studies

Geologists of Geological Survey of India (1864-1865) had firstly made the systematic geologic works as a regional geology of the Southern Shan State including Pindaya Township and Ye-ngan Township.

The geology of Linwe-Pegin area was investigated by several geologists (from 1897 to 1976) on various aspects of its stratigraphy, paleontology and economic aspects. From 1976 to present day, the geology of the research area was continuously studied on purposes of completing student's basic training course as well as aiming of higher degree, such as Master of Science (M.Sc), Master of research (M.Res) and doctoral research (Ph.D).

Materials and Methods

(1) Remote Sensing

- i. Landsat-8 OLI/TIRS Level-1 Data Products are applied for the general evaluation of the study area and alteration zones. Details of the Landsat scene are as follows:
 Landsat Product ID= LC08_L1TP_133045_20190212_20190222_01_T1
 Row/Path = 133/045
 Data Acquired = 5:27:43
 Cloud Cover = 0.01
 Image Quality = 9 for both OLI and TIRS sensors
- ii. SRTM 1-Arc Second Digital Elevation Model
 Product Name = n21_e096arc_v3

(2) Spatial Data

Topographic map, the scale of one-inch map sheet no. () is used as base map for geographic database of the research area. UTM (quarter-inch) and topographic map (quarter-inch) scale are used to identify the significant topographic criteria.

(3) Software

Microsoft Excel 2013 for geostatistical analysis

Global Mapper v.18 (64 bit)

ArcGIS 10.6

ENVI 4.8.

(4) Technical Methods

Using ArcGIS 10.6, band rationing and band combinations of Landsat images are proceeded to export the alteration distribution map. In some cases, geo-statistical procedures are applied using threshold equations to map the alteration anomaly zones for further analysis.

(5) Laboratory Methods

Satellite data of Landsat 7 Thematic Mapper TM were selected from the research. These data are recorded on seven bands with Landsat 7 satellite, the study area is fell within path/row (132/45) with 30 meters ground resolution. Visual image interpretation and digital image processing were applied for classifying images in a base of land cover/land use and to enhance image quality.

In this research, ground control points were selected by following permanent features evenly distributed throughout the area and identified easily both in image and topographic maps. The Universal Transverse Mercator (UTM) projection method is employed in the research area. The scale of Topographic maps used this research area was one-inch.

In this research, the false colour composite (R: G: B=4:5:3) was made for land use/land cover interpretation. TM images are analyzed to identify the major structural patterns and lithology by using ENVI 4.8.

The detailed stratigraphic measurement was made of the, the Linwe Formation.

Rock samples and ore samples were collected at stratigraphic horizon along the measured sections of Linwe Formation.

Identifying the rocks thin sections with low-powdered petrographic binocular microscope and ore polish sections with ore microscope.

Regional Stratigraphy

The stratigraphic sequence of the Paleozoic rocks are exposed in the present area. The area is composed of rocks of Ordovician to Permian except the Devonian age. Most units are mainly composed of carbonate and subordinately of clastic sedimentary rocks. Myint Lwin Thein (1973) classified the Lower Paleozoic rocks of the western part of the Southern Shan State as a Ordovician rocks (the Pindaya Group) including three formations and one member such as Lokeyin Formation (Early Ordovician), Wunbye Formation (Middle Ordovicia), Nan-on Formation (Late Ordovician) and Tanshauk Member (Late Ordovician). Myint Lwin Thein (1973) had also classified the Silurian rocks as the Minbayataung Group with two formations and

one member such as Linwe Formation, Wabya Formation of the Early Silurian age and Taungminggyi Orthoquartzite Member (Late Early Silurian) age. Figure (2).

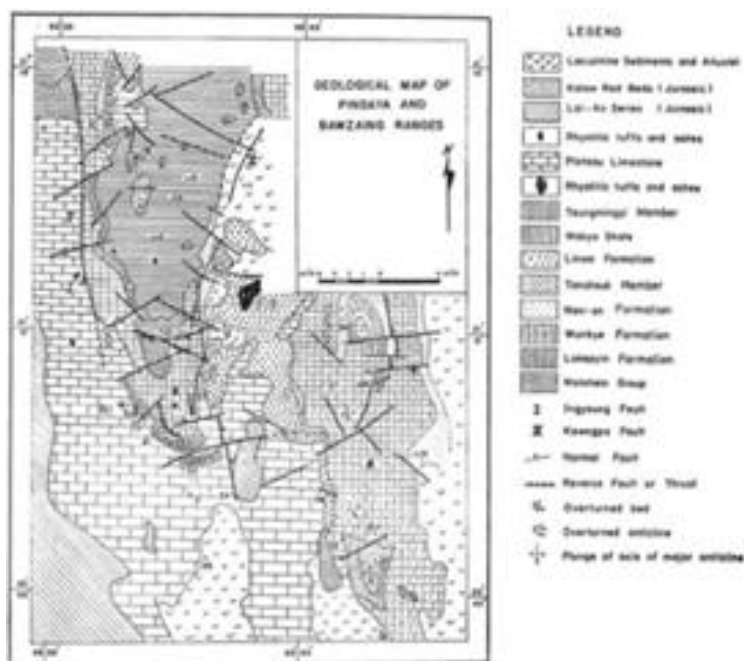


Figure 2 Regional Geological Map of the Study Area((Myint Lwin Thein, 1973)

Regional Structures

The Pegin-Linwe area forms part of the Western Limb of south plunging anticline of Pindaya Range. The regional structural trend is nearly N-S and they are sub-parallel to the topographic trends and minor structural alignments nearly coincide with the major trend. Faults are well developed in the present area, including longitudinal fault and cross fault. The major faults are generally trending in N-S direction. Karani fault is trending in NNW-SSE and occurred at northeast of the study area. Ingyi-Ingyaung fault is trending in NNW-SSE and occurred at western part of study area. Linwe-Pegin fault is nearly N-S in direction and pass through from north (Pegin Monastery) to south (Linwe monastery).Figure (13).

Rock Units in the Study Area

General Statements

The study area is mainly composed of Ordovician to Permian rocks. Most of the type sections are classified by Pascoe (1959), Myint Lwin Thein (1973), Mitchell, A.H.G (1976).

Lokepyin Formation

The Ordovician rock of Lokepyin Formation is mainly made up of yellowish to buff color siltstone which are well exposed at western part of the study area. Figure(3).



Figure 3 Siltstone beds and Orthid brachiopods under Shwe Guu Pagoda in Ingyi Village

Wunbye Formation

Wunbye Formation is mainly composed of limestone with silt patches limestone, dolomite, oolitic limestone, micritic limestone and yellowish siltstone. Barrow structures are also distinct. This formation is well exposed at central portion of the study area. Figure (4)



Figure 4 Burrowed Limestone of Wunbye Formation at Location 062715, (Photo Facing 278) and Actinoceras

Nan-on Formation

Nan-on Formation is especially composed of yellow to buff, subindurated to soft, thin to medium bedded, fossiliferous calcareous siltstone and shale and this formation is exposed at central portion of the study area. Figure (5)



Figure 5 Yellow to Buff colored siltstone with *Spiriferina* Brachiopod of Nan-on Formation(N 21 °14' 31", E 96° 33' 37")

Tanshauk Shale Member

The Tanshauk Member is a marker bed lying between the Nan-on Formation and the Linwe Formation of Mibayataung Group. This unit is well exposed at Tanshauk village and vicinity of Nan-on village. Figure (6)



Figure 6 Purple color shale and Star shape stems of Tanshauk Member at location: N 21° 14' 56", E 96° 33' 48", (photo facing – 68)

Linwe Formation

The Linwe Formation is composed of purplish and grey phacoidal limestone and buff to grey micaceous siltstone. Figure (8)

This unit was named after Linwe village, Ye-ngan Township, Shan State (South) by Myint Lwin Thein (1973).

Type Section

The type section of the Linwe Formation is located W of Linwe monastery, Linwe village, Ye-ngan Township, Shan State (South)

Distribution and Thickness

This unit is widely distributed in Kyauktaw, Pegin, Linwe, NE of Tanshauk, Nan-on and N of Hsin-Sa-Pya villages. We measured the exposed stratigraphic thickness of mineralized limestone unit of Linwe Formation (from 078729 to 087729) and (from 074723 to 087729) (Figure 7).

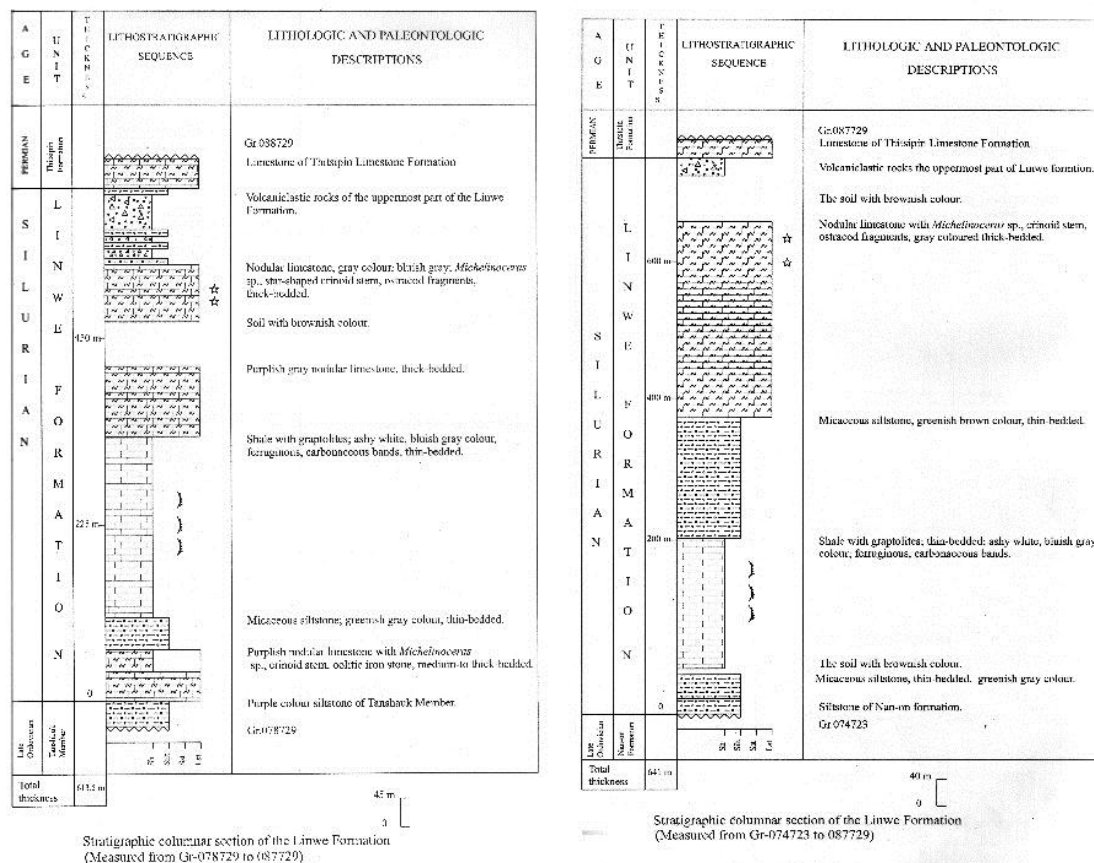


Figure 7 Stratigraphic Measured Sections of Linwe Formation

Lithology

It chiefly consists of medium to thick-bedded, grey-coloured limestone with nodular appearance (phacoidal texture, Fig-), micaceous shale, graptolite-bearing shales (Fig-), micaceous siltstones and black shales are occurred as minor amounts. Wavy bedding nature is common in phacoidal limestones. Coal seams with minor sulfur are found in the Linwe shale unit Figure (10).

Fauna Content and Age

A large number of graptolites are found (Figure-). *Michelinoceras* sp. and crinoid stems are common. Trilobites are found in micaceous siltstone .Figure(12). According to these fossils, it suggests the age of Early Silurian.

Stratigraphic Relationship

The Linwe Formation underlines conformably with Tanshauk Member and it overlies faulted contact with the Mixed Clastic Carbonate.

Correlation

This unit is correlated with Nyaungbaw Formation of Shan State (North).

Depositional Environment

The Linwe Formation might be deposited under shallow warm marine conditions.



Figure 8 Grey-Coloured Phacoidal Limestone Found in Linwe Formation (Location: 082723) (Facing: 290°)



Figure 9 *Michelinoceras* Fossil Found in the Phacoidal Limestone of Linwe Formation (Location: in front of Linwe Monastery) (Facing: 86°) (Location: 082712) (Facing: 349°)



Figure 10 Coal Seams with Minor Sulfur in the Shale of Linwe Formation (Location: 076712) (Facing: 260°)



Figure 11 Graptolite-Bearing Shale Outcrop of the Linwe Formation (Location: 082712, Mwe-Taung)



Figure 12 Trilobite found in micaceous siltstone unit of Linwe Formation (Kyauk Taw Village)

Thitsipin Limestone Formation

The Thitsipin Limestone Formation is exposed at the east of Linwe, Pegin and east of Tanshauk village. The Thitsipin Limestone consists of light to darkgray, bedded to massive limestone and wackestone with abundant of coral fossils, brachiopods, fusulinids and bryozoan. Figure(13). Locally has been dolomitized and it is intensively brecciated.



Figure 13 Limestone outcrop of Thitsipin Formation (N21° 11' 31", E96° 24' 31")

Nwabangyi Dolomite Formation

It is characterized by brecciated dolomite which is light to dark bluish colour, massive to poorly bedded, and highly brecciated. Figure (14)

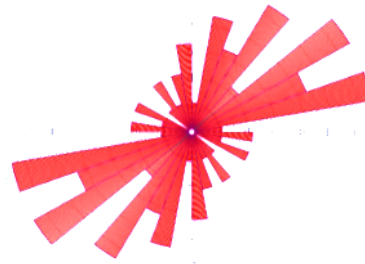


Figure 14 Criss-cross joints on dolomite of Nwabangyi Formation (N21° 11' 34", E96° 24' 34")

Structures of the study area

Pegin-Linwe fault, Thisipin-Karani fault and Ingyi-Dalabin fault are longitudinal faults of the study area .The general trend of these major longitudinal faults is NNE-SSW and NNW-SSE in direction. Figure (15)





Calculation Method ... Frequency
 Class Interval 10 Degrees
 Filtering Deactivated
 Data Type Bidirectional
 Rotation Amount 0 Degrees
 Population 46
 Maximum Percentage ... 13 Percent
 Mean Percentage 5.9 Percent
 Standard Deviation ... 3.69 Percent
 Vector Mean 46.52 Degrees
 Confidence Interval .. 33.51 Degrees

Figure 16 Joint Rose Diagram of Linwe Formation

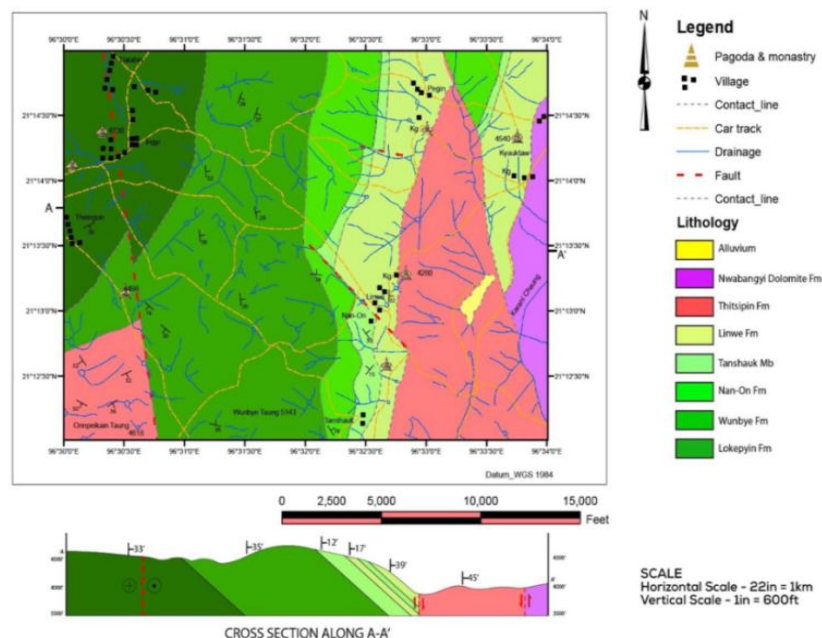


Figure 17 Geological Map of Linwe-Pegin Area

Results and Discussions

For the purpose of detection of mineralization in the study area, it is essential to evaluate the alterations produced by mineralization. In this case, both Landsat-8 and ASTER (Advanced Spaceborne Thermal Emission and Reflection Radiometer) images are used for alteration zone detection. The raw data of those two image types are radiometrically corrected separately, later

these two processed are compared for confirmation of detection of alteration zones in the study area.

Landsat-8 OLI images are converted from their digital numbers to TOA (Top of Atmosphere) reflectances using the equation:

$$\rho\lambda' = ML * Q_{cal} + AL$$

Where: $\rho\lambda'$ = TOA Planetary Spectral Reflectance, without correction for solar angle. (Unitless)

M_p = Reflectance multiplicative scaling factor for the band (REFLECTANCE_MULT_BAND_n from the metadata).

A_p = Reflectance additive scaling factor for the band (REFLECTANCE_ADD_BAND_N from the metadata).

Q_{cal} = Level 1 pixel value in DN

Next, using the solar elevation angle information from the metadata, the conversion of TOA reflectance is calculated as follows:

$$\rho\lambda = \frac{\rho\lambda'}{\sin(\theta_{SE})}$$

Where: $\rho\lambda$ = TOA planetary reflectance

$\rho\lambda'$ = TOA Planetary Spectral Reflectance

θ_{SE} = Local sun elevation angle; the scene center sun elevation angle in degrees is provided in the metadata

The following combination band ratios: Band 4/ Band 2 (Ferrugination), Band 5/ Band 6 (Fe+Mg) and Band 6/ Band 7 (OH-bearing and carbonate minerals) are continued to pansharpen using 15-meter resolution panchromatic Landsat-8 images for better visualization of alteration map.

For the ASTER images, the images are preprocessed and rescaled to 30-meter resolution and the following band combination of Band 6 (SWIR), Band 2 and Band 1 (2 VNIRs) is processed for gossan/alteration/host rock delineation.

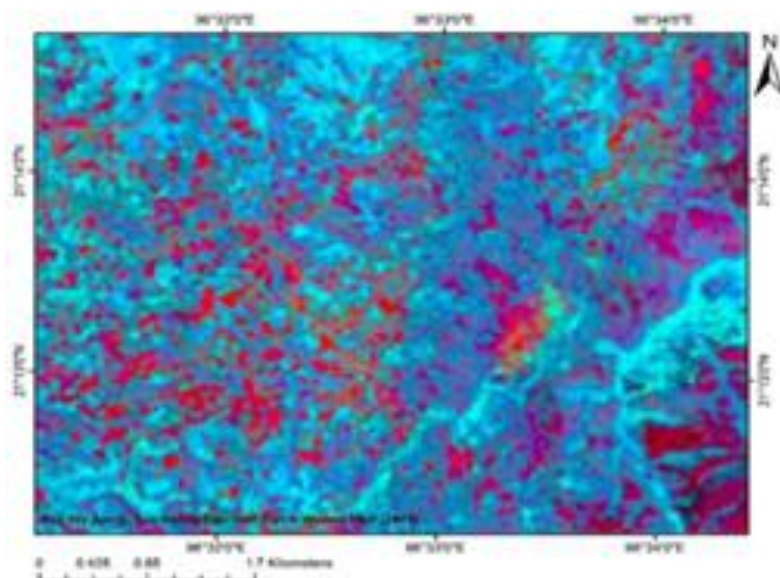


Figure 18 Alteration map by band combination of 4/2, 5/6, 6/7 of the study area using Landsat-8 (red = Fe, green = Dolomitization or formation of sanded dolomite, blue=limestone)

According the alteration map by Landsat-8 images, many ferruginations are observed due to alteration of limestones into laterites. Most of the study area is covered with limestone area (more obvious in eastern part of the area which indicates the Nwabangyi Dolomite Formation). The green colour, a signature of Mg, shows dolomitization, thus also gives the evidence of the presence of mineralization). Figure (18). In the alteration map by ASTER data, many cyan tint pixels (alterations) are observed which the evidences of possible locations of mineralization area. The gossan shows with white or grey tint colour. And the rest of the area is host rock of brown colour. Figure (19)



Figure 19 Alteration map by band combination of 6, 2, 1 of the study area using ASTER L1 products (cyan= alteration, brown = host rock, grey tint = gossan (Fe))

Linwe Village Lead Occurrence (New Finding)

Lead Occurrence (1)

This lead occurrence is situated at ½ mile northwest of Linwe Monastery (Location: Latitude 21°13'16", Longitude 96°32'23"). This occurrence of lead mineralization is assumed to be new finding of lead occurrence as there has been no data mentioned or proof about the existence of this occurrence. There are many cross faults with trending direction N10W and S10E in the studied area. Linwe Formation and Nan-on Formation are cut by minor fault (NW-SE trending cross fault) which is faulted stream. Lead mineralizations observed at Linwe phacoidal nodular limestone that is well exposed along the NW-SE trending faulted stream. Figure (15) and Figure (20).



Figure 20 Occurrence of Lead mineralization in Linwe Village at Lat 96° 32' 23'', Long 21° 13' 16'', Linwe Formation

Lead Occurrence (2)

In the northwestern part of Linwe village, lead mineralization in phacoidal limestone unit of the Linwe Formation observed at GPS locations $21^{\circ} 12' 49''$ N, $96^{\circ} 32' 45''$ E (4070'), $21^{\circ} 12' 54''$ N $96^{\circ} 32' 42''$ E (4390'), $21^{\circ} 12' 59''$ N $96^{\circ} 32' 42''$ E (4150') and $21^{\circ} 12' 60''$ N $96^{\circ} 32' 43''$ E (4210') near the NW-SE trending cross fault zone. In these outcrops, mineralized phacoidal limestone s are highly brecciated and highly weathered and altered. Figure (21)



Figure 21 Lead mineralization in Linwe Phacoidal limestone

Position of Ore Bodies to the Host Rock

The Wunbye deposit can be regarded as stratabound and the deposit is found to be definitely stratigraphically controlled at Wunbye hill, Ywangan township, Shan State (South). The galena is observed to have mostly occurred in the lower Wunbye Formation whereas galena associated with barite commonly occur in middle Wunbye Formation. But the Linwe ore bodies are highly concordant and crosscuts the regional strike of Linwe Formation at high angle. The mineralization controlling fracture has been NW-SE in direction. Most of the Linwe ore bodies have been following NW-SE trending faulted stream that is pre mineral fault. On the surface, the mineralization can be followed the brecciated zone. The ore are disseminated, fracture fillings with no significant replacement of the host rock. The mineralization is structurally controlled with individual district, which is Linwe village at Linwe Formation.

Style of Mineralization

In the occurrences of lead mineralization in two new findings, there are four style of mineralization such as (i) dissemination (ii) fracture –fillings (iii) replacement and (iv) solution collapse breccias. Figure (22)



(i) dissemination



(ii) fracture –fillings



(iii) replacement

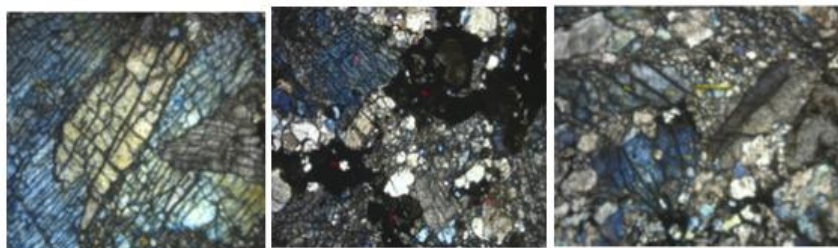


(iv) solution collapse breccias

Figure 22 Lead in Linwe Phacoidal Limestone

Petrography of Linwe Limestone

Under microscope, this rock is found to be medium grained with crystalline texture. Calcite grains are highly deformed and brecciated. Many cracks are observed in each calcite crystal. Lead mineralization fill in cracks of deformed calcite crystals. Figure (23)



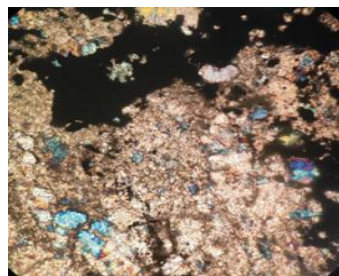
(5X) (Between XN)

(5X) Pb –Lead, Ca - Calcite

Figure 23 Thin section of brecciated limestone with lead mineralization

Ore Textures

In the Linwe deposit, the most common textures revealed are (1) open-space filling, and cavities texture and (2) replacement. Figure(24).



open-space filling (cavities filling texture)



open-space filling (fracture filling)



Replacement texture (may be ?)

Figure 24 Ore texture of Linwe lead deposit

Conclusions

1. The host rock is confined to the Linwe Formation of Silurian in the middle part of study area especially southeastern part of Linwe monastery.
2. The present study provides reevaluation of the structural geology of the research area. Resent study in the Linwe area, has significantly improved our knowledge of recognizing a lead mineralization in phacoidal limestone of Linwe Formation (Early Silurian) mainly occurred in nearly NW-SE trending fault zone.
3. The mineralization of the Linwe area is found to be definitely structurally controlled
4. The galena is observed to have mostly occurred in fault with brecciated zone. In the alteration map by ASTER data, many cyan tint pixels (alterations) are observed which the evidences of possible locations of mineralization area.
5. The common wall rock alteration of Linwe lead mineralization may be dolomitization and the formation of sanded dolomite based on the alteration map by using aster and Landset 8 images.
6. Most of the Linwe ore bodies have been followig NW-SE trending faulted stream that is pre mineralization fault.

7. On the surface, the mineralization can be followed the brecciated zone. Styles of mineralization occur as fracture filling and solution collapse breccia.
8. Lead mineralization fill in cracks of deformed calcite crystals. Texture of lead sulphide minerals are mostly related to open-space filling of breccias and fractures.
9. This fault zone and lead mineralization were previously mapped and designated by Tun Naing Zaw et.al., (2017) as a possible structural control. Lead mineralization in the Linwe area is epigenetic in origin.
10. Sandy dolomite beds make the orebodies changed to a friable sandy nature and leaching of the carbonate rocks result in thinning of some of the favourable beds to form residual shales in some ore bodies, causing fractures to be opened in rocks for ores deposited.
11. Lead deposit in the Linwe Formation is hosted by sedimentary rock deposited during the later stage of at least two overprinting extensional events.
12. Hydrothermal activity and alteration also acted as a heterogeneity focusing of dilational deformation and final stage of mineralization. Reactivated fault thereby accounting for the longevity of the hydrothermal system responsible for the alteration and mineralization at Linwe Formation.
13. Analysis of the kinematic controls on lead mineralization in Linwe Formation is structurally controlled may enable other prospective structures in the near Linwe area to be identified.
14. Need to seek possible means and ways for further exploration of Pb mineral deposits in the Linwe area.

Acknowledgements

We would like to express my thanks to Dr. Phoe Kaung, Rector, University of Yangon, for his permission to submit the research paper. Special hearty thanks are due to Dr. Ohm Thwin, Professor (Retired), Department of Geology, University of Yangon, for his discussions and suggestion. We thank to second year honours students and final year students for their field surveys carried out in the research area. Last, but not the least, we extend our gratitude to the unforgettable villagers and local people of our research area for their valuable helping during the field trip.

References

- Amar, B.I., (1975). Stratigraphy of some of upper Paleozoic and Mesozoic carbonate rocks of the Eastern Highlands, Burma, and Newest Stratigraphy. 4(1): 46-70. Stuttgart.
- Aleks Kalinowski and Simon Oliver (October 2004). *ASTER Mineral Index Processing Manual, Remote Sensing Application, Geoscience Australia*
- Aye Ko Aung, (2006). Revision of the Paleozoic stratigraphy of the Shan State, Dagon University, Department of Geology, 57P, (Unpublished).
- Aye Ko Aung, Kyaw Zay Myint, Kyaw Ko Ko and Aung Aye Lin, (2006). A new Carboniferous unit of the western part of southern Shan State, Myanmar. Dagon University Research Journal, vol.1, no.1, 8-14.
- Borstad Associates, (2008). *Using ASTER in mineral exploration. Unpublished Borstad Associates report*
- Brunshweiler, R.O, (1970). Contribution to Post-Silurian Geology of Burma (Northern Shan State and Kayah State) Jour.Geol.Soc. Australia, 17:59-79
- Clegg, E.L.G., (1952). The Cretaceous and associated rocks of Burma. Rec. Geol. Surv. India, vol-49, 1-101.
- Das, S, (2004). A manual on clinical surgery. Calcutta, India. South Edition 478P.
- Department of the Interior, U.S.Geological Survey, (Version 4.0, April 2019), *Landsat 8(L8) Data Users Handbook*

- Folk, R.L, (1989). Practical petrographic classification of the limestone, Bull. Amer. Asso. Petro Geok, V 43-38P.
- Hassan Mohy, Islam Abou El-Magd and Fawzy F. Basta (9 December 2015) *Newly Improved Band Ratio of ASTER Data for Lithological Mapping of the Fawakhir Area, Central Eastern Desert, Egypt, Indian Society of Remote Sensing 2016, D.O.I 10.1007/s12524-015-0539-0.*
- Jones, E.J, (1887). Notes on Upper Burma. Rea. Geol. Surv. India, 204:170-194, Calcutta
- Keller, E.A, (1988), Environmental Geology. Merrill Publishing Company, Fifth Edition, 540P.
- La Touche, T.H.D, (1913). Geology of northern Shan State. Mem. Geol. Surv. India 39(2):1-379
- Mouhssine WAHI, Kamal TAJ-EDDINE and Noureddine LAFTOUHI (2013), *ASTER VNIR & SWIR Band Enhancement for Lithological Mapping - A case study of the Azegour Area (Western High Atlas, Morocco), Journal of Environmental and Earth Science, Vol 3, No.12, 2013. ISSN 2224-3216 (Paper) ISSN 2225-0948 (Online)*
- Niyeh, M.M., Jafarirad, A., Karami, J. and Bokani, S.J. (2017) *Copper, Zinc, and Lead Mineral Prospectivity Mapping in the North of Tafresh, Markazi Province, Central Iran, Using the AHP-OWA Method. Open Journal of Geology, 7, 533-558. <https://doi.org/10.4236/ojg.2017.74037>*
- Pettijohn. F. J., (1956). Sedimentary Rocks 2ndEdn. Oxford Book Co., 718P
- Pour, Amin & Hashim, Mazlan. (2015). *ASTER and Landsat TM Data for Geological Mapping Application: A Case Study from Esfandagheh Ophiolite Complex, South of Iran.*
- Second Year Hons Students(2014 intake) 2018. Geological Field Report of Linwe-Pegin Area, Ye-ngan Township, Shan State (South)
- Yang, Min & Ren, Guangli & Han, Lin & Yi, Huan & Gao, Ting. (2018). *Detection of Pb-Zn mineralization in west Kunlun using Landsat 8 and ASTER remote Sensing data. Journal of Applied Remote Sensing. 12. 1. 10.1117/1.JRS.12.026018.*

ORE MINERALOGY AND GEOCHEMICAL INVESTIGATION OF LEAD MINERALIZATION IN KYAUKTAP AREA, KALAW TOWNSHIP, SHAN STATE (SOUTH)

Kyaw Thu Oo¹ and May Thawe Aye²

Abstract

Kyauktap area, the study area is situated about 17 kilometres north of Heho, Kalaw Township, Taunggyi District. Regionally, the Precambrian rocks of Chaungmagyi Group are surrounded by Lower Paleozoic rocks. The study area is located in the southern part of Bawsaing Range that lies in the southwestern part of the Shan Plateau. Sedimentary rocks of the Wunbye Formation, Nan-on Formation of Pindaya Group (Ordovician age) and Linwe Formation of Mibayataung Group (Silurian age) cropped out in the study area. According to petrographic classification, Wunbye Formation can be divided into six microfacies: Oolitic Dolomatized Grainstone, Dolomitic Limestone, Crystalline Limestone, Oolitic-Pelloidal Grainstone, Pelloidal-Bioclastic Wackestone, Micrite or Limemudstone, and Ferruginous Lime Mudstone of Linwe Formation. The lead mineralization is confined to the carbonate rocks of Wunbye Formation of Middle Ordovician age. Absence of igneous rocks is conspicuous. Two types of wallrock alteration are dolomitization as the main alteration, and silicification as subordinate, which predate the ore mineralization. The major ore minerals are galena and barite, and its associated minerals are sphalerite, pyrite, chalcopryrite, covellite and anglesite. The gangue minerals are calcite, dolomite and quartz. Both open-space fillings (veinlets, disseminations, fracture fillings and solution collapse breccias) and replacement (irregular patches to massive aggregates) styles are the nature of ore mineralization. Lead mineralizations are localized by both structural and lithostratigraphical controls. There are two occurrences of lead mineralization in the study area. Pb values range from 3.746% to 58.34%. The content of Zn ranges from 0.0% to 16.45%, Cu ranges from 0.0% to 0.024%, Ba ranges from 0.0% to 0.729% in the study area. Based on the geological, geochemical and mineralogical characteristics, the lead mineralizations in the study area are carbonate-hosted, stratabound deposits, and epigenetic in origin and may be regarded as one of the sub-types of the Mississippi Valley-Type (MVT) deposits.

Introduction

Location, Size and Accessibility

The study area is located about 18 kilometres north of Heho and it is bounded by Latitudes 20°50'00"N 20°52'30"N and Longitude 96°46'10"E-96°48'40"E. (UTM map sheet no. 2096/03, about 25 square kilometres). It can be accessible from Heho by motorcycle and motorcar. Location map of the study area is shown in figure 1

¹ Student, Geology Department, University of Yangon, Myanmar

² Associate Professor, Geology Department, University of Yangon, Myanmar

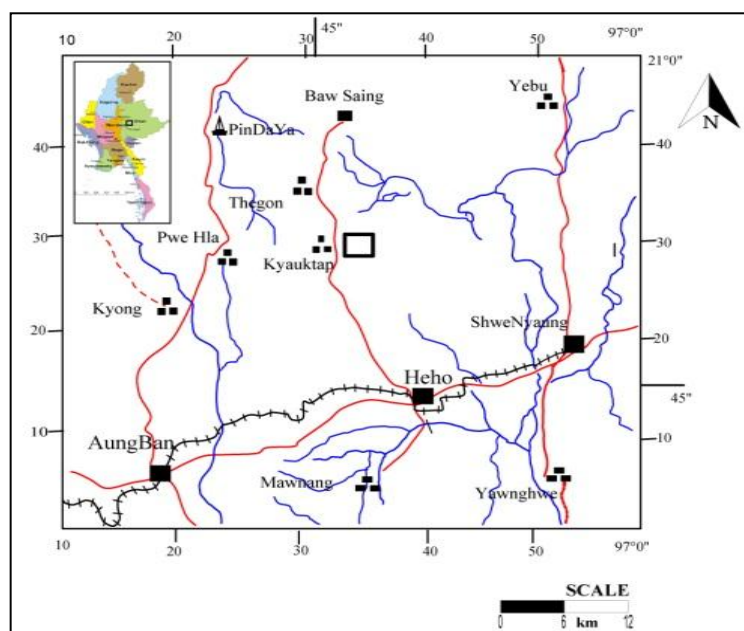


Figure 1 Location map of the study area, Kalaw Township, Shan State (South)

Scope and Objectives

The major purposes of the study area are to prepare fairly detailed geological map of the study area, determine the petrography of the rocks and study ore genesis and ore deposit type of lead mineralization in the study area.

Methods of Study

- (1) Preliminary Study: Studies of previous literature on Kyauk tap area and its environs.
- (2) Field Study: Systematic traversing, mapping, sampling and recording of rock units.
- (3) Laboratory Techniques: Ore Microscopy and X-Ray Diffraction, X-Ray Fluorescence are used in this research.

Geology and Petrography

Regional Geology

Almost complete sequence of the Lower Paleozoic units are exposed in Kyauktap and its environs. (Figure 2)

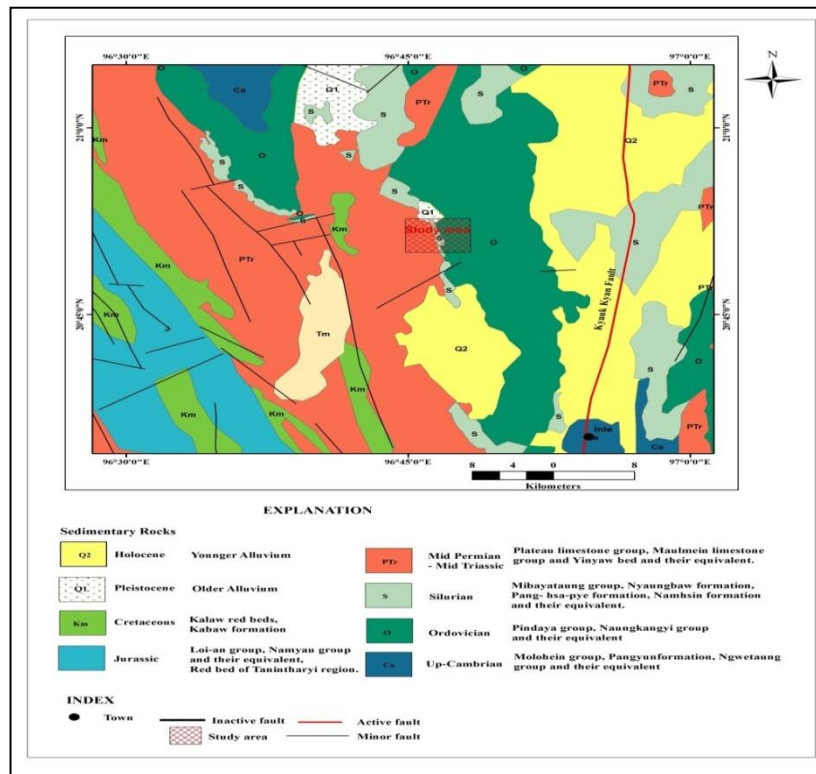


Figure 2 Regional Geological Map (Myanmar Geoscience Society, 2014)

Regional Geological Structure

Regionally, the structure of Bawsaing-Heho area is double plunging anticline (Myint Lwin Thein 1972). The investigated area is located on the western limb of south plunging anticline. The dip amount ranging from 27° to 37° on the eastern portion and on the western portion it varies from 37° to 50° because of tectonic movements, the faulting were developed. Regional structural map is shown in (Figure 3).

Table 1 Rock Unit Sequence of Regional and Environs of the Study Area
(After Myint Lwin Thein, 1973 & Garson *et al.*, 1976)

Group	Formation	Age
Plateau Limestone Group	<u>Nattiek</u> Formation	Middle Triassic
	<u>Nwabangyi Dolomite</u> Formation	Late Permian to Early Triassic
	<u>Thitsipin</u> Limestone Formation	Middle Permian
Unconformity		
<u>Mibayataung</u> Group	<u>Taungmingyi</u> Member	Late Silurian
	<u>Wabya</u> Formation	Late Silurian
	<u>Linwe</u> Formation	Early Silurian
<u>Pindaya</u> Group	<u>Tanshauk</u> Member	Late Ordovician
	<u>Nan-on</u> Formation	Late Ordovician
	<u>Wunbye</u> Formation	Middle Ordovician
	<u>Lokepyin</u> Formation	Early Ordovician
<u>Molohein</u> Group	<u>Myet-ye</u> Formation	Late Cambrian
	<u>Pandaung</u> Formation	Early Cambrian
<u>Chaungmagyi</u> Group		Precambrian

Geology of the study area

The study area is located in the nearly southern part of Bawsaing range. It is mainly comprises the Pindaya Group (Ordovician age) and Mibayataung Group (Silurian age). Sampale location map of the study area can be seen in Figure 4 and the geological map and cross section of the study area shows in Figure 5. The stratigraphic classification of the study area is adopted from Myint Lwin Thein (1973) for Lower Paleozoic rocks. In the study area, Wunbye Formation, Nan-on Formation of Pindaya Group, and Linwe Formation of Mibayataung Group were observed. Detailed stratigraphic succession of the present study area is shown in Table 2.

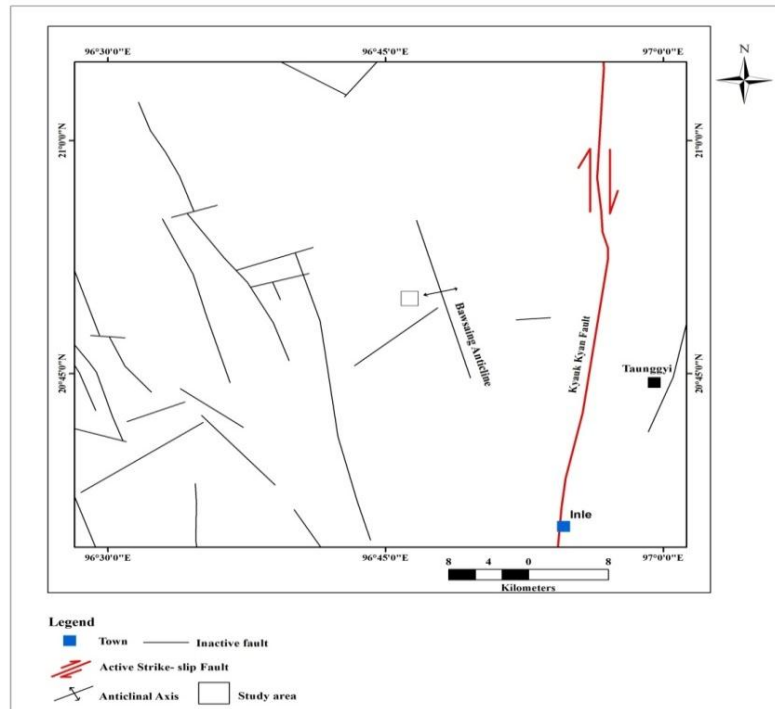


Figure 3 Regional Geological Structural Map (From Tectonic Map of Myanmar and Surrounding Regions, Soe Thura Tun, 2007)

Pindaya Group

Wunbye Formation (Middle Ordovician)

Fine grained, grey to dark grey coloured, massive limestones medium- to thick-bedded and with typical burrow structure are shown in Figure(6 &7). Hand specimen and thin section photomicrograph of oolitic- dolomitized grainstone is shown in Figure (8 & 9), dolomitic limestone in Figure (10 & 11), crystalline limestone in Figure (12 & 13), Oolitic-peloidal grainstone in Figure (14 & 15), Peloidal-bioclastic Wackestone in Figure (16 &17) and Micrite limestone in Figure (18 &19).

Nan- On Formation (Late Ordovician)

Yellow to buff, sub-indurated to soft, thin to medium bedded siltstones (Figure 20), mudstones and marlstones (Figure 21). Phacoidal limestone is shown in Figure (22 &23). Hand specimen of ferruginous lime mudstone is shown in Figure 24 and its thin section photomicrograph (Figure 25).

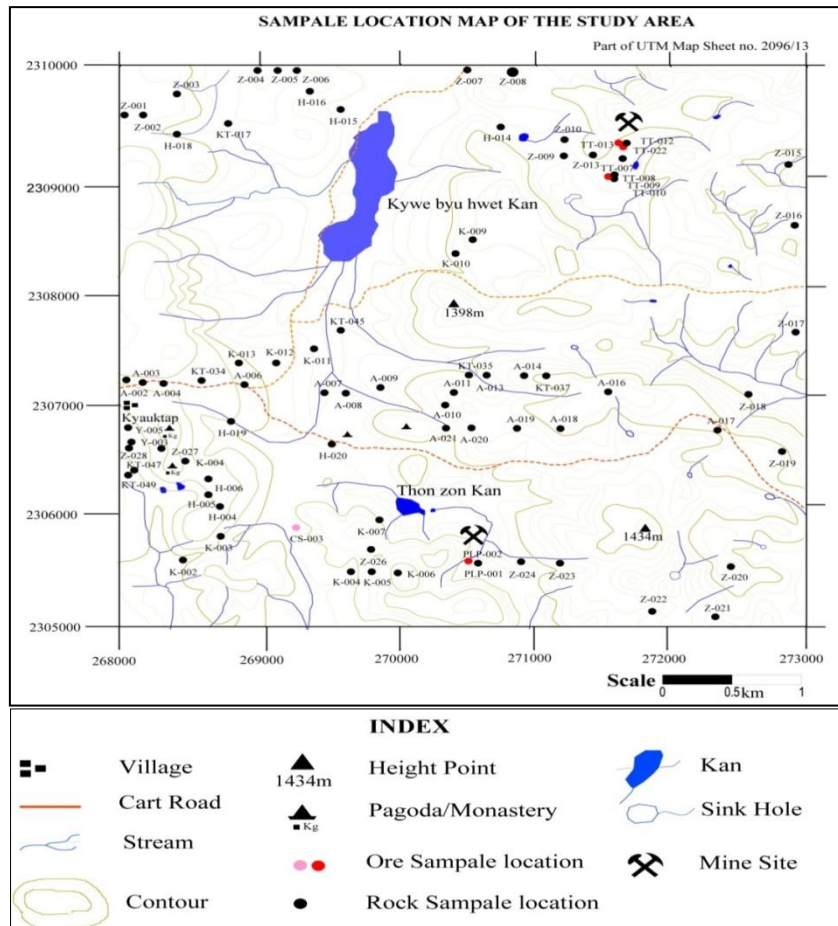


Figure 4 Sample location map of the study area

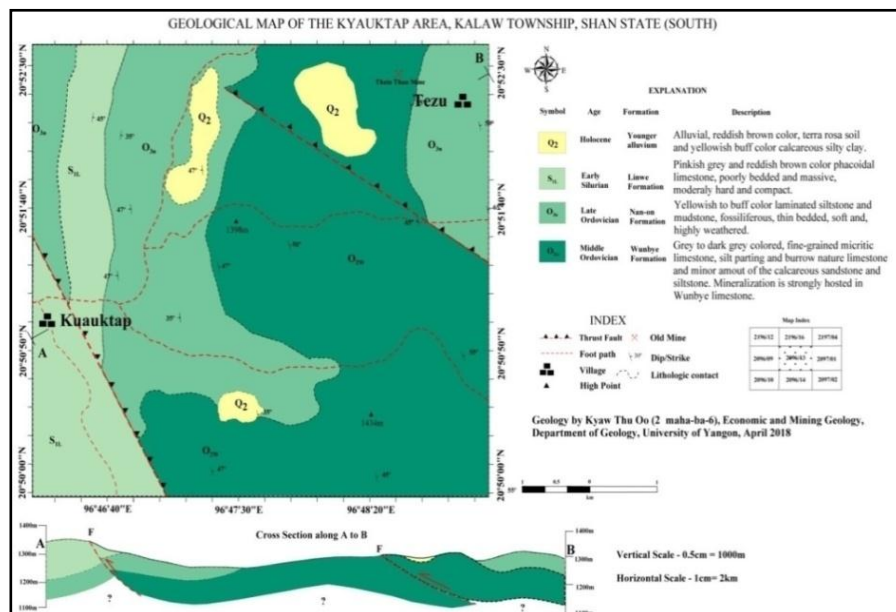


Figure 5 Geological map and cross section of the study area

Table 2 Detail stratigraphic succession of study area.

Group	Formation	Age	Lithology	Occurrence
<u>MibayaTaung</u>	<u>Linwe</u>	Early <u>Siluriun</u>	Pinkish grey and reddish brown <u>colouredphacoidal</u> limestone	West and southwest of the study area
<u>Pyindaya</u>	Nan-on	Late Ordovician	Yellow to buff coloured, <u>liminated</u> silt stone and mudstone	West, northwest and northeast of the study area
	<u>Wunbye</u>	Middle Ordovician	Grey to dark coloured, fine-grained to <u>micritic</u> , silt parting and burrow nature limestone and minor amount of the grain calcareous sandstone an silt stone	Central portion of the study area

Mibayataung Group**Linwe Formation (Early Silurian)**

Purple, pink and grey color, phacoidal limestones, argillaceous limestones, calcareous mudstones and shale.

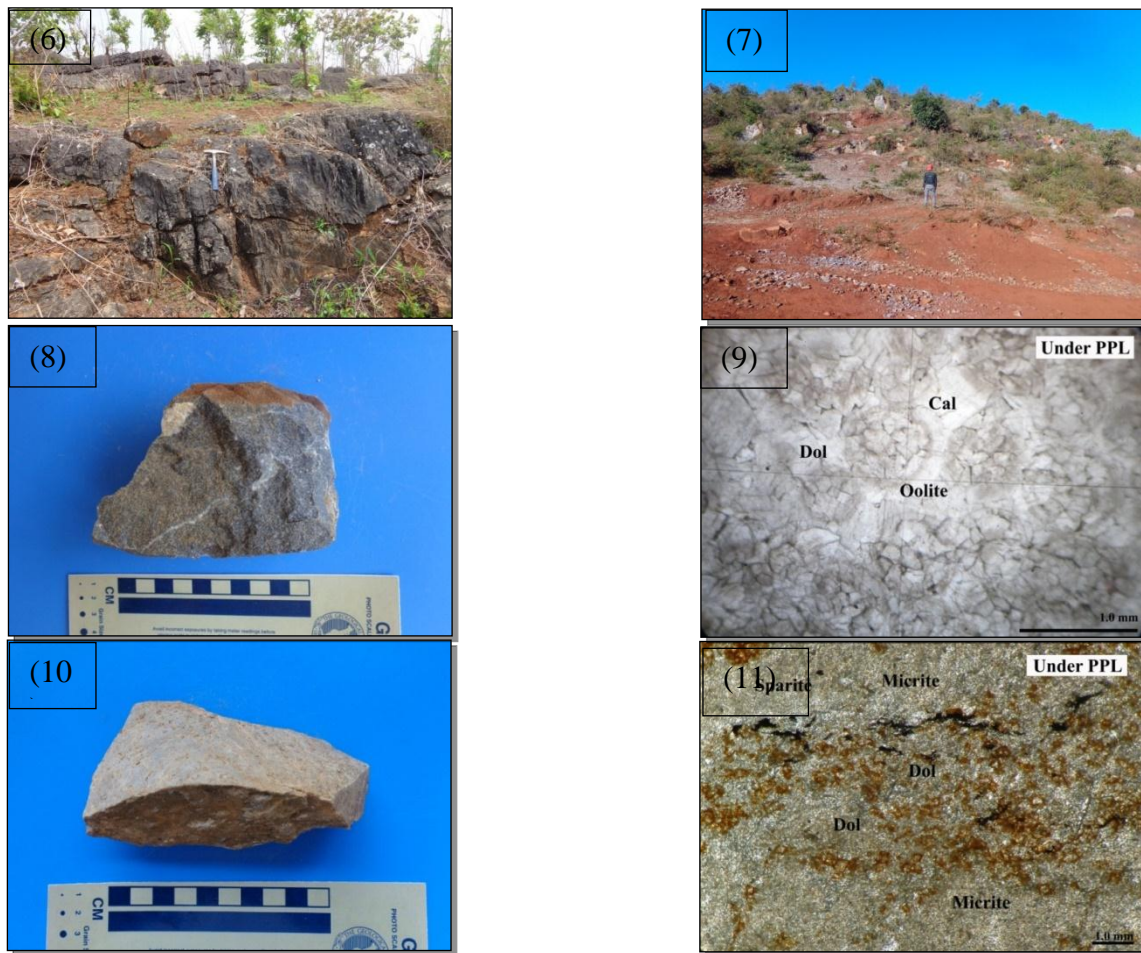


Figure 6 Light grey to dark grey, medium- to thick-bedded limestone, Location: 47Q 271074 E2307332 N, Facing 110°. Figure (7) Massive, finely crystalline, grey to bluish grey limestone, , Location: 47Q 269395 E 2309826 N, Facing 85° Figure (8) Medium - to thick-bedded, bluish grey limestone, Location: 47Q 269395E 2309826N. Figure(9) Oolitic-dolomitized grainstone , thin section photomicrograph of Sample No.KT-TT-017, Under PPL Figure(10) Medium to thick bedded, Pale yellow to reddish brown limestone Location: 47Q 270115 E2307313 N. Figure(11) Dolomitic limestone, thin section photomicrograph of Sample No.KT-TT-037 Under PPL

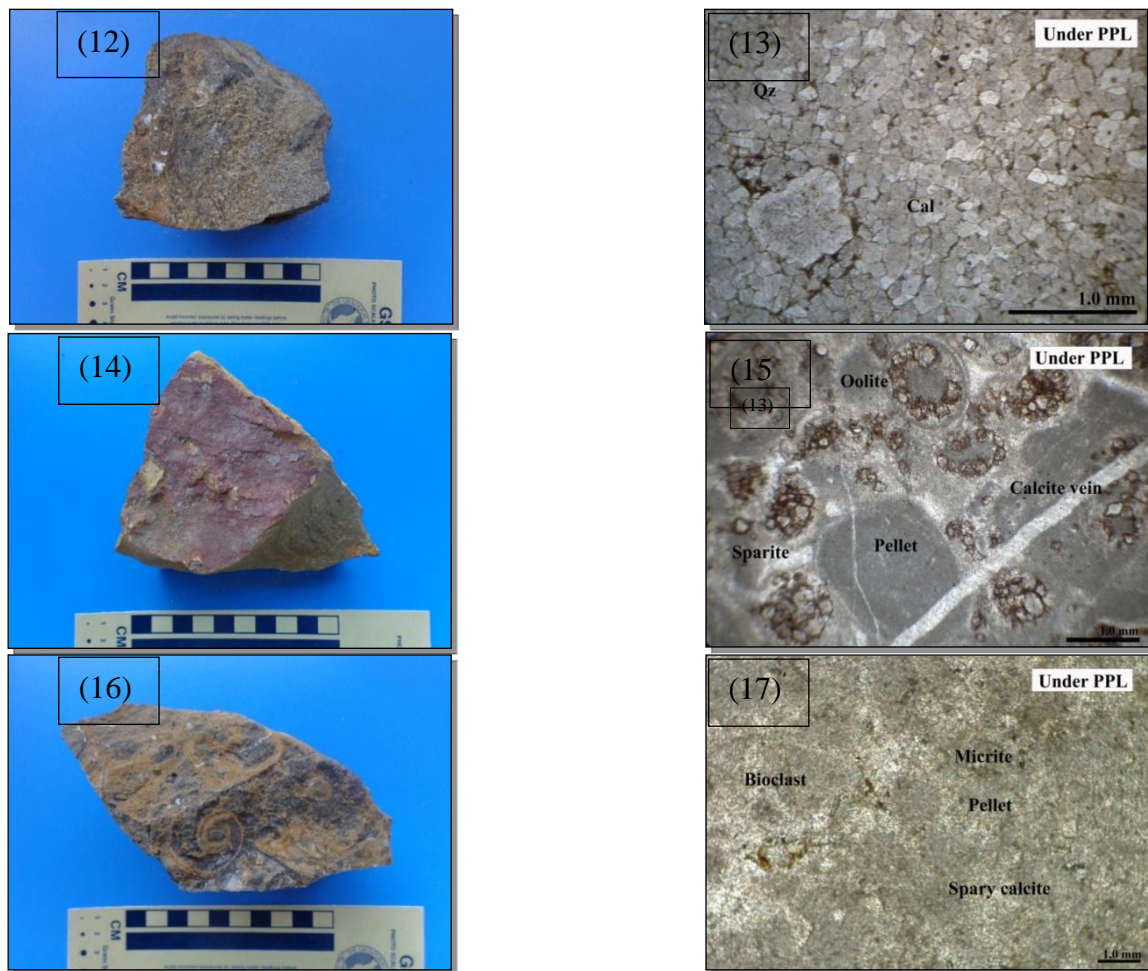


Figure 12 Medium to thick bedded, brown to dark grey limestone, Location: 47Q 269712 E 2307714 N Figure(13)Crystalline limestone, thin section photomicrograph of Sample No. KT-TT-045, Under PPL Figure(14) Medium to thick bedded, grey or blue grey limestone, Location: 47Q 270749 E 2307361 N Figure(15) Oolitic-peloidal grainstone, thin section photomicrograph of Sample No. KT-H- O35 Under PPL. Figure(16) Medium- to thick-bedded, grey or darkgrey limeatone, Location: 47Q 268743 E 2307301 N. Figure(17) Peloidal-bioclastic Wackestone , thin section Photomicrograph of Sample No. KT-H-O34 Under PPL

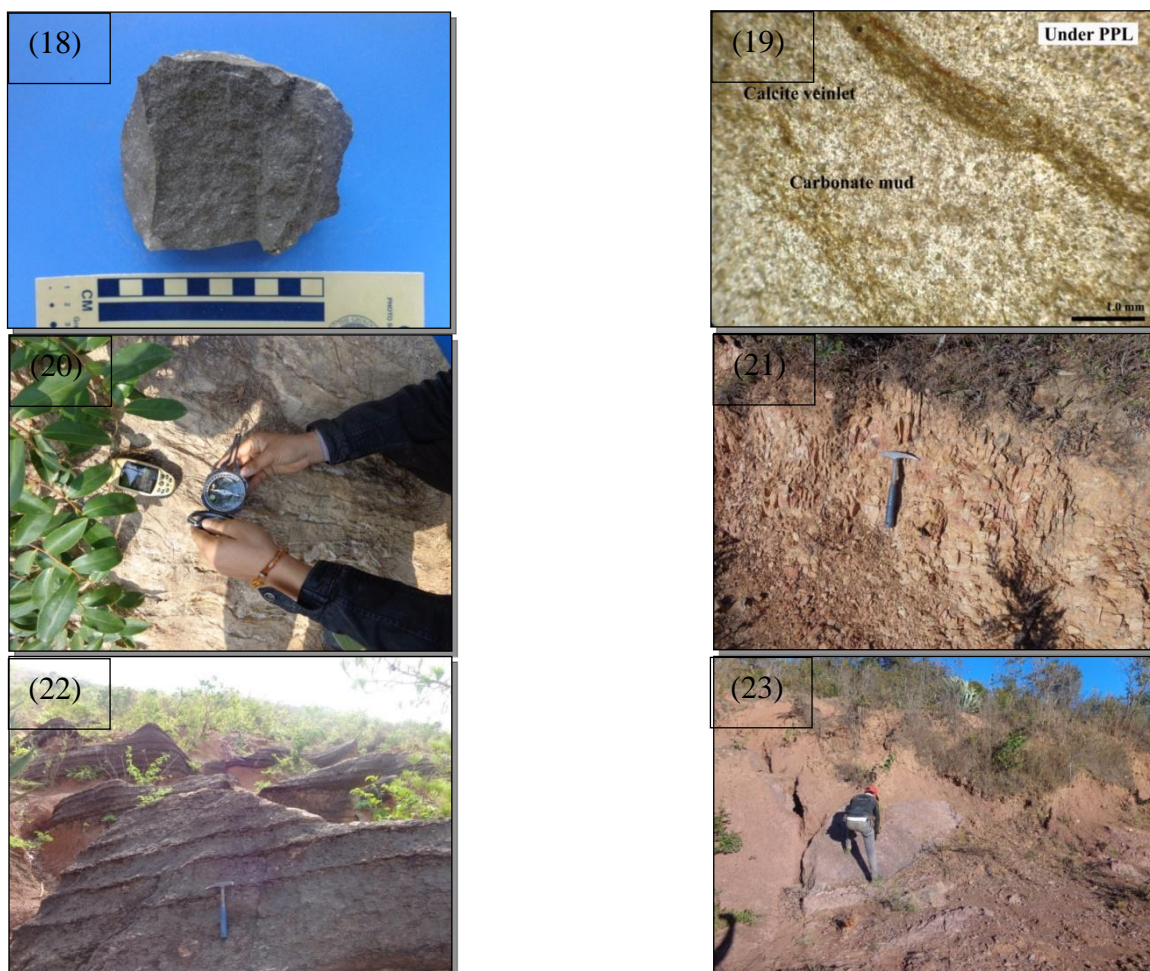


Figure 18 Medium- to thick-bedded, grey or dark grey limestone, Location: 47Q 267913 E 2306622 N Figure(19) Micrite, thin section photomicrographs of Sample No.KT-H-047 Under PPL Figure(20) Poorly bedded siltstone, Location; 47Q 268098 E 2307305 N , Facing 340° Figure(21) Thin bedded marlstone, Location: 47Q 268585E 2306268 N, Facing 55° Figure(22) Grey phacoidal limestone, Location: 47Q 268105 E 2308424 N Facing 270° Figure(23) Phacoidal limestone near Kyauktap village Location:47Q 268584E 2306327 N Facing 55°

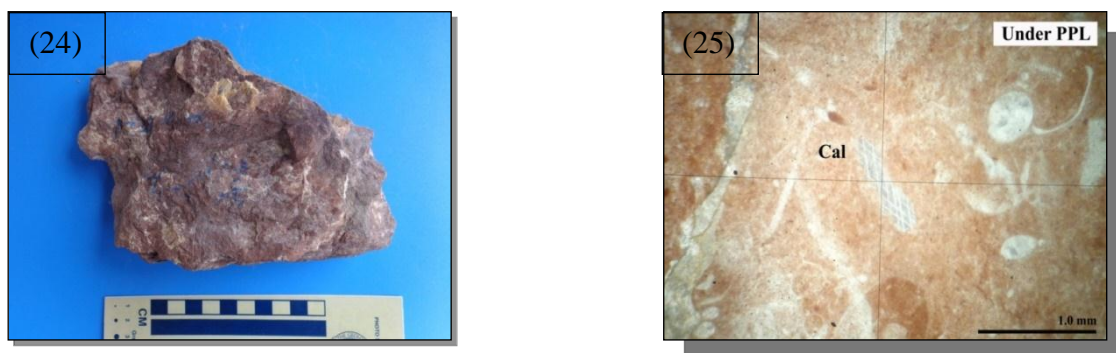


Figure 24 Massive, and grey, pink and purple limestone, Location: 47Q 268150 E 2308424 N Figure(25) Ferruginous lime mudstone, thin section photomicrograph, Sample No.KT-H-049Under PPL

Alteration

There are two type of alteration; dolomatization (Figure 26 A & B) and silicification (Figure 27 A & B), the former one is mainly occurred and the latter is occurred as subordinately. Sulphide mineralization is post-date the wallrock alterations.

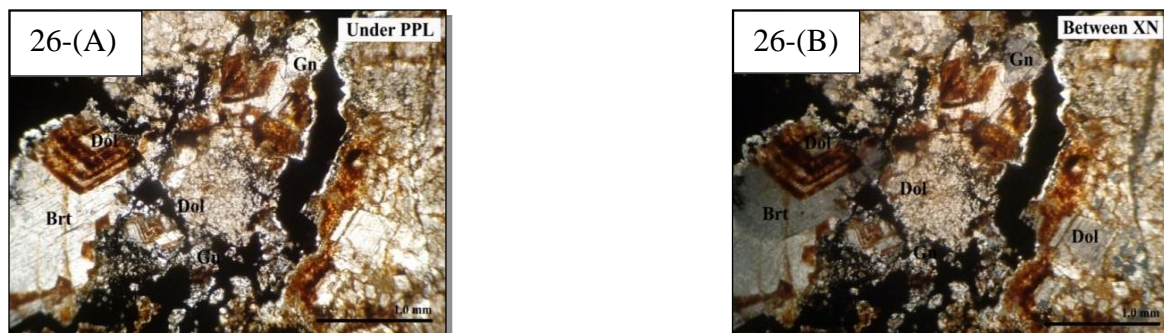


Figure 26 Thin section Photomicrographs showing dolomitization with Pb mineralization Under PPL & Between XN (Dol= Dolomite, Gn= Galena, Brt=Barite)

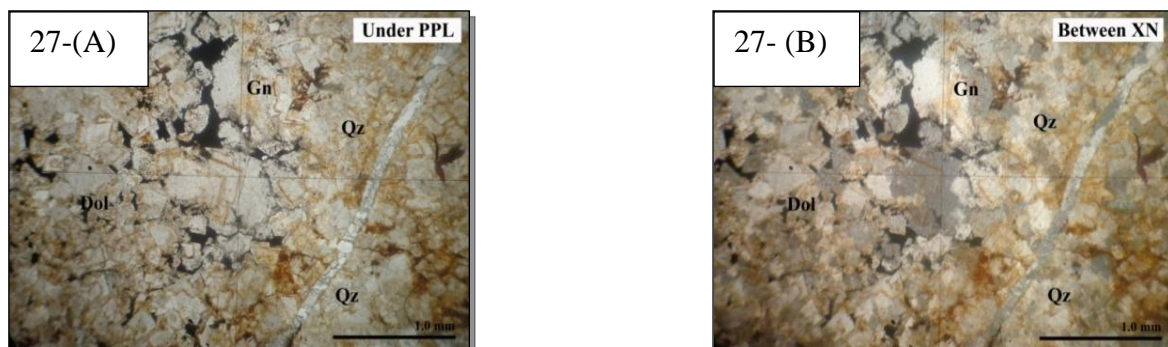


Figure 27 Thin section Photomicrograph showing silicification with Pb mineralization (Under PPL & Between XN) (Dol=Dolomite, Gn=Galena, Qz= Quartz)

Mineralization

There are three occurrences of lead mineralization; Thein Than lead occurrence and Pyae Hlan Paing lead occurrence, they are mainly produced lead sulphide ore (Galena-PbS) and Myae Ni Taung lead occurrence (Figure 30), which is produced lead carbonate ore (Cerussite-PbCO₃). The mineralization mainly occurred as veinlets (fracture filling) and disseminated in the host rock are shown in (Figure 28, 29 & 31). The major ore mineral is galena and associated minerals are sphalerite, pyrite, anglesite, covellite and little or no amount of argentite.

Mineralization style

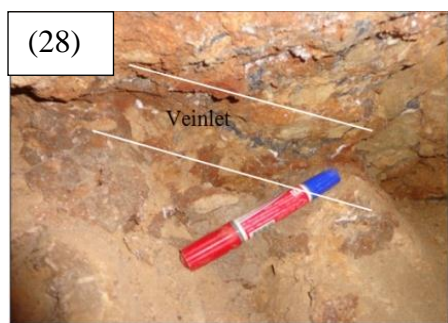


Figure 28 Fracture filling of Pb veinlets in host dolomitic limestone (Thein Than Occurrence)

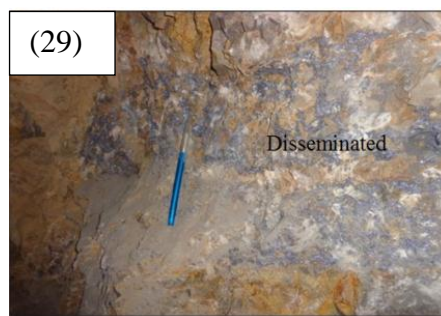


Figure 29 Disseminated Pb mineralization in host rock (Thein Than Occurrence)



Figure 30 Myae Ni Taung artisanal mine (vertical shaft)

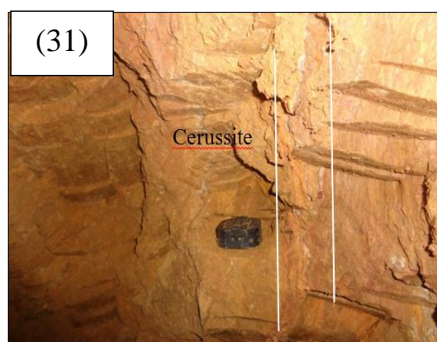


Figure 31 Disseminate or aggregate of lead carbonate (Myae Ni Taung Occurrence)

Ore Mineralogy

Galena (PbS)

It is the most common lead ore mineral and constantly associated with sphalerite and at some places with barite. In hand specimen, it shows cubic form and occurs as fine grained aggregate crystal with lead grey to silvery colour and shows submetallic lustre. Under microscope, it exhibits bright white colour and numerous triangular pits and absence of internal reflection (Figure 32 A & B).

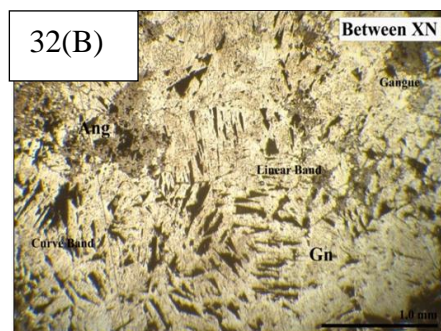
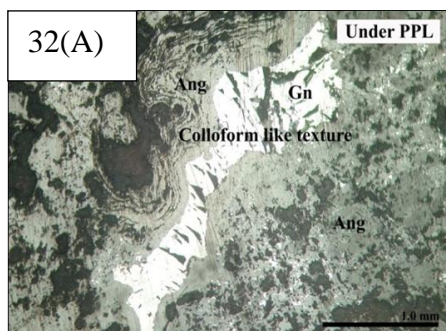


Figure 32 (A) Photomicrograph showing Galena ore (Gn=Galena, Ang=Anglesite), Under Reflected Light, (B) Between X.N.

Anglesite (PbSO_4)

Under ore microscope anglesite shows pale grey colour and situated along the crack and cleavage of galena. It is occasionally found in place, as a result of oxidation of lead sulphide to lead oxide and then galena has been replaced by anglesite with curving inward texture. (Figure 32 A)

Sphalerite (ZnS)

Under microscope sphalerite is observed by its gray colour with brown tint and yellowish brown to reddish brown internal reflection. It occurs as irregular anhedral masses in galena and other gangue minerals. It is harder than galena recognize by its higher relief in polish section. (Figure 33)

Pyrite (FeS_2)

It occurs in the main mineralized zone as tiny isolated crystals with subhedral to anhedral form in galena and host rocks. The earliest pyrite was probably formed during the late diagenesis of the host rock and late pyrite was formed during the hydrothermal stage associated with the galena and sphalerite mineralization. It can be distinguish by its reflectance, polishing hardness and its yellowish colour. (Figure 34)

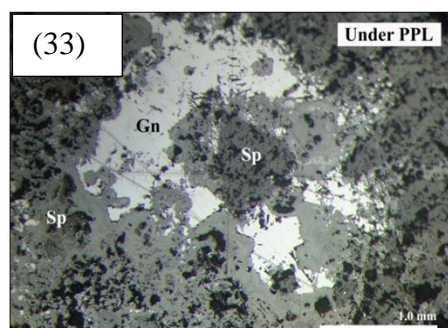


Figure 33 Photomicrograph showing Sphalerite with galena (Gn=Galena, Sp=Sphalerite), Under Reflected Light

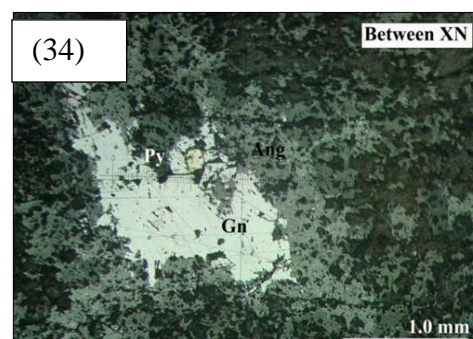


Figure 34 Photomicrograph showing subhedral to anhedral pyrite (Py=Pyrite, Gn= Galena) Under Reflected Light

Chalcopyrite (CuFeS_2)

It is a iron copper sulfide mineral and has brassy to goldern yellow colour. It is hard to see in hand specimen. Under ore microscope, it shows yellow coloured and its reflectance is less than that of pyrite. (Figure 35)

Covellite (CuS)

It is altered from chalcopyrite as a result of oxidation and shows indigo blue colour and at some portion it is partially mixed with chalcopyrite. (Figure 36)

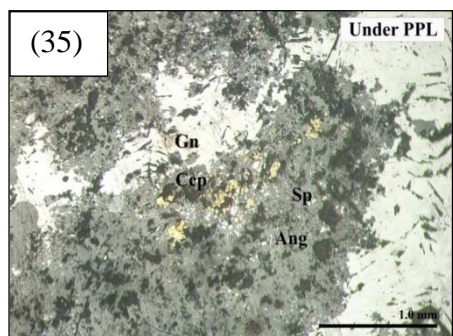


Figure 35 Photomicrograph showing Yellowish coloured chalcopyrite mineral in the lead ore (Gn=Galena, Sp=Sphalerite, Ccp=Chalcopyrite, Ang=Anglesite) Under Reflected Light

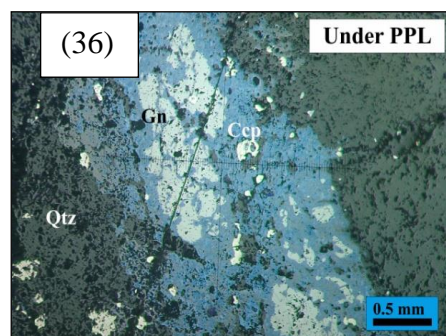


Figure 36 Photomicrograph showing indigo blue coloured covellite mineral in the lead ore. (Gn=Galena, Ccp=Covellite, Qtz=Quartz) Under Reflected Light

Paragenesis

Mineral	Early	Middle	Late
Pyrite	_____	_____	
Chalcopyrite	_____	_____	
Sphalerite	_____	_____	
Galena	_____	_____	
Covellite			_____
Anglesite			_____
Cerussite			_____

Geochemical Investigation

Seven representative ore samples are collected from Thein Than lead occurrence and these sample were tested by X-Ray Fluorescence (XRF) analysis method. These results from geochemical analysis were treated by geostatistical software and the following dendrogram is constructed by weight pair group method.

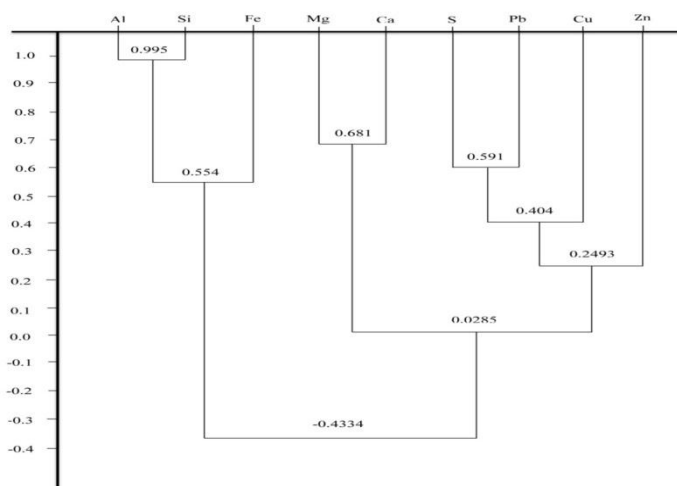
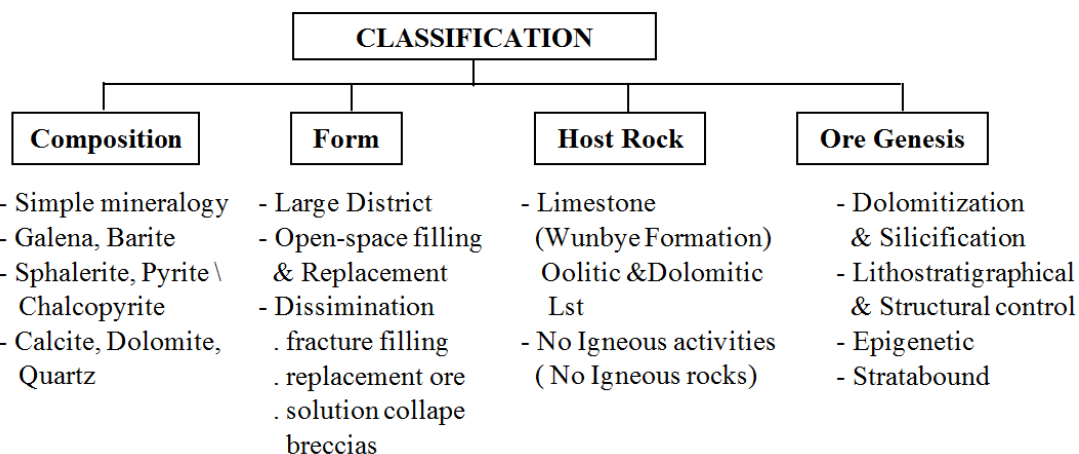


Figure 36 Dendrogram constructed by weighted pair group method

Ore Deposit type of Kyauktap Area



Due to all the above deposit features, the type of ore deposits is Carbonate-hosted, stratabound deposits and epigenetic in origin one of the sub-types of the Mississippi Valley-Type (MVT) deposits

Summary

The study area, Kyauktap is situated about 18 kilometer north of Heho, Taunggyi District, Shan State (South). The covering area is approximately 25 square kilometers. Regionally, it is situated in the southwestern part of Shan Plateau. The major structure, Bawsaing Range, regarded as a south-plunging anticline where the Precambrian rocks of Chaungmagyi Group are surrounded by Early Paleozoic rocks. The study area comprises the Pindaya Group of Ordovician age (Wunbye, Nan-on Formations) and Mibayataung Group of Silurian age (Linwe Formations). The ore occurrences have simple mineralogy that consists of galena, barite, sphalerite, pyrite, chalcopyrite, covellite and anglesite with little or no amounts of argentite. Dolomite, calcite and quartz are gangue minerals. Lead mineralization is spatially hosted by oolitic and dolomitic limestones. Texture of sulphide minerals are mostly related to open-space fillings of breccias, fractures and vugs and replacement of carbonate host rocks. Wallrock alterations took place after the formation of the carbonate host rocks mainly as dolomitization and silicification as subordinate process. They definitely predate the ore mineralization. So that the ore deposits are epigenetic in origin. The ore deposits occurred in the zones of highly brecciated dolomite, collapse breccias, bedding planes, faults and fractures, and these zones are arranged in linear patterns. Both structural controls and lithostratigraphical controls are important parametres for lead mineralization. Therefore they are stratabound deposit type. There is no igneous rocks and igneous activities in and around the ore deposits in the study area, so these ore mineralization cannot be attributed by magmatic ore forming process. As a result of above finding and reliable conclusions, the lead mineralization in the study area is carbonate hosted, stratabound deposit and epigenetic in origin and most probably belong to one of the sub-type of the Mississippi Valley-Type (MVT) deposit.

Acknowledgements

I would like to acknowledge all the respectful teachers of Department of Geology, University of Yangon. I would like to thanks deeply the members, who helps me in the literature review work, field work and drawing and applying geological software.

References

- Aung Than (2013): *Occurrence of Lead Mineralization in Shwe Taung-Yebok Area, Ywangan Township, Shan State (South)*, MSc Thesis, Department of Geology, University of Yangon. (Unpublished). 148p
- Hnin Min Soe, (2008): *Economic Geology of North Ywangan Township, Taunggyi District, Shan State (South), Myanmar*, PhD Dissertation, Department of Geology, University of Yangon. (Unpublished). 168p.
- Myint Lwin Thein, (1979): “Barite and Galena Occurrences in the Ordovician Rocks of the Western part of the Shan Plateau”, A paper read at Burma Research Congress.
- Thein Min Swe, (2017): *Occurrence of Lead Mineralization in the Mogyo Taung, Thapanbin Area, Ywangan Township*, M.Sc. Thesis, Department of Geology, University of Yangon. 89p

GEOLOGY AND ORE GENESIS OF LEAD-ZINC-COPPER MINERALIZATION IN MYINHE TAUNG -YASAGYI AREA, YWANGAN TOWNSHIP, SHAN STATE (SOUTH)

Aye Khaing¹ and May Thawe Aye²

Abstract

Myinhe Taung-Yasagyi area is located about 35 km southeast of Ywangan Township, Taunggyi District, Shan State (South). Regionally the study area mainly composed of sedimentary rocks of the Pindaya Group (Wunbye Formation) of Ordovician age, Mibayataung Group (Linwe Formation) of Silurian age and Plateau Limestone Group (Nwabangyi Formation) of Mid-Permian-Triassic. The Ganaingya fault is the major structure which is trending nearly NW-SE. The present research work involves the carbonate rocks of the Wunbye Formation (Middle Ordovician age) which hosts the lead-zinc-copper ore mineralization. In the study area, four lead-zinc-copper prospects are associated with the dolomitic limestone of Wunbye Formation. The lead sulfide mineralization is confined to the carbonate rocks of Wunbye Formation. The wallrock alteration zones are narrow, with dolomitization as the main alteration, and silicification as subordinate, which happen after the ore mineralization. The ore mineralogy is relatively simple where galena and barite form major constituents with minor amounts of sphalerite, pyrite, chalcopyrite, tetrahedrite, covellite, malachite and azurite. The gangue minerals are calcite, dolomite and quartz. Open-space fillings and replacement (irregular patches to massive aggregates) nature of ore mineralization are present. The lead-zinc-copper mineralization is localized by both structural and lithostratigraphical controls. Lead values range from 0.108% to 34.22% in Myinhe Taung near Yasagyi village. The contents of zinc range from 0.009% to 1.337%, copper ranges from 0% to 7.164% and barite ranges from 0% to 41.82% in the study area. Based on the geological, geochemical and mineralogical characteristics, the lead sulphide mineralizations in the study area are carbonate-hosted, stratabound, and epigenetic in origin and may be regarded as one of the sub-type of the Mississippi Valley-Type (MVT) deposits.

Keywords: Wunbye Formation, carbonate-hosted stratabound deposit, Mississippi Valley-Type

Introduction

Location, Size and Accessibility

The study area is located about 35 kilometres southeast of Ywangan and it is bounded by Latitudes 20°56'16"N 20°59'04"N and Longitude 96°34'32"E-96°36'51"E. (UTM map sheet no. 2096/09, about 20 square kilometres). Location map of the study area is shown in figure 1.

¹ Student, Ph D, Department of Geology, University of Yangon

² Associate Professor, Department of Geology, University of Yangon

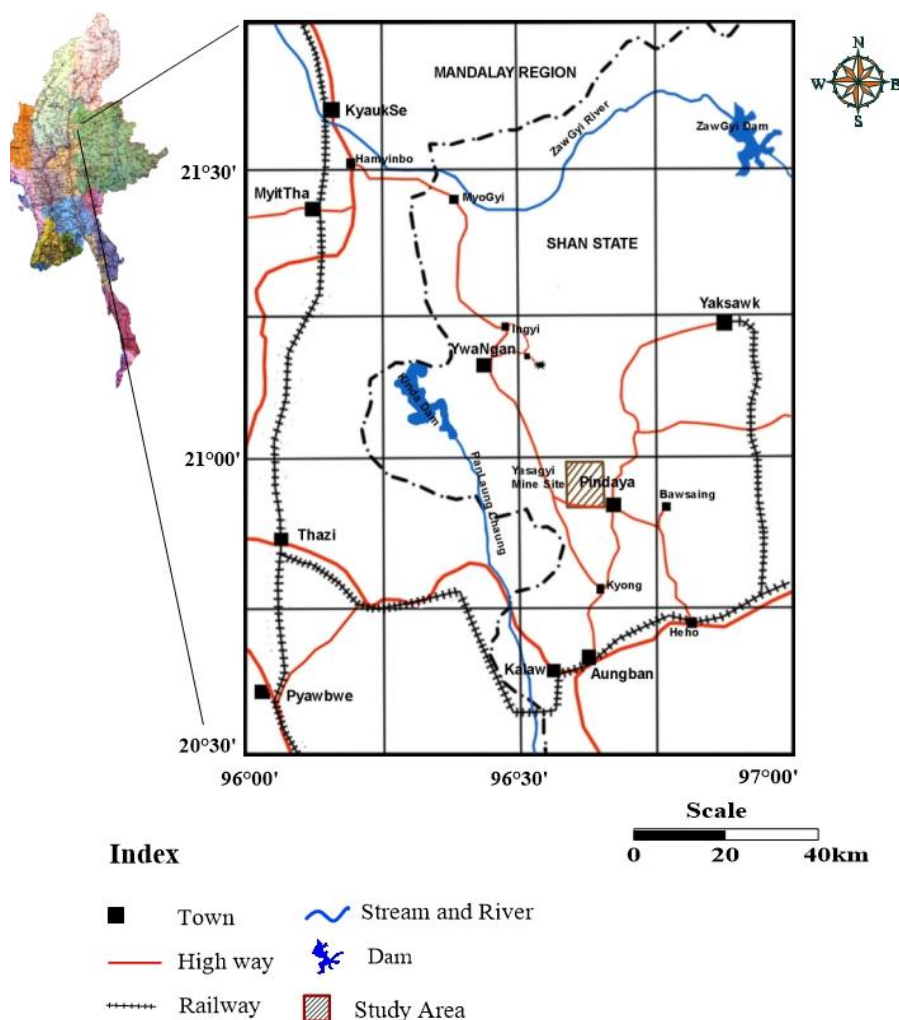


Figure 1 Location map of the study area, Ywangan Township, Shan State (South)

Scope and objectives

The major purposes of the study area are to prepare fairly detailed geological map of the study area, determine the petrography of the rocks and study ore genesis and ore deposit type of lead-zinc-copper mineralization in the study area.

Methods of study

- (1) Preliminary Study: Studies of previous literatures on Myinhe Taung-Yasagyi area and its environs.
- (2) Field Study: Systematic traversing, mapping, sampling and recording of rock units.
- (3) Laboratory Techniques: Ore Microscopy and X-Ray Diffraction, X-Ray Fluorescence are used in this research.

Geology and Petrography

Regional geology

Almost complete sequence of the Lower Paleozoic units are exposed in Myinhe Taung-Yasagyi area and its environs. (Figure 2)

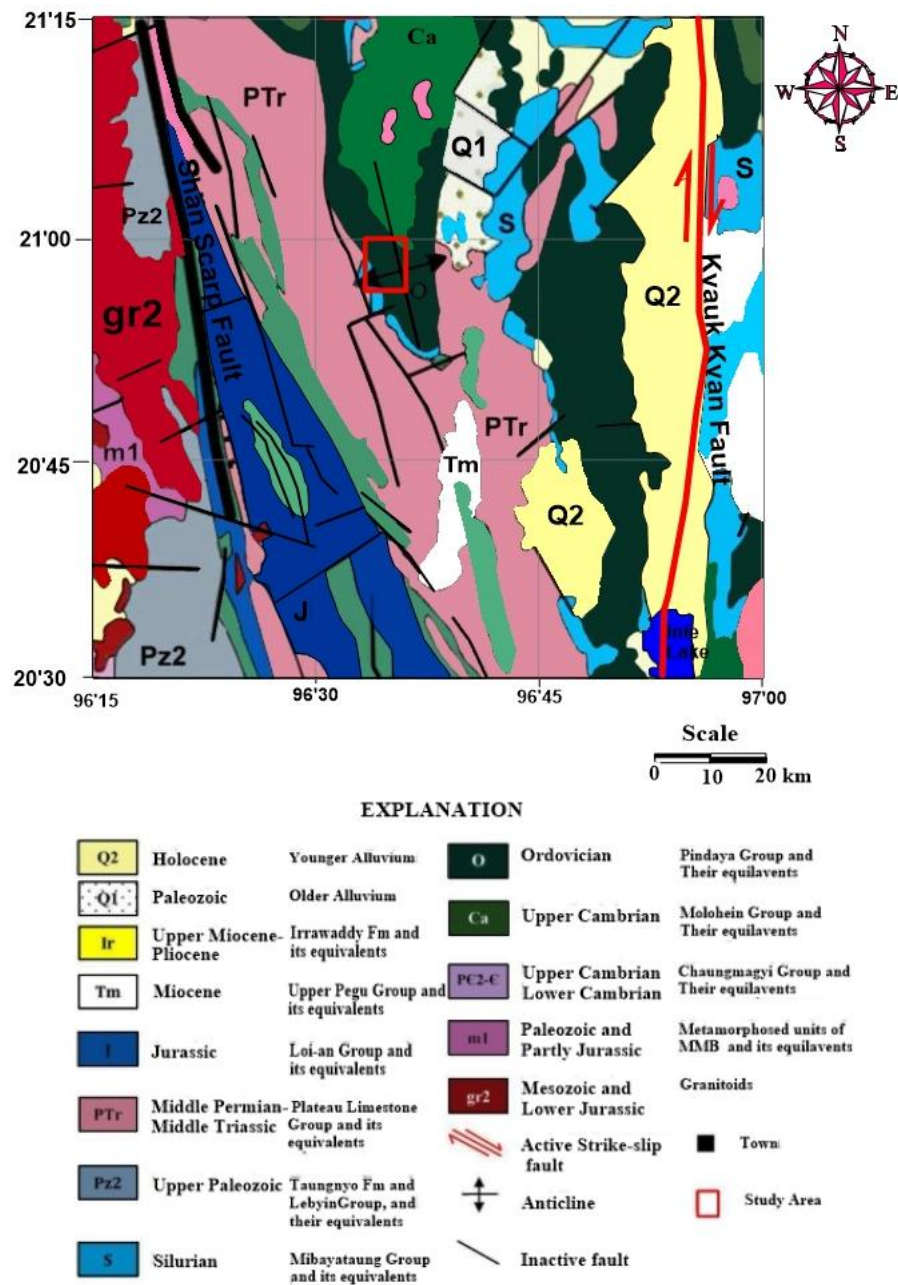



Figure 2 Regional Geological Map (MyanmarGeoscience Society, 2014)

Table 1 Rock Unit Sequence of Regional and Environs of the Study Area (After Myint Lwin Thein, 1973 & Garson *et al.*, 1976)

Group	Formation	Age
Plateau Limestone Group	Nattiek Formation	Middle Triassic
	Nwabangyi Dolomite Formation	Late Permian to Early Triassic
	Thitsipin Limestone Formation	Middle Permian
Unconformity		
Mibayataung Group	Taungmingyi Member	Late Silurian
	Wabya Formation	Late Silurian
	Linwe Formation	Early Silurian
Pindaya Group	Tanshauk Member	Late Ordovician
	Nan-on Formation	Late Ordovician
	Wunbye Formation	Middle Ordovician
	Lokepyin Formation	Early Ordovician
Molohein Group	Myet-ye Formation	Late Cambrian
	Pandaung Formation	Early Cambrian
Chaungmagyi Group		Precambrian

Regional geological structures

The investigated area is located on the western limb of south plunging anticline. The prominent faults are Shan Scarp Fault and Kyaukkyan Fault. They are trending N-S to NNW-SSE direction, that is more or less parallel to regional trend of the rock units. The other faults are trending NE-SW direction, E-W direction and NW-SE direction. (Table 1)

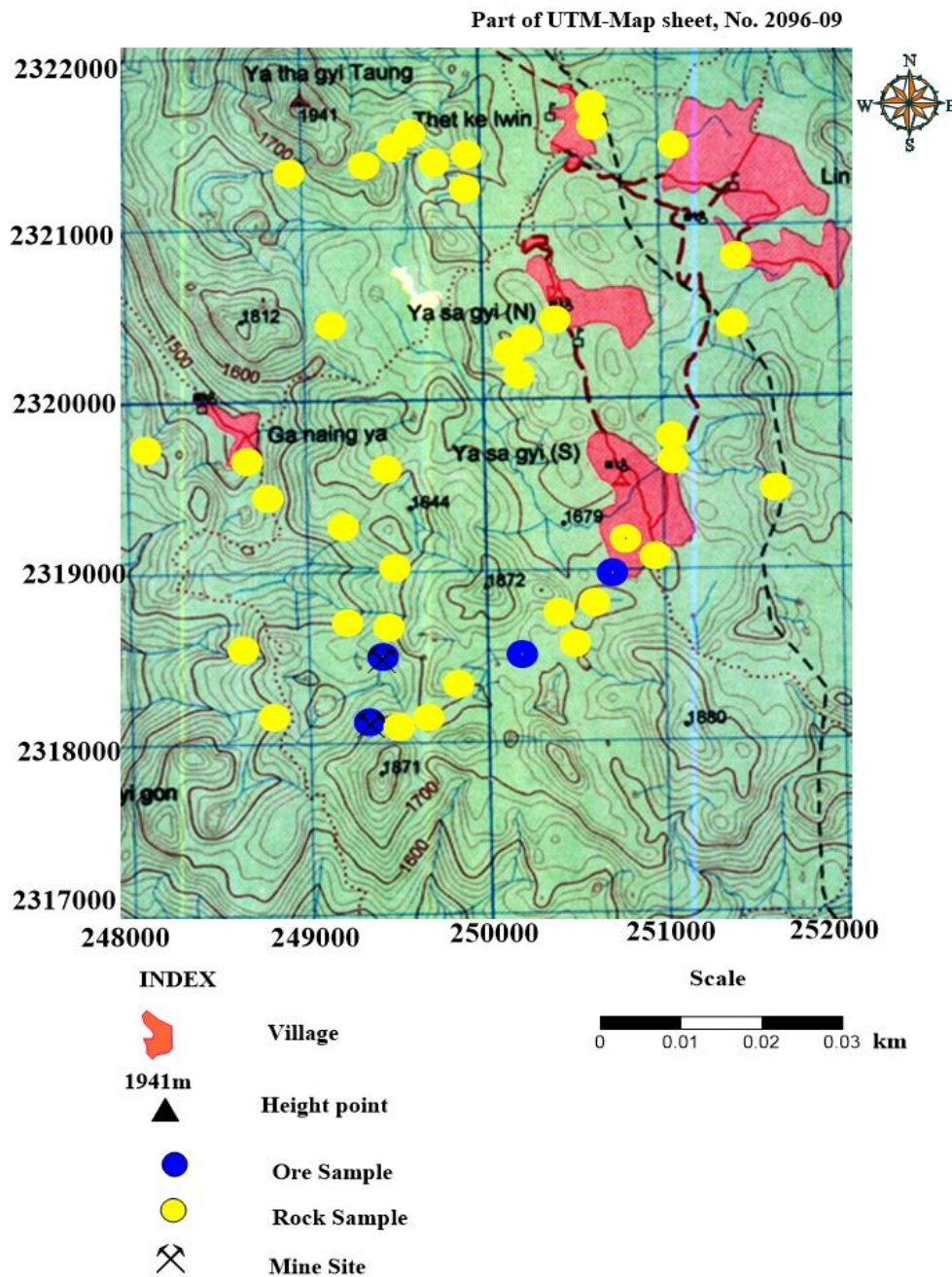


Figure 3 Sample location map of the study area

Geology of the study area

The study area is located in the nearly western part of Pindaya anticline. It is mainly comprises the Pindaya Group (Ordovician age) and Mibayataung Group (Silurian age). Sample location map of the study area can be seen in Figure 4 and the geological map and cross section of the study area shows in Figure 5. The stratigraphic classification of the study area is adopted from MyintLwinThein (1973). In the study area, Wunbye Formation of Pindaya Group, Linwe Formation of Mibayataung Group and Nwabangyi Formation of Plateau Limestone Group were observed. Detailed stratigraphic succession of the present study area is shown in Table 2.

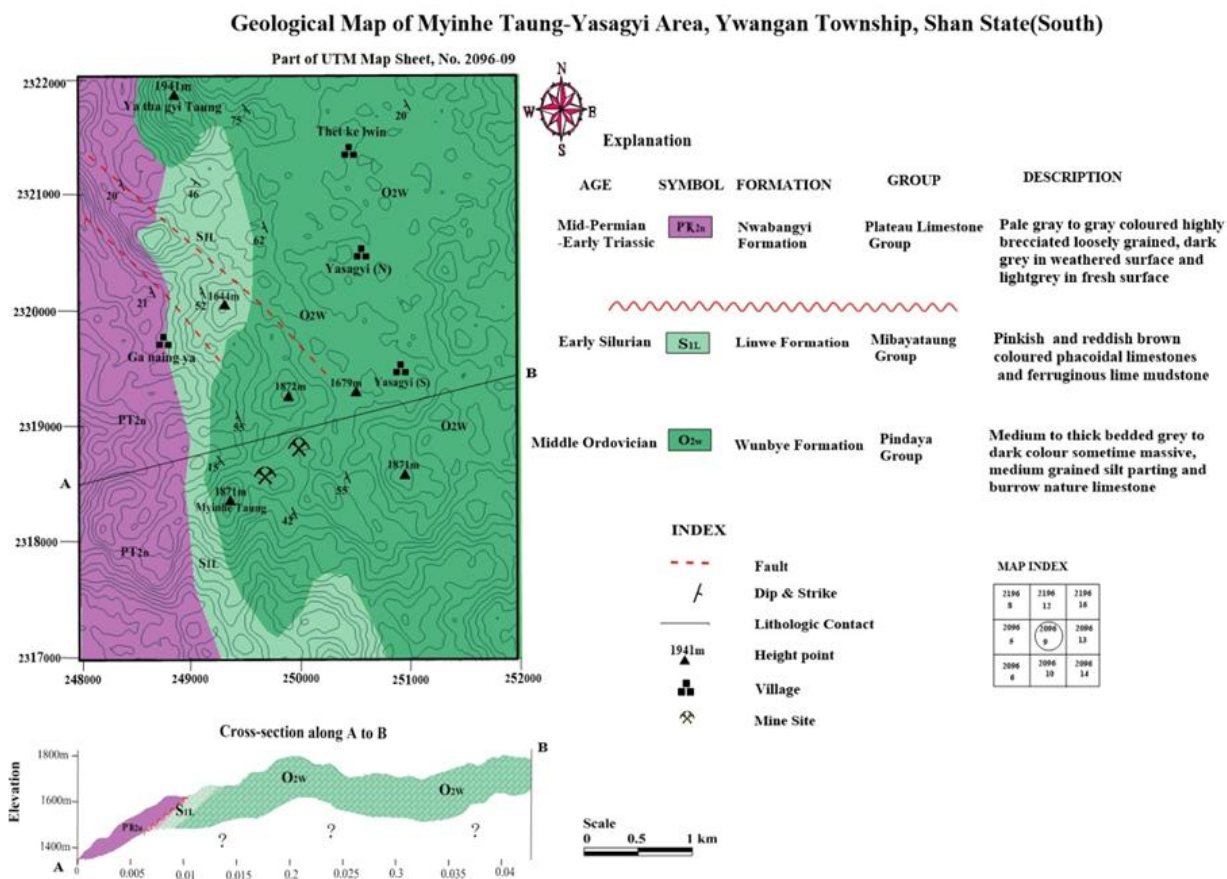


Figure 4 Geological map and cross section of the study area

Table 2 Detail stratigraphic succession of study area.

No	Group	Formation	Age
3	Plateau Limestone Group	Nwabangyi Formation	Middle Permian to Early Triassic
	Unconformity		
2	Mibayataung Group	Linwe Formation	Early Silurian
1	Pindaya Group	Wunbye Formation	Middle Ordovician

Pindaya Group

Wunbye Formation (Middle Ordovician)

Fine grained, grey to dark grey coloured, medium to thick-bedded and massive limestones with typical burrow structure shown in Figure 5 & 6. Rhomb shape dolomite mineral in dolomitic limestone is shown in Figure 8. Hand specimen of dolostone and coarse-grained crystalline texture (PPL) are shown in Figure 9 & 10.



Figure 5 Outcrop nature of limestone (Wunbye Formation, Location: 47Q 0250175 E 2320339 N



Figure 6 Outcrop nature of thick-bedded limestone, Location: 47Q 0249701 E 2321482N



Figure 7 Hand specimen of reddish brown limestone, Location: 47Q 0249887E 2318333N

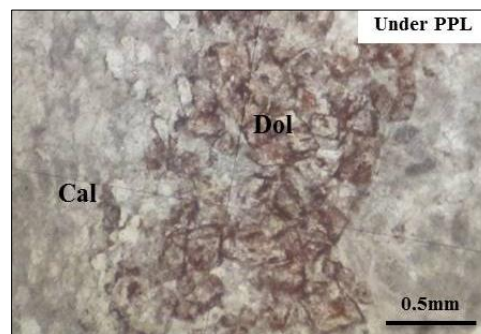


Figure 8 Photomicrograph of rhomb shape dolomite mineral in dolomitic limestone, Sample No.YSG-R-10



Figure 9 Hand specimen of dolostone, Location: 47Q 0250127E 2320220N

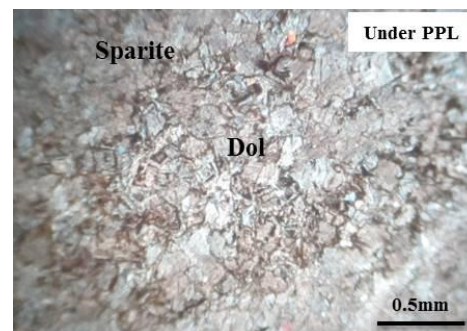


Figure 10 Photomicrograph of medium to coarse-grained crystalline texture, Sample No.YSG-R-17



Figure 11 Hand specimen of Limestone (Wunbye Formation), Location: 47Q 0249701E 2321482N

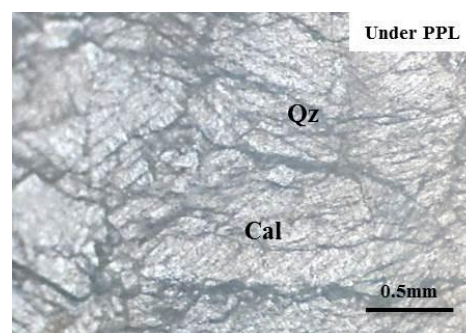


Figure 12 Photomicrograph showing 80% of crystalline calcite grains, Sample No.YSG-R-27



Figure 13 Hand specimen of Limestone (Wunbye Formation), Location: 47Q 0249201E 2321582N

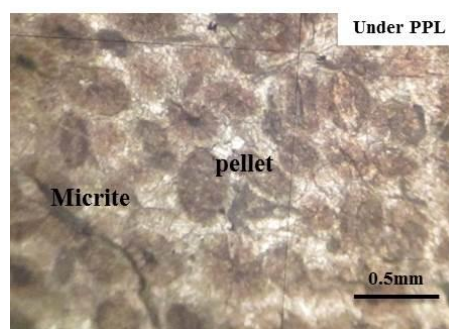


Figure 14 Photomicrograph showing dolomite and a minor amount of pellet, Sample No.YSG-R-33



Figure 15 Hand specimen of Limestone (Wunbye Formation), Location: 47Q 0250395E 2318573N

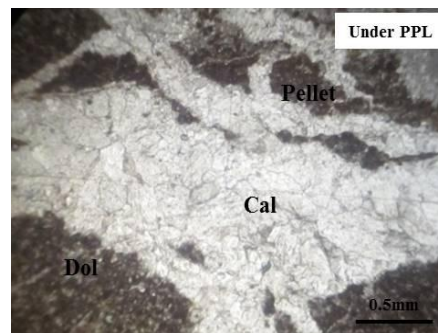


Figure 16 Photomicrograph showing subrounded shape of pellets or peloids, Sample No.YSG-R-7

Minor amount of pellet and subrounded shape of pellets or peloids under PPL are shown in Figure 14 & 16. Hand specimen of pink and purple limestone and *Ostracod* funnas inferruginous lime mudstone (Linwe Formation) are shown in Figure 17&18.

Mibayataung Group

Linwe Formation (early Silurian) Purple, pink and grey color, phacoidal limestones, ferruginous lime mudstones are exposed near the monastery of Ganaya village.



Figure 17 Photograph showing hand specimen of pink and purple limestone (Linwe Formation) Location: 47Q 249064E 2320456N

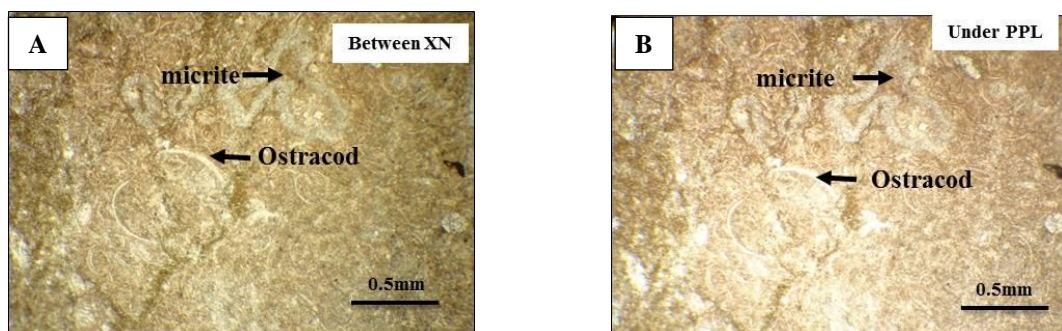


Figure 18 Photomicrograph of ferruginous lime mudstone (A and B) showing *Ostracod* funnas inferruginous lime mudstone (Linwe Formation), Sample No.YSG-R- 54

Nwabangyi Formation

Petrographic classification of limestone used in the present study are adopted from Dunham (1962). Hand specimen of dolomitie (Nwabangyi Formation) and its subhedral to euhedral with planar boundries (Nwabangyi Formation) are shown in Figure 19(A/B) & 20(A/B).

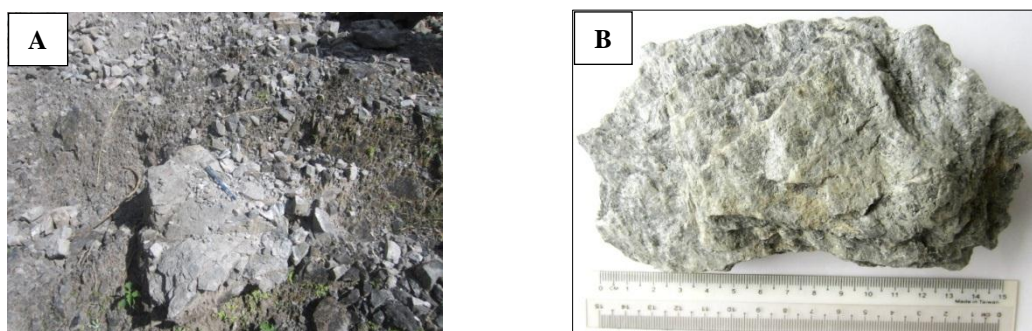


Figure (19-A/B) Photograph showing hand specimen of dolomitie (Nwabangyi Formation), Location: KD 488 182

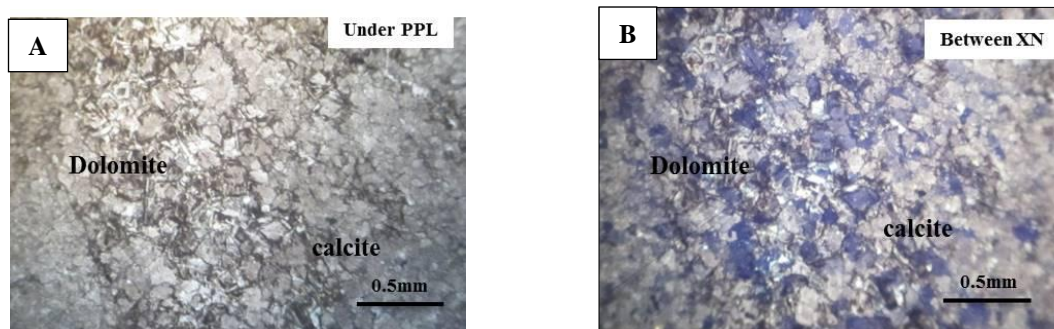


Figure 20 Photomicrograph of dolomite (A and B) showing subhedral to euhedral with planar boundries (Nwabangyi Formation), Sample No. YSG-R- 61

Alteration

In the study area, main host rock is limestone. By the field observation and microscopic study, the dominant alteration is dolomitization accompanied by minor silicification. Dolomitization with Pb mineralization (Thin section) is shown in Figure 21(A /B). Silicification with Pb mineralization (Thin section) is shown in Figure 22(A /B).

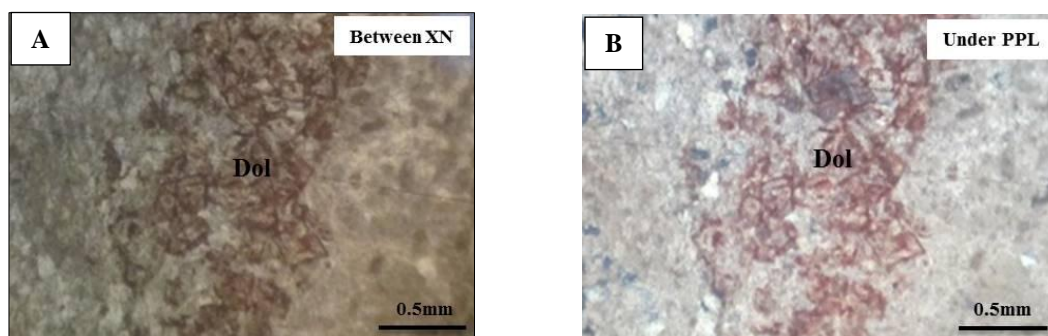


Figure 21 Photomicrograph showing dolomitization (A and B) with Pb mineralization (Thin section) (Dol= Dolomite)

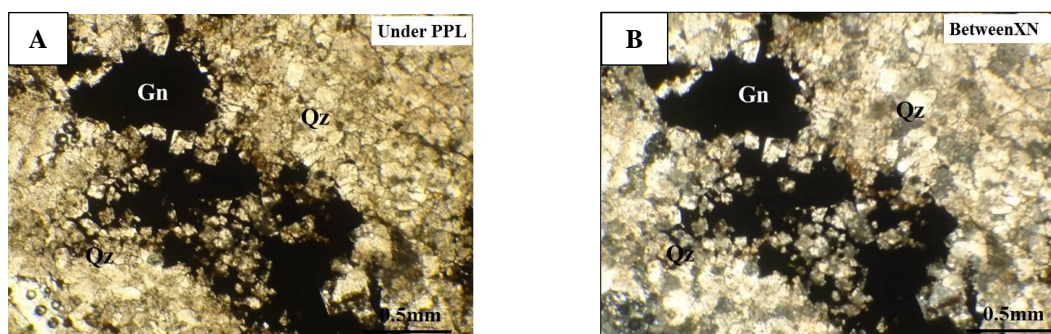


Figure 22 Photomicrograph showing silicification (A and B) with Pb mineralization (Thin section) (Gn= Galena, Qz= Quartz)

Mineralization

In the study area lead and copper ore mineralization can be found at two localities.; Myinhe Taung Lead and Copper Occurrences, they are mainly produced lead sulphide ore (Galena-PbS) and lead carbonate ore (Cerussite-PbCO₃). Yasagyi Copper Occurrences; which consist of azurite and malachite minerals found on the rock surface. In the study area, main copper ore are tetrahedrite.

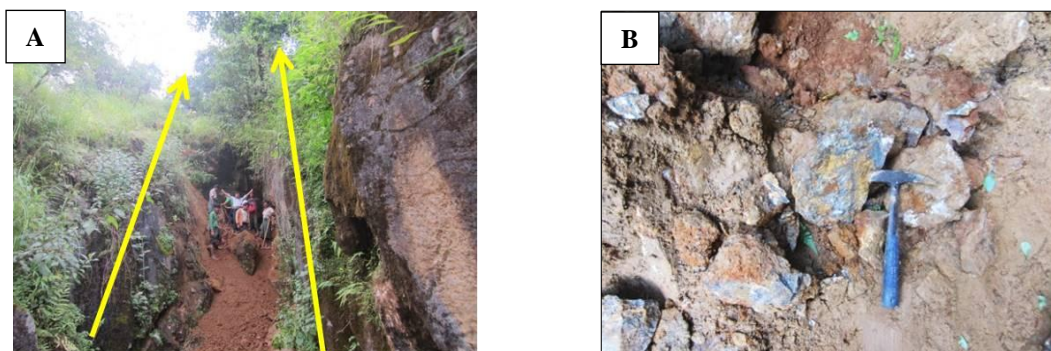


Figure 23 Photograph showing long trench Mine site-1(A and B) (facing NE) at Myinhe Taung; Location 47Q 249350E 2318199N

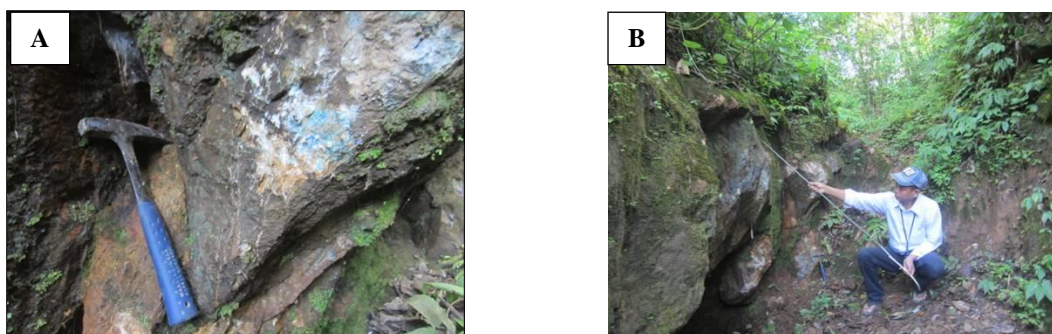


Figure 24 Photograph showing copper ore veinlet(A and B) near Yasagyi(S) village, Location: 47Q 243683 E 2347071N

The mineralization mainly occurred as veinlets (fracture filling) and disseminated in the host rock. The major ore mineral is galena and associated minerals are sphalerite, pyrite, azurite, malachite, covellite and little or no amount of argentite. Long trench Mine site-1 copper ore veinlet(A and B) near Yasagyi(S) village are shown in Figure 23(A /B) and Figure 24(A /B).

Ore Mineralogy

Galena (PbS)

The primary lead ore as galena can be observed in the Wunbye Formation. It is constantly associated with sphalerite and barite. Galena (PbS) is the most common lead ore mineral. Under ore microscope galena is characterized by light or light-grey colour and high reflectivity. It is also readily identified by the presence of triangular pits in Figure (25).

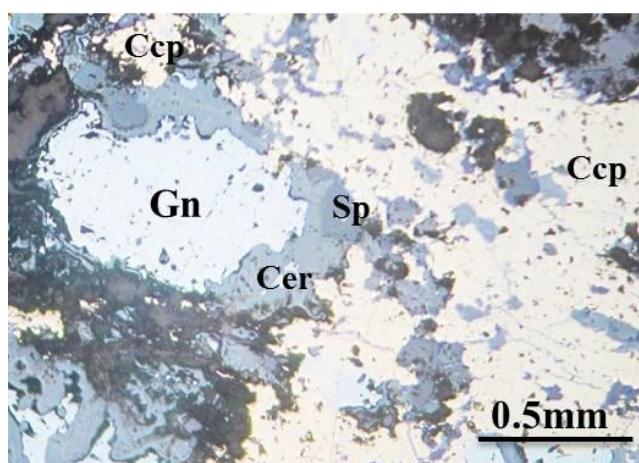


Figure 25 Photomicrograph showing galena with sphalerite (Under Reflected Light) (Gn=Galena, Sp=Sphalerite, Cer=Cerussite, Ccp=Chalcopyrite)

Cerussite (PbCO₃)

Cerussite is a lead carbonate mineral, usually found in oxidized zone of lead ore deposits. It is a very common weathering product of galena and other lead ore minerals. Its colour is colourless, white, gray blue or green. It shows colourless in transmitted light as well as vitreous, pearly, dull and earthy lustre. Under microscope, cerussite is observed as pale gray minute grains filled along the crack and cleavage of galena in Figure (25).

Sphalerite (ZnS)

The sphalerite is light-grey in colour with low iron content. It occurs as irregular anhedral masses in galena and other gangue minerals. In the study area, the sphalerite is characterized by its gray colour with brown tint and yellowish brown to reddish brown internal reflection under the microscope Figure (25).

Tetrahedrite

Under ore microscopie, tetrahedrite is the most common copper ore. It shows olive grey colour, medium relief and fairly internal reflection. Tetrahedrite occurs as groundmass. Irregular grain of chalcopyrite (Ccp) and tennantite(tn) are guest in the groundmass. Sphalerite(sp) is replaced in the groundmass of tetrahedrite(td). In Fig. (6.26), tetrahedrite(td) is replaced by chalcopyrite(Ccp).

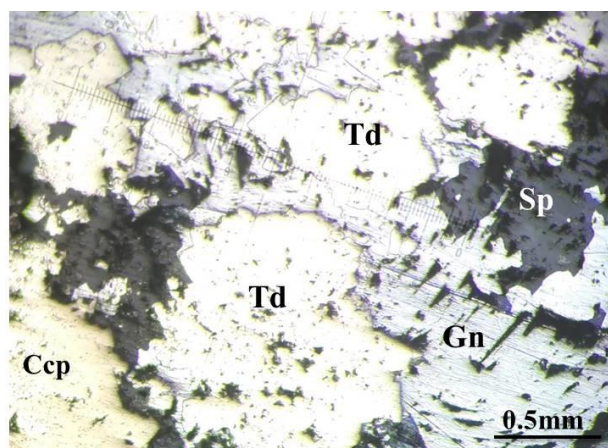


Figure 26 Photomicrograph showing tetrahedrite (Td) (Gn = Galena, Sp = Sphalerite, Ccp = Chalcopyrite) (Under Reflected Light)

Paragenesis

The purpose of the paragenetic study is to understand the principles of ore deposition, character of the minerals deposited during each period, and the trace elements they contain and shown in (Table-3).

Table 3 The Paragenetic Sequence of Ore Minerals in the Study Area

Mineral	Early	Middle	Late
Barite	_____	_____	_____
Pyrite	_____	_____	_____
Chalcopyrite	_____	_____	_____
Tetrahedrite	_____	_____	_____
Sphalerite	_____	_____	_____
Galena	_____	_____	_____
Covellite	_____	_____	_____
Malachite	_____	_____	_____
Azurite	_____	_____	_____

Geochemical Investigation

Fourteen representative ore samples were selected randomly from the occurrences of carbonate-hosted galena and copper mineralization and oxidized breccia zones. X-Ray Fluorescence analysis is conducted to determine the lead and other metals at Ministry of Science and Technology laboratory (Pyin Oo Lwin). Statistical data of the study area is shown in Table 4 and dendrogram of Myinhe Taung-Yasagyi Lead-Zinc-Copper Prospects is also shown in Figure 27.

Table 4 Statistical data of the study area

No	Element	Mean (\bar{X}) Value	Standard deviation (S) value	Threshold ($\bar{X}+2S$) value	Range	
					Minimum	Maximum
1	Pb	4.760	7.296	19.352	0.000	22.220
2	Zn	0.264	0.423	1.11	0.009	1.337
3	Cu	0.855	2.022	4.899	0.000	7.164
4	Fe	1.564	1.725	5.014	0.179	5.398
5	S	2.694	3.021	8.736	0.0859	8.274
6	Ba	12.430	15.891	44.212	0.000	41.82

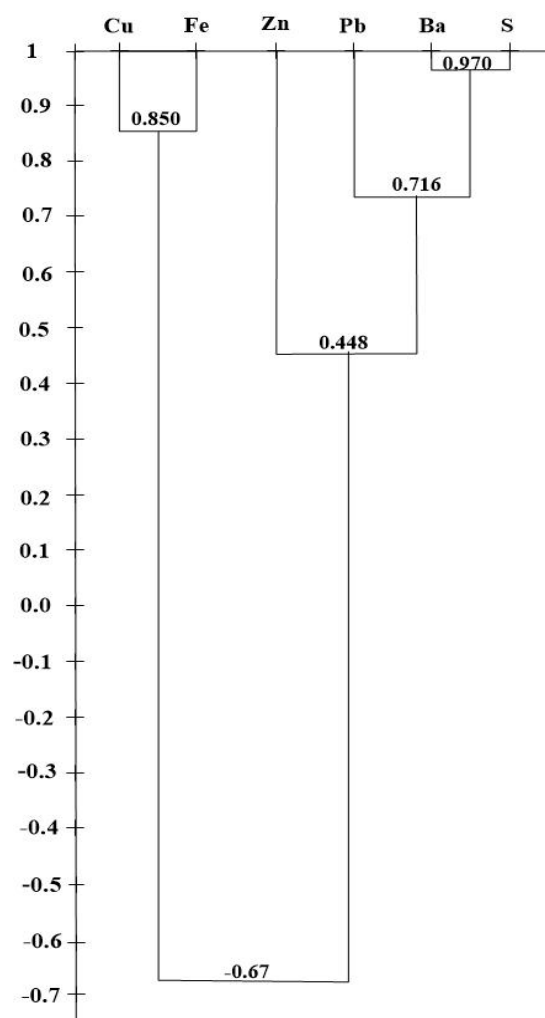


Figure 27 Dendrogram of Myinhe Taung-Yasagyi Lead-Zinc-Copper Prospects

Ore Deposit Type of The Myinhe Taung-Yasagyi Area

The carbonate-hosted base metals deposits in Myinhe Taung – Yasagyi area occurred within the dolomitic limestone of Wunbye Formation of Middle Ordovician age. A cluster of lead-copper deposits in the study area are found along on the western flank of the Pindaya Range and formed in a shallow marine environment. The Lead prospects have simple mineral assemblages comprising galena, barite, sphalerite, tetrahedrite, pyrite, chalcopyrite, azurite and malachite. The ore deposits occur in the zones of highly brecciated dolomite, collapse breccias, bedding plane, faults and fractures and these zones are arranged in linear patterns suggesting a distinct structural control. All the above deposit features strongly indicate that the lead-zinc-copper mineralization of Myinhe Taung-Yasagyi area probably belong to one of the sub-types of the Mississippi Valley-Type (MVT) deposits with their own slightly different characteristics.

Summary

The study area, Myinhe Taung-Yasagyi area is located about 35 kilometres southeast of Ywangan, Taunggyi District, Shan State (South). Area of coverage is approximately 20 square kilometres. Regionally, it is situated at the western part of Pindaya Range. The study area is located between the Shan Scarp Fault and Kyaukyan Fault. The highest peak is Yathagyi Taung 1941m. The study area comprises the Pindaya Group of Ordovician Age (Wunbye, Formation), Mibayataung Group of Silurian Age (Linwe Formation) and Plateau Limestone Group of Mid-Permian-Triassic Age (Nwabangyi Formation). The present research work involves the carbonate rocks of the Wunbye Formation (Middle Ordovician age) which hosts the lead ore mineralization. The wallrock alteration zone is narrow where dolomitization alteration forms the main alteration predating the lead sulfide mineralization and silicification is subordinate. Most of the lead ore mineralized host rocks are dolomitic limestone as well as oolitic limestone. The major constituents are galena, barite, and minor as malachite and azurite, and also with minor amount of sphalerite, pyrite and chalcopyrite, tetrahedrite, covellite and cerussite. Lead-Zinc-Copper mineralization extensively occurred in Myinhe Taung range in three distinct styles, namely, disseminations, fracture fillings (veinlets) and replacement ores (irregular patches to massive aggregates). From the above mentioned findings and plausible conclusions, the lead sulfide mineralizations in the study area are carbonate-hosted, stratabound, and of epigenetic in origin and most probably belong to one of the sub-types of the Mississippi Valley-Type (MVT) deposits.

Recommendation

Currently, local miners are mining artificially lead sulfide ore at Myinhe Taung and Yasagyi area. Moreover lead sulfide ore prospects need further and more detailed explorations whether to make them minable lead deposits. There are distinct and useful structural and lithostratigraphical ore guides that could help for any future exploration activity in the study area. As structural controls, regionally the NNW-SSE and NNE-SSW trending lineations, locally faults and fractures are well examined the lead prospects. As lithostratigraphical controls, both regionally and locally oolitic limestone and dolomitic limestone within the Wunbye Formation of Middle Ordovician age are also important.

Acknowledgements

We would like to acknowledge all the respectful teachers of Department of Geology, University of Yangon. We also would like to thanks deeply to the members, who helps us in the literature review works, field works, drawing and applying geological softwares.

References

- Hnin Min Soe, (2008): *Economic Geology of North Ywangan Township, Taunggyi District, Shan State (South), Myanmar*, PhD Dissertation, Department of Geology, University of Yangon. (Unpublished). 168p.
- Myint Lwin Thein, (1973): The Lower Paleozoic Stratigraphy of Western part of the Southern Shan State, Burma: *Geol. Soc. Malaysia, Bulletin No. 6*, pp. 143-163.
- Myint Lwin Thein, (1979): Barite and Galena Occurrences in the Ordovician Rocks of the Western part of the Shan Plateau, A paper read at Burma Research Congress.
- San Win, (2016): Geology and Geochemical Investigation of Lead Mineralization in the West of Yebu Area, Thazi Township, *MSc Thesis, Department of Geology, University of Yangon*. 89p.
- Thein Min Swe, (2017): Occurrence of Lead Mineralization in the MogyoTaung, Thapanbin Area, Ywangan Township, *M.Sc. Thesis, Department of Geology, University of Yangon*. 89p

PRELIMINARY STUDY OF LEAD MINERALIZATION AT TAUNG GAUNG AREA, MADAYA TOWNSHIP, MANDALAY REGION, MYANMAR

Aung Ye Ko^{1,2}, Day Wa Aung³ and Ohn Thwin⁴

Abstract

Taung Gaung area is situated in Madaya Township, Mandalay Region, Myanmar. It is located approximately 30 km to the northeast of Mandalay, and 26 km northwest of Pyin-Oo-Lwin. The study area, falling in the Shan-Thai Block, lies in the eastern margin of Mogok Metamorphic Belt (MMB) and between the Sagaing Fault in the west and the Shan Scarp Fault in the east. Ordovician limestone is the main ore host rock in the Taung Gaung area. The regional trend of the rocks is generally N-S with dips either to the east or west forming asymmetrical anticlines and synclines. The major faults also trend N-S following the regional trend. The Ordovician limestone unit trends N-S and is broadly folded into a major anticline. The colour of limestone along the mineralization zone changes from pale blue to yellowish brown due to the effect of alteration. The mineralization follows the anticlinal axis of the major anticline, characterized by shearing and brecciation. The dominant alteration is dolomitization accompanied by minor silicification. Others are pyritization and limonitization. The principal ore mineral in Taung Gaung lead deposit is galena associated with sphalerite and minor amounts of anglesite, cerussite, jalpaite, marcasite and pyrite. In a separate paragenesis, copper as chalcopyrite, tetrahedrite - tennantite, covellite, chalcocite and azurite-malachite are also found in this area. The gangue minerals include limonite, siderite, ankerite, barite, dolomite, calcite and quartz. By the field observation and under microscopic study, several styles of mineralization were found to have formed under variable conditions, such as lead-zinc minerals occurring as disseminations, replacement ore, fracture - fillings and mineralized solution collapse breccias.

Keywords – Taung Gaung, Ordovician limestone, anticline, dolomitization, galena, tetrahedrite-tennantite.

Introduction

This paper is mainly based on the first author's third year field work and laboratory studies for his Ph.D Degree. Taung Gaung area is situated in Madaya Township, Mandalay Region. It is located approximately 30 km to the northeast of Mandalay, and 26 km northwest of Pyin-Oo-Lwin. The area lies west of the Shan Plateau where the topography is of rolling hills with the elevation around 270 m above mean sea level. The area is drained by parallel Yechi Chaung and Kyauk Kwe Chaung flowing from south to north. Location map of the study area is shown in Fig.1. The panoramic view of the Taung Gaung Taung is shown in Fig. 2.

Aim and Methods of Study

The major purpose of the study area is to determine the mineralogical characteristics of the ore minerals, alteration and mineralization. This study consists of two main stages, field work and laboratory work. During the field work, ore samples were collected randomly and selectively from the mineralized area at Taung Gaung lead deposit. The laboratory work consists of ore microscopy and Scanning Electron Microscopy (SEM) - Energy-Dispersive X-ray Analyzer (EDX) analysis.

¹ Lecturer, Science and Technology Research Center (Pyin Oo Lwin), Myanmar

² Ph.D Candidate, Department of Geology, University of Yangon, Myanmar

³ Dr, Professor & Head, Department of Geology, University of Yangon, Myanmar

⁴ Dr, Part-Time Professor, Department of Geology, University of Yangon, Myanmar

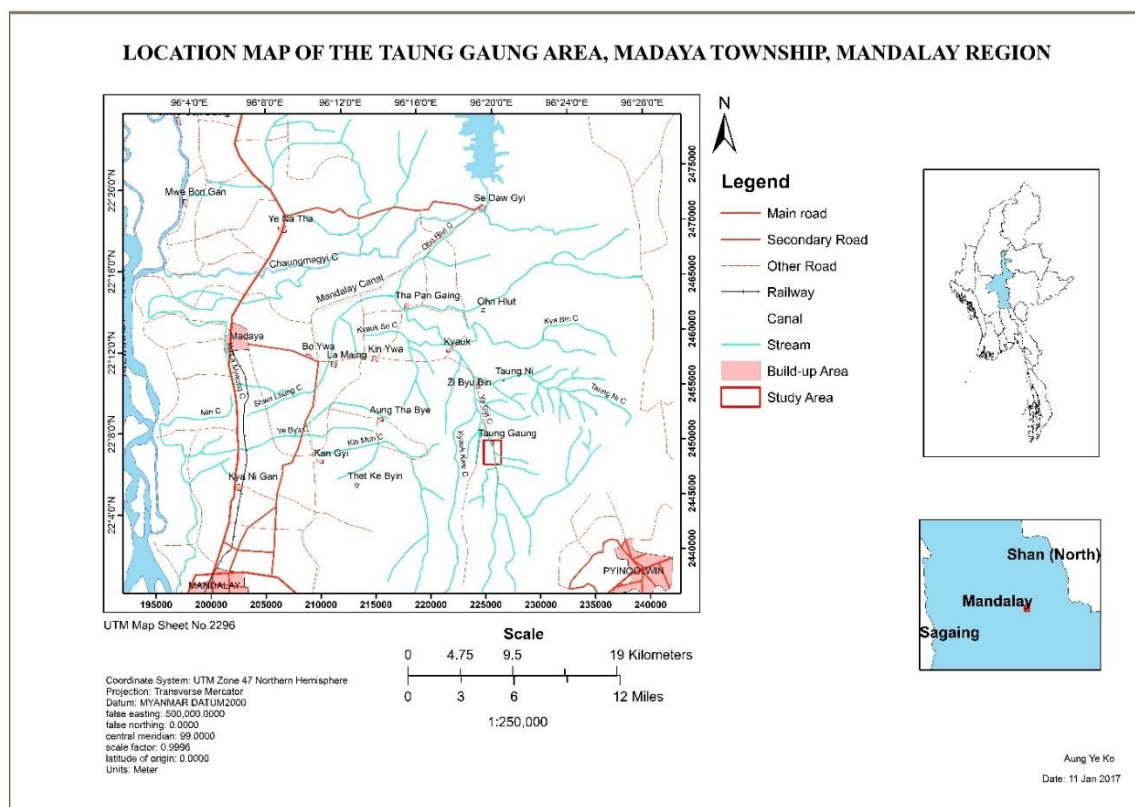


Figure 1 Location Map of the Taung Gaung Area, Madaya Township, Mandalay Region

Geological Background

With increased knowledge in plate tectonics, it is now generally accepted that Myanmar (Burma) is geologically built up of two main parts, the Eastern Part or Shan-Thai Block (Bunopas & Vella, 1983) or Sibumasu Terrane (Metcalf, 1984) (Kachin Highlands, Shan Plateau, Tenasserim Ranges, East Himalayan Syntaxis, Mogok Metamorphic Belt, etc.) and the Western Part or Burma Platelet or Burma Microplate (Curry et al., 1979) or West Burma (Searle et al., 2007) with its accretionary prism of Indo-Burman Ranges or Western Ranges (Naga and Chin Hills and Arakan Yoma). Sagaing Fault, a major right lateral strike-slip fault of 1500 km length (Win Swe, 2013. Soe Thura Tun & Watkinson, I.M.2017) geotectonically separates these two parts from the middle. Both parts belong to the larger Asian Plate. India Plate is subducting beneath Burma Microplate, and thus, in the Andaman Sea, forms an east-dipping curvilinear oblique subduction zone that continues onshore along the Western margin of the Indo-Burman Ranges.

The study area, falling in the Shan-Thai Block, lies in the eastern margin of Mogok Metamorphic Belt (MMB) and between the Sagaing Fault in the west and the Shan Scarp Fault in the east. It occupies the western marginal zone of Shan Plateau to the east of the Central Myanmar Basin (Fig.3). The MMB consists of metamorphosed sedimentary sequences of Precambrian to Carboniferous age. Basement sediments are intruded by Jurassic to Tertiary age granitoids. Regional stratigraphy of the research area and its environs is shown in Fig. 4. Stratigraphic rock units include Mogok Group, Chaungmagyi Group, Pangyun Group, Naungkangyi Group and Upper Plateau Limestone.

The geology of the Taung Gaung area is quite simple. It is composed of the Chaungmagyi Group of Mauk Kaw quartzite trending North-South and Ordovician limestone, comparable to the Wunbye Formation of Southern Shan State (Khin Maung Shwe, 1973). It mainly consists of limestone and dolomitic limestone with a general trend N-S. The limestones are fairly crystalline and grey to bluish grey in colour. Burrow textures are abundantly observed on both weathered and fresh surfaces of limestone. Dolomitic limestones are usually medium- to thick-bedded. Geological map of the Taung Gaung area and its environs is shown in Fig.5. The regional trend of the rocks is generally N-S with dips either to the east or west forming asymmetrical anticlines and synclines. The Ordovician limestone unit trends N-S and is broadly folded into a major anticline. The western limb of the anticline has been eroded away. The major faults also trend N-S following the regional trend. The dip amounts vary from (32° and 46°).



Figure 2 Panoramic View of the Taung Gaung Taung
Location: 96°20'2.372" E and 22° 07' 24.425" N (Facing: South)

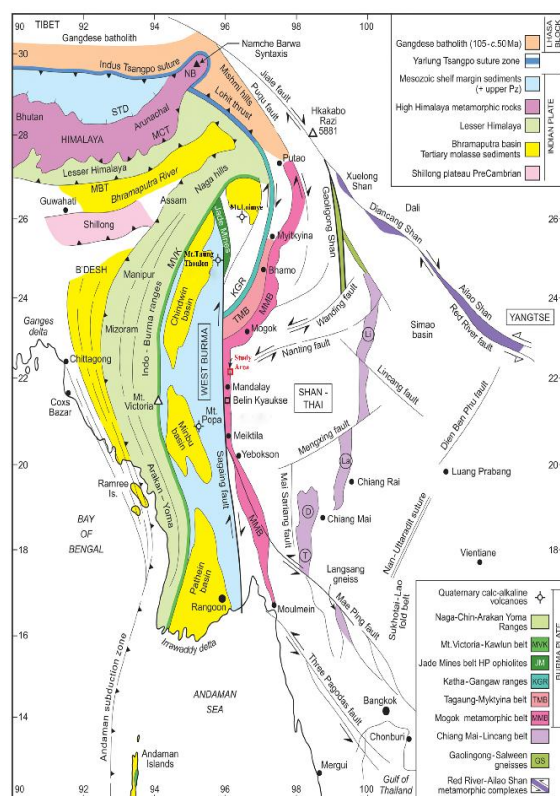


Figure 3 Geological map of Myanmar and surrounding areas showing major structures, faults and Terrane boundaries

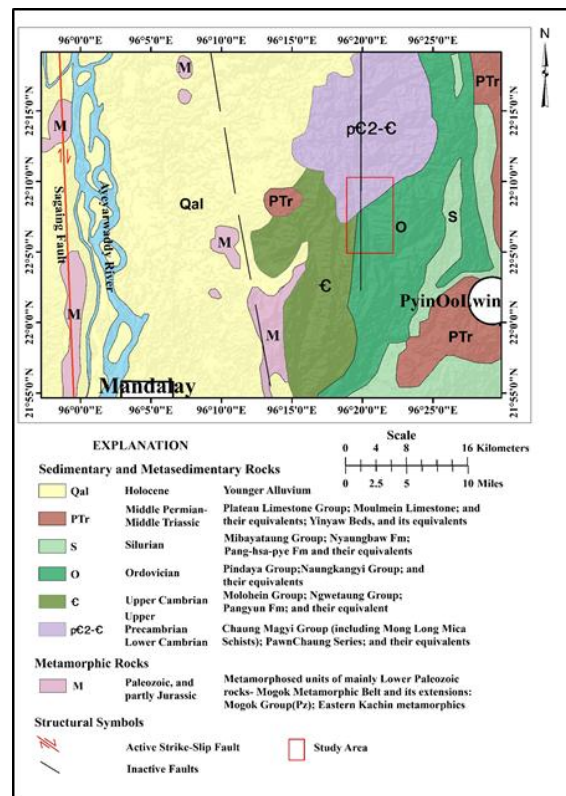


Figure 4 Regional geological map of the study area and its environs (After MGS, 2014)

(Modified after Searle et al., 2007)

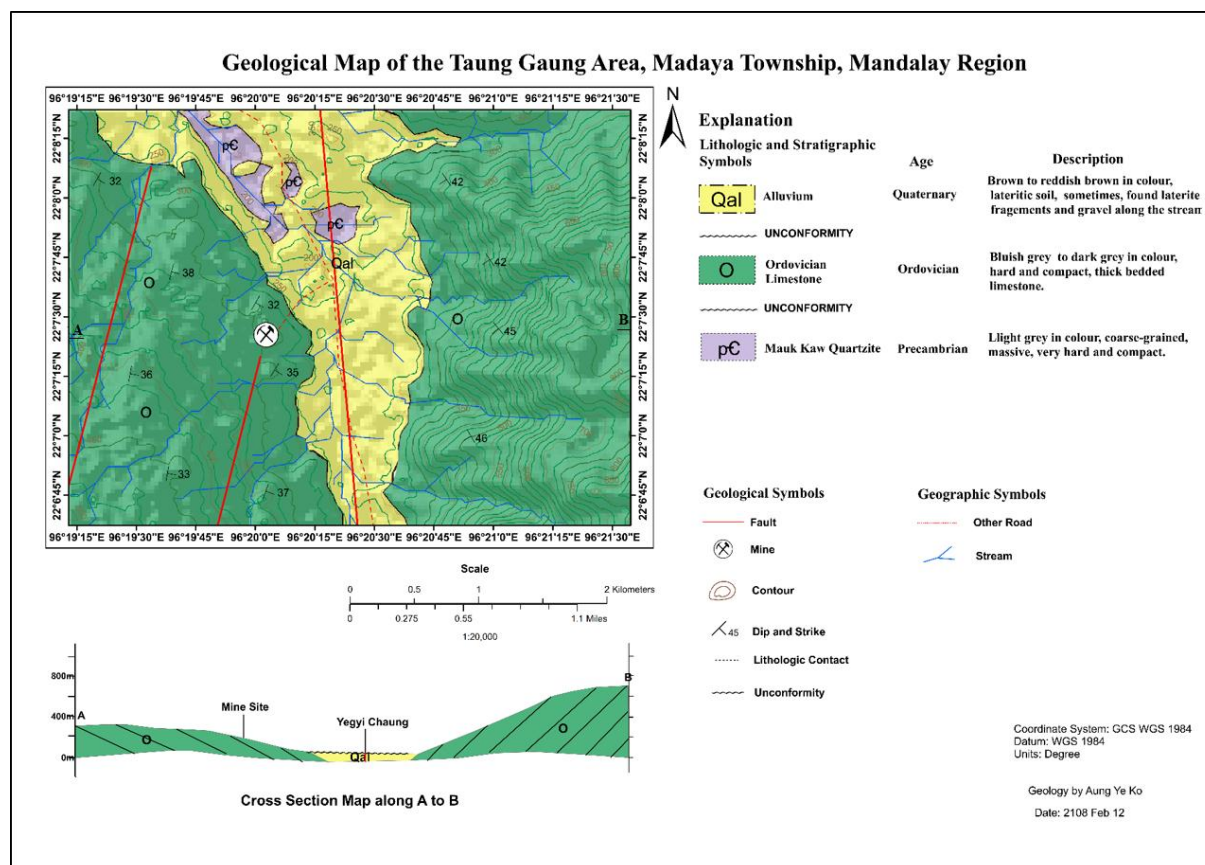


Figure 5 Geological Map of the Taung Gaung Area and its environs, Madaya Township, Mandalay Region, Myanmar

Alteration

Ordovician Limestone is the main ore host rock in the Taung Gaung area. The mineralization of the galena is observed to occur in the oolitic with dolomitic limestones (Fig.6,7,8 and 9). By the field study and microscopic study, the dominant alteration is dolomitization accompanied by minor silicification. Others are pyritization and limonitization.



Figure 6 Highly jointed, brecciated, and criss-cross joint pattern in dolomitic limestone, **Location:** 96°20'7.372" E and 22° 07' 28.425" N (Facing : East)



Figure 7 Grey coloured, medium- to thick-bedded, and highly-jointed dolomitic limestone, **Location:** 96°20'7.372" E and 22° 07' 28.425" N (Facing : East)



Figure 8 Outcrop nature of oolitic limestone with oolitic texture,
Location: 96°21'5.3"E and 22° 08' 27.425" N (Facing : East)



Figure 9 Grey coloured, thin-bedded oolitic limestone
Location: 96°21'5.37"E and 22° 08' 27.425" N (Facing : East)

Dolomitization

Dolomitization is the process by which limestone is altered into dolomite; when limestone comes into contact with magnesium-rich water, the mineral dolomite, calcium and magnesium carbonate, $\text{CaMg}(\text{CO}_3)_2$, replaces the calcite (calcium carbonate, CaCO_3) in the rock, volume for volume.

In the Taung Gaung area, most of the mineralized limestones are oolitic as well as dolomitic limestones. The lead mineralization in the oolitic, dolomitic limestone is later than the secondary dolomitization. The dolomitization is mainly associated with lead mineralization. The dolomitization with Pb mineralization of the study area is shown in Fig. 10 and 11.

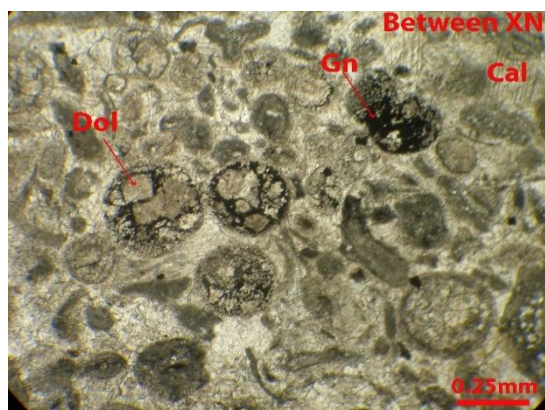


Figure 10 Dolomitization with Pb mineralization in oolitic limestone (Thin-section) (Gn = Galena, Dol = Dolomite, Cal = Calcite)

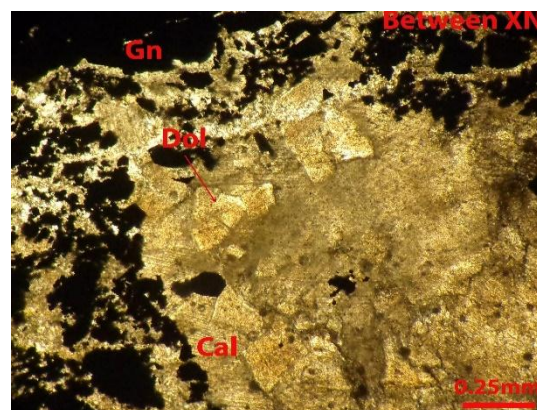


Figure 11 Dolomitization with Pb mineralization in dolomitic limestone (Thin-section) (Gn = Galena, Dol = Dolomite, Cal = Calcite)

Silicification

Silicification is another type of wallrock alteration in Taung Gaung area. The silicification of carbonate rocks is a diagenetic process that involves the major replacement of carbonate minerals by silica minerals. A general geochemical and thermodynamic requirement for the silicification of carbonates is the existence of pore fluids that are supersaturated with respect to the silica phase precipitated, and undersaturated with respect to the carbonate mineral dissolved (Hesse, 1989).

In the study area, silicification is commonly associated with the mineralization. The smaller or minute quartz grains occurring as intergranular grains are anhedral and show wavy extinction. The silicification and mineralization in the carbonate rocks is shown in Fig. 12 and 13. The silicification is not dominant in my study area.

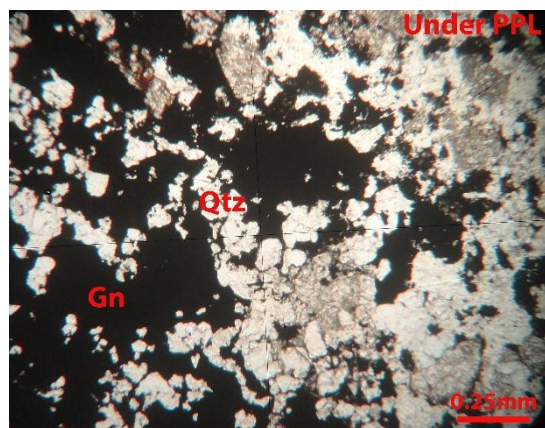


Figure 12 Silicification with Pb mineralization in carbonate rock (Thin-section) (Gn = Galena, Qtz = Quartz)

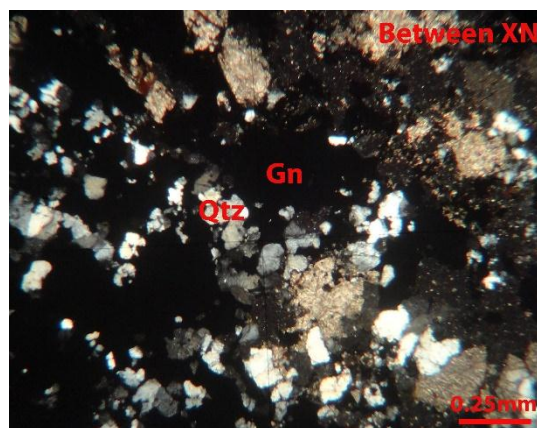


Figure 13 Silicification with Pb mineralization in carbonate rock (Thin-section) (Gn = Galena, Qtz = Quartz)

Pyritization

Pyritization is also another type of wallrock alteration in Taung Gaung area. The pyritization of carbonate rocks is a diagenetic process that involves the major replacement of carbonate minerals by pyrite mineral. Pyrite forms as rounded to elliptical crystals, disseminated in the host rock and ores. The earliest pyrite was probably formed during late diagenesis of the host rock and late pyrite was formed during the hydrothermal stage associated with galena and sphalerite (Fig.14 and 15).

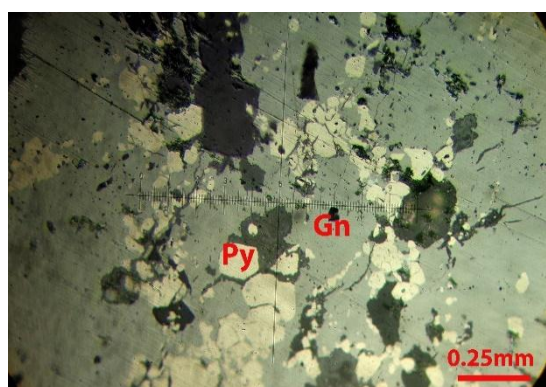


Figure 14 Pyritization with Pb mineralization in oolitic and dolomitic limestone (Polished-section) (Gn = Galena, Qtz = Quartz)

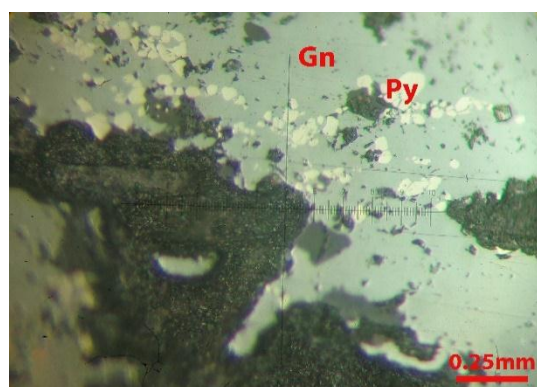


Figure 15 Pyritization with Pb mineralization in oolitic and dolomitic limestone (Polished-section) (Gn = Galena, Qtz = Quartz)

Limonitization

Many lead-zinc sulphides deposits when exposed to weathering undergo oxidation. They are inclined to break down forming new minerals and compounds or go into solution either whole or in part. Pyrite (FeS_2) is a common hypogene sulphide associated with lead-zinc ores and upon

oxidation, it generates sulphuric acid and generally leaves limonite as gossans. A gossan capping at Taung Gaung orebody is shown in Fig. 16, 17, 18 and 19. Oxidation and mineralization at Taung Gaung orebody is shown in Fig.20 and 21.



Figure 16 A Gossan capping the Taung Gaung orebody (Location: 96°20'2.0" E and 22° 7' 27.982" N) Facing: East



Figure 17 Pseudomorphs and coatings on the walls (Location: 96°20'2.049" E and 22° 7' 27.982" N) Facing: East



Figure 18 Gossans in Taung Gaung orebody



Figure 19 Azurite-malachite associated with limonite

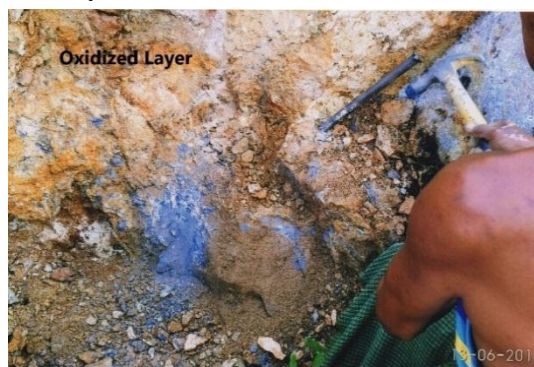


Figure 20 Oxidation and mineralization in Taung Gaung orebody (Location: 96°20'2.079" E and 22° 7' 27.282" N) Facing: East



Figure 21 Oxidation and mineralization in Taung Gaung orebody (Location: 96°20'2.019" E and 22° 7' 27.582" N) Facing: East

Mineralization

The Ordovician limestones are the host to mineralization. The colour of limestone along the mineralization zone changes from pale blue to yellowish brown due to the effect of alteration.

The mineralization follows the anticlinal axis of the major anticline, characterized by shearing and brecciation. Mineralization is in the form of disseminations and as thin stringers of fine galena in the shear planes. The geology and mineral occurrence map of the Taung Gaung area is shown in Fig.22.

Two local workings have exposed the mineralization at Taung Gaung Lead deposit. One at Bawdwingyi, about 1000 m south of Taung Gaung village. One old adit driven along the mineralized zone (7 m wide 3 m high and 30 m long) have exposed thin stringers of galena occupying the entire exposure of the adit. Fig.23. Bawdwinlay is situated about 150 m south of Bawdwingyi. The mineralization of Bawdwinlay is similar to that at Bawdwingyi. One old adit in Bawdwinlay is shown in Fig.24. The lead deposit is said to have been worked before World War- I by German brothers.

In Bawdwingyi, galena associated with barite, siderite, azurite, malachite, etc. occurs as vein and veinlets in the Ordovician limestone beds. The veins are about 7 to 14 centimetres thick and about 30 meters long. Well bedded grey limestone with speckles of disseminated galena and flakes of pyrites have low grade. Such speckles and stringers are found at the lower part of the section of Bawdwingyi tunnel. The upper part has coarsely crystalline white calcitic bands just above which are small stringers of rich galena, especially along the contact with the overlying altered zone. Galena is more coarsely crystalline than in fresh limestone. Other metallic deposits include stains of azurite and malachite occurring in small amounts in the oxidized zone. The mineralized lead ore area at Bawdwingyi mine is shown in Fig.25 and 26. Lead and copper ore samples at Bawdwingyi mine are shown in Fig.27 and 28.

In Bawdwinlay, galena associated with copper ore traces occurs as vein and veinlets in an old adit along the mineralized zone (4 m wide and 2 m high). Barite, quartz and calcite occur as gangue minerals. This type of deposit may be designated as fissure-filling, because the mineralization is observed only along the joints of massive limestone. The lead ore samples at Bawdwinlay mine are shown in Fig. 29 and 30.

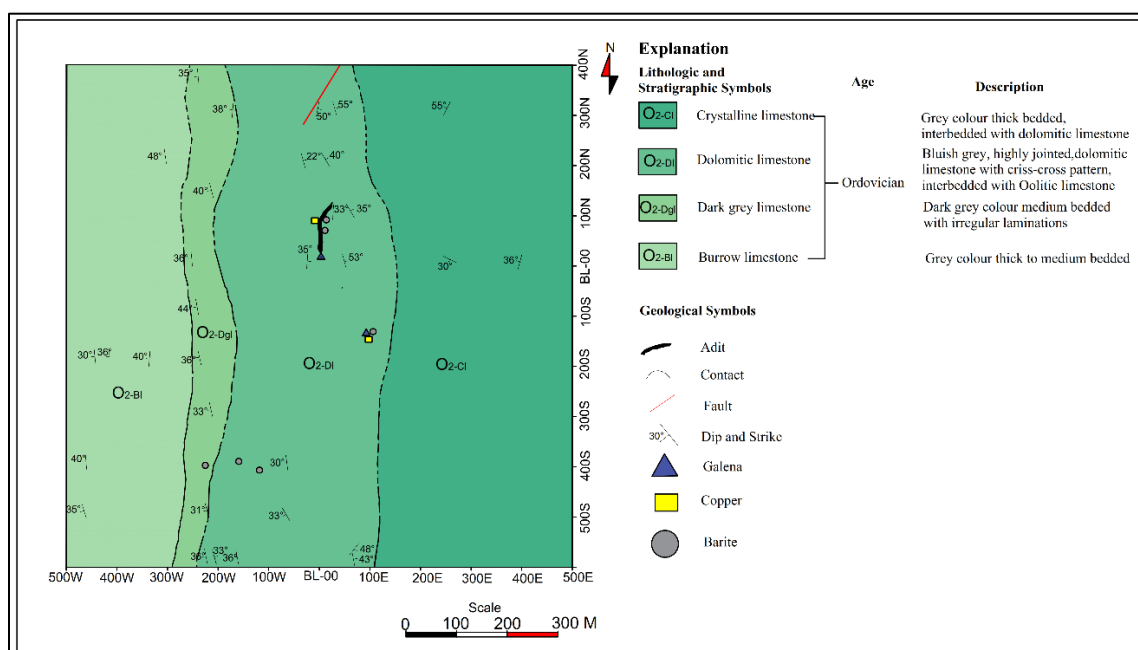


Figure 22 Geology and Minerals Occurrence Map of Taung Gaung Area (Modified after San Thu, Aung Pwa and Kyi Shwin,1980)

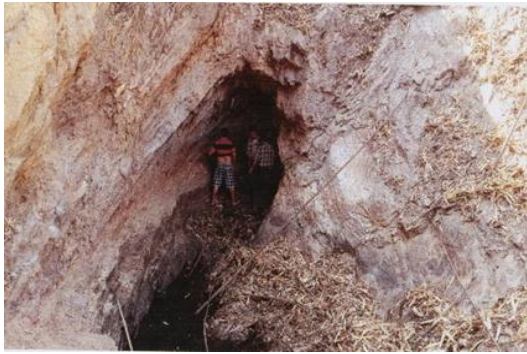


Figure 23 Adit at Bawdwingyi Mine (Location: $96^{\circ}20'2.048''$ E and $22^{\circ} 7' 27.982''$ N) Facing: East



Figure 24 Adit at Bawdwinlay Mine (Location: $96^{\circ}20'2.745''$ E and $22^{\circ} 7' 23.448''$ N) Facing: East



Figure 25 Mineralized lead ore zone at Bawdwingyi Mine (Location: $96^{\circ}20'2.0''$ E and $22^{\circ} 7' 27.982''$ N) Facing: SE



Figure 26 Mineralized lead ore zone at Bawdwingyi Mine (Location: $96^{\circ}20'2.0''$ E and $22^{\circ} 7' 27.982''$ N) Facing: SW



Figure 27 Lead ore samples at Bawdwingyi Mine



Figure 28 Copper ore samples at Bawdwingyi Mine



Figure 29 Lead ore samples at Bawdwinlay Mine



Figure 30 Lead ore samples at Bawdwinlay Mine

Ore Mineralogy

The ore mineralogy of the study area is rather simple, and the principal ore mineral is galena associated with sphalerite and minor amounts of anglesite, cerussite, jalpaite, pyrite and marcasite. In a separate paragenesis copper as chalcopyrite, tetrahedrite-tennantite, covellite, chalcocite and azurite-malachite also occur in this area. The gangue minerals include siderite, ankerite, barite, dolomite, calcite and quartz. The ore minerals of Taung Gaung lead deposit are shown in Fig.31, 32, 33, 34, 35, 36, 37, 38, 39, 40, 41, 42, 43, 44, 45 and 46.

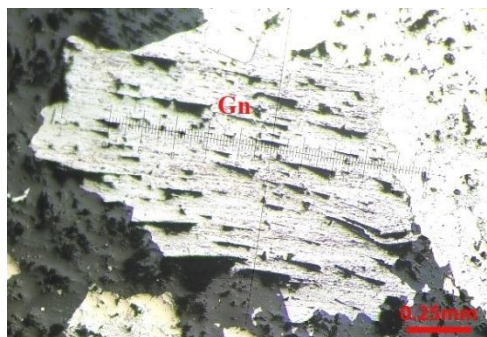


Figure 31 Perfect triangular cleavage pits of galena (Polished Section)

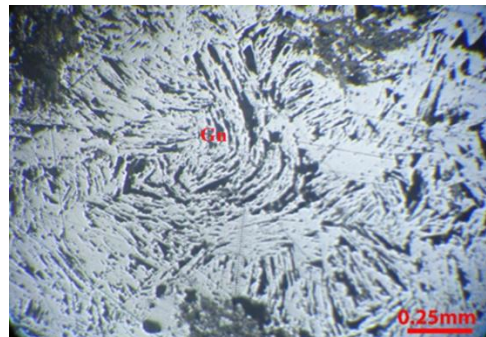


Figure 32 Extremely wavy, curved and displaced triangular cleavage pits of galena due to deformation (Polished Section)

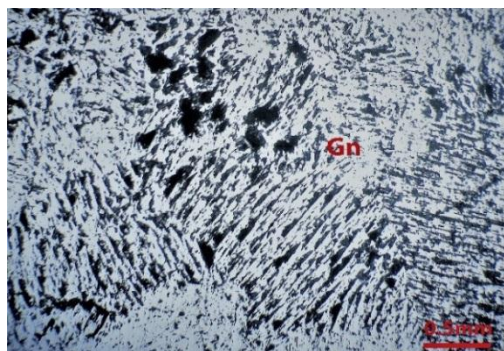


Figure 33 Dendritic patterns of galena (Gn = Galena) (Polished Section)

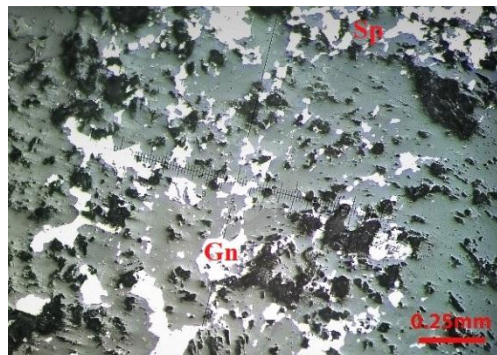


Figure 34 Disseminated patterns of galena in calcite (Gn=Galena) (Polished Section)

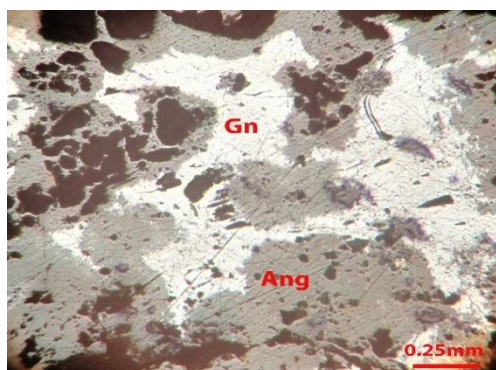


Figure 35 Galena is replaced and rimmed by intergrown anglesite (Gn = Galena, Ang = Anglesite) (Polished Section)

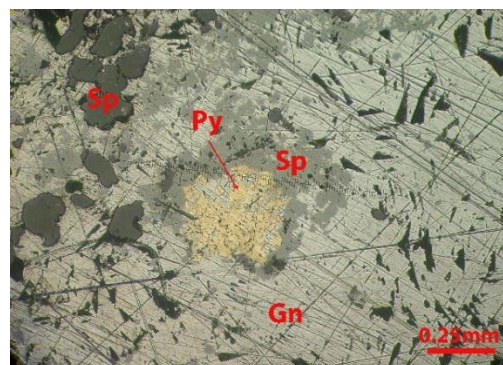


Figure 36 Pyrite isolated grains are formed as inclusions in galena and sphalerite (Gn = Galena, Sp = Sphalerite, Py = Pyrite) (Polished Section)

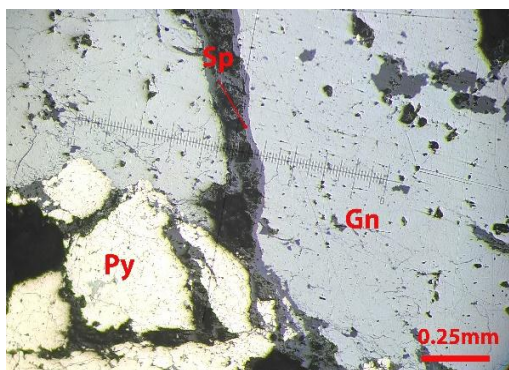


Figure 37 Sphalerite occurs as vein along the grain boundaries of galena (Sp=sphalerite, Gn=galena, Py= Pyrite) (Polished Section)

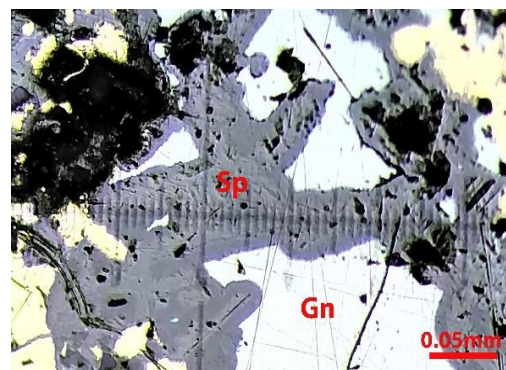


Figure 38 Skeletal structure of sphalerite in galena (Sp = sphalerite, Gn = galena) (Polished Section)

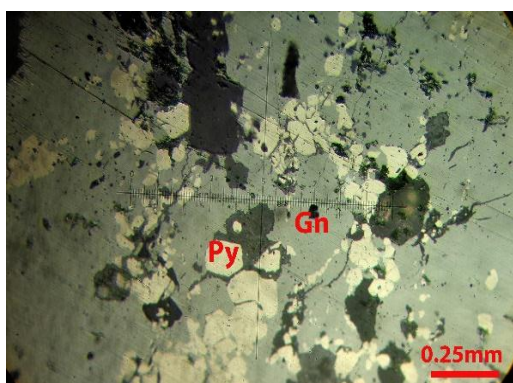


Figure 39 Disseminated pyrite in galena (Py = Pyrite, Gn = galena) (Polished Section)

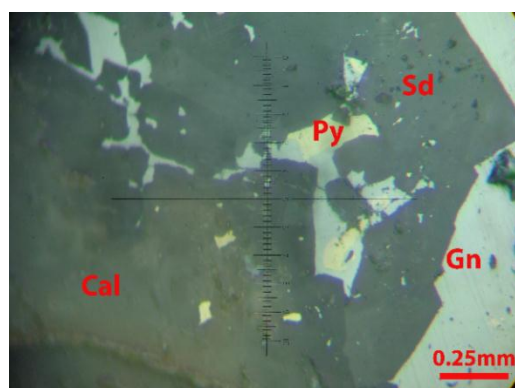


Figure 40 Siderite associated with pyrite, galena and calcite (Sd =Siderite, Py = Pyrite, Gn = galena) (Polished Section)

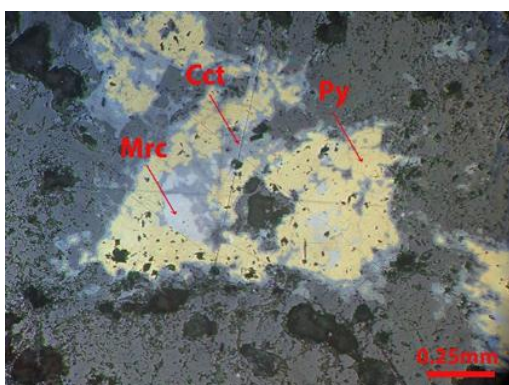


Figure 41 Marcasite embedded in pyrite, pyrite is enclosed by chalcocite and they are replaced by gangue-calcite and dolomite (Py = Pyrite, Cct = Chalcocite, Mrc = Marcasite) (Polished Section)

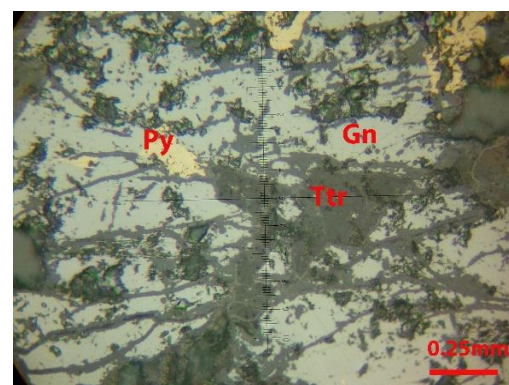


Figure 42 Tetrahedrite veins and veinlets are formed as inclusions in galena (Gn = galena, Ttr = tetrahedrite, Py = Pyrite) (Polished Section)

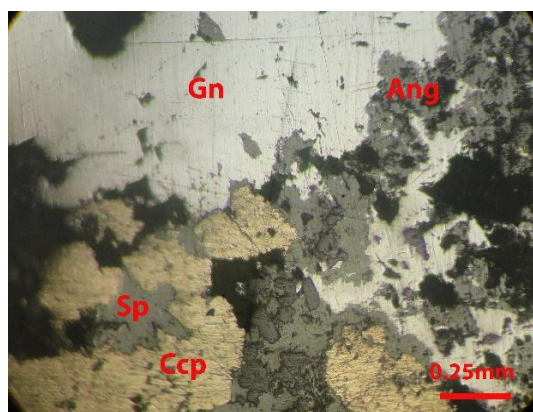


Figure 43 Galena associated with angelinite, sphalerite and chalcopyrite (Gn = Galena, Ang = Angelinite, Sp= Sphalerite, Ccp = Chalcopyrite) (Polished Section)

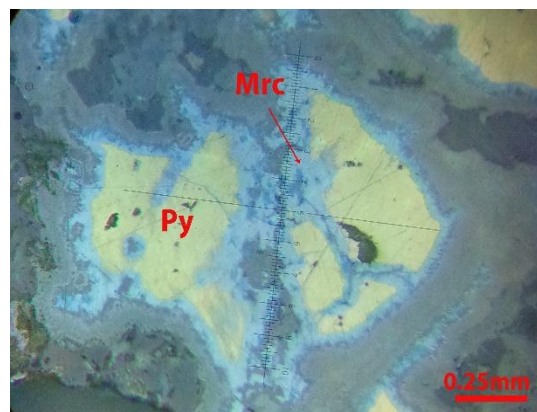


Figure 44 Marcasite is replaced and rimmed by pyrite which occurs zonal replacement texture (Mrc = Marcasite, Py = Pyrite) (Polished Section)

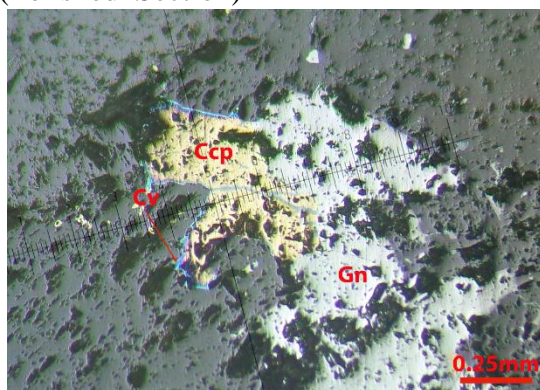


Figure 45 Covellite associated with galena and chalcopyrite (Cv =Covellite, Gn= Galena, Ccp= Chalcopyrite (Polished Section)

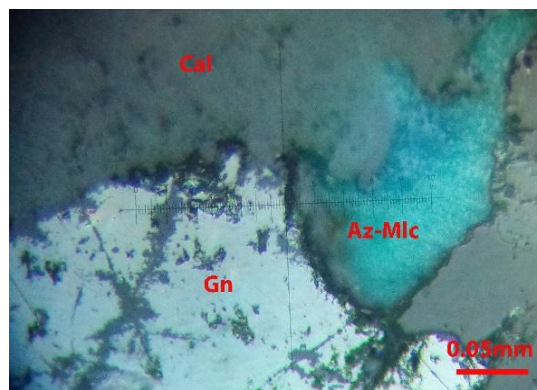


Figure 46 Galena associated with azur-malchite and gangue- calcite (Gn = Galena Az-Mlc = Azur-Malchite, Cal= Calcite) (Polished Section)

SEM-EDX Analysis of Ore Minerals

Scanning Electron Microscopy (SEM) provides detailed high resolution images of the sample by rastering a focused electron beam across the surface and detecting secondary or backscattered electron signal. An Energy Dispersive X-Ray Analyzer (EDX) is also used to provide elemental identification and quantitative compositional information. Back scattered electron imaging by Scanning Electron Microscope was used in order to attempt to explain the characteristics of gold and associated ore minerals.

Analysis of TGO-01 ore sample

In TGO-01 ore sample from Taung Gaung area, spectrum-1 is quartz, spectrum-2 is galena and spectrum-3 is sphalerite which are classified based on their chemical composition and ratio of constituent elements (Fig.47). Sphalerite and quartz formed as inclusions in the galena that formed the replacement texture. Table.1 shows the elemental composition of constituent elements of all spectra of the TGO-01 ore sample (using EDX). The SEM-EDX data graphs of the TGO-01 ore sample are shown in (Fig.48,49 and 50).

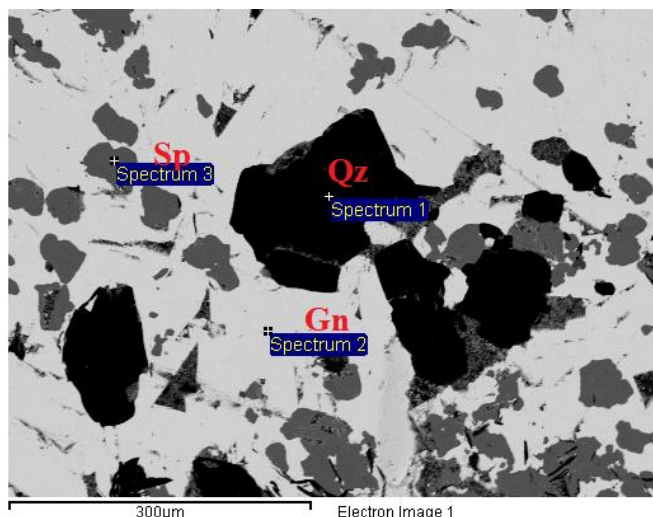


Figure 47 Back Scattered Images of galena, sphalerite and quartz of the TGO-01 ore sample

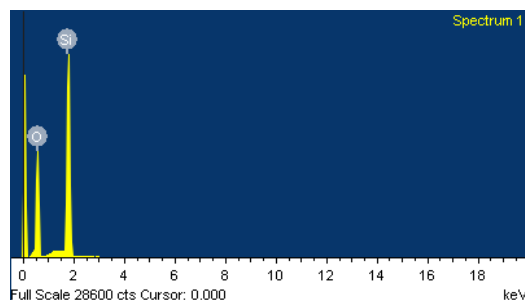


Figure 48 SEM-EDX Data Graphs of the Quartz

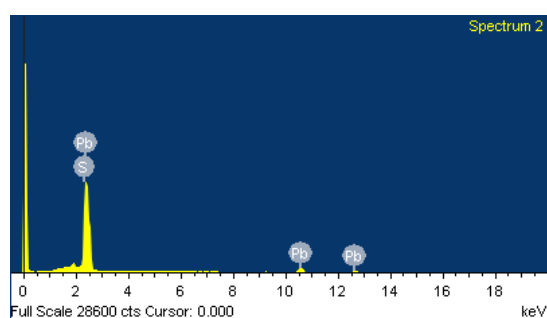


Figure 49 SEM-EDX Data Graphs of the Galena

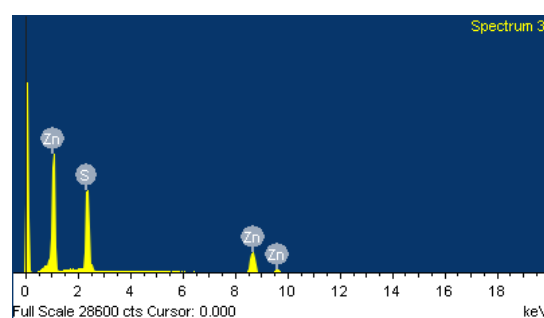


Figure 50 SEM-EDX Data Graphs of the Sphalerite

Table 1 Chemical composition of the TGO-01 ore sample (using EDX)

Spectrum	O	Si	S	Zn	Pb	Total	Mineral
Spectrum 1	62.00	38.00				100.00	Quartz
Spectrum 2			13.41		86.59	100.00	Galena
Spectrum 3			36.24	63.76		100.00	Sphalerite

Analysis of TGO-02 ore sample

In TGO-02 ore sample from Taung Gaung area, spectrum-1 is galena, spectrum-2 is anglesite, spectrum-3 is cerussite, spectrum-4 is barite and spectrum-5 is also anglesite which are classified based on their chemical composition and ratio of constituent elements (Fig. 51). Galena is closely associated with the anglesite, cerussite and barite which show the intergrowth texture. Table. 2 shows the elemental composition of constituent elements of all spectra of the TGO-02 ore sample (using EDX). The SEM-EDX data graphs of the TGO-02 ore sample are shown in (Fig.52,53,54,55 and 56).

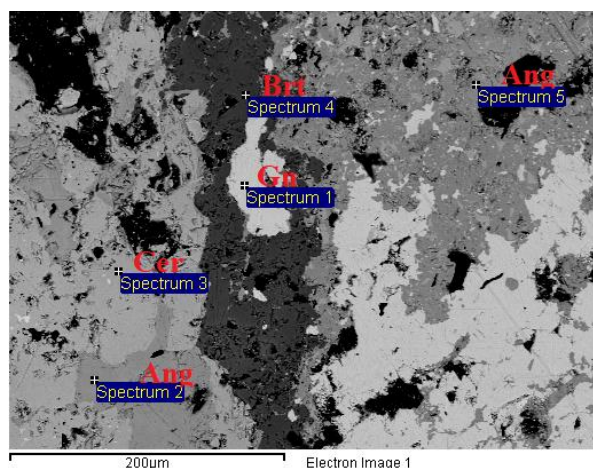


Figure 51 Back Scattered Images of galena, anglesite, cerussite and barite of the TGO-02 ore sample

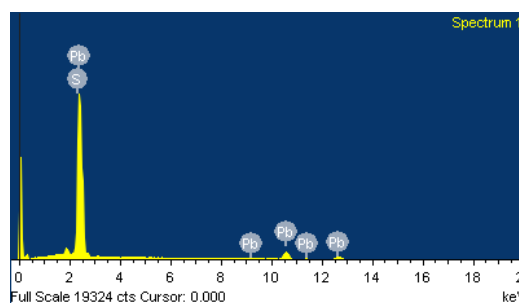


Figure 52 SEM-EDX Data Graphs of the Galena

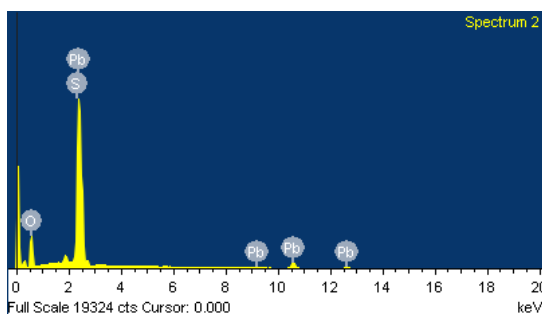


Figure 53 SEM-EDX Data Graphs of the Anglesite

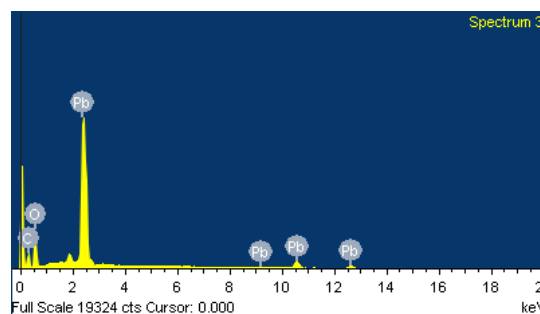


Figure 54 SEM-EDX Data Graphs of the Cerussite

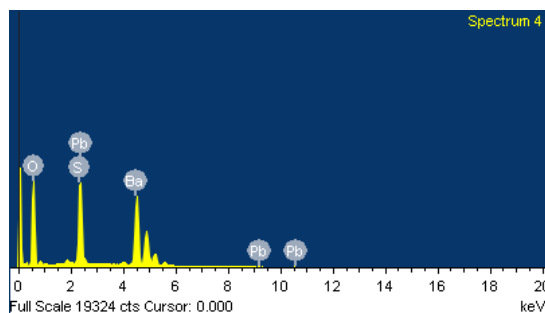


Figure 55 SEM-EDX Data Graphs of the Barite

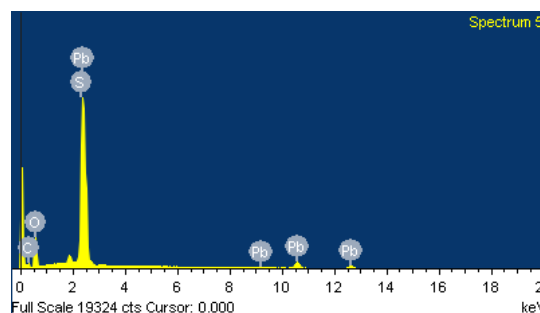


Figure 56 SEM-EDX Data Graphs of the Anglesite

Table 2 Chemical composition of the TGO-02 ore sample (using EDX)

Spectrum	C	O	S	Ba	Pb	Total	Mineral
Spectrum 1			15.7		84.3	100	Galena
Spectrum 2		26.64	11.43		61.93	100	Anglesite
Spectrum 3	11.85	21.32			66.83	100	Cerussite
Spectrum 4		29.56	13.64	55.36	1.43	100	Barite
Spectrum 5	7.24	23.84	10.72		58.2	100	Anglesite

Analysis of TGO-03 ore sample

In TGO-03 ore sample from Taung Gaung area, spectrum-1 is jalpaite, spectrum-2 is tennantite, spectrum-3 is calcite and spectrum-4 is tetrahedrite which are classified based on their chemical composition and ratio of constituent elements (Fig. 57). Jalpaite occurs along the grain boundaries of tetrahedrite- tennantite which formed the zonal texture. Jalpaite and tetrahedrite-tennantite are replacement of calcite that formed the replacement texture. Table. 3 shows the elemental composition of constituent elements of all spectra of the TGO-04 ore sample (using EDX). The SEM-EDX data graphs of the TGO-03 ore sample are shown in (Fig. 58,59,60 and 61).

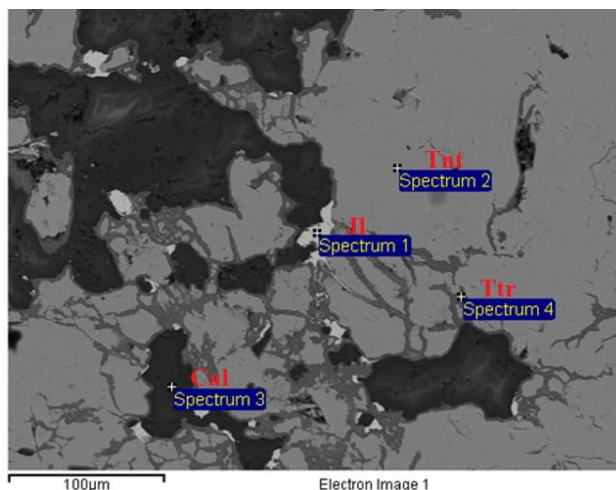


Figure 57 Back Scattered Images of jalpaite, tennantite, calcite and tetrahedrite of the TGO-03 ore sample

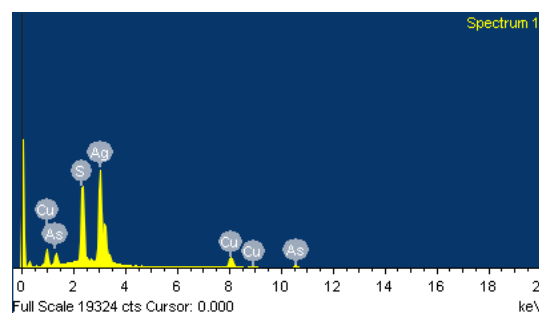


Figure 58 SEM-EDX Data Graphs of the Jalpaite

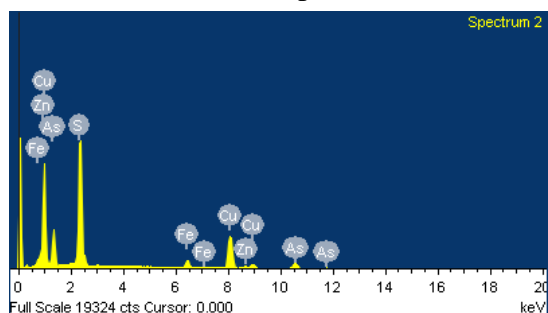


Figure 57 SEM-EDX Data Graphs of the Tennantite

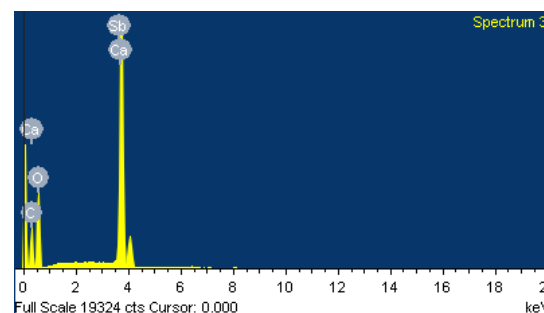


Figure 58 SEM-EDX Data Graphs of Calcite

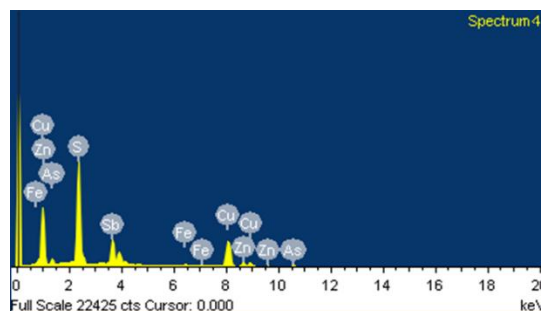


Figure 61 SEM-EDX Data Graphs of Tetrahedrite

Table 3 Chemical composition of the TGO-04 ore sample (using EDX)

Spectrum	C	O	Ca	Cu	Sb	Ag	Zn	As	Fe	S	Total	Mineral
Spectrum 1				14.0		61.41		6.52		18.07	100.00	Jalpaite
Spectrum 2				42.08			2.85	20.06	4.43	30.57	100.00	Tennantite
Spectrum 3	12.18	51.59	33.61		2.62						100.00	Calcite
Spectrum 4				37.55	24.15	4.10	5.58		1.03	27.40	100.00	Tetrahedrite

Deformation after Mineralization

In ore microscopic study, most of the galena display deformed structures (Fig. 32 and 33). Their growth zones and the cleavage sets are curved.

In SEM-EDX study, the calcite mineral grains are observed to be large. The other mineral grains nearby are seen as mostly fine-grained. Recrystallization is inferred to be caused by the orogeny producing the large calcite crystals. It may be partly due to metamorphism (Fig.51 and 57).

Ore Texture

The ore textures were examined under an ore microscope referring to the description of Edwards, A.B., (1954), Cameron (1966), Craig & Vaughan (1981) P.Picot and Z.John (1982) and Roger Taylor (2009).

Polished sections of ores from the Taung Gaung lead deposit were studied under the reflecting microscope and SEM-EDX analysis in order to identify the minerals and determine their texture and sequence of deposition. Textures observed in polished sections and SEM-EDX analysis may indicate the order in which the minerals were deposited and lead to inferences regarding the origin of the ore deposit. Ore textures vary with the type of deposit, structural controls, wallrock alterations and the physical and chemical conditions of the ore fluids.

The common ore textures found in the galena are dendritic pattern in (Fig.33), disseminated pattern in (Fig.34) and replacement texture in (Fig.35). The prominent cleavages sets are clearly seen in galena in (Fig.31).

In the sphalerite, rimmed replacement and disseminated structures are observed. The sphalerite grains are rimmed by the galena and the disseminated patterns of the sphalerite are dispersed in the galena in (Fig.36) and (Fig.47). The vein or veinlet textures of sphalerite are formed in the grain boundaries of galena and gangue-calcite in (Fig.37). The skeletal structure of sphalerite is observed in the galena in (Fig.38). In other minerals, the replacement textures, the disseminated patterns and the veins or veinlets textures are commonly observed.

Generalized Mineral Paragenetic Sequence

The time sequence of deposition of minerals in a rock or mineral deposit is known as its “paragenetic sequence” (Anthony, 1987). The information obtained on the consistence of textural relationships, field observations, both microscopic studies and SEM - EDX studies, such as intergrowth, replacement and cross-cutting features of associated minerals and their assemblages in the study area, provide a basis for interpreting and determining the generalized mineral paragenetic sequence for ore and gangue minerals of Taung Gaung lead deposit as shown in (Fig.62).

In gangue minerals, calcite, dolomite and quartz were deposited in all stages while siderite, ankerite and limonite were formed in post-mineralization (stage-iv), and barite was formed in both main mineralization (stage-iii) and post-mineralization (stage-iv).

In ore minerals, galena, sphalerite and chalcopyrite were deposited in main mineralization (stage-ii and stage-iii) while anglesite, cerussite, jalpaite, covellite, chalcocite, azurite- malachite, tetrahedrite – tennantite and marcasite were formed in post- mineralization (stage-iv), and pyrite was formed in all stages.

Mineral	Pre Mineralization	Main Mineralization		Post Mineralization
	Stage-I	Stage-II	Stage-III	Stage-IV
Gangue minerals				
Calcite	-----	-----	-----	-----
Dolomite	-----	-----	-----	-----
Quartz	-----	-----	-----	-----
Barite			-----	-----
Siderite				-----
ankerite				-----
Limonite				-----
Ore Minerals				
Galena		-----	-----	
Sphalerite		-----	-----	
Anglesite				-----
Cerussite				-----
Jalpaite				-----
Chalcopyrite		-----	-----	
covellite				-----
chalcocite				-----
Azurite- Malchite				-----
Tetrahedrite- Tennantite				-----
Pyrite	-----	-----	-----	-----
Marcasite				-----

Figure 62 Generalized Mineral Paragenetic Sequence for Ore and Gangue Minerals of Taung Gaung Lead Deposit

Style of Mineralization

By the field study and microscopic study, several styles of mineralization were formed under variable conditions, with lead minerals occurring as;

1. Disseminations
2. Replacement ore
3. Fracture-fillings and
4. Mineralized solution collapse breccias

Disseminated ore are widespread with euhedral galena grains in the host rock (Fig. 63 and 64).

Replacement ore is the commonest style of mineralization where the pore spaces of the rock have been replaced by fine-grained galena. The replacement ores carry good grades having a potential for mining (Fig.66).

Fracture-filling ores usually accompany the replacement ores where small fractures and joints in the bedding planes are filled with coarse-grained galena (Fig.65).

The style of mineralization associated with the solution collapse breccias of open-space filling. Galena is found as open-space filling between angular dolomite fragments in the ore-hosting breccias. Open-space mineralization is characterized dominantly by pink sparry dolomite and euhedral galena, minor pyrite and calcite (Fig.67 and 68).

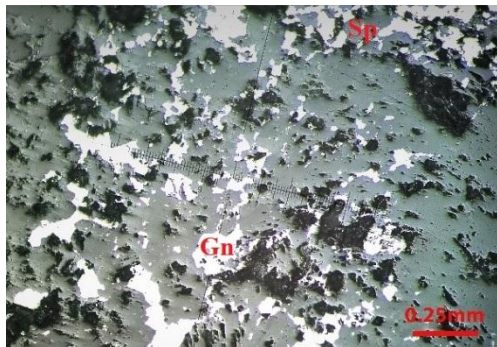


Figure 63 Disseminated lead ore in Bawdwingyi Mine

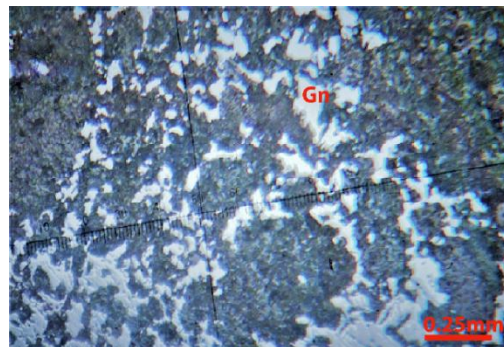


Figure 63 Disseminated lead ore in Bawdwingyi Mine

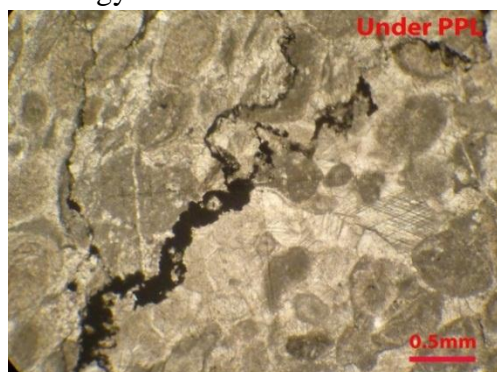


Figure 65 Fracture-fillings Style of lead ore

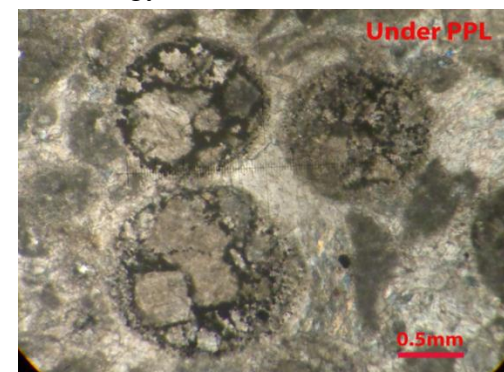


Figure 66 Replacement Style of lead ore

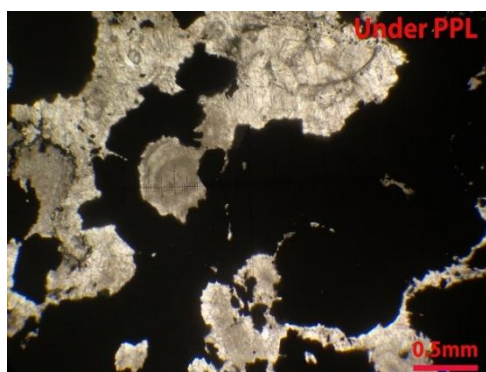


Figure 67 Mineralized solution collapse breccias of open space filling



Figure 68 Mineralized solution collapse breccias of open space filling

Conclusion and Discussion

Taung Gaung area is located in central Myanmar, 37 km to the northeast of Mandalay. It mainly consists of Ordovician limestone and dolomitic limestone with a general trend of N-S. The principal ore mineral is galena associated with sphalerite and minor amounts of anglesite, cerussite, jalpaite, pyrite and marcasite. In a separate paragenetic sequence, copper occurs as chalcopyrite, tetrahedrite - tennantite, covellite, chalcocite and azurite-malachite. The gangue minerals include limonite, siderite, ankerite, barite, dolomite, calcite and quartz.

In ore microscopic study, most of the galena display deformed structures. Their growth zones and the cleavage sets are curved. In SEM-EDX study, the calcite mineral grains are observed to be large. The other mineral grains nearby are seen as mostly fine-grained. It may be partly due to metamorphism. The common ore textures found in the galena are dendritic pattern, disseminated pattern and replacement texture. In sphalerite, rimmed replacement texture, disseminated structures, vein or veinlet textures, skeletal structure and network texture are observed. In other minerals, the replacement textures, the disseminated patterns and the vein or veinlet textures are commonly observed.

In gangue minerals, calcite, dolomite and quartz were deposited in all stages while siderite, ankerite and limonite were formed in post-mineralization (stage-iv), and barite was formed in both main mineralization (stage-iii) and post-mineralization (stage-iv). In ore minerals, galena, sphalerite and chalcopyrite were deposited in main mineralization (stage-ii and stage-iii) while anglesite, cerussite, jalpaite, covellite, chalcocite, azurite- malachite, tetrahedrite – tennantite and marcasite were formed in post- mineralization (stage-iv), and pyrite was formed in all stages.

By field observation and under microscopic study, several styles of mineralization were found to have formed under variable conditions, such as lead-zinc minerals occurring as disseminations, replacement ore, fracture - fillings and mineralized solution collapse breccias.

Acknowledgements

I wish to express my heartfelt thanks to Dr. Day Wa Aung, Professor and Head of Geology Department, University of Yangon for his guidance and interest in writing this paper. I am indebted to Dr. Ohn Thwin, Part-Time Professor, Department of Geology, University of Yangon for his close supervision throughout this research work. I am also deeply grateful to U Than Htay, Deputy Director General (Retired), Department of Geological Survey and Mineral Exploration, Ministry of Mines for his critical reading and improvement of the manuscript.

References

- Anthony M. E., (1987): *An Introduction to Ore Geology*. Blackwell Scientific Publications. London. 358p.
- Bunopas, C. & Vella, P.(1983). "Tectonic and geologic evolution of Thailand." Proceedings on a Workshop on Stratigraphic Correlation of Thailand and Malaysia. Geological Society of Thailand. Bangkok/ Geological Society of Malaysia, Kuala Lumpur, I, 307-322.
- Cameron,E.N., (1966). *Ore Microscopy*. John Wiley & Sons, Inc. U.S.A. 293p.
- Craig, J.R. & Vaughan, D.J., (1981): *Ore Microscopy and Ore Petrography*. John Willey and Sons. 406 p.
- Curry J.R., Moore D.G., Lawver L.A., Emmel F.J., Raitt R.W., Henry M. & Kieckhefer R. (1979). "Tectonics of the Andaman Sea and Burma." In: Watkins J.S., Montadert L. & Dickerson P.W. (eds) Geological and Geophysical Investigations of Continental Margins. AAPG, Memoirs, 29, 189–198.
- Edwards, A.B., (1954). *Textures of the ore minerals and their significance*. Aus.Inst. Min.Met.Melbourne.
- Hesse, R., (1989). Silica diagenesis: origin of inorganic and replacement cherts. *EarthSci. Rev.* 26, 253–284.
- Khin Maung Shwe., (1973). *The Geology of Sedaw-Taung Gaung Area, Mandalay District*. M.Sc Thesis, Department of Geology, University of Mandalay (Unpublished)
- Metcalf, I., (1984). *Stratigraphy, palaeontology and palaeogeography of the Carboniferous of Southeast Asia*. Mem. Soc. Geol. France No. 147, pp. 107–118.
- P. Picot and Z. Johan ; translation by J. Guilloux, reviewed by D.H. Watkinson, (1982)., *Atlas of ore minerals*. Paris : B.R.G.M. ; Amsterdam : Elsevier.458p.
- Roger G. Taylor (2009): *Ore Textures Recognition and Interpretation*. Springer, London, New York. 278 p.
- Searle, M. P., Noble S. R., Cottle, J. M., Waters, D. J., Mitchell, A. H. G., Tin Hlaing, Horstwood, M. S. A., (2007). "Tectonic evolution of the Mogok metamorphic belt, Burma (Myanmar) constrained by U-Th-Pb dating of metamorphic and magmatic rocks."
- Soe Thura Tun & Watkinson, I.M.(2017). "The Sagaing Fault, Myanmar" In:Barber, A.J., Khin Zaw & Crow,M.J. (eds) *Myanmar: Geology, Resources and Tectonic*. Geological Society, London, Memories, 48, 413-441, <https://doi.org/10.1144/M48.19>.
- Win Swe, (2013). "The Sagaing Fault of Myanmar": a brief overview. *Geology of Sagaing Fault in Commemoration of 9th Anniversary of MGS*. Myanmar Geosciences Society, Yangon, Myanmar, p.1-20.

SPHALERITES COMPOSITION AND SULPHIDATION STATE OF POLYMETALLIC EPITHERMAL QUARTZ VEINS AT SORIPESA PROSPECT AREA, SUMBAWA ISLAND, INDONESIA

Win Khant^{*}

Abstract

The Soripesa prospect area is located at Maria village, Wawo district, Bima region in the eastern part of Sumbawa Island, Indonesia. This area is related with Cenozoic Calc-alkaline volcanic inner Banda-Sunda Arc. There have five main polymetallic epithermal quartz veins in the Soripesa prospect area, namely, Rini vein, Jambu air vein, Dollah vein, Merpati vein, and Arif vein. The dominant lithology is a lithic-crystal tuff of andesitic and dacitic composition and bedded limestone. Elemental compositions of sphalerites were analysed using Scanning Electron Microscope with energy-dispersive X-ray (SEM-EDX) method to identify their environment of ore deposition. Detected elements in sphalerite are Zn (63.48 wt.%), S (33.3 wt.%), Fe (1.04 wt.%), Ga (0.7 wt.%), Ge (0.54 wt.%), Cd (0.7 wt.%), and Ag (0.2 wt.%). Au content is below detection limit in all sphalerite. Ga/Ge ratios of sphalerites geothermometry indicate that the formation temperatures of sphalerite are between 180°C and 240°C. Based on the Fe mole %, sulfur activity (a_{S_2}) is a little higher and between 10^{-10} – 10^{-11} . Sphalerite are found in pyritic ore fields and low temperature condition. Sulfur activity and formation temperature plots show that ore-forming processes are formed under intermediate sulphidation state of epithermal system.

Keywords: Soripesa prospect area, Tectonic setting, Mineralization, Sulphidation state

Introduction

The Soripesa prospect area is located at Maria village, Wawo district, Bima regency, West Nusa Tenggara Province, Sumbawa Island, Indonesia. The research area is related with the eastern part of Sunda-Banda arc (Neogene). Sunda-Banda arc is the longest in Indonesia, extending from North Sumatra through Java, Bali, Lombok, and Sumbawa, to east Damar (Carlile and Mitchell, 1994). The prospect area is mainly occupied by andesitic and dacitic volcanoclastic rocks and small portion of Tertiary bedded limestones. There have five quartz veins in the Soripesa prospect area including Arif vein, Dollah vein, Jambu Air vein, Merpati vein, and Rini vein, trending nearly north-south. The main ore minerals are chalcopryrite, azurite, malachite, sphalerite and galena forming as polymetallic epithermal quartz veins.

Epithermal Au and Ag deposits of both vein and bulk-tonnage styles may be broadly grouped into high-, intermediate-, and low-sulphidation types based on the sulphidation states of their hypogene sulfide assemblages (Sillitoe and Hedenquist, 2003). In high-sulphidation epithermal deposits, the sulphidation stage ranges from high for copper-rich enargite-bearing assemblages to intermediate for the later gold-rich tennantite-tetrahedrite+pyrite assemblages, with similarities to and overlap with the base metal veins. In intermediate-sulphidation epithermal deposits, the full range of intermediate-sulphidation states is represented by the assemblage pyrite+chalcopryrite+sphalerite+tetrahedrite (Einaudi, et al., 2003). The purpose of this paper is to identify the environment of ore deposition, ore genesis, and ore forming processes of polymetallic epithermal quartz veins at Soripesa prospect area, East Sumbawa, Indonesia.

^{*} Dr, Lecturer, Department of Geology, Banmaw University

Tectonic setting and regional geology

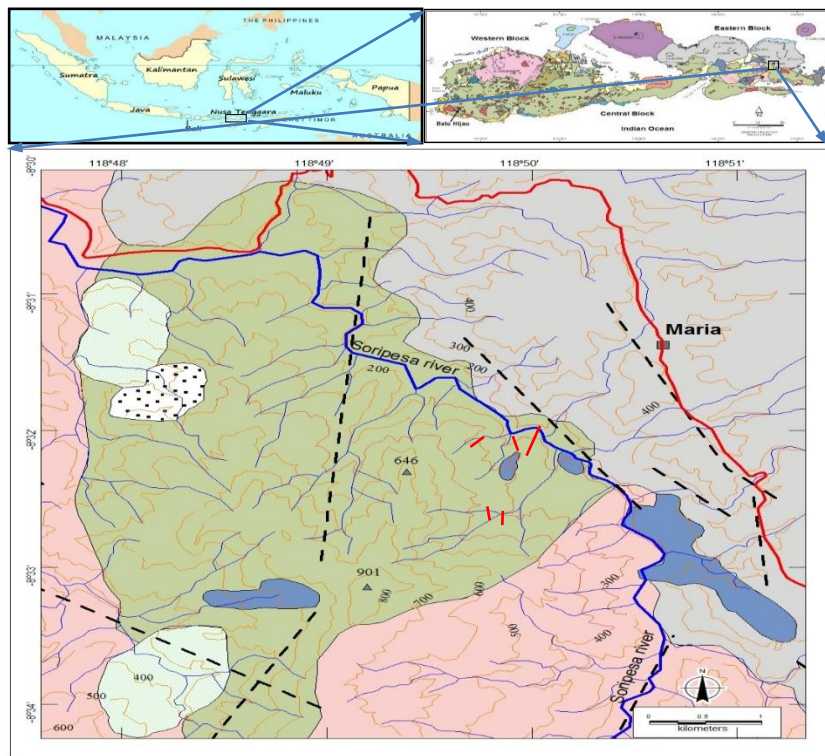
The Sumbawa Island forms as a part of the Cenozoic Calc-alkaline volcanic inner Sunda-Banda arc, which is still active up to present. Sunda-Banda island arc is a volcanic arc formed by the interaction of plate subduction slab in the form of Indo-Australia with Asian plate. The shape of the island arc is now being modified in the east due to collision with the Australian–New Guinea continental margin, including West Flores to East Sumbawa and Alor (Hamilton, 1979).

The East Sumbawa area is largely underlain by andesitic to basaltic lava and breccia of the Lower Miocene, with intercalations of tuff and limestone, and fresh pyroclastic sequences (Noya, et.al., 2009). This sequence is overlain in parts by dacitic tuff and bedded limestone of the Middle Miocene. These units have been intruded by numerous small to medium bodies in the Middle to Upper Miocene including andesite, dacite, diorite, trachyte and syenite (Fig. 1). A signature type of epithermal and porphyry copper mineralization can be recognized in those rock units.

The northern part of Sumbawa Island is dominated by the eruptive products of the active Tambora and Sangeang volcanoes, comprising of lahar, volcanic bomb and lapilli. Sumbawa Island, regionally, is intersected by NW-SE and NE-SW trending structures. However, the formation of quartz veining, alteration and mineralization at Soripesa Prospect are related to the N-S faulting (Noya, et.al., 2009).

Mineralization

The main vein zones which are associated with precious metals (Au-Ag) and base metals (Cu, Pb, Zn) are Rini, Jambu Air, Merpati, Arif, and Dollah epithermal quartz veins (Figure 4). They are nearly vertical ($>70^{\circ}\text{C}$), 1–16 m thick with individual vein to 1000 m length. The vertical outcrop of Rini vein can be observed in the field and it may reach up more than 200 m. The quartz vein and alteration area have a size of $6.7 \times 4.7 \text{ km}^2$ or ± 3150 hectares (Noya, et.al., 2009). Quartz textures of those veins belong to typical characters of low-sulphidation epithermal system and they can help to identify the morphology of veins such as face controlled and parallel-controlled. These parallel-controlled and face-controlled indicate that the epithermal quartz veins in the Soripesa prospect area are formed at the near surface (Khant, et.al., 2012a). Within the veins, multiphases, vuggy, colloform, bedded to massive textures with chalcopyrite, galena, sphalerite, malachite, azurite, chalcocite, pyrite, and iron oxide minerals are observed. Weak to moderate clay-pyrite alteration intensively developed in the volcanic rocks, especially in the west side of Soripesa. It could be influenced by NW–SE trending structures and andesite to porphyry dacite intrusive rock. The common alteration minerals in this prospect area are quartz, epidote, chlorite, pyrite, illite, and smectite. Minor amount of other alteration minerals are kaolinite, alunite, rutile, and anatase (Khant, et.al., 2012a). Temperature sensitive minerals include Ca-silicates such as epidote and chlorite (stable above $200\text{--}240^{\circ}\text{C}$), near the base of the epithermal environment. At the edges of the quartz veins develop silica clay-chlorite alteration; outward has changed to chlorite-epidote \pm magnetite as the halo alteration.



EXPLANATION

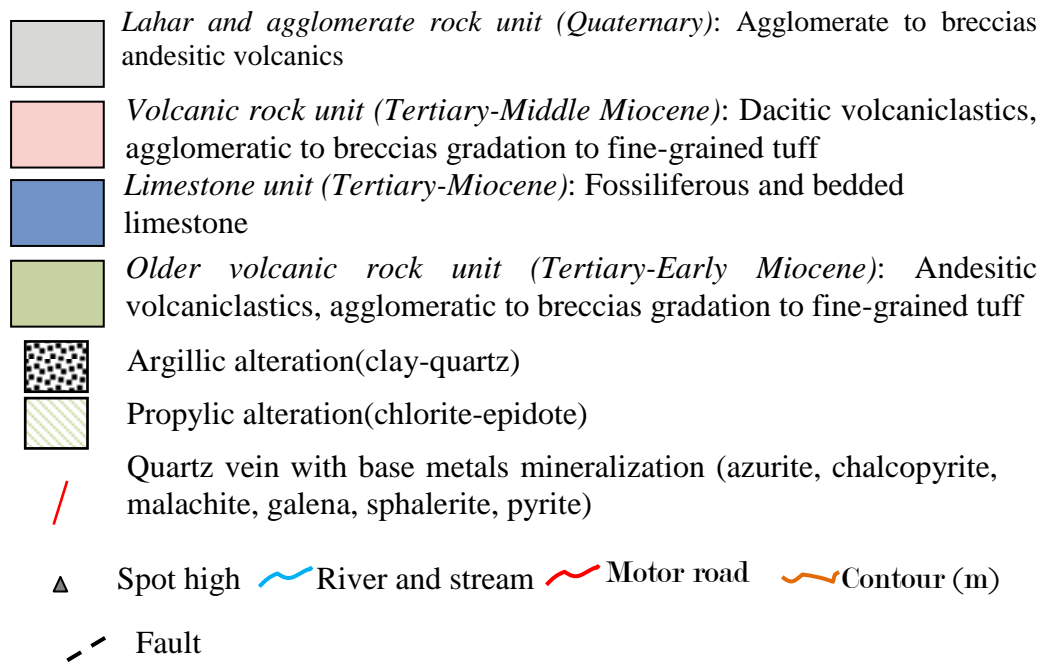


Figure 1 Geological map of the Soripesa prospect area (modified after [5]).

Material and Methods

Scanning electron microscopy with energy-dispersive X-ray analysis (SEM-EDX)

For SEM-EDX analyses, 10 sphalerite minerals in polished sections were used to identify mineral chemistry by using a SHIMADZU SS-550 SEM with a Genesis 2000 energy dispersion spectrometer (EDX) at the Center of Advanced Instrumental Analysis, Kyushu University. SEM-EDX analysis has been conducted on some ore samples such as pyrite, galena, sphalerite, azurite, malachite, iron ore minerals, and some unknown ore minerals for elemental identification and compositional information. It can also detect the content of Ag-Au ratio and other important minor elements. Major and minor element compositions of sphalerite ore minerals in this research area can be also compared with other deposits. Based on the elemental compositions, ore minerals can be estimated and identified their ore genesis, and ore forming processes.

Results and Discussions

Minor Elements in Sphalerite

Sphalerite is one of the most useful indicators of the environment of ore deposition because of its refractory nature, wide distribution in natural environments, and wide range of composition resulting from substitution of Zn by Fe (Misra, 1999). Detected minor elements in sphalerite are Fe (1.04 wt.%), Ga (0.7 wt.%), Ge (0.54 wt.%), Cd (0.7 wt.%), and Ag (0.2 wt.%). Au content is below detection limit in all sphalerite. Table (1) shows the elemental composition (wt.%) of sphalerite minerals. Table (2) shows the elemental composition (at.%) of sphalerite minerals

The cadmium content of sphalerite seems to be independent of the conditions of formation; there is no clear indication of systematic differences in sphalerites from low-temperature and high-temperature deposits (Fleischer, 1956). Jonasson and Sangster (1978) investigated the Zn/Cd ratios of sphalerites from some sulphide ores in Canada and concluded that the Cd contents and Zn/Cd ratios in sphalerites vary with the genetic types of deposit (Table 3). The Zn/Cd ratios (average 93.34) in sphalerite from the Soripesa prospect area are close to Zn/Cd ratios (104-214) of sphalerites from hydrothermal deposits (including volcano-hydrothermal deposits) and skarn-hydrothermal deposits. In low iron content of sphalerite, Cd content is towards higher, and higher iron content of sphalerite lesser cadmium amount.

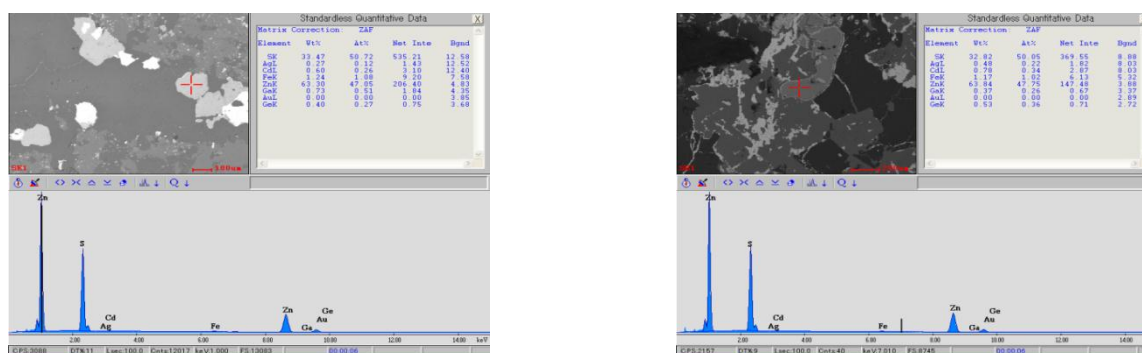


Figure 2 Elemental composition of some sphalerite minerals under SEM-EDX analyses.

Table 1 SEM-EDX analyses of element composition (wt%) of sphalerite minerals.

Element composition (normalized wt%) of Sphalerite minerals										
No.	Samples	Zn	S	Fe	Ga	Ge	Cd	Ag	Au	Zn/Cd
1	Av3-9	62.82	34.14	1.08	0.68	0.29	0.65	0.34	<0.01	96.65
2	Av3-10	63.22	33.81	1.21	0.71	0.54	0.50	<0.01	<0.01	126.44
3	Av3-11	63.30	33.47	1.24	0.73	0.40	0.60	0.27	<0.01	105.50
4	Av3-12	62.29	35.27	0.56	0.65	0.36	0.63	0.25	<0.01	98.87
5	Rvo1-1	64.31	32.62	1.11	0.50	0.48	0.64	0.34	<0.01	100.48
6	Rvo1-2	63.81	33.21	0.93	0.83	0.25	0.71	0.26	<0.01	89.87
7	Rvo1-3	63.38	33.38	0.84	0.59	0.71	0.83	0.27	<0.01	76.36
8	Rvo1-4	64.07	32.00	1.10	0.92	0.65	0.86	0.40	<0.01	74.50
9	Rvo1-5	63.79	32.24	1.17	1.06	0.84	0.77	0.12	<0.01	82.84
10	Mvo4-4	63.84	32.84	1.17	0.37	0.92	0.78	0.48	<0.01	81.85
	Avg	63.48	33.30	1.04	0.70	0.54	0.70	0.27	<0.01	93.34

Table 2 SEM-EDX analyses of element composition (at%) of sphalerite minerals.

Element composition (normalized at%) of Sphalerite minerals									
No.	Samples	Zn	S	Fe	Ga	Ge	Cd	Ag	Au
1	Av3-9	46.48	51.49	0.93	0.47	0.19	0.28	0.15	<0.01
2	Av3-10	46.82	51.05	1.05	0.50	0.36	0.21	<0.01	<0.01
3	Av3-11	47.05	50.72	1.08	0.51	0.27	0.26	0.12	<0.01
4	Av3-12	45.70	52.75	0.48	0.45	0.24	0.27	0.11	<0.01
5	Rvo1-1	48.14	49.78	0.98	0.35	0.32	0.28	0.15	<0.01
6	Rvo1-2	47.56	50.45	0.81	0.58	0.17	0.31	0.12	<0.01
7	Rvo1-3	47.21	50.69	0.73	0.41	0.48	0.36	0.12	<0.01
8	Rvo1-4	48.25	49.13	0.97	0.65	0.44	0.38	0.18	<0.01
9	Rvo1-5	47.90	49.36	1.03	0.75	0.57	0.34	0.06	<0.01
10	Mvo4-4	47.75	50.05	1.02	0.26	0.36	0.34	0.22	<0.01
	Avg	47.29	50.55	0.91	0.49	0.34	0.30	0.12	<0.01

Table 3 Zn/Cd ratios in sphalerites from this research and other deposits.

Type of deposit	Zn %	Cd%	Zn:Cd	Reference
This paper	63.48	0.70	93.34	
Mississippi Valley type	61.10	0.15	398	Jonasson and Sangster (1978)
Alpine type	61.95	0.20	315	Dill (1979)
Volcano-sedimentary Pb-Zn deposit	58.40	0.11	531	Vokes (1976)
Metamorphosed sedimentary Pb-Zn deposit	55.16	0.22	252	Both (1940)

There is general agreement by most workers (Stoiber, 1940 and Fleischer, 1956)) that the gallium content is most likely to be high in sphalerites from low-temperature deposits such as those of Mississippi Valley type and in those from low-temperature quartz veins. In this research, average Ga content (0.7 %) in sphalerites is very high and it means that they may be formed under low temperature condition.

Nearly all of the investigators agree that sphalerite from low-temperature deposits such as those of the Mississippi Valley type tend to be higher in germanium content than those from mesothermal or high-temperature deposits but many exceptions have been noted. In this research, average content of Ge (0.54%) is also very high.

Vaughan and Craig (1997) suggested that a zinc concentrate from a pyritic ore may contain 61-63 wt% Zn, but a concentrate from a pyrite-pyrrhotite ore will often contain only 51-58 wt% zinc and be considerably less valuable. The average content of Zn is 63.48 wt% in sphalerite of this research. It means that sphalerites from this research are related with pyritic ore condition.

Sphalerite Geothermometry

A very interesting recent development is the Ga/Ge geothermometer using sphalerite (Moller, 1985). Ga/Ge can be used to determine temperatures in the source regions of ore solutions and to estimate the degree of mixing of hot parental ore fluids with cool, near surface waters (Evans, 1993). For the study on Ga/Ge geothermometers, we sought geothermometers in the analyzes, obtaining values for Ge and Ga contents in the sphalerites of the study area. 10 samples were simultaneously detected levels for these two elements. The application of these geothermometer results of calculating the logarithm follows:

$$\log [(Ga/Ge) f] = \log [(Ga/Ge) sph] \quad (1)$$

Note that: f - mineraliser fluid; sph - sphalerite.

Determining the values of $\log (Ga/Ge)$ for the analyzes of sphalerite minerals, we obtain the values in the ranges between -0.4 to 1.15. These values are applied to the chart geothermometer Ga/Ge, based on geothermometer of Al/Si, and in this case that of muscovite-chlorite-quartz, given the degree of metamorphism. The chart shows the values of temperatures between 180°C to 240°C. Figure 3 presents the projection of the respective analysis chart that correlates the ratio Ga/Ge with the temperature. This graph is based on geothermometers known systems of Al/Si and published data for reasons of Ga/Ge in many geological systems (Moller, 1985 and 1987).

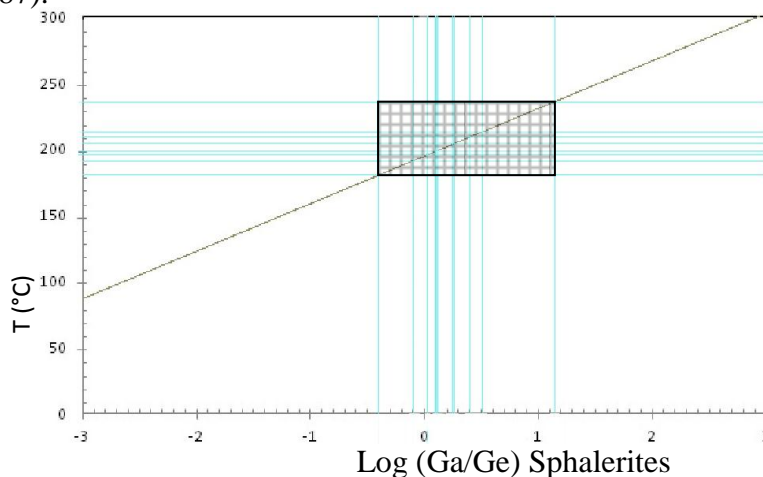


Figure 3 Graph showing the dependence between Ga/Ge ratios in sphalerite and formation temperature. This graph is based on existing Al/Si geothermometers. The musc-chlo-qtz line is the chlorite geothermometer in the Si/Al system (Marquest and Noronha, 2012). Shade area is referred to Ga/Ge ratio (-0.4 to 1.15) and formation temperature (180-240°C).

The results point to low temperatures of formation of the deposit, reaching the values obtained by the method of Ga/Ge between 180°C and 240°C. Marques and Noronha (2012) considers that the presence of Ge is higher in sphalerites that are formed at low temperature. The temperature differences observed between the two geothermometers can be related to the mixing and circulation of fluids late and/or pre-fluid surface Moller, 1985 and 1987). Based on the fluid inclusion data from quartz (host minerals), ranges of homogenization temperature for Merpati Vein is 182°C - 279°C, Rini vein is 185°C -266°C, Dollah vein is 212°C -300°C, Arif vein is 216°C -300°C, and Jambu Air vein is 233°C -297°C (Khant et.al., 2012d).

Sulphur Activity and Sulphidation State

Kullerud (1953) suggested that the FeS content of sphalerite gave a direct measurement of its temperature of deposition. Average Fe content (1.04%) of sphalerite in this research is very low. Mole % FeS in sphalerite is also very low and between 1 – 2%. In Zn-Fe-S of low pressure system, this value (1-2%) falls in pyrite+chalcopyrite field (Fig. 4). Within the pyrite field the decrease in FeS content of sphalerite with increasing sulphur activity (a_{S_2}) is much greater resulting in a close spacing of isopleths near the pyrite-pyrrhotite buffer and in very low FeS contents in sphalerite at high a_{S_2} (10^{-9} – 10^{-11}).

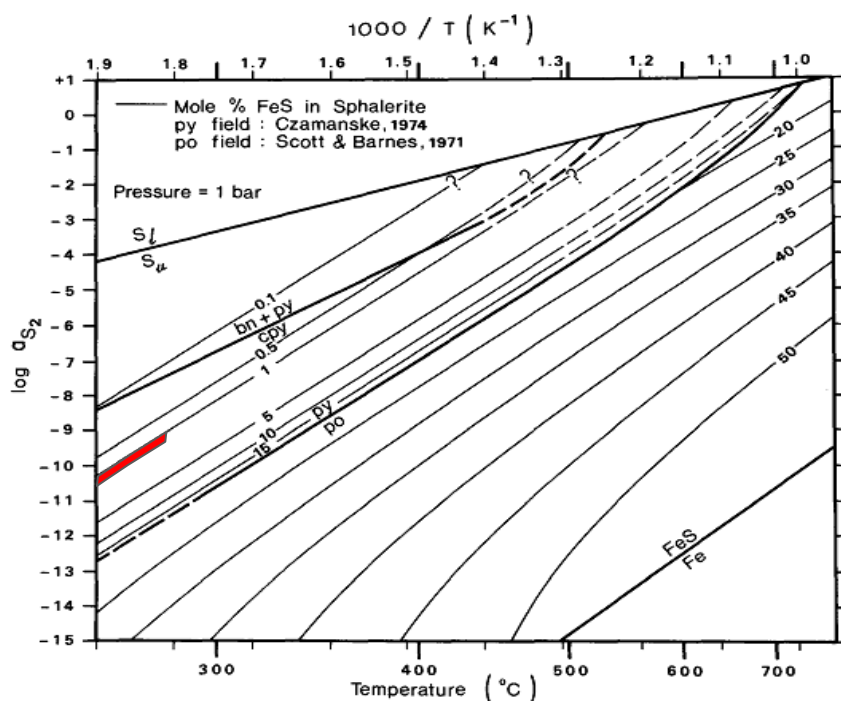


Figure 4 Phase relationships for the Fe-Zn-S system at 1 bar compiled from Barton and Toulmin (1966), Scott and Barnes (1971) and Czamanske (1974) in (Scott, 1983). Red line represents sulfur activity of sphalerite from Soripesa prospect area using Mole % FeS in sphalerite and formation temperature of sphalerite. Abbreviations: bn=bornite; cpy=chalcopyrite po=pyrrhotite; py=pyrite; S_l=liquid sulphur; S_v=sulphur vapour.

In a qualitative sense, it is commonly found that sphalerites formed at high a_{S_2} have a honey yellow to light brown colour with their low FeS contents whereas sphalerites formed at

low a_{S_2} and within the pyrrhotite field are dark brown to black (Scott, 1983). Those factors mean they may be formed in low temperature condition. Based on sulphur activity and temperature, it indicates that plots are fallen in intermediate sulphidation state, pyrite+chalcopyrite field, and magmatic hydrothermal compositional field (Fig. 5). Therefore, epithermal quartz veins at Soripesa prospect area are formed under intermediate-sulphidation state of the fluid condition.

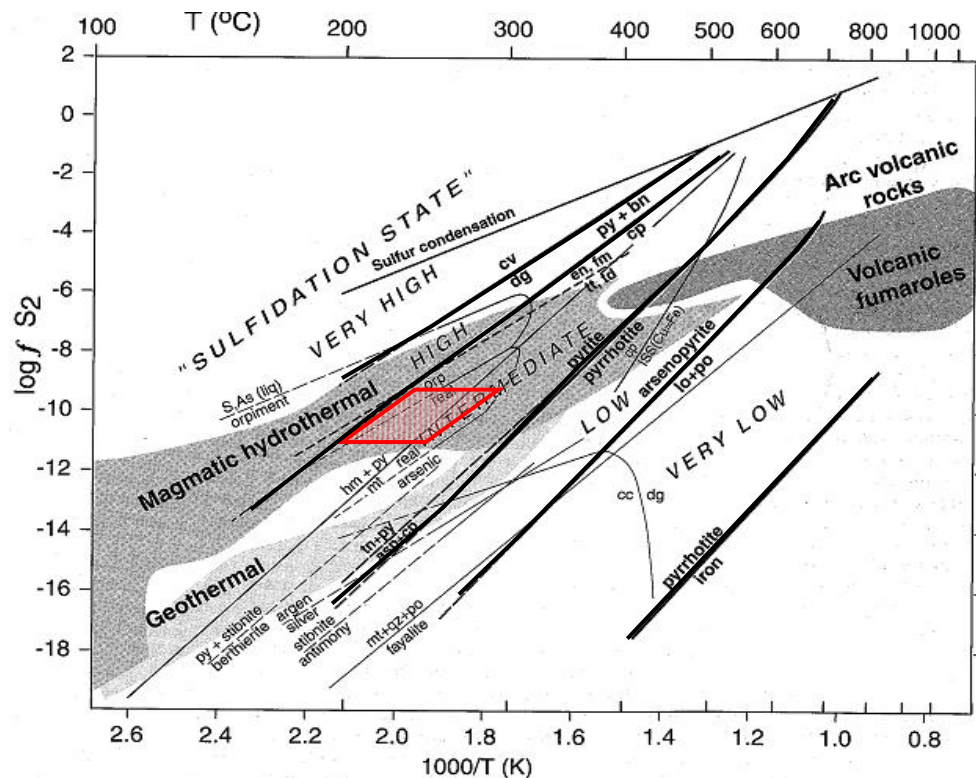


Figure 5 f_{S_2} - T diagram showing the variety of sulfide assemblages in epithermal deposits that reflect sulphidation state from very low through low and intermediate to high and very high. Compositional fields of arc volcanic rocks, high temperature volcanic fumaroles, magmatic-hydrothermal fluids, and geothermal fluids are shown, as discussed by (Einaudi, et.al., 2003 and Sillitoe and Hedenquist, 2003)). Red area is referred to the intermediate sulphidation state of epithermal quartz veins at Soripesa prospect area.

Conclusion

In this research, element composition (average) in sphalerites are Zn (63.48 wt.%), S (33.3 wt.%), Fe (1.04 wt.%), Ga (0.7 wt.%), Ge (0.54 wt.%), Cd (0.7 wt.%), and Ag (0.27 wt.%). Au content is below detection limit in all sphalerite. The Zn/Cd ratios (average 93.34) of sphalerite from this research area are close to Zn/Cd ratios (104-214) of sphalerites from hydrothermal deposits (including volcano-hydrothermal deposits. Average content Ga (0.7%) in sphalerites is very high and it means that they may be formed under low temperature condition. The average content of Zn is 63.48 wt.% in sphalerite of this research. It means that sphalerites from this research are related with pyritic ore condition.

Determining the values of $\log (Ga/Ge)$ for the analyzes of sphalerite minerals are in the ranges between -0.4 to 1.15. The results point to low temperatures of formation of the deposit and estimated formation temperature are between 180°C and 240°C. Mole % FeS in sphalerite is

also very low and between 1% to 2%. In Zn-Fe-S of low pressure system, this value (1-2%) falls in pyrite+chalcopyrite field. Within the pyrite field the decrease in FeS content of sphalerite with increasing sulphur activity (a_{s_2}) is much greater resulting in a close spacing of isopleths near the pyrite-pyrrhotite. FeS contents and formation temperature shows a little high sulphur activity (a_{s_2}) ($10^{-9} - 10^{-11}$). Data from Sulphur activity and formation temperature indicates that ore forming condition is assumed under intermediate sulphidation state, pyrite+chalcopyrite field, and magmatic hydrothermal compositional field.

Acknowledgements

Firstly, we would like to thank to AUN/SEED-Net and JICA for their financial supporting. Second, we are thankful to Indominig Group for their permission to collect samples from their project area. Finally, many thanks to Geology Laboratory members, Kyushu University, Japan for making SEM-EDX analyses.

References

- Carlile, J.C., and A.H.G. (1994) Mitchell, "Magmatic arcs and associated gold and copper mineralization in Indonesia." *Journal of Geochemical Exploration*, vol.50, pp 91-142,
- Sillitoe, R.H., and J.W. Hedenquist (2003) "Linkages between Volcanotectonic Settings, Ore-Fluid Compositions, and Epithermal Precious Metal Deposits." *Society of Economic Geologists*, Special Publication, 10, pp 315-343.
- Einaudi, M.T., J.W. Hedenquist, and E.E. Inan (2003) "Sulfidation State of Fluids in Active and Extinct Hydrothermal Systems: transitions from Porphyry to Epithermal Environments." *Society of Economic Geologists*, Special Publication, vol.10, pp 285-313.
- Hamilton, W. (1979) *Tectonics of the Indonesian region*. U.S. Geol. Surv.
- Noya, Y., O. Effendy, Z. Hamdan Abidin, and Y. Pakaya, (2009) "Geological background and economic prospect of the Soripesa deposit, east Sumbawa." *Proceeding PIT IAGI Semarang, 2009. The 38th IAGI annual Convention and Exhibition Semarang*.
- Khant, W., I W. Warmada, A. Idrus, L.D. Satijadji, and K. Watanabe, (2012a) "Alteration Mineralogy and Quartz Textures of Polymetallic Epithermal Quartz Veins at Soripesa Prospect Area, Sumbawa Island, Indonesia." *2nd Asia Africa Mineral Resources Conference Bandung*, pp 14-17.
- Misra, K.C. (1999) *Understanding Mineral Deposits*. Kluwer Academic Publisher.
- Fleischer, M. (1956) "Minor Elements in Some Sulfide Minerals." *Economic Geology*, 50th Anniversary Volume, pp 970-1024.
- Jonasson, I.R., and D.F. Sangster (1978) "Zn:Cd ratios for sphalerites separated from some Canadian sulphide ore samples." *Geol. Surv. Canada*, Vol.78-1B, pp 195-201.
- Dill, H., (1979) "Lagerstattenkundliche Untersuchungen zur Entstehung der pyritführenden Blei-Kupfer-zink-Lagerstätte Accessa (SW-Toskana)", *Mineral Deposita*, Vol.13, pp 57-80,.
- Vokes, F.M., (1976) "Caledonian massive sulphide deposits in Scandinavia: A comparative review." In: *Handbook of stratabound and stratiform ore deposits*, Vol.6, Wolf, K.H. (ed.), pp 79-128.
- Both, R.A. (1973) "Minor element geochemistry of sulphide minerals in the Broken Hill lode (NSW) in relation to the origin of ore." *Mineral Deposita*, Vol. 8, pp 349-369.
- Stoiber, R.E. (1940) "Minor elements in Sphalerite" *Economic Geology*, Vol.35, p. 501-519,.
- Warren, H.V., and Thompson, R.M., Sphalerites from western Canada. *Economic Geology*, Vol.40, pp. 309-335, 1945.

- Vaughan, D.J., and J.R., Craig (1997) “*Sulfide Ore Mineral Stabilities, Morphologies, and Intergrowth Texture*”, In Barnes H.L. (ed.), *Geochemistry of Hydrothermal Ore Deposits*, John Wiley & Sons, pp 367-434.
- Moller, P. (1985) “Development and application of the Ga/Ge-Geothermometer for sphalerite from sediment hosted deposits” In Germann K. (ed.), *Geochemical aspects for Ore Formation in Recent and Fossil Sedimentary Environments*”, pp.15-30.
- Evans, A.M. (1993) *Ore Geology and Industrial Minerals: An Introduction*, Blackwell scientific publications, 3rd ed.
- Möller, P. (1987) “Correlation of Homogenization Temperatures of Accessory Minerals from Sphalerite-bearing Deposits and Ga/Ge Model Temperatures” *Chemical Geology*, Vol.61, pp 153-159.
- Marques de Sá, C. and F. Noronha (2012) “Ga/Ge in Sphalerite Geothermometer - Application to Braçal Deposit” *Comunicações Geológicas* vol. 99, 1, pp 5-10.
- Khant, W., I W., Warmada, A., Idrus, L.D., Satijadji, and K., Watanabe, (2012b) “Fluid inclusion study of the polymetallic epithermal quartz veins at Soripesa prospect area, Sumbawa island, Indonesia” *Journal of Southeast Asian Applied Geology*, Vol. 4(2), pp 77-89.
- Kullerud, G. (1953) “The FeS-Zns system: a geological thermometer” *Nor. Geol. Tidsskr.*, Vol. 32, p. 61-147.
- Scott, S.D. (1983) “Chemical behaviour of sphalerite and arsenopyrite in hydrothermal and metamorphic environments.” *Mineralogical magazine*, vol. 47, pp 427-435.

CHROMITE MINERALIZATION AT SAISAQUINE WORKSITE, THABEIKKYIN TOWNSHIP, MANDALAY REGION

Hnin Min Soe^{1*}

Abstract

The study of chromite deposits especially at Saisaquine worksite (Local name) is situated in the Thabeikkyin Township, Mandalay Region. The ophiolite rock suite of this area belongs to the Tagaung- Myitkyina Belt of Upper Ayeyarwady Province which extends from the study area (Saisaquine worksite) Tagaung in the south to Myitkyina area in the north. Lithologic mapping in the ultramafic complex is difficult because of later modifications induced by extensive serpentinization and thermal metamorphism. Podiform chromite ores are main mineralization and they are hosted in serpentinized dunite and harzburgite. Mineralizations style occurred as irregular pocket or lens-shaped and fracture filling. Subcordant to discordant nature of the ore bodies which respect to their enclosing rocks and mostly found as massive and granular aggregates ores. Texturally, clot and pull-apart can be observed under microscope. In the field podiform chromitites can be seen as diverse types: they are massive, banded and disseminated, spotted or antiorbicular and nodular types. Nodular structure is characteristically of podiform chromite deposits and also as Alpine-type ultramafic rocks and primary magmatic feature. Low TiO₂ content indicates that the parental magma is a primitive Boninitic melt. The major objective of this paper is to review a chromite mineralization at Saisaquine worksite especially for major and minor elements by X-ray Analytical Microscope (XGT) method. Geochemically, MgO, major oxide content in chromitite ore is 9.32 to 29.8 in wt% by XRF chemical analysis and X-ray powder patterns are used for the identification of chromite mineral species: magnesio chromite is attempted. Due to sporadic podiform chromite deposits of Saisaquine worksite area is a favourable for medium-scale mining operation.

Keywords: *Saisaquine worksite, Chromite Deposits, X-ray Analytical Microscope, Magnesiochromite*

Introduction

Location, Size and Accessibility

The study area is situated between latitude 23° 30' N and 23° 38' N, and longitude 96° 05' E and 96° 12' E. It falls in 93 A/2, one inch topographic map and UTM map sheet No.2396(02) see in (Fig.1). The area lies in the Thabeikkyin Township, Mandalay Region and covers about (45) square kilometers. The study area can be reached from Mandalay by car. The satellite image shows the physiographic nature of the study area see in (Fig.2) and (Fig.3) shows 3D view of the study area, looking N.

* Dr, Professor, Department of Geology, University of Mandalay, Myanmar

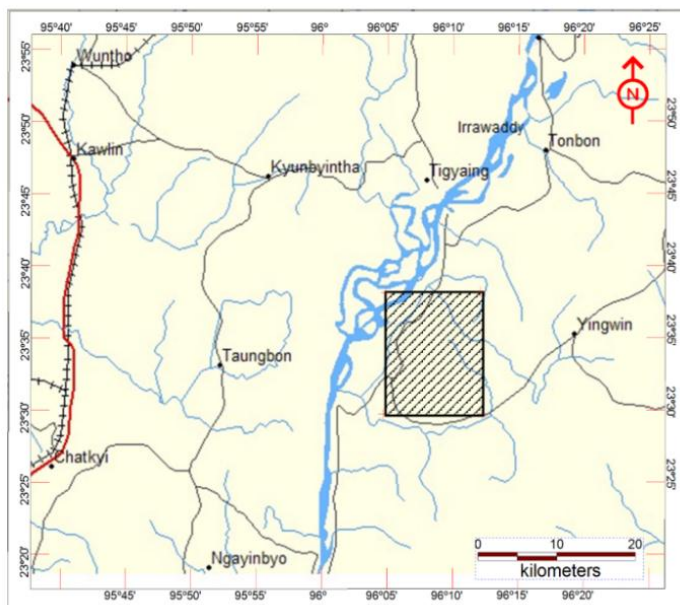


Figure 1 Location map of the study area.

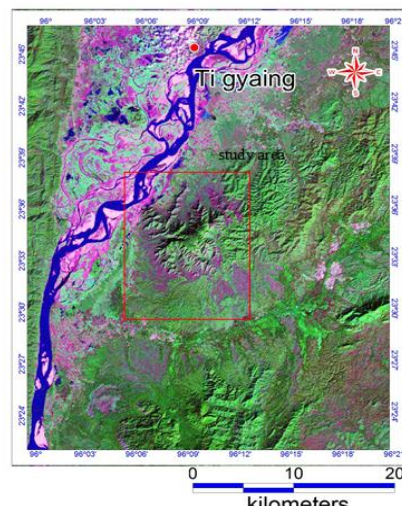


Figure 2 Satellite image of the study area.(Google Earth)

Purpose and Scope

The current research work is expected to contribute the following.

1. To construct the modified geological map of the study area.
2. To discuss the petrography and mineralogy of the Saisaquine worksite chromites.
3. To study the geochemistry and petrogenesis of the Saisaquine worksite chromites.

Methods of Study

Field Investigation

In the field, detailed outcrop mapping was carried out by using Brunton compass-type traverses. Representative samples of ores and host rocks were collected for subsequent analytical work and laboratory investigation. The GPS was used to locate the important outcrops, sample locations and measuring the geological structures and other necessary data.

Laboratory Investigation

The following works were done in the laboratory;

- (1) Polished and thin sections of rocks and ore samples were studied under microscope through transmitted and reflected light.
- (2) Identification of chromite mineral species by X-ray diffraction (XRD) analysis.
- (3) Chemical analysis of rock and ore samples for major and minor elements by X-ray fluorescence analysis (XRF) and X-ray Analytical Microscope (XGT).

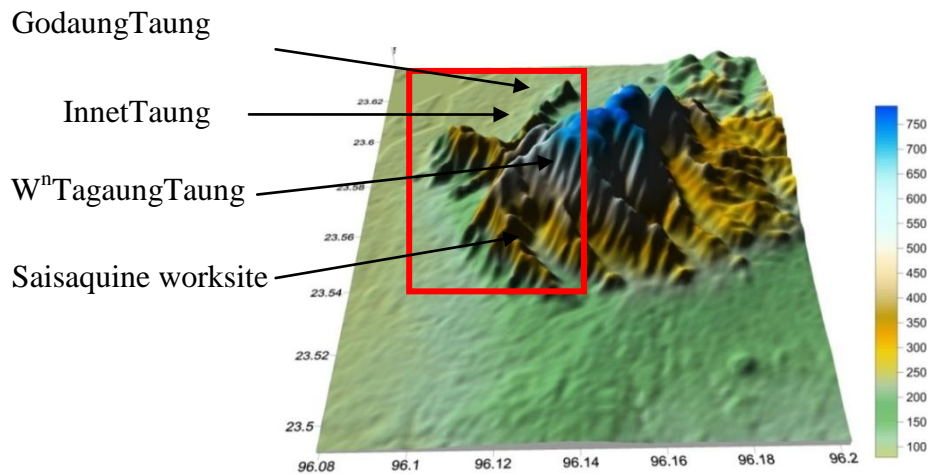


Figure 3 3D view of the study area, looking N.

Regional Geologic Setting

The study area is situated 12 miles south of Tigyaing in the east bank of the Irrawaddy River. This area also located in the southern part of the Tagaung-Myitkyina Belt of Upper Ayeyarwady Province (Mitchell *et al*, 1993).

The study area falls in the western edge of the Shan-Tennasserim Block and the eastern marginal zone of the Central Cenozoic Belt. The study area falls within the Mandalay-Jade Mine Ophiolite Belt according to Hutchison (1989). This ophiolite belt is situated along the western margin of the Sino-Burma Ranges (Fig. 4).

Ayeyarwady River runs nearly N-S directions, which flows north to south. The well-known Sagaing Fault, a right lateral strike-slip fault is trending nearly north-south to the west of the study area. According to Myint Thein *et al.*(1983) the Ngapyawdaw Chaung Formation and the Male Formation lie to west of the study area. Mesozoic age, Katha Metamorphics occupied in north of this fault.

To the south of this area is occupied by the complexes structure and lithology of Mogok Series of La Touche (1913). Twinnge-Momeik Fault is the southern boundary of this area. It separates the rocks of the study area in the north from those of the Mogok Belt in the south. The Katha-Gangaw Range running from Mogaung at the north through Naba-Katha to Tigyaing at the south, dies out to a plain at Tigyaing about 23 km north of the study area.

Stratigraphy

The study area comprises a sequence of ultramafic, sedimentary and metasedimentary rocks. The rock units are generally extended roughly NNE-SSW. The stratigraphic sequences of the study area are established by Than Than Oo (2006). The modified geological map of the study area is shown in (Fig 4).

Rock sequence and distribution of the study area (After Than Than Oo, 2006)

Six different stratigraphic units are recognized in the study area on the basis of lithology, stratigraphic position and fauna content and these units (from younger to older) are;

Stratigraphic Succession	Age
Sedimentary rocks	
Alluvial	Recent
Nickel laterite soil	Pleistocene
Fanglomerate	Pleistocene
Male Formation	Lower- Middle Eocene
Baingbin Conglomerate	Paleocene
That-tu Bedded Chert	Cretaceous
Metasedimentary rocks	
Twegauk schist	Cretaceous?
Igneous rocks	
Ultramafics	Early Jurassic?

Petrography and Mineralogy of Chromite Ore

Types of Chromites

Podiform chromitites of study area are texturally diverse. They are massive type, banded and disseminated type, spotted or antiorbicular type and nodular type.

(a) Massive Type

Massive chromitites typically have sharp contact with the enclosing dunite (Fig.5). Massive chromitites are hard and compact, steel grey to deep black in colour, and have a high specific gravity. They are coarse-grained rocks; composed of more than volume percent chromites. Individual chromite grains are mostly 1 to 5 mm interlocking euhedral, subhedral, or anhedral chromites containing very small quantity of talc or serpentinized olivine filling up the interspace.

(b) Banded and Disseminated Type

Disseminated chromitites grains about 20-70 volume percent are more or less uniformly scattered in dunite and peridotite. The chromites are arranged in persistent layers alternating with layer of altered silicate or serpentine (Fig.6). Small euhedral chromite grains with sharp margins enclosed within single crystallization of partly altered olivines were described as early magmatic by Chakraborty (1973) and Varma (1965). Both olivine and chromite in the banded chromites are considered as the products of in-situ crystallization where both the minerals scattered simultaneously.

(c) Spotted or Antiorbicular Type

Spotted chromites are widespread in this area. Spotted chromites are transitional type between massive and banded chromites. In chromitiferous dunite unit in which euhedral and subhedral chromites are partially or totally filled the interstices of the olivine (Fig.7). These textures are the result of the settling together under gravity of coarse cumulus and finer cumulus of chromites, followed by adcumulus (Wager *et al*, 1960).

(d) Nodular Type

Nodular texture is a critical feature that distinguishes podiform deposits from stratiform deposits (Thayer, 1964). Nodular chromites consist of rounded or ellipsoidal chromite aggregates; interlocked subhedral to anhedral chromite aggregates, usually massive in nature (Fig.8). The structure range from sphere to oblate and vary in size from about 2 mm to 20 mm in the longest dimension. The nodules are embedded in dunite or serpentine in a manner of pebbles in conglomerate. It is characterized by concave-convex embayment of grain boundaries. Core of some nodules are intergrown with silicates. Various mechanisms have been proposed to explain the origin of this structure.

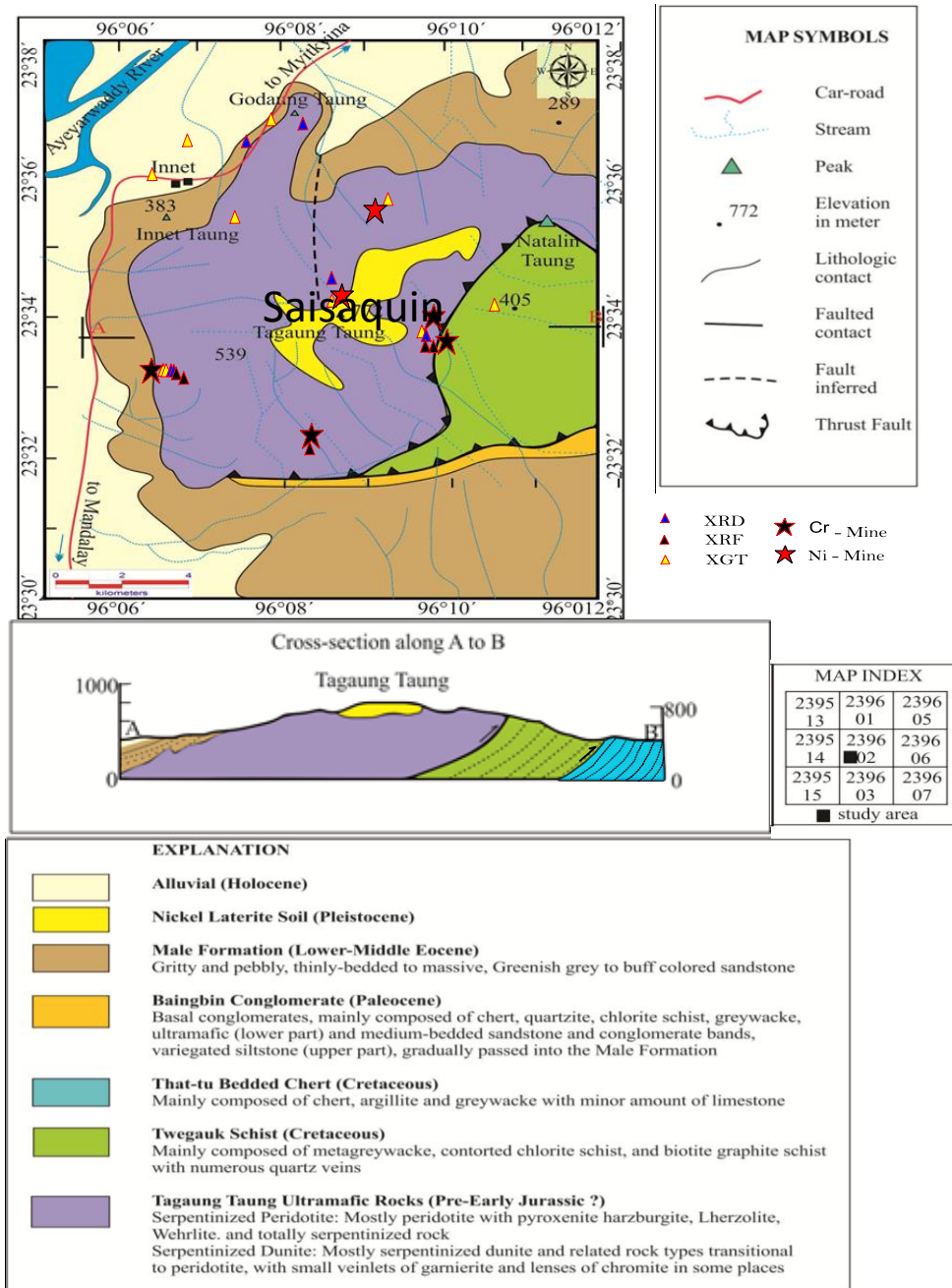


Figure 4 Geological map of the study area (Modified after Than Than Oo, 2006).



Figure 5 Massive chromitites enclosed in dunite exposures, western part of study area.



Figure 6 Serpentine (green) & chromites (black) are arranged in alternating layers.



Figure 7 Spotted type chromitites formed by partially or totally fill the interstices between olivine grains at Saisaquine worksite.



Figure 8 Nodular type chromitites consist of rounded or ellipsoidal chromite aggregates in a matrix of serpentine at Saisaquine worksite area.

Megascopic Description

Chromites are composed of chromian spinel and silicate matrix with various proportions. The predominant ore mineral are chromites with the primary silicates like olivine, enstatite and diopside. Olivine, antigorite, tremolite, kammerite and uvarovite are the gangue minerals for this mineralization. Generally, the chromitites occur as compact and massive, (Tiger ore) and granular aggregates with subordinate amounts of silicate gangue matrix, (Leopard ore). Chromitites ore can be found as opaque, jet black to dark grayish, with a brownish black, brilliant shining and submetallic to dull in color.

Microscopic Description

In thin section, the chromite grains show zonal oxidation extending from the opaque to translucent reddish brown in the centre of the grains. Some translucent chromites have opaque borders and fracture networks. Cracking and crushing are common in it. The silicate inclusions are very characteristic in chromitites (Fig.9). Inclusions of olivines, orthopyroxenes, clinopyroxenes and sulphides are found in chromite grains.

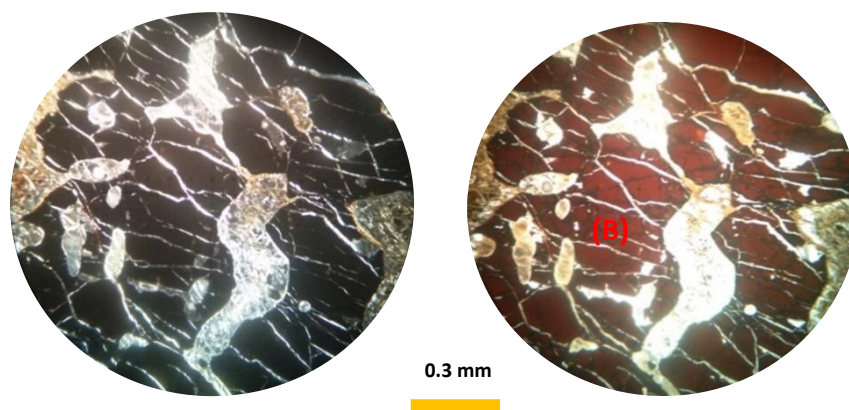


Figure 9 Photomicrograph showing silicate inclusions occurred in chromite crystal, pyroxene, olivine grains and vein serpentines (A) PPL and (B) XN.

Textures of Chromitites

Clot texture

Segregation of finer subhedral or subrounded grains in the interspaces of coarsely granular chromite mosaic was described as clot texture by Mukherjee (1969) (Fig.10). Varma (1965) considered as xenolithic inclusions of late magmatic chromite surrounded by coarsely crystalline hydrothermal chromites. According to Mukherjee (1969), the fine grained clots are formed by rapid cooling of the residual chrome rich liquid.

Pullapart texture

Pullapart texture is very characteristic of massive chromites. Pull-apart texture is well-exposed in coarse-grained chromite normal to the axis of stretching (Fig.11). The chromite grains are fractured and the fracture planes being commonly filled up with serpentine gangue.

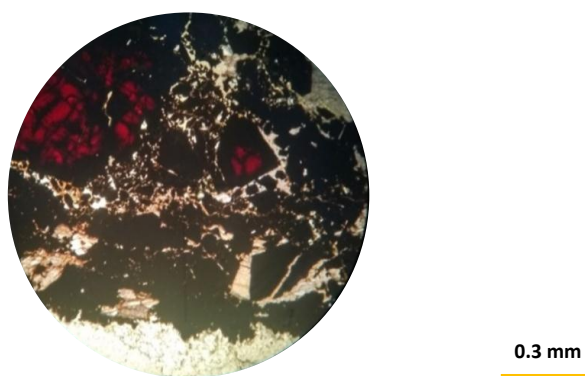


Figure 10 Finer grains in the interspaces of coarsely chromite mosaic can be seen as clot texture, between (XN).

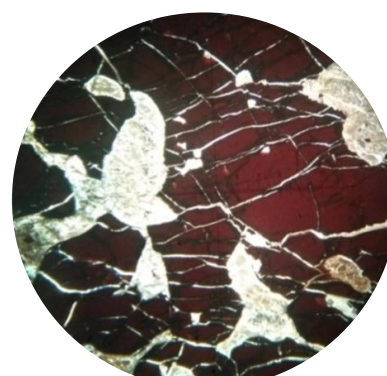


Figure 11 Fractured and the fracture planes of chromite grains are filled up with serpentine gangue, forming pull-apart texture.

Chromite Mineralization

The study area is entirely made up of a massive ultramafic complex which was emplaced in the tectonic zone by an up thrust movement. Serpentinites and highly fractured dunites are dominant ultramafic members. Widespread chromite mineralization is hosted in dunite and surround area, Saisaquine (local name) (Fig.12) and Kyauklaung stream sections (Fig.13),

occupying the south and southwest of the study area. Faults and fractures are the evident of structural controls mineralization in this area. The chromite deposits occurred as floats, fragments and lenticular ore body (podiform) but the major concentration are seen in the dunite. According to the field evidence, along the Kyauklaung Chaung section is the potential area for future chromite exploration.

Saisaquine worksite chromite ore is generally found as deep blackish in color, pods and pockets shaped, irregularly distributed in the ultramafic rock (Fig.14). Size and shape are very variable and unpredictable. Two types of chromite ore are observed, such as (1) Primary and (2) Secondary (placer). Primary ore are (1) Massive (Tiger ore) deep blackish in color, (2). Impure chromite ore (Leopard ore) black and (3) Chrome dioxide dark (Black mixed with greenish colour). (U Hla Myint, U Maung Maung Htwe, U Maung Maung,1997).

Chromium content is more in massive ore (Tiger ore) (Fig.15) than leopard ore. They are occurred in different places or intimately in some places. Massive ore is always overlain by leopard ore (Fig.16). Massive type chromite ore is associated with dunite and occurred as lenticular (podiform) (Fig. 17) about a few feet long too many masses. Some occurrences show well developed pullapart texture indicating tectonic influence on chromite mineralization. The average chromium content is about 52.03 % (MU Research Center,2018).



Figure 12 Chromite mineralization at Saisaquine (local name) open pit mine.



Figure 13 Chromite mineralization near the Kyauklaung stream section.



Figure 14 Close-up view of **Pockets-shaped** chromite (deep blackish) in the study area.



Figure 15 Massive ore (Tiger ore) has more chromite than Leopard ore in the study area.



Figure 16 Impure chromite ore (Leopard ore) is less chromite content in the study area.



Figure 17 Lens-shaped chromite found near the car road in the study area.

Geochemistry and Petrogenesis of the Saisaquine Worksite Chromitites

Geochemical Characterization of Chromitites

Analytical procedure

Chemical composition of chromites was determined by XRF and XGT systems with an energy dispersive spectrometer at the Mandalay University's Research Center and XRD analyzed data at Department of Atomic Energy, Ministry of Science and Technology. Analyses were performed on polished and thin sections which represent to both rocks and ore samples.

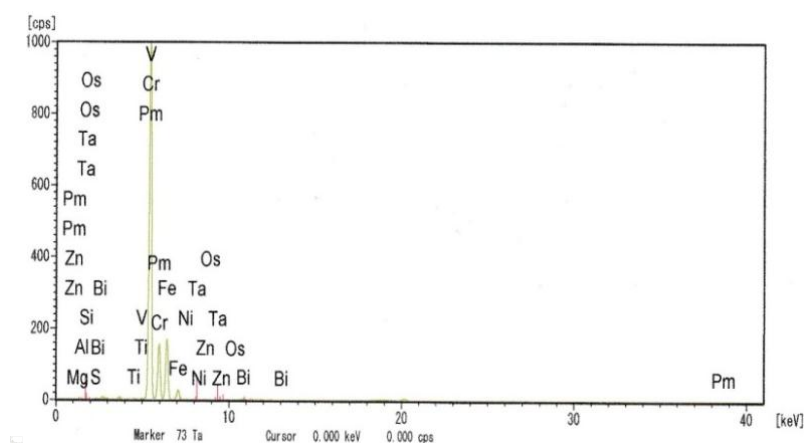
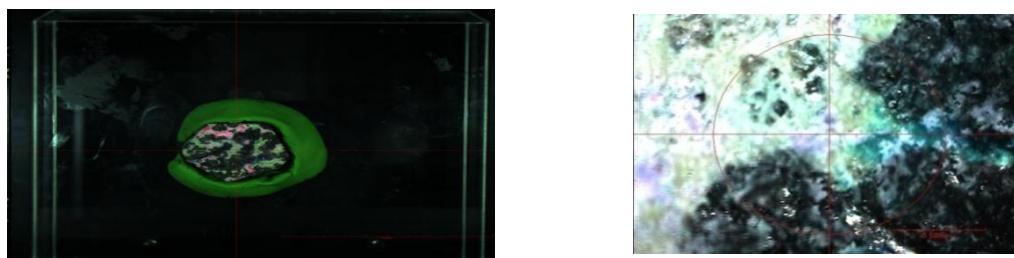
Experimental results and discussions

The chromitites of Saisaquine worksite are composed of both chromite and serpentinized olivine. The chromitites composition ranges from 38 to 52 volume percent chromite. Representative chemical results by X-ray Analysis of chromitite ores from study area is shown in Table-A and the content of Mg element is noticeable. X-ray pattern is illustrated in (Fig.18) and XGT photomicrographs of Cr with Mg, Fe, Al and Ni are shown in (Fig. 19,20,21,22 and 23).

XRF chemical data of representative chromite concentrates with significant amount from the study were carried out and show a broad range of major oxide content; 0.48 to 4.28 wt % Cr_2O_3 ; 0.26 to 0.67 wt% NiO, 0.42 to 10.3 wt % Al_2O_3 ; 4.71 to 27.7wt% Fe_2O_3 ; 9.32 to 29.8 wt % MgO in Table-B.

Table (A) The Chemical Results of gangue and ore minerals in the study area examined under X-ray Analytical Microscope (XGT)

Elements	S ₁	S ₂	S ₃	S ₄	S ₅
Mg	8.28 %	12.03%	8.11%	13.69%	11.22%
Al	7.57	14.65	6.93	5.83	6.45
Si	3.26	6.72	5.35	8.60	3.16
K	0.09	0.06	-	-	-
Sc	0.28	-	-	-	-
Ti	0.06	0.05	0.17	0.18	0.11
V	0.10	0.11	0.07	0.06	0.08
Cr	51.47	38.68	51.01	49.07	52.03
Fe	15.66	16.18	17.56	16.13	15.02
Ni	0.27	0.28	0.25	0.36	0.16
Zn	0.04	0.11	0.08	0.02	0.04
Pm	12.53	11.15	9.86	5.61	11.10
Ta	0.07	0.00	0.01	0.01	0.01
Bi	0.32	-	0.18	0.42	0.19
S	-	-	0.43	0.01	0.40
Os	-	-	-	-	0.04
Total	100	100	100	99.99	100

**Figure 18** XGT pattern of the chromitite at Saisaquine worksite**Figure 19** Sample-(A1b). XGT photomicrograph of Cr with Mg, Fe, Al and Ni.

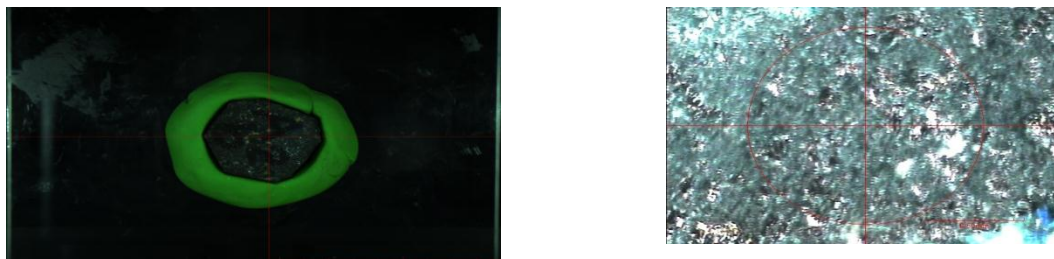


Figure 20 Sample-(A2b). XGT photomicrograph of Cr with Mg, Fe, Al and Pm (promethium).

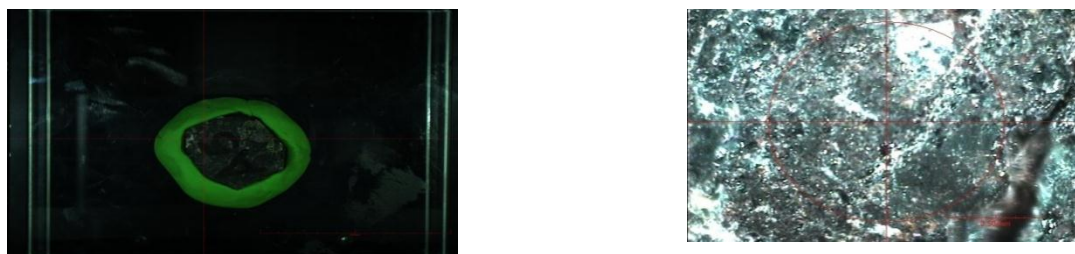


Figure 21 Sample-A5. XGT photomicrograph of Cr with Mg, Fe, Al and P

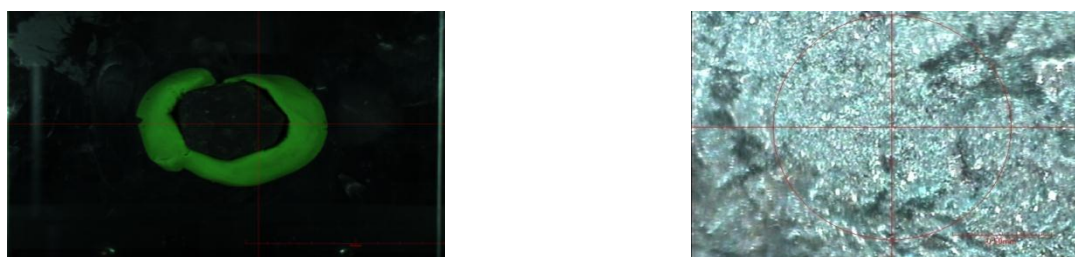


Figure 22 Sample-(B20a). XGT photomicrograph of Cr with Mg, Fe, Al and Pm.

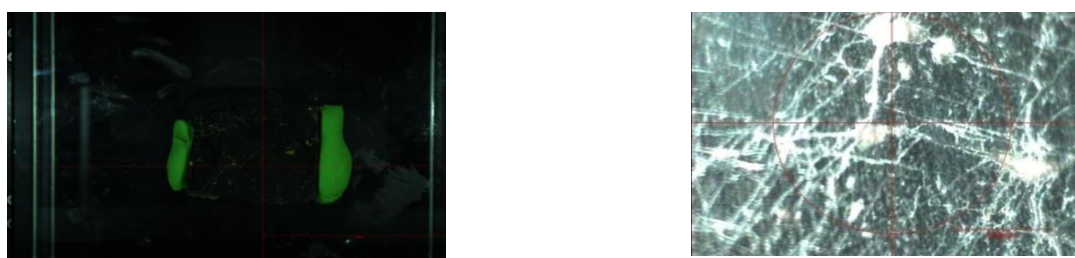


Figure 23 Sample-(E5). XGT photomicrograph of Cr with Mg, Fe, Al and Pm.

Table (B) XRF Chemical composition results of ultramafic rocks.(Major elements in wt%)

Oxide	F8	D8	F7	E2	F5	C3	C5
MgO	26.2	23.0	25.7	14.2	27.2	29.8	9.32
Al ₂ O ₃	1.35	1.22	0.428	10.3	1.35	0.813	1.07
SiO ₂	55.5	58.8	58.6	52.6	54.7	54.9	56.4
P ₂ O ₅	0.118	0.0926	0.101	0.0760	0.0878	-	-
Cl	0.0271	0.0919	0.0590	-	0.0253	-	0.0018
K ₂ O	0.104	0.157	0.141	0.297	0.112	0.103	0.122
CaO	0.437	1.01	0.381	12.9	1.31	0.682	0.521
V ₂ O ₅	0.0294	-	-	-	-	-	-
Cr ₂ O ₃	2.39	0.488	0.536	4.28	0.980	0.522	0.547
MnO	0.187	0.214	0.214	0.0799	0.207	0.194	0.409
Fe ₂ O ₃	13.1	14.3	13.2	4.71	13.5	12.3	27.7
NiO	0.519	0.612	0.582	0.261	0.546	0.668	3.85
ZnO	0.0114	-	0.0131	-	-	0.0141	-
SO ₃	-	0.0791	0.0367	-	0.0102	-	-
CO ₂ O ₃	-	0.0318	0.0299	-	-	-	-
TiO ₂	-	-	-	0.268	-	-	-
Total	99.855	99.3865	100	99.9719	100	99.9961	99.9408

Petrogenesis of the Host Rocks

Dunite and serpentized-dunite of ophiolite suite are the main host of chromite ores in the study area. The formation of ophiolites will be explained in terms of their igneous development demonstrating that ophiolites occurred as closely associated assemblages. Their origins are polygenetic. Ophiolites are generated in several tectonic environments characterized by distinct sets of chemical signature. There are differences between the two major types of ophiolites; Mid Ocean Ridge (MOR) and Supra-Subduction Zone (SSZ). Discussion will be based on the variations of the degree of partial melting between these two ophiolite groups.

Mineral identification by XRD analysis

The representative chromite samples were analyzed in the XRD laboratory of the Department of Atomic Energy, Ministry of Science and Technology. X-ray powder patterns are the only certain means of identifying chromite mineral species. The X-ray diffraction (XRD) powder patterns are illustrated in (Fig.24), magnesiochromite species can be observed.

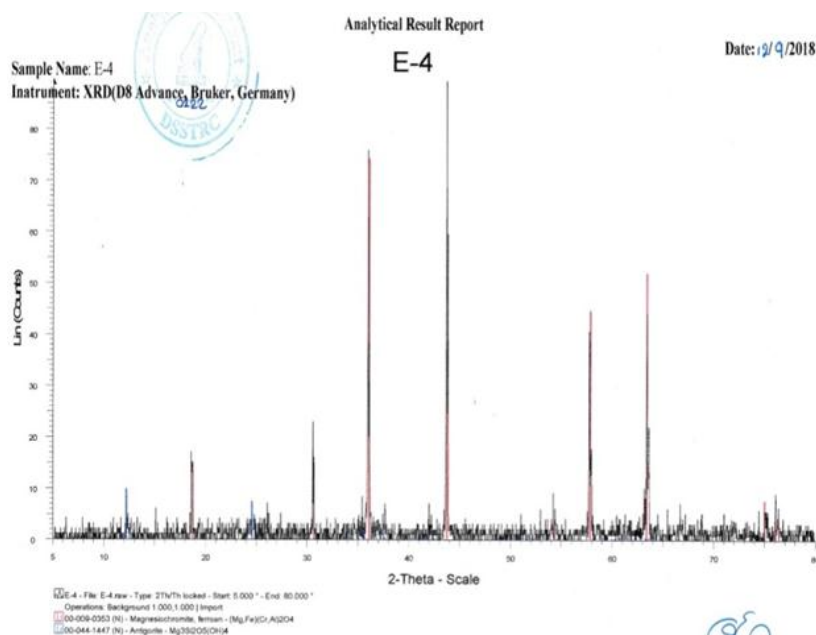


Figure 24 Contain major amount of magnesio- chromite and minor amount of antigorite.

Statistical Treatment of Geochemical Data from Saisaquine Worksite

The geochemical distribution pattern of the elements around the chromite mineralization is the basis for the development of the geochemical exploration techniques which shows about the associated minerals. The X-Ray analytical microscope (XGT) and X-Ray Fluorescence (X.R.F) results at Saisaquine Worksite chromite mining is shown in table (A and B). The elements of PbO, ZnO, CaO, MgO, SiO₂ and Fe₂O₃ were determined. These results from geochemical analysis were treated by statistical method using geostatistical software by calculating the values of Mean (\bar{X}) and Standard Deviation (S).

Distribution of Chromite: The concentration of chromite in ore samples ranges from 38.68% to 52.03%. The mean value of chromite is 48.45% and standard deviation is 5.578%.

Distribution of Nickle: The concentration of nickle in ore samples ranges from 0.168% to 0.36%. The mean value of nickle is 1.55% and standard deviation is 2.347%.

Nickle has negative correlation with chromite. R square linear is 0.093. The chromite and nickle frequency histograms of chemical results and the variation diagram of negative relationship between chromite and nickle are shown in (Fig 25- A,B,C).

Distribution of Titanium: The concentration of titanium in ore samples ranges from 0.05% to 0.18%. The mean value of chromite is 0.11% and standard deviation is 0.06%. Titanium has positive correlation with chromite. R square linear is 0.221. The chromite and titanium frequency histograms of chemical results and the variation diagram of positive relationship between chromite and titanium are shown in (Fig 26- A,B).

Distribution of Silica: The concentration of silica in ore samples ranges from 0.05% to 0.18%. The mean value of silica is 0.11% and standard deviation is 0.06%. Silica has negative correlation with chromite. R square linear is 0.093. The silica frequency histograms of chemical

results and the variation diagram of negative relationship between chromite and silica are shown in (Fig 27- A,B).

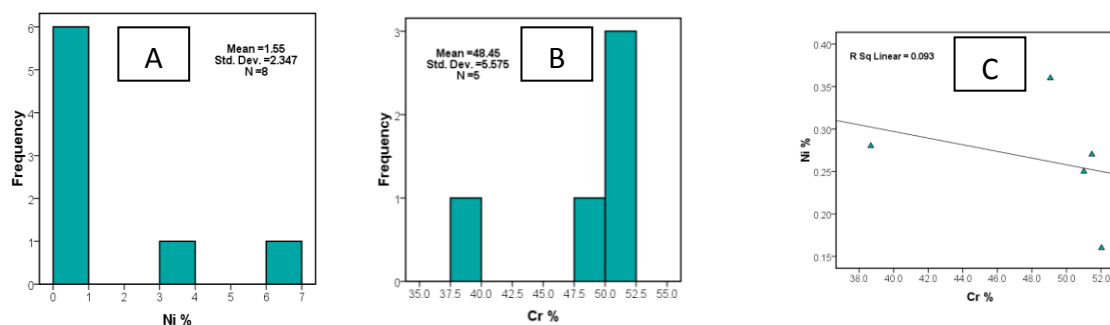


Figure 25 (A,B,C) Chromite and nickel frequency histograms and variation diagram of negative correlation between chromite and nickel.

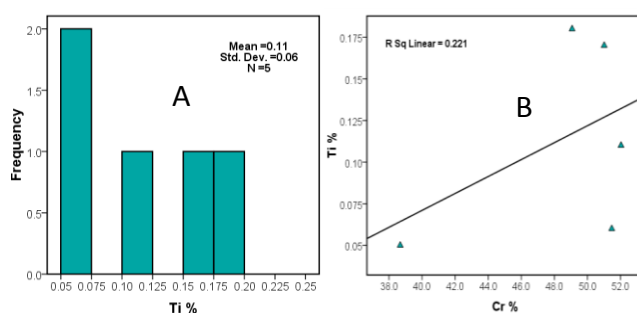


Figure 26 (A,B) Titanium frequency histogram and variation diagram of positive correlation between chromite and titanium.

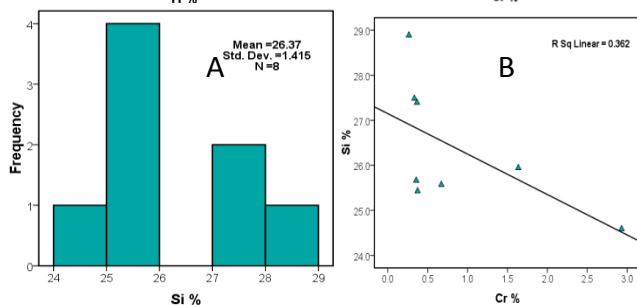


Figure 27 (A,B) Silica frequency histogram and variation diagram of negative correlation between chromite and silica.

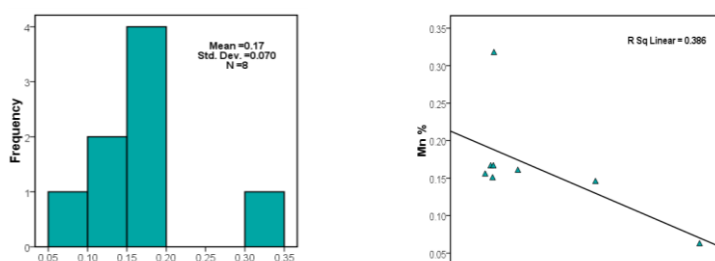


Figure 28 (A,B) Manganese frequency histogram and variation diagram of negative correlation between chromite and manganese.

Distribution of Manganese: The concentration of manganese in ore samples ranges from 0.079% to 0.409%. The mean value of manganese is 0.17% and standard deviation is 0.070%.

Manganese has negative correlation with chromite. R square linear is 0.386. The manganese frequency histogram of chemical results and the variation diagram of negative relationship between chromite and manganese are shown in (Fig 28- A,B).

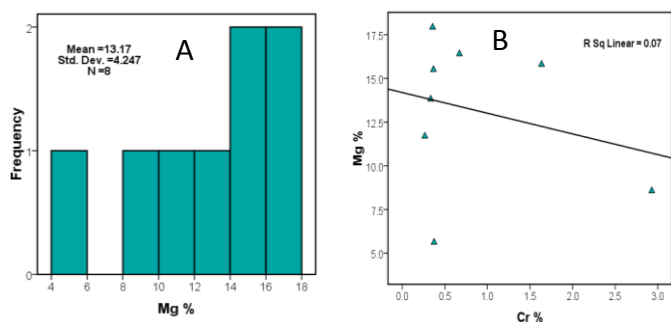


Figure 29 (A,B) Magnesium frequency histogram and variation diagram of negative correlation between chromite and magnesium.

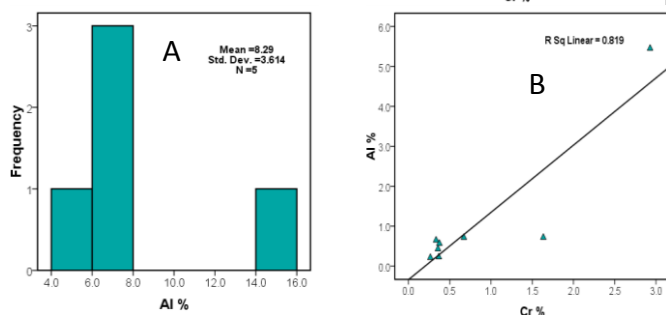


Figure 30 (A,B) Aluminum frequency histogram and variation diagram of positive correlation between chromite and aluminum.

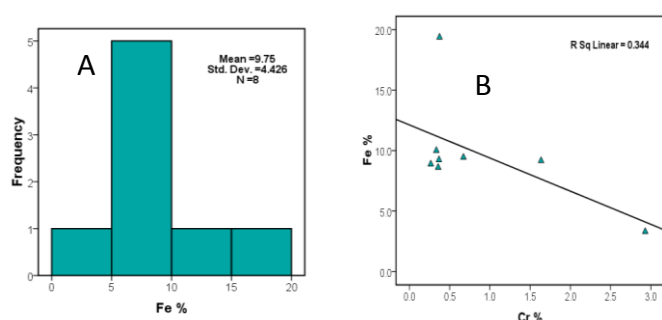


Figure 31 (A,B) Iron frequency histogram and variation diagram of negative correlation between chromite and iron.

Distribution of Magnesium: The concentration of magnesium in ore samples ranges from 8.11% to 13.69%. The mean value of chromite is 13.17% and standard deviation is 4.247%.

Magnesium has negative correlation with chromite. R square linear is 0.07. The chromite and magnesium frequency histograms of chemical results and the variation diagram of negative relationship between chromite and magnesium are shown in (Fig.29- A,B).

Distribution of Aluminium: The concentration of aluminium in ore samples ranges from 5.83% to 14.65%. The mean value of aluminium is 8.29% and standard deviation is 3.614%.

Aluminium has positive correlation with chromite. R square linear is 0.819. The aluminium frequency histograms of chemical results and the variation diagram of positive relationship between chromite and aluminium are shown in (Fig.30- A,B).

Distribution of Iron: The concentration of iron in ore samples ranges from 15.02% to 17.56%. The mean value of iron is 9.75% and standard deviation is 4.426%.

Iron has negative correlation with chromite. R square linear is 0.344. The iron frequency histogram of chemical results and the variation diagram of negative relationship between chromite and iron are shown in (Fig.31- A,B).

Cluster Analysis of ore samples at Saisaquine Worksite Area

Cluster analysis of elements in ore samples is performed by the weighted pair group method. This investigation is based on eight ore samples results of X.R.F analysis from Saisaquine Worksite chromite deposit, as shown in above Table. The constructed dendrogram is

shown in (Fig.32).The dendrogram drawn through cluster analysis of ore samples from Saisaquine Worksite chromitedeposit indicates that six associations of elements are observed in the clusters.

The first group of associated elements is Fe –Mn (0.997) and the second group is Cr –Al = (0.905). The third cluster, Ni-Si = (0.614) and fourth cluster is SiNi-FeMn = (0.170). Fifth cluster is Fe Mn Si Ni Mg = (-0.245) and Sixth cluster is Fe Mn Si Ni Mg Al Cr = (-0.488).

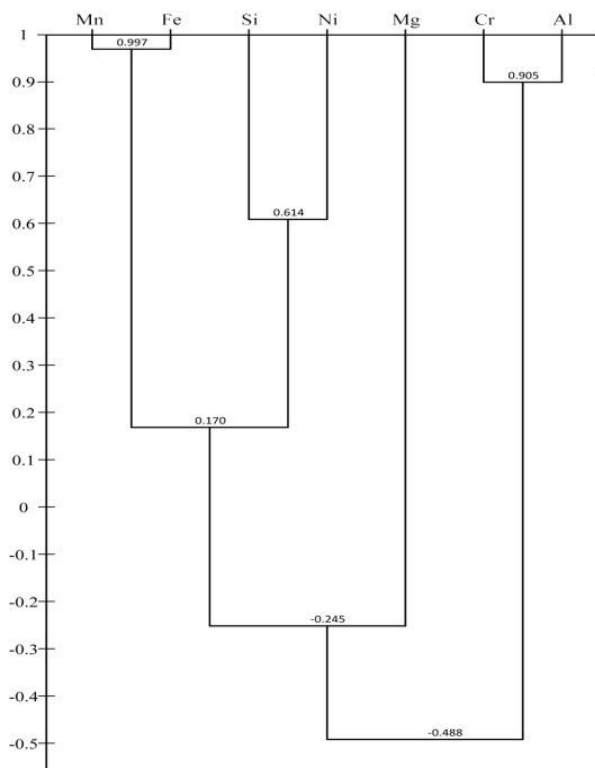


Figure 32 Dendrogram constructed by weight pair group method at Saisaquine Worksite chromite mineralization.

Conclusions

The Saisaquine worksite area lies within latitudes 23° 30' N and 23° 38' N, and longitude 96° 05' E and 96° 12' E. It falls in the UTM map sheet No.2396-02, one-inch topographic map N0. 93-A/2. The study area occupies in the Thabeikkyin Township, Mandalay Region.

The Saisaquine worksite ultramafic rocks are occupied nearly half of the study area. The major rock types are dunite, peridotite (harzburgite, lherzolite) and serpentinite. Most of them are partially to completely serpentinite. Serpentinites are alteration products from ultramafic rocks such as dunite and harzburgite. Harzburgite and dunite predominate over the other rock types. Mineralization host rock are serpentinitized-dunite body near the harzburgite unit.

The chromitites are of the orogenic Alpine- type or the Podiform type that occurred as lens-shaped, nodular disseminated and massive forms. The ore bodies are small, erratic but occurred over and extensive area at Tagaung Taung area. Many of the orebodies are subcordant to discordant. The chromitites are composed of chromium spinel and silicate matrix. Chromite is the predominant ore mineral with olivine and serpentine (antigorite).

Texturally, Pull-apart texture is characteristic of the massive varieties, developed normal to the axis of stretching and the fracture commonly filled with serpentine gangue. Clot texture is segregation of finer subhedral or subrounded grained in the interspaces of coarsely granular chromite mosaic.

The geochemistry and the petrogenesis of the chromitites of the Saisaquine worksite area with a significant chemical data available from the analyzed samples studied by the aid of XRD, XRF and XGT systems. The petrogenesis of the ophiolites will be explained in terms of their igneous development and their polygenetic origins.

Low TiO₂ content in XRF results indicates that the parental magma is a primitive Boninitic melt. Geochemically, MgO, major oxide content in chromitite ore is 9.32 to 29.8 in wt% by XRF chemical analysis and X-ray powder patterns give the identification of chromite mineral species: magnesio chromite specie is identified. According to the field observation and chemical data, sporadic podiform chromite deposits of Saisaquine worksite area is a favourable for medium-scale mining operation.

Acknowledgements

Firstly, I am deeply indebted to Dr. Thida Win, Rector, University of Mandalay for her allowing to write this paper. I would like to extend my deep gratitude to Dr. Than Than Nu, Professor and Head, Department of Geology, University of Mandalay, for her encouragement to do this research.

References

- Chakraborty, K.L., (1973) Some characters of the bedded chromite deposit of Kelrangi, Outtack District, Orissa, India. *Mineral Deposita* (Berl), vol. 8, pp. 73-80.
- Hutchison, C.S., (1989) The Palaeo-Tethyan Realm and Indosinian Orogenic System of Southeast Asia in *Tectonic Evolution of the Tethyan Region*, p. 585-643, Kluwer Academic Publisher.
- La Touche. T. H.D., (1913) Geology of the Northern Shan State. *Mem. Surv. India*, vol. 39
- Myint Thein, Kyaw Tint and Kan Saw, 1983. Geology of the part of the Eastern Margin of the Central Burma Belt between Sagaing and Tagaung, *unpub. report*.
- Mitchell, A. H. G., (1993) Cretaceous-Cenozoic tectonic events in the western Myanmar (Burma)-Assam region in *Journal of the Geological Society of London*, vol. 150, p. 1089-1102.
- Mukherjee, S., (1969) Clot texture developed in the chromitites of Nausahi, Keonjhar District, Orissa, India; *Econ. Geol.* Vol. 64, p. 329-337.
- Than Than Oo, (2006) *Economic Geology of the Chromitites of the TagaungTaung Area, Thabeikkyin Township, Mandalay Division*, Ph.D Thesis, Y.U, unpub.
- Thayer, T.P., (1964) Principal features and origin of podiform chromitite deposits and some observation on the Guleman-Soridag District, Turkey: *Econ. Geol.* Vol. 59, p. 1497-1524.
- U Hla Myint, U Maung Maung Htwe, U Maung Maung, (1997) Report on detailed geological mapping in the Tagaung Taung area.
- Varma, O.P., (1965) Periods of crystallization and alteration of chromite from Keonjhar, Orissa. *Proc. Min. Geol. Met. Inst. Ind.*, vol. 62, pp. 67-79.
- Wager, L.R., Brown, G.M., and Wadsworth, W. J., (1960). Types of igneous cumulates: *Jour. Petrology*, vol. 1, p. 73-85.

WALL-ROCK ALTERATIONS AND ASSOCIATED HYDROTHERMAL QUARTZ TEXTURES IN ANTIMONY DEPOSITS OF THABYU AREA, KYA-IN-SEIKKYI TOWNSHIP, KAYIN STATE

Than Htoo Aung¹, Tun Naing Zaw², Than Than Oo³, Ohn Thwin⁴

Abstract

The research area is located in the southernmost part of Kayin State, near Myanmar-Thai border, Kya-in-seikkyi Township. In the research area, antimony mineralization is observed in the fracture zones which are NNW-SSE trending in the metasedimentary rock units of Taungnyo Formation. The common types of hydrothermal wall-rock alterations of ore deposits in the research area are silicification, vuggy silica (vuggy quartz) alteration, argillic alteration, propylitic alteration, and pyritization/sulphidation. Quartz (chalcedony and vuggy), calcite, pyrite, hematite, barite and sericite are the alteration products. Hydrothermal alteration around the mineral deposits commonly forms alteration halos. Classification of quartz textures observed in the mineralized veins and wall-rocks of the research area are –primary growth texture, recrystallization texture, and replacement texture. . Primary growth textures of vein quartz are (1) Chalcedonic texture, (2) Comb texture and (3) Crustiform texture. Recrystallization texture of quartz in the mineralized veins can be classified into moss texture. Replacement textures represent partial or complete pseudomorphs of other minerals by silica minerals within veins. The samples from the mineralized vein are show bladed texture under microscope. The consistent pattern of distribution of textures and consistent assemblages of textures can be used to define a vertical textural zoning model. Thus model should be capable of determining vertical position within a boiling epithermal vein system and predicting the locus of mineralization. The mineralogy and some chemical composition of alterations and hydrothermal quartz textures of antimony mineralization of research area provide an indication of proximity of mineralization and provide information on reservoir and fluid characteristics.

Keywords: wall-rock alteration, hydrothermal quartz textures, antimony deposits, Thabyu area

Introduction

The Thabyu area is located in the southeastern part of Kayin State, near Myanmar-Thai border about 400 kilometres Southeast of Yangon and 160 kilometres Southeast of Mawlamyaing and about 11 kilometers north of Phayathonzu. It is located at north Latitude 15° 33' to 15° 35' and East Longitude 98° 25' to 98° 26' and between vertical grid no. 380-440 and horizontal grid no. 130-200 of topographic map index no. 95 I/6 (Figure .1). It is covered about 8 square km.

In the Thabyu area, the antimony mineralization is hosted in the slate, phyllite and quartzite of the Taungnyo Formation which occurred on the eastern limb of local anticlinal structure along the western side of NW-SE trending Tele-Chaung and continues along the Lenpya-Chaung in the north having the length about 5km.

¹ Dr, Lecturer, Department of Geology, Loikaw University, Loikaw, Myanmar

² Dr, Lecturer, Department of Geology, University of Yangon, Yangon, Myanmar

³ Pro-rector, Magway University, Magway, Myanmar

⁴ Professor (retired), Department of Geology, University of Yangon, Yangon, Myanmar

Moulmein Limestone

In the Thabyu area, thick-bedded to massive, grey to dark grey coloured calcitic limestone, laminated limestone, dolomitic limestone and dolomite are occur in the Moulmein Limestone. The calcitic limestones unit is mostly fine to medium-grained, medium to thick bedded, light grey when fresh and yellowish grey when weathered. Individual bed thickness varies from place to place ranging from 10 cm to 25 cm. Several calcite veinlets are observed throughout the unit and slightly dolomitized in some places. It is poorly fossiliferous and some unidentifiable fossil fragments are observed. Laminated limestone unit is well-exposed along the crestal portion of study area. It is thick-bedded to massive, fine- to medium-grained, light to dark grey in colour and laminated.

Dolomitic limestone with minor dolomite is mostly observed among the limestone units of Moulmein Limestone Group. Dolomitic limestone unit is fine to medium-grained, thick to massive and show crystalline texture, light grey to grey on fresh surfaces and dark grey colour in weathered outcrop. Strongly dolomitized limestone shows criss-cross joints on its surface and some are brecciated and form karst topography.

Antimony Mineralization

In the Thabyu area, mine No. 1, 1.7, 2, and 3, where most of the quartz-stibnite-barite veins are found as lenses in the NW-SE trending fracture zone of slate, phyllite and quartzose sandstone unit of Taungnyo Formation and disseminated within the alteration zone and host rocks. The mineralization zones strike between 300° and 325° , dip between 60° and 75° to the northeast parallel with the alignment of Tele-chaung which is probably a fault aligned stream running NW-SE.

Large antimony mineralized veins having 2-3 metres width and about 30 metres high in surface exposure occur parallel or slightly parallel to the foliation plane of quartzite and phyllite units of Taungnyo Formation generally dipping northeast at 65° to 75° . Therefore, the directions of these veins are aligned parallel to the major NNW-SSE structural trends of host rocks. The mineralization zone can be traced along the Tele-chaung and through Lampha Chaung about 10 kilometres. There are about 10 separate worksites within the Thabyu area.

A chain of lenticular ore bodies have been found along the general strike of the ore vein. The chief mineral is stibnite and chalcopryrite, saphlerite and galena are occur as accessories. Mainly quartz (vuggy quartz, chalcedonic quartz) and other calcite, barite and pyrite are observed as vein minerals. In Mine-No.1, such mineralization is associated with barite.

Hydrothermal Wall-Rock Alteration

In the study area, as the antimony ore bearing solution penetrate along and between the impervious layers of metasedimentary rock units (slate, phyllite and quartzite) of Taungnyo Formation, the wall rock alterations are less common in the mineralization area. However, some hydrothermal alterations such as kaolinization and sulphidation observed along mineralized veins and nearby area and some are observed under microscope. The nature of alteration products controlled by such factors as (1) the characters of the original rocks, (2) the characters of invading fluid and (3) the temperature and pressure conditions at which the reaction took place (Park and Mac Diarmid, 1970).

The common types of hydrothermal wall-rock alterations of ore deposits in the Thabyu area are; (1) Vuggy silica (vuggy quartz) alteration, (2) Silicic alteration, (3) Argillic alteration, (4) Propylitic alteration, and (5) Pyritization/sulphidation.

Vuggy /Silica (vuggy quartz) Alteration

This alteration typically occurs in the structural zones or as replacement bodies in permeable lithologies. This extreme form of leaching is more common at higher epithermal levels. The mineral assemblages occur in this type of alteration are quartz, hematite, pyrite and barite. Vuggy quartz alteration is characterized by fine-grained quartz with numerous open spaces that may be partly filled by a variety of minor minerals. Vugs in the alteration zone may be filled by late quartz, sulphides, sulphates or sulphur. Vuggy quartz is characterized by the fine grained quartz with numerous open-spaces that may be filled by variety of minor minerals.

In thin section, quartz forms a dense mosaic texture. Vugs are lined with euhedral quartz and other minerals and may be filled (Figure .2). Quartz may contain irregular clots of rutile, pyrite and other sulphides. In some cases, quartz is cut by veinlets of secondary quartz.

Silicic Alteration

Quartz, chalcedony, barite, pyrite, and hematite are mineral assemblages of silicic alteration. This type of alteration represents the addition of silica to the rock, resulting in the replacement or more commonly, fill to vugs created during leaching. Silicification is common in high-sulphidation system at porphyry to epithermal deposits (Arribas, 1995). It sometime confused with quartz stock-work veining (Figure. 3, 4 & 5). Silicification caused greater compactness and hardness of the altered rocks.

Argillic Alteration

Argillic alteration or argillization refer to the dominance of clay minerals (kaolinite/dickite) altered from K-feldspar of the country rock. It can occur as zone of alteration between advanced argillic alteration and propylitic alteration, particularly in the high sulphidation epithermal setting. It occurs as surface expression around the ore deposits which are hosted in the feldspathic sandstone of the study area (Figure .6& 7).Kaolinite may form during supergene weathering. Kaolinization could have weakened the country rock.

Propylitic Alteration

Calcite is a common gangue mineral occurring as open-space fill and associated with quartz, pyrite, barite and sericite. Calcite forms over a wide temperature range, and its stability is mainly sensitive to aqueous CO₂ concentrations. It occurs both at proximal and distal to low sulphidation epithermal mineralization where it is characteristic of propylitic assemblages. In open space, calcite deposit in response to boiling and exsolution of CO₂. Platy calcite occurrence is intimately associated with epithermal mineralization (Thompson and Thompson, 1996). Rhombic and scalenohedron forms occur in massive coarse calcite (Figure .8) that typically fills late open-spaces formed subsequent to metal deposition.

Sulphidation or Pyritization

Pyrite minerals occur as euhedral to anhedral crystals in polished section and they are the most abundant sulphide mineral of the mineralization zone. Euhedral pyrite occurred in quartz veins, vesicles and fractures and as disseminated in wall-rock groundmass (Figure .9). Very fine-grained pyrite in vein quartzs is intergrown with very small amorphous stibnite particles along the quartz veinlets.

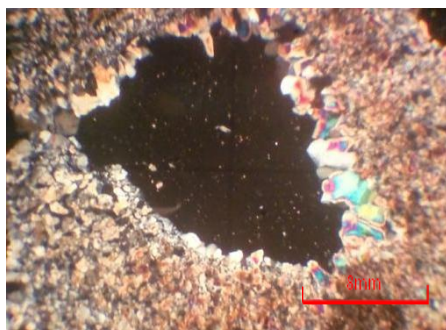


Figure 2 Vuggy quartz (open-space lining quartz) formed next to the alteration of chalcedonic quartz (fine-grained cryptocrystalline quartz) (Between XN)

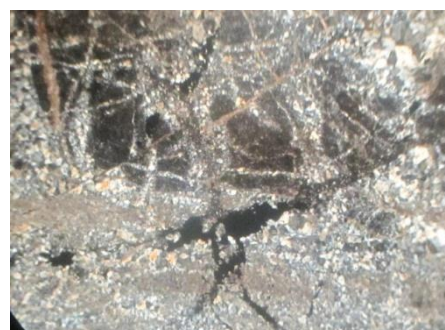


Figure 3 Silicification of country rock within the fracture zone and silica flooding by means of small vein-lets stock-work structure. (Between XN)



Figure 4 Cryptocrystalline variety of silica (chalcedonic quartz) filling in the cavity and lining along crystalline quartz rim. (Between XN)

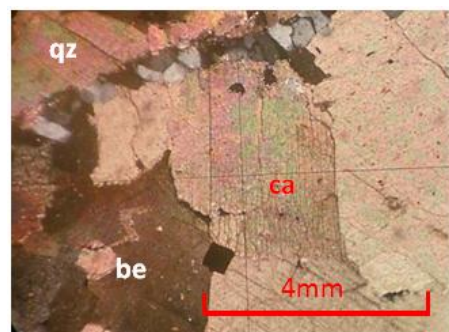


Figure 5 Silicic alteration mineral assemblages; quartz (qz), calcite (ca), barite (be) and pyrite (py), (Between XN)



Figure 6 The kaolinization (argillic alteration), Loc – 416166, Facing – NW

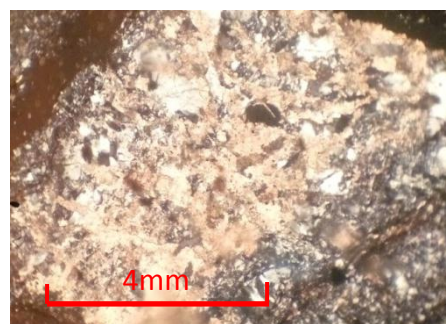


Figure 7 The incomplete kaolinization of potash-feldspar that occurs in the wall rock of feldspathic sandstone of deposited area. (Between XN)

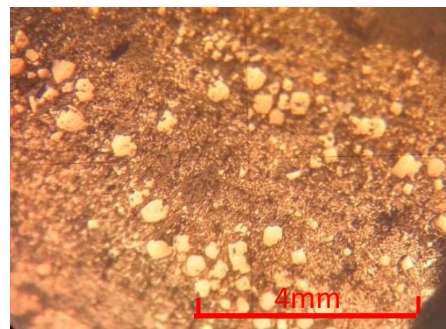
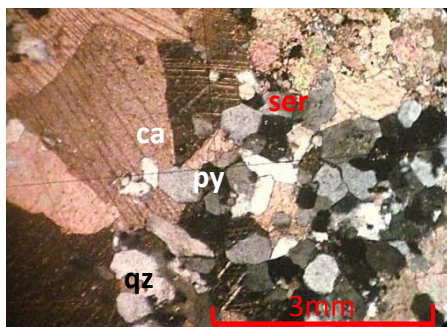


Figure 8 Propylitic alteration mineral assemblages such as calcite (ca), quartz (qz), sericite (ser) and pyrite (py). (Between XN)

Figure 9 Microphotograph showing euhedral pyrite grains scattered through the wall-rock ground mass (Polished section, Under PPL)

Hydrothermal Quartz Textures

General Characteristics

The textures of vein quartz offer not only a rapid reconnaissance tool to evaluate the character of mineralizing environments but also a means of identifying mineralized loci within vein systems (Dowling & Morrison, 1990). In simple veins there is a consistent pattern of distribution of textures and consistent assemblages of textures that can be used to define a vertical textural zoning model. Thus the quartz model should be capable of determining vertical position within a boiling epithermal vein system and predicting the locus of mineralization.

Classification of quartz textures observed in the mineralized veins and wall-rocks of the study area are -(1) Primary growth texture, (2) Recrystallization texture and (3) Replacement texture

Primary Growth Textures

Primary growth texture represents the open-space filling. There is a textural subdivision of the primary growth textures into those characteristic of cryptocrystalline quartz and those characteristic of crystalline quartz. Primary growth textures of vein quartz found in the study area are (1) Chalcedonic texture, (2) Comb texture and (3) Crustiform texture.

Chalcedonic texture

It is cryptocrystalline quartz with a waxy lustre and commonly a fibrous microscopic habit. Massive chalcedonic quartz is a uniform dense aggregate of cryptocrystalline quartz (Figure ure .10). Massive chalcedonic texture forms under conditions of intermediate silica super-saturation with respect to quartz. Low temperature (below about 180° C) during and after deposition is responsible for low crystallinity maintained in this texture.

Comb texture

Comb texture represented by groups of parallel or subparallel crystals oriented perpendicular to vein walls thus resembling the teeth of a comb. Normally crystals have euhedral terminations at their free ends (Figure .11). Comb texture is typically formed in open space from a hydrothermal solution which is slightly super-saturated with respect to quartz, but under-saturated with respect to chalcedony (Fournier, 1985). This slight silica super-saturation is

possibly brought about by slow cooling of the system and uniform growth from multiple nuclei along a vein wall.

Crustiform texture

It is successive bands oriented parallel to vein walls and defined by differences in mineralogy, or texture, colour (Figure .12). Some are concentric crustiform bands surrounding isolated rock fragments. Crustiform texture is common that is considered a diagnostic feature of epithermal veins (Buchanan, 1981). Repetitive bands of different composition or texture reflect fluctuating concentrations of elements in solution and fluctuating fluid conditions during precipitation. These fluctuations are commonly ascribed to periodic boiling of hydrothermal fluid.

Recrystallization Texture

Recrystallization textures reflect the transformation of amorphous silica or chalcedony to quartz. They are most commonly associated with cryptocrystalline quartz textures and may partly obscure them where recrystallization is extensive. In the study area, recrystallization texture of quartz which has been observed in the mineralized veins which can be classified as moss texture.

Moss texture

It resembles fine botryoidal (grape-like) aggregates with a massive irregular form similar to moss vegetation. In thin-section, individual spheres typically have a cryptocrystalline core and a crystalline rim. In the core, impurities or fluid inclusions define a concentric or radiating pattern and in the rim the extinction is radiating (Figure .13).

Replacement Texture

Replacement textures represent partial or complete pseudomorphs of other minerals by silica minerals within veins. The samples taken from the mineralized vein shows bladed texture under microscope.

Bladed texture

It is crystalline or cryptocrystalline quartz aggregates arranged in a bladed or platy form (Figure .14&15). They are parallel within a group but adjacent groups may have different orientations thus giving parallel bladed. Parallel bladed texture could result from replacement of granular calcite by quartz along repeated lamellar parting planes.



Figure 10 Chalcedonic cryptocrystalline texture, a uniform dense aggregate of cryptocrystalline quartz (Between XN)

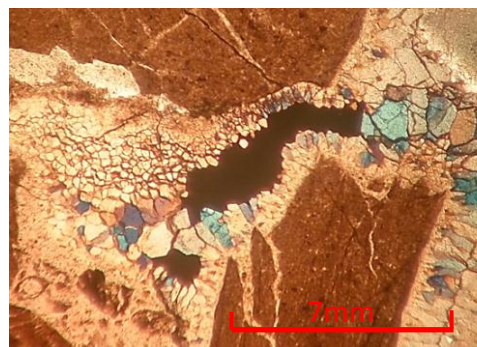


Figure 11 Comb texture, euhedral teeth of a comb terminating at their free ends. (Between XN)

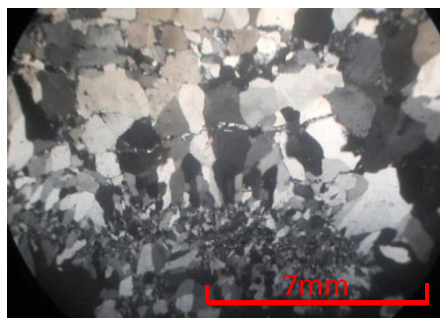


Figure 12 Crustiform texture which is successive bands oriented parallel to vein walls and defined by differences in mineralogy, or texture, colour, (Between XN)



Figure 13 Moss texture: aggregate of spheroidal cryptocrystalline core and crystalline rim forming botryoidal (grape-like) texture. (Between XN)



Figure 14 Bladed texture: parallel bladed could result from replacement of granular calcite by quartz along repeated lamellar parting planes, (Between XN)

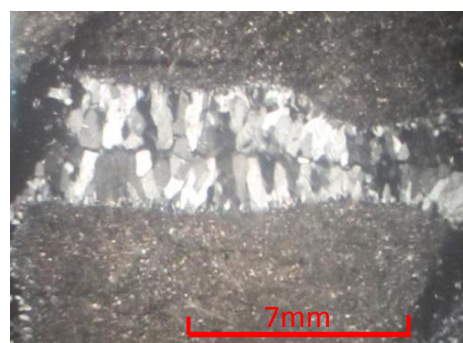


Figure 15 Microphotograph showing crystalline quartz aggregates arranged in a bladed or platy form. (Between XN)

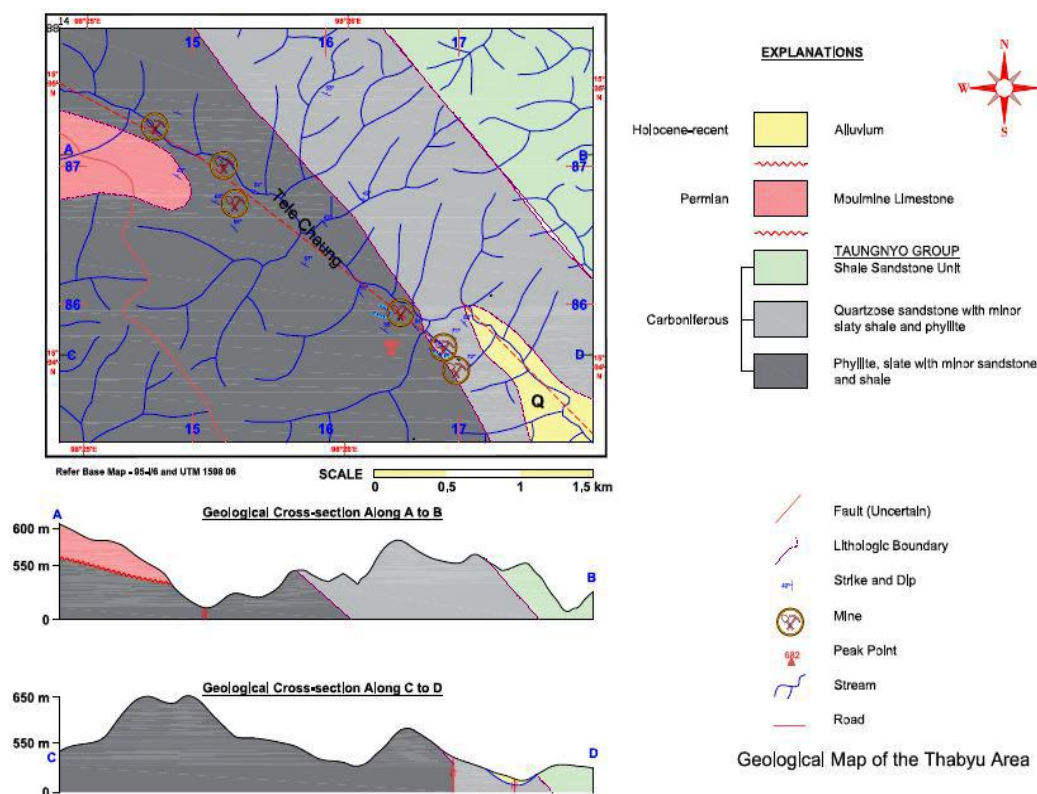


Figure 16 Geological map of the Thabyu Mine area.

Conclusions

In the research area, quartz (chalcedonic and vuggy), calcite, pyrite, hematite, barite and sericite are the alteration products of mineralization. The common types of hydrothermal wall-rock alterations of ore deposits in the study area are silicification, vuggy silica (vuggy quartz) alteration, argillic alteration, propylitic alteration, and pyritization/sulphidation. Classification of quartz textures observed in the mineralized veins and wall-rocks of the study area are –primary growth texture, recrystallization texture, and replacement texture.

Chemically interaction between the intruding ore bearing hydrothermal fluids and wall-rocks of fracture zone occur and then formation of wall-rock alterations are produced i.e. silicification, recrystallization etc. Much of the ground preparation that takes place prior to the introduction and deposition of ores is really chemical. The effects of temperature and pressure are important in the deposition of ores. Moreover, quartz textures (vuggy texture), mineral association and nature of hydrothermal alterations point to an epithermal system at temperatures between 200° C and 80° C.

Acknowledgements

The author would like to thank Dr. Htay Aung (Acting Rector) and Dr. Soe Myint Thein (Pro-Rector) of Loikaw University for their permissions to do this research project. The author is also deeply indebted to Dr. Toh Toh Win Kyi (Professor), Head of the Department of Geology, Loikaw University for her encouragement to carry out this research. I also thank Professor Dr Ohn Thwin (Retired), Department of Geology, Yangon University, Dr Than Than Oo, Pro-Rector, Magway University and Dr Tun Naing Zaw, Lecturer, Department of Geology, Yangon University for their helpful suggestions.

References

- Arribas, A., Jr., (1995), *Characteristics of high-sulfidation epithermal deposits, and their relation to magmatic fluids*, in Thompson, J.F.H., ed., *Magmas, Fluids and Ore Deposits: Mineralogical Association of Canada*, short course volume 23, P. 419-454
- Buchanan, L. J., (1981), Precious metal deposits associated with volcanic environments in the southwest: Arizona *Geol.Soc. Digest*, v. 14, p. 237-261
- Dowling, K. & Morrison, G.W., (1990). Application of quartz textures to the classification of gold deposits using North Queensland examples: *Econ. Geol. Monograph* 6, pp 324-355
- Fournier, R.O., (1985). The behavior of silica in hydrothermal solutions in Berger, B. R. & Bethke, P. M. eds, *Geology and geochemistry of epithermal systems, Reviews in Econ.Geol.* v.2, p. 45-51
- Park, C. F. and MacDiarmid, R. A., (1964). *Ore Deposits*. W, H. Freeman and Company, San Francisco and London.
- Thompson, A. J. B. and Thompson, J.F.H., (1996), *Atlas of alteration: A Field and Petrographic Guide To Hydrothermal Alteration Minerals*, Geological Association of Canada, Alpine Press Ltd, Vancouver, British Columbia. Pg-100

GRANODIORITE-HOSTED GOLD DEPOSIT IN THE MAGYIBIN-KABA AREA, PINLEBU TOWNSHIP, SAGAING REGION

Zaw Win¹, Maung Maung Naing², Min Aung³ and Cho Cho Lwin⁴

Abstract

The research area, granodiorite-hosted gold deposit, is situated within the Pinlebu Township, Sagaing Region, Northern Myanmar. It is bounded by latitude 24° 3' 30" to 24° 12' 30"N and longitude 95° 32' 00" to 95° 40' 00"E and falls in UTM map 2495-12. The research area consists chiefly of the various igneous rock types which form a batholith and sedimentary units. Ore deposits of gold are hosted in the Kanzachaung batholith (Wuntho massif) especially as granodiorite and diorite body. Five gold deposits were observed at Magyibin and Kaba area, productive gold deposits are MG-1, MG-2, KB-1, KB-2 and KB-3. Most of mineralized quartz veins, fracture filling, are recognized in the fracture zone of granodiorite body and diorite body. Quartz veins in the research area contain gold (Au), lead (PbS) and copper (CuSO₄). The mineralized quartz veins show lenticular and banded nature. In some places, pinch and swell structures are noted. Economically the main ore mineral is gold. The mineralogy of the vein is relatively simple and can be recognized into three paragenetic stages. Stage-1 and stage-2 are main mineralization stages and stage-3 is post- ore forming stage. Ore deposit of the research area is hydrothermal origin source of hydrothermal ore fluid is considered to be meteoric water and magmatic water. It is reasonable to conclude that mineralization in the present area might have been formed at the late stage of or after the intrusion.

Keywords: Granodiorite, fracture filling, hydrothermal origin

Introduction

Location, Size and Accessibility

The research area is situated within the Pinlebu Township, Sagaing Region, Northern Myanmar. It is bounded by latitude 24° 3' 30" to 24° 12' 30"N and longitude 95° 32' 00" to 95° 40' 00"E and falls in one-inch topographic map 83 P/12 (Fig. 1 and 2). It covers approximately 80 square miles. The research area can be reached from Kawlin by car, which is situated on Mandalay-Myitkyina railway line, 155 miles from Mandalay and 180 miles from Myitkyina. Road connecting the area with Pinlebu can be used during the dry season only.

Geological Background

The research area lies on the northerly trending Central Volcanic Line (Volcanic Arc) related to the subduction zone of the collision of India and Eurasian plates. Along the line are the Upper Cenozoic volcanoes, volcanic and plutonic rocks (pre-Oligocene) and igneous rocks (probable Upper Mesozoic to Lower Tertiary) (Chhibber, 1934).

¹ Dr, Associate Professor, Department of Geology, Panglong University

² Dr, Rector, Department of Geology, Yadanabon University

³ Dr, Prorector (Retired), Department of Geology, Maubin University

⁴ Dr, Associate Professor, , Department of Geology, Panglong University

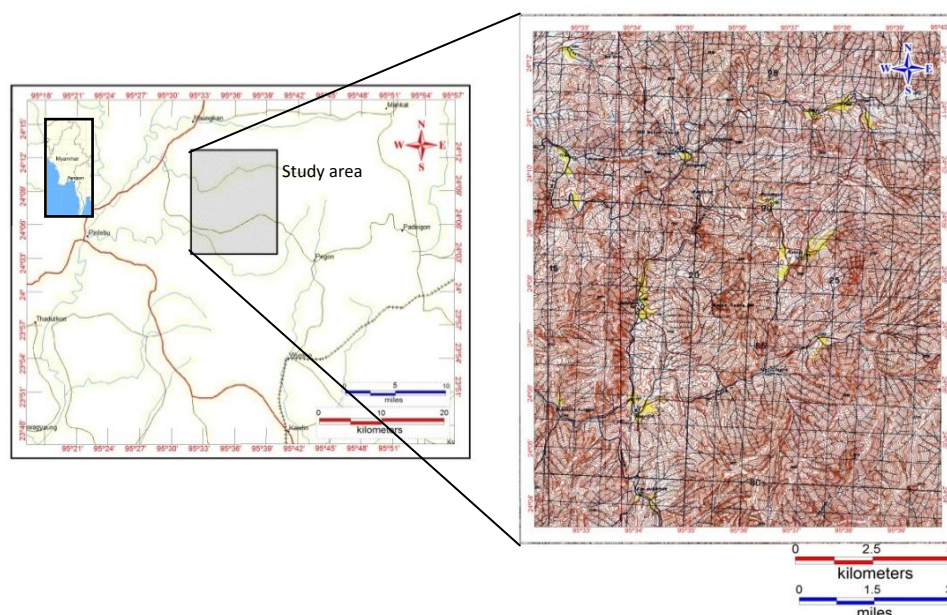


Figure 1 Location map of the research area

The western part of the research area includes part of the eastern limb of the Chindwin syncline. A well-known major fault, Sagaing Fault (Win Swe 1970) is situated to the eastern part of the research area. The Geological Survey and Exploration Project (BUR.72.002) of the United Nations (UN project), and the Development of Geological Survey and Mineral Exploration (DGSE), of the Ministry of mines carried out reconnaissance survey and geological mapping in this area.

Methods of study

The present research includes field methods and laboratory investigations and employs the three methods to achieve the objectives of the research. The three methods are (a) landsat image and aerial photographic interpretation were made before doing field trip, (b) detailed studies of outcrops and sampling applying the GPS II Plus method and (c) using the ore microscope to analysis the ore texture and mineral paragenetic sequence.

General Geology

Geomorphologically as well as tectonically, Myanmar can be subdivided into four North-South trending major tectonic domains from west to east. They are the Arakan (Rakhine) Coastal Area, Indo-Burman Ranges, Inner-Burman Tertiary Basin, and the Sino-Burman Ranges (Bender, 1983). The study area occupies the Central Volcanic Line that is classically interpreted as the volcanic arc separating the fore arc basin in the west and the relatively thin back arc basin in the east.

Generally, the research area consists chiefly of the various igneous rock types which form a batholith and sedimentary units. The Kangan Formation occupies the north-western part, and the eastern part of the research area is mainly composed of igneous units of Kanzachaung batholith such as granodiorite and diorite. The north and north-western flank of the study area is formed of the Mawgyi andesite.

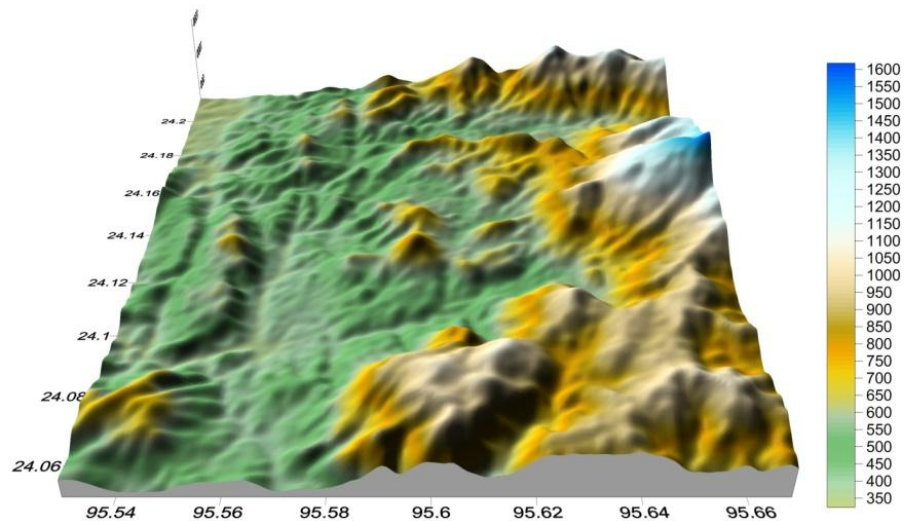


Figure 2 3D view of the study area (looking north)

The sequence of the rock units of the study area is described in the table (1) based on the field relationship, correlation and radiometric dating. The simplified geological map of the Magyibin-Kaba area is shown in figure (3) (Based on UNDP project, 1979).

Table 1 Rock sequence of the study area

Rock Unit	Age
Sedimentary Rock Units	
Alluvium ^^^^^^^^^^^^^^^^^^^^	Recent
Mansigale Group	Unconformity
Kangon Formation	Early Eocene
Igneous Rock Units	
Kanzachaung Batholith	Late Cretaceous
Veins and dykes of aplite, pegmatite and andesite	
Granite	
Biotite granodiorite	
Hornblende biotite granodiorite	
Diorite	Early Cretaceous
Mawlin Formation	
Mawgyi andesite	

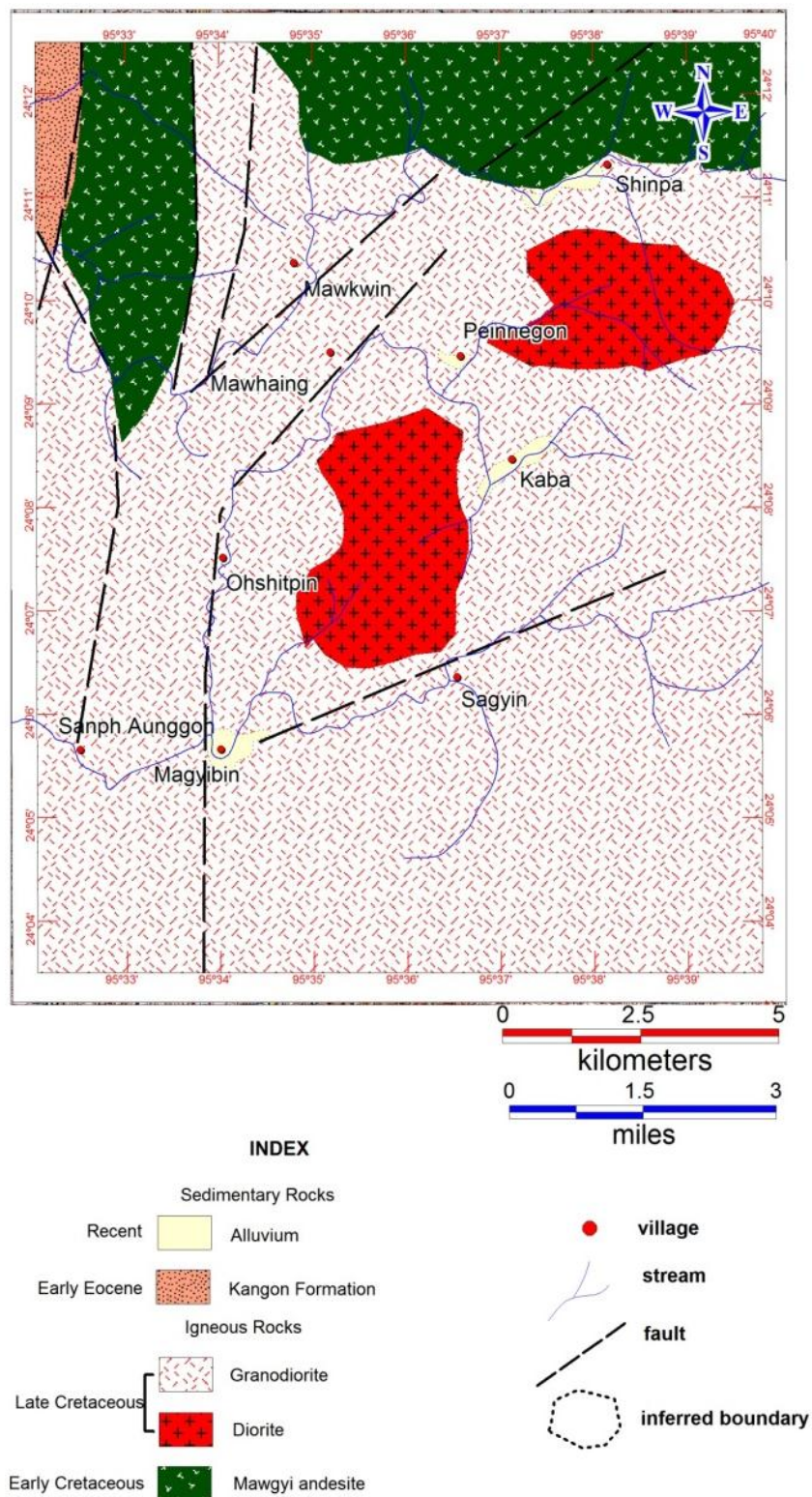


Figure 3 Geological map of the study area (modified after United Nations, 1978)

Occurrence of Gold Deposits

Distribution of Gold Deposit at the Magyibin-Kaba Area

Gold ore deposits in the research area are hosted in the Kanzachaung batholith (Wuntho massif). Five gold deposits were observed at Magyibin-Kaba area and their distribution is shown in figure (4). The mineralized gold vein occurrences are predominantly hosted in the granodiorite and diorite body. In many places, the veins follow the fracture filling. Some mineralized quartz veins are recognized in the fracture zone of granodiorite body. The most productive gold deposits in Magyibin-Kaba area are MG-1, MG-2, KB-1, KB-2 and KB-3.

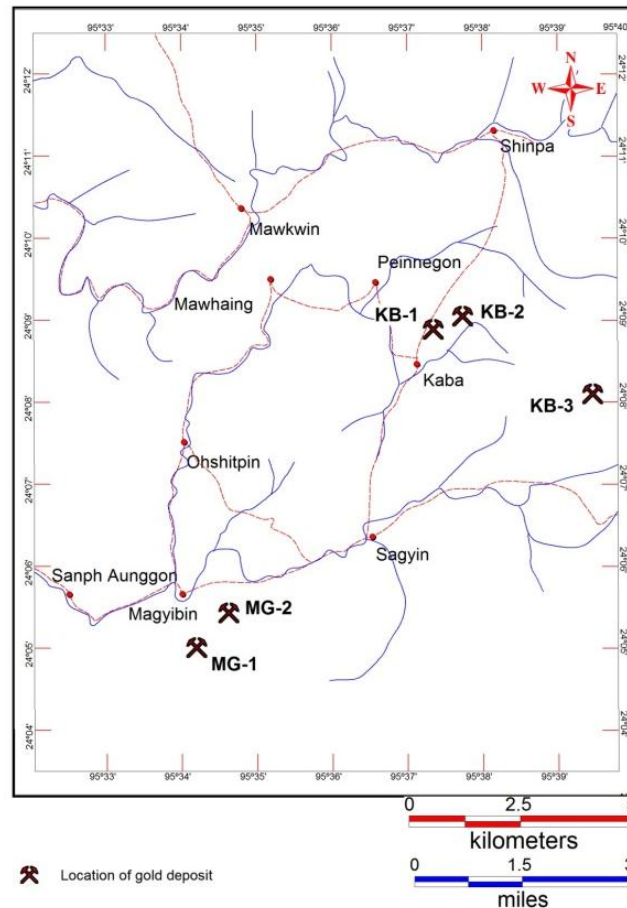


Figure 4 Location of gold mines and salt springs in the study area

Gold Mine of MG-1

This gold mine (KB-1) (N 24° 6' 02.22", E 95° 35' 21.3") is located at the ½ mile south-east of the Magyibin village and stands at the elevation of 1428 ft. The gold mineralization at MG-1 is related to 240° / 35° SW direction quartz veins and veinlets. At the second level of the main shaft (about 300 ft), the thickness of the quartz veins vary from a few centimeters to 90 cm and dip westward (Fig. 5). The quartz vein is associated with the pyrite, chalcopyrite, sphalerite, galena and other sulfide minerals. The MG-1 mine is run from the inclined shaft. The wall-rock is soft, friable and loose due to the alteration. Gossan zone occurs within 20-30 ft below the surface. The MG-1 gold mine is situated beside the Magyibin Fault which is trending NE. The vein related alteration is characterized by silification, sericitization and chloritization.

Gold Mine of MG-2

The MG-2 gold mine (N 24° 05' 28.9", E 95° 34' 39.9") is situated ½ mile south of the Magyibin village and stands at the elevation of the 1264 ft (Fig.6). The host rock of the MG-2 gold mine is hornblende biotite granodiorite. The mineralized quartz veins occur at the main shaft of 90 ft and is 1 - 3 cm thick. The strike of the quartz veins is 120° / 5°-10° SW direction. It occurs as a fracture filling type. The quartz vein is associated with the sphalerite galena and other sulfide minerals. It is characterized by the occurrence of gold flake in hand specimens (Fig. 7). The mineralized gold veins are found together with calcite and show vuggy texture. The clear microcrystalline quartz is relatively coarse compared to the milky quartz. The quartz vein is associated with the galena, sphalerite, pyrite and other sulfide minerals.

Gold Mine of KB-1

The KB-3 gold mine (N 24° 09' 04.10", E 95° 37' 29.9") is situated at the 1 mile north of Kaba village and stands at the elevation of 2014 ft. The mine is run by the inclined shaft. The host rock of the mineralization is the diorite body. It is soft, friable and brecciated. The strike of the veins is 216° / 20°- 27° NW direction and veinlets cross-cut the diorite body. The thickness of the veins varies from 5 to 20 cm and shows the wall-rock alteration. Some veins show lens-shaped or pinch and swelling structure (Fig. 8). Some veins and veinlets contain gold grains a few millimeters in diameter, gold is generally dispersed in sulfide minerals. Quartz veins display crustiform- colloform, drusy and comb textures (Fig. 9). A crustiform-colloform symmetrically banded quartz vein sample belongs at least 10 cm thick. The gold-bearing quartz vein is associated with the pyrite, arsenopyrite, galena and other sulfide minerals.

Gold Mine of KB-2

The KB-2 gold mine (N 24° 09' 03.10", E 95° 37' 50.0") is situated 1 mile north of Kaba village and stands at the elevation of 1980 ft. Host rock is dark grey diorite. It is mined by the inclined shaft. The strike of the vein is 190° and the dip amount is 20°-30° NW direction. The alteration halo occurs below and above the mineralized quartz veins (Fig. 10). Above the mineralized vein, gossans zone occurs in the form of the iron cap (Fig. 11). This vein is mainly composed of galena, sphalerite, pyrite and other sulfide minerals. The thickness of the quartz vein varies from 10- 20 cm. The alteration is characterized by silicification, sericitization and chloritization.

Gold Mine of KB-3

The KB-3 gold mine (N 24° 07' 39.8", E 95° 38' 49.6") is run at the site 3 miles east of Kaba village. This gold mine is operated by the inclined shaft along the fault plane (Fig. 12). Host rock is hornblende biotitegranodiorite and it is associated with the brecciated quartz vein. The thickness of the quartz vein is about 25 cm and trends 154° / 35° NW direction. The mineralized quartz vein is highly brecciated, brittle and hard. Wall-rock alteration is characterized by the sericitization and clay alteration.



Figure 5 Photograph showing the bifurcate and lens-shape of auriferous veins at MG-1 (N 24° 6' 02.22", E 95° 35' 21.3") (west facing)

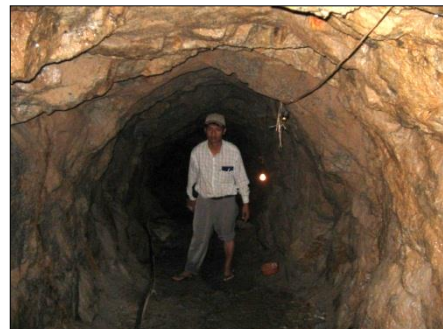


Figure 6 Exploration adit of No.2 gold deposit of MG-2 (west facing) (N 24° 6' 02.22", E 95° 35' 21.3")

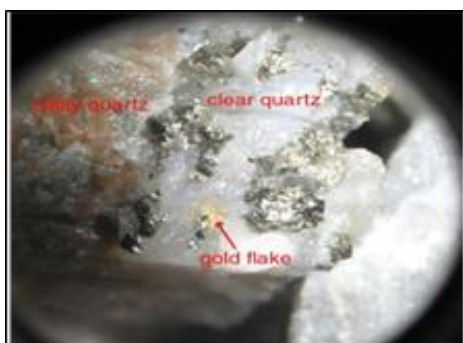


Figure 7 Photograph showing the gold flakes associated with the clear quartz, milky quartz and pyrite minerals of the MG-2 gold mine (10X)(N 24° 05' 28.9", E 95° 34' 39.9")



Figure 8 The pinch and swelling of auriferous quartz vein at KB-1 gold mine (N 24° 09' 04.10", E 95° 37' 29.9") (west facing)

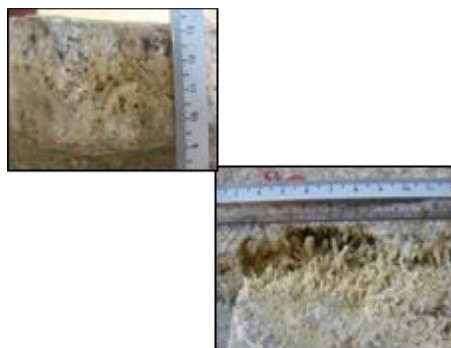


Figure 9 Photograph showing the drusy and comb textures of the gold bearing quartz vein at KB-1 gold mine (N 24° 09' 04.10", E 95° 37' 29.9")



Figure 10 Alteration formed along the auriferous quartz vein at KB-2 gold mine (N 24° 09' 03.10", E 95° 37' 50.0") (north facing)



Figure 11 Photograph showing the yellow, earthy hematite gossan at KB-2 gold mine (N 24° 09' 03.10", E 95° 37' 50.0") (west facing)



Figure 10 Auriferous quartz vein along the fracture zone of granodiorite body at KB-3 gold mine (N 24° 07' 39.8", E 95° 38' 49.6") (east facing)

Ore Mineralogy

The major ore constituents of quartz veins in the study area are gold, lead and copper. The major ore minerals are pyrite, chalcopyrite, sphalerite, galena and arsenopyrite with lesser amount of chalcocite, bornite and arsenopyrite. Economically the main ore mineral is gold.

Therefore polished section and thin section of mineralized rock samples (15 double polished and thin sections) are prepared. The mineralizing veins at MG -1, MG -2, KB-1, KB-2 and KB-3 gold mines are composed of gold and sulfides minerals.

Sphalerite (Zn Fe)S

Grain size ranges from 0.5 mm to 2 mm and occurs as gray color irregular anhedral masses along with pyrite, galena and chalcopyrite. It contains randomly oriented grains of exsolved chalcopyrite. Late stage sphalerite veins are injected into quartz and pyrite minerals. In some specimens, the sphalerite minerals cross cut the galena, and enclose the quartz and galena minerals (Fig. 13).

Chalcopyrite (CuFe) S₂

It occurs as minor constituent of ore minerals in the study area. Anhedral patches of grain size ranges from 0.5 mm to 2 mm, yellow to brassy yellow colored chalcopyrite is formed in pyrite and apex of the galena minerals. It also occurs as inclusion and exsolved grains in pyrite and sphalerite (Fig. 13&14). Most of the chalcopyrites are found along the grain boundaries and within the galena minerals.

Gold (Au)

Bright yellow gold is observed as disseminated specks within the pyrite, chalcopyrite, sphalerite and galena. Some gold minerals occur along the grain boundaries of pyrite which is associated with the galena and gangue minerals (Fig. 15). Sometimes, gold flakes occur within the gangue minerals like quartz. It is characterized by its "golden" color, lack of fracture and very high reflectance and paleochroism. Some minute gold grains are encapsulated in pyrite which renders the gold ore refractory. Most of the visible gold is bright yellow in color, suggesting that it has a relatively high fineness.

Galena (PbS)

Galena occurs as anhedral to euhedral form. In some specimens, euhedral grains of galena are found associated with the gangue mineral quartz (Fig. 16). The perfect cleavage is usually visible and triangular pits (Fig. 16) are observed as characteristic feature. The average grain size is 0.5 to 2 mm. In some specimens, curved cleavage pits occur as a result of post depositional deformation. Galena associated with chalcopyrite is set in pyrite. Sometimes, galena and sphalerite minerals are replaced by the gangue minerals like quartz.

Pyrite (FeS₂)

Grain size of pyrite ranges from 0.1 mm to 2 mm and it occurs as yellowish white irregular coarse-grained and often euhedral crystals (Fig. 16). Small fractures of pyrite are partly replaced and filled by chalcopyrite. Discrete grains of pyrite occur in quartz vein. Pyrite is the most abundant sulfide mineral. In one section, annealed texture of recrystallized monomineralic pyrite is seen. Coarse pyrite is commonly fractured and cemented by sulfide minerals such as galena and sphalerite and by gangue minerals quartz and calcite (Fig. 14). The early formed pyrite cubes occur as relic crystals in anhedral chalcopyrite and sphalerite. Pyrite is also found as small disseminated grains throughout the vein and as aggregates of small cubes.

Arsenopyrite (FeAsS)

Arsenopyrite occurs as small white colored subhedral to euhedral grains marginal to gold. It is embedded in pyrite. It is characterized by white color rhomb form and anisotropism.

Chalcocite (Cu₂S)

Chalcocite occurs as blush white disseminated grains and veinlets in the pyrite. In some specimens, chalcocite is found replacing the cleavage and boundaries of the galena (Fig. 7.8). It is also found along the sphalerite, galena and chalcopyrite grain boundaries.

Bornite (Cu₅FeS₄)

Bornite has pinkish to purplish color. It occurs as irregular aggregates and as coating or lamella intergrowth with chalcopyrite. It is altered to covellite on grain boundaries and its core. It is also dispersed in sphalerite together.

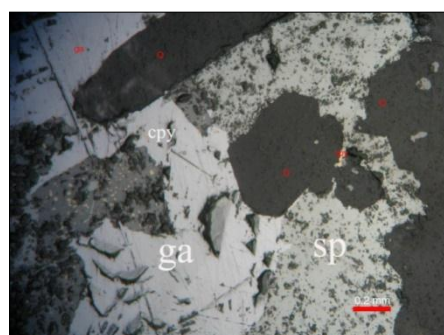


Figure 13 Photomicrograph showing sphalerite (sp), galena (ga) and quartz mineral (Q) from the KB -1 gold mine (N 24° 6' 02.22", E 95° 35' 21.3")

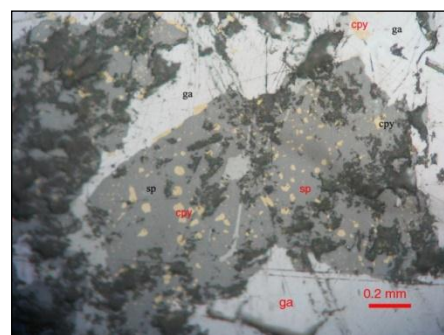


Figure 14 Photomicrograph showing chalcopyrite (cpy) diseases within the sphalerite (sp) and along the edges of galena (ga) from the KB -1 gold mine (N 24° 6' 02.22", E 95° 35' 21.3")

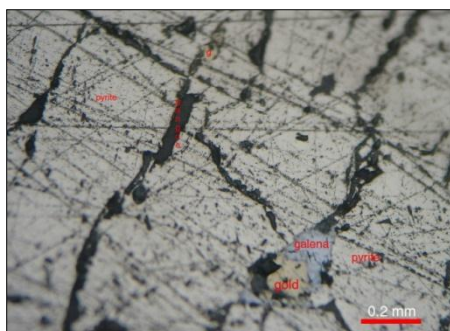


Figure 15 Photomicrograph showing fracture-filling of electrum (g) associated with galena (ga) and quartz within the pyrite (py) from the KB-1 gold mine (N 24° 09' 04.10", E 95° 37' 29.9")

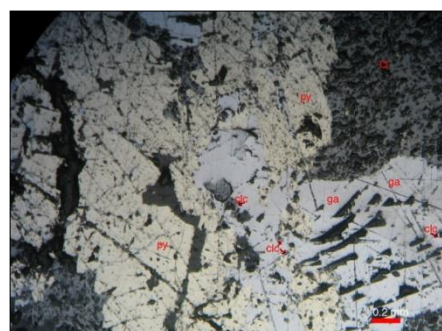


Figure 16 Photomicrograph showing chalcocite (clc) replacing galena (ga) along the grain boundaries and cleavages from the KB -3 gold mine (N 24° 6' 02.22", E 95° 35' 21.3")

Paragenesis

The mineralogy of the vein is relatively simple and can be recognized into three paragenetic stages. Stage-1 and stage-2 are main mineralization stages and stage-3 is post-ore forming stage. In stage-1 quartz and pyrite with minor amounts of sulfide minerals were formed. Precious metal and sulfide mineral are mainly precipitated stage-2. Generally, white to clear crystalline quartz is most abundant in stage-1 and stage-2. The vein width of the stage-1 is relatively in small comparison with the stage-2. Stage-2 is the most important paragenetic stage and thickness of the veins varies from 2 cm to 25 cm in the research area. Hydrothermal solutions are terminated in stage-1 and stage-2 by onset of fracturing and brecciation event along the mineralized veins. Finally, barren hydrothermal solutions were deposited lean or cross-cutting the stage-1 and stage-2. Generalized paragenetic sequence of the vein minerals of the study area is shown in Table (2).

Table 2 Generalized paragenetic sequence of ore and gangue minerals in the research area

Minerals	Stage 1	Stage 2	Stage 3
Quartz	—	—	—
Adularia		—	
Sericite		—	
Calcite			—
Pyrite	—	—	
Arsenopyrite		—	
Chalcopyrite		—	
Galena		—	
Sphalerite		—	
Gold		—	
Bornite		—	
Covellite		—	
Chalcocite		—	

Conclusion

In the research area, precious and base metal mineralization of is hosted by diorite and granodiorite units which were intruded by later intrusion of andesite dykes and apalite dykes. Therefore, these metals might be scavenged from hydrothermal solution which is probably as a result of late stage magmatic differentiation during the emplacement of intrusions

Therefore, the mineral deposit of the present area is of hydrothermal origin (both mesothermal and epithermal) and source of hydrothermal ore fluid is considered to have an igneous source combined with the meteoric water. It is reasonable to conclude that the precious and base metal mineralization of the study area might have been formed more or less associated with the intrusion.

Acknowledgements

We would like to express our thanks to Dr New Nwe Yin, the Acting Rector of Panglong University for her kind permission and advice to carry out this research work .We wish to express our sincere gratitude to our supervisors, Dr Maung Maung Naing, Rector of Yadanabon University and Dr Min Aung, Prorector (retired) of Maubin University, for their enthusiastic guidance, valuable criticism and close supervision for this research paper.

References

- Bender, F., (1983). *Geology of Burma*. Gebruder Borntraeger, Berlin.
- Chhibber, H. L., (1934a). *The Geology of Burma*, London, Mac Millan. Pp. 538.s
- Chhibber, H. L., (1934b). *The Mineral Resources of Burma*, London, Mac Millan, P 520.
- D.G.S.E, (1976). *Geology and Exploration Geochemistry of the Pinlebu-Banmauk Area*, (unpublished report No.2).
- Evans, A. M., (1980). *An Introduction to Ore Geology*, p 227, Blackwell Scientific Publications, Oxford.
- Heald, P., N. K. Foley, and D. O. Hayba, (1987). Comparative anatomy of volcanic-hosted epithermal deposits: Acid-sulfate and adularia-sericite types. *Economic Geology*, V82, p 1-26.
- KhinMaungMyint, (1982). A petrological study of the Okkan- Ainggyi Area, west of Kawlin, *M.Sc (Thesis)*, Mandalay University (unpublished).
- Noetling, F., (1894). *Note on the geology of Wuntho, Upper Burma*.
- Ross, L. J., (2005). *Introduction to Ore-Forming Processes*, p 368, Blackwell.
- Sawka, W. N., B.W. Chappell., and R. W. Kistler., (1990). Granitoid Compositional Zoning by Side-wall Boundary Layer Differentiation: Evidence from the Palisade Crest Intrusive Suite, Central Sierra Nevada, *Journal of Petrology*, Vol.31, Part 3, pp. 519-553.
- Seward, T. M., (1973). Thio complexes of gold and transport of in hydrothermal ore solution. *Geochemicaet Cosmochimica Acta*, 37, 337-399.
- United Nations, (1978a). Geology and exploration geochemistry of the Pinlebu-Banmauk Area, Sagaing Division, northern Burma, United Nations Development Programme, New York, *Technical Report, UN/ BUR/72/002, No. 2*.
- United Nations, (1979). Mineral Exploration in Selected Areas, Burma, United Nations Development Programme, New York, *Technical Report, UN/ BUR/72/002, No. 6*.
- Win Swe, (1970). Rift feature at the Sagaing Taung ridge, paper read at 5th Burma Research Congress.

SEQUENCE STRATIGRAPHIC IMPLICATION OF THE NAPENG FORMATION EXPOSED AT NAPENG – NAMON AREA, KYAUKME TOWNSHIP, NORTHERN SHAN STATE

Cho Cho Lwin¹ and Zaw Win²

Abstract

Napeng-Namon area is mainly consisting of carbonate and siliclastic sedimentary rocks of Late Permian to Late Triassic age. In this paper, lithofacies and sequence stratigraphy of the Late Triassic of Napeng Formation are studied in detail. The sequence boundary between Nwabangyi Dolomite Formation and Napeng Formation is type I sequence boundaries (SB) which is represented by a significant unconformity. In the present study, the Napeng section contains stacked depositional cycles consisting of characteristic succession of sedimentary facies and facies associations. Based on detailed measurement, these siliclastic-carbonate facies are deposited by shallow marine tidal current. Seven fourth-order shallowing upward, parasequence cycles can be recognized by environmental changes within Napeng section; by the graduality of the change in lithology, facies composition and faunal content. Features formed during the transgression, such as hardgrounds, iron-stained surface, and mollusk bearing siltstone are more prominent than the subaerial exposure features. Sequence in these outcrops display fewer paleokarst features and more pyritized and erosional hardgrounds at flooding surfaces and transgressive surfaces. The deposition of the Late Triassic (Napeng Formation) can be regarded as the progradational stacking pattern with some aggradations and these homoclinal ramp stack may show vertical accretion, but individual sequence seldom develop in a keep-up style.

Keywords: shallowing upward, transgression, progradation, homoclinal ramp

Introduction

The Napeng-Namon area is situated about 7 miles, south-east of Kayukme, northern Shan State. In Napeng-Namon area, most shallow marine sections of Late Triassic age were formed in mixed carbonate-siliclastic systems, and shallow marine limestones as a homoclinal ramp, which has been studied from a sequence-stratigraphic view point of Napeng Formation. Sequence stratigraphy is a powerful tool for explaining the relationships of allostratigraphic units that analyses the sedimentary response to base-level changes. Through the recognition of boundary surfaces, genetically related facies (system tracts) can be identified. Lithofacies can be correlated accounting to where each unit is positioned along an inferred curved that represents base-level fluctuations.

From the establishment of the fundamental concepts of sequence stratigraphy by Vail *et al.* (1977), the relation between sediment supply and carbonate production, and accommodation space largely determines the facies distribution. The purpose of this paper is to express and discuss data on lithofacies, depositional systems and sequences stratigraphy and a detailed analysis of the evolution, anatomy and sedimentology. The studied sedimentary sequences belong to the Late Triassic units (Napeng Formation) of Napeng- Namon area are shown in Fig. (1)

¹ Dr, Associate Professor, Department of Geology, Panglong University

² Dr, Associate Professor, Department of Geology, Panglong University

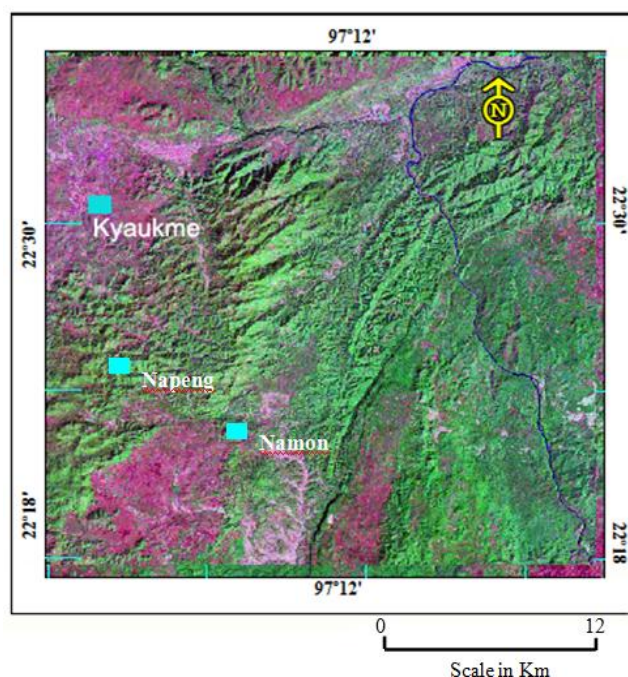


Figure 1 Satellite image of the study area and its environs. (Source: Google Earth, 2010)

Methods of Study

The studied transect in Napeng-Napong car road section, Napeng-Naungleng road section and west of Naungleng section, exposed at Napeng-Namon area, is based on large outcrops that expose most or the entire Napeng Formation (Late Triassic). Identification of the sedimentary facies must depend on thin sections of some samples obtained from outcrops.

Petrographic classification of Dunham (1962) and Embry and Klovan (1971) are used in the present study. Microscopic description is based on Adams and Mackenzie (1984). The paleoenvironments and their vertical distribution were identified on the basis of microfacies analysis, microfauna and macrofauna content in the Late Triassic units. The sequence stratigraphic interpretation follows classic concepts (e.g Van Wagoner *et al.*, 1988; Vail *et al.*, 1991; Handford and Loucks, 1993 in Weidlich *et al.*, 2003) with emphasis on carbonate and siliciclastic system.

The key measured sections were carried out by bed by bed analysis and details of associated mineralization and the more important fauna in each unit. Sequence boundaries, parasequence boundaries and maximum flooding surface were emphasized in each measured section.

Sequences Stratigraphic Implication and Interpretation

The sequence stratigraphic interpretation is mainly based on the sedimentary facies analysis and section measurements were done in well-exposed representative rock units and their interpretation with regard to sedimentary dynamics. The sequence boundaries marine flooding surfaces and depositional systems tracts were achieved by using the sedimentologic column and facies analysis. Water depth is measured between the sea-level change (change in accommodation) and change in sediment supply (Myers and Milton, 1996). The facies changes in the study area depend on the tectonic movement, the basin topography, sediment source shifting and sea-level change. The sedimentary sequences developed in the Napeng-Namon area indicate

that the south-eastern part is shallower than the north-western part because of the higher topography of south eastern portion.

Therefore, deepening trends are considered as Transgressive System Tracts (TST), whereas shallowing trends are held to be Highstand System Tracts (HST). Moreover, the change from deepening to shallowing is interpreted to be maximum flooding surface (mfs).

The sudden superposition of transgressive beds upon prograding one is thought to represent a cycle boundary (CB). Seven, fourth-order shallowing upward depositional sequences are recognized in the Napeng succession (Fig.2). Parasequence stacking patterns were identified on the basis of vertical trends in facies composition. As a result, this study focused on depth trend to identify stacking patterns, much as is commonly alone in siliciclastic sequence stratigraphic studies (Van Wagoner et al, 1990).

Detailed measured-section and distribution of facies association of the Napeng Formation exposed at Napeng-Napong and Napeng-Naungleng sections.

In Napeng-Namon area, the common cycles that are typified are upward coarsening cycles. At the top of Napeng-section, mostly packstone and wackestone passes into mudrocks and then shale and siltstone as shallow-marine tidal and wave prograded across platforms. Variations of the sedimentary patterns are due mainly to sea-level changes reflected by the up and down movement across the ramp. So, these shallowing upward cycles appear to be the dominant cycle type on unrimmed shalves, especially homoclinal ramps through the geological record (Lohman., 1976).

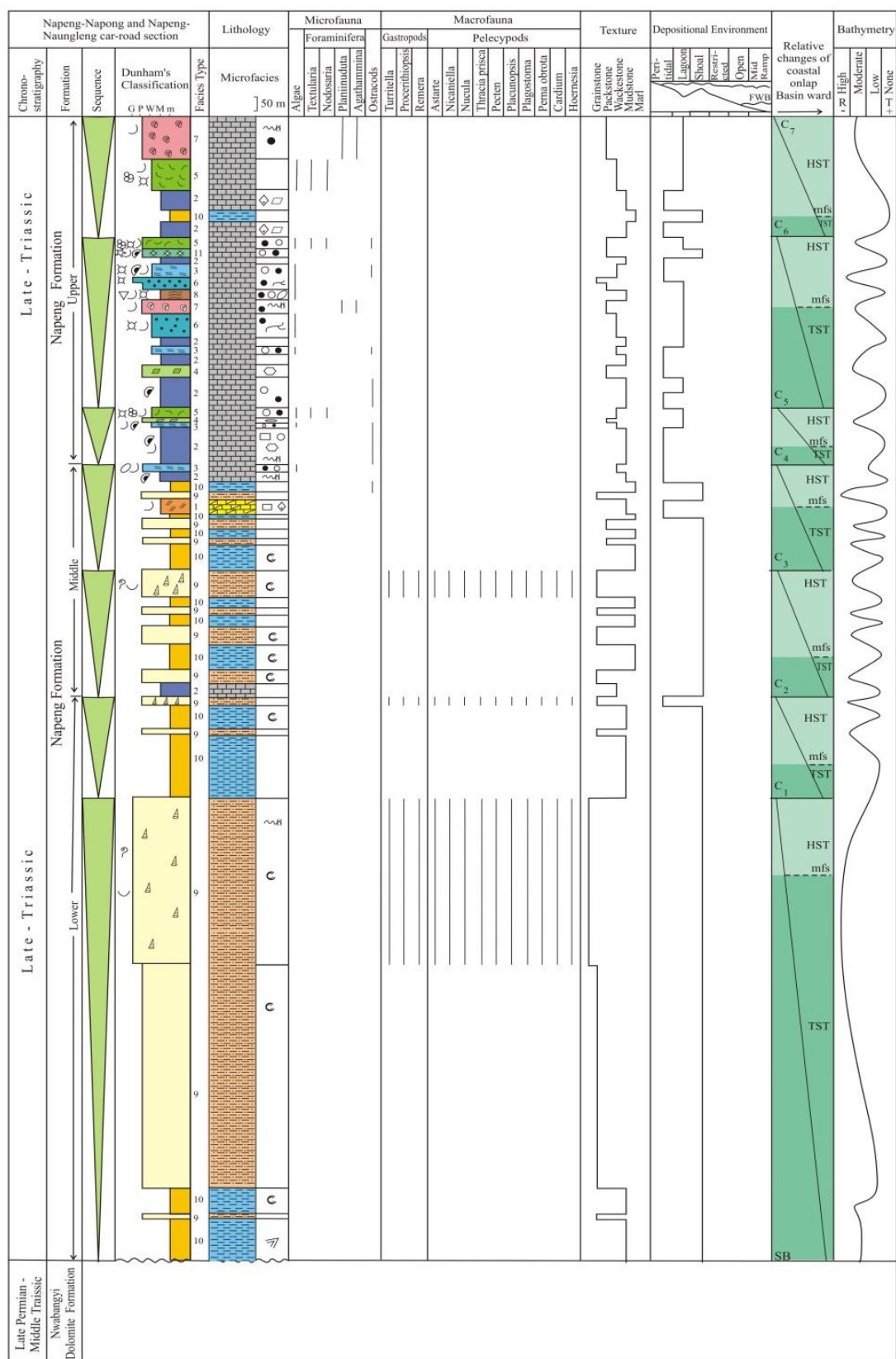
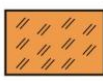

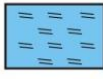
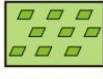









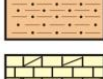
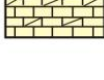


Figure 2 Sequence stratigraphic interpretation of the Late Triassic sections of Napeng Formation exposed at Napeng-Namon Area


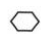

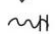









Legend

m : Marl
 M : Mudstone
 W : Wackestone
 P : Packstone
 G : Grainstone






Facies and Lithology

	Dolomitic mudstone-wackestone
	Mudstone
	Peloidal-bioclastic wackestone-packstone
	Gypsiferous mudstone-packstone
	Bioclastic wackestone-packstone
	Peloidal wackestone-packstone
	Wackestone-packstone with miliolids
	Algal mudstone
	Mollusk-bearing siltstone
	Marl
	Skeletal packstone
	Limestone
	Mudstone
	Siltstone
	Dolomitic limestone



Sedimentary Structures

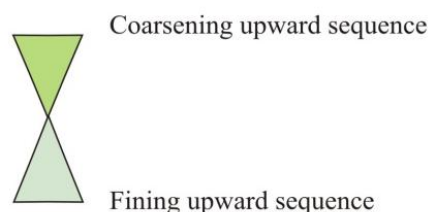
	Pyrite
	Gypsum
	Dolomite
	Hardground
	Stylolite
	Tepee structure
	Lamination
	Fenestrae / Birdeyes
	Pellet
	Intracast
	Concretion
	Calcisphere
	Dessication crack



Microfauna

	Ostracod
	Foraminifera
	Algae
	Echinoderm
	Shell fragment

Macrofauna

	Gastropod
	Bivalve / pelecypod



	Cycle Boundary (C)
	Maximum Flooding Surface (mfs)
T	Transgression
B	Regression

Abbreviations

HST	- Highstand Systems Tract
TST	- Transgressive Systems Tract
mfs	- Maximum Flooding Surface

Field Expression of Sequences

Seven fourth order depositional sequences are recognized in the Late Triassic exposed on the northern and north-eastern parts of the study area. These sequences are realized and correlated on the basis of parasequence stacking patterns and by apparent features of sequence boundaries and transgressive surfaces. The most prominent stratigraphic features of contact

between Nwabangyi Dolomite Formation and Napeng Formation is type I sequence boundaries (SB) which is represented by a significant unconformity (Fig.3). Recognition of this unconformity and its significance as a sequence boundary can be related to changes in eustatic sea level, global climate and oceanic state.



Figure 3 Photograph showing the unconformity between Napeng Formation and Nwabangyi Dolomite Formation at the base of the Ngwetaung Hill.

Eleven microfacies are defined in the Napeng Formation on the basis of detailed sedimentologic and macrofossils logging of sedimentary structures, Flügel's (2010) model and Wilson's (1975) classification. Terminology and definition introduced by Dunham (1962) are used in this paper. The microfacies distinguished are: 1. Dolomitic mudstone-wackestone, 2. Mudstone, 3. Peloidal-bioclastic wackestone-packstone, 4. Gypsiferous mudstone-wackestone, 5. Bioclastic wackestone-packstone, 6. Peloidal wackestone-packstone, 7. Wackestone-packstone with miliolids, 8. Algal mudstone, 9. Mollusk bearing siltstone, 10. Marl and 11. Skeletal packstone.

The depositional environment of the Napeng Formation is interpreted as a shallow carbonate platform with a gentle slope. Much of the Napeng Formation in the Napeng-Namon area was deposited in peritidal, lagoon and shoals in an inner ramp environment.

Depositional Sequences and Cycle Boundaries and Transgressive Surfaces

Seven cycle boundaries are identified in the Late Triassic sediments, which can be divided into seven parasequences: (CB-1 to CB-7) (Fig. 2). Cycle boundaries are demarcated by contact between the progradational parasequence sets (Highstand) and retrogradational parasequence sets (Transgressive). It is apparent that the sudden superposition of transgressive beds upon prograding one is thought to represent a cycle boundary (CB). Based on this fact, in the Napeng succession, the cycle boundaries are marked on the top surface of the shallowing upward cycles. In other word, the boundary is placed at the thickening upward or coarsening upward cycles. It is designated by dolomite (diagenetic caps) and depositional cycles such as changes from lithofacies, grain size and bed thickness (Fig.4,5&6). Shallowing upward Late Triassic units have been used by their vertical outcrop (Fig.7). The indicator for the evidence of subaerial exposure is the presence of hardground surfaces (Fig.8&9). Therefore, sequence boundaries have to be inferred from major shift of depositional systems and stacking patterns. The Napeng succession are the inner ramp sequence and show little potential for vertical (keep-up) growth during flooding event.



Figure 4 An outcrop showing grey color, fossiliferous limestone in middle part of the Napeng section.

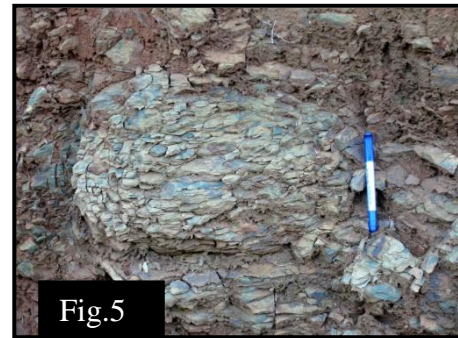


Figure 5 Concretionary clay in siltstone exposed at the lower part of the Napeng section.

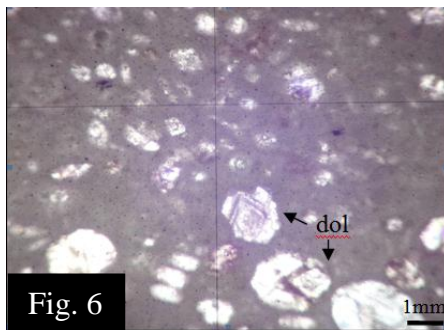


Figure 6 Photomicrograph showing dolomite (dol) (diagenetic cap) indicating the sequence boundaries in Bioclastic wackestone-packstone facies. Under PPL.



Figure 7 An outcrop photograph showing the thickening upward sequence of Napeng section.



Figure 8 Photograph showing erosional hardground with iron-stained surface at sequence boundary in the middle part of Napeng section.



Figure 9 Photograph showing burrowed Limestone with erosional surface at the middle part of Napeng section.

Maximum Flooding Surface (mfs)

The maximum flooding surface represents the last of the significant flooding surfaces found in the transgressive system tract. The mfs coincides with maximum abundance of fossils, intense bioturbation (Vail ., 1991).

In this study, mfs are defined by using change in lithologic unit, or change in facies, the presence of intense bioturbation (Fig.10) mostly indicates the beginning of progradation. In many

other carbonate studies, mfs imply a slow drop in rates of accommodation from the rapid rates during the TST to the slow rates during the early HST.



Figure 10 Intense bioturbation indicating the maximum flooding surface (mfs) in the upper part of the Napeng Formation at Napeng-Namon area.

System Tracts

A sequence can be subdivided into distinctive units that are called system tracts. The term systems tract was first introduced by Brown and Fisher (1977), as a linkage of contemporaneous depositional environments. Transgressive systems tract (TST) and highstand systems tract (HST) are observed in the study area whereas the lowstand systems tract is missing because of no distinctive exposures are recognized.

Transgressive System Tracts (TST)

The transgressive systems tract consists of a retrogradational set of parasequences. It is underlain by the TS and overlain by the mfs. The TST is bounded at the base by transgressive surface display features attributable to subaerial exposure (Fig.11). In the Napeng successions, the TST is capped by black carbonaceous shale (Fig.12) and iron-stained surfaces.

The TST in the cycle-1 characterized by shoal and lagoonal facies sediments of marl, siltstone and mollusk bearing siltstone. The TST of cycles 2, 3 and 4 are composed of the alternation of marl and siltstone sediments. This system tract, cycles 1, 2, 3 and 4 start the aggradational stacking patterns, in this condition the rate of sediment supply subequal to the rate of accommodation. The cycle-5 is made up of peritidal carbonates facies to lagoonal facies and TST of this cycle also indicate that the aggradational stacking pattern. The TST of the cycle-6 is characterized by the paritidal to lagoonal facies. The last cycle-7 is typically comprised of peritidal carbonate to shoal facies sediments. This last cycle provide that aggradational stacking patterns to progradational sediment supply which is greater than rate of accommodation space.

Highst and System Tract (HST)

Highstand systems tracts are defined by either aggradational or progradational parasequence sets. The mfs is the basal surface of the system tract. The top surface of the HST is transgressive surface as well as cycle boundaries CB (Fig. 13). The aggrading HST occurs when the rate of sediment supply closely matches the amount of accommodation space being created by rising sea-level (Emery & Myers, 1996). These highstand tracts are capped by karstic surface and intense bioturbation which become more pronounced upwards within the stack as the upper sequence boundary is approached.



Figure 11 Photograph showing erosional surface indicating the sedimentation break on siltstone at Napeng area.



Figure 12 Photograph showing black carbonaceous shale indicating the marine transgression in the lower part of Napeng section.

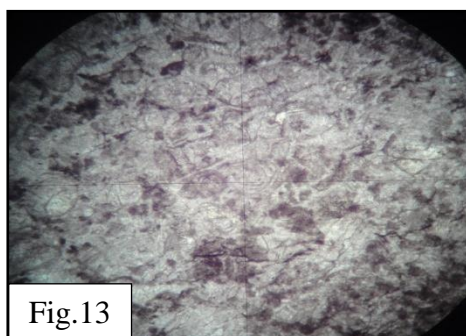


Figure 13 Photomicrograph showing intense bioturbation in wackestone-packstone with miliolids facies exposed at the upper part of the Napeng section. Under PPL.

In the Napeng succession, the HST in cycle-1, 2 and 3, is characterized by shoal and open-marine facies and the aggradational parasequence sets occur. Therefore, the sediment supply and rate of creation of topset accommodation volume are roughly balanced. The HST cycles – 4, 5, 6 and 7 are mainly composed of parasequences of peritidal, lagoonal and shoal facies. Therefore, when the early stage of these system tracts is interpreted as rate of sediment supply exceeds rate of accommodation and later these are roughly balanced. The Napeng-Namon area, HST cycle is described by peritidal to shoal facies. In measured section, HST is typified by both aggradational and progradational stacking patterns.

Discussion

In Napeng-Namon area, according to the occurrences of significant unconformity, the sequence boundary between Nwabangyi Dolomite Formation and Napeng Formation may be type I sequence. According to the lithofacies analysis, eleven facies are categorized in Napeng Formation at Napeng-Namon area. These were grouped into three facies associations representing as peritidal, lagoonal and shoal and slightly open-marine environments.

Seven fourth-order shallowing upward, parasequence cycles can be recognized by environmental changes within the section. The facies variations were used for the sequence stratigraphic interpretations of the succession. In the description of the section, deepening trends (retrogradational stacking) are considered Transgressive Systems Tracts (TST), shallowing trends (progradational stacking) are held to be Highstand System Tracts (HST), and the change from deepening towards shallowing is interpreted as maximum flooding surface (mfs). Cycle

boundaries were recognized abrupt from shallowing-upward to deepening-upward reflect to an increase in sea-level fluctuation. Such shifting of parasequence boundary is marked by the transgressive surface and beginning of the transgressive system tract. In the Napeng section, the lowstand system tract is missing.

Many of the cycle boundaries coincide with transgressive surface which are associated with pyrite, iron-stained surface and hardground surface and surface display intense bioturbation. The deposition of the Late Triassic units exposed in Napeng-Namon area can be regarded as the progradational stacking pattern with some aggradations and these ramp stack may show gross vertical accretion, but individual sequences seldom develop in a keep-up style.

Acknowledgements

We wish to express our sincere gratitude to Dr Nwe Nwe Yin, the Acting Rector of Panglong University for her permission. We are grateful to Dr Zaw Win, Associate Professor and Head of Geology Department, Panglong University for his encouragement. Moreover, we would like to express our thanks to the Myanmar Academy of Arts and Science. Thanks are also due to all local people of the Napeng village for their valuable help throughout the field trip. Finally, all teaching staff from Geology Department, Panglong University are highly thanked for their cooperation.

References

- Adams, A.E., MacKenzie, W.S., and Guilford, C., (1984). *Atlas of Sedimentary Rocks under the Microscope*, Longman Group Limited, 104p.
- Brown, L.F. and Fisher, W.L., (1977). Seismic stratigraphic interpretation of depositional systems: Examples from Brazil rift and pull-apart basins. *Am. Assoc. Petrol. Geol. Mem.* **26**: 213-248.
- Dunham, R.J. (1962). Classification of Carbonate rocks according to depositional texture. *Amer. Assoc. Petr. Geol. Mem.* No.1., P.108-121
- Embry, A.F. and Klovan, J.E., 1971. A Late Devonian reef tract on northeastern Banks island, N.W.T. *Bulletin of Canadian Petroleum Geology* **19**: 730 -781.
- Emery, D. and Myers, K., (Eds.), (1996). *Sequence stratigraphy*. Blackwell, Oxford, p. 211-233.
- Flügel, E., (2010). *Microfacies of carbonate rocks*, 2nd. Edition, Springer- London, 984p
- Lohmann, K.C., (1976). Lower Dresbachian (Upper Cambrian) platform to deep-shelf transition in eastern Nevada and Western Utah: an evaluation through lithologic cycle correlation: Brigham Young University, *Geological Studies*, V.23, P. 860- 878.
- Myers, K., Milton, N.Y., (1996). Concepts and principles of sequence stratigraphy: In Emery, D., Myers, K. (Eds.), *Sequence stratigraphy*. Blackwell, Oxford, P.11-41.
- Vail, P.R., Mitchum, R.M., Todd, R.G., Widmer, J.M., Thompson, S., Sangree, J.B., Bubba, J.N. and Hatlelid, W.G., (1977). Seismic stratigraphy and global changes of sea level, In Payton, C.E., ed., *Seismic stratigraphy – applications to hydrocarbon exploration: AAPG Memoir*, 26, P.49-212.
- Van Wagoner, N.A., Mudle, P.J., Cole, F.E., and Daborn, G., (1990). Siliceous sponge communities, biological zonation, and recent sea level change on the Aratic margin: Ice Island results: *Canadian Journal of Earth Sciences*, V.26, P.2341-2364.
- Weidlich, O. and M. Bernecker, (2003). Supersequence and composite sequence carbonate platform growth: Permian and Triassic outcrop data of the Arabian Platform and Neo-Tethys. *Sedimentary Geology* **158**: 87-116.
- Wilson, J.I., (1975). *Carbonate Facies in Geologic History*: Berlin, Springer. Verlag. 471p.

-SEDIMENTOLOGY OF MOULMEIN LIMESTONE IN KAWKALUT-HNIDON AREA, KYAIKMARAW TOWNSHIP, MON STATE

Nandar Myint Maung¹, Day Wa Aung², and Tun Tun Zaw³

Abstract

The study area is situated in the southeastern part of Kyaikmaraw Township, Mon State. It lies between latitude 16° 20' 30" N to 16° 23' 00" N and longitude 97°44' 42" E to 97° 47' 24" E of one inch topographic map no. 94H/15. The present research mainly emphasized only on the carbonate sedimentology of the Middle to Late Permian Moulmein Limestone. Kawkalut-Hnidon Hills are composed of micritic limestone, fossiliferous limestone, dolomitic limestone and crystalline limestone. It was measured about 175 m and 200 m in thickness in details for microfacies analysis and were recognized into six microfacies; algal wackestone to packstone, dolomitic mudstone, mudstone, microbial grainstone, peloidal grainstone and peloidal packstone. These microfacies were grouped into three microfacies associations which represent three different depositional environments such as supratidal, intertidal and subtidal environments. The sequence stratigraphic interpretation of the Kawkalut section line indicates that eight metre-scale fourth-order shallowing upward parasequence cycles and three, metre-scale fourth-order deepening upward parasequence cycles. In the global Permian sea level, the slow falling of sea level also representing to Middle to Late Permian time which superimpose by lower order smaller cycles.

Keywords: Moulmein Limestone, Microfacies, Parasequence Cycles, Sea Level

Introduction

The research area is situated in the southeastern part of Kyaikmaraw Township, Mon State. It lies between latitude 16° 20' 30" N to 16° 23' 00" N and longitude 97°44' 42" E to 97° 47' 24" E of one inch topographic map no. 94H/15 and areas covering approximately 16 km² (6.25 square miles) (Fig.1). Physiographically, two different topographic units can be classified in the study area such as two isolated rolling hilly regions and flat alluvial plains (Fig.2). In the western part, Kawkalut Taung is about one mile long and 688 ft high above sea level. At the eastern part, Hnidon Taung is about 1.5 mile long and 802 ft high. Regionally, the investigated area lies on the southern part of Shan-Taninthayi Massif (Eastern Highlands), falls in the easternmost geotectonic belt of Burma and northern continuation of Taninthayi ranges. It belongs to the Moulmein Limestone of Middle to Late Permian age. Structurally, Hpa-pon fault and Three-pagoda fault are situated at the northern and southern part of the area and their trend is nearly NW-SE direction (Fig.3). Thin sections were prepared for petrography and get visual estimation of the constituent mineral grains. In addition to volume percent of rock constituents, it was done by using Terry and Chilingier's reference chart (1955). And then, make analysis of petrofacies by using Folk (1959) and Dunham (1962) classifications, microfacies [Adams and Mackenzie (1984), Scholl (2003)] and finally interpret the depositional environment.

Stratigraphy

Maung Thein (2014) described "Moulmein Limestone" at Middle to Late Permian time is gradational contact with Taungnyo Formation. The present work deals with the rocks of the Moulmein Limestone.

¹ Dr, Lecturer, Department of Geology, Mawlamyine University

² Dr, Professor and Head, Department of Geology, University of Yangon

³ Dr, Lecturer, Department of Geology, Mawlamyine University

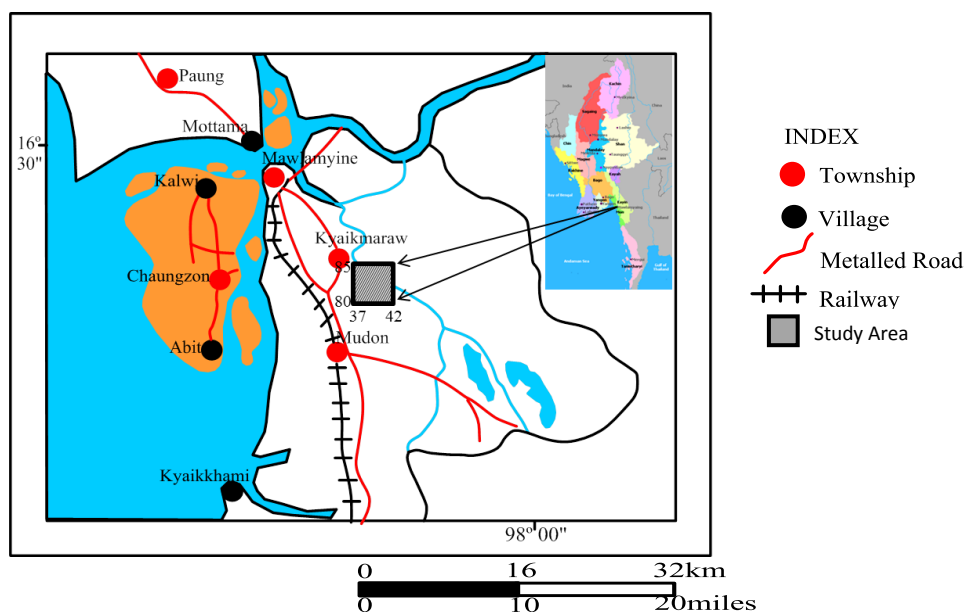


Figure 1 Location map of the study area

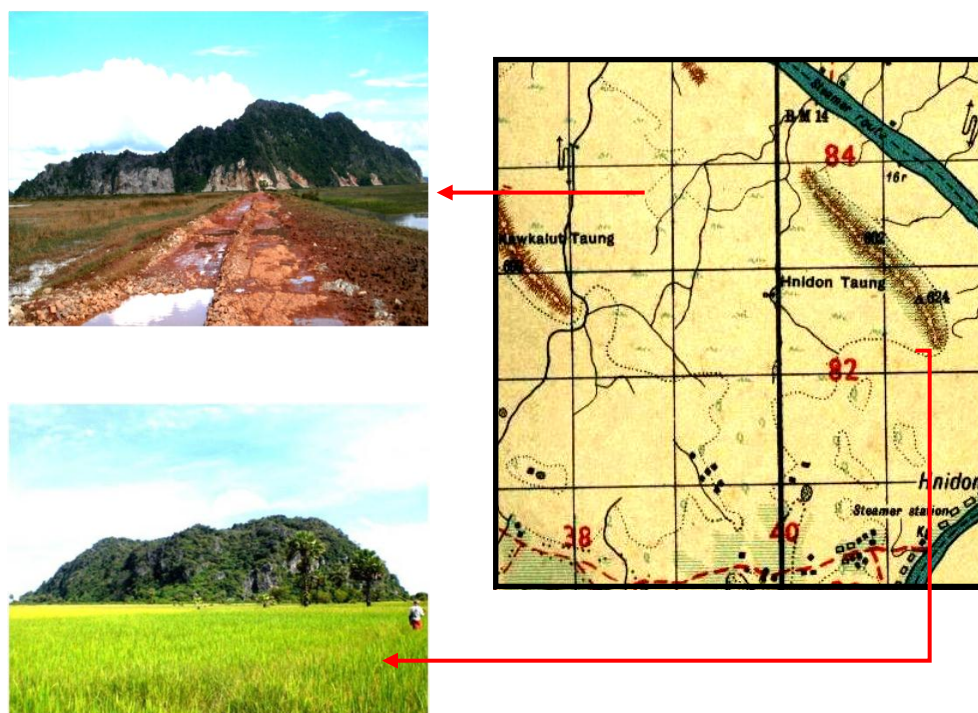


Figure 2 Kawkalut Hill (facing 75°) and Hnidon Hill (facing 5°) rising up in the alluvial land

Limestone of Kawkalut Hill

Kawkalut Hill Limestone is cropped out at the southeastern part of Kyaikmaraw Township and the eastern part of Taungnyo Range. It is exposed as isolated hill. Their trend is generally in NW-SE and dipping west with a dip amount of 50° to 75°.

In the lower part of Kawkalut Hill section line, light grey to dark grey-colored, thick-bedded, fine-grained micritic limestone are interbedded with fine-grained dolomitic limestone with wavy calcite veinlets (Fig.4). The middle part is mainly composed of dark grey-colored, fine-grained, micritic limestones (Fig.5) are intercalated with medium-grained limestone. Micritic

limestone with stromatolite is found in the middle part of Kawkalut Hill. The upper part consists of light grey to dark grey coloured, fine-grained fossiliferous limestone with rugose coral (Fig.6). The approximate stratigraphic thickness of Kawkalut Hill Limestone is about 574 ft (175m).

Limestone of Hnidon Hill

Sabe and Pagan Tunnels located at the northern and eastern part of Hnidon Hill. The trend of hill block is generally in NW-SE and dipping west with a dip amount of 25°.

At the southern part of Hnidon Hill, there is light grey-coloured, medium to thick-bedded, fine-grained micritic limestone in the lower and upper part interbedded with light grey to grey-coloured, fine to medium-grained dolomitic limestone. In the middle part, light grey to grey-coloured, medium to thick-bedded, fine to medium-grained limestone are interbedded with fine-grained micritic limestone with wavy laminations. The uppermost part is massive, grey to dark grey-coloured, fine-grained micritic limestone and dolomitic limestone (Fig.7). The approximate stratigraphic thickness is about 656 ft (200 m).

Carbonate Microfacies Analysis of Kawkalut and Hnidon Hills

Moulmein Limestone in the research area, the section lines can be categorized into (6) microfacies respectively.

Algal wackestone to packstone (microfacies -1)

Under the microscopic study, this microfacies consists of carbonated mud and some bioclasts. Allochembioclasts are included approximately 15 to 55 percents of the total rock volume. Bioclasts are algae, stromatolite, foraminifera, ostracods, gastropod, crinoids and unidentified shell fragments. Among them, densely radiating structure of tubules and shrubby plant forms of *Microbial* blue green algae and *Mizzia* green algae are found. Fragment of *Mizzia* green algal grain, outling of the grain with micritic sediment and infilling of original pores are sparry calcite cement. Laminated and contorted stromatolite (loferite) which preserved irregular lamination and elongate (birdseye or fenestral) pores (Fig.8). Crinoids showing the unit extinction (single crystal extinction), traces of pores structure and the axial canal and are surrounded by micrite envelope and filled with sparite. Foraminiferal tests show a variety of shapes and sizes. *Miliolina sp.* like tubular foraminifera is found. Micrite-walled endothyraceans were small Fusulinina, often with a well-developed inner fibrous layer. The rounded, circular-shaped exteriors of these grains made them easy to transport and orient, and as such they can be useful paleocurrent indicators. Thick-shelled gastropod, in which the original shell has been replaced by calcite and the internal are filled with algae and micrite. Orthochemmicrite are range from 15 to 40 percents and sparite is range from 25 to 50 percents of the framework. Peloids contain less than 5 percents of total rock volume.

Due to the presence of bioclasts (algae), micrite and sparite, the rock can be called biomicrite to biosparite using Folk's classification (1959, 1962). The rock can also be called algal wackestone to packstone using Dunham (1962).

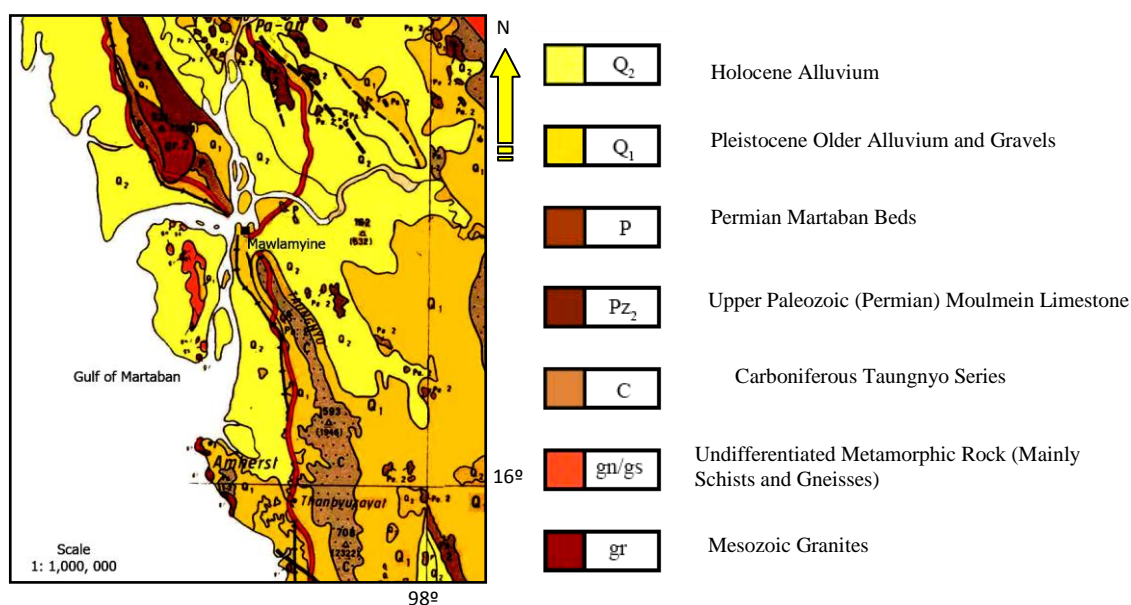


Figure 3 Regional Geological Map of the Study Area (From Geological Map of Myanmar, 1977)



Figure 4 Dolomitic limestone with wavy calcite veinlets in the lower part of Kawkalut Hill (Loc. 377829) (facing-west)

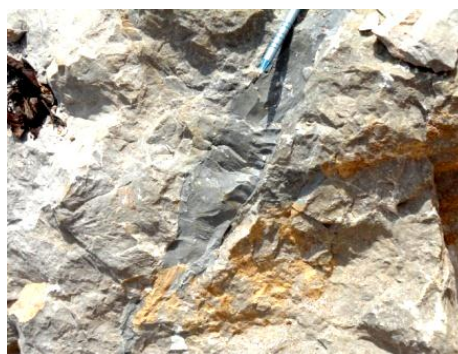


Figure 5 Fine-grained micritic limestone intercalated with medium-grained limestone in the middle part of Kawkalut Hill (Loc. 378828) (facing- southwest)



Figure 6 Rugose coral with fossiliferous limestone in the uppermost part of Kawkalut Hill (Loc.380826) (facing-northwest)



Figure 7 Massive nature of dolomitic and micritic limestone in the upper part of Hnidon Hill (Loc. 414823) (facing- west)

Dolomitic mudstone (microfacies-2)

Microscopically, allochems are very rare, and usually consists of brachiopod fragments, crinoids and algae. They are ranging from 3 to 5 percents of the total rock volume. Orthochemmicrite are 20 to 85 percents of the total volume of rock. These are made up of entirely of equant, granular, aphanocrystalline to cryptocrystalline mosaic of dense carbonate mud. Coarsely euhedral dolomites in micrite are also found. Microstalactitic or pendent fabrics were precipitated in the micrite (Fig.9). Dolomites are second in abundance. Dolomites place 15 to 75 percents of the total rock volume. Sparry calcite occurred from 3 to 5 percents of the rock.

Thus, the rocks of microfacies can be called dolomitic micrite (Folk, 1959, 1962). According to the limestone classification of Dunham (1962), the rock can be designated as dolomitic mudstone.

Mudstone (microfacies -3)

Microscopically, this mudstone facie is mainly made up of micrite. Bioclasts are included approximately 3 to 7 percents of the total rock volume. They are crinoids, ostracode, foraminifera and fossil fragments. Umbrella void in mudstone, the presence of some microcrystalline material on the roof of the cavities and calcite cements are filled with the fossil fragments and the remaining of geopetal pore space (Fig.10). Orthochem of micrite are range from 80 to 95 percents of the framework and sparites contain a little amount and which are filled in fossil fragments. Microstylolites are commonly observed in this microfacies. Dolomite contains 5 to 12 percents and calcite veinlets and selenites are present.

So carbonate mud are mainly present in this rock, the rocks can be called micrite by using the limestone classification of Folk (1959, 1962). According to Dunham's (1962), the limestone of this microfacies can be named as mudstone.

Microbial grainstone(microfacies -4)

Petrographically, allochem bioclasts range from 35 to 65 percents, peloids are less than 10 percents and orthochem of sparite are 25 to 65 percents of the total rock volume. Bioclasts are blue-green and green algae, brachiopod, echinoid plates, ostracode and foraminifera. The more irregularly shaped clumps of blue-green algae (*Microbial*) (Fig.11) and dasycladacean green algae (*Mizzia*) are the most common type among the bioclasts. Less complete fragments of brachiopod shell outline by micrite envelop and are smoothly curved and filled with blue-green algae. Gastropod test which shows the inside of the shell is filled with fine sediment of calcite. The original void space was partly filled calcisilt and remaining portion with coarse crystalline calcite. Little dolomites are found in some specimen. Five types of foram are found. Among them, Fusulinid foraminifer has the dark micrite wall.

Thus, the rock may be called as biosparite (Folk, 1959, 1962). According to Dunham's classification, it can be designated as bioclastic grainstone or microbial grainstone.

Peloidalgrainstone (microfacies -5)

Petrographically, allochem of bioclasts (algae) contain 13 to 23 percents, peloids are 17 to 55 percents and orthochem of sparite are 35 to 62 percents of the total rock volume. Bioclasts are algae, foraminifera, bryozoan and crinoid plates. Discoidal crinoid plates are thickest at their margins and the internal pores are completely filled with micritic carbonate giving the grains a

characteristic dusty or speckled appearance. Grains that have micritic internal structure like pellet, but that has diverse and irregular shapes and sizes or vague remnants of internal fabric are generally termed peloids (Fig.12). Finely peloidal rock in which individual peloids are, for the most part, distinct and some peloids are less distinct and are considered under cements. These peloids must have been followed by relatively sparry calcite cementation. The peloids ranges from 0.1mm to 0.01mm in length, and width ranges from 0.15mm to 0.01mm.

Thus, the rock may be called as pel-sparite (Folk, 1959, 1962). According to Dunham's classification, it can be designated as peloidal grainstone.

Peloidalpackstone (microfacies -6)

According to the microscopic study, allochemical bioclasts consist of algae, echinoid plates, gastropod and foraminifera which are 10 to 30 percents of the total rock volume. A variety of shapes and sizes of peloids are range between 15 to 65 percents. *Mizzia sp.* dasycladacean green algae and larger grains are pellet mud, which show the typical ellipsoidal shape in the middle part of the section line (Fig.13). The grains are peloids, probably algae in origin which shows some relict internal structure but with a variety of shapes and sizes. Many of the smaller grains are structureless. Uniformly grain size of peloids was associated with a lithified cyanobacterial mat in the upper part of the section line. A large echinoderm fragment with characteristic single crystal and the grain is surrounded by calcite overgrowths that formed in optical continuity with the grain which has irregular shape and lack of a central canal. Longitudinal section of gastropod, the exterior of the shell has been encrusted with calcite and the body chambered has been filled with micrite. The circular to cigar –shape cross-section of these spiral forms, the chamber structure and the microgranular walls with barely visible perforations all are the characteristic of small fusulinid foraminifera. Orthochem occupy 15 to 40 percents of sparry calcite and 10 to 35 percents of microcrystalline calcite. Dolomite contains 10 percents and calcite veinlets are present.

The rocks are made up of allochem grain of peloids and orthochem of sparry calcite and micrite. Therefore the rock can be named as pelmicrite to pelsparite (Folk, 1959, 1962) and peloidal packstone (Dunham, 1962).

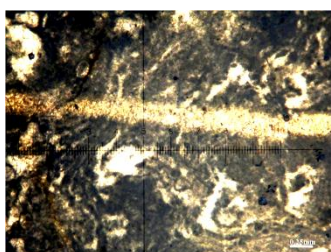


Figure 8 Laminated and contorted stromatolite (loferite) which preserved irregular lamination and elongate (birdseye or fenestral) pores in algal wackestone to packstone, PPL

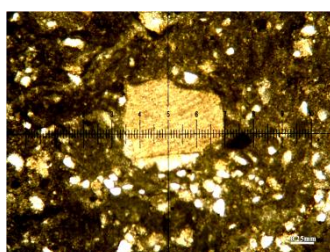


Figure 9 Microstalactitic or pendent fabric were precipitated in the micrite and anhedral to subhedral dolomite crystal in dolomitic mudstone, PPL

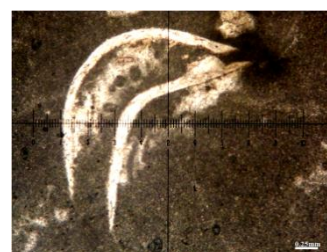


Figure 10 Umbrella void in mudstone, the presence of some microcrystalline material on the roof of the cavities and calcite cements are filled with the fossil fragments and the remaining of geopetal pore space, PPL

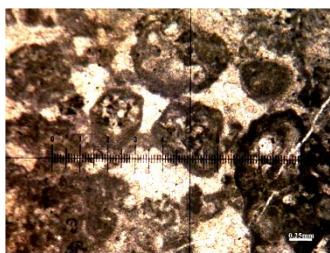


Figure 11 The more irregularly shaped clumps of blue-green algae in microbial grainstone, PPL

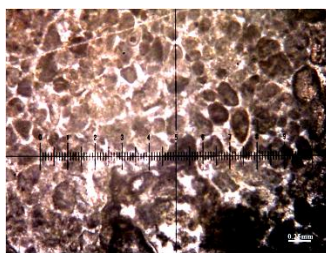


Figure 12 Grains that have micritic internal structure like pellet, but that has diverse and irregular shapes and sizes or vague remnants of internal fabric in peloidal grainstone, PPL

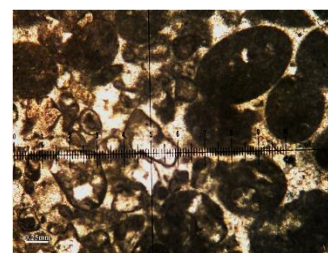


Figure 13 Larger loose grains are pellet muds, probably faecal in origin, show the typical ellipsoidal shape in peloidal packstone, PPI

Facies association and recognition of paleodepositional environment

Triangular plot of the rocks show that deposition had been taken place in the supratidal, intertidal and subtidal environments of Moulmein Limestone in Kawkalut and Hnidon Hill section lines (Fig. 14 and 15). Three major depositional environments are identified in the study area on the basis of grain types, physical and biogenic sedimentary structures, and vertical facies relationships as shown in table (1), (2) and (3). The possible depositional model of Kawkalut and Hnidon Hill is acquired by the study of microfacies and their respective association (Fig.16). Petrographic characteristics and depositional environments of the Kawkalut and Hnidon Hill Limestone are shown in (Fig.17 & 18).

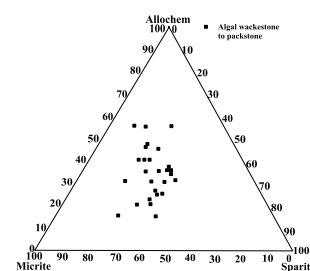
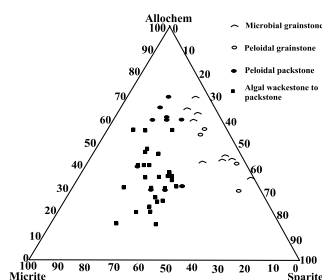
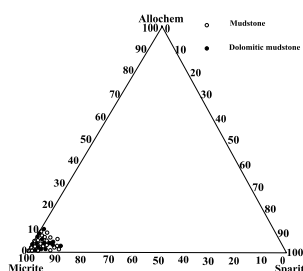


Figure 14 Triangular plot of supratidal, intertidal and subtidal environments of Moulmein Limestone in Kawkalut Hill section line (after Folk, 1959)

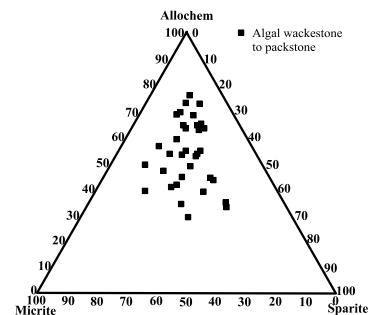
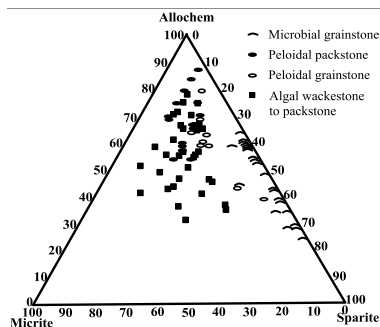
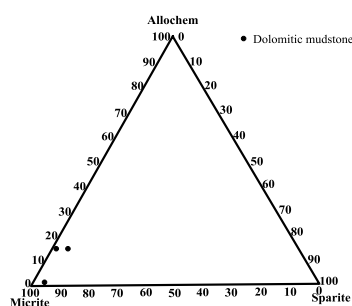


Figure 15 Triangular plot of supratidal, intertidal and subtidal environments of Moulmein Limestone in Hnidon Hill section line (after Folk, 1959)

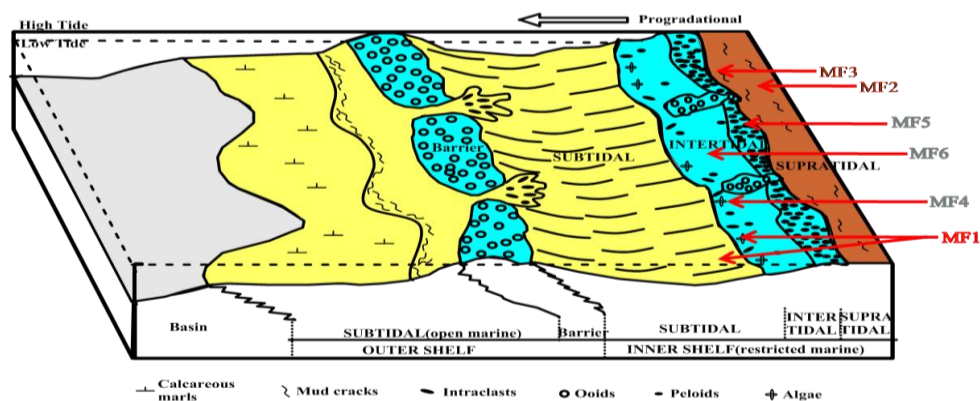


Figure 16 The possible depositional model of Kawkalut and Hnidon Hills Limestone

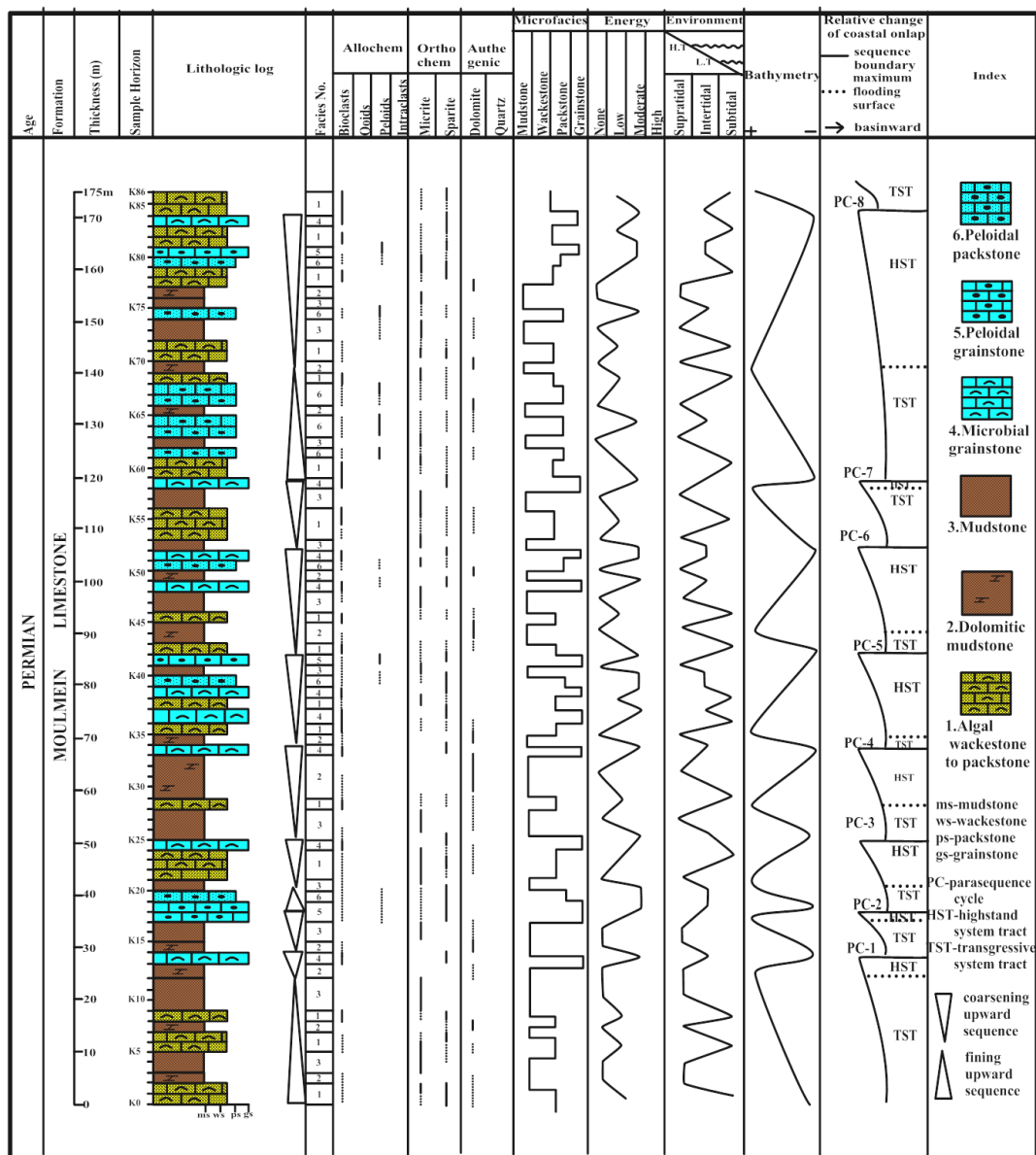


Figure 17 Petrographic characteristics and depositional environments of Moulmein Limestone at the Kawkalut Hill section (measured from Loc. 377830-378827)

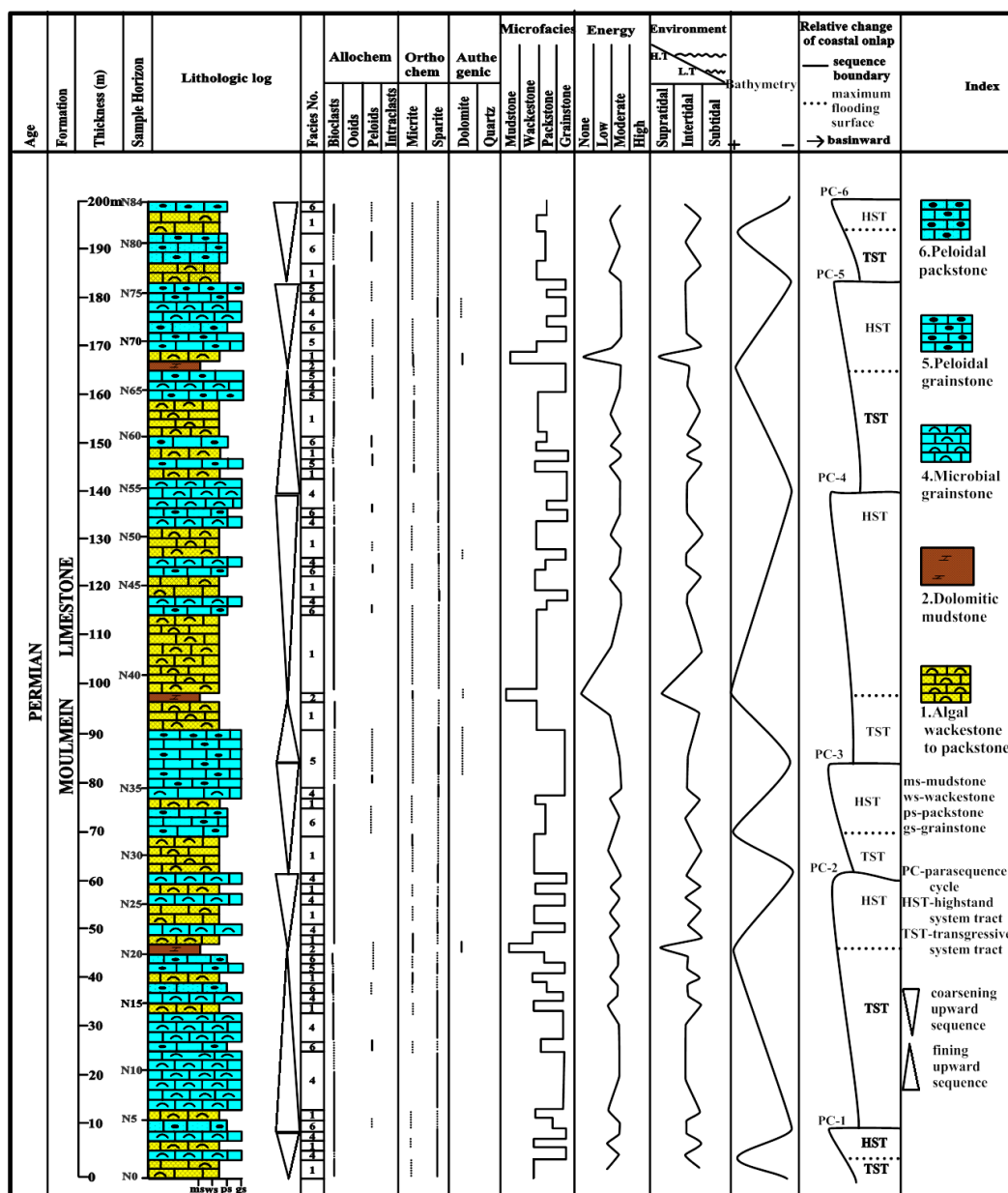


Figure 18 Petrographic characteristics and depositional environments of Moulmein Limestone at the Hnidon Hill section (measured from Loc. 377830-378827)

Table 1 Microfacies association and characteristic features of supratidal environment in Kawkalut and Hnidon Hill Section Lines

Supratidal	
Microfacies	Characteristic features
Dolomitic mudstone (microfacies- 2) Mudstone (microfacies- 3)	carbonate mud , high content of dolomite, dark colour, dolomite exhibit hypidiotopic to idiotopic fabric, gypsum (selenite), microstatitic or pendent cement, none energy, thick- bedded

Table 2 Microfacies association and characteristic features of intertidal environment in Kawkalut and Hnidon Hill Section Lines

Intertidal	
Microfacies	Characteristic features
Microbial grainstone (microfacies-4) Peloidal grainstone (microfacies-5) Peloidal packstone (microfacies-6) Algal wackestone to packstone (microfacies- 1)	Mostly bioclasts such as large brachiopod and gastropod, stromatolite, peloids, packstone, grainstone, moderate to high energy large

Table 3 Microfacies association and characteristic features of subtidal environment in Kawkalut and Hnidon Hill Section Lines

Subtidal	
Microfacies	Characteristic features
Algal wackestone to packstone (microfacies- 1)	Bioclasts, bryozoans, crinoids, stromatolite wackestone, lamination, low energy

Sequence Stratigraphy

Sequence Stratigraphic Interpretation of Kawkalut Hill Section Line

In this section line, eight, metre- scale fourth-order shallowing upward parasequence cycles and three, metre-scale fourth-order deepening upward parasequence cycles are recorded (Fig.17). The parasequence cycle boundaries PC-1 to PC-8 are tentatively defined at the changes of lithologic units. The PC-1, PC-3, PC-4, PC-6, PC-7 and PC-8 cycle boundaries are contact with microbial grainstone (MF-4). The PC-2 and PC-5 cycle boundaries are regarded by peloidal grainstone (MF-5). Dolomitic mudstone and mudstone are overlying on the cycle boundaries PC-1 to PC-8.

Maximum flooding surface (mfs) forms the boundary between the transgressive and highstand systems tract. In the study area, maximum flooding surfaces are defined by using argillaceous units (dolomitic mudstone and mudstone).

The transgressive systems tracts are noticed at the cycles PC-1 to PC-8. In the cycle PC-1, PC-3 and PC-8, the transgressive systems tracts progressively fining upward and are composed of dolomitic mudstone and mudstone facies. These facies display retrogradational stacking pattern which suggested that the rate of sediment supply is less than the rate of accommodational space (Emery and Myers, 1996).

In the cycle PC-2, the transgressive systems tracts are dolomitic mudstone and mudstone facies. These mudstone facies display aggradational stacking pattern which suggested that the rate of sediment supply is equal to the rate of accommodational space.

In the cycle PC-4 and PC-5, this is made up of mudstone and dolomitic mudstone facies. The transgressive systems tracts of these cycles express progradational stacking pattern which indicate that the rate of sediment supply is greater than the rate of accommodation space.

In the PC-6, transgressive systems tract is characterized by algal wackestone to packstone and dolomitic mudstone facies. The transgressive systems tract of these cycle displays retrogradational stacking patterns repeatedly occurred. The rate of sediment supply is less than the rate of accommodation space.

The transgressive systems tract of PC-7 is collected of mudstone and algal wackestone to packstone facies. These cycles are occupied by progradational stacking patterns initially occurred and retrogradational stacking patterns are observed in later. The rate of sediment supply is greater than the rate of accommodation space in early stage and less in later stage.

The high systems tract of PC-1 consists of dolomitic mudstone and microbial grainstone facies. These grainstone facies represents cycle boundary. The highstand systems tract of this cycle, the progradational stacking patterns occurred which indicate that the rate of deposition is greater than the rate of accommodation space.

The high systems tracts of PC-2 and PC-7 consist of peloidal grainstone and microbial grainstone facies. These grainstones represent cycle boundaries. The highstand systems tract of this cycle, the progradational stacking patterns occurred which indicate that the rate of sediment supply is greater than the rate of accommodation space.

In the PC-3, highstand systems tract is characterized by algal wackestone to packstone and microbial grainstone facies. These grainstone represents cycle boundary. These cycles are occupied by retrogradational stacking patterns. These features indicate that the rate of sediment supply is less than the rate of accommodation space.

The highstand systems tract of PC-4 is composed of dolomitic mudstone and microbial grainstone facies. This grainstone represents cycle boundary 4. These cycles are occupied by progradational stacking patterns. This feature indicates that the rate of sediment supply is greater than the rate of accommodation space.

In the PC-5, highstand systems tract is characterized by algal wackestone to packstone, microbial grainstone, peloidal packstone, mudstone and peloidal grainstone facies. This grainstone represents cycle boundary 6. The highstand systems tract of these cycles initially display retrogradational stacking patterns repeatedly, and followed by progradational stacking patterns in later. Thus the rate of deposition is less than the rate of accommodation space in early stage, greater in later stage.

In the PC-6, highstand systems tract is characterized by algal wackestone to packstone, mudstone, microbial grainstone, dolomitic mudstone and peloidal packstone facies. This grainstone represents cycle boundary 6. These cycles are repeatedly occupied by retrogradational stacking patterns initially and progradational stacking patterns are observed in later. These features indicate that the rate of sediment supply is less than the rate of accommodation space in early stage and greater in later stage.

In the PC-8, highstand systems tract is characterized by algal wackestone to packstone, mudstone, peloidal packstone, dolomitic mudstone, peloidal grainstone and microbial grainstone facies. This grainstone represents cycle boundary. This cycle is occupied by four repeated retrogradational stacking patterns. These features indicate that the rate of sediment supply is less than the rate of accommodation space.

Stratal stacking patterns of Kawkalut Taung related to shorelines trajectories can be observed in figure 19.

Parasequence Stacking Pattern

In the Middle to Late Permian time, global sea level history was also provided by the deposition of Moulmein limestone forming a peritidal carbonate platform giving a fashion of shorter sea level oscillation. The lacks of clastic strata and without pronounced drop in sea level are very strong support to the deposition in a stable sea level. In the global Permian sea level, the slow falling of sea level also representing to Middle to Late Permian time which superimposed by lower order smaller cycles.

Conclusion

From the present study, the limestones of Kawkalut and Hnidon Hills are composed of micritic limestone, dolomitic limestone, fossiliferous limestone and crystalline limestone according to field assessment. Microscopic analysis reveals the rock types of Kawkalut and Hnidon Hills are grouped into six microfacies. Dolomitic mudstone and mudstone are deposited in supratidal environment. Algal wackestone to packstone, microbial grainstone, peloidal grainstone and peloidal packstone are deposited in intertidal environment. Algal wackestone to packstone is deposited in subtidal environment. In sequence stratigraphic interpretation of the study area, eight, metre- scale fourth-order shallowing upward parasequence cycles and three, metre-scale fourth-order deepening upward parasequence cycles of Kawkalut Hill can be recognized. After the completion of Moulmein Limestone deposition, the slow falling of sea level also representing to Middle to Late Permian time which superimposed by lower order smaller cycles.

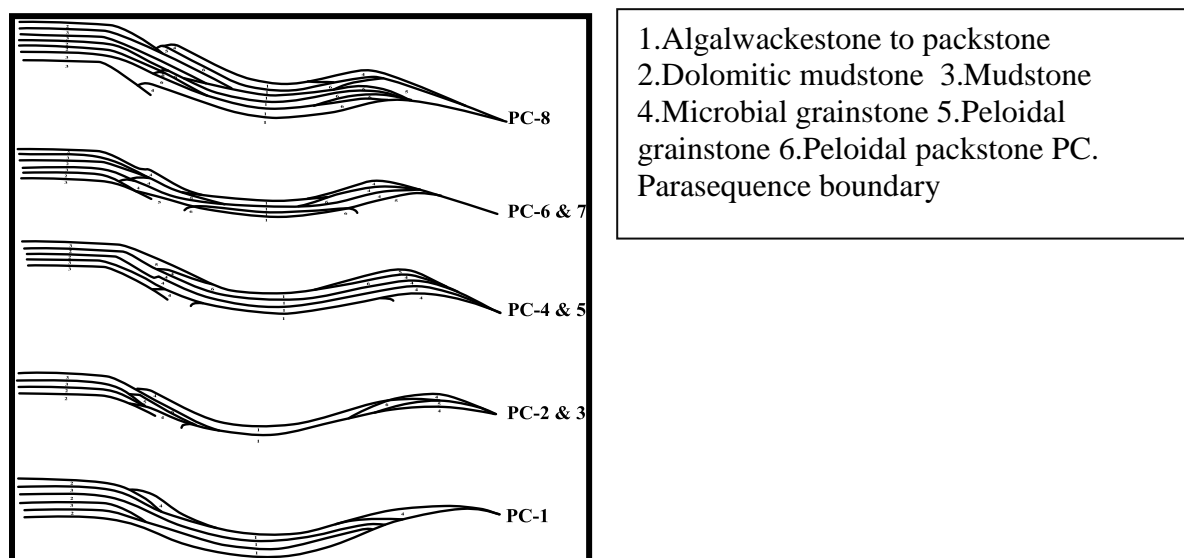


Figure 19 Stratigraphic stacking patterns of Kawkalut trajectories (from Catuneanu et al. 2010)

Acknowledgements

Appreciation is due to Dr Aung Myat Kyaw Sein (Rector of Mawlamyine University) and Professor Dr Yin Yin Aye (Head of Geology Department, Mawlamyine University), for permission to carry out my research work.

References

- Adams, A.E., and W.S. Mackenzie, (1984). *Atlas of sedimentary rocks under the microscope*, Longman Scientific & technical, John Wiley & Sons, Inc., 104 p.
- Catuneanu, O., et. al., (2010). *Sequence stratigraphy*: common ground after three decades of development. *First Break* **28**, 21–34.
- Dunham, R.J., (1962). *Classification of carbonate rocks according to depositional texture*, p. 108-121, in W.E. Ham, Ed., *Classification of Carbonate Rocks*: Tulsa, Okla, America Association of Petroleum Geologists, Mem., 1, 279 p.
- Folk, R.L., (1959). Practical Petrographic Classification of Limestone. *Bull. Amer. Asso. Petrol. Geol.* **43**. 1-38.
- Meyers, J., (1980). Compaction and Mississippian Skeletal Limestones, Southwestern New Mexico: *Jour. Sedi. Petrology*, v. 50, 457-474.
- Oldham, T. (1856). Notes on the coal field and tin- stone deposits of the Tenasserim Provinces. *Sel., Rec. Geol., Govt. India*, 10: 31-67.
- Scholle, P.A. and D.S. Ulmer- Scholle, (2003). *A color Guide to the Petrography of Carbonate Rocks: Grains, Texture, porosity, diagenesis*, AAPG Memoir 77, 459 p.
- Terry, R.D. and Chiling, G.V., (1955). Summary of concening some additional aids in studying sedimentary formation by Shvetsov. M.S.: *Jour. Sed. Petrology*, v. 25, 229-234.
- Tucker, M.E., (1991). *Sedimentary Petrology*. Blackwell Scientific Publications, 227 p.

OCCURRENCE OF GLAUCONITE AND PHOSPHATE IN THE SEDIMENTS FROM AYEYARWADY CONTINENTAL SHELF

Ko Yi Hla¹, Day Wa Aung², Moe Moe Lwin³ and TunTun Zaw⁴

Abstract

The study area is located in the northern part of Andaman Sea; bounded by Latitude 13° 25' N and 15° 40' N and Longitude 93° 15' E and 97° 45' E occupies the south and southwest oceanic area of Myanmar. Ayeyarwady continental shelf is a part of an area of a complex geological setting in Andaman basin, located in the south of Ayeyarwady delta surrounded by land area in north and east. In the present study, the formation and association of glauconite and phosphate were systematically studied. Sand of the study area is arkosic sand and lithic arkosic sand in composition derived from continental block and magmatic arc, subduction complex provenances. In the sediments, the glauconite constitutes 1 – 15.5 % of the total detrital fraction in some stations. The glauconite of biotite origin, fecal pellet conversations, foraminifera cavity fillings and replacements also occur. Phosphate constitutes 1 – 10 % of the sediment as replacement of bioclast, micro coprolite phosphate pellet and cement. The phosphates are formed in the shelf edge and slope where upwelling current favors the formation of phosphate. The association of glauconite and phosphate is and they were formed from during slow sedimentation in transgressive phase forming the condense horizon. Therefore, the shelf, shelf edge and slope area are the best fit for the formation of glauconite and phosphate in the present sea-level condition.

Keywords: glauconite, phosphate, transgressive phase, condense horizon.

Introduction

Location and size of the study area

The study area is located in northern Andaman Sea. It is bounded by Latitude 13 degree 25 minute N and 15 degree 40 minute N and Longitude 93 degree 15 minute E and 97 degree 45 minute E, occupies the south and southwest oceanic area of Myanmar. The area extends N-S in 225 km and E-W in 450 km respectively. The area extent of study area is approximately 101250 km². The study area is bounded by southern part of Ayeyarwady delta and Gulf of Martaban, and western part of Tanintharyi coast. Therefore, the area occupies the oceanic area around the Myanmar coast of northern Andaman Sea. The location map of the study area is shown in (Fig.1).

Glauconite

Glauconite is yellowish green, dark green to greenish black colored, usually consisting of ovoid and/or lobate shape, sand size smooth grains, presented in sand of the study area.

Glauconite constitutes (1) % to (15.5) % of the total detrital fractions. The forms of glauconites are various. Likewise, a few quartz inclusions are present in some glauconite. Under microscopic examination, flaky materials in glauconite are randomly oriented but some are properly oriented in nature (Figs. 2, 3, 4 and 5). Sometimes, the included very fine silt size quartz is haphazardly arranged (Figs. 6 and 7). In some cases, no distinct internal structures are to be

¹ Dr, Professor, Department of Geology, Mawlamyine University

² Dr, Professor and Head, Department of Geology, University of Yangon

³ Dr, Associate Professor, Department of Geology, Mawlamyine University

⁴ Dr, Lecturer, Department of Geology, Mawlamyine University

observed. Some glauconites are also frequently seen as internal fillings a few foraminifera tests as cavity fillings. Moreover, some labile grains stained and replaced by glauconite are observed as replacement glauconite. In addition, some glauconite coatings on some detrital grains are found. Most grains are weakly pleochroic.

Ovoid grains with shrinkage cracks as mentioning with their evolving stages are nascent, slightly evolved, evolved and highly evolved grains. In some case, no distinct internal structures are observed but the outer boundary of grain showing cracks or lobes and these cracks showing wedge-shaped aperture. In some horizons, the replacement of volcanic rock fragments, siltstone fragments, fauna fragments, and feldspars by glauconite with greenish staining is noted (Figs. 8 and 9). A few of the phosphate (collophane) grains associated with glauconite are well marked. The concentric glauconitic coating or glauconitized grain is also noted.

Glauconite content is conspicuously higher in lower shelf area. The glauconitic content decreases towards Ayeyarwady Delta and Gulf of Martaban.

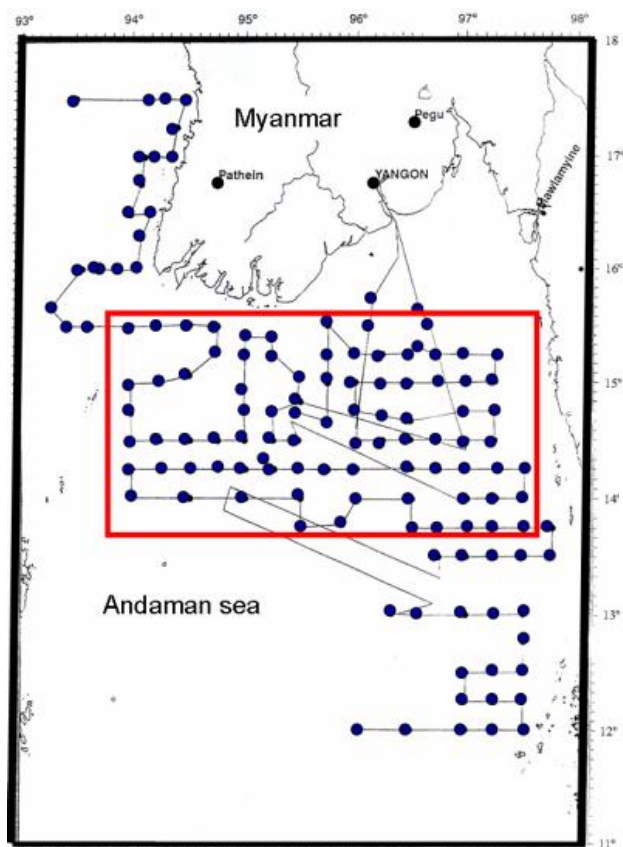


Figure 1 Location map of the study area with sample location and geophysical lines.



Figure 2 Photomicrograph showing glauconite grain with minute flakes (under PPL) (Sp. 63).

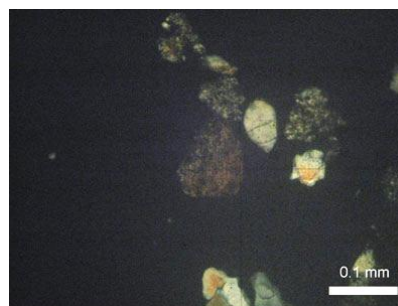


Figure 3 The same view with Fig.2 (between XN).

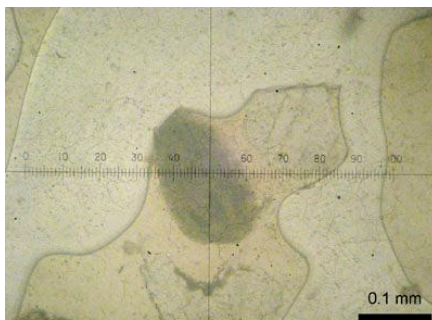


Figure 4 Photomicrograph showing glauconite grain with alignment of flaky material (under PPL) (Sp. 65).

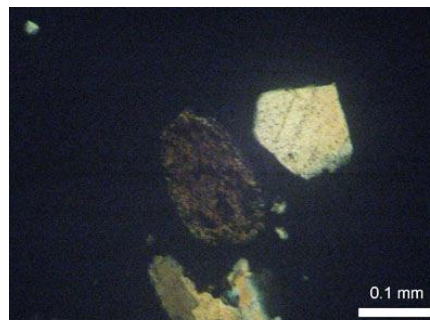


Figure 5 The same view with Fig.4 (between XN).

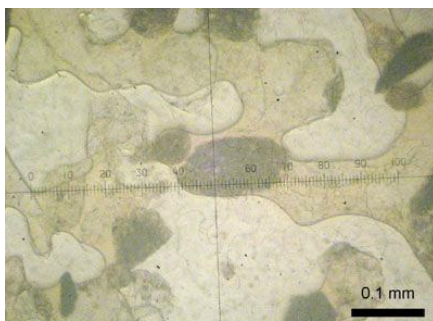


Figure 6 Photomicrograph showing well rounded glauconite grain with faint alignment of flaky material (under PPL) (Sp. 77)

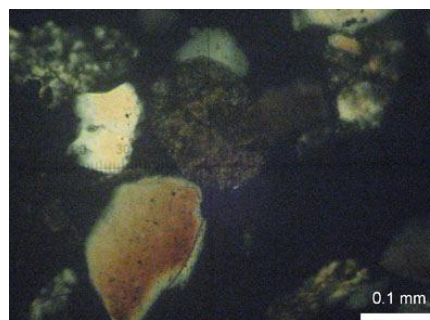


Figure 7 The same view with Fig.6 (between XN)

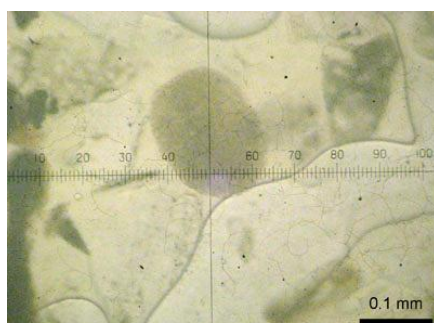


Figure 8 Photomicrograph showing ovoid glauconite grain with some minute inclusion of quartz and feldspar grains (under PPL) (Sp. 63)

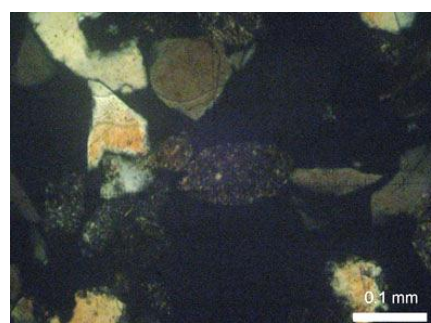


Figure 9 The same view with Fig.8 (between XN)

Formation of Glauconite

The origins of glauconite have been discussed by many authors and put many theories and postulations. These are (1) fecal pellet conversion, (2) Foraminifera cavity filling, (3) alteration of biotite, and (4) clay pellet agglomeration in the sea (Ehlmann, et al, 1963). The most common methods of glauconite formation are internal moulds, fecal pellets, replacement of carbonate skeletal fragments and the coating and replacement of mineral or rock grains (Odin and Fullagar, 1988).

Glaucanisation of mineral grains or rock fragments can occur with quartz, feldspar, mica, calcite, phosphate and volcanic glass common minerals to be replaced or coated by glauconite. Replacement of the mineral grain occurs along fissures or cleavage planes and tends to produce vermicular morphology (Odin and Fullagar, 1988).

In the present research area, glauconite altered from biotite, fecal pellet and foraminifer's cavity fillings are recorded (see fig. 78 .10.). Galliher (1935) concluded that the glauconites are the derivatives of biotite by a process of submarine weathering. The present material of glauconites is stated by Hein, et al, (1974) match with the glauconites under discussion. Glauconite pellets which appear to have cleavages were probably derived from minerals with cleavages like coarse-grained feldspar or biotite.

Glauconite pellets without cleavages, but containing inclusion of silt size quartz and feldspar were probably altered from fecal pellets.

A third group belongs to the alteration product of clay minerals trapped within the microfossil tests. Ehlmann, et al. (1963) stated that the glauconites are the alteration product of mud filled foraminifera test. Foraminifer tests are the dominants host for internal moulds and the glauconite is precipitated directly into the test or replaces clay-sized material previously deposited in the test. Fecal pellets are also common, particularly in modern sediments, and are produced by filter feeding or soft-bodied organisms which consume mud. Glauconite appears to form in the pores of these pellets and slowly replaces the muddy material within the pellet (Odin and Fullagar, 1988).

Glauconites are formed only in marine water of normal salinity. It requires slightly reducing (Cloud, 1955), and weakly oxidizing condition (Chilingar, 1956), in the area of slow sedimentation.

Galliher (1935) stated that the formation of glauconite is favored in black mud and sands in anaerobic environment, where "oxidation" may occur, at the surface of the sediments.

Hadding (1932) suggested that the glauconite is always marine, always sub-littoral, and always a shallow sea formation. As a rule these are formed in agitated water, under decrease deposition and never form in highly oxygenous water.

Lochman (1949) presented that the glauconite essentially needs a moderately anaerobic environment.

Debrabant and Paquet (1975) stated that the glauconites usually associated with phosphates pellets and pyrites. This means that the prevailing of reducing condition present.

The replacements, the concentric coating and the highly evolved glauconites are the products of submarine glauconitization process directly from seawater. (Amorosi, 1995).

Cloud (1935) stated that glauconites are formed only in marine water with normal salinity under slightly reducing condition. It also requires weakly oxidizing condition.

Galliher (1935) stated that the formation of glauconite is favored in black mud and sands in anaerobic environment, where oxidation may occur, at the surface of the sediments.

The glauconite is always marine, always sub-littoral, and always a shallow sea formation. As a rule these are formed in agitated water under decreased deposition and never form in highly

oxygenous water. Therefore, the glauconite with concentric coatings is suggested to be formed under that condition.

Moreover, the glauconite essentially needs a moderately anaerobic environment and the rocks commonly associated with pyrite and siderite. So, the occurrence of pyrite associated with glauconites in some intervals is thought to be of reducing condition (Day Wa Aung, 1993).

Amorosi (1995) stated that the glauconites usually associated with phosphatic pellets and pyrites, which can also be documented in shelf sand of the area.

Odin and Matter (1981) mentioned that the parent of material of glauconites is carbonate particles, argillaceous (Kaolinitic) fecal pellets, infilling of foraminifer's tests, various mineral grains and rock fragments that pass gradually into the commonly occurring green grains, which is undoubtedly acceptable statement.

On a larger scale, the formation of glaucony is governed by the availability of iron and potassium and the balance between detrital influx and winnowing. (Odin and Matter, 1981).

Low accumulation rates expose grains to the open marine environment for sufficient long times (10^6 years) for highly evolved glaucony (Odin and Matter, 1981). This means that the glauconitization is early diagenetic event under slow sedimentation in open marine with slightly reducing, mildly oxidizing condition.

There are four main stages of glauconite formation: nascent, slightly evolved, evolved and highly evolved (Odin and Fullagar, 1988). At the nascent stage the glauconite is just beginning to form and is iron rich with K_2O contents of 2-4%. Slightly evolved glauconite has K_2O contents of 4-6% and most of the original grain (mineral, fecal pellet, clay has been replaced (Odin and Fullagar, 1988). Glauconite grains reach the evolved stage when their K_2O contents are 6-8% and all of the original grains structure and texture have been lost. In highly evolved grains of glauconite any cracking of the grains is filled to produce smooth surfaces and the K_2O content is greater than 8% (Odin and Fullagar, 1988). The glauconite infilling the cracks have less K_2O and are less evolved as result. Based on K_2O content, most of the glauconite falls within the evolved stage (five out of seven samples).

The ideal conditions for glauconite formation occur between 65 degree S and 80 degree N on continental shelves (<500 m water depth) with pH conditions that are slightly alkaline (7-8 pH) and a water temperature between 15 and 20 degree C (McRae, 1972). A slightly reducing environment with bacterial decomposition of organic matter is favored on modern shelves glauconite formation is often associated with areas of reduced sedimentation and relict sediment (McRae, 1972).

Phosphate

Of some interest at present are the phosphorus deposits found on the shelves off the coasts of many countries of the world. Thus, phosphorus deposits have been found off Peru, Chile, Mexico, the west and east coasts of the United States, off Argentina, South Africa, Japan, and on the submerged parts of several islands around the Indian Ocean (Mero, 1966)

Phosphate consists of 1 to 10 % of sediment of the Ayeyarwady continental shelf. The phosphate occur in the study area are mostly collophane. The replacement of bioclast (Figs. 10, 11), cavity filling in fossil chambers (Fig. 12), micro coprolites phosphate pellet and cement

(Fig.13). Phosphate constitutes in shelf sediments of the study area. The association of glauconite and phosphate materials is conspicuously seen. It is light yellow to brown in color and isotropic between XN (Fig. 11). The form of phosphate such as micro coprolite, replacing of fauna and cement (Figs. 14, 15, 16, 17) are noted. The sediment of the study area yield different concentration especially in the shelf edge area. The sediments closed to the Ayeyarwady delta and shallow areas yield a trace amount of phosphates.

In the present research, the phosphate occurs as bioclast replacement, cavity filling in fossil chambers, phosphatized fecal pellet, and phosphate grains. It shows yellow in color under ppl and isotropic between XN. Some bioclasts are partially or totally replaced by phosphate is well marked.

In the area, the phosphate occurs as cement and minute particles disseminating in sediments. Most of these phosphates occur in the sediment of shelf-edge and slope areas of the study area. Dispersed phosphate, biogenic fragments, coprolites, and pellets are noted. In thin section, skeletal phosphate is distinguished by its light-yellow to brown color and presence of a microstructure of regularly arranged canals (canaliculi) and growth lines.

Coprolites are commonly present in bioclastic phosphorites. They are generally spherical to elongate fecal pellets, up to 20 mm in diameter, composed of collophane.

Phosphatised skeletal fragments are broken rounded grains than in thin section re brown in plane light and anisotropic under cross-polarized light.

Origin of marine phosphorites

The marine phosphorite generally occurs in areas of slow sedimentation, on outer continental shelves and slopes, particularly on the tops and sides of local ridges and banks, on fault scarps and flanks of submarine canyons. Phosphate nodules and crusts generally occur at depths from 60 to 300 m (Tucker, 1991)

The phosphorite is developing on the upper continental slope as replacements of benthic foraminifera. Obliteration of the foraminifer's structure by the replacement leads to the production of phosphorite pellets.



Figure10 Photomicrograph showing glauconite in fossil chamber (under PPL) (Sp. 75)

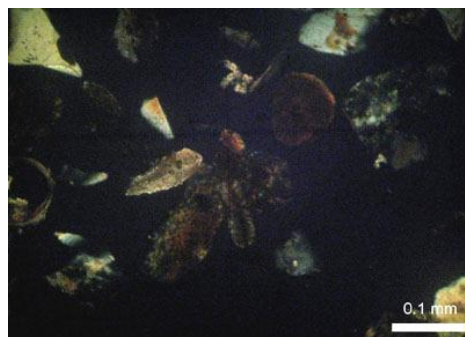


Figure 11 The same view with Fig.10 (between XN)

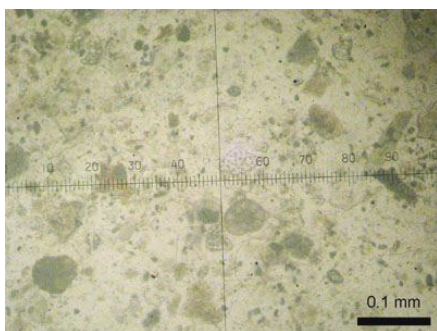


Figure 12 Photomicrograph showing forams and phosphate (under PPL) (Sp. 103)

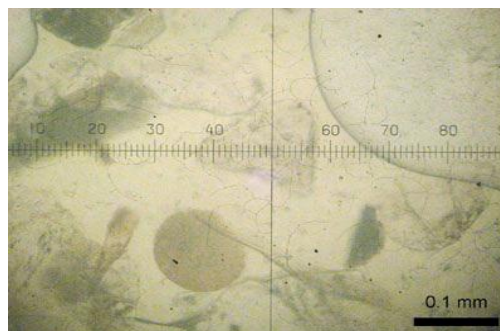


Figure 13 Photomicrograph showing yellowish colored, rounded phosphate pellet (under PPL) (Sp. 77)

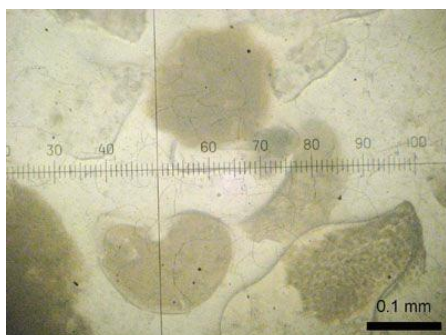


Figure 14 Photomicrograph showing the Phosphate replacement of bioclast (under P.P.L) (sp.77).

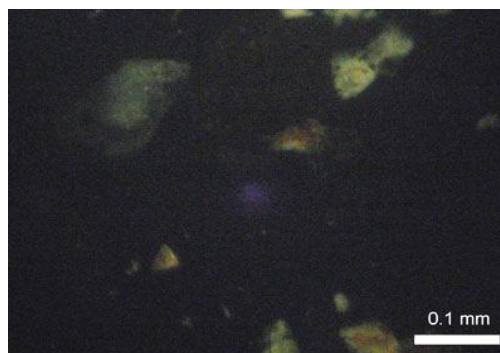


Figure 15 The same view between X.N. (sp.77).

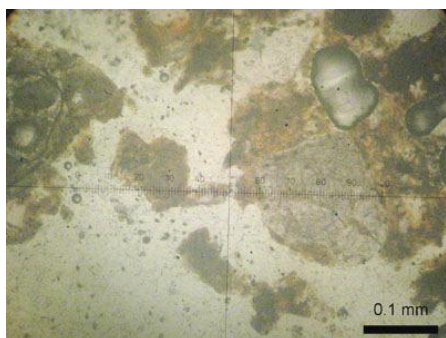


Figure 16 Photomicrograph of the Phosphate replacement foraminifer's shell and phosphate cement (sp.112)



Figure 17 The same view between X.N. (sp.112)

One popular mechanism has been upwelling, whereby cold waters containing nutrients rise from the depths towards the surface. Upwelling currents lead to high organic productivities and phytoplankton growth in surface waters which in turn results in organic rich (and so phosphate-enriched) sediments and oxygen-deficient waters overlying the sea floor.

Low sedimentation rates prevailed during phosphogenesis, and this is reflected in the associated sediments which may be organic-rich mud rocks, cherts, pelagic limes, hard grounds and glauconite. Ancient phosphorites are common constituents of condensed sequences. It occurs in condensation with very low rates of accumulation.

Although it was once thought that phosphorus was precipitated directly from sea water, perhaps as some type colloid, data from sites of active phosphorus formation indicate that much is being formed within the surface sediments, largely by replacement and impregnation of grains. The bacterial decay of organic matter in the sediment liberates phosphate which is precipitated in pellets and coprolites, and replaces siliceous and calcareous skeletons and lime mud, eventually giving rise to nodular masses of phosphorite. Micaceous and detrital clays may absorb phosphate into their lattices. The role of the phytoplankton is the crucial in transporting the phosphate from upwelling currents and near-surface waters to the sea floor.

Many of the phosphorite deposits of the geological record formed when sea level was relatively high or were associated with short-lived transgressions. During these times, shallow, fertile, shelf seas promoted phytoplankton blooms, which led to poorly oxygenated shallow sea floors where organic matter (with its PO_4^{2-}) could accumulate.

Therefore, in the Ayeyarwady continental shelf, the phosphate deposition is formed in sea-level rise period. This is documented that the deposition of phosphate is confined in the shelf edge and slope area where the phytoplankton is flourished and upwelling prevails.

In the oceanic environment, phosphorus is relatively rare with an average of only 70 ppb in both organic and inorganic forms and surface water is further deplete of inorganic phosphorus by phytoplankton activity (Phillip, 1986). Phosphate-enriched water is mainly introduced to the shelf and slope through upwelling which increases the surface water concentration and, as a result, phytoplankton activity. Phosphate is incorporated into the sediment through the introduction of phytoplankton remains, which through decomposition result in the accumulation and concentration of inorganic phosphate in oxygen-poor sediments. Phosphate accumulation predominantly occurs in areas of upwelling currents and the optimum water depth for phosphate formation is from 30-200m (Phillip, 1986; Parrish et al., 2001; Coles et al., 2002).

Most phosphate minerals are formed close to the sediment/ water interface by precipitation from interstitial waters (Bentor, 1980) and phosphatization took place under anoxic conditions where interstitial waters become greatly enriched in phosphate compared with the concentration of phosphate in bulk sea water. Decomposition of organic phosphate causes the dissolved phosphate concentration in the interstitial water to rise (Berner, 1974).

These organic-rich sediments accumulated along the continental shelf, which had considerable bathymetric relief (Edman and Surdam, 1984). A widespread oxygen-minimum zone coincided either continually or frequently with the sea floor as deposition progressed, and upwelling was both strong and persistent (Edman & Surdam, 1984).

Thus the association of authigenic phosphate minerals with organic-rich sediments may be a consequence of the chemical reactions that are prerequisites for the precipitation of calcium phosphates (Edman and Surdam, 1984). The dissolution of fossil fragments immediately following the precipitation of calcium phosphates was probably related to removal of calcium from the pore water by the calcium phosphate minerals. As precipitation of apatite began, the concentration of calcium ion decreased, which resulted in the dissolution of the calcareous fossils.

Glaucinite and phosphate association

Glaucinite and phosphate minerals occur in varying quantities in sediment continental margin of Ayeyarwady continental shelf. Glaucinite, in particular, comprises a significant component of the siliciclastic-rich sediment with. Glaucinite-phosphate associations are common features in marine environments with many examples known from continental margins in the rock record (e.g. Shublik Formation, Arctic Alaska (Parrish et al., 2001); Helvetic Shel, north Africa (Notholt and Jarvis, 1990)) and in the modern (e.g. East Australian continental margin, (James et al., 2004); outer continental shelf, Cape Canyon, South Africa, (Compton et al., 2004).

Glaucinite is commonly associated with phosphate (McRae, 1972; Odin and Fullagar, 1988). These samples imply low sedimentation rates, which allowed a glauconite-phosphate association to form on the upper slope (Phillip, 1986).

Both phosphate and glauconite require slightly reducing conditions and organic decomposition and along with these analyses this indicates that phosphate and glauconite are being precipitated simultaneously on the Ayeyarwady continental shelf area. Slow deposition of phosphate and glauconite in condensed sections is common and often associated with sea level rise (Compton, 1989).

The skeletal grains are replaced by carbonate apatite. Both francolite and dahllite have been identified in these phosphorites, and glauconite is frequently found too.

Glaucinite has also been inferred to be present both at the base of the transgressive systems tract (Baum and Vail, 1988). (Van Wagoner et.al. 1990; Vail et.al., 1991) and in the entire TST (Transgressive Systems Tract) (Mitchum and Van Wagoner, 1991).

Autochthonous glauconite in common at various stratigraphic levels in the transgressive systems tract (TST) and the lower highstand systems tract (HST), showing an upward increase (TST) and then decrease (HST) in abundance and maturity (Amoros,1995).

According to Amorosi (1995), glauconite can occur in most depositional sequences but is generally most common in the deposits of the transgressive systems tract (TST). The intrabasinal clasts such as glauconite and phosphate mostly occur in transgressive episode (Zuffa, 1980) (Fig.18). The condensed section can be distinguished by the higher concentration of glauconite (Fig.19). Therefore, the high glauconite concentration in study area can be regarded as TST which attained present sea level position (Fig.19). In condensed sections very high concentration of glauconite occur compared to the over- and underlying deposits. Differing rates of supply of siliciclastic sediment is the primary control on the presence of glauconite in depositional sequences and, as such, glauconite is considered one of the most reliable indicators of low sedimentation rates (Amorosi, 1995).

Phosphate grains, with abundant skeletal material, are common in condensed sections where the glauconite concentration and compositional maturity is greatest with dark green, evolved and highly evolved glauconite grains widespread.

Whichever, the relative sea level rise must have been rapid to promote the very low sedimentation rates conducive to glauconite formation (Amorosi, 1995). It can be concluded that, after the regression, which form the formation of relict sand followed by a sea level transgression which affecting present sea-level favors the formation of glauconite.

Summary and Conclusion

The study area is located in northern part of Adman Sea bounded by latitude 13° 25' N and 15° 40' N and longitude 93° 15' E and 97° 45' E occupies the south and southwest oceanic area of Myanmar. The area extent is approximately 101250 km².

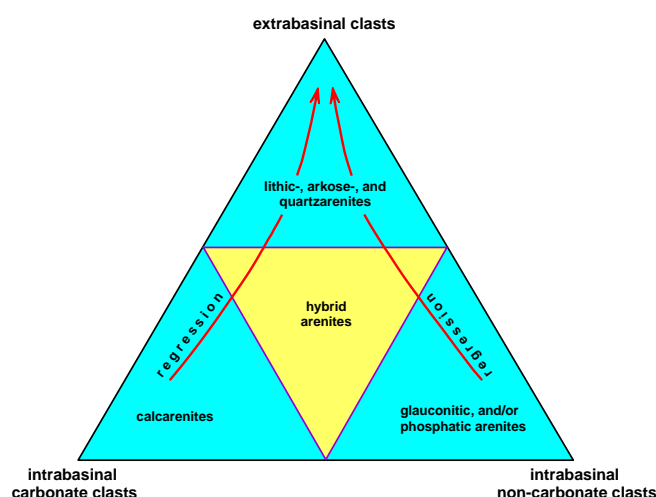


Figure 18 Triangle showing possible changes in the proportion of extra-basinal and intra-basinal, framework grain composition of sandstones due to changes in the relative sea level (after Zuffa, 1980).

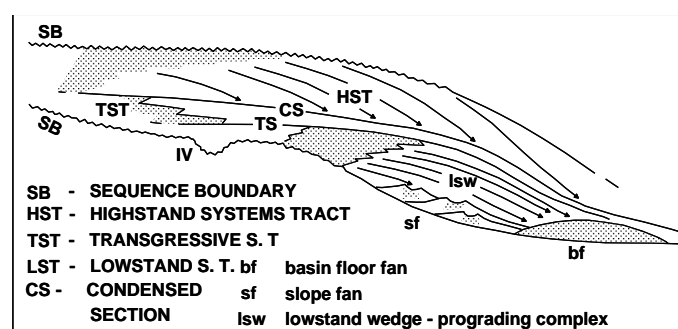


Figure19 A sequence stratigraphic context showing the marine condensation (after Walker, 1992)

Ayeyarwady continental shelf is part of an area of a complex geological setting in Andaman basin, located in the south of Ayeyarwady delta surrounded by land area in north and east. Ayeyarwady continental shelf has a tidal range between 4m-7m is located in tropical climate and the Ayeyarwady, Thanlwin and Sittaung rivers flow into the study area. The glauconite and phosphate are especially focused as authigenic minerals of the study area. Glauconite constitutes 1-15.5% of the total detrital fraction in some station. The glauconite of biotite origin, fecal pellet conversions, foraminifera cavity fillings and replacements also occur.

Phosphates constitute 1-10% of the sediment as replacement of bioclast, micro coprolite phosphate pellet and cement. The phosphates are formed in the shelf edge and slope where upwelling current favours the formation of phosphate. The association of glauconite and phosphate are conspicuously occur in shelf edge sediment. They were formed during slow sedimentation in transgressive phase forming the condensed horizon. The formation of glauconite needs normal salinity, slightly reducing and weakly oxidizing condition in marine environment. It requires, 7-8 pH condition that is slightly alkaline condition, therefore it can form only in

marine water. Therefore it can be concluded that glauconite and phosphate mostly occur in transgressive episode. In the present sea-level, the shelf, shelf edge and slope are the best fit for the formation of glauconite and phosphate.

Acknowledgements

We are deeply thankful to Professor Dr Yin Yin Aye, Head of Geology Department, Mawlamyine University for her kind permission to carry out this research.

References

- Amorosi, A. (1995) Glaucony and Sequence Stratigraphy: A Conceptual Framework of Distribution in Siliciclastic Sequence: *Jour. Sed. Res.* V. B65, No. 4, p.419-425.
- Bender, F. (1983) *Geology of Burma*: Stuttgart, Berlin.
- Berner, R.A. (1974) Kinetic models for the early diagenesis of nitrogen, sulfur, phosphorus, silicon in anoxic marine sediments, in E.D. Goldberg, ed., *The sea, vs.*, New York, John Wiley and Sons, p.427-450.
- Chhibber, H. L. (1934) *The Geology of Burma*: 538 pp, London Mac Millan.
- Cloud, P. E., JR., (1953) Physical limits of Glauconite formation. *Bull. Amer. Assoc. Petrol. Geol.* V. 39, no.4, p. 485-491.
- Curray, J.R., Moore, D. G. et al, (1979) *Tectonic of the Andaman Sea and Burma*.

SEQUENCE STRATIGRAPHY OF TAUNGNYO FORMATION IN THE SOUTHERN PART OF MAWLAMYINE AREA, MON STATE

Moe Moe Lwin¹, Day Wa Aung² and Ko Yi Hla³

Abstract

The study area is situated in Mawlamyine and Mudon Townships, Mon State. It is mainly composed of Early Carboniferous to Early Permian clastic sedimentary rocks comprising shales, mudstones, pebbly mudstones, sandstones, gritty sandstones, conglomerate and pebbly greywacke. Nine lithofacies of Taungnyo Formation are recognized; (1) dark grey color thick-bedded mudstone facies, (2) dark color pebbly sandstone facies, (3) dark color pebbly mudstone facies, (4) conglomeratic gritty sandstone facies, (5) gritty sandstone facies, (6) medium to thick-bedded sandstone facies, (7) thin to medium-bedded sandstone facies, (8) thin-bedded sandstone with shale interbedded facies and (9) sandstone and mudstone interbedded facies. It is divided into three lithofacies associations; (1) pebbly greywacke-pebbly mudstone-shale association which represents upper and lower fan sequence, (2) conglomerate-gritty sandstone-sandstone-shale association represented upper fan and mid fan sequence and (3) sandstone-shale association representing mid fan channel and basin plain of lower fan sequence. By studying the rocks of Taungnyo Formation it is characterized by high velocity turbidity current, low density turbidity current, fine-grained sandstone with low velocity and coarse-grained sandstone with high velocity turbidity current of submarine fan environment. Taungnyo Formation was formed as a submarine fan and taken place in the deep sea. This is forming as a sand-rich and mixed sand-mud turbidite system. Growth and deposition of a turbidite system are intimately tied to a cycle of eustatic or relative sea-level change. During a maximum regression, the shore line moved basinward and the fluvial system placed on the exposed shelf area and most of the sediments were deposited in continental slope area. This regression is also coincided with the global sea level drop.

Keywords: Taungnyo Formation, turbidite system, maximum regression, Sequence

Introduction

Location, size and accessibility

The study area is located in Mawlamyine and Mudon Townships, Mon State. It is bounded by Latitudes 16° 21' N to 16° 30' N and Longitudes 97° 38' E to 97° 43' E, and are located partly in one inch topographic maps No. 94 H/ 10, 11 and 15. It can be easily accessed by car (Fig 1).

Physiography

The Taungnyo range can be physiographically divided into two divisions such as the hill ranges of southeasterly trending Taungnyo range in the middle and the rest is young flat alluvial plain. The eastern and western parts of the ranges are also covered by alluvial plains of Mawlamyine, Kyaikmaraw and Mudon Townships. Isolated hill blocks of Moulmein Limestones also stand out in the low lying alluvial plain on both sides of the Taungnyo range. Regional structural trend is NNW-SSE direction (Fig. 2).

¹ Dr, Associate Professor, Department of Geology, Mawlamyine University

² Dr, Professor and Head, Department of Geology, University of Yangon

³ Dr, Professor, Department of Geology, Mawlamyine University

Regional geologic setting

The study area is located in the central portion of Mon State occupies Shan-Taninthayi block. In this area, clastic sedimentary rocks were folded and it is conformably overlain by Moulmein Limestones in both eastern and western part of the range. Regional structural trend of these rocks is NNW-SSE direction and has been stratigraphically correlated with Lebyin Group of Southern Shan State. The Taungnyo Group and Mawchi Series were regarded as homotaxial and part of Mergui Series which is ranging in age from Silurian to Lower Carboniferous (Haq and Thein, 1969). The fauna found in Zwegabin range, south of Hpa-an reveals that the age of fossils-bearing sandstones of Taungnyo Group is Upper Carboniferous (Brunnschweiler, 1970). Generally Taungnyo Series is resting conformably on Mergui Series and overlain by Moulmein Limestones exposed along the eastern and western part of Taungnyo range (Brunnschweiler, 1970). Regional geological map of the study area is shown in Fig (3).

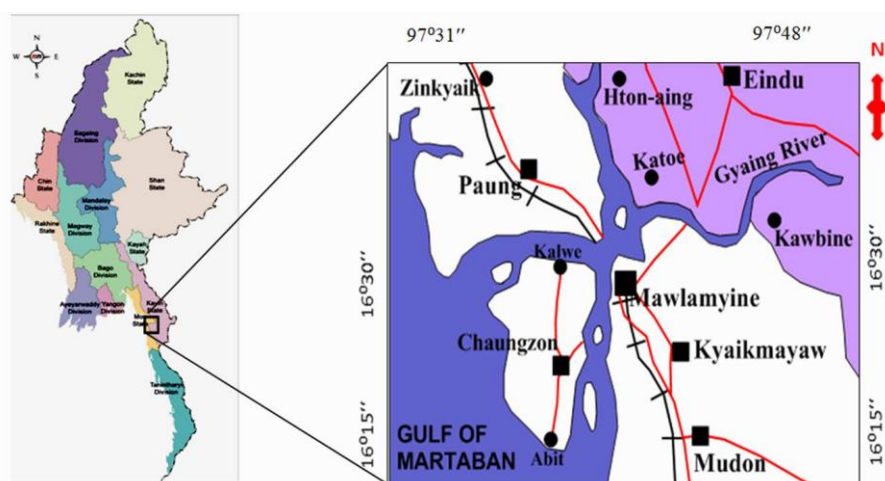


Figure 1 Location map of the study area.

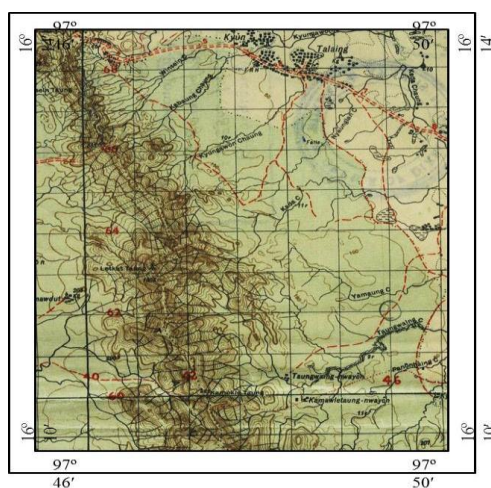


Figure 2 Topographic map of the study area.

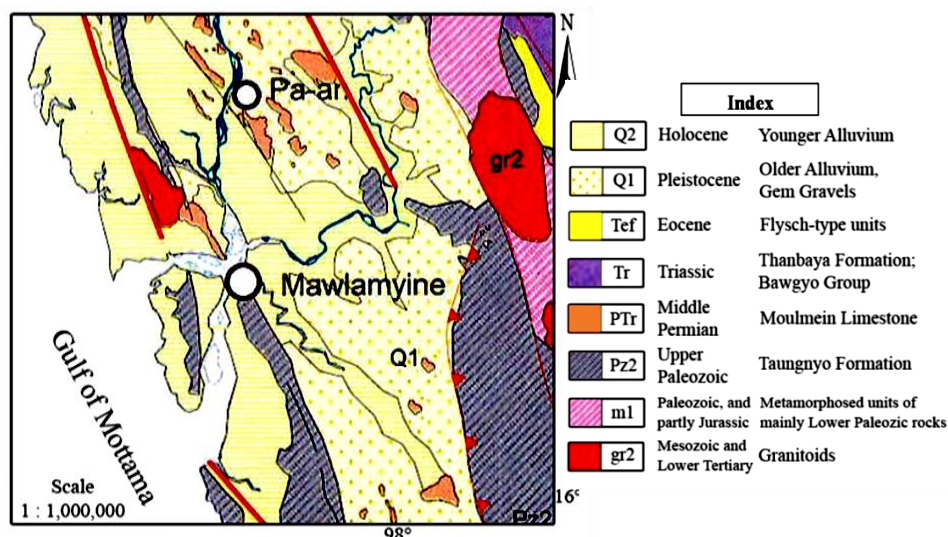


Figure 3 Regional Geological Map of the Study Area.(From Geological Map of Union of Myanmar, 2014)

Stratigraphy

The study area lies in a part of Shan-Taninthayi Block. It is composed of clastic sedimentary rocks of Early Carboniferous to Early Permian Taungnyo Formation which is overlain by Moulmein Limestone. According to the lithologic characteristics and bed thickness, the Taungnyo Formation is divisible into three different subunits such as unit 1, 2 and 3. The stratigraphic succession is shown in Table (1).

Table 1 Stratigraphic succession of Taungnyo Formation.

	Age	Subunits	Dominant lithology
Taungnyo Formation	Early carboniferous to Early Permian	Unit 1	Thin to medium-bedded, coarse-grained sandstone interbedded with shale and mudstone
		Unit 2	Medium to thick-bedded, medium to coarse-grained sandstone interbedded with shale and mudstone, paddy mudstone, pebbly mudstone, pebbly sandstone, grit and conglomerate
		Unit 3	Thick-bedded to massive fine to medium-grained sandstone with shale and mudstone

Sedimentology

Facies analysis

There are nine lithofacies were differentiated on the basis of grain sizes, lithology and sedimentary structures. They are; (1) dark grey coloured thin-bedded to massive mudstone facies(Fig. 4), (2) dark grey coloured pebbly sandstone facies(Fig. 5), (3) dark grey coloured pebbly mudstone facies(Fig. 6), (4) conglomeratic gritty sandstone facies(Fig. 7), (5) gritty sandstone facies (Fig. 8), (6) medium to thick-bedded sandstone facies(Fig. 9), (7) thin to medium-bedded sandstone facies(Fig. 10), (8) fine-grained laminated sandstone with shale intercalated facies(Fig. 11), and (9) thin to medium-bedded sandstone and mudstone interbedded facies(Fig. 12).

Facies (1) Dark grey coloured thin-bedded to massive mudstone facies

Description

This facies is mainly consisting of grey to dark grey coloured mudstone. In some localities dark grey coloured mudstone consists of laminations (Fig.4). In some grey coloured mudstone abundant fossilized brachiopod shell as living position are well preserved. Sometime, pyrite occurs in this facies. This facies is vertically associated with thick-bedded to massive sandstone facies and fine-grained sandstone interbedded with shale facies and thin to medium-bedded sandstone. It is similar with Bouma's T_a division.

Interpretation

Dark grey coloured mudstone in this facies was deposited in low energy environment where the finer particles settle out of suspension (Reineck and Singh, 1980). The pyrite associated with dark grey shale display the reducing environment far enough from shore lines and has settle on the sea floor. This facies may be deposited in the basin floor of the lower fan environment.

Facies (2) Dark grey coloured pebbly sandstones facies

Description

This facies is composed mainly of medium to thick-bedded and massive dark grey coloured pebbly sandstones (Fig 5). Pebbles are subangular to well rounded, and sizes range from 1cm to 5cm in diameter. They are vertically associated with dark grey coloured sandstones, pebbly mudstones and gritty sandstones. This facies is similar to Bouma's T_a division.

Interpretation

The sandstone with pebbles is the deposit of high density turbidity current (Lowe, 1982). During river floods or slump and slide, main long distance transport took place debris flow and high concentration turbidity current (Walker, 1987). The observed character of this facies could be assigned to a gravelly high density turbidites. Pebbly wacke and massive sandstones are deposited near the mouth of the submarine canyon according to Stanley & Kelling, 1967.

Facies (3) Dark grey coloured pebbly mudstones facies

Description

This facies is consisted mainly of grey to dark grey coloured, fine-grained, thin to medium-bedded and thick-bedded to massive pebbly mudstones (Fig 7). This facies is vertically and laterally associated with thin to medium-bedded gritty sandstones, medium to thick-bedded dark coloured pebbly sandstones and thin to medium-bedded mudstone. Pebbles are subrounded to well rounded and size ranging from 1cm to 3cm in diameter. Some pebbly mudstone deposits possess large rock blocks with sizes ranging from about cobble to boulder. Clasts are randomly oriented. This facies is similar with Bouma's T_a division.

Interpretation

These pebbles are carried by rivers as bed load and moved on the muddy surface (Stanley, 1969) when increase rates of deposition during flood periods possibly cause to a trigger failure and moving masses downward on the very steep side to be an unstable area. The deposit shows

no internal evidence of slump (Walker, 1992) also observed in various continental margins may be the deposits of submarine canyon especially in the mouth (Gorsline, Emery, 1959). Thus, pebbly mudstone deposits represent high velocity plastic mass-flow downslope movement under the influence of gravity (Crowell, 1957).

Facies (4) Conglomeratic gritty sandstone facies

Description

This facies is mainly composed of white to light grey and buff to reddish brown colored, coarse to very coarse-grained, medium to thick-bedded conglomeratic gritty sandstones (Fig 8). Observed internal structure is only graded bedding. This facies is vertically associated with medium to thick-bedded sandstone and gritty sandstone. They are clast supported conglomerate and having different rock types and pebble size ranges from 0.3 cm to 10 cm in diameter.

Interpretation

This facies was deposited in the braided channel of upper fan. This interval is composed of graded conglomerates and sandstone resembling the graded stratified conglomerate facies of Walker (1975, 1977) and Hein & Walker, (1982). The coarser sediments may be restricted to thalweg channels. In such area (braided channels of upper fan), gravels and boulder may be deposited (Haner, 1971, Clearly & Condly, 1974). Therefore, the area of deposition of conglomerate may be upper fan valley and channel.

Facies (5) Gritty sandstone facies

Description

This facies is consisted of coarse-grained, white to light grey, light grey to buff colored, thin to medium and medium to thick-bedded gritty sandstones (Fig 9). This facies is vertically and laterally associated with conglomeratic gritty sandstones, medium to thick-bedded sandstone, dark grey coloured pebbly mudstones and shale. Recognized internal structures of this facies are lamination, mud drapes, graded bedding, small scale planar and trough cross bedding. This facies is similar with Bouma's T_{a-c} division.

Interpretation

The facies is assumed to be deposited in the braided channel of mid fan area. Gritty sandstone (show normal graded bedding) interval has been deposited from dispersed pressure and or turbulent suspension. Cross-stratification and flat-layered gritty sandstone and thick-bedded sandstone reflect traction sedimentation beneath high density flow (Reading, 1986). This facies is probably deposited in braided channel of middle fan submarine environment (Walker, 1982).

Facies (6) Medium to thick-bedded sandstone facies

Description

This facies is mainly composed of buff to light grey, medium to coarse-grained, medium to thick-bedded sandstone (Fig 10). In some locality, sandstones grade upward into massive character. It is vertically associated with thin to medium-bedded sandstones, gritty sandstone and buff to light grey shale. Laminations, ripples, low angle planar cross-bedding and mud drapes are observed as internal structures. This facies is similar to Bouma's T_{b-d} division.

Interpretation

Thick-bedded to massive sandstone can be recognized in many places and probably indicate channel filling and suggest the possibility of gradual lobe shifting with lobe margin replacing lobe center depositional environment of mid fan (Mutti, Ricci and Lucchi, 1972). Due to lateral shifting of a lobe in the mid fan region, it is possible that thickening and coarsening upward sequence are repeated (Mutti, Ricci and Lucchi, 1972).

Facies (7) Thin to medium-bedded sandstone facies

Description

This facies is mainly consist of buff to white coloured, fine to medium-grained and thin to medium-bedded sandstone (11). Laminations, planar cross beddings, and rip-up mud clasts and ripple boundings are observed as internal structures. It is vertically associated with medium to thick-bedded sandstones, fine-grained thin-bedded sandstone with shale intercalation and light grey to buff and reddish colored shale. This facies is similar with Bouma's T_{b-c} division.

Interpretation

Thining upward and finer grained are recorded, similar to fluvial deposits in abandoned channel of mid fan environment (Mutti, Ricci and Lucchi, 1972). Evenly laminated sand can be produced in the plane-bed phase of high flow regime (Reneick and Singh, 1980). This facies is deposited probably in braided channel of mid fan lobe.

Facies (8) Fine-grained laminated thin-bedded sandstone with shale intercalated facies

Description

This facies consists of buff to light grey color, very fine to fine-grained, thin-bedded sandstones and shale intercalation (Fig 12). Laminations, small scale ripples, ripped-up mud clasts and cross bedding are recognized in this facies. It is vertically associated with buff to light grey shale and thin to medium-bedded sandstone. This facies is similar with Bouma's base missing T_{c-d} division.

Interpretation

This facies would be deposited in the incised channel deposits of new supra fan lobe as proposed by Walker (1982). Low-density flows are generally thought to transport largely clay and silt-sized particles. Mixed sand-mud depositional system consists of well developed channel-levee systems and deposition lobes. Thin-bedded sandstone intercalated with poorly sorted clayey silt and mud layers are fan valley similar to channel levee of the lower fan environment.

Facies (9) Thin to medium-bedded sandstone and mudstone interbedded facies

Description

This facies is mainly composed of white to light grey colour, fine to medium-grained thin to medium-bedded sandstone with shale interbedding (Fig 13). Laminations and ripped-up mud clasts are recognized as sedimentary structures. This facies is vertically associated with mudstone facies, thin to medium-bedded sandstone facies, medium to thick-bedded sandstone facies and gritty sandstone facies). This facies is similar to Bouma's T_{b-d} interval.

Interpretation

Interbedding of mudstone and thin, fine-grained turbidites and thinning upward succession was compared with channel fills on the delta plain and was interpreted as the fills of submarine channel. This facies is characterized by monotonous alternation of sharp-based sandstones and interbedded mudstone of Walker (1992). The overbank flow from the channel contains fine silt and mud which spread out as a fine-grained turbidity current away from the channel to form a submarine channel levee.

According to Walker's (1978) facies models and sub marine fan environment, facies F2, F3 and F4 were deposited with high density grain flow in feeder channel of upper fan. Facies F5, F6, F7 and F9 were deposited in the incised channel, on channel margins or on levee and on lobe area of a channel margins in the mid-fan region. Facies F1 and F3 were deposited in basin floor and levee area of lower fan (Fig 13). There are three facies associations termed, conglomerate-gritty sandstone-sandstone-shale association, pebbly greywacke-pebbly mudstone-shale association and sandstone-shale association.



Figure 4 Lamination in dark grey colour thick-bedded to massive mudstone.



Figure 5 Nature of dark grey coloured pebbly sandstone facies showing various size of pebbles.



Figure 6 Rounded sandstone pebble embedded in thick-bedded to massive dark color pebbly mudstone.

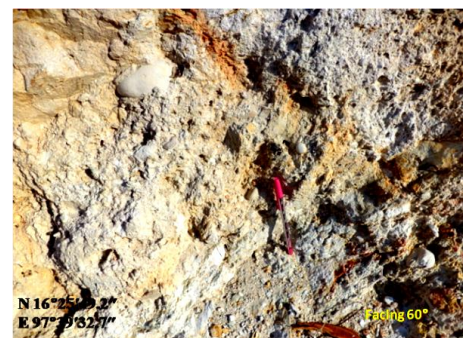


Figure 7 Nature of medium to thick-bedded conglomeratic gritty sandstone.

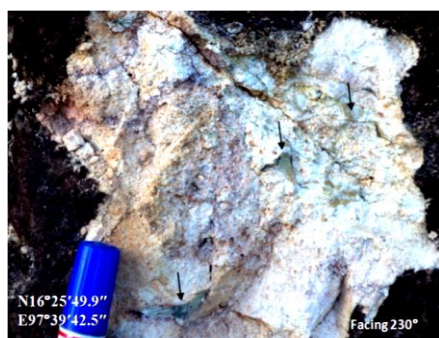


Figure 8 Mud clasts (arrows) in medium to thick-bedded gritty sandstone.



Figure 9 Nature of thick-bedded to massive sandstone facies.



Figure 10 Nature of medium to thick-bedded sandstone facies.



Figure 11 Nature of mudstone and thin-bedded sandstone intercalation facies.



Figure 12 Nature of thin to medium-bedded sandstone interbedded with mudstone facies.

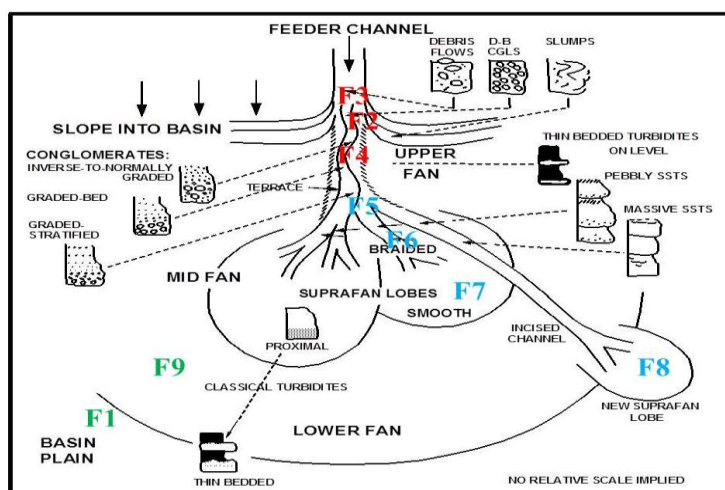


Figure 13 Facies analysis and depositional environment of the rocks of Taungnyo Formation in submarine fan model (Walker, 1978).

Sequence stratigraphy

Relative sea-level order and cycle

The study area is mainly composed of clastic sedimentary rocks of Early Carboniferous to Early Permian age. So duration of the deposition of Taungnyo Formation is about 90 million year by geological age. There are four orders of stratigraphic cycles are depicted (Duval et al., 1992) (Fig. 14). The continental encroachment cycle is defined by the very largest scale (> 50 million years). So, sea level cycle order of Taungnyo Formation is related to first order according to stratigraphic cycle. First-order continental encroachment cycles are considered to be controlled by tectono-eustasy, i.e. changes in ocean basin volume related to plate tectonic cycle (Pitman, 1978).

Sequence stratigraphic implication and general statement

The facies study of Taungnyo Formation revealed that the majority of depositional facies is sediment gravity flow in origin. This leads to conclude that Taungnyo Formation is accumulated as sand-rich and mixed sand-mud turbidite system. Although, the lower boundary of the Taungnyo Formation is not observed in the study area, the upper boundary with Moulmein limestone is an unconformity existed as a sequence boundary. In the Early Carboniferous to Early Permian age, the deposition of Taungnyo Formation taken place in the deep sea. During a maximum regression, the shore line moved basinward and the fluvial system placed on the exposed shelf area and most of the sediments were deposited in continental slope area. Moreover, the presence of high content of extrabasinal grains indicates that the deposition taken place in regressive phase (Zuffa, 1980) (Fig 15). This regression is also coincided with the global sea level drop (Fig 16).

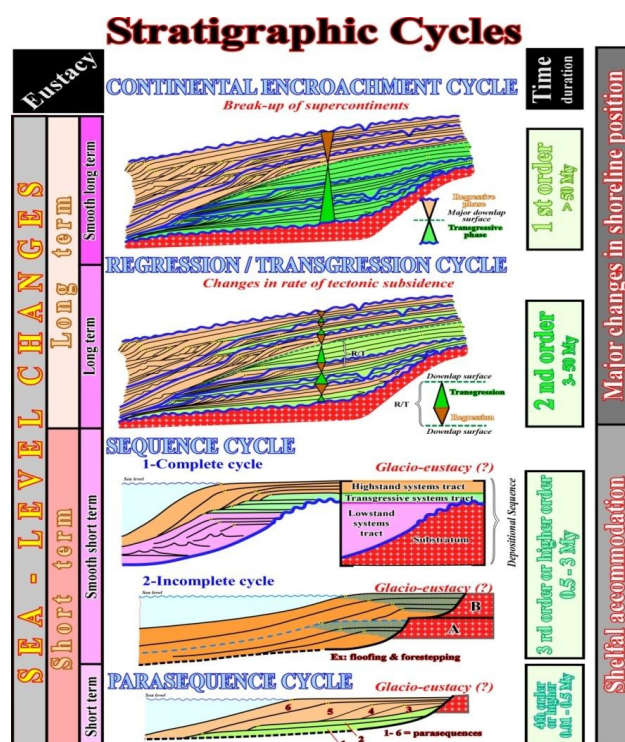


Figure 14 Hierarchy of stratigraphic cycle. (After Duval et. al., 1992)

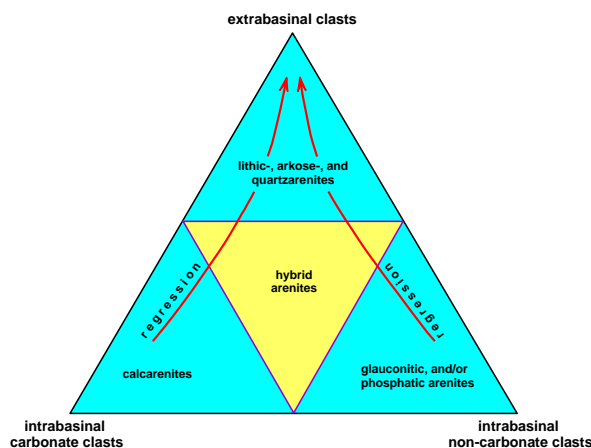


Figure 15 Triangle showing possible changes in the proportion of extra-basinal and intra-basinal, framework grain composition of sandstones due to changes in the relative sea level (after Zuffa, 1980).

Sand-rich fan and ramp systems are dominated by up-dip channel sand bodies pass down-dip into channelized fan lobes (Reading and Richards, 1994). The systems are largely dominated by massive to internally graded high-density turbidites, with only thin-bedded turbidites forming fan abandonment and fringe deposits. Mid fan deposits are dominated by abrupt changes from shale into thick, amalgamated sandstones.

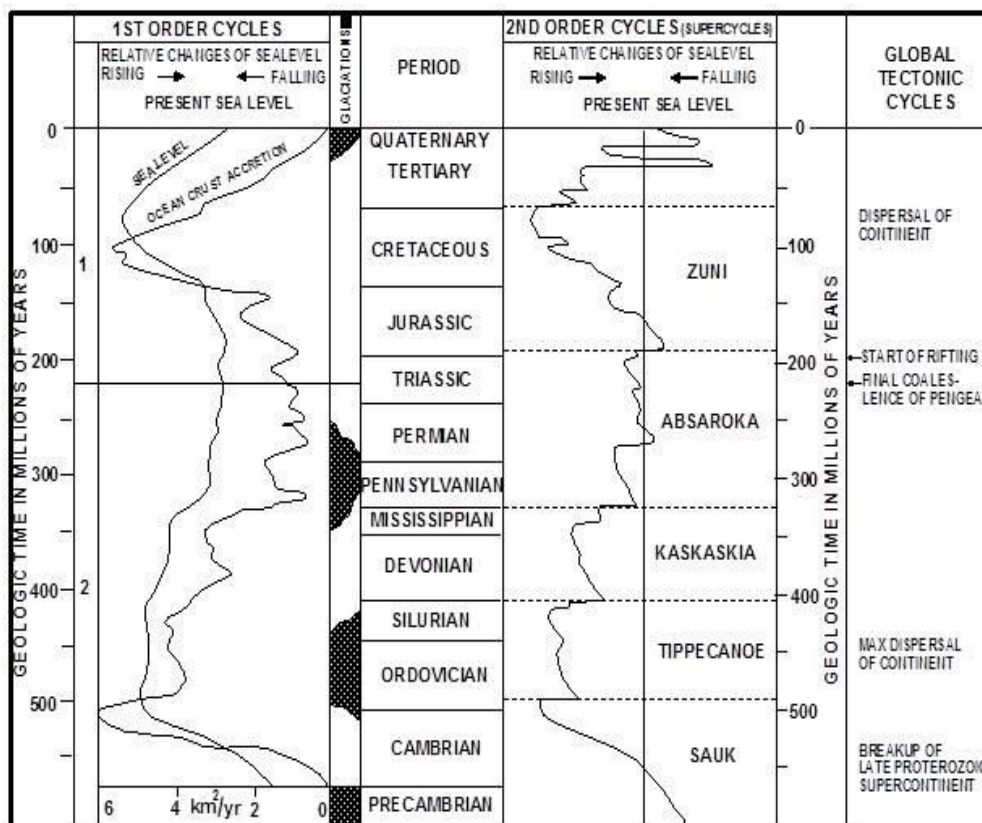


Figure 16 Eustatic sea level variation during the Phanerozoic (after Walker, 1992).

Lowstand System Tract

It is a basal system tract in a type 1 depositional sequence. In the stratigraphic sequence of the study area, Taungnyo Formation was deposited as submarine fan environment. The lower part of the formation is characterized by high velocity gravel rich deposits such as gritty sandstones and pebbly mudstone. It is a characteristic feature of LST deposits may result in low sinuosity (braded) channel. Gravel rich slope apron are derived from reworking, mass wasting and catastrophic submarine rock fall avalanches associated with high-angle slope and scarps. Sediments are often poorly sorted prior to deposition. These coarse-grained facies commonly interbedded with turbidite sandstone and mudstone (Surlyk, 1978; Ineson, 1989).

When relative sea-level falls at the offlap break, the river incise into the previously deposited topsets; the alluvial plain, coastal plain and/or shelf deposits of the previous sequence. These rework sediments and fluvial load from the hinterland are delivered directly onto the previous high stand clinoform slope. This is an inherently unstable situation, the sedimentation processes are dominated by large-scale slope failure resulting in bypass of the slope and deposition of submarine fan in the basin. These processes continue to dominate the sedimentary record while relative sea-level is falling and the river system is forced incise.

The rate of rises of relative sea-level is initially low and together with the limited topset area of the prograding system. This will be outpaced by sediments supply next system tract (transgression) will be formed (Fig 17).

Transgressive System Tract

It is deposited during relative sea-level rise when topset accommodation volume is increasing faster than the rate of sediment supply. The transgressive system tract passes distally into a condensed section characterized by extremely low rates of deposition and the development of condensed facies such as glauconitic, organic rich and/or phosphatic shales or pelagic carbonates. Highstand system tract of Taungnyo Formation in this study area is characterized by high-velocity turbulence gravity flow deposits as pebbly mudstone. The depositional product of these systems reflects a wide variety of mass flow processes and includes non-channelized chaotic boulder/cobble beds and intraformational rotational slump of fine-grained interbedded sandstones and mudstones with exotic clasts.

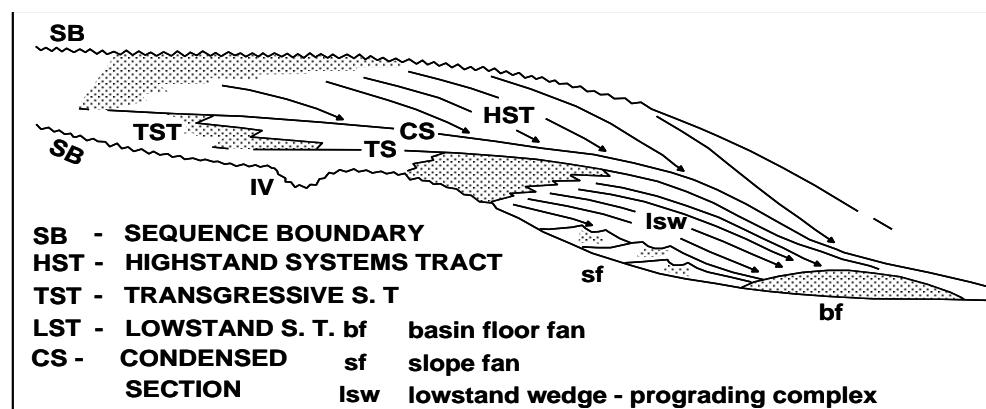


Figure 17 Submarine fans in a sequence stratigraphic context (After Walker, 1992).

Acknowledgements

We are deeply thankful to Professor Dr Aung Myat Kyaw Sein, Rector, University of Mawlamyine for his kind permission to carry out this research. I sincerely thanks to Dr Yin Yin Aye, Professor and Head of Geology Department, University of Mawlamyine for her kind permission of our researchworks.

References

- Bouma, A.H, (1962) *Sedimentology of some flysch deposits: A graphical approach to facies interpretation*. Elsevier, Amsterdam, 168 p.
- Brunnschweiler, R.O., (1970) *Contributions to the post-Silurian geology of Burma (Northern Shan State & Karen State)*; Geol. Soc. Australia.
- Emery, D. and Myers, K. J. (1996) *Sequence stratigraphy*, editors: Oxford, Blackwell Science, 297 p.
- Galloway, W.E. (1989) Genetic stratigraphic sequences in basin analysis: architecture and genesis of flooding surface bounded depositional units. *Am. Assoc. Petrol. Geol. Bull.*, 73, 125-142.
- Kolla, V. and Perimutter, M.A. (1993) Timing of turbidite sedimentation on the Mississippi fan. *Am. Assoc. Petrol. Geol. Bull.*, 77, 1129-1141.
- Kyaw Min., (1997) *Geology of Taungnyo Area, Mawlamyine, Mudon and Kyaikmayaw Townships*. M.Sc. Thesis. University of Mawlamyine.
- Leicester, P., (1930) *Geology of Amherst district* Rec-Geol. Surv. India, V.63, Pt.1 (Dir Gen. Rep).
- Lowe, D.R. (1979) Sediment gravity flows: their classification and some problems of application to natural flows and deposits. In: *Geology of Continental Slopes* (ed. by K.J. Doyle & O.H. Pilkey). Special Publication, Society of Economic Paleontologists and Mineralogists, Tulsa, 27, 75-82.
- Lowe, D.R. (1982) Sediment gravity flows II: depositional models with special reference to the deposits of high density turbidity currents. *J. Sediment. Petrol.*, 52, 279-297.
- Middleton, G.V. and Hampton, M.A. (1973) Sediment gravity flows: mechanics of flow and deposition. In: *Turbidites and Deepwater Sedimentation* (ed. by G.V. Middleton & A.H. Bouma). Society of Economic Paleontologists and Mineralogists, Los Angeles, pp. 1-38.
- Posamentier, H.W. and Vail, P.R. (1988) Eustatic controls on clastic deposition I. – sequence and systems tract. Models. In: *Sea-level Changes: An Integrated Approach* (ed. by C.K. Wilgus, B.S. Hastings, C.G. St. C. Kendall, H.W. Posamentier, C.A. Ross & J.C. Van Wagoner). Special Publications, Society of Economic Paleontologists and Mineralogists, Tulsa, USA, 42, 109-124.
- Reading, H.G., (1981) *Sedimentary Environments and Facies*: Oxford Blackwell Sci- Publications.
- Reading, H.G. and Richards, M. (1994) Turbidite systems in deepwater basin margins classified by grain-size and feeder system. *AAPG Bulletin* 78, 792 - 822.
- Reineck, H.E., and Singh, I.B., (1980) *Depositional Sedimentary Environment*: Springer- Verlag, N.Y.
- Time and Facies. American Association of Petroleum Geologists Methods in Exploration Series, Tulsa, 7, 55 pp.
- Walker, R.G. (1978) Deep water sandstone facies and ancient submarine fans: models for exploration for stratigraphic traps. *Am. Assoc. Petrol Geol. Bull.*, 62, 932-966.
- Walker, R.G. (1992) Turbidites and submarine fans. In: Walker, R.G. & James, N.P. (eds) *Facies models – response to sea-level change*. Geological Association of Canada, 239 – 263
- Zuffa, G.G. (1980) Hybrid arenities: their composition and classification. *Journal of Sedimentary Research* 50, 21-29.

INTERPLAY OF CEMENTATION, MECHANICAL AND CHEMICAL COMPACTION IN EARLY SILURIAN PHACOIDAL (NODULAR) LIMESTONES OF THE PINDAYA RANGE, SOUTHERN SHAN STATE

Yin Min Htwe^{*}

Abstract

The phacoidal (nodular) limestones of early Silurian age were studied in three selected areas on the Pindaya Range of Southern Shan State. In Yegyanzin area, the limestones are entirely crinoidal; the Linwe area are red crinoidal limestones, grey ostracoda limestones and lime mudstones; while the Thayetpya area consists of grey ostracoda limestones and lime mudstones. The limestones commonly show evidence of early lithification taken place near the sediment/water interface.

Petrographic observation of both mud and grain-supported facies being rich in crinoids, brachiopods, trilobites, thin-shelled bivalves enabled the reconstruction of the diagenetic evolution. Some layers, underwent a phase of early lithification, acquired a rigid framework that prevented deformation and rearrangement of grains during later burial. In the mud-supported facies, the effects of subsequent mechanical and chemical compaction are easily recognizable. Mechanical compaction includes overburden pressure, flattened burrows, fossil breakage, shrinkage pores and transformation from wackestone to packstone fabrics. The response to chemical compaction varied with texture; grain-supported sediments developed fitted fabrics whereas in mud-supported sediments stylolitic seams were generated. As a result of these diagenetic processes, laterally extensive stylolites would have developed in these phacoidal limestones.

Introduction

This paper describes compaction mechanisms in limestones and relationships among cementation, mechanical compaction, and chemical compaction are considered as the complex diagenetic history of the purple and grey phacoidal (nodular) limestones of the early Silurian age. Petrological observations of both mud-supported facies (Thayetpya area) and grain-supported facies (Yegyanzin and lower parts of Linwe area) which are rich in thin-shelled bivalves, crinoid and brachiopod enabled reconstruction of the diagenetic evolution. Difference in the original composition and texture of sediment certainly influence the development of burial diagenetic features. To clarify the effects of these differences, I focused on particular lithologies composed mainly of one kind of skeletal grain for an initial comparative study of compacted and uncompacted textures. The location map of the present study area is shown in Figure (1).

^{*} Dr, Professor and Head, Department of Geology, Maubin University

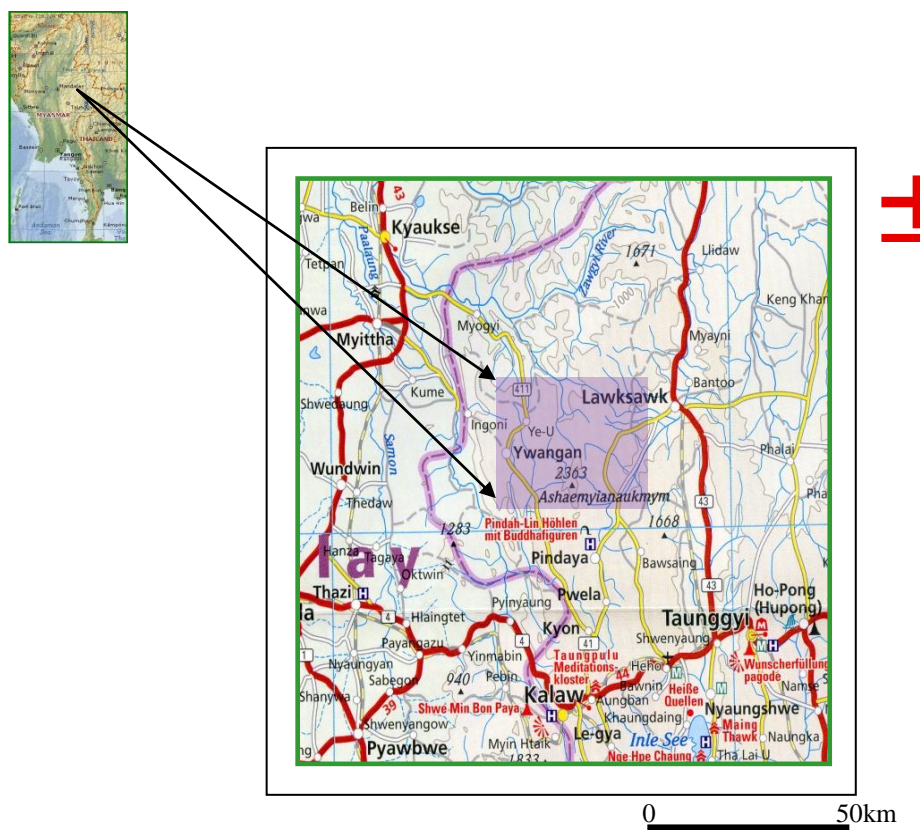


Figure 1 Location map of the study area

Materials and Methods

The petrographic study was based on nearly 90 samples obtained from the three studied areas. In the phacoidal limestone, only indirect method can be used because direct measurement of deformation objects of known original size and shape is not possible. Two parameters of carbonate sediments have been used: percentage of clay and percentage of grains which are not modified by diagenesis. On the basis of these considerations, Ricken (1986) mathematically related the percentage of compaction, K , rock porosity, n , carbonate content of the rock, C , and the standardized non carbonate fraction NC_d (i.e., the clay content in the original uncompacted sediments).

Lithofacies Description

Crinoidal Limestones

These crinoidal limestones can be observed in the Yegyanzin area. They are pink to purple, medium-bedded, argillaceous seam in some horizon, thickening-upward sequence (Fig. 3a). They have sand-sized crinoid fragments, with lesser amounts of brachiopods, bryozoans, trilobites, and other allochem. Two types of crinoidal limestones can be distinguished: crinoid-dominated zones, with syntaxial overgrowth cements and rim cements and few pressure solution feature: less crinoid-rich rocks which are lack of substantial cementation. In the first type, syntaxial overgrowths on crinoids are abundance and minor sparry calcite cement is seen on microcrystalline substrates. In the second type, cementation is minor, both crinoidal and other allochem grains are fitted in an interlocking pressure solution mosaic.

Phacoidal Limestones

These phacoidal limestones are encountered in the Linwe area. The limestones are purple colour phacoidal limestone at lower horizon and grey colour phacoidal limestone at upper horizon. Phacoidal limestone (0-25 m thick units) consists of medium-bedded, purple bioclastic wackestone and mudstone with some bioclastic packstone (Fig. 3b). Fossils are very poorly sorted and are highly diverse. The packstone contain 5 to 30 percent fine-grained matrix which reduces visible pore spaces. Cementation on brachiopod fragment mask in matrix indicates early lithification, acquired a rigid framework that prevented deformation and rearrangement of grains during later burial.

Bioclasts-bearing limemudstones

These bioclasts-bearing lime mudstones are observed in the Thayetpya area. The limestones are grey, medium-bedded limestones contains less than 10 percent allochems, most of which are ostracods and large brachiopod and trilobite, slightly phacoidal appearance (Fig. 3c). The bioclasts are sometimes attained their size as large as 1 mm and these fragments are cemented by bladed calcite.

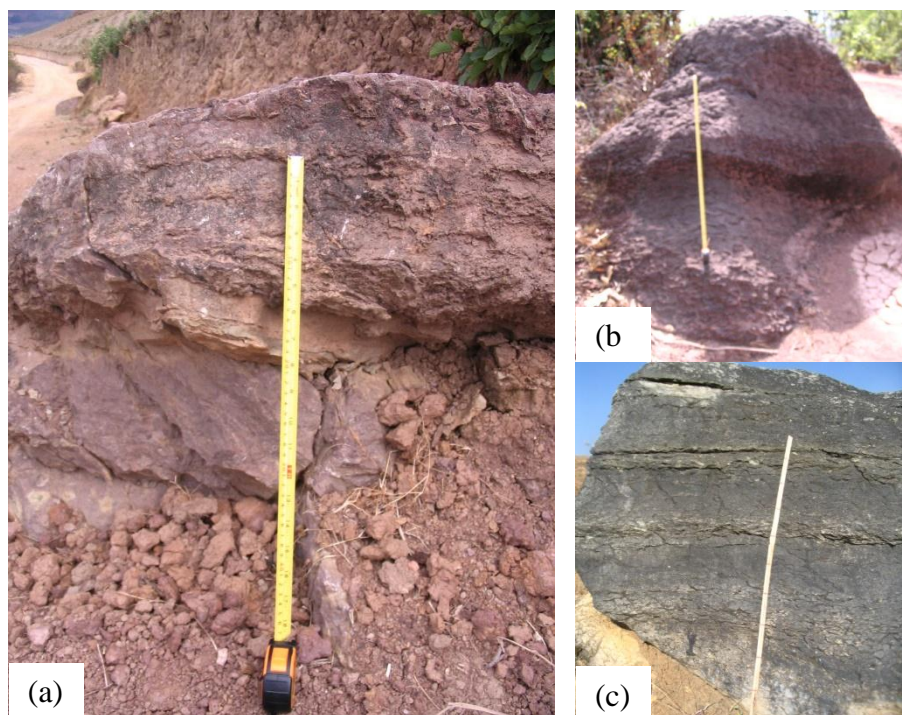


Figure 3 Outcrops of the Silurian limestone from (a) Yegyanzin area (b) Linwe area and (c) Thayetpya area

Discussion

There are three fundamental styles of diagenesis in the phacoidal limestones: cementation, mechanical compaction and chemical compaction.

Cementation

Early cementation affected on bioclastic grains is recognized. The type of cement depends particularly on Mg/Ca ratio and salinity of the solutions. In the crinoidal grainstone, early cements consist of clearly recognizable syntaxial overgrowths and rim cement (Fig. 4). In

the phacoidal wackestone and grey bioclastic mudstone, early cements are bladed cement on brachiopod fragments. A growing body of evidence obtained by petrographic study suggests that much of the cement in ancient peritidal, shallow-marine, and platform-margin limestone may also have formed during deep-burial diagenesis (Sam Bogg, 2009). Cementation can take place when pore fluids are supersaturated with respect to the cement phase and there are no kinetic factors inhibiting the precipitation.

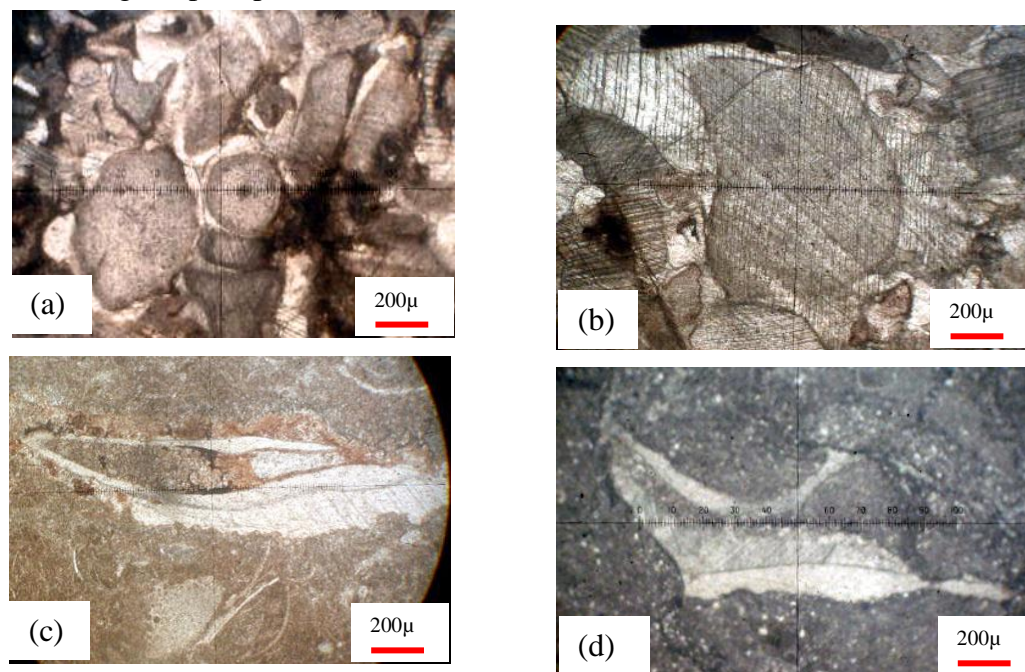


Figure 4 Types of cements (a) rim cement (b) syntaxial overgrowth (c) bladed cement (d) bladed cement within nodule

Effects of Mechanical compaction

Physical compaction may affect loss of porosity and numerous other effects on sediments. Most of the mechanical compaction is fossil breakage and wackestone to packstone. Breakage of the most part is readily apparent and separated by fine sediments (Fig. 5). The extent of porosity loss and thinning of bed and other mechanical compaction effects is related to the degree of early cementation in the sediments. If extensive intergranular cementation takes place in either the seafloor or shallow meteoric diagenetic environments, compaction effects are moderated (Moore, 2001 in Sam Bogg, p.432). It is assumed that sand-size crinoid fragments floating in mud, that is wackestones, have been forced together so that grains are in contact and intergranular spaces filled with mud; a packstone had been produced simply by mechanical compaction (Fig. 5).

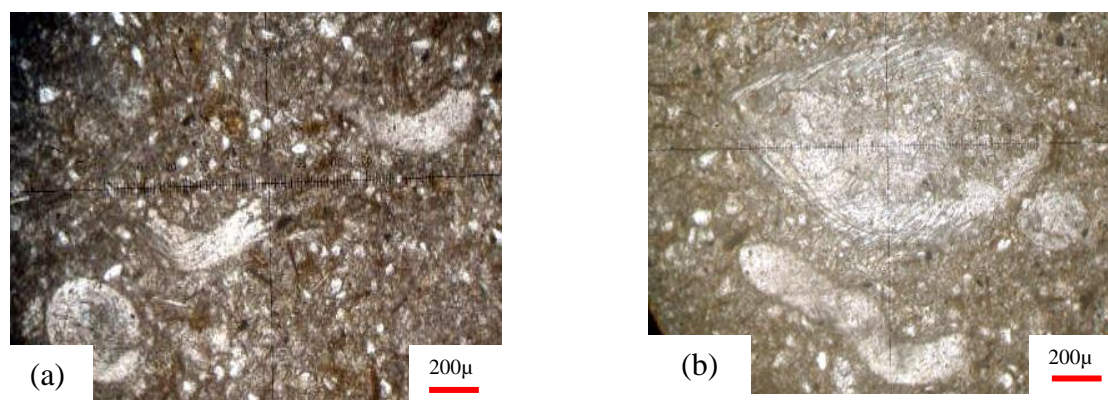


Figure 5 Mechanical compaction (a) fossil breakage (b) fossil twist

Effects of Chemical compaction

The most obvious chemical compaction in the crinoidal limestones of Yegyanzin area is stylolites, solution seams and grain-to-grain solution. Grain-to-grain pressure solution at the contact points of individual grains can result in the formation of interpenetrating or sutured contacts (Fig. 6).

Creation of these features is accompanied by reduction in bulk volume of the rocks and subsequently loss in porosity. Pressure solution begins after mechanical compaction is essentially complete and a stable grain framework has been created. Load or tectonic stress transmitted to grain-to-grain contact points or surfaces causes dissolution at the contact. Solid calcium carbonate is changed to liquid creating a solution film. Calcium and bicarbonate ions released into solution move away from the stressed contact point or surface by solution transfer toward adjacent areas of pore space.

Stylolites are serrated boundaries between units; the boundaries usually have an accumulation of clay, iron oxides, and/or organic matter. In general, solution seams are smooth, undulating boundaries between units, lacking the sutured form of stylolite. They also have an accumulation of clay or other material. These three types of pressure solution features are stylolite, wispy seam and solution seam. Stylolite are sutured surface of interpenetrating columns that are laterally continuous surface and amplitude ≥ 1 cm. Wispy seam is converging and diverging sutured to undulose surfaces that are laterally discontinuous and insoluble residue accumulation along individual surfaces ≤ 1 mm. Solution seam is undulose surfaces, laterally continuous and insoluble accumulate.

The important of “fitted fabric” texture as a major category of pressure solution features was recognized by Logan and Semeniuk (1976). Fitted fabric pressure solution differs from pressure solution along stylolites and solution seams in that fitted fabric dissolution occurs pervasively throughout a zone affecting all grains whereas stylolites and solution seams are planar features.

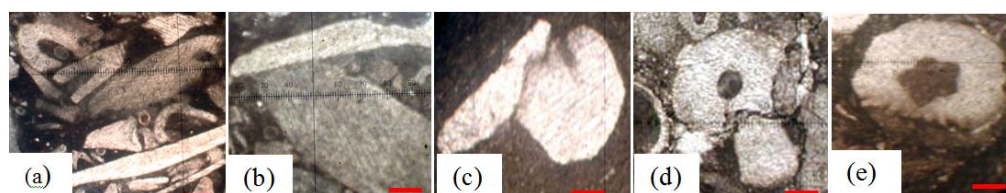


Figure 6 Grain to grain solution (a) point contact (b) line contact (c,d) concavo-convex contact (e) suture contact, scale bar = 100 μ m

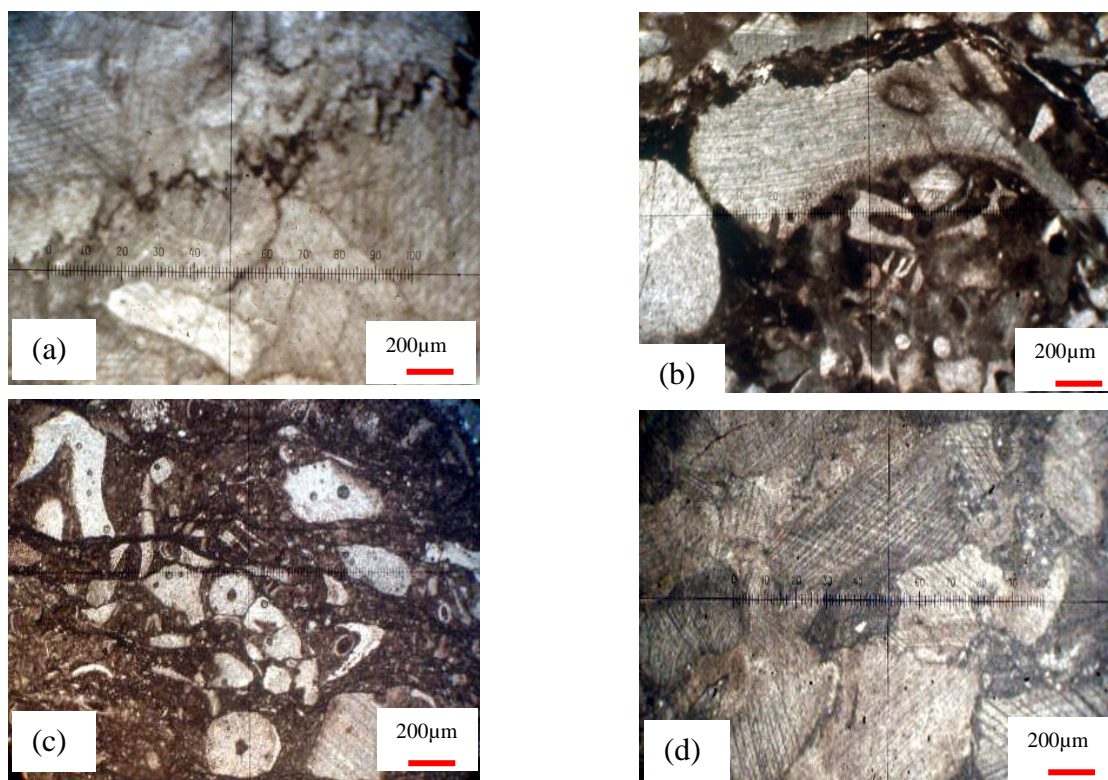


Figure 7 Kinds of pressure solution features (a) stylolite (b) wispy seam (c) solution seam (d) fitted fabric

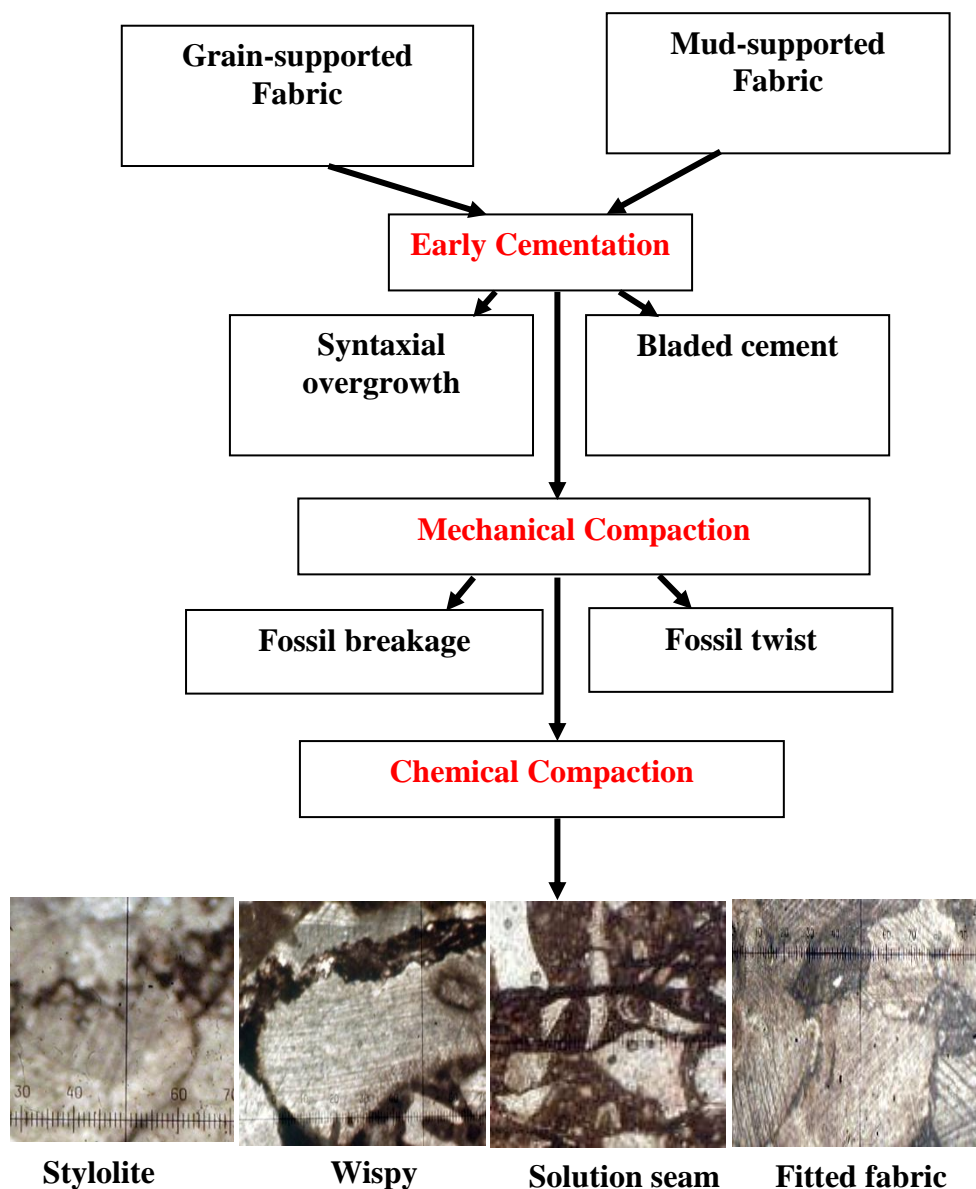
Results

The Interplay among the sedimentation, bioturbation and cementation reached the highest complexity in the phacoidal limestone; burrowing was active and changed in sedimentation style in crinoidal limestones, and sedimentation may have ceased for long enough to allow complete cementation on bioclasts in phacoidal limestones and bioclastic lime mudstone.

Clays disseminated in carbonate mud would not become organized into anastomosing microstylolite-like seams simply by physical compaction. These are a product of pressure dissolution of carbonate. Organic layers resulting from soft-sediment compaction might initiate chemical compaction during and after cementation resulting stylolites. Stylolitization would proceed further with increasing depth of burial.

In the grainstones, early cements consist of clearly recognizable syntaxial overgrowths and rim cement. In the wackestones, early cements are obviously larger bioclastic fragments. Besides, stylolite and fitted fabric are common in crinoidal grainstones whereas wispy seam and solution seam are observed in packstone-wackestone.

Some layers, underwent a phase of early lithification, acquired a rigid framework that prevented deformation and rearrangement of grains during later burial.



Conclusion

The phacoidal (nodular) limestones of early Silurian age were studied in three selected areas on the Pindaya Range of Southern Shan State. In Yegyanzin area, the limestones are entirely crinoidal; the Linwe area are red crinoidal limestones, grey ostracoda limestones and lime mudstones; while the Thayetpya area consists of grey ostracoda limestones and lime mudstones. The limestones commonly show evidence of early lithification taken place near the sediment/water interface.

Petrographic observation of both mud and grain-supported facies being rich in crinoids, brachiopods, trilobites, thin-shelled bivalves enabled the reconstruction of the diagenetic evolution. Some layers, underwent a phase of early lithification, acquired a rigid framework that prevented deformation and rearrangement of grains during later burial. In the mud-supported facies, the effects of subsequent mechanical and chemical compaction are easily recognizable. Mechanical compaction includes overburden pressure, flattened burrows, fossil breakage,

shrinkage pores and transformation from wackestone to packstone fabrics. The response to chemical compaction varied with texture; grain-supported sediments developed fitted fabrics whereas in mud-supported sediments stylolitic seams were generated. As a result of these diagenetic processes, laterally extensive stylolites would have developed in these phacoidal limestones.

Acknowledgements

I would like to express thanks to Dr Aung Kyaw, Rector of Maubin University, Dr Win Myint Thein, Pro-rector and Dr Lwin Lwin Myint, Pro-rector, Maubin University for their kind permission and advice to carry out this research work.

References

- Adams, A.E., & MacKenzie, W.S., (1998), *A Colour Atlas of Carbonate Sediments and Rocks under the Microscope*, Manson Publishing, London, 180p.
- Boggs, S., Jr., (2009), *Petrology of Sedimentary rocks*, 2nd ed., Cambridge University press, p. 1- 600.
- Buxton, T.M. & Sibley, D.F., (1981), Pressure solution features in a shallow buried Limestone. *Journal of Sedimentary Petrology*, v.51, p.19-26.
- Myint Lwin Thein, (1973), The Lower Paleozoic Stratigraphy of Western Part of the Southern Shan State, Burma: *Geological Society of Malaysia*, Bull. 6, p.143-163.
- Richen, W., (1986), Diagenetic bedding: a model for marl-limestone alternation; *Lecture Notes in Earth Sciences*, v.6, Berlin, Springer-Verlag, 210p.
- Richen, W., (1987), The Carbonate Compaction Law: a new tool: *Sedimentology*, v.34, p.571-584.
- Shinn, E.A. & Robbin, D.M., (1983), Mechanical and Chemical Compaction in fine-grained shallow-water limestones, *Journal of Sedimentary Petrology* v.53, p.595-618.
- Wanless, H.R., (1979), Limestone response to stress: pressure solution and dolomitization. *Journal of Sedimentary Petrology*, v.49, p.437-462.
- Scholle, P.A. & Ulmer-Scholle, D.S., (2003), *A Colour Guide to the Petrography of Carbonate Rocks*, AAPG, Memoir 77, 474p.
- Yin Min Htwe, (2011), *Sedimentology of the Silurian Rocks of the Pindaya and Bawsaing Ranges, Shan State (south)*, PhD Thesis, University of Yangon (Unpublished), 174p.

SEQUENCE STRATIGRAPHY OF THE OLIGOCENE LIMESTONES EXPOSED AT HTONDAUNG AREA, THAYET TOWNSHIP, MAGWAY REGION, MYANMAR

Mi Mi Ko¹, Tin Aung Myint & Maung Maung

Abstract

The study area is situated in Thayet Township. The present work mainly emphasizes on the limestone bodies in the Okhmintaung Formation of the area. The carbonate rocks exposed at Thayet area contains stacked depositional cycles consisting of characteristic succession of sedimentary facies and facies associations. The stratigraphic succession starts on delta abandonment phases together with an erosional surface at the base of facies, *Grobigerina* packstone-grainstone facies in the lower part. Delta abandonment phase is indicated by the occurrence of swamp development and the subsequent formation of coal at the base of Limestone. Through the succession, repetitive of inner, middle and outer ramp facies associations are present, and then they are followed by an alternation of shale and sandstone facies at the top. The term "cycle boundary" was used to determine the fourth-order cycles. The individual cycles were numbered 1-5 and the same numbers were used for their respective boundaries. The fourth-order cycles (parasequence sets) can be recognized by environmental changes within section; by the graduality of the change in fauna and the co-occurrence of normal marine perforates and platform-interior imperforates, and a relatively large amount of planktonic foraminifera. The first level or base level 'C-1' of the Limestone shows the shallowing upward, start with basinal blue-grey shale, Globigerinid wackestone, Globigerinid packstone-grainstone, or *Lepidocyclina* packstone. The outer ramp sediment shifted just above outer ramp (basinal shale) sediment within the section. The cycle 'C-2' observes an outer to mid-ramp community of planktonic fauna in the lower part, and a gradual shift from a planktonic dominated fauna toward perforate larger benthic one of the mid-ramp in the upper. The cycle 'C-3' of the lower part consists of the retrogradation of the facies belts (from mid-ramp sediment to algal shoal of the inner ramp) marks the following TST aggradation and slow progradation of the corresponding HST. The cycle 'C-4' consists of bluish-gray shale with high amount of planktonic foraminifera (*Globigerina* sp., *Globotruncana* sp., *Nodosaria* sp.). The upper shows inner to mid-ramp sediments containing a rich perforate foraminifera (*Lepidocyclina* sp., *Operculina* sp.) packstone-grainstone containing coal and gypsum bearing shale. The base of the 'C-5' consists of yellowish brown calcareous shale with lime bands. The upper part shows middle to inner ramp sediments having rich in benthonic foraminiferal assemblages.

Keywords: carbonate rock, depositional cycles, ramp facies associations

Introduction

Location and Accessibility

The study area is located at about 4 miles southwest of Thayet Township. It lies between North Latitude 19° 15' and 19° 18' and East Longitude 95° 7' and 95° 11' within the one inch-map of 85 M/3. Being situated on the western bank of Ayeyarwady River, study area is accessible throughout the year. Location maps of Thayet area is shown in Figs. (1a).

¹ Dr, Associate Professor, Department of Geology, Mawlamyine University

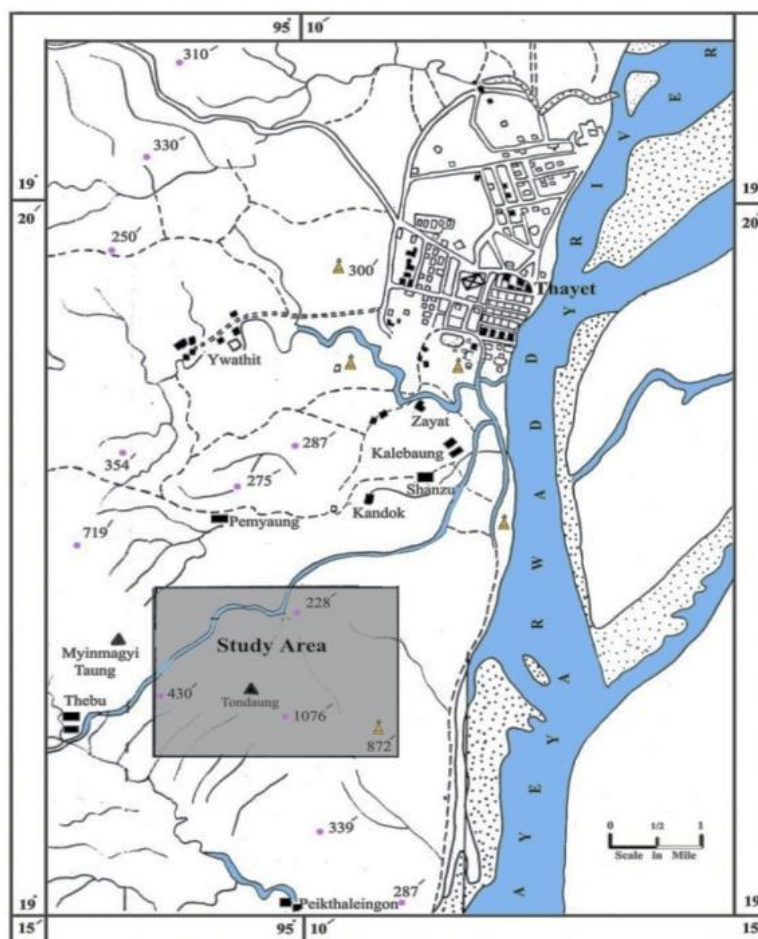


Figure 1 (a) Location map of the Thayet-Tondaung area.

Regional Geologic Settings

The present area is located in the Central Lowland. The Thayet areas near 19° 30' North Latitude have most of the stratigraphic and structural characters of both the Central Basin and Pyay Embayment Basin. So, it is interpreted here that the Thayetmyo area, including the study area, may be regarded as a transitional area between the Central Basin and Pyay Embayment Basin belonging to the Central Cenozoic Belt consisting mainly of the Tertiary sediments (Aung Khin and Kyaw Win, 1969). More specifically, Thayet area and its environs are mainly composed of the rocks of the Lower Pegu Group (Oligocene), the Upper Pegu Group (Miocene) and Irrawaddy Formation (Pontian to Pliocene). As a result, the present study is mainly emphasized on the limestone bodies (carbonate rocks) of the area. It is exposed along the NW-SE striking in the Okhmintaung Formation. The stratigraphic units generally dip east with local variations near folds and faults. Structurally, NW-SE trending anticlinal and synclinal structures are dissected by faults. Lime hill is about one mile long in NW- SE direction and about a quarter mile wide, forming as an anticlinal structure plunging toward both NW and SE direction.

The core of anticline is occupied by the limestones and interbedded shales of the Okhmintaung Formation, forming the elevated part on the western bank of the Ayeyarwady River (Fig.1b & 1c).



Figure 1 (b) Land-sat image of the study area. (Source: Google Earth, 2008)

Methods of Study

The geology map is chiefly based on the work of the previous workers and one-million-scale map, and modification has been done wherever necessary. Besides, rock samples were taken for the purpose of making thin sections. Photographs and sketches were taken wherever necessary. Sequence stratigraphy of the limestone outcrops were measured in the field.

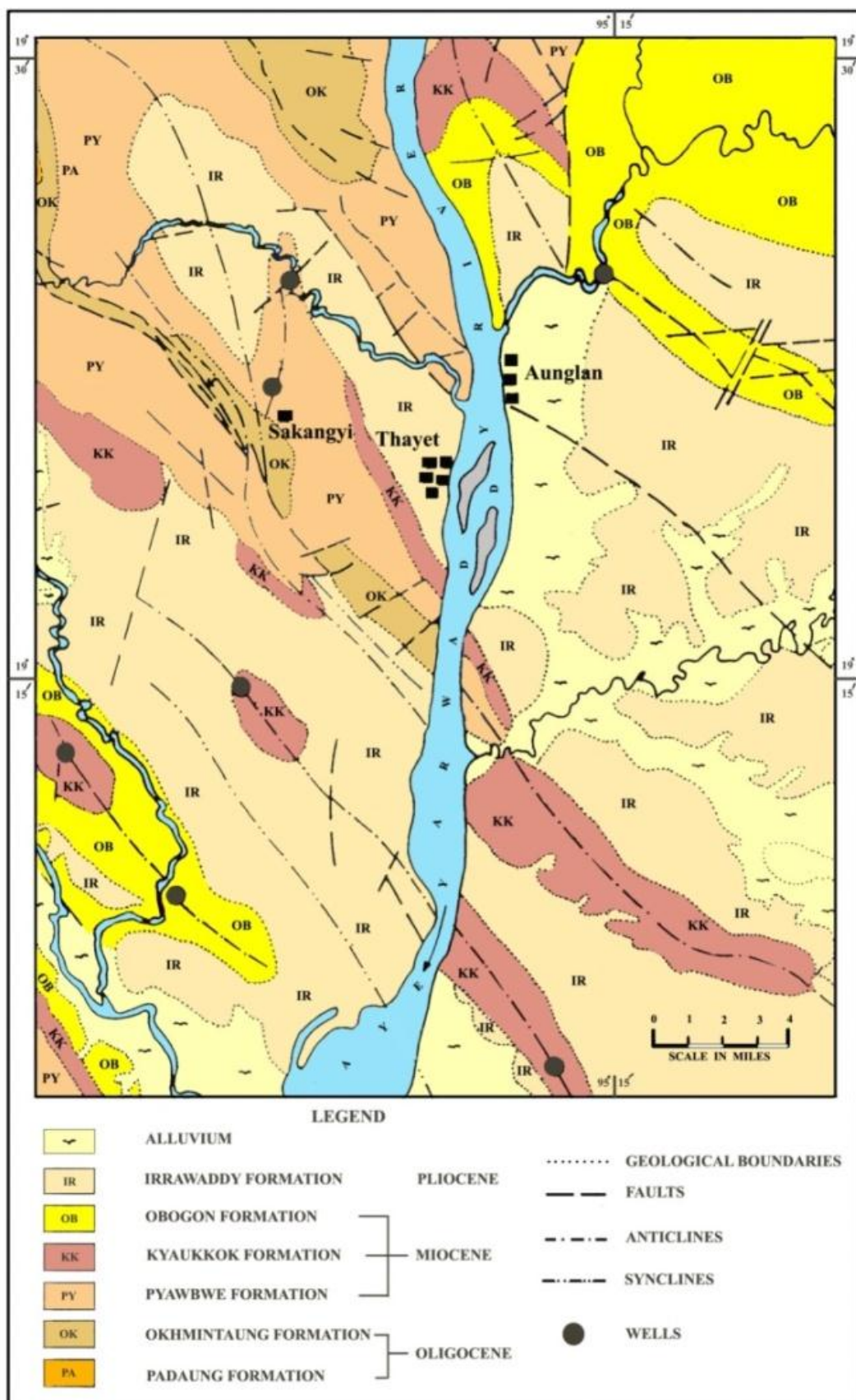


Figure 1 (c) Geological map of the Thayet-Tondaung area and its environs. (Modified from Chit Saing, 2003)

Result

Depositional Sequence and Cycle Boundaries and Transgressive Surfaces

In the present Tondaung area, the stratigraphic succession starts on delta abandonment phases together with an erosional surface at the base of facies *Grobigerina* packstone-grainstone facies in the lower part. Delta abandonment phase is indicated by the occurrence of swamp development and the subsequent formation of coal at the base of Tondaung Limestone (Fig.2).



Figure 2 (a-b) Yellowish gray shale containing coal layers exposed in Thayet area.

These carbonate facies are interrupted by fluvial incursion, based on the detailed measurements. Coal bearing shale beds indicate the shallow condition. The lower part of the succession indicates a marine transgression from fluvial through a tidal or estuarine to ramp environment with some fluctuations. Besides, foraminiferal fossils recorded from facies associations also support to confirm the marine transgression. The individual cycles were numbered 1-5 and it is here to say that the same numbers were used for their respective boundaries. Sequence boundaries in the Tondaung, are thought to be placed at the contact between progradation parasequence sets (Highstands) and retrogradational parasequence sets (Transgressive). It is apparent that the sudden superposition of transgressive beds upon prograding one is thought to represent a cycle boundary (CB). Based on this fact, in the Tondaung succession, the cycle boundaries are marked on the top surface of the shallowing and thickening upward cycle.. The indicator for the evidence of subaerial exposure is the presence of hardground surfaces (Fig.3).



Figure 3 Photomicrographs of Globigerinid Wackestone containing *Globigerinia* and planar hardground with irregular surface probably formed by dissolution.

Features related to Transgression

Most cycle boundaries coinciding with transgressive surfaces especially occur at C1, C2, & C5 in which hard ground surfaces are developed. In the field, these surfaces can be easily visible by the presence of iron-stained surface and ionized bands (Fig.4a). Several of these surfaces combined with sequence display a horizon of intense burrowings suggesting the transgression period (Fig.4b). The edges of the burrows are well defined and sharp, suggesting a firm substrate.

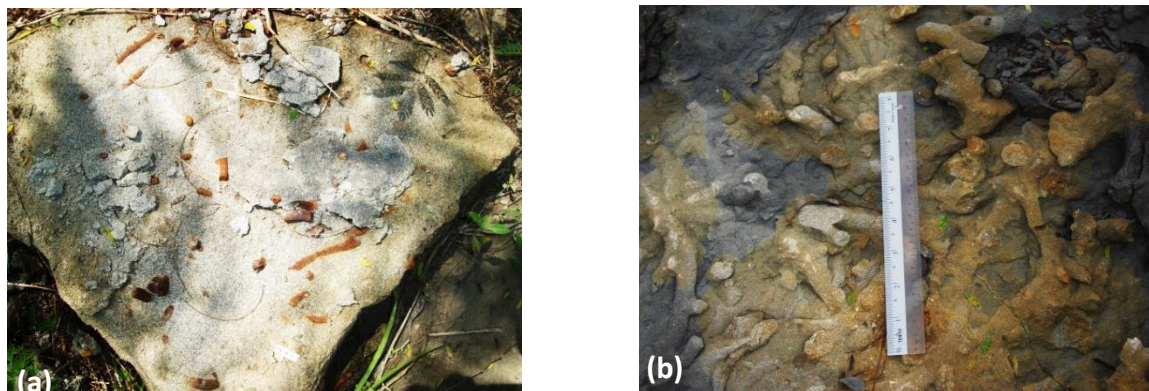


Figure 4 (a) Ionized bands and iron stain surface and (b) Intense burrowing in Oligocene Limestone.

Maximum Flooding Surface (mfs)

The marine flooding surface represent the time of maximum flooding on the ramp and is marked by shift from retrogradational to aggradational or progradational parasequence sets (Zwart et.al. 1994). The mfs coincides with maximum abundance of fossils (intense bioturbation) (Vail et al.1977). It is difficult to locate the position of mfs exactly within measured section. In this study, mfss have to be probably defined by using the changes in lithologic unit or in facies, the presence of intense bioturbation (Fig.5a,b), and transgression pointing at the beginning of progradation.

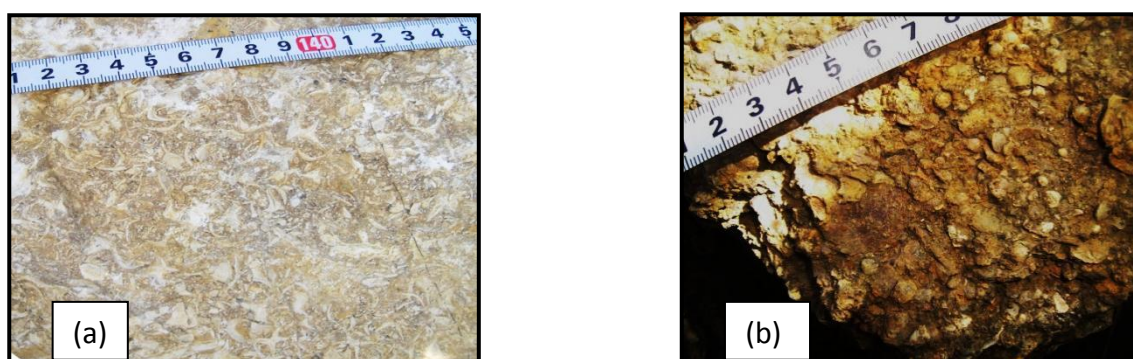


Figure 5 (a) Shell fragments in creamy limestone and (b) Pelecypods in buff color silty limestone at Tondaung mine, indicating maximum flooding surface.

System Tracts

Lack of Lowstand System Tracts

The lowstand systems tract may include two distinct parts, the lowstand fan (basin-floor submarine fan) and the lowstand wedge (Tucker et al.1993). In the present area, these features are missing or absent, so it is thought to be considered as lacking in lowstand system tract.

Transgressive System Tracts (TST)

It is characterized by retrogradational parasequence (deepening trend) of the ramp. It is underlain by the transgressive surface and overlain by the maximum flooding surface. In another way, the TST is bounded at the base by transgressive surface display features attributable to subaerial exposure (Fig.6). The basal surface of the TST is a marine flooding surface with the indication of abrupt deepening (Burchette et.al. 1990).

Highstand System Tract (HST)

Highstand Systems Tracts are defined by either aggradational or progradational parasequence sets. The mfs is the basal surface of the system tract (See also Fig.6). The top surface of the HST is transgressive surface as well as CB. The HST consists of an aggradational to progradational set of parasequences that overlies the maximum flooding surface and is overlain by the next sequence boundary. In Thayet-Tondaung area, HST cycle is described by shallow to deep subtidal facies. In measured section, HST is typified by both aggradational and progradational stacking patterns.

Cyclicity

It is observed that the carbonate ramp of Tondaung has a clear picture of cyclicity not only in megascopic but also in microscopic scales. The features that found on megascopic contain alternation of hard and soft lithologies and upward thickening or shallowing cycles (Fig. 7).

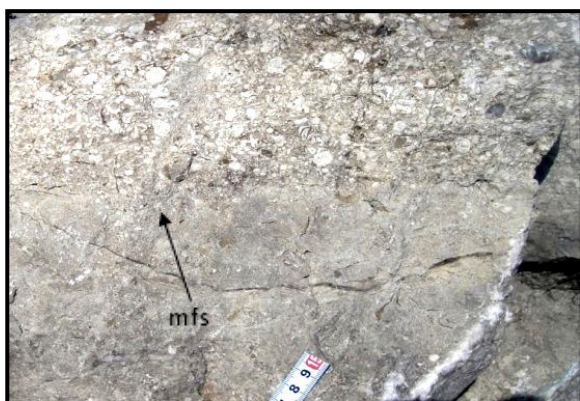


Figure 6 Intense bioturbation indicating the maximum flooding surface (mfs) at Thayet area.



Figure 7 Thickening upward cycle of buff color silty limestone at Thayet area.

Discussion

Cycles of the Thayet-Tondaung Section

Five cycles could be recognized in Thayet area (C1-C5), separated by cycle boundaries.

The first level (or) base level of cycle 'C-1' of the Tondaung Limestone shows the shallowing upward, start with basinal blue grey shale, Globigerinid wackestone, Globigerinid packstone grainstone, or *Lepidocyclina* packstone (Fig.8a). The lower part of the section is alternately composed of blue gray shale, forams wackestone-packstone and forams packstone-grainstone. The presence of planktonic foraminifera (*Globigerina*) is usually found in the shallow-deep transtitional fore reef zone.

The cycle 'C-2' observed in the basal part, predominance of an outer to mid-ramp community of planktonic fauna, and in the upper part a gradual shift from a planktonic dominated fauna toward perforate larger benthic one of the mid-ramp. The lower part is interpreted as a TST whereas the upper part as a HST. The boundary between the lower and upper part is marked by a sharp, sudden change in fauna and lithology; gray packstone containing abundant planktonic (*Globigerina*) is substituted by creamy skeletal lime sand with predominance of perforate (*Lepidocyclina* sp, *Amphistegina* sp.) The faunal assemblages suggest that there were no effective burrier present, the boundary and change in fauna at the TST/HST transition (mfs).

The cycle 'C-3' of the lower part consists of retrogradation of the facies belts (from mid-ramp sediment to algal shoal of the inner ramp) marks the following TST aggradation and slow progradation of the corresponding HST.

The lower part of the sequence starts with carbonaceous shale overlain by well bedded *Lepidocyclina* packstone- grainstone to red algae foraminifera grainstone. The lower part is regarded as TST on the outer ramp, basinal shale; the upper part is interpreted as a HST deposition in an inner ramp algal shoal and capped by iron-staining packstone (Fig. 8b) and meteroic diagenetic.

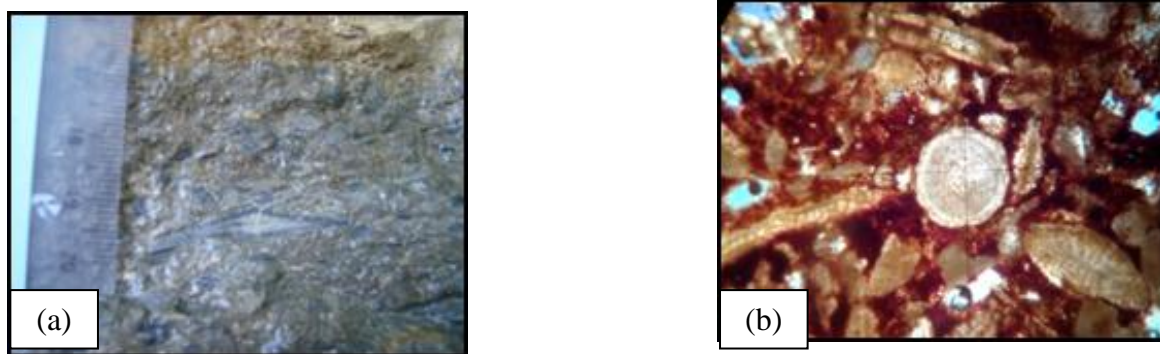


Figure 8 (a) Light grey, thick-bedded limestone containing abundant *Lepidocyclina* exposed in the middle part of measured section. (b) Photomicrographs of ironized bioclastic grainstone in which iron cement is coating on the detrital grains. Scale bar is 0.1mm.

The basal sequences of the cycle 'C-4' consist of bluish gray shale with high amount of planktonic foraminifera (*Globigerina* sp, *Globotruncana* sp, *Nodosaria* sp). The upper shows inner to mid-ramp sediment contain a rich perforate foraminifer (*Lepidocyclina* sp, *Operculina* sp) packstone-grainstone, containing coal, and gypsum bearing shale. This associations is typical of deltic and marginal marine fauna of gastropod, pelecypod and bryozoan, echinoderm etc.),

separated by coastal marine shale, delta plain organic clay and coals, mark local transgressive phase related to local delta lobe abandonment.

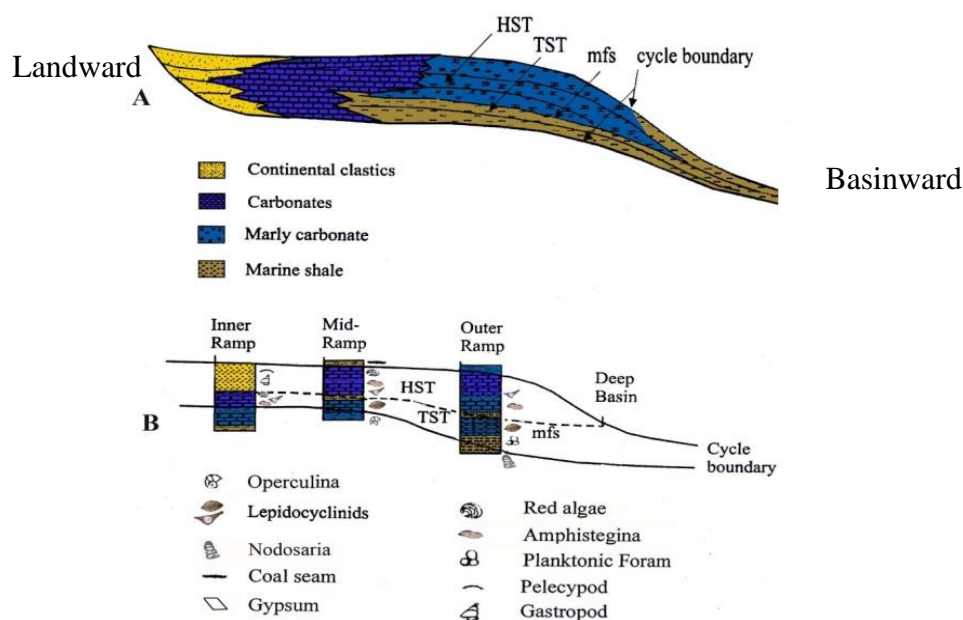
The base of the cycle 'C-5' consists of yellowish brown calcareous shale with lime bands. The upper part shows middle to inner ramp sediments containing rich benthonic foraminiferal assemblages indicating a sharp sudden change boundary between lower and upper. In contrast, the yellowish brown calcareous shale of middle ramp is substituted by well bedded sandy packstone to grainstone with abundant benthic foraminifers, pelecypods and gastropods fossils. Then, carbonates were deposited following a transgression brought about by compaction of overlying deltic sediments. Considering the base of middle ramp is interpreted as a TST and the upper inner - ramp is interpreted as HST.

After that, mixing of siliciclastic-carbonate facies is formed at the top of the Tondaung section. A mixed siliciclastic-carbonate facies point out that siliciclastic facies prograded basinward or progradational parasequence sets of the late highland.

Model of Sequences

The observed sedimentary cycles in Htondaung area were interpreted with a sequence stratigraphic ramp model (Fig.9). This model is derived from sequence stratigraphic ramp models (Vail et.al 1977) but highly modified for the specific conditions observed in Tondaung area.

Once fourth-order depositional sequence is shown with system tracts and associated facies distribution in Fig.9a. Three simplified sections through one cycle are displayed for the outer ramp, the mid-ramp and the inner ramp. The three depositional systems combine to form five sequences are observed in Thayet-Htondaung area (see also Fig. 9b).



TST - Transgressive Systems Tracts, HST - Highstand Systems Tracts, mfs – Maximum flooding surface

Figure 9 Empirical Model for a depositional fourth order cycle on the carbonate ramp of Tondaung area. (a) Distribution of facies in system tracts and (b) three typical sections for inner, middle and outer ramp (Not to scale).

Summary and Conclusion

The Thayet- Tondaung section shows a clear cyclicity on megascopic scale. Five fourth-order shallowing upward, parasequence cycles can be recognized by environmental changes within the section. In the description of the section, deepening trends (retrogradational stacking) are considered Transgressive systems Tracts (TST), shallowing trends (progradational stacking) are held to be Highstand System Tracts (HST), and the change from deepening towards shallowing is interpreted as maximum flooding surface (mfs). The sudden superposition of transgressive beds upon prograding one as thought to represent a Cycle Boundary (CB). Cycle boundaries recognized in this study were initially identified abrupt shift from shallowing trend to deepening trend response to increase in water depth and the lowstand systems tract is missing. As a result, this study focused on depth trends to identify stacking patterns. Progradational stacking was indicated by a net shallowing upward trend through a series of parasequences. Retrogradational stacking is despite upward shallowing within each of component parasequences. Many of the cycle boundaries that coincide with transgressive surface have hardground developed on them, usually with pyrite and iron-stained surface, and surface display a horizon of intense burrowing. The three depositional systems combine to form five sequences are observed in Thayet area.

Acknowledgements

The author would like to thank Dr. Htay Aung (Acting Rector) and Dr. Soe Myint Thein (Pro-Rector) of Loikaw University for their permissions to do this research project. The author is also deeply indebted to Dr. Toh Toh Win Kyi (Professor), Head of the Department of Geology, Loikaw University for her encouragement to carry out this research. My deeply thanks are due to Dr Myint Thein, Rector (retired), Dr Than Than Nu, Professor (Head of Department), Department of Geology, Mandalay University, and U Maung Maung, Professor (Head of Department) (retired) for their valuable suggestion, constructive comment and interest. This paper could not be completed without the cooperation of responsible personnel from Tondaung Mine during our field trip.

References

- Aung Khin and Kyaw Win, (1969). Geology and hydrocarbon prospects of Burma Tertiary Geosyncline, *Union of Burma Science and Technology Journal*, v.2, p. 53-81.
- Buchette, T.P. and Wright, V.P., (1990), Carbonate ramp depositional systems. *Sediment Geol.*, 79: p 3-57.
- Chit Saing, (2003). Oligocene and Miocene microfossils of Myanmar. Unpublished Ph.D. Thesis, Department of Geology, Yangon University, 137p.
- Tucker, M.E., Calvet, F., and Hunt, D., (1993), Sequence stratigraphy of carbonate ramps: system tract, models and application to the Mushelkalk carbonate platform of eastern Sapain. *Int. Assoc. Sedimentol.*, Sepc. Publ.
- Vail, P.R., Mitchum, R.M., Todd, R.G., Widmer, J.M., Thompson, S., Sangree, J.B., Bub, J.N. and Hatlelid, W.G., (1977), Seismic stratigraphy and global changes of sea level, In Payton, C.E., ed., *Seismic stratigraphy – applications to hydrocarbon exploration: AAPG Memoir*, 26, P.49-212.
- Zwart, E.W., Fouke, B.W., and Everts, A.J.W., (1994), Evidence for subaerial exposure of a carbonate platform from fluid inclusion studies (vercors, SE France): application and techniques (abstract) fifth Biennial pan American Conference on Research on Fluid Inclusions 19-21 May 1994, p.127-128.

DISCOVERY OF THE MIDDLE DEVONIAN (GIVETIAN) RUGOSE CORALS FROM THE MAYMYO FORMATION, PYINOOLWIN AND HSIPAW TOWNSHIPS

Khaing Khaing San*

Abstract

Five species of Middle Devonian (Givetian) rugose corals are firstly described from the Pwepon Limestone of the Maymyo Formation at Pwepon (Pyinoolwin Township) and Kongtha (Hsipaw Township) areas. The Pwepon Limestone consists of grey to dark grey, well-bedded, hard micritic limestone intercalated with argillaceous limestone, siltstone and shale. This limestone in Pwepon and Kongtha areas is considered as the sandwiched unit of the Maymyo Formation. The Pwepon Limestone is richly fossiliferous including Eifelian and Givetian rugose coral faunas. The later, never reported before, include two new species: *Argutastrea pweponsensis* sp. nov., *Hexagonaria carinata* sp. nov. and three previously described species *Grypophyllum postprimum postprimum* from Late Givetian of Schweln-Kalk, NW Sauerland, Germany, *Disphyllum dispar* from Givetian, Dosey Limestone, Broken River Province, North Queensland, Australia and *Disphyllum caespitosum* from Givetian, Cürten Formation, Eifel Hill, Germany. The Myanmar Givetian species are compared with those from Europe and Australia.

Keywords: Middle Devonian, Pwepon, Kongtha, rugose corals

Introduction

Marine Middle Devonian limestone is formerly as the very limited exposed unit in Myanmar (Padaukpin and Pwepon area). Two new discovered fossiliferous units of Middle Devonian age in Lashio area and Hsipaw area, northern Shan State provide an insight into changing lithology and faunal occurrences. The Pwepon area, Pyinoolwin Township is the occurrence of a slighter younger coral dominated Middle Devonian limestone, recorded in that area and is assigned to the Pwepon Limestone (Figure 1). Another occurrence of Pwepon Limestone continuously exposed along Mandalay – Lashio car-road mile post (156/3) in Kontha area, Hsipaw Township contains a diverse rugose coral fauna representing an in situ assemblage of complete and unfragmented specimens. Fossils recorded from this area are abundant rugose and tabulate corals and numerous brachiopods.

This study is primarily concerned with the systematatic description of the Middle Devonian (Givetian) rugose corals from the Pwepon Limestone of the Pyin Oo Lwin Township and Hsipaw Township. Five species are identified and described in this paper.

* Dr, Professor, Department of Geology, Yadanabon University

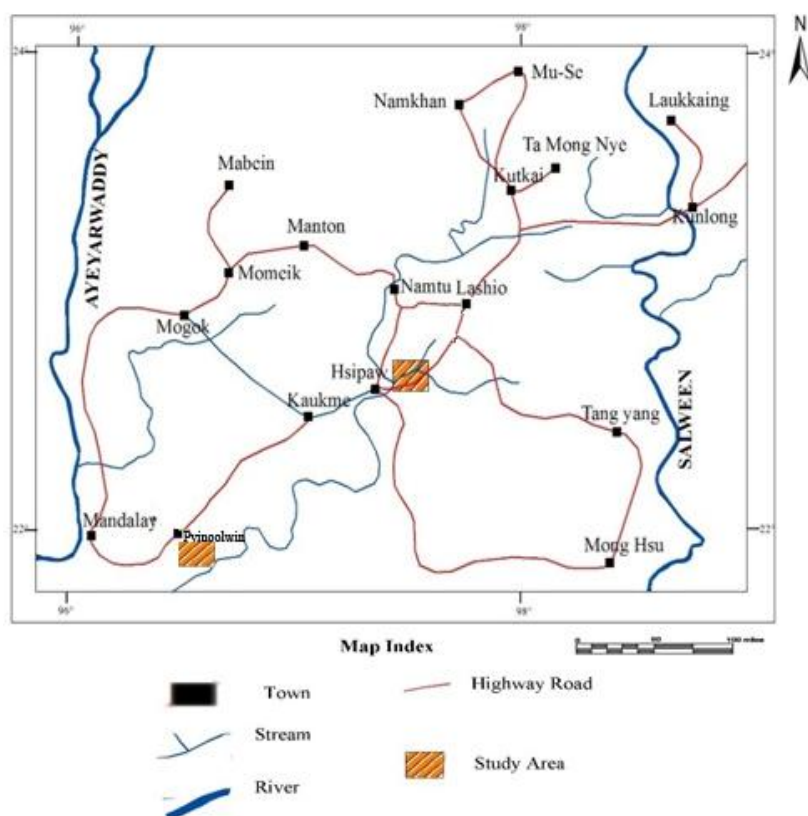


Figure 1 Location map of the Study area.

Stratigraphy of the Pwepon Limestone

The Pwepon Limestone is restricted to expose in northern Shan State. The Pwepon area is located about 5 miles SE of Pyinoolwin which also lies between latitudes $21^{\circ} 53' N$ to $22^{\circ} 0' N$ and longitudes $96^{\circ} 30' E$ to $96^{\circ} 35' E$. It occupies the northern part of one-inch topographic map 93 C/9. The coral bearing limestone is situated at the Pwepon cave and its environ, 3473 ft. hill at the eastern part of the Pwepon cave and smooth, isolated hill (3200 ft.) at the western part of Pwepon cave and has the coordinates of $N21^{\circ} 53' E96^{\circ} 33'$.

The Pwepon Limestone is well-bedded, hard, micritic limestone and difficult to struck with hammer. It can be easily struck with hammer and giving the thin layers of small chips when the limestone has been subjected by weathering process. Its topography is very different from the neighborhoods by isolated hills of well-bedded character. The total thickness of the Pwepon Limestone is 174 meters (Figure 2A).

Lithologically, Pwepon Limestone is classified into eight subunits namely dolomitic limestone, micritic limestone, argillaceous limestone, stromatolitic limestone, limestone intercalated with crinoidal limestone, argillaceous limestone intercalated with silty shale or mud, micritic limestone with parallel lamination and silt partings and limestone with chert nodules. The detailed description for measured section of the Pwepon Limestone is shown in Figure 3. It is overlain by dolomitic limestone with relict fossils, argillaceous limestone, ferruginous dolomitic limestone, hematite, calcareous limestone and highly jointed and brecciated dolomitic limestone. The Pwepon Limestone is richly fossiliferous with rugose corals and the other

fossils are the abundant tabulate corals, bryozoans, branchipods and conodonts (Khaing Khaing San, 2005).

Kong tha area is bounded by north latitude $22^{\circ}36'48''$ to $22^{\circ}42'12''$ and East Longitude $97^{\circ}24'$ to $97^{\circ}32'20''$ in UTM map no. 2297 (6 - 10). In this area, Pwepon Limestone is mainly exposed in the south western part. The best exposures of Pwepon Limestone continuously exposed along road cut section at the mile post (156/5) of the Mandalay-Lashio car road ($N22^{\circ}53'36''$ and $E96^{\circ}40'50''$) and (62) meter in thickness (Swe Hnin Maung, 2018).

In this area, the Pwepon Limestone is also the sandwiched unit of the Maymyo Formation which laterally passed into dolomite or dolomitic limestone. It is the escaped unit of the dolomitization. It consists of thin- to medium-bedded, buff colour, grey to black, fine- to medium-grained, soft and indurated, limestone, calcareous limestone, argillaceous limestone, carbonaceous shale and grey shale. Where shale or argillaceous materials is dominated, fossils fragments (Corals and Brachiopods) are most abundantly occurred and easily extracted from this unit. Detailed description for measured section of the Pwepon Limestone is shown in Figure 2B. This Limestone is the fossiliferous unit containing a number of corals (rugose and tabulate) and brachiopods.

The occurrence of faunal assemblage indicates that the age of the Pwepon Limestone in these two areas can properly be designated as the Middle Devonian (Eifelian to Givetian) age.

Systematic Paleontology

Methods of Study

The rugose corals are collected from the coral-bearing horizon of the upper part of the Pwepon Limestone in Pwepon area and Kong tha area. Most of the rugose corals show abrasion but no sign of reworked character. They included in the detrital limestone unit in Pwepon area and argillaceous limestone unit in Hsipaw area. All specimens described herein have been prepared the thin-section. Statistical methods are used for identification of the species.

The suprageneric classification used in this paper follows the classification of Hill (1981) except as noted under the relevant taxa. The rugose coral terminology follows that of Hill (1935, 1956, 1981). In solitary and fasciculate corals, the corallite diameter quoted is the mean diameter as measured in a transverse section. In cerioid corolla, the corallite diameters measured from the middle of one side to the middle of the opposite side.

Known distributions of the genus are summarized so as to indicate their biostratigraphic and paleogeographic significance. Figured specimens have been selected to show both inter- and intra-specific variation. The thin-sections were placed in the negative carrier and the image traced directly into drafting film.

All described rugose corals from Pwepon area are housed in the department of geology, Yadanabon University and from Kong tha area are housed in the department of geology, Lashio University. The repositories of the rugose corals from Pwepon area are prefixed by YDBPP and from Kontha area are prefixed by LSOKT.

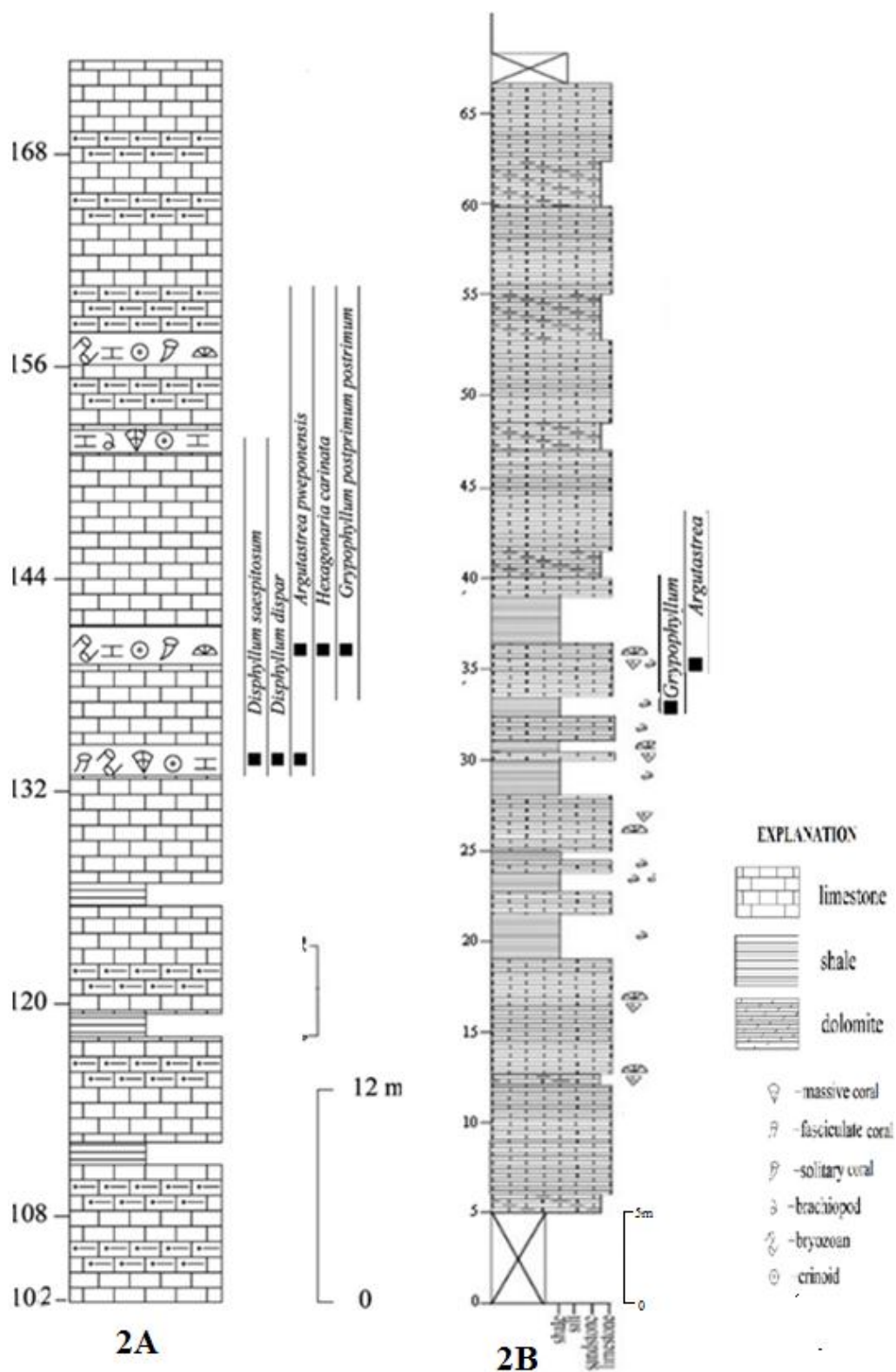


Figure 2 Stratigraphic measured section of the upper part of Pwepon Limestone with the distribution of the rugose corals in Pwepon area (2A) and the Pwepon Limestone with the occurrence of fossils (mile-post 156/3 furlong) along Mandalay -Lashio Car-road in Kontha area (2B).

Result and Discussion

Phylum Coelenterata Frey and Leukart, 1847

Class Anthozoa Ehrenberg, 1834

Subclass Rugosa Milne-Edwards and Haime, 1850

Order Cystiphyllida Wedekind, 1927

Family Ptenophyllidae Wedekind, 1922

Subfamily Ptenophyllinae Wedekind, 1922

Genus *Grypophyllum* Wedekind, 1922

Grypophyllum Wedekind, 1922, p.13

Type species. - *Grypophyllum denckmanni* Wedekind 1922; p.13-14, Text-figs. 13,14; Givetian, Bergisch-Gladbach, Germany.

Remarks. - The present specimens are closely resembled with the genus *Grypophyllum* Wedekind (1922) in the character of non-carinated septa, peripherally thickened and thin inwards, wide dissepimentarium with subglobose dissepiments steeply, adaxially inclined and narrow tabularium with incomplete tabulae, closely spaced and flat with a central depression.

Occurrence. - Middle Devonian for Europe (Germany, United Kingdom, Belgium, France, Czech.- Austria, Urals, N. Zemlya), Asia (Kuzbas NE, USSR, Pakistan, Kwandsi, Myanmar, China), North America (S. Mackenzie).

Grypophyllum postprimum postprimum Birenheide and Lütte, 1990 (Figs. 3.1 - 3.2)

Grypophyllum postprimum postprimum Birenheide and Lütte, 1990, p. 14, pl. 5, figs 31-32

Holotype. - *Grypophyllum postprimum postprimum* Birenheide and Lütte, 1990, SMF WDKD: Kat.- Nr. 7014-7015 (1QS, 1LS; pl.5, figs. 31a-b), Upper Givetian, Schwelm- Kalk; NW-Sauerland, Germany.

Diagnosis - The subspecies of *Grypophyllum postprimum* with flat lying or irregularly curved and closely spaced tabulae and minor septa very short or reduced to spines (modified after Birenheide and Lütte, 1990).

Materials. - Figured specimen MUPP 0559 and LSOKT 250 from Middle Devonian (Eifelian-Givetian), upper part of the Pwepon Limestone PP (D), Maymyo Formation, Pyinoolwin township and Hsipaw Township, Myanmar.

Description. - The material consists of fragment of solitary coralla, which may be cylindrical. Its height and external morphology cannot be observed because it is encrusted in the micritic limestone (MUPP 0559). LSOKT is cylindrical coral, length is 20 -24 mm, diameter ranges between 15- 40mm, gently sloping calical platform and moderately deep calical pit (LSOKT). The septa are non-carinate, slightly dilated throughout their length. Occasionally, they are thicker at the periphery; a triangular thickening may also appear against the outer wall. In some cases, the septa are discontinuous at the periphery or interrupted by a few lonsdaleoid dissepiments. Septa are arranged in two orders with 25-30 in each and peripherally dilated forming a relatively wide peripheral stereozone of 1mm thick. The major septa extend close to the axis of the corallum; their distal ends slightly curved and bilaterally arranged. Minor septa are

very short or reduced to spines and isolated fragments. Dissepiments are mainly concentric in transverse sections. Dissepimentarium consists of 5 to 7 rows of elongate, adaxially inclined dissepiments, with a sharp boundary between the dissepimentarium and tabularium. Tabulae are incomplete, flat lying or irregularly curved and closely spaced. The diameter of the corallum ranges from 13-16mm. The width of the tabularium is 4mm.

Remarks - These specimens are assigned to *Grypophyllum*. This species closely resembles with *G. postprimum postprimum* Birenheide and Lütte (1990), Givetian, Rheinisches Schiefergebirge, Burg-Berg section, Germany described by Schröder (2002), except the later in having rhopaloid major septa and herring-bone dissepiments. This is considered as a specific variation.

Occurrence - This species occurs in Upper Givetian, Schwelm- Kalk; NW- Sauerland, Germany; Givetian, Rheinisches Schiefergebirge, Burg-Berg section, Germany and Middle Devonian (Eifelian-Givetian), Pwepon Limestone, “Maymyo Formation”, Pyinoolwin and Hsipaw townships, Myanmar.

Suborder Columnariina Soshkina, 1941

Family Disphyllidae Hill, 1939

Genus *Disphyllum* De Fromentel, 1861

Disphyllum De Fromentel, 1861, p.302

Type species (SD, by Lang and Smith, 1934). - *Cyathophyllum caespitosum* Goldfuss, 1826, p.60, Pl. 19, fig. 2b; = *Disphyllum goldfussi* (Geinitz, 1846); Givetian, Eifel, Germany.

Remarks. - Birenheide (1978, p.90-91) put the emphasis on the subcerioid nature of the holotype colony of *Disphyllum caespitosum*, the type species of the genus, and assigned this species to *Columnaria* Goldfuss (1829). However, *Columnaria* (type species *C. sulcata* Goldfuss; see Birenheide, 1978, pl.12, fig.4) is cerioid and its dissepiments are so scarce, that they are often not in contact with each other. *Disphyllum* is dendroid, phaceloid to subcerioid commonly with more numerous dissepiments. Even if only one series is present, it forms a continuous zone at the corallite periphery. The forms described here agree exactly with that of the genus *Disphyllum*.

Occurrence. - Early Devonian (Emsian) for Asia (NE USSR); Middle Devonian (Eifelian) for Europe (Belgium), Asia (Myanmar, China); Middle Devonian (Givetian) for Europe (U.K.-Belg.-Ger.-Pol.-Czech.-Aus.) - Asia (Kazakh); Late Devonian (Frasnian) for South China, Tadjikistan.

Disphyllum caespitosum Goldfuss, 1826

(Fig. 3.4)

Disphyllum caespitosum Goldfuss, 1826, p. 60

Holotype. - *Cyathophyllum caespitosum* Goldfuss, 1826 = *Disphyllum caespitosum*, Goldfuss, 1826, Givetian, Eifel, Germany.

Diagnosis. - Colonial rugose corals of *Disphyllum* with 23 major septa at a diameter of 10-12mm. Major septa leaving an axial space of 1-3mm, dissepimentarium composed of globose dissepiments about 3 to 6 rows. Tabulae is incomplete, bizonal (Schröder, 1998).

Materials. – MUPP 0533, MUPP 0578, MUPP 0590 from Middle Devonian (Eifelian-Givetian), upper part of the Pwepon Limestone (PP-D), Maymyo Formation, Pyinoolwin township, Myanmar.

Description. - Coralla is phaceloid to subcerioid and their size unknown because it included in the groundmass. The long, cylindrical corallites are locally in contact, and lateral offsets occur in the colony. The diameter of the corallite ranges from 8mm to 14mm (average 10-11.2 mm in diameter). Septa are 21 to 26 in each order, smooth and non-carinate, peripherally dilated in wedge-shape and embedded into walls and attenuating toward axis, three-fourths as long as the radius, leaving an axial space of 1-3 mm. Minor septa are short, nearly reaching or just extending into tabularium, one-fourth as long as the radius. Trabeculae are coarse monacanth, extending inwards and upwards at a low angle to the horizontal.

The dissepimentarium consists of 2 to 3 rows of small, inclined dissepiments adaxially toward the axis. Tabularium is two-third as wide as the corallite, 4.5-6mm wide and is composed of complete or incomplete, horizontal or slightly convex at centre with down-turned margin and occasionally supplemented with small peripheral tabellae; rather closely, but unevenly spaced, vertically there are 6 to 8 tabulae per 5mm.

Remarks. - This material closely resembles with *D. caespitosum* Goldfuss (1826) described by Schröder (1998, p.41, pl.5, Fig.35) from Givetian, Cürten Formation, Germany in all characters. This species is the type species of the genus. It is also similar to *Disphyllum dushanese* Yü and Liao in Kong and Huang (1978) described by Liao and Birenheide (1989, p.87, pl.4, fig.23) from the Frasnian of Tushan Province of Guizhou, South China but regular axial torsion of the thin major septa can serve to distinguish it from *D. caespitosum*.

Occurrence - This species occurs in Middle Devonian (Eifelian-Givetian), Pwepon Limestone, Maymyo Formation, Pyinoolwin Township, Myanmar; Givetian, Bergisches Land and Sauerland, Ermberg-Rodert Formation, Eifel, Germany.

Disphyllum dispar Aung, 1991

(Fig. 3.3)

Disphyllum dispar Aung, 1991, p.208, pl.31, Fig. 2a-f; pl.32, Figs. 1a,b, 2a,b; pl.33, Figs.1a, b, 2a, b, 3a, b, 4.

Holotype. - *Disphyllum dispar* Aung, 1991, UQF 77635 from UQL5528, limestone lens B26, 400m west of the small creek, 500m south of the Broken River, 1km upstream from the Jack Hills Gorge, Early Givetian, Dosey Limestone; Broken River Province, north Queensland, Australia.

Diagnosis. - Phaceloid to subcerioid *Disphyllum* with cylindrical corallites, 6-9 mm in diameter; increase both parietal and lateral; septa number 38 - 45, consistently dilated in the dissepimentarium. Tabularium wide, consisting of closely spaced complete tabulae; tabularial floors flat, slightly convex or sagging; dissepiments small, single to multiple rows; monacanthine trabeculae (Aung 1991, p.208).

Materials. - MUPP 0541, MUPP 0577 from Middle Devonian (Eifelian-Givetian), upper part of the Pwepon Limestone (PP-D) of, Maymyo Formation, Pyinoolwin township, Myanmar.

Description. - Originally loose phaceloid colony of thin section with four of the cylindrical corallites and two incomplete corallites are available. Isolated corallites with a diameter between 5 and 8mm (average 5.5 to 5.25mm in diameter) are enclosed in limestone. Septa of both orders are 68-72. Major septa are usually short, half to the radius of the corallite, not reaching axis, smooth and non-carinate, peripherally dilated and attenuating in the tabularium. Minor septa are

very short and never reach the tabularium. Trabeculae are monacanth arranged in a broad asymmetrical half fan over the dissepimentarium.

Dissepimentarium is narrow with 1.5mm wide, typically consists of 2-3 rows of globose, small dissepiments, they are almost horizontal in arrangement. Tabularium is broad, 2.5-3mm in diameter about 2/3 of the corallite diameter. It is filled with complete tabulae which are horizontal, or slightly concave or convex, and in some adaxially incline large periaxial tabulae also occurred. Tabulae are rather closely, but unevenly spaced and vertically counting about 4-6 tabulae per 5 mm.

Remarks. - This species closely similar to *Disphyllum gemmiforme* Etheridge (1902) illustrated by Pickett (1967, pl.7, figs. 27-28) from ?Lower Middle Devonian, Cavan Bluff Limestone, near Taemas bridge, New South Wales, Australia but he did not describe it. Hill (1981, p. F280) described the genus *Zelolasma* Pedder (1964) with the type species of *Disphyllum gemmiforme* Etheridge (1902). The transverse section of this species is more or less the same but in the longitudinal section, it has smaller tabularial diameter and more closely spaced tabulae in the tabularium.

Occurrence - This species occurs in Middle Devonian (Eifelian-Givetian), Pwepon Limestone, Maymyo Formation, Pyinoolwin Township, Myanmar and in Early Givetian, Burges Formation, and Dosey Limestone, Broken River Province, north Queensland, Australia.

Subfamily Disphyllinae Hill, 1939

Genus *Argutastrea* Crickmay, 1960

Argutastrea Crickmay, 1960, p.10

Type species (SD, by Hill and Jell, 1970). – *Argutastrea arguta* Crickmay, 1960, Middle Devonian, Can., W. end of Carcajou Ridge, NW. Terr.

Remarks. - The genus *Hexagonaria* is easily distinguished from *Argutastrea* by septa typically carinate with spindle shaped dilation in the dissepimentarium, by calices with broad and flat peripheral platform and by numerous dissepiments, which are in horizontal in layers in the outer part of the dissepimentarium and steeply inclined in its inner part. The collected specimens show radially arranged long major septa, dilated in dissepimentarium with some knobby or spinose carinae, slightly declined dissepiments with monacanthine trabeculae and flat or convex axial tabulae. Therefore, it should be assigned to the genus *Argutastrea*.

Occurrence. - Latest Eifelian to Early Givetian (Australia); Eifelian to Givetian (Germany, Myanmar, China); Givetian (France); Givetian to Frasnian (Belgium); Eifelian to Frasnian (USSR).

Argutastreapweponensis new species

(Figs. 4.1 – 4.3, 5.1)

Name derivation. - This species is firstly found from the Pwepon Limestone.

Diagnosis. - A species of *Argutastrea* with corallites having 36 to 40 septa at a diameter of 5 mm to 10 mm. Septa dilated in the dissepimentarium. Septa of both orders are long, the minor ones traversing the full dissepimentarium.

Materials. - Holotype: MUPP 05145, paratype: MUPP 0575, MUPP 0576, LSOKT 27-30 from Middle Devonian (Eifelian-Givetian), upper part of PP (D) of the Pwepon Limestone, Maymyo Formation, Pyinoolwin and Hsipaw townships, Myanmar.

Description. - The materials consist of cerioid corallum and their size unknown. Calical surface has been strongly weathered; the excavated calices are protruded like a calical boss, which are bordered by a moderately wide, flat calical platform (MUPP 05145, MUPP 0575-0576). LSOKT 027- 030 is colonial massive form, size ranges between 10 – 30 cm and largest form attain 60 cm. The walls between adjacent corallites are straight and sharp, medium line forming the polygonal corallites. There are 36 to 40 septa per corallite. Corallite diameter ranges from 5mm to 10mm (average 7 to 8.2 mm in diameter). The width of the tabularium varies commonly between 3.75 mm and 4.3 mm.

The septa are non-carinate or bear occasionally a few small spinose or knobby carinae. They are slightly thickened in the dissepimentarium-tabularium boundary and thinner in the peripheral and axial part. Sometimes, the septa are more thickened by schlerenchyme. The major septa reach the axis of the corallites or leave a free space in the center of the tabularium, which is usually small. Septa are mostly subequal and some united at the axis. The minor septa are usually long, traversing the full dissepimentarium about the two-third length of the majors. The dissepimentarium is wide composed of numerous, small dissepiments in the periphery and inner part, commonly occurred as the herringbone dissepiments in the transverse section. The dissepimentarium consists of 3 to 7 rows, which have two series; the peripheral dissepiments are large, subglobose and flat or horizontal and the inner dissepiments are small, elongated and adaxially steeply inclined. The tabulae are mostly incomplete with the axial part of flat or convex tabulae and the periaxial part of small, inclined tabulae. The trabeculae are monacanthine that are parallel or diverging upward and inward like a half-fan.

Remarks. - This species resembles *A. sp.* Aung (1991) from Early Givetian, Dosey Limestone, Broken River Province, North Queensland but differs in the later has peripherally dilated wedge-shape, dilated, shorter septa and wider axial area in the tabularium. The present Myanmar species is similar in character with *A. (Pseudohexagonaria) philomena* (Glinski, 1955) described by Schröder (1998) from the Middle Devonian (Eifelian), Junkerberg Formation, Dollendorfer Mulde, Eifel, Germany but it has lonsdaleoid dissepiments in the periphery. This species may possibly be a transitional form between Queensland sp. of *A. sp.* (Aung, 1991) and German, *A. (Pseudohexagonaria) philomena* (Glinski, 1955).

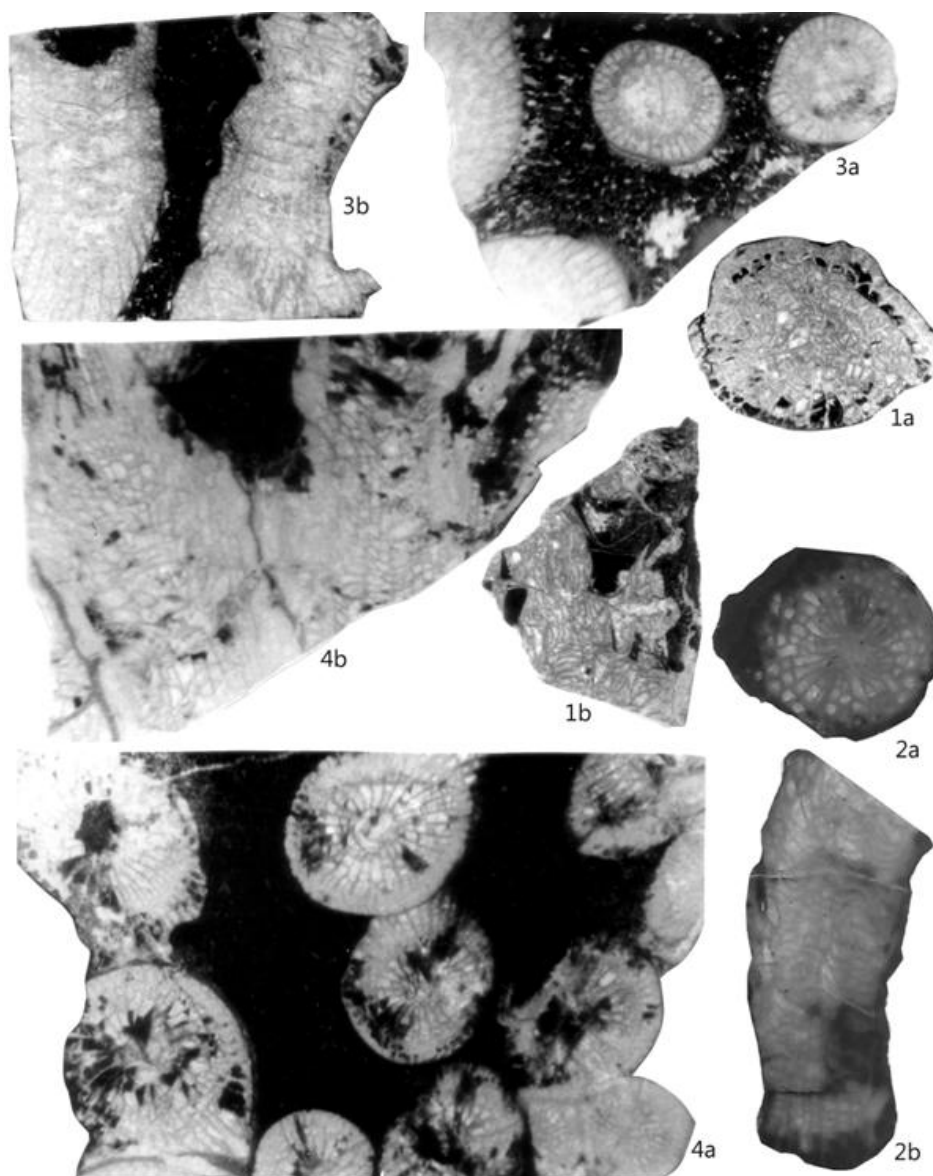


Figure 3 1-2, *Grypophyllum postprimum postprimum*. 1a&1b, transverse and longitudinal sections, MUPP0559, x 2.8; 2a&2b, transverse and longitudinal sections, LSOKT 250, x 2.8; 3, *Disphyllum dispar*. 3a&3b, transverse section x 5 and longitudinal sections x3.5, MUPP0577; 4. *Disphyllum caespitosum* 4a&4b, transverse section x 2.5 and longitudinal sections x3, MUPP0533.

Occurrence - This species occurs in the Middle Devonian (Eifelian-Givetian), Pwepon Limestone, Maymyo Formation, Pyinoolwin and Hsipaw townships, Myanmar.

Subfamily Hexagonariinae Bulvanker, 1958

Genus *Hexagonaria* Gürich, 1896

Hexagonaria Gürich, 1896, p.171

Type species (SD, by Lang, Smith and Thomas, 1940). –*Cyathophyllum hexagonum* Goldfuss, 1826, p. 61, Upper Givetian or Lower Frasnian, Refrath beds, Germany, Bensberg.

Remarks. - The present Myanmar specimens show cerioid, long, dilated in fusiform septa with closely carinae, mostly yarrow, radially arranged and fan shape monacanthine trabeculae,

numerous dissepiments and slightly convex axial tabulae. It closely resembles with the diagnosis of the genus *Hexagonaria*. Thus, it should be assigned to the *Hexagonaria* and this is the first occurrence of the genus *Hexagonaria* in Myanmar.

Occurrence - *Hexagonaria* is a Givetian- Frasnian genus in the worldwide. Middle Devonian for Myanmar; Givetian – Frasnian for Europe (United Kingdom, France, Belgium, Germany, Poland, Urals), Asia (Kuzbas-Yunnan), West Australia, North America (Washington, NW Ter.).

Hexagonariacarinata new species

(Figs. 5.2 – 5.3)

Diagnosis. - A species of *Hexagonaria* with corallites having 30-34 septa at a diameter of 8.5mm. Septa dilated in fusiform and closely carinated with yardarm. Dissepiments are globose, monacanthine trabeculae and incomplete tabulae.

Materials. - Holotype: MUPP 05116, paratype: MUPP 05114 from Middle Devonian

(Eifelian-Givetian), upper part of the Pwepon Limestone (PP-D), “Maymyo Formation”, Pyinoolwin township, Myanmar.

Description. - The materials consist of a cerioid corallum and their size unknown. Calical surface has been strongly weathered. The walls between the adjacent corallite are curved. The corallites are polygonal to hexagonal in shape and are 8mm in diameter but ranging up to 10mm. The septa are long, dilated to fusiform in dissepimentarium-tabularium boundary and become thinner in their periphery and axial ends. The septa are closely carinated mostly with yardarm carinae. The major septa reach more or less to the axis of the corallites, but often leave a small free space 1-1.5mm in the center of the tabularium. The minor septa are usually long about 2/3 lengths of the majors.

The dissepimentarium consists of 4-6 rows of horizontal, subglobose outer dissepiments and 2-4 rows of inner dissepiments, adaxially steeply inclined. The tabulae are incomplete consisting of two series; flat or convex axial tabulae and small, slightly inclined, peripheral tabulae. There are 30-34 septa per corallite. The width of the tabularium varies commonly between 3mm and 3.5mm. Trabeculae are monacanthine, almost parallel and directed upward and inward from periphery like fan-shape.

Remarks. - This species resembles *H. cf. hexagona* Goldfuss (1826) described by Schröder (2002) from Upper Givetian, Burg-Berg section, east Sauerland, Germany but the latter has more septa number and less carinated with knobby or spinose. The Chinese species of *H. beichuanensis* He (1978) described by Liao and Birenheide (1985) from Givetian of Dushan, Province of Guizhou, S. China differs from the present species by larger corallite diameter and more septa number, less carinated septa and flat or horizontal tabulae. According to the present investigation, this specimen differs from other known established species, so it is present investigation, this specimen differs from other known established species, so it is designated to the new species.

Occurrence - This species occurs in the Middle Devonian (Eifelian-Givetian), Pwepon Limestone, Maymyo Formation, Pyinoolwin Township, Myanmar.

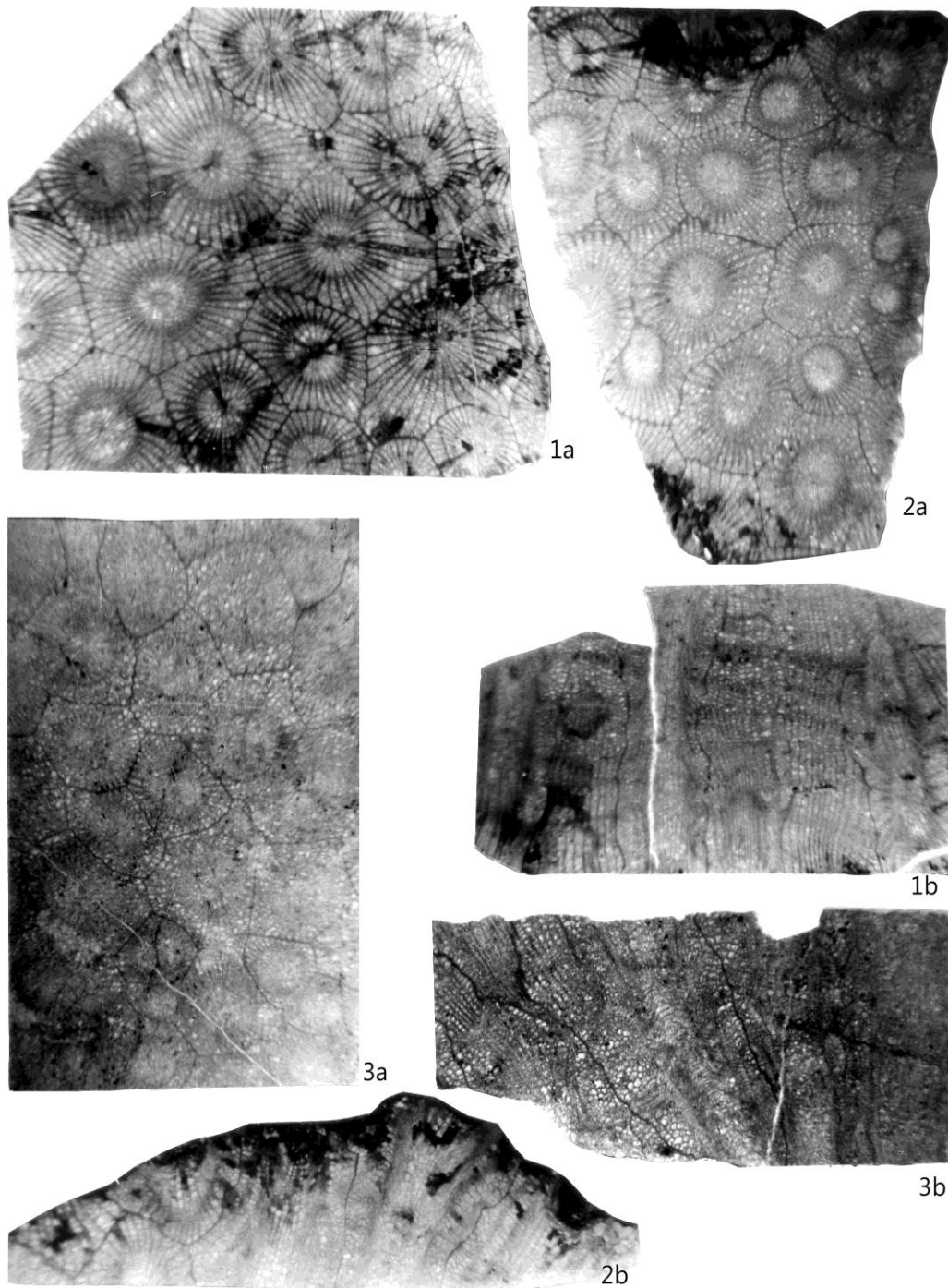


Figure 4-1-3,*Argutastrea pweponensis*. 1a&1b, transverse section x 2.5 and longitudinal sections x 3, MUPP0545; 2a&2b, transverse section x 2.25 and longitudinal sections x 2.7, MUPP0576; 3a&3b, transverse section x 2.2 and longitudinal sections x2.7, MUPP0575

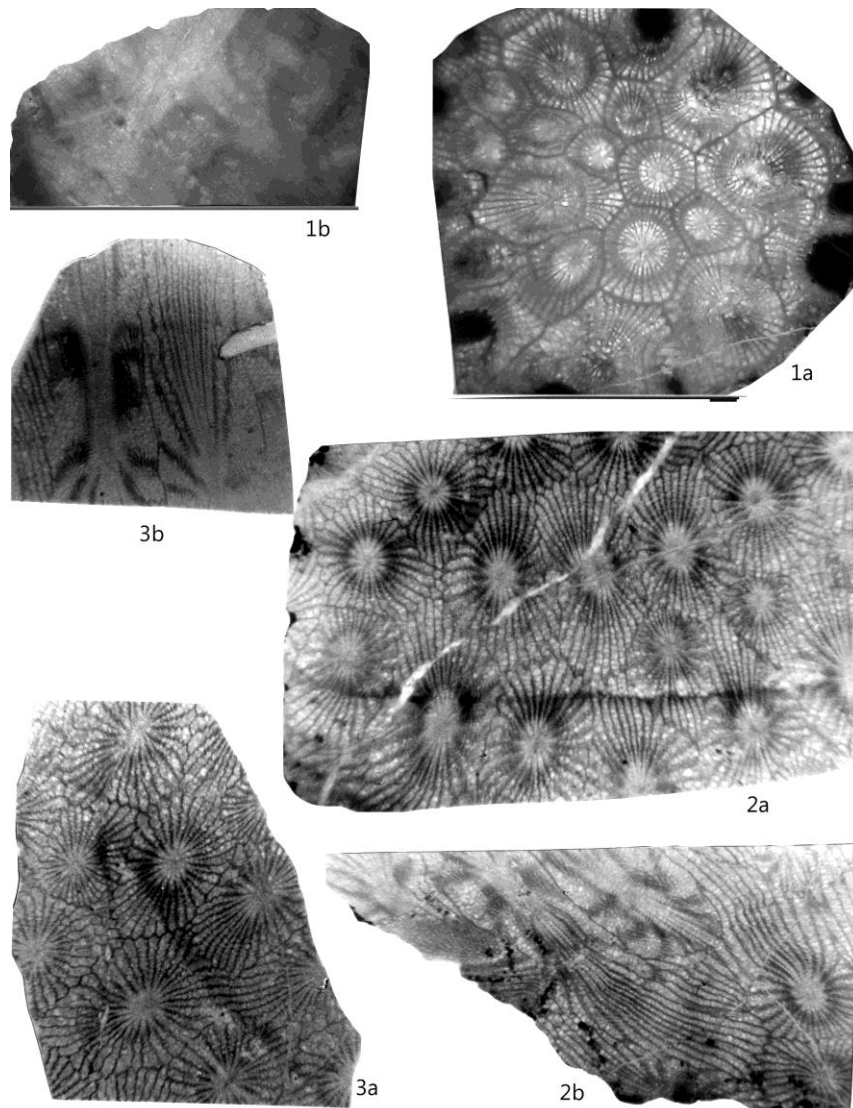


Figure 5-1, *Argutastrea pweponensis*. 1a&1b, transverse section x1 and longitudinal sections x 0.75 , LSOKT 0559,x2.8; 2-3, *Hexagonaria carinata*. 2a&2b, transverse section x3 and longitudinal sections x 2.6, MUPP0516,x2.8; 3a&3b, transverse section x 3 and longitudinal sections x2.6, MUPP0514

Conclusion

The coral fauna characterized by the abundant occurrences of compound corals, such as of the *Grypophyllum*, *Argutastrea*, *Hexagonaria*, and *Disphyllum* dominated by disphyllids in the upper part of the Pwepon Limestone in Pwepon area and Hsipaw area. In this interval, fossils are less abundant and the fossiliferous bioclastic limestone is intercalated in the medium-bedded, light grey to grey, argillaceous limestone and calcareous limestone. The colonial massive forms of rugose corals become much widely distributed in the upper part. The associated fauna are the tabulate corals, brachiopods and bryozoans. The upper most part of the Pwepon Limestone is terminated with thin- to medium-bedded, grey, slightly dolomitized limestone with high calcitization and rare fossil horizon.

Grypophyllum is the first occurrence of Myanmar. It also widely distributed in the world. *Argutastrea* is confined to latest Eifelian to Givetian for Australia, Germany, China and Vietnam.

The new species of *A. powensis* is closely resembled with *A. periclada* Kramer (1982) (in Coen-Aubert and Lütte, 1990) from the Givetian of Törringen Formation, North Eifel Hills, Germany. *Hexagonaria* is a common element of Givetian- Frasnian in the worldwide especially in Europe, Asia, West Australia and North America. *H. carinata* resembles *H. cf. hexagon* Goldfuss (1826) (in Schröder, 2002) from upper Givetian, Burg-Beng section, Germany. *D. caespitosum* Goldfuss (1826) (in Schröder, 1998) is described from Givetian, Curten Formation, Eifel, Germany. *D. dispar* Aung (1991) occurred in early Givetian, Dosey Limestone, Broken River Province, north Queensland.

The composition of the present described rugose coral fauna allows assignment of ages to the limestone where conodont or shelly faunas are absent. The correlation of the faunas of upper part of the Pwepon Limestone and the occurrences from outside Myanmar allows age determination of the coral-bearing sequences as Middle Devonian (Givetian). Their correlation with the standard conodont zonation reaches from the *hemainsatus* to the middle *varcus* zone and has close affinities with contemporaneous faunas of Ardennes, northern France, Rheinisches Schiefergebirge, Eifel Hills and Broken River Province.

Acknowledgements

I greatly appreciate the help of Professor Dr. Marie Coen-Aubert, Belgium and Dr. Stefan Schröder (Geology and Paleontology Institute, Köln University), Germany for their supporting the literatures of the corals. Many thanks are due to Dr. Aye Ko Aung, Professor (Retd.), Department of Geology, Dagon University for his proper guidance and critical reading the manuscript.

References

- Aye Ko Aung. (1991). *Early to Middle Devonian rugose coral and conodont faunas of the Burges Formation, Broken River Province, north Queensland*. Ph.D. Thesis (unpublished), University of Queensland, Australia, 307p.
- Birenheide, R. (1978). *Rugose Korallen des Devon*. Leitfossilien, 2. Gebriider Borntraeger, Berlin, Stuttgart: 265P.
- Birenheide, R. and B.P.Lütte. 1990. Rugose Korallen aus dem Mittel - Givetium (Mittel - Devon) des Rheinischen Schiefergebirges. *Senckenbergiana lethaea*, 70 (1/3):1-28, 5.
- Bulvankar, E.Z. (1958). Devonskie chetyrekhluchevye korally okrain Kuzetskogo basseyna, 2:212, pl.93. *Vsesoyuznyi Nauchno-issledovat'skiy Geologicheskii Institut (VSEGEI)*, (Leningrad). [Devonian tetradiate corals from the Kuznetsk basin].
- Coen-Aubert, M. and B. P.Lütte. (1990). Massive rugose corals from the Middle Devonian of the North Eifel Hills (Rheinisches Schiefergebirge, West Germany). *Geologica et Palaeontologica*, 24:17-39.
- Crickmay, C. H. (1960). *The older Devonian faunas of the Northwest Territories*. 21, 11pl. Evelyn de Mille Books (Calgary).
- De Fromentel, E. (1861). *Introduction à l' etude des polypiers fossils*. Savy, Paris, 357p.
- Ehrenberg, C.G. (1834). Beitrage zur physiologischen Kenntnis der Corallen. Thiere im allgemeinen, and besonders des rothen Meeres, nebst einem Versuche zur physiologischen Systematik derselben. *Königliche Akademie der Wissenschaften zu Berlin, Physiolog Abhandlungen* 1832:225-380.
- Etheridge, R. JR. (1902). Additions to the Middle Devonian and Carboniferous corals in the Australian Museum. *Records of Australian Museum.*, 4:253-262.
- Frey, H. and Leuckart, C.G.F.R. (1847). Beitrage zur Kenntniss wirbelloser Thiere mit besonderer Beruck Sichtung der Fauna des Norddeutschen Meeres: vii +170p. Verlag von Friedrich Vieweg und Sohn (Braunschweig).
- Geinitz, H.B. (1846). *Gudriss der versteinernerungen*, 401-813, Arnold (Dresden, Leipzig).
- Glinski, A. (1955). Cerioide Columnariidae (Tetracoralla) aus dem Eifelium der Eifel und des Bergischen Landes. *Senckenbergiana lethaea*, 36(1/2):73-114.

- Goldfuss, G.A. (1826), *Petrefacta Germaninae*. Erster Theil. -1 (1-4): XS. (nicht pagintert). 1-252. 71 Taf.; Dusseldoaf (Arnz and Comp).
- Goldfuss, G.A. (1829). *Petrefacta Germaniae*, I: 77-164; pl.xxvi-1, Arnz and Co. (Düsseldorf).
- Gürich, G. (1896). Das Paläozoicum des polnischen Mittelgebirges. *Berhandlungen der Russisch kaiserlichen Mineralogischen Gesellschaft zu St. Petersburg*, Ser. 2, 32:1-539.
- He, Y.-X. (1978). Rugosa. In: Southwest China Institute of Geological Science (Edt.): *Atlas of fossils of Southwest China. Sichuan* 1:1-x, 1-617.
- Hill, D. (1939). The Middle Devonian rugose corals of Queensland, 1: Douglas and Drummond Creek., Clermont District. *Proceedings of the Royal Society of Queensland*, 50: 55-65.
- Hill, D. (1956). Rugosa. In: R. C. Moore (ed.), *Treatise on Invertebrate Paleontology, Part F, Coelenterata*, p.F 233-F327, text-fig. 165-221, Geological Society of America and University of Kansas (New York, Lawrence).
- Hill, D. (1981). Rugosa and Tabulata In: Teichert. C. (ed), *Treatise on Invertebrate Paleontology, Part F, Coelenterata*, Supplement. 1: F1 - 429. The Geological Society of America. Inc and University of Kansas, Boulder, Colorado and Lawrence, Kansas.
- Hill, H. (1935). British terminology for Rugose Corals. *Geological Magazine*, 72, 857, 481-619.
- Khaing Khaing San. (2005). *Middle Devonian Rugose Corals of the Padaukpin Limestone, Pyinoolwin Township, Mandalay Division*. Unpublished Ph.D. Thesis, University of Mandalay, 282p.
- Kong Lei and Huang Yunming, (1978), Tetraceralla. In: Gui 2 hou Stratigraphy and Paleontology Work Team (ed) *Atlas of the Paleontology of the Southwestern Region of China, Guizhou*. Vol.1 Cambrian Devonian: 35-161.
- Krämer, T.J. (1982). Cerioide Rugosa aus dem Devon der Bergisch Gladbach – Paffrather Mulde (Rheinisches Schiefergebirge). *Neues Jahrbuch für Geologie und Paläontologie, Monatshefte*, 1982 (11): 648-666.
- Lang, W.D and S. Smith. (1934), 'Ludwig's corallen aus Paläolithischen formationen' and the genotype of *Disphyllum* de Fromentel. *The Annals and Magazine of the Natural History*. Ser 10, 13: 78-81.
- Lang, W.D., S. Smith and, H.D Thomas. (1940). *Index of Paleozoic coral genera*. British Museum, Natural History, London, 231 p.
- Liao, W.-H. and R. Birenheide. (1985). Rugose Korallen aus dem Givetium von Dushan, Provinz Guizhou, S. China. 2: Kolonien der Columnariina. *Senckenbergiana lethaea*, 65(4/6) : 265-295.
- Liao, W.-H. and R. Birenheide. (1989). Rugose corals from the Frasnian of Tushan, Province of Guizhou, South China. *Courier Forschungsinstitut Senckenberg*, 110:81-103.
- Milne-Edwards, H. and J. Haime. (1850). A monograph of the British fossil corals. First Part. Introduction; Corals from the Tertiary and Cretaceous Formations. *Paleontographical Society Monographs*, 3(2): 7.
- Pedder, A.E.H. (1964). Correlation of the Canadian Middle Devonian Hume and Nahanni Formations by tetracorals. *Palaeontology*, 7, (3): 430-451, pl. 62-73.
- Pickett, J. (1967). Untersuchungen zur Familie Phillipsastreidae. *Senckenbergiana lethaea* 48 (1): 1- EED, C. F. R. 1920.
- Schröder, St. (1998). Rugose Korallen und Stratigraphie des oberen Eifelium und unteren Givetium der Dolendorfer Mulde/ Eifel. (Mittel-Devon; Rheinisches Schiefergebirge). *Courier Forschungsinstitut Senckenberg* 208: 135 p.
- Schröder, St. (2002). Neue Daten zur Gattung *Tabulophyllum* Fenton and Fenton 1924 im Devon (Givetium, Frasnium) von Europa und Nord Afrika. *Senckenbergiana lethaea*, 82(2):515-543.
- Soshkina, E. D. (1941). Sistematika srednedevonskikh Rugosa Urala. *Trudy Paleontologicheskii Institut Akademii Nauk SSSR*, 10(4): 1-54.
- Swe Hnin Maung (2018). *Stratigraphy and Paleontology of the Nan-un-Kong-tha area, Hsipaw Township, northern Shan State*. MSc Thesis (unpublished), Lashio University.
- Wedekind, R. (1922). Zur Kenntnis der Stringoppyllen des oberen Mittel Devon.- Sitzungs. *Berichte der gesamten Naturwissenschaften zu Marburg*. 1921(1): 1-16.
- Wedekind, R. (1927). Die Zoantharia Rugosa von Gotland (Bes. Nordgotland). Nebst Bemerkungen zur Biostratigraphie des Gotlandium. *Sveriges Geologiska Undersökning*. Ser. Ca, No. 19, 35p.

FACIES ANALYSIS OF THE KYAUKKOK FORMATION IN THE SIN THE CHAUNG NEAR MILEPOST 240 BETWEEN NAY PYI TAW- MANDALAY HIGH-WAY

Win Win Myint¹, Min Min Khaing² and Thant Sin³

Abstract

The study area is located in the west of Tatkon Township, Mandalay Region. This area is well exposed of the Kyaukkok Formation (Burdigalian), the Obogon Formation (Vindobonian) and the Irrawaddy Formation (Pontian to Pliocene). In the study area, the Kyaukkok Formation is well exposed in the Sinthe Chaung. The Kyaukkok Formation is mainly composed of thin to medium bedded, gray, yellowish brown, fine to medium grained sandstone. Micaceous sandstone hard band are locally exposed. In some place, concretions, ripples and cross-laminations are common in the Kyaukkok Formation. In the present research, primary sedimentary structures are used for the facies scheme. The lithology, nature of the bed base and paleocurrent direction is also used to perform facies analysis to interpret the sedimentary environments. The Kyaukkok Formation of the Sinthe Chaung are divided into seven lithofacies such as thick bedded bluish gray shale facies, sandstone and shale alternation facies, thin to medium bedded sandstone facies, massive sandstone facies, trough cross- bedded sandstone facies, hummocky cross- stratification sandstone facies, and sand- mud interlayer facies. These facies can be grouped as prodelta/ offshore facies association, delta front facies association, delta plain facies association and outer shelf facies association. The Kyaukkok Formation is deposited in subtidal, intertidal, and offshore/ shelf environment.

Keywords – Kyaukkok Formation, Facies Analysis

Introduction

Location and Size

The study area lies between latitude 20° 05' 00" and 20°15' 00" N, longitude 95° 53' 00" and 95° 57' 00" E, along the Nay Pyi Taw - Mandalay High - Way (expressway) between mile post 233 -240, covering one inch topographic map No. 84 p/16 of Myanmar Survey Department (Figure.1). The study area is easily accessible by car all the year.

Physiography

The study area is located in northern part of the Bago Yoma and is mainly covered rolling hills and flat valleys. This rolling terrain is composed of several short ranges usually trending N-S direction. The study area has mainly gradual slopes and small number of steep slopes. The overburden soil covers over a wide area (Figure.2). The Sinthe Chaung is the northern boundary of the study area which is a main stream flowing from NNW-SSE direction. Dendritic drainage pattern is the most common in this area. Drainage pattern is medium to coarse texture in the all areas (Figure.3).

The study area is located in the Central Myanmar Region and semiarid climate is well developed. The rainy season is the most important season, because it takes place the flooding which has large effect on annual output of crop production, settlement pattern and transportation

¹. Lecturer, Department of Geology, Dagon University

². Lecturer, Department of Geology, Dagon University

³. Dr, Lecturer, Department of Geology, Dagon University

especially, Sinthe Chaung and its environs. In the study area, wood, bamboo, banana plant, bushes are observed. The alluvial plain is used as cultivated land, where peddy-fields and garden-fruit are grown.

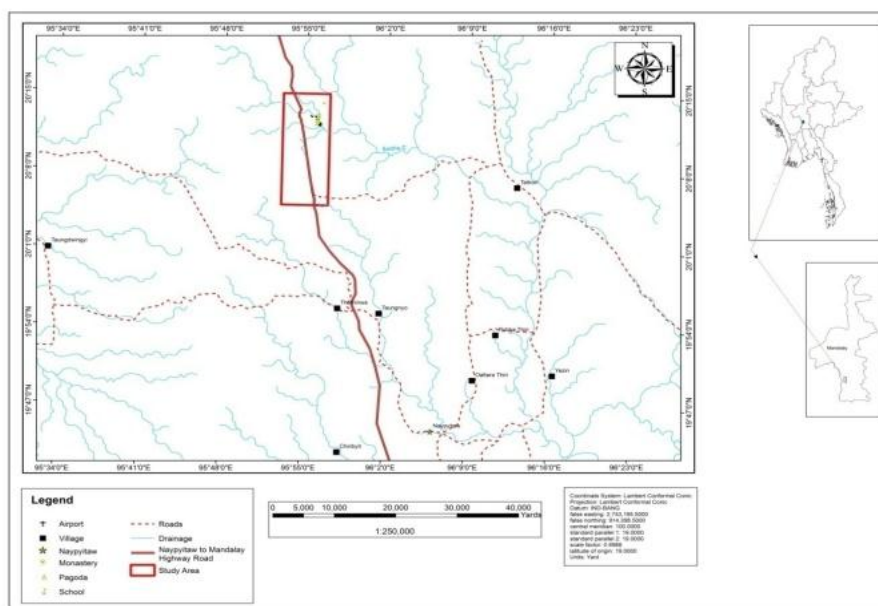


Figure 1 Location map of the study area

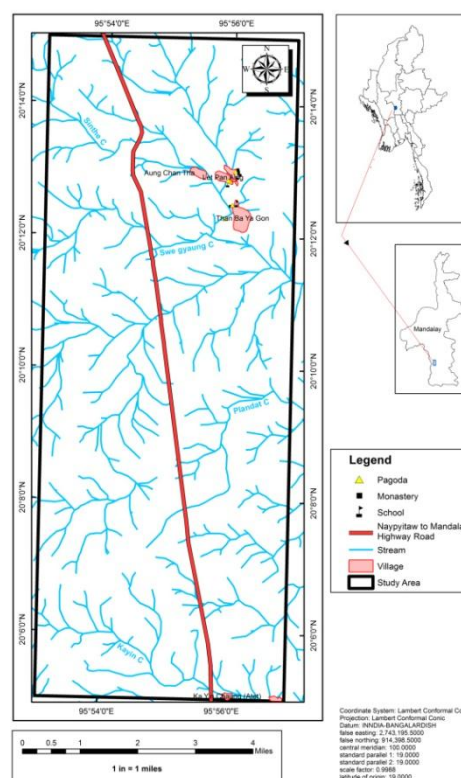
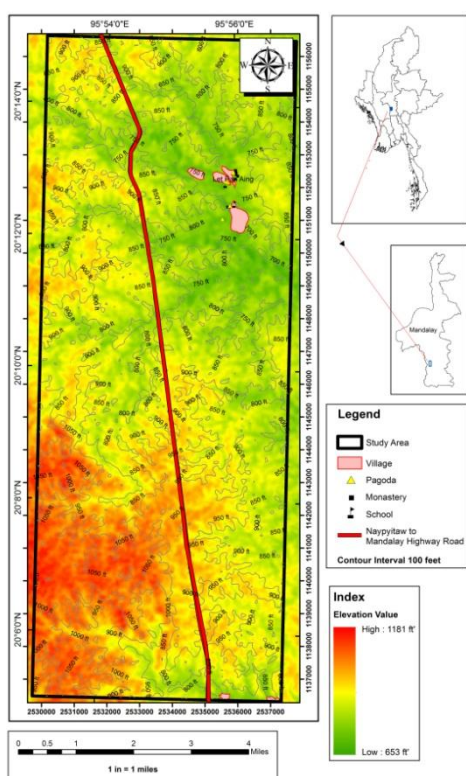


Figure 2 Topographic map of the study area. **Figure 3** Drainage pattern map of the study area

Purpose of Research

The present research has been carried out according to the following objectives:

1. To prepare a fairly detail geological map with appropriate scale.
2. To conduct the sedimentary facies analysis and to interpret the depositional condition
3. To reveal the lithofacies association of the study area.

Material and Methods

The literature review, aerial photo analysis, reconnaissance field checking and also collecting sample were done initially. Based on the sedimentary structures observed in the rock unit of the study area, the facies analysis has been established.

Regional Geology

The study area occupies the hinge of the Eastern trough and Western trough of the Central Cenozoic Belts of Myanmar and situated just east of the Central Volcanic line and well-known Sagaing Fault those runs north-south. The geological formations encountered belong to Pegu group and Irrawaddy Formation. In the study area, Kyaukkok Formation mainly composed of yellowish brown to grayish brown, fine to medium grained sandstone with few alterations of shale and clay. Obogon Formation consists of medium to thick bedded, fine to medium grained, pale yellow to buff colour, soft sandstone and bluish gray to greenish gray shale. Irrawaddy Formation consists of yellowish to pinkish brown coloured, medium to thick bedded, coarse-grained, loosely consolidated sandstone with intercalated very thin bedded siltstone and clay/mudstone. These strata are generally NNW-SSE trending with east dipping but west dipping in some localities. The upper Pegu Group is bounded by an unconformity which occurs in Miocene and Mio-Pliocene Period (Figure 4 &5).

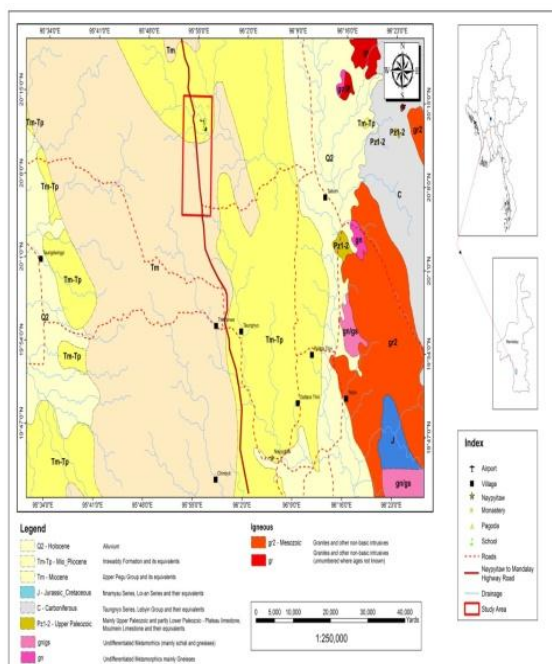


Figure 4 Regional geological map of the study area and its environs
(source: Myanmar Geosciences Society, 2014.)

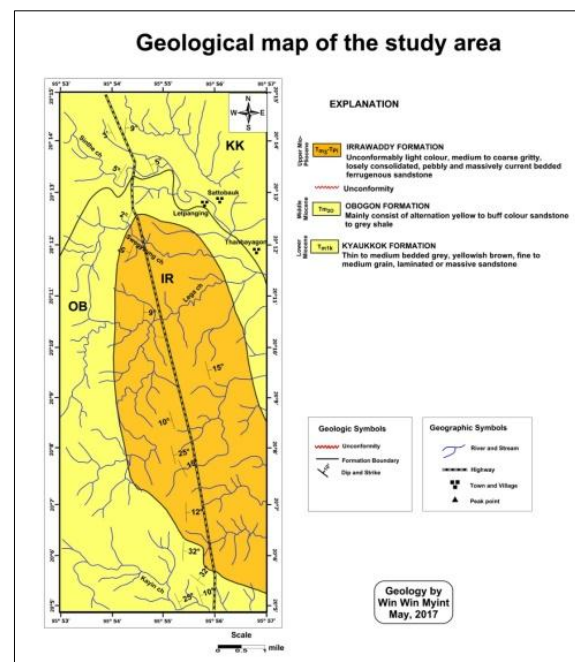


Figure 5 Geological map of the Study area.

Results and Discussion

Sedimentary Facies Analysis

In the study area, the depositional sedimentary features are used for the facies scheme. The lithology, nature of the bed base and paleocurrent direction were used to perform facies analysis and to interpret the sedimentary environments. Moreover, the petrographic characteristics can be used and certain conditions as an aid to the facies analysis.

To analysis the sedimentary facies of Kyaukkok Sandstones, sedimentologic measurements were made along the Sinthe Chaung near milepost 240 between Nay Pyi Taw – Mandalay High-Way.

Classification of Sedimentary Facies

In the study area, measurable exposures are observed. The columnar sections are established for each sedimentary facies. The clastic sedimentary rock sequences of the study area are subdivided into (7) facies as follow. (See Appendix)

They are:	Lithofacies (A)	Thick bedded bluish grey shale Facies
	Lithofacies (B)	Sandstone and shale alternation Facies
	Lithofacies (C)	Thin to medium bedded sandstone Facies
	Lithofacies (D)	Massive sandstone Facies
	Lithofacies (E)	Trough cross-bedded sandstone Facies
	Lithofacies (F)	Hummocky cross-stratification sandstone Facies
	Lithofacies (G)	Sand-mud interlayer Facies

Thick bedded bluish grey shale Facies

Description

This facies is mainly composed of bluish gray color and thin to medium bedded shale and nodular type (Figure.5). Locally, upward increase the shale content is occurred. Desiccational joints and calcareous sand concretion are common. Sand layer intercalated in shale units are also observed. The contacts of two adjacent layers are sharp, erosional and transitional.

Interpretation

Shale can occur away from the coast and settle out of suspension. The settlement of finer particle can be occurred in low energy environments. The presences of sandstone layers denote the storm generated sand layers. The bluish gray shale of nodular type was deposited in prodelta area (Reineck and Singh, 1980). Reading (1981) pointed that these thick accumulations of shale can be occurred in offshore or prodelta area.

Sand and shale alternation Facies

Description

In the study area, the alternations of sandstone and shale layers are widely distributed. Sandstones are gray to yellow, fine to medium grained and parallel laminations are common. Wavy and ripple laminations are also found in some horizons. Sandstones are hard and compact (Figure.6). Shales are bluish gray, thinly lamination and soft. The average thickness of sand bed

is about 6 cm to 30 cm thick and shale is about 1 cm to 2.5 cm. Sharp, erosional and transitional contact is common.

Interpretation

The alternate nature of sandstone and shale bedding resembles the current action and slack water depositional condition. The sand layers are deposited during current and wave activity. Most mud is deposited during period of slack water and just before and after the slack water condition. Alternate deposition of thick sandstone and shale layer can operate in areas other than tidal environments (Reineck and Singh, 1980). Therefore, the alternation of sandstone and shale layers might be formed by the alternation of transgression and regression condition.



Figure 5 Photograph showing thick bedded bluish gray shale exposed in the Sinthe Chaung (N 20° 13' 26", E 95° 54' 48"), facing east.



Figure 6 Photograph showing sandstone and shale alternation in the Sinthe Chaung (N 20° 13' 22", E 95° 54' 26"), facing south-east

Thin to medium bedded sandstone Facies

Description

This facies is mainly consists of thin to medium bedded, fine to medium grained, gray to buff coloured sandstone with thin mud intercalation resting on wavy or slight erosional base (Figure.7). The sandstone beds of this facies are generally wavy laminated. Some of the beds are composed of parallel laminated sandstone whereas wave ripples present on top of some beds. Moreover, the rare case is that the micro deformational features such as flame structure are occurred at the base of some beds intercalated in shale veneer. This facies is generally associated with thick bedded bluish gray facies, and flaser or lenticular-bedded facies. This facies is thickening upward nature.

Interpretation

Thin to medium bedded sandstone of Kyaukkok Formation was deposited in delta front environment. The initially associated wavy laminations were form between the storm wave base and fair-weather wave base (Walker, 1992). The micro-deformational features are indicative of the prodeltaic environment under the high rate of sedimentation. The beds thickness and facies association show that this facies was deposited in lower subtidal or delta front area. The present of sand beds alternative with mud intercalation point out the area of the energy condition and slack water period (Reineck and Singh, 1980).

Massive sandstone Facies

Description

Massive sandstone and some clay are interbedded in these sandstones. Massive sandstone is dark grey in fresh colour and yellow colour in weather surface (Figure.8). Mud pebbles are found. Sandstones are fine to medium grained, moderately hard and compact. The bed thicknesses are variable and coarsening upward nature is the characteristic feature in this facies. Sharp (parallel and erosional) contact is characterized, but in some horizons, transitional contact is also common.

Interpretation

Massive sandstones are representing the abundance of sand supply conditions during high energy regime. The intraformational mud pebbles are commonly concentrated at the base of point bar (Reineck and Singh, 1980). The lithologic character and facies scheme tend to regard that it may be either upper shore face (fore shore) or shallow channel. Therefore it may be deposited in near shore or beach environment.



Figure 7 Photograph showing thin to medium bedded sandstone exposed in the Sinthe Chaung (N 20° 13' 22", E 95°54' 26"), facing south-east.



Figure 8 Photograph showing thick bedded sandstone exposed in the Sinthe Chaung. (N20° 13' 22", E 95°54' 26"), facing south-east.

Trough cross-bedded sandstone Facies

Description

This facies is mainly composed of fine-grained, gray colour, soft to moderately hard sandstone. The primary sedimentary structure is trough cross bedded and wavy laminations (Figure.9). Paleocurrent directions of cross-beds sets show southwest in lower horizon whereas the northeast in the upper part of Kyaukkok Formation. The bed base type of this facies is erosional type. The average thickness of this cross bedding is about 4 to 8 inches in height and 8 to 12 inches wide.

Interpretation

The sandstones with cross bedded on erosional base point out that the depositional environment is channel area where erosive base occurs. The unidirectional paleocurrent indicate that the deposition medium was influenced by river. They are mostly as a result of depositional from migration small current and ripples (Reineck and Singh, 1980). This facies is deposited under shallow marine intertidal environment.

Hummocky cross-stratification sandstone Facies

Description

Hummocky cross-stratification are found in fine to medium grained, gray to dark gray colour, thick bedded to massive sandstones. The hummocky cross-stratification of curving laminations, both convex-up (hummocky) and concave-up (swale) (Figure.10). Base contact is erosional and upper contact is parallel. The thickness of this bed is 6 cm to 15 cm. These beds are truncated each other in this facies. The thickness of this facies is about 10 m.

Interpretation

Hummocky cross-stratification indicated that storms domination dominated facies succession (Walker, 1984). It may be deposited in the middle shelf platform where there was a storm action. Moreover, these were generated in storm condition by geostrophic currents especially in sub-tidal area. Storm deposits are commonly preserved in prograding shore face successions (Dyson, 1995). Cores of possible hummocky cross-stratifications have been obtained from the shore face (Greenwood and Sherman, 1986). Therefore, this facies is deposited in sub-tidal environment under influence of storm.



Figure 9 Photograph showing trough cross bedded sandstone unit exposed in the Sinthe Chaung (N 20° 13' 22", E 95° 54' 26"), facing south-east



Figure 10 Photograph showing wave ripple and small hummocky cross-stratification sandstone exposed in the Sinthe Chaung (N 20° 13' 28", E 95° 54' 16" facing east.

Sand-mud interlaying Facies

Description

Sand-mud interlayer facies composed of flaser, lenticular, and sand/ mud alternate heterolithic beds (Figure.11, 12). The flaser facies comprises the micro cross-laminated sand layers alternating with bluish gray mud concentrating on the trough of the adjacent ripple with unidirectional or bi-directional paleocurrents. Sand-shale ratio is 3:2 in average. The lenticular-bedded sandstone facies is characterized by ripple (linguoid) topped thin-bedded sand-mud alternation.

Both fining and coarsening sequence occur and associate with trough cross bedded sandstone facies and shale facies. Thin sand mud alternation facies comprises various proportions of fine sand and mud with transitional bedding character. This facies can be observed in the Sinthe Chaung.

Interpretation

Flaser, lenticular bedded sandstone facies was confirmed to be deposited in intertidal mixed flat area (Klevin, 1971). These alternate beddings are mostly related to the tidal current and slack water phases (Reineck and Singh, 1980). The bi-directional micro-cross laminated indicates the tidal influence. Moreover, the flaser beddings, lenticular beddings, wavy ripples and finely interlayered sand-mud beddings are the characteristic features of the intertidal mixed flat (Reading, 1980). Under the constant fluctuation but relatively in a low energy condition (Reineck and Singh, 1980).



Figure 11 Photograph showing hummocky cross-stratification sandstone with event horizontal though to be deposited of seismite in the Sinthe Chaung (N 20° 13' 28", E 95° 54' 16"), facing east.



Figure 12 Photograph showing the sand-mud inter layer bedding the sand composed of micro-cross lamination (N 20° 13' 27", E 95° 54' 16), facing east.

Facies Association

A combination of one or more facies which are formed in the same deposition environment at a certain geologic time can be grouped as a facies association. A facies association can be used for the more detailed interpretation of depositions handled the transgressive-regressive episodes. Thus, these facies can be grouped as prodelta/ offshore facies association (thick bedded bluish grey shale facies), delta front facies association (sandstone and shale alteration facies, thin to medium bedded sandstone facies, shale intercalated with sandstone facies), delta plain facies association (massive sandstone facies, trough cross-bedded sandstone facies, hummocky cross-stratification sandstone facies), and outer shelf facies association (sand mud inter layer facies).

Summary and Conclusion

The study area is located in west of Tatkon Township, Mandalay Region. It is mainly composed of Neogene and Quaternary clastic sedimentary rocks. The three lithostratigraphic units namely the Kyaukkok Formation, the Obogon Formation and Irrawaddy Formation have been observed. The present study mainly focused on facies analysis of the (Early Miocene) Kyaukkok Formation. Totally seven sedimentary facies can be divided in this area: (A) Thick bedded grey shale Facies, (B) Sand and shale alteration Facies, (C) Thin to medium bedded sandstone Facies, (D) Massive sandstone Facies, (E) Trough cross-bedded sandstone Facies, (F) Hummocky cross-stratification sandstone Facies, and (G) Sand-mud interlayer Facies. They can be grouped into three lithofacies association; (i) Intertidal Facies Association, (ii) Subtidal Facies association and (iii) Prodelta /Offshore Facies Association. The sandstone of Kyaukkok

Formation was laid down shore face during Early Miocene (Burdigalian). Thus a short term marine regression took place. After then, this area may become deeper in latter transgression period of Burdigalian which is documented by the thick clay unit underlying the sandstones. This transgression was followed by subsequent minor regression leading to be formed the tidal flat sedimentation. The sandstones of the Kyaukkok Formation are economically used as construction and road materials.

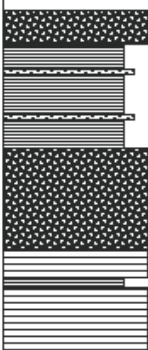



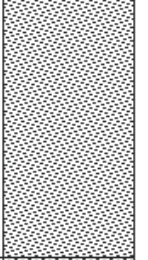




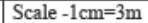
Acknowledgements

I would like to mention my deep gratitude to Dr Daw Kyi Kyi Maw (Professor and Head, Department of Geology) Dagon University, for allowing to submit this research paper and her guidance, support, critical reading of manuscripts and suggestion. I would like to thank Dr. Daw Aye Aye Aung (professor, Department of Geology) Dagon University, for her guidance and suggestion. I am especially grateful to Dr Day Wa Aung (Professor and Head, Department of Geology, University of Yangon) for his valuable guidance and advice. I also thank to all the teachers (Department of Geology, Dagon University) for their literature support and suggestions.

References

- Aung Khin and Kyaw Win (1969). Geology and Hydrocarbons prospects of the Burma Tertiary Geosyncline. Union of Burma Jour.Sci & Tech, V2, No.1.
- Clegg, E.L.G. (1938). The Geology of the part of the Minbu and Theyetmyo District, Burma. Mem.Geol. Surv. India, V-72.
- Dyson, I.A., (1995). A review of storm deposits in geologic al record. PESA Journal. No. 23, P.39-50.
- Greenwood, B. and Sherman, D.J., (1986). HCS in the surf zone: flow parameters and bedding genesis: sedimentology.V-33, 33-45.
- Reading, H. G. (1981). *Sedimentary Environment Facies*: Oxford Blackwell Sci Publications
- Klevin, G. de. V., (1971). Determination of Paleotidal range in clastic sedimentary rocks: Bull. Geol. Soc.Amer., v.82, p. 2582-2592.
- Reineck, H.E.and J.B Singh, (1980). Depositional Sedimentary Environments. Springer Verlag, N.Y.
- Stuart, M., (1912). The Geology of the Henzada District, *Burma Rec. Geol. Surv. India*, v-41, 240-265.
- Walker, R.G., (1984) *Facies Models*: Geosciences Canada. 317 pp.
- Walker, R. G. and P. J. Noel., (1992). Facies Models: Response to Sea level changes, Geological asso. of Canada. 409 p.

Appendix

Age	Formation	Thickness	Lithology	Lithofacies
Early Miocene	Kyaukkok Formation	71.4m		Sand and shale alteration facies (B)
		50.4m		Sand – mud interlayer facies (G)
		46.8m		Sand and shale alteration facies (B)
		36.7m		Bluish grey shale facies (A)
		26m		Massive sandstone facies(D)
		9.5m		Through Cross-bedding sandstone facies (E)
		6.6m		Thin to medium bedded sandstone facies(C)
		5.2m		Bluish grey shale facies (A)
		3.4m		Hummocky cross-stratification sandstone facies (F)
		0m		
Total Thickness		71.4m	Scale -1cm=3m	

Stratigraphic column of Kyaukkok Formation exposed along the Sinthe Chaung
(N 20° 13' 22" to 20° 13' 28" and E 95° 54' 16" to 95° 54' 26")

APPLICATION OF MARKOV CHAIN AND ENTROPY FUNCTION FOR CYCLICITY ANALYSIS OF OLIGOCENE FORMATIONS OF NGAPE-YENAMA AREA, SOUTHERN PART OF MINBU BASIN, MYANMAR

Naw Chel Phaw¹, Tun Naing Zaw², Day Wa Aung³

Abstract

The area under investigation lies between Padan (Minbu District) to the north and Yenama (Thayet District) to the south. The exposed stratigraphic sections in the study area are from Cretaceous Formation at the base to Pleistocene Formation at the top. The main structure of the study area is mainly monocline structure. The main target research interests on Shwezetaw Formation, Padaung Formation, and Okhmintaung Formation. To prove similar cyclic arrangement in the lithofacies of the study area, the Markov property and entropy analysis was applied to test for the presence of order in the sequence of structures or descriptive facies in the Minbu Basin. The presence study is based on the outcrop and stratigraphic columnar section. According Markov Chain analysis, shaly sandstone facies to trough-cross bedded sandstone facies, shaly sandstone facies to thick-massive sandstone facies, shale facies to thinly laminated sandstone facies and arenaceous shale facies can be cyclical in Shwezetaw Formation. Shale facies to thinly laminated sandstone facies can be cyclical before pass to carbonaceous sandstone facies. Transition directed from shale facies to thinly laminated sandstone facies skipping sandy shale in Shwezetaw Formation. No transition from sandy shale to thinly laminated sandstone and carbonaceous sandstone to shaly sandstone. Shale facies to sandy limestone facies can be cyclical in Padaung Formation. Shale facies to massive sandstone facies can be cyclical in Okhmintaung Formation.

Keywords: Lithofacies, Markov chain analysis, cyclicity, transition.

Introduction

The area is located between latitudes 19°46'00"N to 20°04'00" N, and longitudes 94°25'00" E to 94°40'00" E, covering approximately 9.3 miles (15km) in width and 24.8 miles (40 km) in length. It is situated in the western flank of Salin syncline and also situated between Padan to the south and Yenama to the north, Figure (1). There are two major streams which generally flow from west to east and locally named Mann Chaung in the northern part and Sabwet Chaung in the southern part. These streams flow into the Ayeyarwaddy River. Generally, pattern of the main streams and its tributaries are mainly developed parallel to the regional strike, and tectonic structure such as faults and fractures. The topography of the eastern region is characterized by flat lying and the mountainous rugged terrains in the western margin, trending NNW-SSE direction.

¹ Assistant Lecturer, Department of Geology, University of Yangon

² Lecturer, Department of Geology, University of Yangon

³ Professor and Head, Department of Geology, University of Yangon

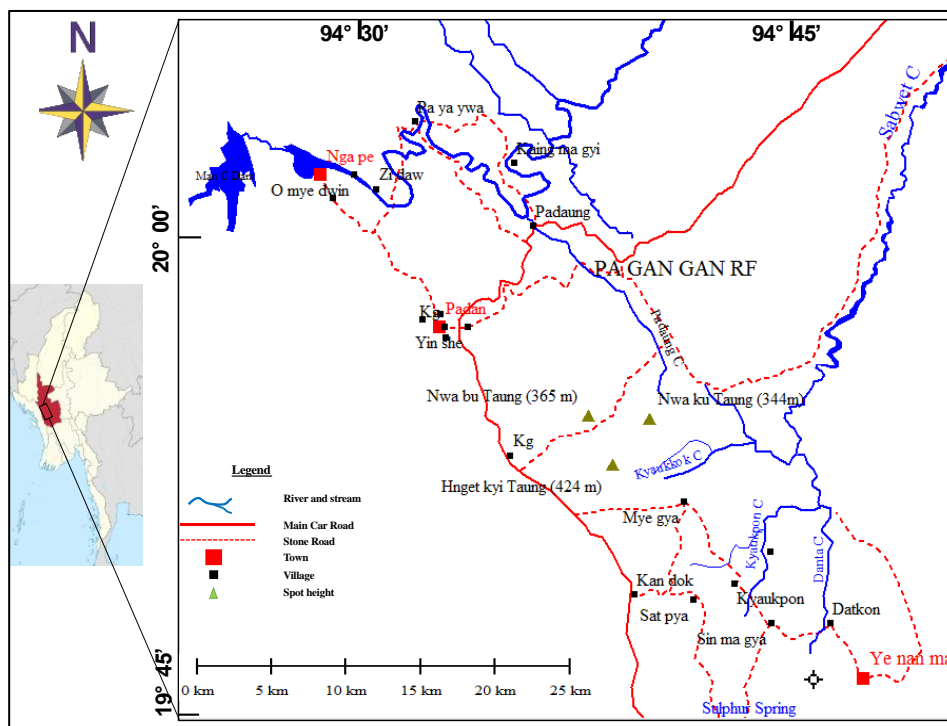


Figure 1 Location map of the study area

Regional Geology

The study area consists of the following formations and the lithostratigraphic correlation is shown in Table (1). This research mainly focused on the Oligocene Formations such as Shwezetau Formation, Padaung Formation, and Okhmintaung Formation.

Shwezetau Formation

Type section of this formation is at the Shwezetau Hill (Shwezetau Pagoda) in the Mann Chaung area. The stratigraphic thickness of the Shwezetau Formation is 3200-4600 ft. It is made up of yellowish brown sandstones interbedded blue gray shales from north to South. The lower part of the Shwezetau Formation is composed of yellowish brown to bluish grey, soft, fine-grained calcareous thinly bedded sandy shale interbedded with bluish grey, carbonaceous shale and sand-shale alternation. The Shwezetau Formation may be assigned to the Early Oligocene age. Shwezetau Formation was deposited in low to high energy conditions. Figure (2A) and figure (2B).

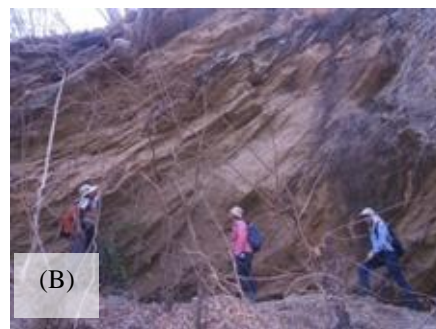
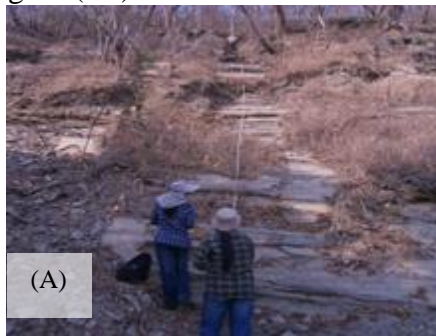


Figure 2 Sandstone unit of Shwezetau Formation; (A) Medium bedded sandstone interbedded with thinly laminated shale in the middle part of Shwezetau Formation at Shwezetau-Nga pe road section, facing NE (Lat: 20° 05' 44"N, Long: 94° 31' 37"E), (B) Medium-to thick-bedded sandstone in the upper part of Shwezetau Formation at Shwezetau Pagoda, facing NE (Lat: 20° 05' 44"N, Long: 94° 31' 40"E)

Padaung Formation

It is well developed along the Mann Chaung and its tributaries. The maximum stratigraphic thickness of the Padaung Formation is 1500- 3200ft. It is composed of massive and lumpy deep bluish gray to gray, nodular sandy shale in which gastropod and lamellibranch shells are embedded. The middle and upper parts of the Padaung Formation are characterized by the development of fossiliferous sandy limestone and yellowish, fine- to medium-grained, medium- to thick-bedded. Vertical and horizontal burrows, larger forams occurred in the sandy limestone. Bluish gray shale, shaly sand and sandy limestone sequence are observed in the middle and upper parts. The age of the Padaung Formation as Middle Oligocene in age. The Padaung Formation is deposited in low energy environment, offshore area. Figure (3A) and (3B).

Okhmintaung Formation

The Okhmintaung Formation occupies a part of the Salin Syncline. It is well exposed at the bank of the Mann Chaung in south of U-Yin and in north of Kaingmagyi villages. The stratigraphic thickness of the Okhmintaung Formation along the Mann Chaung is 2640 ft. It is composed of light yellowish brown, moderately hard, fine to medium-grained sandstones, massive and micro-current bedded with ferruginous gritty and pebbly sandstone lenses.

In the lower part, bluish gray sandstones with concentrated carbonaceous materials and gypsum flakes along the bedding planes. Gastropods and lamellibranches also observed in the sandstone. Fossil bed (3-5 cm thick) is intercalated between sandy shale and sandstone in the middle part. The upper part of this formation is made up of yellowish, fine- to medium-grained, thick-bedded sandstone. Ferruginous concretion and climbing ripples are observed in the sandstone unit and thin gypsum layers are occurred along bedding plane. Okhmintaung Formation is Late Oligocene in age. Okhmintaung Formation was deposited in intertidal to subtidal area in near shore environment. Figure (4A) and (4B).

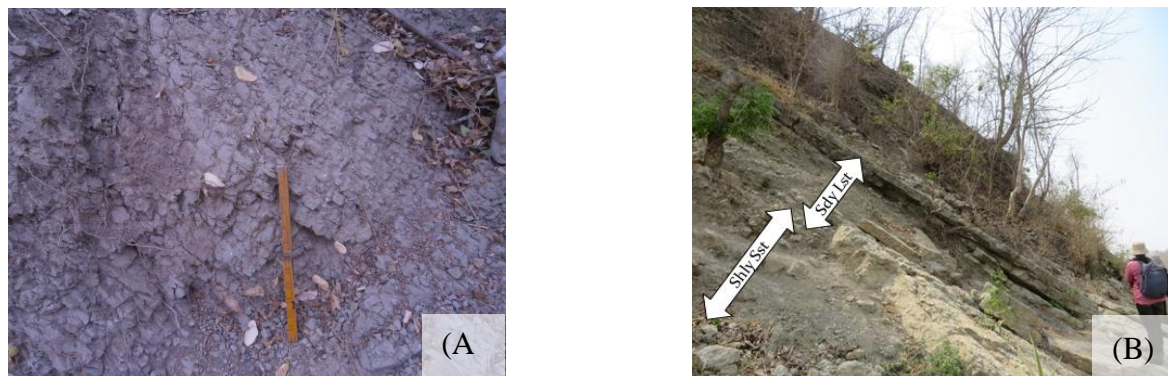


Figure 3 Lithologic unit of Padaung Formation; (A) Light gray and nodular sandy shale in lower part of Padaung Formation near Auk set taw yar, facing WNW (Lat: 20° 06' 43"N, Long: 94° 31' 38"E), (B) Bluish gray shale-shaly sand-sandy lime sequence in the middle part of Padaung Formation near Payaywa, facing WNW (Lat: 20° 06' 51"N, Long: 94° 31' 38"E)



Figure 4 Sandstone unit of Okhmintaung Formation; (A) Sandy upward sandy shale layers in the middle part of Okhmintaung Formation near Uyin Village, facing E (Lat: 20° 03' 51"N, Long: 94° 35' 32"E), (B) Thick-bedded to massive sandstone in the upper part of Okhmintaung Formation near Uyin Village, facing WNW (Lat: 20° 03' 55"N, Long: 94° 35' 40"E)

The general structural trends of the study area is NNW-SSE in direction. All of the beds of formations are nearly NE in directions. Major fold is a broad monoclinal syncline. In the western part of the study area, steep dips towards the east in dip amount of 45° to 60°. In the eastern part of the study area, become gradually shallow to the east towards the Minbu syncline, 20° to 15°. In the southern part of the study area, dip amount of the monocline gradually decrease from 30° to 10°. Monocline is cut-cross by a series of E-W trending cross faults, more abundant in distribution and longer in length to the south of the study area, figure (6).

Table 1 Correlation table of the stratigraphic unit of the Myanmar (Dr Maung Thein, Nov, 2000) and revised May, 2010

GEOLOGICAL AGE		CHIN HILL & N. RAKHINE YOMA		MINBU BASIN	NORTHERN SHAN STATE West East		S. SHAN STATE & KAYAN STATE	KAYAN & MON STATE & TANINTHAYI		
Holocene		Mountain Soil		Alluvium	Terrarossa soil		Terrarossa soil Travertine, cave & lake deposits	Alluvium Laterites		
Pleistocene				Terraces Maw Gravels	Travertine & cave deposits Gem gravels of Mogok					
Pliocene				Irrawaddy Fm	Sand, Pebbles bed, Lignite					
Miocene	L	Pegu Group		Obogon Fm				Oil Shale Of Hthichara Basin		
	M			Kyaukkok Fm						
	B			Pyawbwe Fm						
Oligocene	L			Okhmintang Fm						
	B			Padaung Fm						
				Shwezetaw Fm						
Eocene				Yaw Fm						
	L			Pondaung Fm						
	M			Gwa Fm					Kennedy Fm	Tabyin Fm
	B			Khayingyi Fm					Tilin Fm	
Paleocene									Laungshe Fm	
	L			Ngapali Fm					Paunggyi Fm	
	B								Kabaw Fm	
Cretaceous	L			Nayputang Ls					Paung Chaung Ls	
				Rangfi Fm					Orbitolina Ls	
	B									
				Kalaw Red Bed						

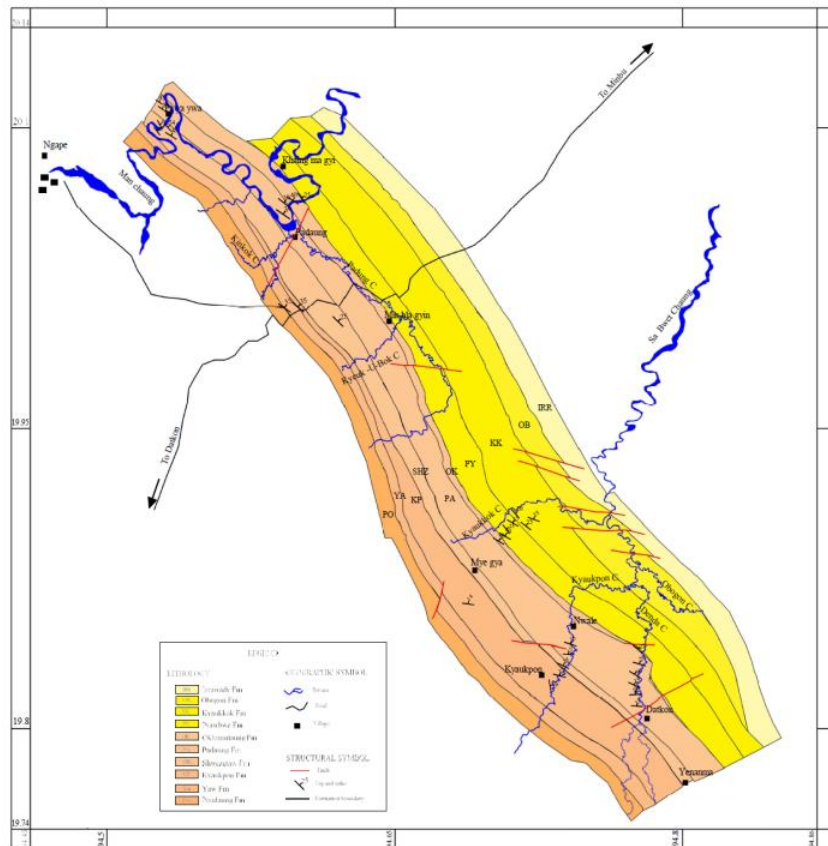


Figure 6 Geological map of the study area (Based on M.O.C, 1982)

Cyclic Sedimentation and facies relationship based on Markov Chain Analysis

Structuring data for Markov chain

Vertical sequence profile

Seventeen lithological sections were considered for studying the vertical and a real distributions of the lithofacies within the research area.

Nature of Data

The data used in the study is different lithofacies in a verticalised inventory log sequence coded into a finite number of states for the statistical analysis. In this study twelve sublithofacies for Shwezetaw Formation, six sublithofacies for Padaung Formation, and six sublithofacies for Okhmintaung Formation are used which are clearly marked in outcrop section as well as in each sedimentary log and this is also done in order to prevent diffusion of transitions between two lithofacies (Maejima, 2004).

For the statistical inter relationships between different lithofacies, following twelve variables were extracted from the ten vertical log successions for Shwezetaw Formation, six variables were extracted from the four vertical log successions for Padaung Formation, and six variables were extracted from the three log successions for Okhmintaung Formation. The lithofacies variables (descriptive characteristics in the previous section) and the symbols used to designate them are as follows:

Sub-lithofacies variations of Shwezetaw Formation

F1 : Shale	F7 : Fossiliferous Sandstone
F2 : Sandstone	F8 : Sandstone with planar lamination
F3 : Sandy Shale	F9 : Low-angle cross-bedded sandstone
F4 : Carbonaceous Sandstone	F10 : Trough cross-bedded sandstone
F5 : Shaly Sandstone	F11 : Thick to massive sandstone
F6 : Current Ripple	F12 : Glauconitic gritty sandstone

Cross-laminated Sandstone

Sub-lithofacies variations of Padaung Formation

- F1: Nodular shale facies
- F2: Cross-bedded sandstone facies
- F3: Gritty sandstone facies
- F4: Sandy shale facies
- F5: Shaly sand facies
- F6: Fossiliferous Sandy limestone facies

Sub-lithofacies variations of Okhmintaung Formation

- F1: Nodular shale facies
- F2: Massive sandstone facies
- F3: Thickening-upward current ripple cross laminated sandstone facies
- F4: Sandy shale facies
- F5: Shaly sandstone facies
- F6: Thick- bedded to massive sandstone facies

Calculation of frequency count matrix (F)

Frequency count matrix is calculated from the vertical sequence profile of sedimentary logs. Since we are using Markov chain which has memory less property i.e. the geologic situation at point (n-1) governs the event that will happen at n. That's why all seventeen sedimentary logs can be used to calculate matrix F without loss of information. Subsequently, data for all logs are added and matrix is structured at the basin level (Tewari et al., 2009). Number of transition from facies i to j is represented in row i and column j of matrix F, which signifies number of times state j followed immediately after state i in the sedimentary logs.

The frequency count matrix is structured into embedded Markov chain (definition below) considering only transition of lithologies and not their thickness as stated elsewhere. Since a transition is supposed to occur only when it results in a different lithology, the diagonal elements are all zero's in the resulting frequency matrix (Tewari et al., 2009).

Analytical procedure

In the present study, the embedded Markov matrix is used for structuring the frequency count matrix (F_{ij}), where i, j is the row and column number respectively. When $i=j$, zero is present in the matrix, this implies that the transition from one facies to another has only been recorded where there is an abrupt change in the lithofacies. The advantage of the embedded Markov matrix over the regular Markov matrix is that it is used to identify an actual order in facies transition, if present, regardless of the thickness of the individual bed (Hota and Maejima, 2004).

Transition frequency matrix (F): It is a two dimensional array which records the frequency of the vertical transitions that occur between the different lithofacies in a given stratigraphic succession. The lower facies of each transition couplet are given by the row numbers of the matrix, and the upper facies by the column numbers.

Upward transition probability matrix (P): The upward transition probability matrix calculates the probability of upward transition of lithofacies in a succession and is calculated in the following manner:

$$P_{ij} = F_{ij} / S_{Ri}$$

Where, S_{Ri} is the corresponding row total.

Downward transition probability matrix (Q): Downward transition probability determined by dividing elements of the transition frequency matrix (F) by the corresponding column total, i.e.

$$Q_{ji} = F_{ij} / S_{Cj}$$

Where, S_{Cj} is the column total. It calculates the probability of downward transition of lithofacies in a given succession i.e probability of facies i overlain by facies j .

Independent trail matrix (R): This matrix represents the probability of the given transition that occur in a random manner and is given by,

$$R_{ij} = S_{Cj} / (S_T - S_{Ri})$$

Where, S_T represents total number of facies transition. The diagonal cells are filled with zeros assuming each transition represent an abrupt change in facies characteristic.

Difference matrix (D): A difference matrix is calculated which highlights those transitions that have a probability of occurrence greater than if the sequence were random. By linking positive values of the difference matrix, a preferred upward path of facies transitions can be constructed which can be interpreted in terms of depositional processes that led to this particular arrangement of facies.

$$D_{ij} = P_{ij} - R_{ij}$$

A positive value in difference matrix indicates that a particular transition occurs more frequently and a negative value indicates that it occurs less frequently. In difference matrix the values in each rows of the matrix sum to zero. If the values are close to zero, a vertical succession with little or no 'memory' indicates independent nature of deposition of facies in a basin.

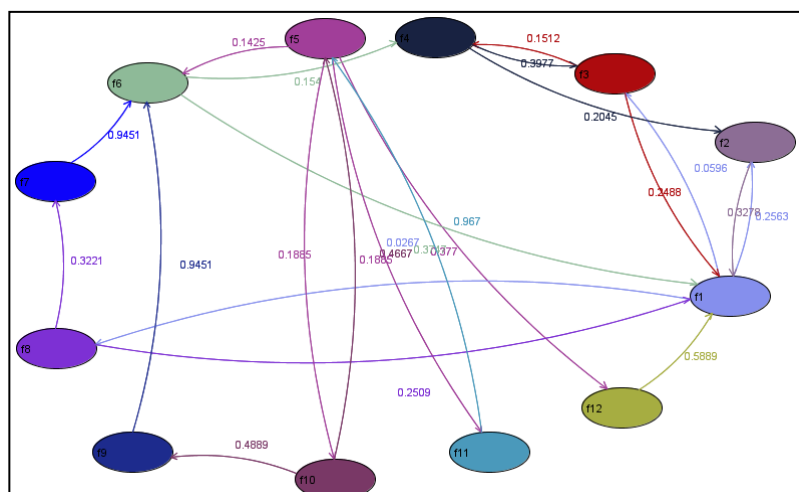
Expected frequency transition matrix (E_{ij}) of Shwezetaw Formation

	f1	f2	f3	f4	f5	f6	f7	f8	f9	f10	f11	f12
f1	0	0.396825	0.238095	0.063492	0.079365	0.079365	0.015873	0.047619	0.015873	0.031746	0.015873	0.015873
f2	0.506494	0	0.194805	0.051948	0.064935	0.064935	0.012987	0.038961	0.012987	0.025974	0.012987	0.012987
f3	0.448276	0.287356	0	0.045977	0.057471	0.057471	0.011494	0.034483	0.011494	0.022989	0.011494	0.011494
f4	0.397959	0.255102	0.153061	0	0.05102	0.05102	0.010204	0.030612	0.010204	0.020408	0.010204	0.010204
f5	0.402062	0.257732	0.154639	0.041237	0	0.051546	0.010309	0.030928	0.010309	0.020619	0.010309	0.010309
f6	0.402062	0.257732	0.154639	0.041237	0.051546	0	0.010309	0.030928	0.010309	0.020619	0.010309	0.010309
f7	0.386139	0.247525	0.148515	0.039604	0.049505	0.049505	0	0.029703	0.009901	0.019802	0.009901	0.009901
f8	0.393939	0.252525	0.151515	0.040404	0.050505	0.050505	0.010101	0	0.010101	0.020202	0.010101	0.010101
f9	0.386139	0.247525	0.148515	0.039604	0.049505	0.049505	0.009901	0.029703	0	0.019802	0.009901	0.009901
f10	0.39	0.25	0.15	0.04	0.05	0.05	0.01	0.03	0.01	0	0.01	0.01
f11	0.386139	0.247525	0.148515	0.039604	0.049505	0.049505	0.009901	0.029703	0.009901	0.019802	0	0.009901
f12	0.386139	0.247525	0.148515	0.039604	0.049505	0.049505	0.009901	0.029703	0.009901	0.019802	0.009901	0

Probabilities difference matrix (d_{ij}) of Shwezetaw Formation

	f1	f2	f3	f4	f5	f6	f7	f8	f9	f10	f11	f12
f1	0	0.230905	0.055229	-0.054054	-0.040541	-0.040541	-0.045828	-0.013514	0.016451	-0.013514	-0.013514	-0.013514
f2	0.318741	0	-0.139535	-0.0171	-0.034884	-0.005472	-0.028728	-0.011628	-0.023256	-0.011628	-0.011628	-0.011628
f3	0.304582	-0.268194	0	0.105121	-0.028302	-0.028302	-0.04717	-0.009434	-0.018868	-0.009434	-0.009434	-0.009434
f4	-0.439655	0.189655	0.396552	0	-0.025862	-0.025862	-0.043103	-0.008621	-0.017241	-0.008621	-0.008621	-0.008621
f5	0.564103	-0.307692	-0.102564	-0.034188	0	-0.025641	-0.042735	-0.008547	-0.017094	-0.008547	-0.008547	-0.008547
f6	-0.447368	-0.315789	-0.105263	-0.035088	0.473684	0	0.122807	-0.008772	-0.017544	-0.008772	-0.008772	-0.008772
f7	0.356522	-0.313043	-0.104348	0.165217	-0.026087	-0.026087	0	-0.008696	-0.017391	-0.008696	-0.008696	-0.008696
f8	-0.428571	-0.302521	-0.10084	-0.033613	-0.02521	-0.02521	0.957983	0	-0.016807	-0.008403	-0.008403	-0.008403
f9	0.230769	-0.307692	-0.102564	-0.034188	-0.025641	-0.025641	-0.042735	0.324786	0	-0.008547	-0.008547	-0.008547
f10	-0.428571	-0.302521	-0.10084	-0.033613	-0.02521	-0.02521	0.957983	-0.008403	-0.016807	0	-0.008403	-0.008403
f11	-0.432203	-0.305085	-0.101695	-0.033898	-0.025424	0.474576	-0.042373	-0.008475	-0.016949	0.491525	0	-0.008475
f12	-0.428571	-0.302521	-0.10084	-0.033613	-0.02521	0.97479	-0.042017	-0.008403	-0.016807	-0.008403	-0.008403	0

Facies relationship diagram of Shwezetaw Formation using Walker Method



Cyclicity of Shwezetaw Formation

According to the Markov chain analysis, Shwezetaw Formation have cyclicity from shale facies to trough cross-bedded sandstone facies, shaly sandstone facies to thick-bedded to massive sandstone facies, shale facies to sandstone with horizontal planar lamination facies, shale facies to sandy shale facies may be cyclical before passing to carbonaceous sandstone facies.

Moreover, there have no transition from sandstone facies to sandy shale facies, carbonaceous sandstone facies to shaly sandstone facies, and sandstone with horizontal planar lamination facies to low angle cross-bedded sandstone facies.

Then, transition directed from shale facies to sandy shale facies skipping sandstone facies. In this study, current action from offshore to lower shoreface can be cyclical before pass to Lower intertidal region in the Shwezetaw Formation.

Transition matrix (F matrix) of Padaung Formation

	f1	f2	f3	f4	f5	f6
f1	0	0	2	30	0	0
f2	1	0	0	0	0	0
f3	0	2	0	0	0	0
f4	25	0	0	0	2	2
f5	2	0	0	0	0	0
f6	2	0	0	0	0	0

Probability matrix (P matrix) of Padaung Formation

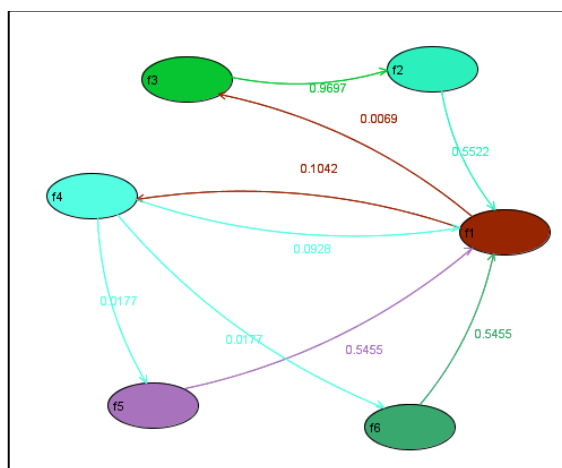
	f1	f2	f3	f4	f5	f6
f1	0	0	0.0625	0.9375	0	0
f2	1	0	0	0	0	0
f3	0	1	0	0	0	0
f4	0.862069	0	0	0	0.068966	0.068966
f5	1	0	0	0	0	0
f6	1	0	0	0	0	0

Expected frequency transition matrix (E_{ij}) of Padaung Formation

	f1	f2	f3	f4	f5	f6
f1	0	0.055556	0.055556	0.833333	0.055556	0.055556
f2	0.447761	0	0.029851	0.447761	0.029851	0.029851
f3	0.454545	0.030303	0	0.454545	0.030303	0.030303
f4	0.769231	0.051282	0.051282	0	0.051282	0.051282
f5	0.454545	0.030303	0.030303	0.454545	0	0.030303
f6	0.454545	0.030303	0.030303	0.454545	0.030303	0

Probabilities difference matrix (d_{ij}) of Padaung Formation

	f1	f2	f3	f4	f5	f6
f1	0	-0.055556	0.006944	0.104167	-0.055556	-0.055556
f2	0.552239	0	-0.029851	-0.447761	-0.029851	-0.029851
f3	-0.454545	0.969697	0	-0.454545	-0.030303	-0.030303
f4	0.092838	-0.051282	-0.051282	0	0.017683	0.017683
f5	0.545455	-0.030303	-0.030303	-0.454545	0	-0.030303
f6	0.545455	-0.030303	-0.030303	-0.454545	-0.030303	0

Facies relationship diagram of Padaung Formation using Walker Method

Cyclicality of Okhmintaung Formation

According to the Markov chain analysis, Okhmintaung Formation has cyclicality from nodular shale facies (f1) to massive sandstone facies (f2), and from massive sandstone facies (f2) to thick-bedded to massive sandstone facies (f6). Moreover, there have no transition from thickening-upward current ripple cross laminated sandstone facies (f3) to thick-bedded to massive sandstone facies (f6). Therefore, prodelta to delta front can be cyclical in the Okhmintaung Formation.

Summary and Conclusions

According to the Markov chain analysis, current action from offshore to lower shoreface can be cyclical before pass to Lower intertidal region in the Shwezetaung Formation.

In Padaung Formation, prodelta to shallow marine condition can be cyclical by transgression and regression. Moreover, prodelta to delta front can be cyclical in the Okhmintaung Formation.

Acknowledgements

The authors are greatly indebted to Dr Phoe Kaung (Rector, University of Yangon) for his kind permission undertake this research. We are deeply grateful to U Than Htut, Chief Research Officer (Retd.), Myanmar Oil and Gas Enterprise, for his kind help, give valuable advice and discussion.

References

- Formations of Talchir Basin, Orissa, India: A Statistical Analysis of Subsurface Logs, *Gondwana Research* 7(2):353-362.
- Hattori, I., (1976). Entropy in Markov chain and discrimination of cyclic pattern in lithologic successions. *Math Geol* 8: 477-497.
- Hnin Hnin Swe, (2011). Sedimentology and sequence stratigraphic analysis of the Shwezetaung and Padaung Formations in Minbu-Ngape Area, M.Sc Thesis, Unpublished, University of Yangon, Department of Geology, 88p.
- Hota and Maejima, (2004). Comparative Study of Cyclicality of Lithofacies in Lower Gondwana
- Maung Thein, (2000). Summary of the geological history of Myanmar, Unpublished paper, p.8.
- Miall AD, (1973). Markov chain analysis applied to an ancient alluvial plain succession. *Sedimentology* 20: 347-364.
- Tewari RC, Singh DP, Khan ZA (2009) Application of Markov chain and Entropy analysis to lithologic succession – an example from early Permian Barakar Formation, Bellampalli coalfield, Andhra Pradesh, India. *J Earth Sys Sci* 18: 583–596.

GEOCHEMICAL ANALYSIS OF SANDSTONE OF LAUNGSHE FORMATION IN THE ALE BAN AREA, TILIN TOWNSHIP, MAGWAY REGION

Kyaw Khaing¹ and Day Wa Aung²

Abstract

The present study mainly focuses on the Geochemistry of Clastic sedimentary rock mainly on the sandstones of Early Eocene Laungshe Formation exposed in the northernmost part of the Minbu Basin, Tilin, Magwe region. The study attempts to constrain their source rocks, palaeo-weathering and tectonic setting of the provenance. The study area mainly consists of Tertiary Clastic Sedimentary rocks. Selected samples from the research area were analyzed using X-ray Fluorescence (XRF) for major oxides and some trace elements to know the chemical composition of sandstone and to classify the sandstone. Lithologically, the Laungshe Formation is mainly composed of thinly laminated dark grey to bluish grey shale intercalated with thin to medium-bedded sandstones. By the XRF analysis, sandstones of the Laungshe Formation fell within the litharenite zone. The analysis also points out that most of the sandstones are Fe-sand composition. By the discriminant diagram the Laungshe sandstones samples indicating the mafic igneous provenance. Moreover, sandstones of The Laungshe Formation were deposited in the active continental margin shifted to the downward of the oceanic island arc field. Additionally, the average CIA and CIW values of Laungshe sandstones indicate extreme degree of chemical weathering might have taken place in the source area.

Keywords: Litharenite, Mafic igneous provenance, Active continental margin

Introduction

The research area, northernmost part of the Minbu Basin, is located at 16 km east of Tilin, Magwe region. It lies between latitudes 21° 36' N and 21° 44' N and longitudes 94° 09' E and 94° 17' E in UTM-No 2194-02 and 2194-06. The location map of the study area is shown in figure (1). Tilin is easily accessible from Pakokku by car. The western part of the study area can be easily accessible by car from Pakokku to Tilin throughout the year but the eastern part of the study area is less accessible in rainy season.

The research area is a mountainous and forested region and the ranges are running north-south direction. Because of the sandstone dominant and shale dominant formation, this area shows ridge and valley topography. The whole area is occupied by thick soil cover and cultivation is good. The study area is swampy during rainy season. It lies between Pondaung range and the eastern flank of the Chin hill. Three dimensional map of the study area is shown in figure (2).

¹ Assistance Lecturer, Department of Geology, Pakokku University

² Dr, Professor and Head, Department of Geology, University of Yangon

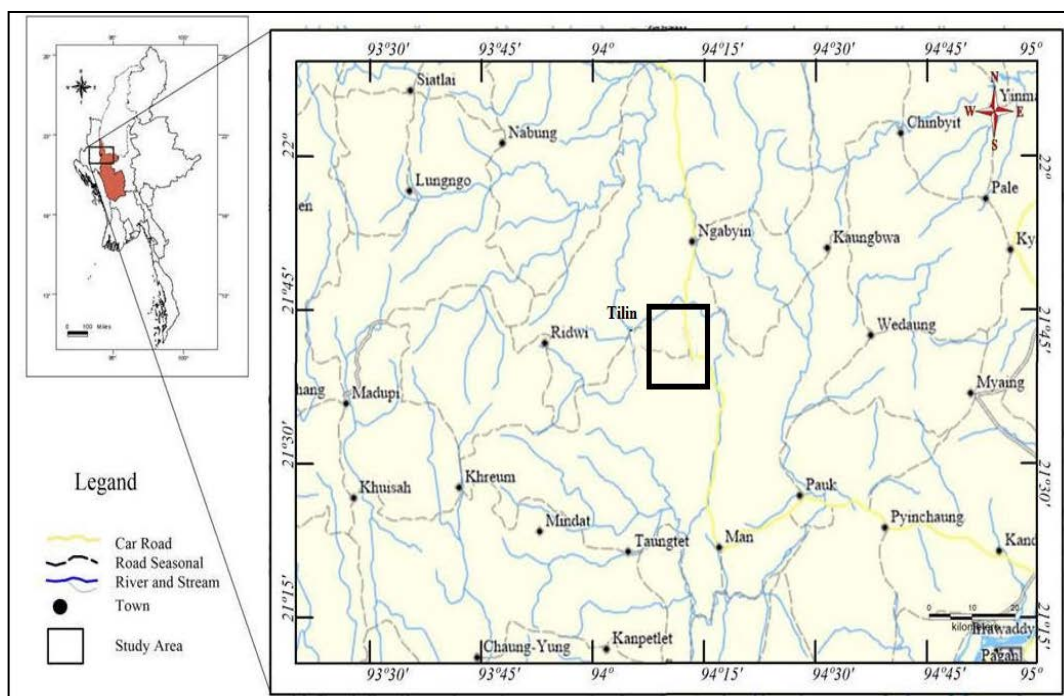


Figure 1 Location map of the study Area

Methodology

The X-ray Fluorescence (XRF) analysis conducted to know the chemical composition of sandstone and to classify the sandstone. The samples collected in the field were performed chemical analysis as X-ray Fluorescence. This method is most widely used analysis techniques in the application of quantitative major element analysis, minor and trace element analysis (Hutchison, 1974). Selected samples from the research area were analyzed using X-ray Fluorescence (XRF) for major oxides and some trace elements. In this research, X-ray Fluorescence (XRF) analyses were be done to interpret the chemical classification and weathering of the clastic sediments.

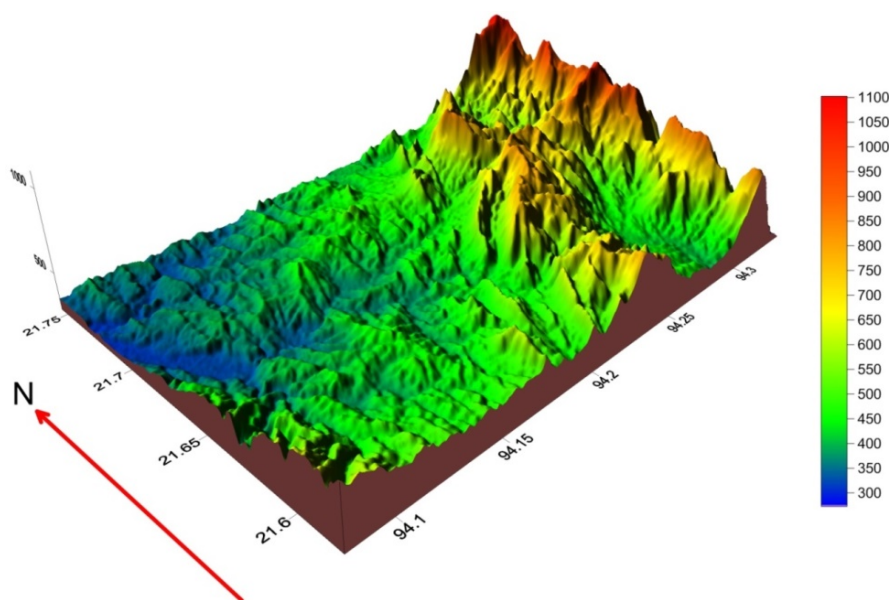


Figure 2 3D Map of the Ale ban Area, Tilin Township

Geochemical Analysis of Sandstone

Geochemical data are useful in the analysis of provenance studies, tectonic setting of basin, weathering, transport and erosion of sediments, depositional and diagenetic processes (Rollison, 1993). In geochemical analysis, the mineralogical and chemical composition of clastic sedimentary rocks are controlled by various factors, including (1) the composition of their source rocks, (2) environmental parameters influencing the weathering of source rocks (e.g., temperature, rainfall and topography), (3) duration of weathering, (4) transportation mechanism of clastic material from source region to depocenter, (5) depositional environment and (6) post-depositional processes (e.g., diagenesis and metamorphism).

The present study examines the geochemistry of sandstones including Laungshe Formations attempts to constrain their source rocks, palaeoweathering and tectonic setting of the provenance. Owing to limitations of analytical facilities, the present work is based on chemical analyses data of major elements of the investigated sandstones of the study area. The geochemical composition (Wt %) of Laungshe sandstones are shown in the Table (1).

Table 1 Chemical Composition of Laungshe Sandstone

Element	LS-2	LS-6	LS-8	LS-10	LS-14	LS-20	LS-22	LS-24	LS-36	LS-42
SiO ₂	48.07	55.14	61.2	59.74	57.58	56.9	60.86	60.59	41.87	60.85
Al ₂ O ₃	13.22	14.61	13.71	15.68	14.65	13.72	12.79	13.8	12.42	14.99
Fe ₂ O ₃	6.062	6.811	5.051	4.785	5.701	4.793	5.918	5.984	5.17	5.05
Na ₂ O	1.12	1.1	1.47	1.3	1.28	1.12	1.49	1.58	1.24	1.39
K ₂ O	1.06	1.16	1.01	1.08	0.997	1.11	0.899	0.89	1.19	1.29
SO ₃	0.044	0.033	0.045	0.03	0.032	0	0.047	0	0	0.031
TiO ₂	0.765	0.633	0.533	0.765	0.578	0.76	0.594	0.541	0.686	0.736
CaO	5.516	2.261	1.784	0.414	2.482	0.449	0.0948	0.496	16.5	0.3
MnO	0.179	0.102	0.237	0.0591	0.198	0.0345	0.0948	0.044	0.271	0.0339
Cr ₂ O ₃	0.0832	0.0432	0.0653	0.0966	0.0719	0.119	0.129	0.0511	0.0525	0.103
SrO	0.0223	0.0205	0.0142	0.0109	0.0162	0.0102	0.0118	0.0109	0.0387	0.0107
P ₂ O ₅	0.044	0.071	0.0775	0.074	0.103	0.046	0.056	0.07	0.123	0.036
ZrO ₂	0.0212	0.0122	0.0131	0.0191	0.0128	0.0187	0.0187	0.0128	0.0267	0.017
CuO	0.006	0	0	0	0	0	0	0	0	0.006
Rb ₂ O	0.004	0	0	0.003	0	0	0	0	0.003	0.004
ZnO	0.0099	0.0096	0.0078	0.0088	0.009	0.0085	0.0085	0.0079	0.0089	0.0099
NiO	0.0116	0.0126	0.01	0.0117	0.0099	0.0143	0.0126	0.0115	0	0.0126
FeO	0	0	0	0	0	0	0	0	0	0
MgO	1.63	1.827	1.52	1.87	1.861	1.36	1.38	1.581	2.835	2.143

Geochemical classification of sandstones

The composition of sandstone can be got from XRF analysis. To conduct XRF analysis, 10 sandstone samples were taken from the selected layer of sandstones from Laungshe Formation.

Sandstones are classified and named variously based on their chemical composition. In the present study, sandstones were classified according to the scheme proposed by Pettijohn *et al.* (1972) and Herron (1988). Although Pettijohn *et al.* (1972) classified the sandstones based on the bivarious log (Na₂O/K₂O) versus log (SiO₂/Al₂O₃) diagram. Herron (1988) proposed the bivariate log (Fe₂O₃/K₂O) versus log (SiO₂/Al₂O₃) diagram. Herron also examined the importance of the major oxide variables and classified the clastic rocks mainly as Fe-sands with little portions on the wacke zone. The results of log ratio are plotted on the diagrams of sandstone

classification. The geochemical classification diagrams of Pettijohn *et al.*, (1972) (figure-3) pointed that Laungshe sandstones fell within the litharenite zone. However one sample of Laungshe sandstone is greywacke. Herron (1988) (figure-4) also pointed out Laungshe sandstones are Fe-sand except one samples of sandstone.

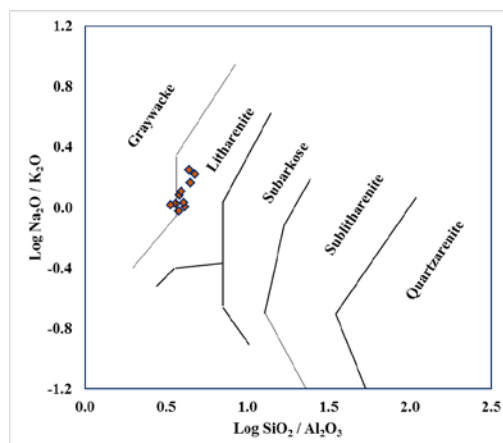


Figure 3 Chemical classification diagram of Pettijohn *et al.* (1972) of Laungshe sandstones

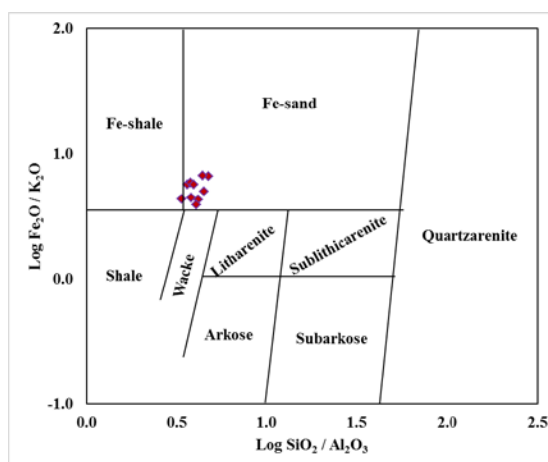


Figure 4 Chemical classification diagram of Herron (1988) of Laungshe sandstones

Source rock lithology and tectonic provenance

In the published literature several major-, trace-, rare-earth element-based discrimination diagram are proposed to decipher the source rock of the siliciclastic sedimentary rocks (eg., Taylor and McLennan, 1985; Roser and Korsch, 1988; McLennan *et al.*, 1993; Condie, 1993; Gu *et al.*, 2002; Cingolani *et al.*, 2003; Asieudu *et al.*, 2004). In order to use major element of provenance interpretations we considered the discriminant functions of Roser and Korsch (1988), which use Al_2O_3 , TiO_2 , Fe_2O_3 , MgO , CaO , Na_2O and K_2O contents as variables. In the discriminant diagram (figure-5), the Laungshe sandstones samples plot in the field of mafic igneous provenance. The Al_2O_3 and TiO_2 contents of the siliciclastic sedimentary rocks are considered as significant indicators of their provenance. During weathering of source rocks, Al and Ti remain essentially immobile, owing to solubility of their oxides and hydroxides in low temperature aqueous solutions (e.g., Stumm and Morgan, 1981; Yamamoto *et al.*, 1986; Sugitani *et al.*, 1996). It is well known that in normal igneous rocks Al resides mostly in feldspars and Ti in mafic minerals (e.g., olivine, pyroxene, hornblende, biotite, ilmenite).

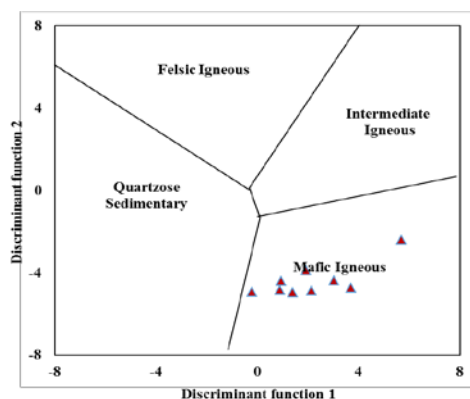


Figure 5 Discriminant function diagram for the provenance signation of the Laungshe sandstones using major elements, Roser and Korsch (1988)

Several studies have shown that the chemical composition of siliciclastic sedimentary rocks are significantly controlled by plate tectonic settings of their provenances and depositional basins, and as a result, the siliciclastic rocks from different tectonic settings possess terrain-specific geochemical signatures (Bhatia, 1983; Bhatia and Crook, 1986; Roser and Korsch, 1986). Among the various tectonic setting discrimination diagrams, the major element-based discrimination diagrams of Bhatia (1983) and Roser and Korsch (1986) are widely used. In the discrimination diagram of Bhatia (1983) and Roser and Korsch (1986) the bivariate, including discriminant functions, are based on immobile and variable mobile major elements, including Na_2O and K_2O .

In the present study, the discrimination diagrams proposed by Bhatia (1983) used to discuss the tectonic setting by the major element geochemistry of sandstone samples. The Laungshe sandstones were deposited in the active continental margin (figure 6c). However, in the diagrams of Bhatia 1983 (figure 6a and b), some of the Laungshe sandstones are shifted to the right of the oceanic island arc field because of Fe composition is high.

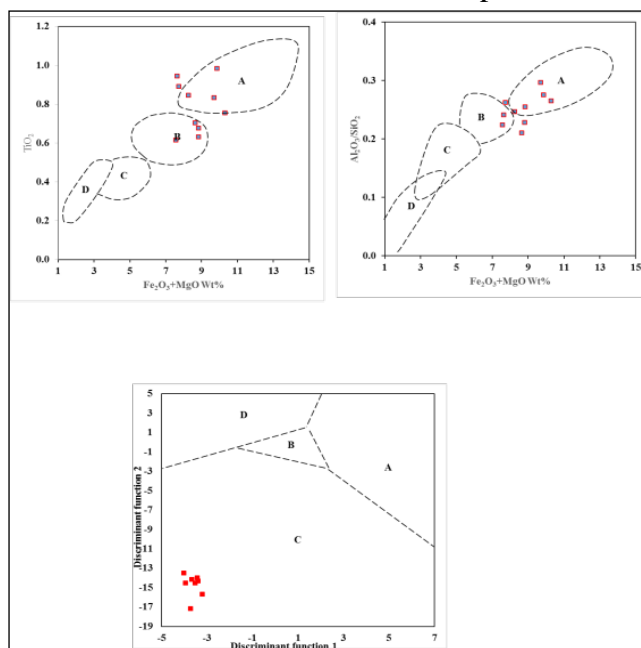


Figure 6 Plot of the major element composition of the Laungshe sandstone on the tectonic setting discrimination diagrams of Bhatia (1983). a: $\text{Fe}_2\text{O}_3 + \text{MgO}$ vs TiO_2 ; b: $\text{Fe}_2\text{O}_3 + \text{MgO}$ vs $\text{Al}_2\text{O}_3/\text{SiO}_2$; c: discrimination diagram. A: Oceanic island arc, B: Continental island arc, C: Active continental margin, D: Passive margin.

Geochemical weathering of source area

Intensity of chemical weathering of source rocks is controlled mainly by source rock composition, duration of weathering, climatic and rates of tectonic uplift of source region. About 75% of the labile materials of the upper crust is composed of feldspars and volcanic glass and chemical weathering of these materials ultimately results in the formation of clay minerals (e.g., Nesbitt and Young, 1982, 1989; Taylor and McLennan, 1985). During chemical weathering Ca, Na and K are largely removed from source rocks.

The degree of source rock weathering is quantified variously. A few indices of weathering have been proposed based on molecular proportion of mobiles and immobiles element oxides (Na_2O , CaO , K_2O and Al_2O_3). Among the known indices of weathering/alteration the Chemical index of Alteration (CIA; Nesbitt and Young, 1982) is well established as a method of quantifying the degree of source weathering. Source weathering and elemental redistribution during diagenesis also can be assessed using Chemical Index of weathering (CIW; Harnois, 1988). The weathering effects can be evaluate in terms of the molecular percentage of the oxide components, using the formulae of chemical index of weathering ($\text{CIW} = [\text{Al}_2\text{O}_3 / (\text{Al}_2\text{O}_3 + \text{CaO} + \text{Na}_2\text{O})] \times 100$); (Harois, 1988) and chemical index of alteration ($\text{CIA} = [\text{Al}_2\text{O}_3 / (\text{Al}_2\text{O}_3 + \text{CaO} + \text{Na}_2\text{O} + \text{K}_2\text{O})] \times 100$); (Nesbitt and Young, 1982). The CIA and CIW are interpreted in similar way with values of 50 for unweathering upper continental crust and roughly 100 for highly weathered materials, with complete removal of alkali and alkaline-earth elements (McLennan, 1993). Low CIA values (i.e. 50 or less) also might reflect cool and/or arid conditions (Fedó *et al*, 1995).

According to CIA values, the Laungshe sandstone of the degree of source weathering varies from 40 to 85% (average= 75.6%). CIW values suggest the degree of source weathering in the range from 39 to 79% (average= 80%). Average CIA and CIW values indicate extreme degree of source weathering.

Mobility of elements during the progress of chemical weathering of source material and post-depositional chemical modifications of the sandstones can be evaluated by plotting the molar proportions of Al_2O_3 , $\text{Na}_2\text{O} + \text{CaO}$ and K_2O in A-CN-K ternary diagram (Nesbitt and Young, 1982). Weathering trends might be predicated to be parallel to the A-CN join towards the composition of Al_2O_3 and Na and Ca are removed by chemical weathering of plagioclase feldspars. The average values of Laungshe sandstones indicate extreme degree of chemical weathering (figure-7)

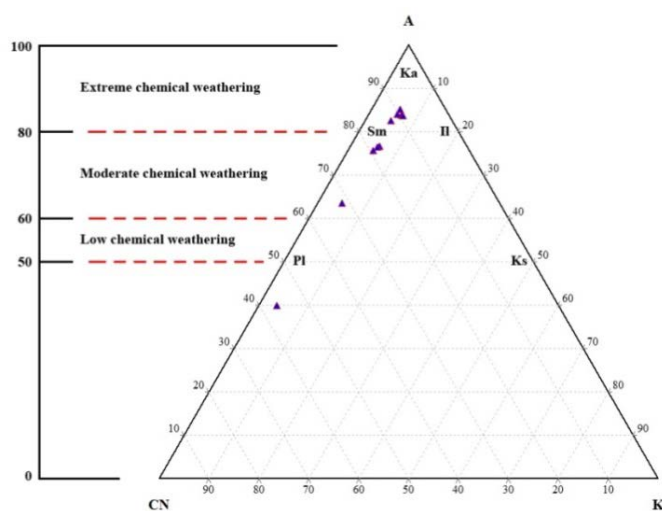


Figure 7 A-CN-K ternary Laungshe sandstone of weathering diagram A= Al_2O_3 ; CN= $(\text{CaO} + \text{Na}_2\text{O})$; K= K_2O (Nesbitt and Young, 1982)

Conclusion

The research area, northernmost part of the Minbu Basin, is located at 16 km east of Tilin, Magwe region. It lies between latitudes 21° 36' N and 21° 44' N and longitudes 94° 09' E and 94° 17' E in UTM-No 2194-02 and 2194-06. The present study examines the geochemistry of sandstones including Laungshe formations attempts to constrain their source rocks, palaeoweathering and tectonic setting of the provenance. Laungshe sandstones fell within the litharenite zone. However one sample of Laungshe sandstone is greywacke. The Laungshe sandstone samples plot in the field of mafic igneous provenance. The Laungshe sandstones were deposited in the active continental margin. The average values of Laungshe sandstones indicate extreme degree of chemical weathering.

Acknowledgements

I would like to express our gratitude to Dr Win Win Maw, Professor and Head, Pakokku University, for her permission and departmental facilitates and Dr Thin Thin Han, Professor, Department of Geology, Pakokku University. I am greatly thankful to Dr Day Wa Aung, Professor and Head, University of Yangon, for his guidance and invaluable suggestions. I would like to state my thanks to Dr Paike Htwe, Lecturer in Geology Department, Pakokku University for his helpful during field trip, valuable suggestion. Finally, I wish to thank to all teachers in Geology Department, Pakokku University, for their help and encouragement throughout the course of this research work.

References

- Bhatia, M. R., (1983), Plate tectonics and geochemical composition of sandstones: *Journal of Geology*, 91, 611-627.
- Bhatia, M. R., Crook, K. A. W., (1986), Trace element characteristics of greywackes and tectonic setting discrimination of sedimentary basins: *Contributions to mineralogy and Petrology*, 92, 181-193.
- Fedo, C. M., Nesbitt, H. W., & Young, G. M., (1995), Unraveling the effects of potassium metasomatism in sedimentary rocks and paleosols, with implication for paleoweathering conditions and provenance, *Geology*, 23, p.921-924.
- Harnois, L., (1988), The CIW index: A new chemical index of weathering: *Sedimentary Geology*, 55, 319-322.
- Herron, M. M., (1988), Geochemical classification of terrigenous sands and shales from core or log data: *Journal of sedimentary Petrology*, 58, 820-829.
- Hutchison, C. S., (1974), Laboratory Hand Book of Petrographic Techniques.
- McLennan, S. M., (1993), Weathering and global denudation: *The journal of Geology*, 101, 295-303.
- Nesbitt, H. W., Young, G. M., (1982), Early Proterozoic climates and plate motions inferred from major element chemistry of lutites: *Nature*, 299, 715-717.
- Pettijhon, F. J., Potter, P. E., Siever, R., (1972), *Sand and Sandstone*: New York, Springer-verlag.
- Roser, B. P., Korsch, R. J., (1986), Determination of tectonic setting of sandstone-mudstone suites using SiO₂ content and K₂O/ Na₂O ratio: *Journal of Geology*, 94, 635-650.
- Roser, B. P., Korsch, R. J., (1988), Provenance signatures of sandstone-mudstone suites determined using discriminant function analysis of major-element data: *Chemical geology*, 67, 119-139.
- Taylor, A. S., McLennan, S. M., (1985), the continental crust: its composition and evolution: Oxford, Blackwell, 312 p.

SEDIMENTARY FACIES ANALYSIS OF THE KALAW FORMATION IN THE TIGYIT AREA, SOUTHERN SHAN STATE, MYANMAR

Wai Wai Lwin¹, Day Wa Aung², Htay Lwin³

Abstract

The study area is located in the Pinlaung Township, Southern Shan State. The study area is mainly composed of Cenozoic to Mesozoic clastic sediments and subordinate amount of Paleozoic and Mesozoic carbonate rocks. The sedimentary rocks are Nwabangyi Dolomite Formation (Late Permian to Early Triassic), Natteik Formation (Middle Triassic), Loi-an Group (Jurassic), Kalaw Formation (Cretaceous), and Hsi-hkip Formation (Pliocene). The Kalaw Formation is well exposed in the eastern and western parts of the study area mainly found at Myatheintan range and Tayoketaung range with the total thickness of Kalaw Formation is estimated about 645 m (21, 10 feet). Kalaw Formation comprises the clastic sequences of conglomerate, sandstone, siltstone, and subordinate shale. Kalaw Formation is divisible into three different members: Lower conglomerate-sandstone member, Middle sandstone-shale member, and Upper conglomerate member. Kalaw Formation consists of six lithofacies such as Massive clast-supported conglomerate, Massive matrix-supported conglomerate, Planar cross-bedded conglomerate, Ripple laminated sandstone, Thin-bedded sandstone interbedded with siltstone, and Massive siltstone respectively. These facies are representing of the Alluvial Fan Association, Channel Association, Overbank Association, and Flood Basin Association. The clastic sequences of the Kalaw Formation were deposited in the debris-flow dominated alluvial fan environment.

Keywords- *lithofacies, clast-supported conglomerate, matrix-supported conglomerate, alluvial fan*

Introduction

The study area is located in the Pinlaung Township, Southern Shan State and lies between (20° 24' N to 20° 30'N) and (96° 40'E to 96° 45'E). The location map of the study area is shown in figure (1). The study area is situated in the tectonic province of Shan-Tanintharyi Block or in the Eastern Highlands of Myanmar. In the study area, the Mesozoic clastics of Loi-an Group, and Kalaw Formation are bounded in the eastern part by the carbonate sediments of the Nwabangyi Dolomite Formation and; Natteik Formation in the central part by Hsi-hkip Formation. The main purpose of the present study is to interpret the depositional environment of Kalaw Formation exposed at the study area and to reconstruct the depositional model of the Kalaw sediments by carrying out the facies analysis.

Materials and Methods

The detailed stratigraphic measurements were carried out along the Tayoketaung and Myatheintan Range, Tigyt area, Southern Shan State. The examination and identification of lithofacies analysis of Kalaw Formation were done according to Miall (1978), Reading (1994), Reineck and Singh (1980), Tucker (2001), and Walker (1979).

¹ Assistant Lecturer, Department of Geology University of Yangon

² Dr., Professor & Head, Department of Geology University of Yangon

³ Dr., Professor & Head, Department of Geology University of Yangon

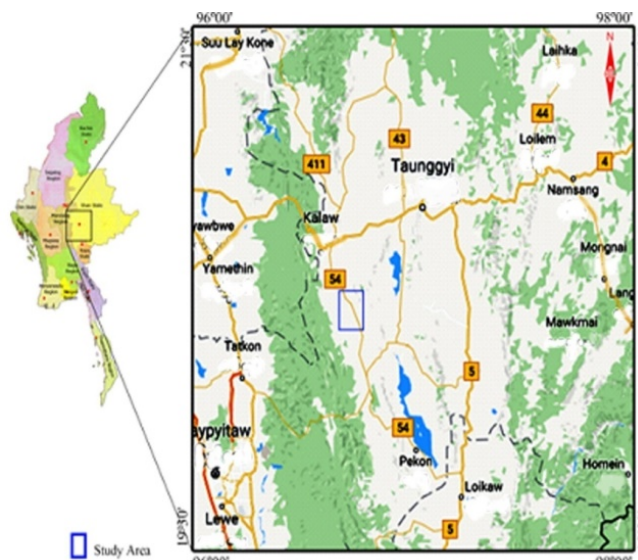


Figure 1 Location map of the study area

Results

A facies is a body of rock and it is defined on the basis of its distinctive lithologic features including colour, bedding, composition, texture, fossils and sedimentary structure (Reading, 1994). Each lithofacies represents on individual depositional environments. Therefore, lithofacies may be grouped into lithofacies associations or assemblages which are characteristics of particular depositional environment (Miall, 1978).

Facies Description and Interpretation

Facies A: Thick-bedded, Clast-supported Conglomerate (Gci)

Facies A is characterized by thick-bedded, clast-supported conglomerate Figure 2. Thickness of a single bed varies 100 cm to 300 cm. Such conglomerates commonly are characterized by lenticular beddings and erosional surfaces with conspicuous relief. The clasts are subangular to rounded, poorly sorted and granule to cobble size up to 15 cm in diameter. The clast types are sorting is generally very poor. Subangular to subrounded pebbles have without preferred orientation, but sometimes platy grains are oriented vertically. The pebbles are of polymic type consisting of limestone clasts of the Plateau Limestone; red sandstones, siltstones, and quartzose sandstones of the Loi-an Group; and a few amount of igneous rock fragments. Clast-supported conglomerates are the predominant facies of stream flow or water-laid deposits within a proximal fan. This facies is interpreted as bed load deposition from stream flows entrenched into a fan (according to Miall, 1978).

Facies B: Thick-bedded Matrix-supported Conglomerate (Gm)

This facies is characterized by thick-bedded, matrix-supported conglomerate with assortment of many kinds of clasts Figure 3. Thickness of a single bed varies from 100- 300 cm. It can be traced laterally for a few meters with a non-erosional base. The clast size is ranging from a fraction of 0.5 cm to more than 15 cm in diameter. Sorting is generally very poor. Subangular to subrounded pebbles have without preferred orientation. These pebbles are cemented by reddish silty and sandy matrix. Facies B is well exposed at the Myatheintan Taung, and Tayoke Taung. Matrix-supported conglomerates are more characteristics of debris-flow or mud-flow deposits. The sediments were deposited by gravity-induced movement at sediment-

water mixture, in which large sediment blocks were embedded in a fine-grained matrix. According to Bull (1977) (in Walker, 1979), debris-flows form on steep slope (more than 10°) with lack of vegetation, during short periods of very abundant water supply.

Facies C: Planar Cross-bedded Conglomerate (Gp)

This Facies is characterized by thick, polymic, clast-supported to matrix-supported conglomerate Figure 4. Large scale planar type cross-bedding are commonly present. The polymic clasts are poorly sorted and ranging in size from granule to pebble. Individual beds vary in thickness from 30 cm to 100 cm. These deposits never make thick layers, and they are invariably discontinuous. The nature of contact is sharp, flat, and concave. Horizontally laminated sandstone wedges are present. Facies C accumulates as discontinuous lenticular patches in the deeper parts of the channel showing lateral accretion. Coarse-grained, poorly sorted sediment seems to favor the formation of linguoid or longitudinal bar.

Facies D: Ripple-laminated Sandstone (Sr)

This facies is reddish brown colored, very fine-grained, well-sorted, and micaceous sandstone consists predominantly of current-ripples Figure 5. Individual beds range in thickness from 10 cm to 50 cm. The boundaries are sharp and commonly non-erosional. Ripple-laminated sandstones usually occur towards the tops of the channel units. They reflect relatively weak currents. The small wavelength and amplitude of ripple bedforms suggest the deposition in shallow water (Tucker, 2001). Thus, the facies D is a product of ripple migration and deposition (Reineck and Singh, 1980).

Facies E: Thin-bedded Sandstone Interbedded with Siltstone (Fl)

Facies E is characterized by thinly bedded, very fine-grained sandstones and siltstone interbeds Figure 6. The sandstone of this facies is 3 cm to 10 cm thick beds with very small ripples. Red colored, thinly laminated siltstones are interbedded with these sandstones. As this lithofacies is a multicycles of thin sandstone and siltstone, this facies represents an overbank or waning flood deposits. This interbedded assemblage is more likely suggestive of deposition by vertical accretion and may represent levee and splay deposits.

Facies F: Massive Siltstone (Fm)

Facies F is composed of thick-bedded to massive, soft and friable red siltstone which is intercalated with thin-bedded red shale Figure 7. This facies is interpreted as the deposit of subaerial waning flood flows and subaqueous suspension sedimentation. Color is a valuable indicator of the drainage state of the floodplain and the level of the water table. Red color suggests an oxidizing early diagenetic regime (Reading, 1994).

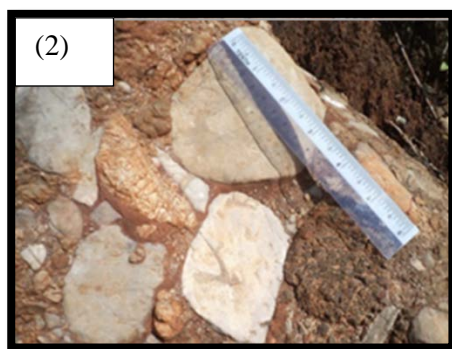


Figure 2 Reddish brown colored, massive, clast-supported conglomerate of Kalaw Formation at Tayoke Taung (N. 20°26' 12.1" and E. 96°43' 35.8")



Figure 3 Reddish brown colored, massive, matrix-supported conglomerate of Kalaw Formation at Tayoke Taung (N. 20°26' 12.1" and E. 96°43' 35.8")



Figure 4 Reddish brown colored, clast-supported conglomerate to matrix-supported conglomerate with planar cross-bedding at Myatheintan Taung (N. 20°26' 12.1" and E. 96°43' 35.8")



Figure 5 Reddish brown colored, very fine-grained, well sorted sandstone consists predominantly of current ripples at Myatheintan Taung (N. 20°26' 12.1" and E. 96°43' 35.8")

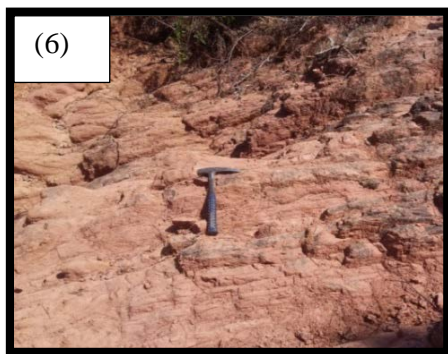


Figure 6 Reddish brown colored, thin-bedded, very fine-grained sandstone interbedded with siltstone at Myatheintan Taung (N. 20°26' 12.1" and E. 96°43' 35.8")

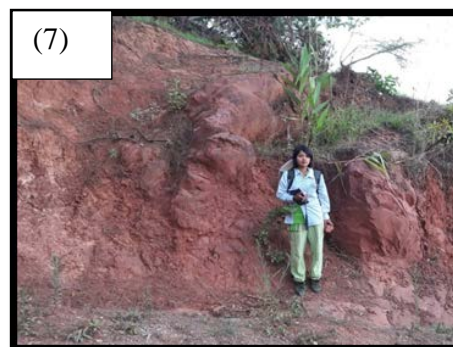


Figure 7 Red colored, massive siltstone intercalated with red shale at Tayoke Taung (N. 20°28' 5" and E. 96°43' 37")

Lithofacies Association of Kalaw Formation

Facies associations are the essential building blocks of facies analysis. Individual facies vary in their interpretative value. Thus facies have to be interpreted, at the environmental level, by reference to their neighbors and are consequently grouped together as facies associations that are genetically or environmentally related. According to Miall (1978), two or more facies of the measured section are grouped into a facies association Figure 8. Four facies associations can be established here:

- (1) Alluvial Fan Association
- (2) Channel Association
- (3) Overbank Association, and
- (4) Flood Basin Association

(1) Alluvial Fan Association

An alluvial fan is a fan-shaped body of rather coarse detrital sediments, poorly sorted, built up by a mountain stream at the base of a mountain front where a steeper slope passes abruptly into a gentler slope.

Alluvial fan lithofacies association consists mainly of sediment gravity flow elements (SG), and less commonly of the gravel bar and bedform (GB), architectural elements of Miall (1985). These deposits comprise three facies, facies A, B, and C which are made up of clast to matrix-supported conglomerates with minor sandstones. Lithofacies A, B, and C occur as thick tabular units. Facies A is the most dominant facies. These conglomerates are uncommonly grade up into coarse sandstone of facies C.

Massive, polymic paraconglomerate of facies B is the result of deposition by debris flows in alluvial fan and massive, polymic orthoconglomerate of facies A deposited in ephemeral alluvial fan channels.

(2) Channel Association

Braided channels are marked by successive divisions and rejoining of the flow around alluvial islands. These channels have active and inactive channels which occupy the deeper part of the river bed. Channel deposits including channel lag and channel bar deposits are formed mainly from the activity of river channels.

Channel association comprises mainly gravel bars and bedforms and subordinate downstream accretion deposits. Gravel bars of coarser-grained channel lag deposits, facies A and C, were firstly formed in the channel and later they become buried by the sandstone sheets of channel bar deposits. This facies association is the result of deposition by deposition of bedload and by deposition of migrating sinuous crested dunes under the lower flow regime condition.

(3) Overbank Association

Sediments of the overbank association are deposited on the river banks and are produced during flood periods. Natural levees are wedge-shaped ridges of sediments bordering stream channels. During high floods large quantities of flood water and sediment is diverted into an adjacent flood basin. Water may follow distinct channels cut across the bank through the natural levee deposits. These water-cut channels are crevasses.

Overbank lithofacies association consists mainly of the laminated sand sheets, architectural elements of Miall (1978). This facies association generally follows bar sediments and is a group of facies D, and E which is fine-grained sediment deposited from suspension by flood water. Facies D was buried by finely thin-bedded sandstone interbedded with siltstone of facies E formed with decreasing water level (lower flow regime).

(4) Flood Basin Association

Flood basin is the lowest lying part of a river flood plain. It is elongated and running parallel to the channel. It acts as settling basin, in which suspended fine-grained sediment settles down from overbank flows after the coarser sediments have been deposited on levees and crevasse splays.

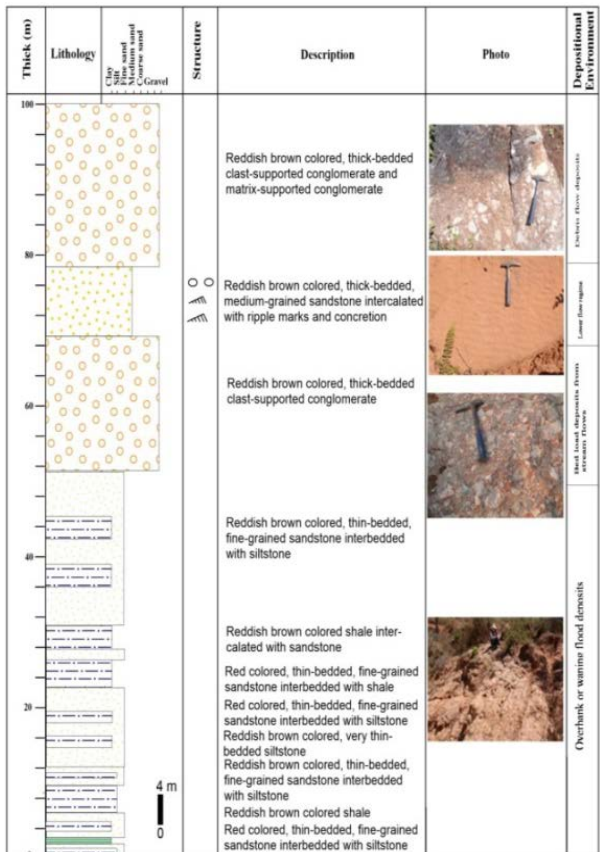
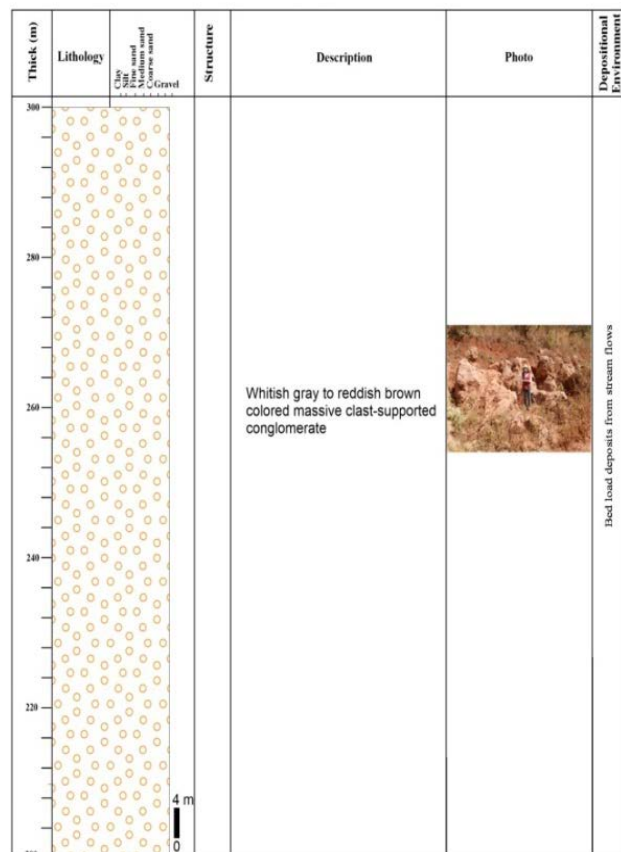
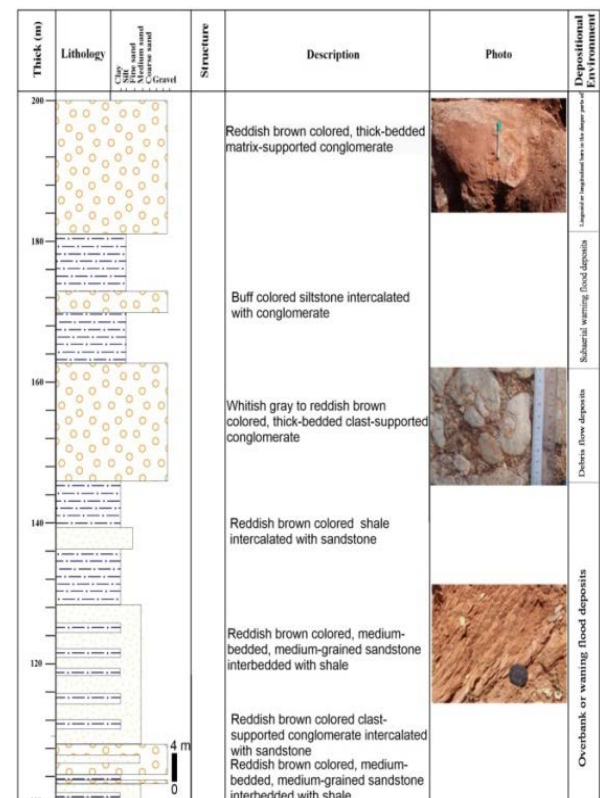
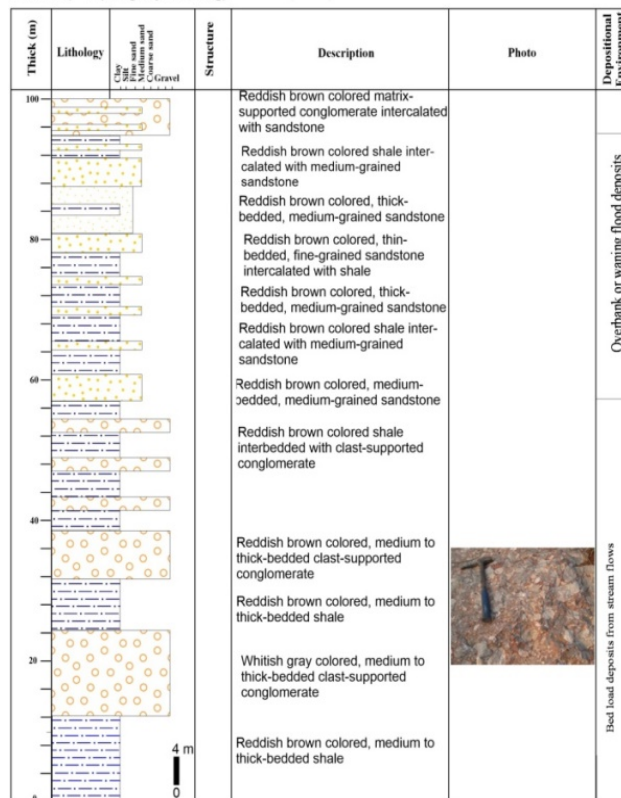
Lithofacies D, E, and F are grouped together as flood plain association. Massive siltstone of facies F is dominant. Flood basin deposits in the study area are rather thin and are sandwiched

between channel deposits. This deposit is characterized by negligible organic matter content, somewhat reddish in colour. Flood basin deposit represents the long-continued accumulation of fine-grained suspended sediment.

Table 1 Lithofacies of Kalaw Formation exposed at the Tigyt Area

	Facies	Grain size	Bed Thickness (cm)	Structures	Boundaries	Interpretation
A	Massive clast-supported conglomerate	Granule to cobble, diameter up to 15 cm	100-250 cm	Massive	erosional	Bed load deposits from stream flows
B	Massive matrix-supported conglomerate	Granule	100-250 cm	Massive	Sharp and erosional	Debris flow deposits
C	Planar cross-bedded conglomerate	Granule to pebble	30-100 cm	Planar cross-bedding	Sharp and erosional	Lower flow regime
D	Ripple laminated sandstone	Fine-grained	10-50 cm	Current ripple	sharp	Ripple migration and deposition (lower flow regime)
E	Thin-bedded sandstone interbedded with siltstone	Very fine-grained	3-15 cm	Lack	sharp	Overbank or waning flood deposits
F	Massive siltstone	Silt size	10-300 cm	Massive	sharp	Waning flood deposits

Location/Date : (20°25' 59.6" - 20° 26' 10.3" & 96° 43' 28" - 96° 43' 30.0")
 Formation : Kalaw Formation
 Measured by : (Along Tayoke Taung)



Discussion

A facies analysis of the Mesozoic clastic of Kalaw Formation has revealed four facies associations assigned to two major depositional environments, which are:

- (1) Debris flow dominated alluvial fans that spread sediments westward from the fault-bounded basin margin and
- (2) A gravelly braided river, prograding south

These two major environments are illustrated in the depositional model Figure 10. The right hand side of the model is a belt of coalescing alluvial fans with lobes of debris flow in the upper fan areas. Under favourable conditions thick deposits of alluvial fans are produced and preserved as marginal facies of the basin of deposition (Reineck and Singh, 1980). The alluvial fans in the study area are dominated by debris flow deposits (Facies B) with relatively fewer water-laid deposits (Facies A). As alluvial fan sediment essentially represents the conglomerate of local provenance (older rock fragments of Nwabangyi Dolomite Formation, Natteik Formation, and Loi-an Group), there is little transport and sorting. Presence of large siltstone and carbonate clasts which were susceptible to weathering suggests that sediment underwent weathering and transport prior to deposition on the fans. Red coloration occurs in alluvial fan deposits, and point to a semi-arid paleoclimate. Therefore, the alluvial fan sedimentation in the study area was strongly influenced by two factors: the semi-arid climate and the active tectonic setting.

These fan deposits are associated with gravelly braided river deposits of mountainous region. Three facies associations; channel association, overbank association, and flood basin association assigned to a gravelly braided river system. In this system, massive, clast-supported conglomerate (Facies A) is the predominant facies in conglomerate units. Planar cross-bedded conglomerate (Facies C) makes up about 20% of the conglomerate. These conglomerate units grade into finer-grained sediments. The coarser-grained character of channel lag and bar deposits can be assumed that the sediment transport and sediment discharge were rather high. The graded size –gradually decreases upwards, and the degree of sorting improved upward. But, in some sequences, fine-grained sandy layers are intercalated in the coarsest and bars. This shows the variability of sequences due to rapid shifting of channels and bars. The development of thin flood basin deposits which were sandwiched between channel deposits indicates the braided nature of streams with their rapid rates of lateral migration.

The above facies assemblages are probably resembles the proximal reaches of gravelly braided river (comparable to Donjek type of Miall, 1978). Deposits of this type are characteristic of climatic extremes (semi-arid), in which large amounts of coarse detritus are produced, and plant cover is sparse.

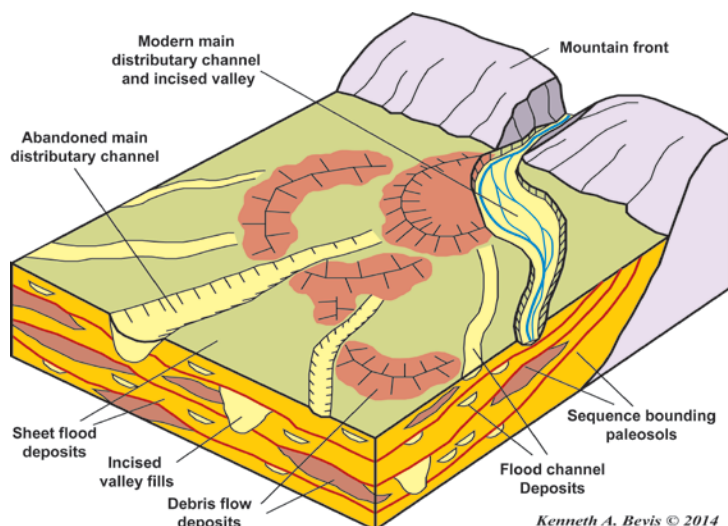


Figure 10 Depositional Model of debris flow-dominated alluvial fans and a gravelly braided river for the sedimentary sequences of Kalaw Formation (based on Kenneth A. Bevis @ 2014)

Summary and Conclusion

The study area is located in the Pinlaung Township, Southern Shan State and lies between (20° 24' N to 20° 30'N) and (96° 40'E to 96° 45'E). In the Tigyt area, the Mesozoic clastics of Loi-an Group, and Kalaw Formation are bounded in the eastern part by the carbonate sediments of the Nwabangyi Dolomite Formation and; Natteik Formation in the central part by Hsi-hkip Formation. In the Kalaw Formation, six lithofacies can be classified and grouped into four lithofacies associations. On the basis of facies associations, the depositional environment of the Kalaw Formation may be regarded as debris-flow dominated alluvium fan deposits and braided river deposits.

Acknowledgements

I am greatly indebted to Dr. Htay Lwin, Professor, Geology Department, University of Yangon, for his encouragement and permission to perform this research paper. I would like to express my thanks to my supervisor, Dr. Day Wa Aung, Professor and Head of Geology Department, University of Yangon, for his creative guidance and invaluable suggestions. Special thanks are also due to the responsible personnel of the Tigyt Town. for their helps and facilities throughout the field works.

References

- Amos, B.J., (1975). Stratigraphy of some of the Upper Paleozoic and Mesozoic carbonate rocks of the Eastern Highlands, Burma: *Newsl. Stratigr.*, V.4, p.47-70.
- Aung Win Swe, (2010). Geology of the Southern Part of the Kalaw-Pinlaung Basin, Southern Shan State, *PhD Dissertation*, Department of Geology, University of Mandalay, (Unpublished), p107.
- Bender, F., (1983). *Geology of Burma*, Gebruder Brontraeger, Berlin, p. 293.
- Brown, J.C. And V.P. Sondhi, (1933). The geology of the country between Kalaw and Taunggyi, southern Shan State, Burma. *Rec. Geol. Surv. India*, V.67, No. 2, p.166-247.
- Chhibber, H.L., (1934). *Geology of Burma*, Macmalling, London, p538.
- Garson, M.S., A.H.G., Mitchell and B.J., Amos, (1976). Geology of the area around Nyaungga and Ye-ngan, southern Shan State, Burma. *Overseas Mem. Inst. Geol. Sci.* No.2, 72p.
- G. I. A. C., (1999). The Tectonics of Myanmar, Final report, in GIAC Project. 1996-1999, p. 108.
- Miall, A.D., (1978). Fluvial Sedimentology; and historical review, In Miall, A.D., ed., *Fluvial Sedimentology*, Canadian Society of Petroleum Geologists, Memoir.
- Khin Maung Latt, (1980). Stratigraphy and structure of the eastern Thazi and western Kalaw area. Upb. M.Sc. Thesis. Rangoon University, p.130.
- Khin Maung Win, (1978). Geology and stratigraphy of the Kalaw-Aungban area, Southern Shan State. M.Sc. Thesis. Rangoon University, p. 115.
- Kyi Soe, (2006). The Stratigraphic Paleontology of the Jurassic and Cretaceous Units of the Western part of the southern Shan State, *PhD Dissertation*, Geology Department, University of Yangon, (Unpublished), 107p.
- Nichols, G. J., (2009). *Sedimentology and Stratigraphy* (2nd ed): John Wile & Sons, New York.
- Pettijohn, F.J., (1987) *Sedimentary Rocks*. 3rd ed: New York, Harper&Row.
- Reading, H. G., and M. Richards, (1994) *Turbidite systems in deep-water basin margins classified by grain size and feeder system*. Bull. Am.Ass. Petrol. Geol.,v. 78, p. 792-822.
- Reineck, H. E. and Singh, I.B., (1980): *Depositional Sedimentary Environments*: Springer- Verlag, New York.
- Tucker, M.E, (2001). *Sedimentary Petrology*. An Introduction to the Origin of Sedimentary Rocks (3rd edition) Blackwell Science.
- Walker R.G, (1979) *Facies Model*, p-98, Printed by Ainsworth Press Limited, Kitchener, Ontario.
- Wolfart, R.U., U Myo Win, Saw Boiteau, U Myo Wai, U Peter UK Cung, and U Tint Lwin, (1984). Stratigraphy of the western Shan Massif, Burma. *Geologisches Jahrbuch*, Heft 57, Hannover, 3-93

CORRELATION OF SHEAR WAVE VELOCITY (Vs) AND SPT-N VALUE OF VARIOUS SOIL DEPOSITS FOR CHANAYETHARZAN TOWNSHIP IN MANDALAY DISTRICT

Tun Tun Win¹, Myo Thant², Than Than Nu³, Pyi Soe Thein⁴, Tin Naing Tun⁵
& Win Min Than⁶

Abstract

The research area, Chanayethazan Township is a main population center in Mandalay District and lies in near the seismically active Sagaing fault. Nowadays, geotechnical and geophysical techniques are widely used for evaluating dynamic soil properties and seismic hazard analysis. The dynamic loading of soil in the present area are evaluated by shear wave velocity (Vs) using geotechnical (mainly SPT) and geophysical (mainly microtremor HVSr) methods. At some places obtaining only SPT data or only Vs value, we are difficult to predict the true correlation. The purpose of this paper is to establish the new formulas for the shear wave velocity (Vs) and SPT-N values relationships of the various soil types. Fifteen data pairs were employed to assess relation between Vs and SPT-N values. Although most correlations of other areas are comparable and in good trend, these correlations for the present area are directly disallowed because of different practice of SPT and shear wave investigation works. Thus, present research based on previous literature and observed data was attempted to establish new correlations between Vs and SPT-N for various soil types of the study area. The proposed data will be aid for seismic hazard analysis and engineering purposes of Chanayethazan Township.

Keywords: shear wave velocity (Vs), numbers of blows from standard penetration test (SPT-N) value, microtremor horizontal vertical spectral ratio (HVSr).

Introduction

The research area, Chanayethazan Township is a main population center of Mandalay District and lies in near the seismically active Sagaing fault. The hazardous effects of earthquake are significantly affected by the local site effects of soil under dynamic loading. Nowadays, geotechnical and geophysical techniques are widely used for evaluating dynamic soil properties and seismic hazard analysis. The dynamic properties of soil in the present area can be estimated using shear wave velocity (Vs) resulted from both borehole (SPT-N values) data and microtremor horizontal vertical spectral ratio (MHVSRs) data.

Shear wave velocity (Vs) can be also used for various applications such as liquefaction potential analysis, earthquake site response, foundation stiffness assessment and soil compaction (Park, B, C., et al, 1997). Thus, average shear wave velocity to a depth of 30 m (V_{s30}) is essential for evaluation of seismic site characteristic in the study area. Now, standard penetration tests blow count number (SPT-N) value and the shear wave velocity (Vs) are the most common methods for determining the earthquake related hazards all over the world. Thus, many attempts in worldwide have been made to correlate values of Vs with available soil parameters (SPT- N value). Although the empirical correlations of previous researchers between SPT-N and Vs is

¹ Lecturer, Department of Geology, University of Mandalay

² Professor, Department of Geology, University of Yangon

³ Professor, Department of Geology, University of Mandalay

⁴ Lecturer, Department of Geology, Yadanabon University

⁵ Assistance Lecturer, Department of Geology, University of Mandalay

⁶ Assistance Lecturer, Department of Geology, University of Mandalay

convincing with notably worldwide agreement, these correlations are directly disallowed because of different practice of SPT and shear wave investigation works due to various geological conditions. In the present area, the own empirical correlations of SPT-N & Vs for the different soil types have not been reported in the literature. Therefore, Vs–N relationship for various soil types of Chanayethazan Township in Mandalay district has been investigated. Sometimes microtremor survey is not easy to obtain Vs value in all the locations of the research area because of noisy conditions. At this condition, standard penetration test is better than microtremor survey. On the other hand, sometimes the penetration test cannot be performed conveniently and reliably at all depths and in all soils such as those with large grain size, i.e., gravelly soils these sites may give unrealistic high N-value. Thus, a new correlation between SPT-N and Vs needs to establish for research area. An empirical relation (Vs & SPT-N) applicable to all the fifteen-pair sites was evaluated based on the existing correlations of previous researchers and observed data. By using empirical regression analysis, the present research was established the new formulas for SPT-N and Vs values relationships of the various soil types i.e. all soils, sandy soils and clayey soils for estimation of seismic hazard analysis.

Site Investigations

The site investigations were carried out using both geotechnical mainly standard penetration test (SPT) and geophysical mainly microtremor survey. In the present research, 15 boreholes and 40 microtremor investigation points are used to conduct subsurface survey in the study area. Among them, all the 15 pair sites was evaluated for empirical relation SPT-N & Vs. The laboratory tests of sample were collected from all these sites. The locations of the fifteen-pair points are shown in Fig. 1.



Figure 1 Location map of investigation sites

Methodology

Subsurface investigations of the present area were carried out by using 40 microtremor points and 15 drilled boreholes. For the study area, 15 data pairs were employed to develop empirical relations between Vs & SPT-N values for different soils using regression analysis. The site investigations at 15 boreholes points of the study area were examined about 30 m depth of surface layer. N value was obtained from geotechnical field data as SPT method. Vs profiles resulted from SPT-N values were presented seven layers and Vs models obtained from microtremor HVSR data were constructed four layers. The combination of the two Vs model profiles are shown in Fig. 2.

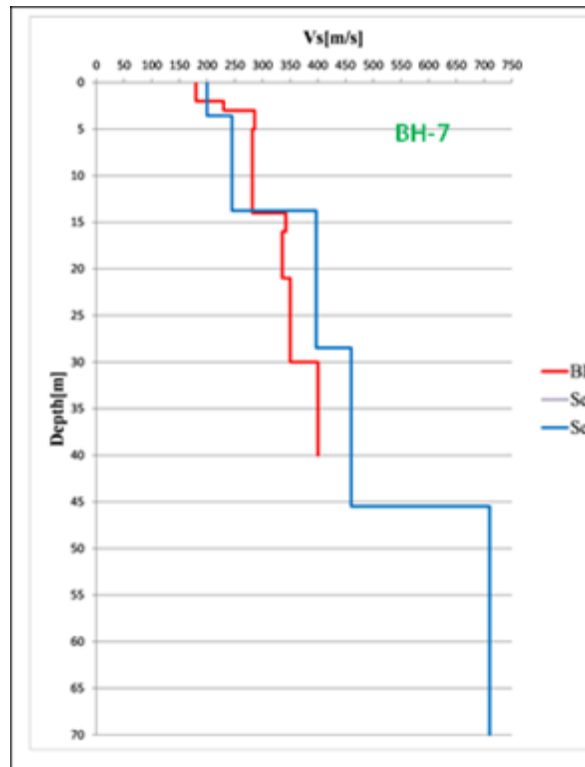


Figure 2 Comparison of Vs profiles resulted from SPT-N (red line) and microtremor (HVSR) data (blue line)

Estimation of shear wave velocity to a depth of 30m using SPT data

The SPT dataset is used to develop subsurface describing the distribution of time-averaged shear wave velocity, Vs30, across the study area. Target profile depths of 5, 10, 20, 30 m were considered to allow for an assessment of the distributions of soil stiffness with depth across the region. Vs30 values are computed for each target depth. The evaluated Vs30 for each site of the study area are calculated in the following equation.

$$Vs30 = \frac{\sum d_i}{\sum t_i} \frac{\sum d_i}{\sum \frac{d_i}{v_{si}}}$$

Where v_{si} is shear wave velocity, d_i thickness of i^{th} layer and t_i one way travel time in i^{th} layer

Estimation of shear wave velocity to a depth of 30m using MHVRs method

Shear wave velocity is an important parameter for estimation of the dynamic properties of soil in the shallow subsurface. In the present study, V_{s30} is calculated as the following equation;

$$V_{s30} = \frac{30}{\sum_{i=1}^N \frac{h_i}{V_i}}$$

Where, V_{s30} is the shear wave velocity of upper 30m, h_i and V_i denote the thickness (m) and shear wave velocity of the i -th layer, in a total of N , existing in the top 30m.

Regression analysis

For the regression analysis of the present area, N values were estimated above suitable depth of SPT borehole and the shear wave velocity profile was developed based on the layer formations observed from SPT and MHVRs testing by using 15 pair data. Many researchers as listed in table (1) were proposed their own empirical correlation between V_s and SPT- N value for various categories of soil (i.e. all soils, sand and clay) at different locations. The present correlations V_s and SPT- N were examined based on previous literature and observed data using regression analysis. The predicted correlation in the form of a power-law relationship between V_s and SPT resistance can be used as the following equation.

$$V_s = a N^b$$

where V_s is shear wave velocity, N is SPT- N value, a and b are coefficients varying for different locations and types of soil.

Table 1 V_s - N correlations given by other researchers

Researchers	All soil(ms^{-1})	Sand(ms^{-1})	Clay(ms^{-1})
Hanumantharao and Ramana	$V_s = 82.6N^{0.430}$	$V_s = 79.0N^{0.434}$	-
Maheshwari et al.	-	$V_s = 95N^{0.300}$	-
Ohba and Toriumi	$V_s = 84N^{0.310}$	-	-
Imai	$V_s = 91N^{0.340}$	$V_s = 80.6N^{0.331}$	$V_s = 80.2N^{0.292}$
Ohta and Goto	$V_s = 85.35N^{0.348}$	$V_s = 88.0N^{0.340}$	-
Jafari et al	$V_s = 121.0N^{0.270}$	$V_s = 88.0N^{0.330}$	$V_s = 100.0N^{0.330}$
Seed and Idriss	$V_s = 61N^{0.500}$	-	-
Lee	-	$V_s = 57.4N^{0.490}$	$V_s = 114.4N^{0.310}$
Sykora and Stokoe	-	$V_s = 100.5N^{0.290}$	-
Okamoto et al	-	$V_s = 125.0N^{0.300}$	-
Pitilakis et al	-	$V_s = 162.0N^{0.170}$	$V_s = 165.7N^{0.190}$
Athanasopoulos	$V_s = 107.6N^{0.360}$	-	-
Raptakis et al	-	$V_s = 123.4N^{0.290}$	$V_s = 184.2N^{0.170}$
Hasancebi and Ulusay	$V_s = 90N^{0.309}$	$V_s = 90.8N^{0.319}$	$V_s = 97.9N^{0.269}$
Uma Maheswari et al	$V_s = 95.64N^{0.301}$	$V_s = 100.53N^{0.265}$	$V_s = 89.31N^{0.358}$
Esfahanizadeh et al	-	$V_s = 107.2N^{0.34}$	-
Fatehnia et al	-	$V_s = 77.1N^{0.355}$	$V_s = 77.1N^{0.355}$

Results and Discussion

For the present area, the observed data for estimating the best relationships were also used in the above power function equation. By result data, range of SPT-N values is 2 to 20 and average range of V_s is >120 to <400 ms^{-1} . This analysis is almost performed by computer program. The new equations developed for the correlation between V_s and SPT-N values of the study area are shown in table (2). The coefficient of determination (R^2) is used to analyze how difference in two variable. R^2 range is 0 to 1 i.e, 0% to 100% probability of the two sets of variables.

Table 2 Summary of the proposed relationships in Chanayetharzan Township

Type of soil	correlation	R^2
All soils	$V_s = 90.9N^{0.352}$	0.9874
Sandy soil	$V_s = 97.6N^{0.325}$	0.9894
Clayey soil	$V_s = 113.55N^{0.28}$	0.9918

All Soil

Fig (3) shows the graphical validation of the regression analysis for all soil based on comparison of previous researchers and observed data. N values were placed ≤ 20 for regression analysis. This correlation was compared with nine researchers such as Hanumantharao and Ramana(2008), Ohba and Toriumi(1970), Imai(1977), Ohta and Goto(1978), Jafari et al(2002), Seed and Idriss(1981), Athanasopoulos(1995), Hasancebi and Ulusay(2007), and Uma Maheswari et al(2009). According to research data, the new regression equation for all soil is similar to Imai (1977), and Hasancebi and Ulusay (2007). Fig (3) shows the empirical correlation between V_s and SPT-N for all soil based on observed data of the study area using regression analysis and the proposed relation is $V_s = 90.9N^{0.352}$. The coefficient of determination (R^2) is 0.9874 which is a strong correlation between SPT-N and V_s value.

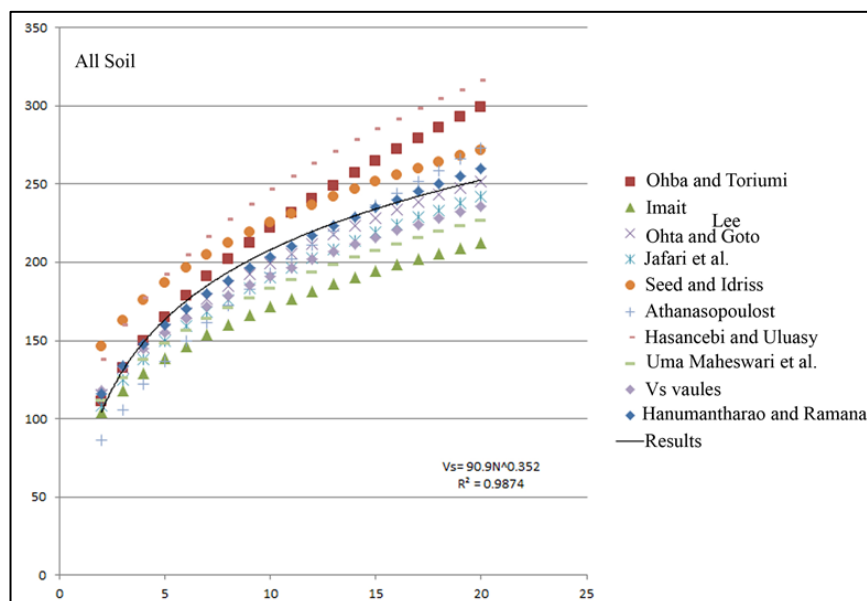


Figure 3 Comparison of the proposed regression formula with current correlations between SPT-N and V_s value for all soil types based on other worldwide relations and observed data

Sandy Soil

The predicted correlation between SPT value and shear wave velocity for sandy soil is compared with the existing correlations given by other researchers as shown in Fig (4). The comparisons of the results of the present study are made with the equations recommended by fourteen other researchers as shown in table (1). Fig (4) shows correlation between V_s and N for sandy soils and proposed relationship of sandy soil is $V_s = 97.6N^{0.325}$. The coefficient of determination obtained (R^2) was 0.9894 which is a good correlation between SPT- N and V_s . There is a considerable more scatter below the fitted (results) line. According to fig (4), the new regression equation for sandy soil is similar to Sykora and Stokoe.

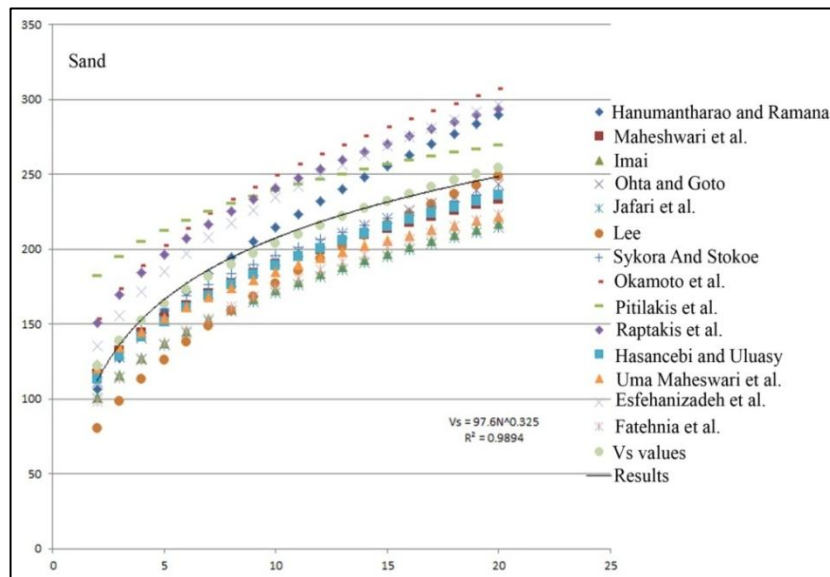


Figure 4 Comparison of the proposed regression formula with current correlations between SPT- N and V_s value for sandy soil

Clayey Soil

Similar to other soil types, the correlation was developed using a simple regression analysis for the existing database. In Fig. 5, the proposed relationship of V_s and SPT- N for clayey soils is compared with the equations recommended by eight other researchers as shown in table (1). Fig (5) shows comparison between uncorrected V_s and uncorrected N for clayey soils is developed and the proposed relation is $V_s = 113.55N^{0.28}$. The coefficient of determination is $R^2 = 0.9918$ which is quite high value as compare to that for other soil types. Therefore, the relationship for clayey soils is bit different than other soils (table.2). It can be observed that the result of the present study is closed to that of Jafari et al.

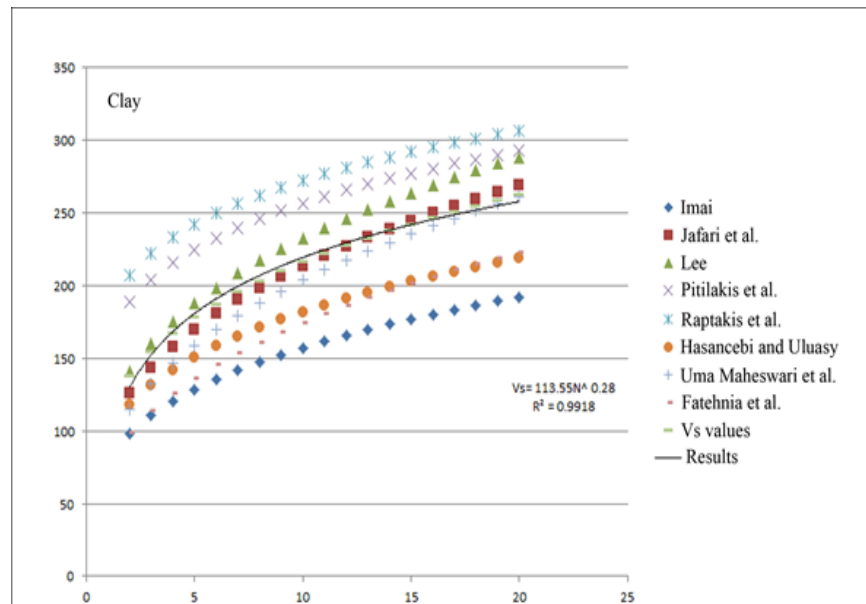


Figure 5 Comparison of the proposed regression formula with current correlations between SPT-N and Vs value for clayey soil

Conclusions

For the study area, 15 data pairs were employed to develop empirical relations between Vs & SPT-N values for different soils using regression analysis. By result data, range of SPT-N values is 2 to 20 and average range of Vs is >120 to <400 ms^{-1} . Direct measurement of Vs is time consuming and costly, therefore many researchers have been trying to update empirical relationships between Vs and other geotechnical properties of soils such as SPT Blow count, SPT-N.

All of present results obtaining from SPT and Vs are to assess the dynamic properties of soil. Although most of the previous correlations are comparable and in good trend, direct application to other regions are disallowed because of different practice of SPT and shear wave investigation works. The differences exist in the earlier predicted correlations because of the site investigation error and chance in geological conditions or soil strata in the study area. Such relationships are not reported previously for the present area. Hence, present researcher were attempted to establish new correlations between Vs and SPT-N for various soil types of the study area such as all soils, sandy soils and clayey soils. The present correlations Vs and SPT-N were examined based on previous literature and observed data using regression analysis. According to our result data, the present correlations are reliable with other relations. By the coefficient of determination (R^2) values, the new regression equations of the present area give good prediction performances. Hence, the present results can be effectively used for studying the seismic site response and engineering properties of soil in the study area.

Acknowledgements

We would like to thank Professor Dr. Myo Min, Department of Geology, University of Mandalay for his valuable suggestions and advices in preparation for the research paper. We are deeply thankful to Professor Hiroshi Kawase, Tokyo University in Japan for his constructive suggestions and supporting the microtremor machine to measure geophysical survey for the study area.

References

- Athanasopoulos, G.A. (1995), "Empirical correlations V_{so}-NSPT for soils of Greece": a comparative study of reliability, *Proceedings of the 7th International Conference on Soil Dynamics and Earthquake Engineering Computation Mechanics Publications, Southampton, Boston*, pp 19–25
- Boore, D.M., Joyner, W.B and Fumal, T. E. (1997), Equations for Estimating Horizontal Response Spectra and Peak Acceleration from Western North American Earthquakes: A Summary of recent Work, *Seismological Research Letters*, Vol. 68, No. 1, 128-153.
- Bour, M., Fouissac, D., Dominique, P and Martin, C. 1998. "On the Use of Microtremor Recordings in Seismic Microzonation", *Soil Dynamics and Earthquake Engineering*, Vol. 17, No. 7-8, pp. 465-474
- Esfahanizadeh, M., Nabizadeh, F., Yazarloo, R. (2015), Correlation between Standard Penetration (NSPT) and Shear Wave Velocity (V_s) for Young Coastal Sands of the Caspian Sea, *Arab J Geosci* 8:7333–7341.
- Fatehnia, M., Hayden, M and Landschoot, M. (2015), "Correlation between Shear Wave Velocity and SPT-N values for North Florida Soils", *Elec J Geotech Eng* 20:12421–12430 *Int. J. of Geosynth and Ground Eng.* (2016) 2:9 pp. 11 of 11 9123.
- Hanumantharao, C & Ramana, G.V. (2008), "Dynamics Soil Properties for Microzonation of Delhi, India". *J Earth Syst Sci* 117(S2):719–730
- Hasancebi, N & Ulusay, R. (2007), Empirical Correlations between Shear Wave Velocity and Penetration Resistance for Ground Shaking Assessments, *Bull Eng Geol Environ* 66:203–213
- Imai, T. (1977), P- and S-wave Velocities of the Ground in Japan, *Proc IX Int conf Soil Mech Found Eng* 2:127–132
- Jafari, M.K., Shafiee, A & Razmkhah, A. (2002), Dynamic Properties of Fine Grained Soils in South of Tehran. *Soil Dyn Earthq Eng* 4(1):25–35
- Jhinkwan, H & Jain, P. K. (2016), "Prediction of Shear Wave Velocity Using SPT-N Value" *TROI*, VI.3, Issue 7.
- Kirar, B., Maheshwari, B. K & Muley, P. (2016), Correlation between Shear Wave Velocity (V_s) and SPT Resistance (N) for Roorkee Region, *Int. J. of Geosynth, Ground Eng.* 2016.2-9.
- Krammer, S.L. (1996). *Geotechnical Earthquake Engineering, Prentice-Hall Civil Engineering and Engineering Mechanics Series, Upper Saddle River, NJ: Prentice Hall*, c1996, 1.
- Lee S, H, H. (1990), Regression Models of Shear Wave Velocities in Taipei Basin. *J Chinese Inst Eng* 13:519–532
- Maheshwari, B.K., Mahajan, A.K., Sharma, M.L., Paul, D.K., Kaynia, A.M., Lindholm, C. (2013), Relation between Shear Velocity and SPT Resistance for Sandy Soils in the Ganga Basin, *Int J Geotech Eng* 7(1):63–70
- Nakamura, Y. (1989), A Method for Dynamic Characteristics Estimation of Subsurface Using Microtremor on the Ground Surface, *Quarterly Report of the Railway Technology Research Institute*.
- Ohta, Y & Goto, N. (1978), Empirical Shear Wave Velocity Equations in Terms of Characteristics Soil Indexes. *Earthq Eng Struct Dyn* 6:167–187
- Pitilakis, K.D., Anastasiadis, A & Raptakis, D. (1992), Field and Laboratory Determination of Dynamic Properties of Natural Soil Deposits, *In Proceedings of the 10th world conference on earthquake engineering, Rotterdam*, pp 1275–1280.
- Raptakis, D.G., Anastasiadis, S.A.J., Pitilakis, K.D & Lontzetidis, K.S. (1995), Shear Wave Velocities and Damping of Greek Natural Soils, *In Proceedings of the 10th European conference on earthquake engineering, Vienna*, pp 477–482.
- Seed, H. B., Tokimatsu, K & Harder, L. F. (1985), The Influence of SPT Procedures in Soil Liquefaction Resistance Evaluation, *Geotechnical engineering, ASCE, No.111, Vol.12*.
- Sykora, D. E & Stokoe, K. II. (1983), Correlations of In situ Measurements in Sands of Shear Wave Velocity, *Soil Dyn Earthq Eng* 20(1–4):125–136
- Uma Maheswari, et al. (2010), Use of Surface Waves in Statistical Correlations of Shear Wave Velocity and Penetration Resistance of Chennai soils, *Geotech Geol Eng* 28:119–137

ENVIRONMENTAL GEOCHEMISTRY OF SOLID MINE WASTES FROM KYITAUKPAUK – CHAUNGGYI AREA, SINGU AND THABEIKKYIN TOWNSHIPS, MANDALAY REGION

Zin Mar Kyaw¹, Than Than Nu², Kyu Kyu Mar³

Abstract

The chemical composition of soil and sediments from study area were characterized by high sulfur contents (1118-67500ppm) and high concentration of zinc (70-53600 ppm). Almost soil and sediments samples were observed highly significant concentrations of Cu value than the limit of 36mg/kg in part by EPA. SiO₂ content is high in nearly almost solid samples including soil and rock. According to XRD result, prominent minerals observed quartz, calcite, pyrite and galena. The mean concentration of heavy metal in soils are ranging from S > Zn > Pb > Cu. Through the use of different indices of heavy metal contamination index (I_{geo}) and Enrichment ratios (ER) results indicated that the study area was the most contaminated in As and Hg and followed by S and Cu.

Keywords: EPA, ER and I_{geo}

Introduction

1.1 Background

The high concentrations of potentially toxic elements in mine wastes can pose risks to ecosystems and humans, but these risks can be mitigated by implementing appropriate management or remediation schemes. Successful mine waste characterization is of paramount importance in light of the potential environmental, social and financial impacts from mining landforms constructed from geochemically reactive or erosive mine waste (Smedly et al. 2014).

Sulfur and carbon are commonly measured used in calculations of the acid producing and acid neutralizing potentials (Weber et al. 2005). Measurement of total metals and metalloids is commonly achieved through X-ray fluorescence (XRF) method.

Heavy metals can be present in the soil as a product of the weathering of the natural rocks, or because they come as part of pollution loads generated by human activities such as mining and agricultures may be in study area. It is very important to distinguish between the natural background values and anthropogenic inputs, and to recognize that the background values change from area to area and with the scale of the area investigated. For these reasons the geochemical monitoring of soil is important in the aim of evaluating the natural content of heavy metal in soils, related to parental materials and possible enrichment due to mining activities in study area.

1.2 Study Area

The study area lies in the Thabeikkyin and Singu Townships, Mandalay Region. It is located within one inch topographic maps of 93 B1 & B/2. This area falls within North Latitude 22°39'20" to 22°46'30" and East Longitude 96°00'00" to 96°03'30", area extends about 3.5 miles

¹ Assistant Lecture, Department of Geology, University of Yangon

² Dr, Professor and Head, Department of Geology, University of Mandalay

³ Dr, Associate Professor, Department of Geology, University of Mandalay

from east to west and 5.6 miles from north to south, totally 19.6 square miles and readily accessible throughout the year. The location map of the study area is shown in Fig (1).

The study area forms part of the highly deformed metamorphic rocks of Mogok Belt (Searle and Haq, 1964). Most of the metasedimentary rocks such as Hornblende gneiss, banded biotite gneiss, marble units and diopside calc-silicate rocks which of the age from Precambrian to Mesozoic are widely distributed throughout the whole area. Valuable gold mineralization occurs in marble, biotite gneiss and at or near the contact of marble and biotite microgranite. Principal metallic vein minerals are pyrite, chalcopyrite, sphalerite, lead in addition to gold. Gold veins in gneisses are observed as fissure filling type while more replacement nature occurs in marble unit.

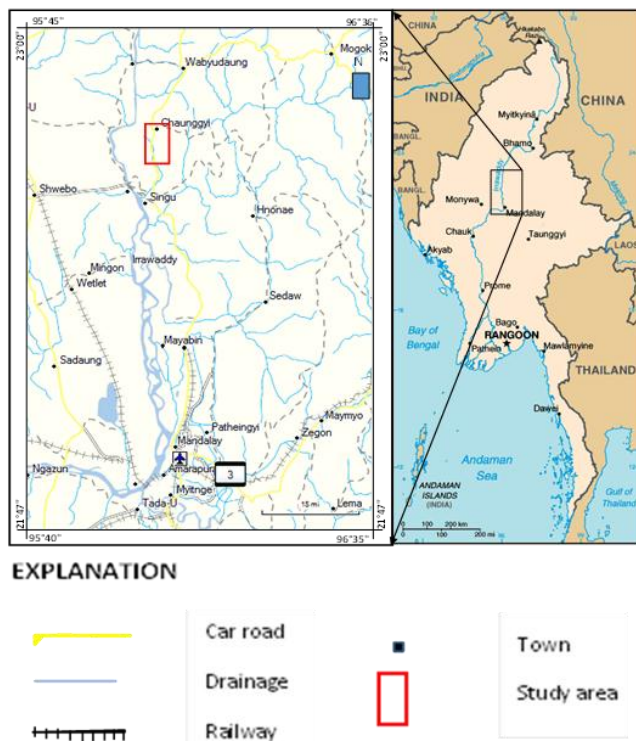


Figure 1 Location map of the study area.

Material and Methods

2.1. Sample Collection and Preparation

Totally, there have thirty-five gold mine sites in the study area; twenty-eight mine sites were existed in Kyitaukpauk area and seventeen were in Chaunggyi area. In the present study, samples collected from seven mine sites which were three from Kyitaukpauk area (SGU-6, SGU-189 and SGU-190) and four from Chaunggyi area (TPK-152, TPK-168 and TPK-171), shown in Fig.(2). In order to access the impacts of gold mining on the surrounding environment, totally of eighteen tailing soil samples, twelve ore sample including ore bearing soils and fourteen waste rock samples were collected in October,2018 and Janauary, 2019, respectively in the vicinity of mine from study area . Tailing soil samples were collected from mine waste dumps and processing sites.

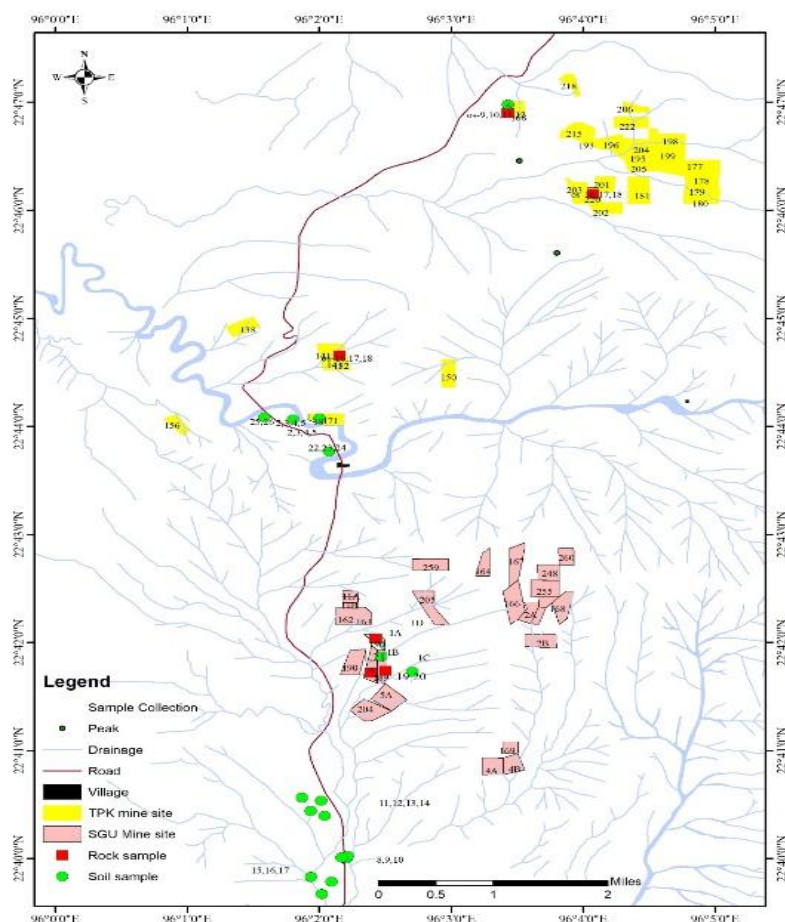


Figure 2 Collected samples location map of the study area.

2.2. Laboratory Works

After sample collection, soil and rock samples were transported to laboratory to analyze the chemical properties of solid mine wastes. XRD (X-ray Diffractometer), XRF (X-ray Fluorescence) and AAS (Atomic Absorption Spectrometer) method were used to analyze the chemical and mineralogical compositions of the collected samples.

Results and Discussion

3.1 Chemical Composition of the Solid Mine Wastes

The SiO_2 content is (2.75–91.1wt%) in rock samples and (21.2 – 53.6wt%) in soil samples, average 50wt% in ore samples and 47wt% in tailings. SiO_2 content is high in nearly almost solid samples including soil and rock. Significantly high concentrations of CaO (90.5 and 89.2wt%) is observed in rock and ore samples while the concentrations of CaO (36.9, 33.6 and 31.3wt%) in soil sample respect. Although average of CaO contents is 21wt% in ore samples, only 3wt% in tailings. High concentration of Fe_2O_3 (42.7 - 57.3 wt%) were observed. The average concentration of Fe_2O_3 is about 7wt% in ore and 15wt% in tailing, respectively.

The chemical composition of soil and sediment samples were characterized by high sulfur contents and high concentration of copper. Almost of soil and sediment samples were observed highly significant concentrations of Cu value than the limit of 36mg/kg in part by EPA (United States Environmental Protection Agency).

The Pb concentration is (0.001 - 291mg/kg) in rock samples and (37.7 - 33500mg/kg) in soil samples, respect. The average concentration of Pb in rock samples is (16.23mg/kg) and (2014mg/kg) in soil sample. Therefore, the difference in Pb concentration is significantly high between rock and soil samples. Not only tailing soil samples except (SS-1) showed significantly higher Pb concentration value (714mg/kg – 2170mg/kg) than the standard limit of 300mg/kg in part by WHO Standard but also significantly observed the 33500mg/kg in soil sample (SS-25).

3.2. Mineralogical Composition of Solid Mine Wastes

Mineralogical examination is essential to understanding process, mineral habit, and reactive minerals that result in ARD (Acid Rock Drainage Potential) and metal leaching from mine-waste piles (Diehl et al., 2006a; Diehl et al., 2006b, Hammarstrom and Smith, 2002). Not only the abundance of sulfur and carbonate minerals but also mode of occurrence of chemical elements and reactive minerals are usually focus on mineralogical investigations. In addition, silicate and aluminosilicate minerals that may have long-term ARD neutralizing potential can be identified and quantified. Blows (1997) developed a mineralogically based sulfide alteration index to quantify the degree of oxidation of mine-waste materials.

X-ray diffraction (XRD) methods can be used in an initial screening to identify mineral phase in mine waste samples. The prominent minerals observed in all soil sample are quartz, calcite, pyrite, pectolite and elpidite. The galena content is significantly observed in waste rock sample (OS-9). The ore minerals sphalerite, galena, whereas copper sulfide minerals chalcopryrite, bornite, covellite, chalcocite and iron sulfide minerals marcasite and arsenopyrite were well observed in the rocks of study area (Thaire Phyu Winn,2002), although not detected in XRD results of present study. Acid generation from oxidation of sulfide minerals, such as pyrite and pyrrhotite in mine waste is one of the most significant issues facing the mining industry. Secondary Fe-bearing oxyhydroxysulfate, hydroxide and oxyhydroxide minerals play a major role in sequestering metals and metalloids from mine wastes (Hudson-Edwards and Dold, 2015).

3.3. Physiochemical characteristics of the solid mine wastes

The pH, EC and Temperature (T) parameters of soils from the study area are shown in table (1). These are able to provide sufficient information to understand the soils capacity to retain heavy metal pollutants.

Results obtained for the soil pH measurement showed a neutral to alkaline pH ranging from 7.13 to 8.2. pH variations are presumed to be related to heterogeneous deposits of sulfidic residues at the surroundings of the mine which can cause a decrease of the pH by corresponding oxidation and formation of sulfuric acid (Barkouch and Pineau, 2016). The medium alkaline pH condition of the tailings could be ascribed to the dominant potential acid-neutralizer or pH buffering minerals such as alumino-silicate minerals and traces of carbonate (i.e. calcite) present within the tailing system (Gitari, et al., 2018).

The electrical conductivity values could be attributed to excessive amount of heavy metal in the soil. High electrical conductivity may occur as a result of poor irrigation, water quality and excessive use of fertilizer. The high values of temperature recorded in the soil samples of study area may have affected carbon turn-over and organic matter.

Table 1 Physiochemical properties of soil samples in study area.

Sr. no.	Sample	pH	EC (μ /s cm)	Temp($^{\circ}$ C)
1	SS-5	7.76	608	29.5
2	SS-8	7.63	191.2	29.7
3	SS-10	7.13	796	29.7
4	SS-11	7.76	155.7	29.7
5	SS-12	7.98	81.7	29.7
6	SS-13	8.06	185.3	29.6
7	SS-14	7.88	222	29.6
8	SS-18	7.64	692	29.6
9	SS-19	8.2	104.5	29.1
10	SS-20	7.27	277	29.3
11	SS-21	7.86	176.6	29.3
12	SS-25	7.74	619	29.3
13	SS-26	7.5	638	29.3
14	OS-18	8.04	193	29.4
MEAN		7.76	7.76	29.55

3.4. Major Element Geochemistry

Table 2 is the summary statistics of the major and trace elements concentrations of solid mine wastes in study area. The table includes the results of present study, along with the crustal averages and soil guideline values for some of the potentially toxic elements by EPA, and the elements concentration of solid materials in study area.

Table 2 Summary of XRF data for major (wt%) and trace elements(ppm) in solid materials from study area, along with published concentrations values of continental crust guideline values for potentially toxic elements.

Soil sample					Rock and ore sample				*Cont. Crust Background value	Soil Guideline value of EPA
No.	Min	Max	Mean	St. Dev.	Min	Max	Mean	St. Dev.		
SiO ₂	21.2	70.76	53.6	12.75	2.75	91.1	64.8	25.39	66	
Al ₂ O ₃	3.98	18.71	11.17	4.64	0.46	18.7	11.4	6.27	15	
Fe ₂ O ₃	2.93	42.73	10.48	10.48	0.23	57.3	3.23	12.58	5	
CaO	1.75	6.09	9.75	9.12	0.09	90.5	6.01	25.01	4.2	
K ₂ O	1.01	6.09	2.78	1.22	0.02	9.43	2.04	3.43	3.4	
MgO	0.96	10.04	2.78	1.88	0.08	4.61	1.11	1.32	2.2	
Na ₂ O	0.21	10.63	3.28	2.84	0.20	3.55	3.49	1.06	3.9	
TiO ₂	0.03	1.76	0.72	0.42	0.01	1.34	0.15	0.38	0.5	
MnO	0.04	0.27	0.14	0.04	0.01	0.39	0.07	0.09	0.1	
Pb	37.7	33500	221.5	6895.15	0.0006	1.11	0.0027	0.24	20	30
S	1118	67500	2960	15973.22						
Hg	20.8	210	30.4	58.02						
Cu	32.6	2510	32.6	608.03					25	22
Zn	37.56	53600	689	13034.29					71	66
Au	12.17	203	31.36	40.51						
Ag	15.2	120	22.9	30.99						
Pt	28.2	444	43.2	132.75						
U	7.72	19.1	13.85	4.074	16.6	95.8	30.6	24.68		
As	12.1	2010	129	402.79	0.0004	1800	2.97	402.79	1.5	

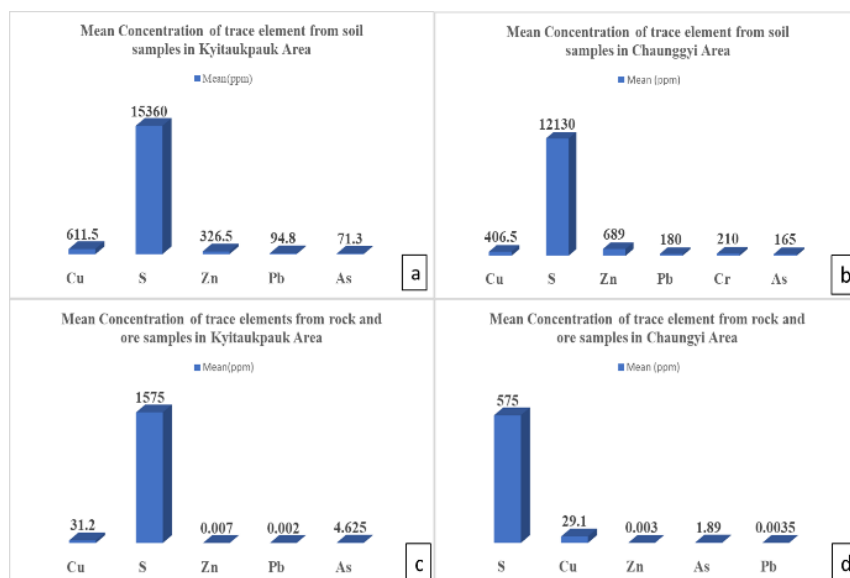


Figure 3 Mean concentrations of oxide in study area, (a & b) for soil and (c & d) for rocks and ore samples.

As can be seen in Fig. (3), the mean concentration in all soil samples SiO_2 , TiO_2 , Al_2O_3 and Fe_2O_3 are 54.35, 1.57, 25.02 and 24.1wt% in Kyitaukpauk area and 35.1, 0.34, 8.25, 23.6 in Chaunggyi area respectively. The result further show that the mean concentration of MgO and CaO are high, and Na_2O , MnO are similar compared to their crustal averages in both area.

3.5. Trace Element Geochemistry

The results of potentially toxic element analysis are summarized in table (2) and Fig (4). The results show that all heavy metal in soil and sediments of study area have mean concentration above the published crustal abundances. The results were also compared with trigger and guideline value for potentially toxic elements in soils and this shows that the mean concentration of As is above the limit set for median soil content. The mining of gold is an important source of As in the environment. The mean concentration of As in rock sample from Kyitaukpauk area is 4.62 mg/kg and Chaunggyi 1.89mg/kg area while 71.3mg/kg and 165mg/kg in soil samples. Chaunggyi area is significantly high the concentration of As in soil sample than Kyitaukpauk area although less concentration in rock and ore samples than Kyitaukpauk area. The Enrichment ratio (ER) in metal and Geoaccumulation Index (I_{geo}) are indicators used to assess the presence and intensity of anthropogenic contaminant deposition on surface soil.

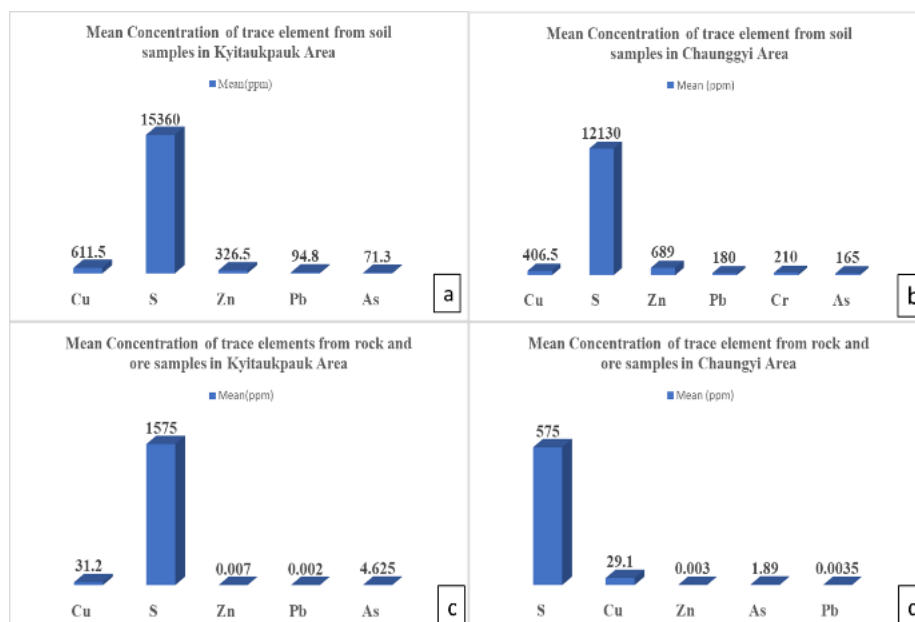


Figure 4 Mean concentrations of trace elements in study area, (a & b) for soil and (c & d) for rock and ore samples.

3.6. Enrichment Ratios

Element enrichment ratios were calculated to evaluate the extent of enrichment and / or depletion of trace elements in the soils of the study area relative to their crustal concentrations. In this study, the Upper Continental Crust concentrations of the elements were used as baseline or background values and the enrichment ratio (ER) was calculated using the equations (Waziri, 2014):

$$ER = C_n / B_n$$

where C_n is the concentration of an element measured in a sample and B_n is the background or baseline concentration, in this study, the upper crustal concentration of the element. The results and define qualities of the enrichment ratios are shown in table (3). The numerical results are different pollution level. Values of 0.5-1.5 suggest that the trace metal concentration may come entirely from natural weathering process (Yongming et al., 2006). However, an ER value >1.5 indicates that a significant portion of the trace metals was delivered from non-crustal materials (Yongming et al., 2006 and Klerks et al., 1989), so these trace metals were delivered by other sources, like point and non-point pollution and biota (Yongming et al., 2006). With ER index, soil quality state can be indicate by different classes in table (3) range from $ER < 2$ (Deficiency to minimal enrichment) to $ER > 40$ (Extremely high enrichment). (Klerks et al., 1989)

Table 3 Contamination categories based on ER values. (Source: Yongming et al., 2006)

Class	ER Value	Soil quality
1	<2	Deficiency to minimal enrichment
2	2-5	Moderate enrichment
3	5-20	Significant enrichment
4	20-40	Very high enrichment
5	>40	Extremely high enrichment

The enrichment ratios are summarized in (table 4 and table 5) and show the factor by which the concentration of elements except As and Cu in the samples of study area exceeds their crustal abundances. An enrichment ratio, ER of 1 indicates that the soil or sediment is neither enriched nor depleted in a particular element relative to the average crustal concentration. On the other hand an ER of >1 or <1 is an indication of enrichment or depletion.

The results (table 4 and table 5) show that As is extremely high enriched element relative to the baseline value, with ER of about 47.5 in Kyitaukpauk to 110 in Chaunggyi area. This is evidence of higher As concentrations obtained in the top soils and sediments. The concentration of Cu and Pb are about 15 times and 12 times respectively its upper crustal concentration.

As shown in (table 4 and table 5), the ER rank of the study area is ranging from $As > Cu > Pb > Zn$ in Kyitaukpauk Area and $As > Cu > Zn > Pb$ in Chaunggyi area.

Table 4 Summary of enrichment ratios, ER for the soil samples from Kyitaukpauk area.

No.	Element	Enrichment ratios, ER			ER Class	Soil Quality
		Min	Max	Mean		
1	Cu	4.28	100.4	22.84	4	Significant enrichment
2	Zn	0.99	12.04	4.6	2	Significant enrichment
3	Pb	1.89	31.75	4.74	2	Significant enrichment
4	As	8.07	225.33	47.53	5	Extremely high enrichment

Table 5 Summary of enrichment ratios, ER for the soil samples from Chaunggyi area.

No.	Element	Enrichment ratios, ER			ER Class	Soil Quality
		Min	Max	Mean		
2	Cu	1.30	74.4	16.26	3	Significant enrichment
3	Zn	2.11	754.92	9.70	3	Significant enrichment
6	Pb	6	1675	9	3	Significant enrichment
9	As	31.33	1340	110	5	Extremely high enrichment

3.7. Index of Geoaccumulation (I_{geo})

One of the method used in estimating the enrichment of concentration of an element above the background or baseline values is to calculate the index of geoaccumulation, I_{geo} proposed by Muller. Muller (1981) has defined seven classes of geoaccumulation Index ranging from class 0 ($I_{geo}=0$, unpolluted) to class 6 ($I_{geo} > 5$, extremely polluted). The highest class (class 6) reflects at least a 100-fold enrichment factor above background. The pollution by using seven enrichment classes based on an increase on the numerical value of the scale are shown in Table (4 and 5).

Table 6 Classes of the index of geoaccumulation, I_{geo} . (Muller, 1981)

Value	Class	Pollution Intensity
>5	6	Extremely polluted
4-5	5	Strongly polluted to extremely polluted
3-4	4	Strongly polluted
2-3	3	Moderately polluted to strongly polluted
1-2	2	Moderately polluted
0-1	1	Unmoderately polluted to moderately
0	0	Unpolluted

The index of geoaccumulation, I_{geo} was calculated for all the samples according to the equations:

$$I_{geo} = \text{Log}_2(C_n/1.5 B_n)$$

where C_n is the concentration of the element measured in a sample and B_n is its concentration in some reference sample or background concentration, which in this study is the average crustal value, while 1.5 is a constant which is introduced to minimize the effect of the variation of background values.

(Table 7 and 8) are shown in summary of the results. Based on the I_{geo} classes in (Table 6), the results of this work show that the study area may have problems relating to As contamination. The mean I_{geo} value of 4.91 and 9.54 for As falls within class 5-6 which is maximum I_{geo} values >5 of the Muller scale, indicating that the soils from this area are extremely polluted with respect to As. Similarly, all samples have I_{geo} values exceed than 6 for Hg corresponding to also extremely polluted conditions, showing that the area has problem with respect to Hg and heavy metal contamination of surface soils and sediments. The mean index of geoaccumulation 1-2 for Zn is indicating no pollution to moderate pollution.

Table 7 Summary of indices of geoaccumulation, I_{geo} for trace elements in soils and sediments from the Kyitaukpauk area.

No.	I_{geo}					Pollution intensity
	Element	Min	Max	Mean	Class	
1	S	0.34	10.24	3.89	4	Strongly
2	Hg	52.28	233.13	89.805	6	Extremely
3	Pb	0.22	12.44	2.09	3	Moderately to strongly
4	Cu	0.86	20.15	4.59	5	Strongly to extremely
5	Zn	0.2	2.42	0.93	1	Unpolluted to Moderately
6	As	1.62	45.22	9.54	6	Extremely

Table 8 Summary of indices of geoaccumulation, I_{geo} for trace elements in soils and sediments from the Chaunggyi area.

No.	I _{geo}					Pollution intensity
	Element	Min	Max	Mean	Class	
1	S	0.43	19.35	3.48	4	Strongly
2	Hg	20.8	151	28.1	6	Extremely
3	Pb	0.69	192.08	1.03	1	Unpolluted to Moderately polluted
4	Cu	0.22	12.44	2.7	3	Moderately to strongly
5	Zn	0.33	119.52	1.54	2	Moderately
6	As	1.57	67.23	4.91	5	Strongly to extremely

Conclusion

The study area Kyitaukpauk- Chaunggyi is significant mineralized zone especially the gold metal in Thabeikkyin- Singu area. There have many gold mines in this area but seven mines can be analyzed in the present study. Therefore, its need to many research in environmental impacts of gold mining for these area. Heavy metal distribution in soils ,mine tailings and waste rock piles from study area were investigated. The ER shows five different classes in the investigated soils: extremely high enrichment is observed for As in both area. Although Cu is more enriched in Kyitaukpauk area than in Chaunggyi, Zn and Pb are more enriched in Chaunggyi area. These elements are directly related to mineral paragenesis and mining activities in study area.

According to I_{geo} results, study area observed in extremely polluted for As and Hg and, strongly polluted for S and Cu. High metal concentrations in the soils of study area are derived, for their most important part, from the geological background of which the soils ultimately derived. The abundance of metals and trace elements in soils also reflect (i) their release from mining and smelting derived particles, and (ii) their partitioning into different soil compartments. The smelting process of gold ore had significant impacts on the enrichment of As and Hg in the mine wastes.

Acknowledgements

I would like to thank Dr. Day Wa Aung, Professor and Head of Department of Geology, University of Yangon for his kind help, valuable guidance, critical reading and precious suggestions. I also appreciate to Mg Myint Kyaw and Mg Zaw Khant Linn for their helping to my field works and also extent to U Kyaw Kyaw Oo and U Khin Mg Htwe, Pyi Thar Naing Co.Ltd, Nga Pyar Pay village, Singu Township for their careful help during in my field work. Thanks are extended to all staffs of Geology Department, and my colleagues, for friendship, helps and for all their support during my academic pursuits.

References

- Barkouch, Y. and Pineau, A., (2016), Impact of Mine Tailings Surrounding Soils: Case Study of Draa Lasfar Marrakech- Morocco, *Environmental Resources Research*, vol.4, No.1,2016
- Blowes, D.W., (1997), The Environmental Effects of Mine Wastes, in the Proceeding of Exploration 97, "Fourth Decennial International Conference on Mineral Exploration", p 887-892
- Diehl, S.F., Hageman, P.L., and Smith, K.S., (2006a), What's weathering? Mineralogy and field leach studies in mine waste, Leadville and Montezuma mining districts, Colorado, in Proceedings of the 7th International Conference on Acid Rock Drainage (ICARD7), St. Louis, Missouri, March 26-30, 2006, p 5.7-527.
- Diehl, S.F., Hageman, P.L., Smith, K.S., Koenig, A.E., and Lowers, H.A., (2006b), What's weathering in mine waste? Mineralogic evidence for sources of metals in leachates, in Proceedings of the U.S. Environmental Protection Agency Hard Rock Mining 2006 conference, Tucson, Arizona.
- Gitari, W.M, Thobakgale, R. and Akinyemi, S.A, (2018), Mobility and Attenuation Dynamics of Potentially Toxic Chemical Species at an Abandoned Copper Mine Tailings Dump, *Minerals* 2018, vol.8, 64.
- Hammarstrom, J.M. and Smith, K.S., (2002), *Geochemical and mineralogic characterization of solids and their effects on waters in metal-mining environments*, Progress on geoenvironmental models for selected mineral deposit types, U.S. Geological Survey, p 8-54.
- Hudson-Edwards, K.A., and Dold, B., (2015), Mine waste characterization, management and remediation, *Mineral* 2015, vol.5, p 82-85.
- Klerks P.L., Levinton, J.S., (1989), Rapid evolution of metal resistance in a benthic oligochaete inhabiting a metal-polluted site, *Biological Report*, Bulletin, p 135-141.
- Lawrence, R.W., and Scheske, M., (1997), A Method to Calculate the Neutralisation potential of Mining Wastes, *Environmental Geology*, vol.32, 100-106
- Lottermoser, B.G.,(2010), *Mine wastes characterization, Treatment and Environmental Impacts*, 3rd edit, Springer, Berlin, Heidelberg.
- Muller, G., (1979), *Schwermetalle in den sedimenten des Rheine* Veränderungen seitt, Umschau, p 778-783.
- Muller, G.,(1981), *Die Schwermetallbelastung der sedimente des Neckars and seiner Nebenfluec: eine Bestandsaufnahme*, Chem. Ztg., p 157-164.
- Parbhakar-Fox, A. and Lottermoser, B., (2017), "Prediction of Sulfidic Waste Characteristics", *Environmental Indicators in Metal Mining*, Springer, Berlin, Heidelberg.
- Smedley, E., Mackenzie, S., Astill, W., Campbell, G. and Haymont, R, (2014), 'Cost effective integrated assessment of mine waste and practical management solutions, in the Proceeding of the "Gold Fields Environmental Management Group Conference", Kalgoorlie.
- Taylor, S.R., McLennan, S.M, (1995), The Geochemical Evolution of Continental Crust, *Review of Geophysics*, vol.33, no.2, p 241-265.
- Thaire Phyu Winn, (2002), *A genetic approach to gold mineralization in the Nweyon-Kantaung area, Singu Township*, M.Sc Thesis, University of Mandalay (Unpublished).
- Wazari, N.M., (2014), Environmental Geochemistry of Soils and Sediments from the Birnin – Gwari Artisanal Gold Mining Area, North-western Nigeria, *Universal Journal of Geoscience* vol.2, no.1, p 18-27.
- Weber, P.A., Thomas, J.E, Skinner, W.M, Smart, St. RC, (2005), A method of determine the acid- neutralisation capacity of rock samples, *The Canadian Mineralogist*, vol.43, p 1183-1192.
- Yongming, H., Peixuan, D., Junji, C., Posmentier E.S., (2006), Multivariate analysis of heavy metal contamination in urban dusts of Xi'an, Cent, China, *Science of Total Environment*, vol. 355, p 176-186.

A STUDY ON LANDSLIDE POTENTIALS AND SLOPE STABILITY OF THE ROAD AT ZWEKABIN RANGE NEAR KHALAUKNOS VILLAGE, HPA-AN TOWNSHIP

Aung Kyaw Myat¹, Day Wa Aung², Hlaing Myo Nwe³ and Aung May Than⁴

Abstract

The research aims to mention the landslide hazard and mitigation measures in the Zwegabin Range. This study road is located at the eastern part of the Zwegabin Range near Khalaunknos Village, Hpa-an Township, Kayin State. This area is mainly composed of cherty limestone and lime-mudstone of Moulmein Limestone (Permian in age). Moreover, the area lies in the Zwegabin-Belin Fault Zone, a right-lateral strike-slip fault. Hilly terrain with steep slopes is found in the most of places at the study route and structurally unstable. The big landslide occurred on 15th, July in 2018 on the road at Zwegabin Range. Rock mass characterization and slope stability analysis are carried out for potential of landslides in the research area to know causes of landslides and preventing systems. In the study, although the behaviors of the rocks are not quite different along the road, the strength and engineering properties of the rocks are varied from place to place. Plane failures and wedge failures commonly occur. Most of the slopes are dangerous attaining stability because some rocks are very weak in geological condition as well as slope condition. According to the slope mass rating (SMR) analysis, most of the slopes are completely unstable and unstable slope conditions. In addition, all slopes have not been supported by suitable retaining structure and systematic drained system. Therefore, preventing systems and controlling techniques should be made to mitigate the causes of landslide.

Keywords: Landslide, plane failure, wedge failure, slope stability, slope mass rating

Introduction

The present study mainly aims to conduct the analysis of the landslide hazards along the road at the base of the Zwegabin Hill near Naunglon (east) village, Hpa-an Township, Kayin State. The geological and geotechnical parameters of the rocks along the road are mainly studied and measured in this research. This area is mainly composed of carbonate sedimentary rocks. The behaviors of the rocks are not quite different along the car-road but not the same. Moreover, the strength and engineering properties of the rocks are varied from place to place because of the structural controls. The big landslide occurs on 15th, July in 2018 at this road.

Location

This area lies between north latitudes 16° 46' 00" to 16° 50' 00" and east longitudes 97° 39' 00" to 97° 43' 00", covering UTM map No. 1697-09. The research road sector along the road is about 1200 m long near Naunglon (east) village, Hpa-an Township, Kayin State which is shown in Figure (1).

¹ Dr, Lecturer, Geology Department, University of Yangon

² Dr, Professor and Head, Geology Department, University of Yangon

³ Dr, Lecturer, Geology Department, Dagon University

⁴ Dr, Professor and Head, Geology Department, Hpa-an University

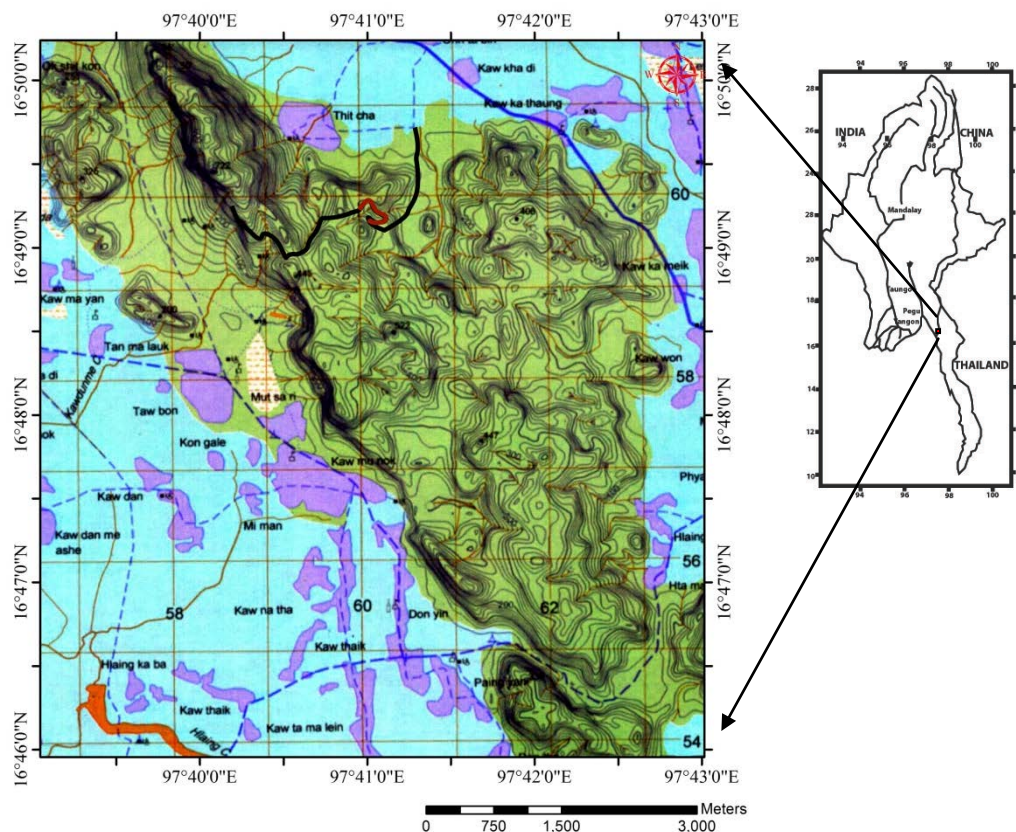


Figure 1 Location map of the research area

Physiography

Physiographically, Zweekabin Range is highly elevated and rugged terrain which is composed of limestone over the whole range (Figure 2). The elevation was divided into four divisions based on their elevations where green colored area shows flat plain and its elevation is less than 300 m. Although the elevations were classified into four, the other three want to designate as highly elevated and rugged terrain where elevation has greater than 300 m because the whole lithology is same. The average elevation is 400 m in this area and the highest peak has at the top of the Zweekabin Range which is elevated about 722 m above sealevel.

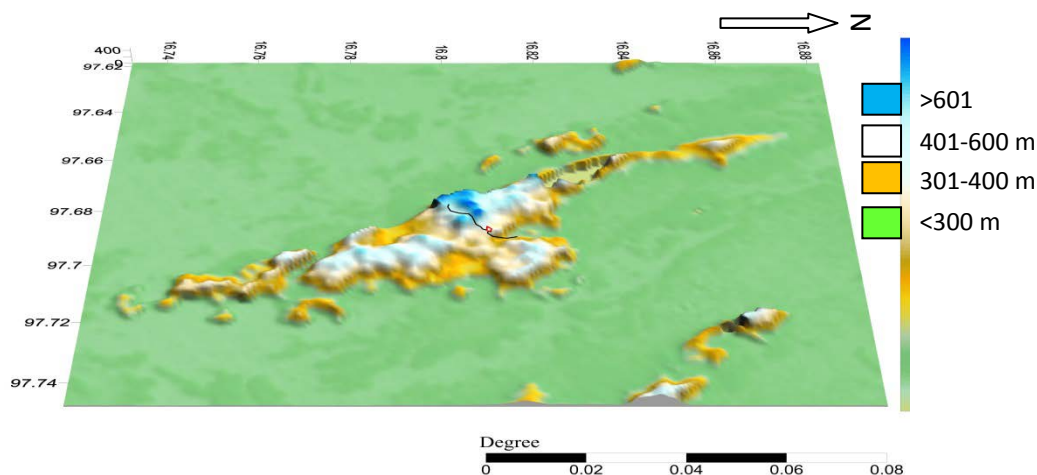


Figure 2 Physiographic map of the research area

Drainage Pattern

In the research area, the centripetal pattern and sub-dendritic pattern are mainly evolved at the central and western part of the research area (Figure 3). The whole area of Zweekabin Range is covered by the centripetal pattern which is reflected by the underlying Moulmein Limestone. Sub-dendritic pattern with fine to medium texture is found at the north-western part of the study area where is covered by the underlying Taungnyo Formation.

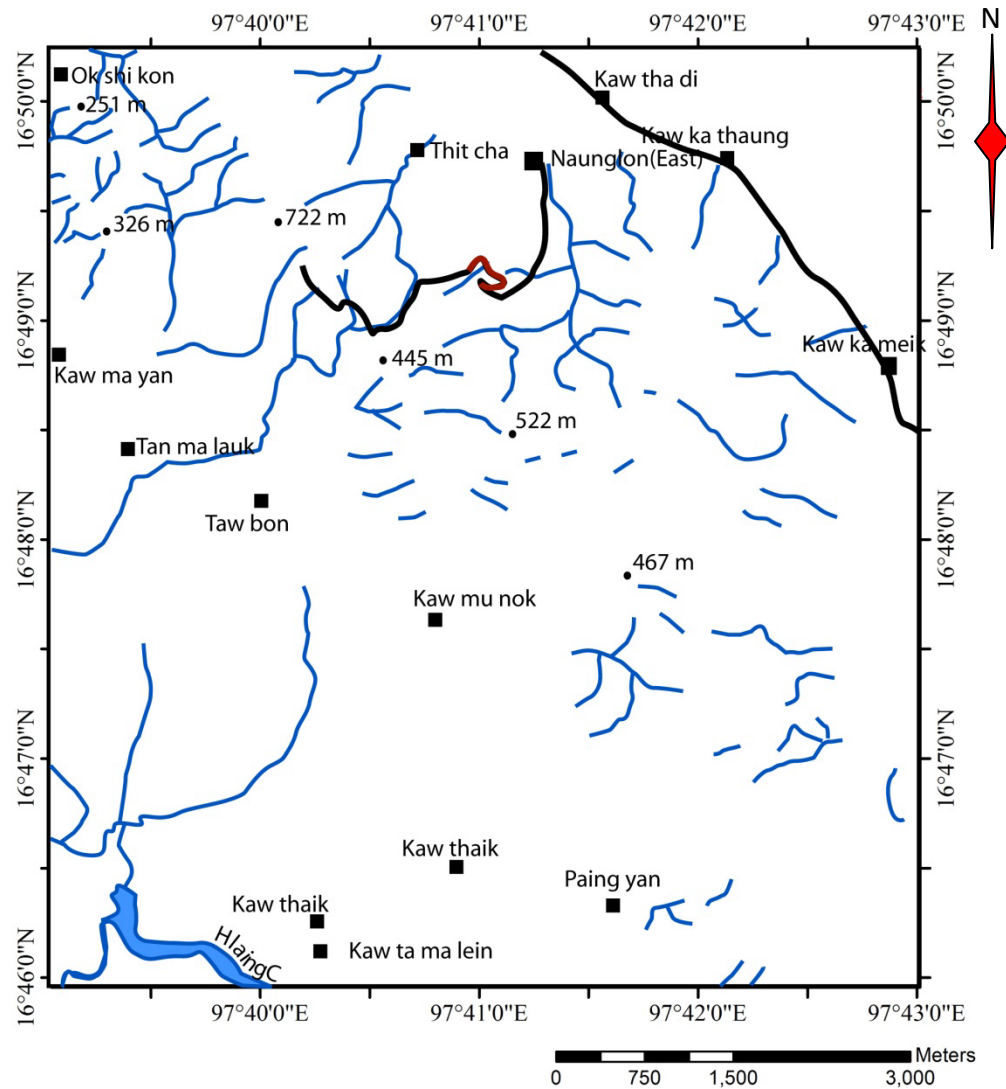


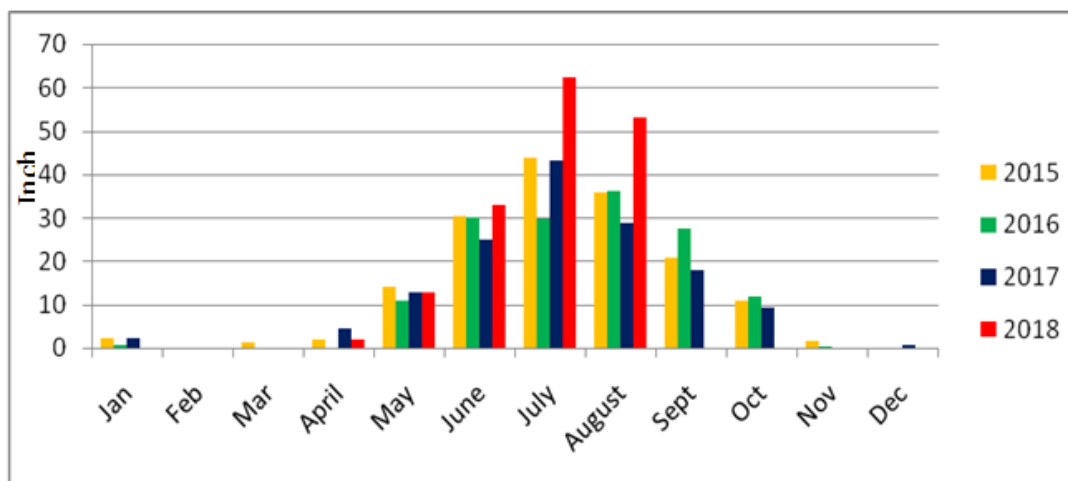
Figure 3 Drainage pattern of the research area

Climate and Rainfall

The climatic condition of the study area is tropical. Rainfall made the rock units as highly weather nature, so rock fall block as risk effect. According the comparative study of rainfall data by using histogram, highly rainfall shows in June, July and August in 2015-2018. The significant rainfall data are highest in July and August, 2018 (Table-1 & Figure 4).

Table 1 Monthly rainfall data of the research area

	Jan	Feb	Mar	April	May	June	July	Aug	Sept	Oct	Nov	Dec
2015	2.24	0	1.42	1.86	14.05	30.52	43.92	35.71	20.77	10.82	1.56	0
2016	0.86	0	0	0.08	11.07	30.25	29.7	36.22	27.51	11.97	0.24	0
2017	2.12	0	0	4.61	12.63	24.93	43.02	28.64	18.00	9.31	0	0.63
2018	0	0	0	1.77	12.91	32.8	62.4	53.00	19.24	12.1	0	0

**Figure 4** Histogram shows comparative study of monthly rainfall data

Regional Geologic Setting

The rocks of Taungnyo Formation (Carboniferous to Early Permian), Moulmein Limestone (Middle to Late Permian) and Alluvium (Quaternary) covered in the study area with different relief which is shown in Figure (13).

The rocks of the Taungnyo Formation are exposed at the northern part of the Zweekabin Range and southern part of the Hpa-an Town. The rocks are mainly composed of clastic units; thin bedded, whitish grey to pinkish colored siltstone intercalated with thinlly laminated shale, partly fine grained nodular sandstone which is shown in Figure (5).

Moulmein Limestone is mostly composed at the Zweekabin Range with gentle dipping. The other isolated hills with karst topography are also composed of Moulmein Limestone. The rocks are consist of medium to thick bedded, grey to dark grey colored lime-mudstone and brecciated limestone of the Moulmein Limestone (Figures 6-8).

Most of the flatplain are covered by reddish brown to yellowish brown colored, thick alluvial soils.

Geological Structures

The research area is mainly characterized by NNW-SSE trending stratigraphic units in eastern part and NW-SE trending in central and western part. Besides, the major longitudinal fault with normal sense occurred at the western flank of the Zweekabin Range which is trending

nearly north-south in direction (Figure 9 & Figure 10). Another thrust fault is also trending parallel with the above normal fault (Figure. 11). Besides, the Zweekabin (east) Fault is trending nearly NW-SE direction at the east part of the Zweekabin range which occurred as the right-lateral strike-slip faults (Figure 12). Moreover, the anticlinal fold is occurred with NNW-SSE trending at the western part of the Zweekabin Range.



Figure 5 Thin bedded, whitish grey to pinkish colored siltstone intercalated with thinlly laminated shale, partly fine grained nodular sandstone of Taungnyo Formation at the northern part of Zweekabin Range



Figure 6 Medium to thick bedded, grey to dark grey colored lime-mudstone of the Moulmein Limestone exposed at the west of Naunglon (East) Village



Figure 7 High pressure radial joint pattern in lime-mudstone with chert nodule at the Naunglon (east) village



Figure 8 Intersection of two normal faults with vertical striation (N16° 57' 00.2", E97°25'51.0", Facing - 260°)



Figure 9 Normal fault scarp at the western part of the Zweekabin Range



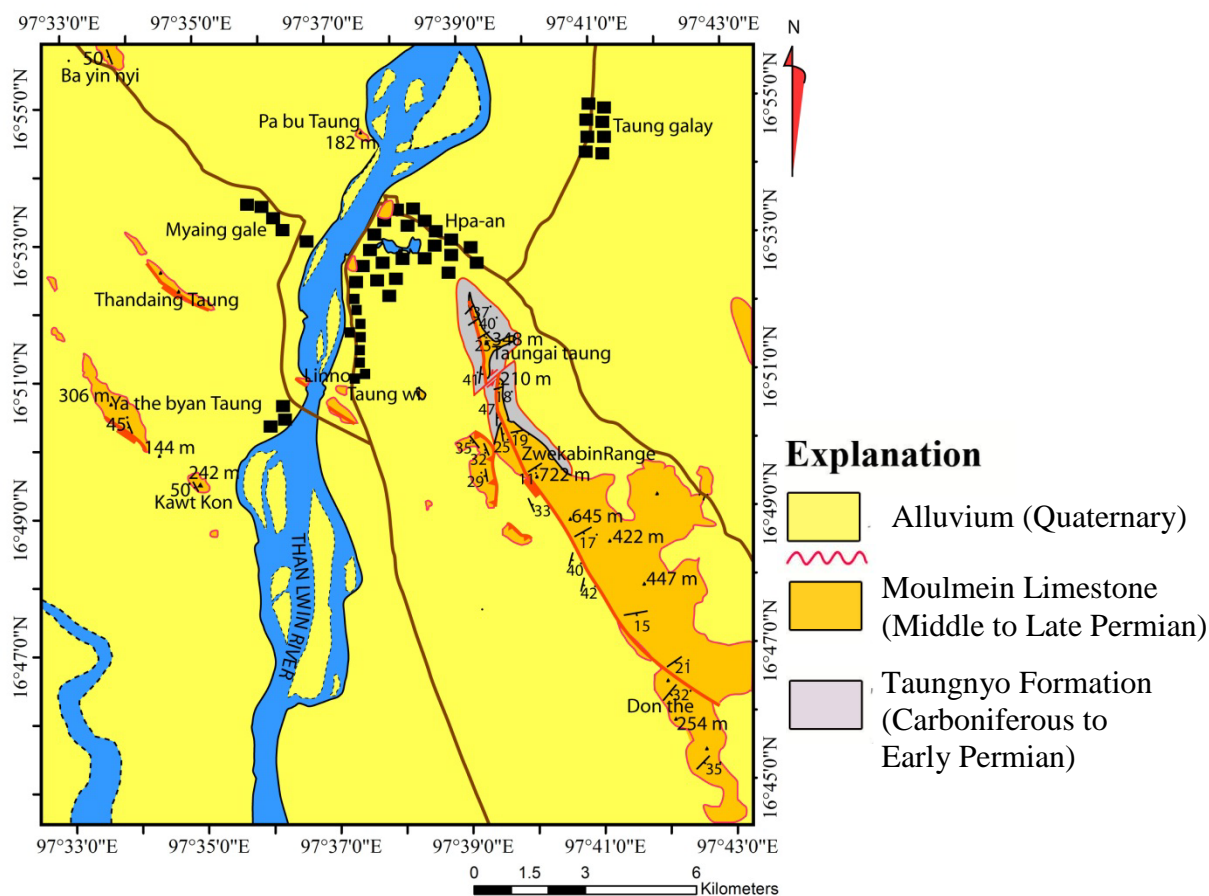
Figure 10 Extensional normal fault planes cutting in calcite vein at the west of Naunglon (East) Village



Figure 11 Thrust sheet at the west of the Zwegabin Range



Figure 12 Strike-slip fault at the east side of the Zwegabin Range



Geology by Aung Kyaw Myat and Aung May Than (2018)

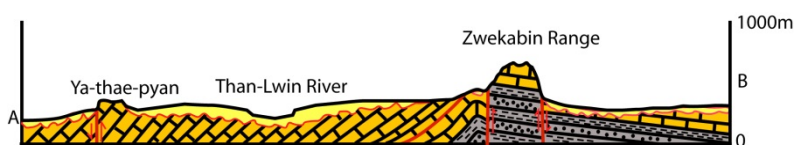


Figure 13 Geological map of the research area

Past Landslides

Annually landslide happens always occur at hilly region of Hpa-an area in rainy season. But many minor landslides are found in this rainy season because of the significant rainfall

effect. Most of the slope failures are formed by the following effects; (a) uncontrolled cutting the slope, (b) coincide with fault line (c) highly rainfall effect and (d) weathering effect. According to the Varnes (1978), there are many types of landslide along the car-road such as rockfall (Figures 14 & 16), debris flow (Figure 17, 18, 19 and 20), creep (15) and size of the landslide is shown in Figure (21).



Figure 14 Rockfall in lime-mudstone of Moulmein Limestone (N16°49'13.1, "E97° 41'11.4", Facing - 170°)



Figure 15 Creep in cherty limestone of Moulmein Limestone (N16°49' 14.6"E97°41'13.6", Facing - 80°)



Figure 16 Rockfall in cherty limestone of Moulmein Limestone (N16°49'14.6"E97° 41'14.3", Facing - 340°)



Figure 17 Debris flow in brecciated limestone of Moulmein Limestone (N16°49'15.4"E97°41'09.6", Facing - 280°)



Figure 18 Rockfall in brecciated limestone of Moulmein Limestone (N16°49'15.4" E97°41'09.6", Facing - 290°)



Figure 19 Debris flow in brecciated limestone of Moulmein Limestone (N16°57'00.2", E97°25'51.0", Facing - 280°)



Figure 20 Big debris flow in the research area (N16°57'00.2", E97°25'51.0")

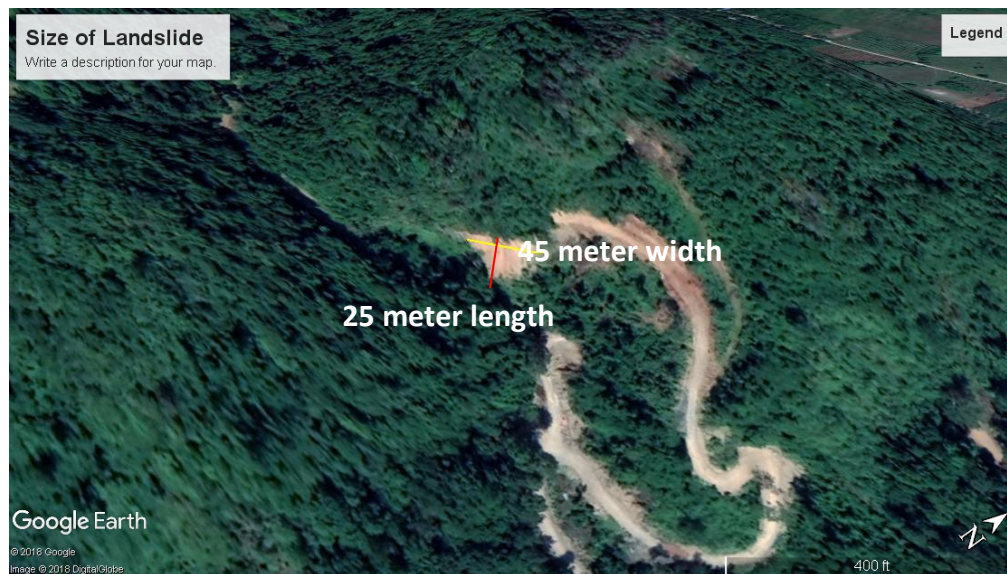


Figure 21 Size of the debris flow on google map

The big landslide is triggered on 15th July, 2018 because of the significant highly rainfall in Kayin State. The width of the landslide scar or debris flow area along the road is 45 meter width and 25 meter length until the base of the mountain. This landslide badly destroyed the road where can't be used in future if the systematic retaining structure and drainage don't use.

Methodology

Landslide classification adopted for this research is that proposed by Cruden and Varnes (1978). The rock mass rating (RMR) was computed according to Bieniawski (1989), with adding rating values for five parameters: i) strength of intact rock, ii) RQD, iii) spacing of discontinuities, iv) condition of discontinuities, and v) water inflow through discontinuities and/or pore pressure ratio.

The volumetric joint count (J_v) has been described by Palmström (1982). It can be measured from the joint set spacings within a volume of rock mass as $J_v = 1/S_1 + 1/S_2 + 1/S_3 + \dots + N_r/5$ where S_1, S_2, S_3 are the joint set spacings and also random joints can be included by assuming a random spacing (N_r) for each of these where N_r = the number of random joints.

The strength of the rock mass is measured by using point load test of laboratory tests. The volumetric joint count was used to measure by using the formula of $J_v = 1/S_1 + 1/S_2 + 1/S_3 + \dots + N_r/5$, where N_r means the numbers of random joints to determine the RQD (Romana, 1993). It is not possible to obtain good correlations between RQD and J_v . In 1982, the formula $RQD = 115 - 3.3 J_v$ was applied, which was presented by Palmström (1982).

Spacing of discontinuities is the distance between them, measured along a line perpendicular to discontinuity planes. Determining the condition of discontinuities is not simple parameter, as it includes several parameters such as (i) roughness, (ii) separation, (iii) filling material, (iv) persistence and (v) weathering of walls. The groundwater which accounts for the influence of the water pressure, with particular reference to the underground excavation are classified either; completely dry, damp, wet and dripping or flowing.

Geomechanics classification of Rock Mass Rating (RMR), Bieniawski (1989) system has been used to find Slope Mass Rating (SMR) (Romana, 1993). The "Slope Mass Rating" (SMR) is obtained from RMR by adding a factorial adjustment factor; depending on the relative orientation of joints and slopes and another adjustment factor depending on the method of rock slope excavation. Field observations and measurements of discontinuities by using this formula $SMR = RMR + (F_1 \times F_2 \times F_3) + F_4$ are the main method for finding the SMR.

The stereographic method of kinematic analysis (Goodman, 1998) and (Jeonggi-gi and Kulatilake, 2001) is mostly useful for assessment of the stability of discontinuity planes. Slope orientation, discontinuity sets orientation and friction angle of the each Formation in the research area are used for kinematic analysis as the three main parameters. Data of the strike and dip values of slopes and discontinuities have been obtained from a discontinuity survey and pole plot, respectively. The slope face is shown as a great circle and the friction angle is represented by an interior circle.

Results and Discussions

A rock mass is composed of a system of rock blocks and fragments separated by discontinuities forming a material in which all elements behave in mutual dependence as a unit. The main features constituting a rock mass are large variations in the composition and structure of rocks as well as in the properties and occurrence of the discontinuities intersecting the rock that lead to a complicated composition and structure of the rock mass.

The following rock mass tests are measured to know the properties or characteristics of the rocks that are observed by field observations, descriptions and indirect test and supported by laboratory test also (Figure 22).

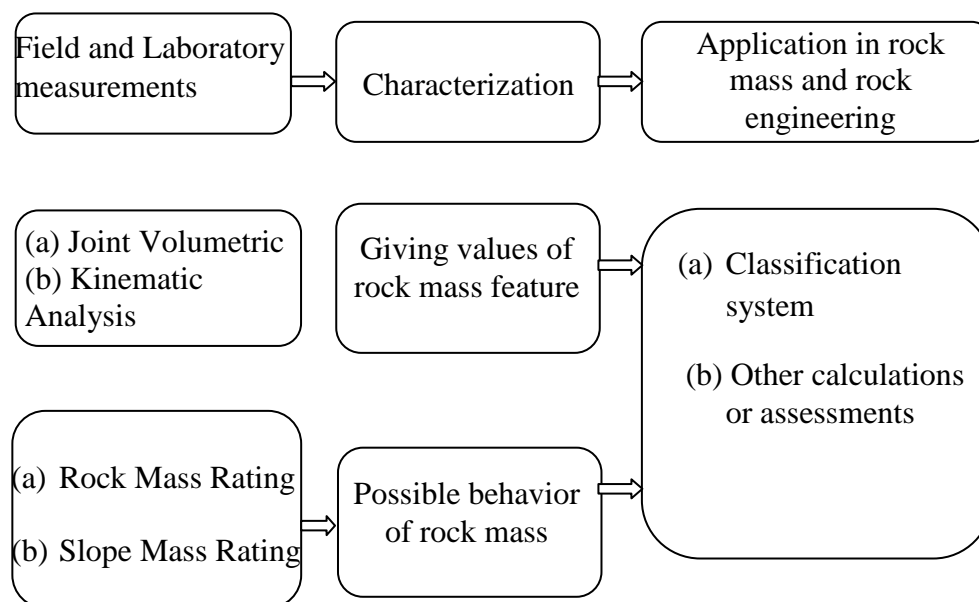


Figure 22 Idealized rock mass analysis diagram for present study

The Characteristic of Discontinuities

Joint Volumetric

The volumetric joint count of the area is a measure measured from the joint set spacings within a volume of rock mass and also random joints can be included by assuming a random spacing (Table 2). It is defined as number of joints per m^3 . The slope site localities map is shown in Figure (23).



Figure 23 Slope site localities map of the research area

Table 2 Joints volumetric counts data in this area

Site No.	Location	Rock Unit	Length (m)	Joint set spacing (m)				(Jv)
				1/J1	1/J2	1/J3	Nr/5	
1	N16°49'13.1" E97°41'11.4"	Lime-mudstone with chert nodules	1	10.25	5.32	4.21	5.67	25.45
2	N16°49'16.4" E97°41'11.4"	Lime-mudstone with chert nodules	1	12.34	7.63	3.23	5.89	29.09
3	N16°49'16.1" E97°41'13.4"	Cherty Limestone	1	14.8	10.23	4.32	2.47	31.82
4	N16°49'14.6" E97°41'13.6"	Cherty Limestone	1	13.3	8.31	2.33	5.15	29.09
5	N16°49'14.6" E97°41'14.3"	Cherty Limestone	1	14.11	9.26	3.21	3.72	30.30
6	N16°49'14.6" E97°41'15.5"	Lime-mudstone	1	13.12	9.43	4.21	2.63	29.39
7	N16°49'15.1" E97°41'09.5"	Lime-mudstone	1	9.21	7.34	4.55	3.14	24.24
8	N16°49'15.4" E97°41'09.6"	Lime-mudstone	1	14.14	9.21	3.23	3.72	30.30
9	N16°49'15.7" E97°41'10.2"	Brecciated limestone	1	12.4	6.34	2.22	4.49	25.45
10	N16°57'00.2" E97°25'51.0"	Brecciated limestone	1	15.5	11.45	3.21	2.57	32.73

Geotechnical Analysis

The geotechnical analyses are made on the basis of rock mass rating and slope mass rating which is shown in Table (3).

Rock Mass Rating

Bieniawski's Geomechanics Classification system provides a general rock mass rating (RMR) increasing with rock quality from 0 to 100. It is based upon five universal parameters: strength of the rock, drill core quality, groundwater conditions, joint and fracture spacing, and joint characteristics.

Table 3 Rock mass rating measuring data in the field

Site No.	Strength	RQD	Joint spacing	Joint condition	Groundwater condition	RMR	Rock Mass Class
1	7	31	5	9	4	56	Fair rock
2	4	19	5	9	7	44	Fair rock
3	4	10	5	15	4	36	Poor rock
4	7	19	5	9	7	47	Fair rock
5	4	15	5	9	4	33	Poor rock
6	4	18	5	15	7	44	Fair rock
7	4	35	5	9	4	58	Fair rock
8	4	15	5	9	4	33	Poor rock
9	7	31	5	9	4	56	Fair rock
10	4	7	5	9	4	29	Poor rock

According to this classification, Sites 3, 5, 8 and 10 are highly jointed and highly weathered rocks that composed of poor rocks as rock mass rating. The conditions of these sites can danger for slope stability if these slope sites don't use the systematic slope treatment. Moreover, the rocks composed of sites 3, 5, 8 and 10 have poor strength according to the rating measured by point load test. Most of the other rock units are moderately jointed and fair rocks.

Slope Mass Rating

The Slope Mass Rating (SMR) is obtained from RMR by adding a factorial adjustment factor; depending on the relative orientation of joints and slopes and another adjustment factor depending on the method of rock slope excavation. The formula of SMR is $RMR + (F_1 \times F_2 \times F_3) + F_4$, where F_1 depends on parallelism between joints and slope face strike, F_2 refers to joint dip angle in the planar mode of failure, F_3 reflects the relationship between slope face and joints dip angles and F_4 refers to the adjustment factor for the method of excavation which has been fixed empirically which is illustrated in Table (4).

Slope mass rating addresses both planar sliding and toppling failure modes, no additional consideration is made for sliding on multiple joint planes. The description of the SMR Class is provided in Table (5).

Table 4 Adjustment rating for joint (after Romana, 1993)

Case	Very Favorable	Favorable	Fair	Unfavorable	Very unfavorable
P $a_j - a_s$	$> 30^\circ$	$30^\circ - 20^\circ$	$20^\circ - 10^\circ$	$10^\circ - 5^\circ$	$< 5^\circ$
T $a_j - a_s - 180^\circ$					
P/T $F_1 = (1 - \sin a_j - a_s)^2$	0.15	0.4	0.7	0.85	1.00
P B_j	$< 20^\circ$	$20^\circ - 30^\circ$	$30^\circ - 35^\circ$	$35^\circ - 45^\circ$	$> 45^\circ$
P $F_2 = \tan^2 B_j$	0.15	0.4	0.7	0.85	1.00
T F_2	1.00	1.00	1.00	1.00	1.00
P $B_j - B_s$	$> 10^\circ$	$10^\circ - 0^\circ$	0°	$0^\circ - (-10^\circ)$	$< -10^\circ$
T $B_j - B_s$	$< 110^\circ$	$110^\circ - 120^\circ$	$> 120^\circ$	—	—
P/T F_3	0	— 6	— 25	— 50	— 60
F ₄ Adjusting factor for excavation method	Natural slope + 15	Pre-splitting + 10	Smooth blasting + 8	Blasting or mechanical 0	Deficient blasting - 8

P- Planar failure

a_s - Slope dip direction

a_j - Defect dip direction

T- Toppling failure

B_s - Slope dip

B_j - Defect dip

Table 5 SMR Classes defined by Romana (1993)

Class	SMR	Description	Stability	Failures	Support
I	81 – 100	Very good	Completely stable	None	None
II	61 – 80	Good	Stable	Some blocks	Occasional
III	41 – 60	Normal	Partially stable	Some joints or many wedges	Systematic
IV	21 – 40	Bad	Unstable	Planner or big wedges	Importance/ Corrective
V	0 – 20	Very bad	Completely unstable	Big planner or soil like	Re-excavation

A total of 10 sites have been selected covering the transportation route for slope mass rating assessment and the results and the rock types are described in Table (6).

Table 6 Slope mass rating measuring data in the field

Site No.	RMR	F1	F2	F3	F4	SMR	SMR Class	Stability
1	56	0.85	1	5	-6	56.85	III	Partially stable
2	44	0.85	1	5	-6	44.85	III	Partially stable
3	36	0.15	1	5	-25	17.15	V	Completely unstable
4	47	0.85	1	5	-6	47.85	III	Partially stable
5	33	0.15	1	5	-25	14.15	V	Completely unstable
6	44	0.85	1	5	-25	25.85	IV	Unstable
7	58	0.85	1	5	-25	39.85	IV	Unstable
8	33	0.15	1	5	-25	14.15	V	Completely unstable
9	56	0.85	1	5	-25	37.85	IV	Unstable
10	29	0.15	1	5	-25	10.15	V	Completely unstable

The SMR values of the 10 sites ranges from Class III to Class V. The SMR Class IV and Class V sites hold significant threat to the commuters as well as the road infrastructure.

Sites 3, 5, 8 and 10 are assessed as completely unstable (Class V) and these sites are the most dangerous for slope stabilization as SMR assessment. Sites 6, 7 and 9 are identified as unstable (Class IV) according to slope mass rating. From field observation, the Class IV sites involve smaller rock fragments having larger volume than the SMR Class III Sites. The last sites 1, 2 and 3 are assessed as partially stable (Class III) and these sites are possible joint related failures.

Kinematic Analysis

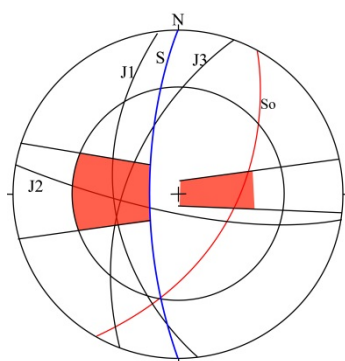
The conventional kinematic analyses for sliding along discontinuities involve constructing the great circles of joints, slope surface, faults, bedding plane, etc. and interpreting the location of intersections. In the kinematic analysis, the relationship between individual great circle and slope inclination is important to assess the slope stability. According to the stereographic projection study, primary and secondary critical possible failure zones can be identified on the stereograph. If the primary critical possible failure zone is in front of the slope face where the cutting by discontinuities planes is inclined less than the slope face, then wedge and plane failures are possible. If the primary critical possible failure zone is in the back side of the slope face, there can be a possible toppling failure. Besides, the side of the primary critical possible failure zone of the slope face is described as the secondary critical possible failure zone.

According to kinematic analyses, Goodman (1998), and Jeongi and Kulatilake (2001), the following determinations have been made based on the relationship of discontinuities, slope faces and friction angle (ϕ) obtained from RMR values by using the stereographic projection as shown in Table (7) and Figure (24).

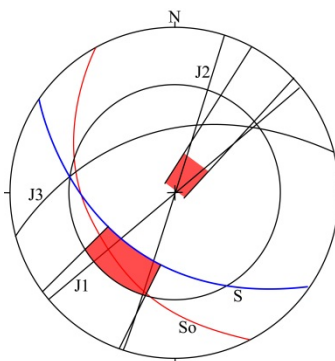
Table 7 Parameters and Results of kinematic analysis of the study area

Site	Site slopes parameters			Discontinuity/ bedding plane or intersection	Mode of Failure	Failure category
	Slope angle	Slope Direction	Frictional angle (ϕ)			
1	70	270	35	So,J1,J2,J3	P,W	Potential
2	46	215	35	So,J1,J2	P,W,T	Potential
3	50	275	25	J3	P	Potential
4	63	220	35	So,J1,J2	P	Potential
5	60	65	25	B,J1,J3	P, T	Potential
6	65	50	35	J1,J2	P	Potential
7	65	50	35	J1,J2	P	Potential
8	70	20	25	B,J1,J2,J3	W,T	Potential
9	69	255	35	J1,J2	W,P	Potential
10	75	265	35	So, J2,J3	W,P	Potential

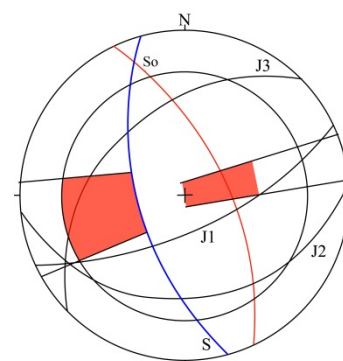
Where W=Wedge Failure, P = Plane Failure, T = Toppling Failure, S_0 = Bedding planes, S= Slope face, J = Joint plane, F = Fault plane



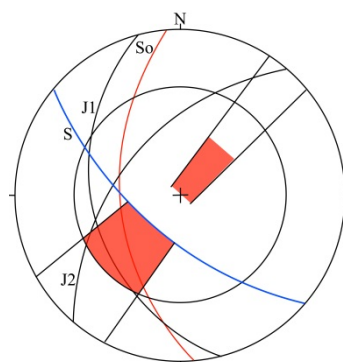
Site (1)



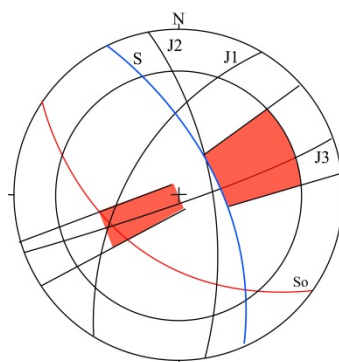
Site (2)



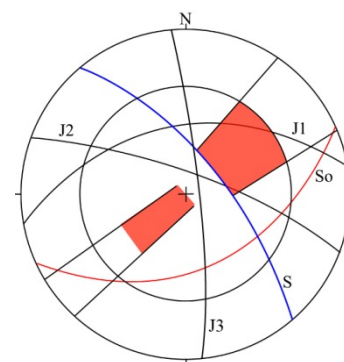
Site (3)



Site (4)



Site (5)



Site (6)

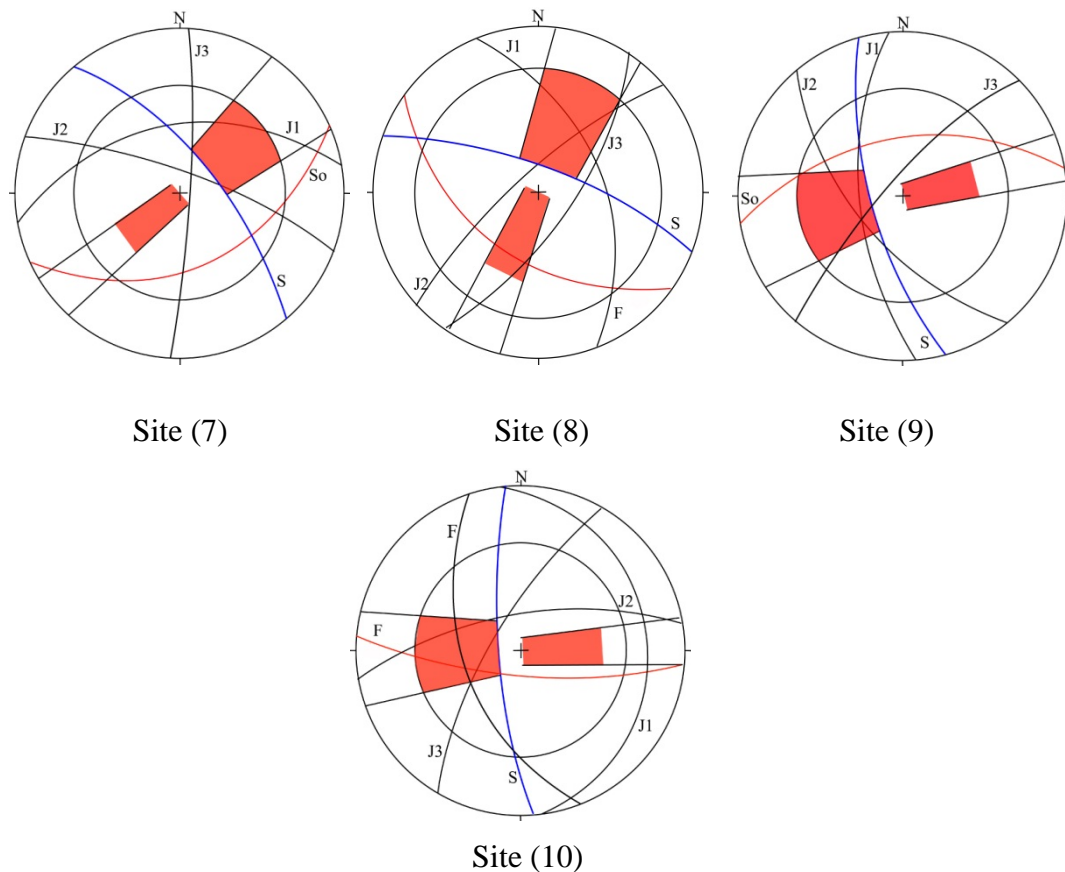


Figure 24 Kinematic analysis of sites (1) to (10) on the relationship of the discontinuities and slope face parameters

Accordingly, most of the slopes possibly have failures and the most prominent failures are wedge failure and planar failure, but some places can have toppling failure. Besides, all these slopes are lack systematic retaining structures and drainpipe.

Conclusions and Recommendations

The present study area is situated along the Car-road, at the base of the Zweekabin Hill near Khalauknos village, Hpa-an Township, Kayin State. This area is mainly composed of carbonate sedimentary rocks especially Moulmein Limestone (Middle to Late Permian) and Alluvium (Quaternary) covered in the study area.

The research area is mainly characterized by NNW-SSE trending stratigraphic units in eastern part and NW-SE trending in central and western part. Besides, the major longitudinal faults with north-south in direction occurred at the eastern and western flank of the Zweekabin Range.

There are many types of landslide along the car-road such as rockfall, debris flow and creep. The big landslide is found on 15th July, 2018 because of the significant rainfall effect which is one of the debris flows.

Moreover, Slope 3, 5, 8 and 10 are highly jointed and highly weathered rocks that composed of poor rocks as rock mass rating. Moreover, the SMR values of the 10 sites have from

Class III to Class V. Sites 3, 5, 8 and 10 are assessed as completely unstable (Class V) and Sites 6, 7 and 9 are identified as unstable (Class IV). These sites are very dangerous to use for transportation. According to the kinematic analysis, most of the slopes possibly have failures and the most prominent failures are wedge failure and planar failure. Besides, the strength and joint condition of rock mass as well as slope condition are also influenced in forming landslide along the road.

It can be recommended that to prevent the slope failures, these slopes should be reduced the slope inclination depends on the orientation and density of discontinuities, planes and mode of failures with systematic retaining structures and drainage pipe. Remedial and mitigation measures seem to be inadequate during the construction of this road. Additional risk assessment study is recommended for prioritizing the necessary mitigation measures and safety of the travellers.

Acknowledgements

Authors wishing to Ko Aung Soe Moe, geologist, geology department, Hpa-an University for his technical support to take the 4k resolution images with drone throughout the preparation of this research are to great extent, acknowledged.

References

- Aung Kyaw Myat and Aung May Than, (2018). Study on Speleothems at the Ba-yint-nyi Cave and Ye-thae-pyan Cave in the Hpa-an Township, Kayin State, Myanmar, *Hpa-an University Research Journal*, Vol.9, No.1, p 154-166.
- Bieniawski, Z.T., (1989). *Engineering Rock Mass Classifications*. John Wiley and Sons, New York, 251pp.
- Goodman, (1998). *Introduction to Rock Mechanics 2nd ed.*, University of California at Berkeley. John Wiley and Sons, Inc., 651pp.
- Jeongi-gi Um and Kulatilake, P. H. S. W. (2001). Kinematic and Block Theory Analysis for Shiplock Slope of the Three Gorges Dam Site in China. *Geotechnical and Geological Engineering*, 19: p. 21-42.
- Palmström A (1982): The volumetric joint count - a useful and simple measure of the degree of jointing. Proc. int. congr. *IAEG, New Delhi*, V.221 - V.228, 198pp.
- Romana, M., (1993). *A geomechanical classification for slopes: Slope Mass Rating*. In: J.A., Hudson (Ed.), *Comprehensive Rock Engineering*. Pergamon Press, London, p 3 – 45.
- Varnes, D.J., (1978). *Slope Movement Types and Processes*. In: Schuster, R. L., and Krizek, R.J., eds., *Landslides, analysis and control*. Transportation Research Board, Nat Acad. Sciences, Spec., Rept., No. 176, p 13-33.

ESTIMATION OF GROUND SETTLEMENT BY EARTHQUAKE INDUCED LIQUEFACTION IN DOWNTOWN AREA, YANGON

Khin Soe Moe¹, Tun Naing², Ma Wai³

Abstract

As Yangon has undergone rapid development and expansion, it is needed to construct various new structures. Most of new constructions are on the alluvial deposit. Alluvial deposits are saturated loose sediments and thus, liquefaction is very liable to occur in Yangon area. For that reason, the estimation of ground settlement by earthquake induced liquefaction is needed to carry out. Liquefaction induced ground settlement is estimated at 120 representative sites in downtown based on the Standard Penetration Test and the laboratory results by semi-empirical method. The aim of this research is to provide potential ground settlement information at different locations of site at various depths for earthquakes magnitudes M_w 7.0 with peak ground acceleration of 0.2 g. It also helps in urban planning, prevention of earthquake hazard and determining the suitable foundation types and designs. The study area includes Latha, Pebedan, Kyauktada, and Botahtaung Townships. According to this research, the liquefaction induced ground settlement in the study area is ranging from 6 cm to 56 cm. The estimated ground settlement reveals that light damage may occur in the Ward (2) of Botahtaung Township, General Administrative Department in Kyauktada Township and Ward No. (8) of Botahtaung Township since they have settlement of 6 cm to 10 cm. So, minor cracks may occur when an earthquake of M_w 7.0 strikes. Most of the downtown area can occur medium settlement of 10 cm to 30 cm. Extensive damage may be along the Strand Road, lower part of Thein Phyu Road and Bo Aung Kyaw Roads where it may be the settlement of 30 cm to 56 cm. Therefore, adequate geotechnical site investigation should be done before construction and suitable earthquake resistant design and ground improvements should be applied for all constructions in the areas with high damage potential.

Keywords: alluvial deposits; liquefaction, settlement, Standard Penetration Test, saturated loose sediment

Introduction

Soil liquefaction describes a phenomenon whereby a saturated or partially saturated soil substantially loses strength and stiffness in response to an applied stress, usually earthquake shaking or other sudden change in stress condition, causing it to behave like a liquid. Typical effects of liquefaction are loss of bearing strength, lateral spreading, sand boil, flow failure, ground oscillation, flotation and settlement. Ground settlements due to soil liquefaction have been one of the major causes for infrastructure damages during an earthquake. It is challenging to predict liquefaction because natural variability of the ground is usually not well understood and the soil behavior is complex and difficult to access.

Yangon is located at the confluence of the Yangon and Bago rivers about 30 km away from the Gulf of Martaban. It is located between Latitude 16.8661° N and Longitude 96.1951° E, which refers to the map index 94 D/1. Research area includes Latha Township, Pebedan Township, Kyauktada Township, and Botahtaung Township and location map of research area is shown in Fig (1).

¹ Lecturer, Department of Engineering Geology, Yangon Technological University

² Dr, Professor and Head, Department of Engineering Geology, Yangon Technological University

³ Assistant Lecturer, Department of Petroleum Engineering, Technological University (Mandalay)

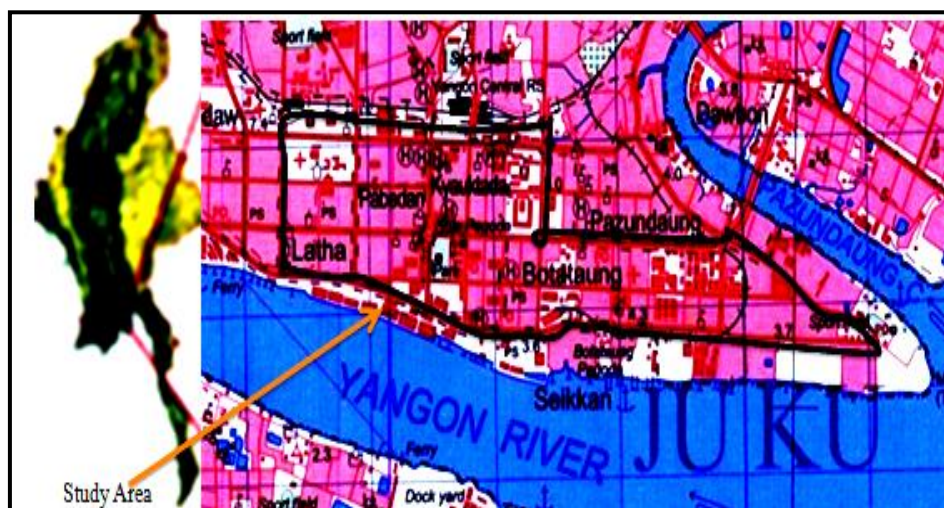


Figure 1 Location map of research area

Method of study

Based on the methodologies for analysis of liquefaction-induced ground deformations, semi-empirical approach is used. Semi-empirical approaches follow a 3-phase methodology, as shown in Fig (2). The first step is typically a liquefaction triggering analysis in which the subsurface layers that are expected to liquefy as a result of scenario ground shaking are identified. The following step is to estimate the shear strain and reconsolidation volumetric strain in these liquefied sub-layers. Finally the ground lateral displacement and settlement are calculated on the basis of the estimated strain components. Representative semi-empirical approaches include the Tokimatsu and Seed (1984), Ishihara and Yoshimine (1992), and Shamoto et al.(1998).

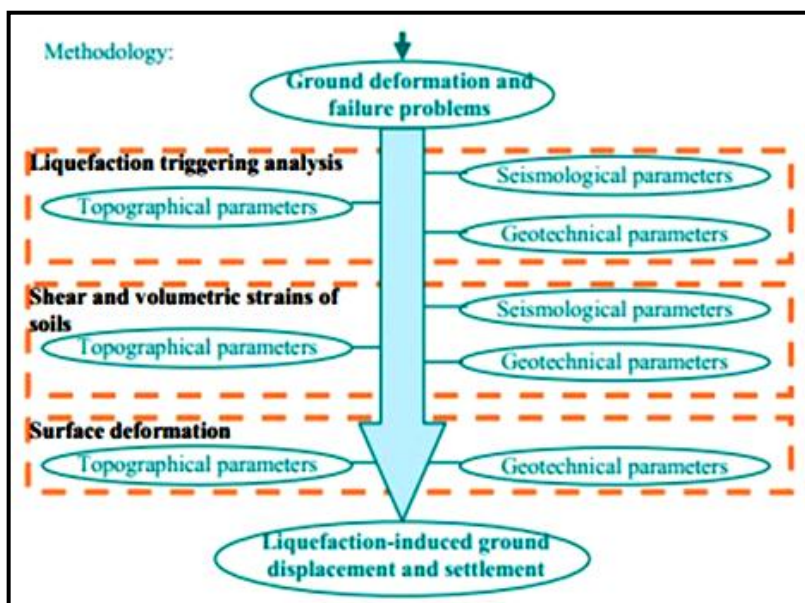


Figure 2 Components of semi-empirical based method

For this research, ground settlement by earthquake induced liquefaction is estimated at (120) representative sites in downtown area by using the borehole records and their standard penetration test results. Based on the SPT value and the laboratory results, estimation of liquefaction induced settlements are carried out by semi-empirical method. Groundwater level is

noted on each bore holes. Liquefaction induced ground settlement at different soil profiles are estimated by using earthquakes moment magnitudes M_w 7.0 with peak ground acceleration 0.2 g. The suitable foundation type and ground improvement method can be chosen by estimating the liquefaction induced ground deformation. The locations of analysed sites in downtown area are shown in Fig (3). The number of projects for analysis of liquefaction induced ground settlement is shown in Table (1).

Table 1 Number of projects for liquefaction induced settlement analysis

No	Township	Number of Projects
1	Latha	13
2	Pebedan	33
3	Kyauktada	31
4	Botahtaung	43
Total		120



Figure 3 Location of project in research area

Topography and regional geology

The topography of the Yangon area can be divided into hilly area, ridge areas, terraces, low lying flat plain, and tidal flat and channel. The research area is situated on the low lying flat plain. In Yangon, three geological rock units such as alluvial deposits, Irrawaddy Formation and Pegu Group can be found. The alluvial deposit is divided into recent alluvium and valley filled deposit. Irrawaddy Formation consists of Danyingon Clay and Arzarnigon Sandrocks. Pegu Group includes Bewsapet Alternations, Thadugan Sandstone and Hlawga Shale. Recent alluvium consists essentially of yellowish grey, bluish grey, brownish grey silt, sand and clays. Most of downtown areas are located on the recent alluvium. Most of the alluvial deposits are saturated loose sediments. Geological map of the Greater Yangon area is shown in Fig (4).

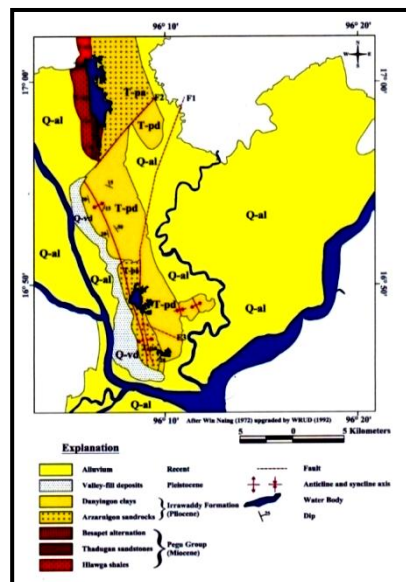


Figure 4 Geological map of the greater Yangon area

Theoretical background

Liquefaction-induced ground settlement is of great engineering significance. There are many mechanisms that can vertical result in liquefaction-induced ground settlements, as shown in Fig (5). Most of these involve settlements as a result of deviatoric ground deformation, but Fig (5) illustrates purely volumetric reconsolidation settlement in level or near level ground. This mechanism of liquefaction-induced settlement is mainly attributed to the densification of sandy and/or silty deposits resulting from the dissipation of excess pore water pressures.

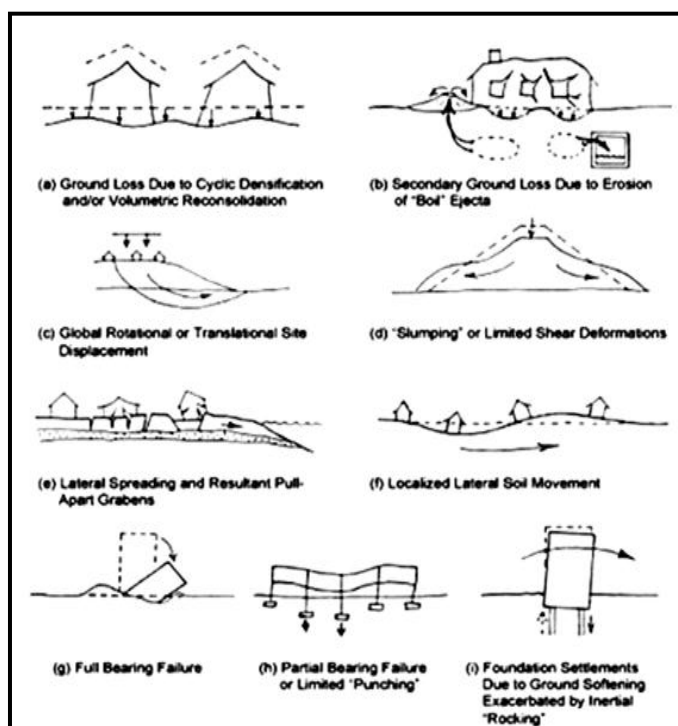


Figure 5 Illustration of liquefaction induced ground settlement mechanisms

Procedure for estimating liquefaction induced ground settlement

Required parameters

The required parameters for the estimating liquefaction induced ground settlement are shown in Table (2).

Table 2 Required parameters

Factor	Parameter
Seismic excitation	M_w , PGA
Topography	Level of gentle sloping ground ($\alpha \sim 0$)
Subsurface condition	SPT N values, Fines content (FC), groundwater level, soil densities, thickness of layer

Determination of corrected SPT N value

Based on SPT Blow count, N_{60} is first normalized for overburden stress at the depth of the test and corrected to a standardized value of $(N_1)_{60}$. To calculate $(N_1)_{60}$, the following equations are used.

$$(N_{60}) = C_E \cdot C_B \cdot C_S \cdot C_R \cdot N \quad (1)$$

$$(N_1)_{60} = C_N \cdot (N_{60}) \quad (2)$$

Where, $(N_1)_{60}$ = Corrected SPT Values

C_E = Hammer Efficiency

C_B = Borehole Diameter Correction

C_R = Rod Length Correction

C_S = Sample Correction

N = Measured SPT N value

C_N = Corrected Factor for Overburden Pressure = $(100 / \sigma'_{v_0})^{0.5}$

Correction for the fine content and soil plasticity is done from $(N_1)_{60}$ value by using Seed and Idriss, (1982) equation.

$$(N_1)_{60,cs} = \alpha + \beta (N_1)_{60} \quad (3)$$

Where, $\alpha = 0$; $\beta = 1$ for $FC \leq 5$

$$\alpha = \exp[1.76 (190/FC^2)] \quad \text{for } 5\% < FC < 35\%$$

$$\beta = [0.99 + (FC^{1.5}/100)]$$

$$\alpha = 5; \quad \beta = 1.2 \quad \text{for } FC \geq 35\%$$

Determination of cyclic stress ratio (CSR)

According to the Seed and Idriss (1972), the cyclic stress ratio for magnitude $M_w = 7.0$ earthquake is calculated by using the following equation.

$$CSR = 0.65 r_d (\sigma_{v0} / \sigma'_{v0}) (\alpha_{max} / g) \quad (4)$$

where, CSR	=	Cyclic Stress Ratio
α_{\max}	=	Peak horizontal ground acceleration (ft/s^2 or m/s^2)
g	=	Acceleration due to gravity
σ_{vo}	=	Total vertical Stress (lb/ft^2 or kPa)
σ'_{vo}	=	Vertical Effective Stress (lb/ft^2 or kPa)
r_d	=	Stress Reduction with Depth = $1 - (0.012 z)$
z	=	Depth from Ground Surface

Determination of reconsolidation volumetric strain ($\epsilon_v\%$)

Reconsolidation volumetric strain (ϵ_v) is determined by the following chart.

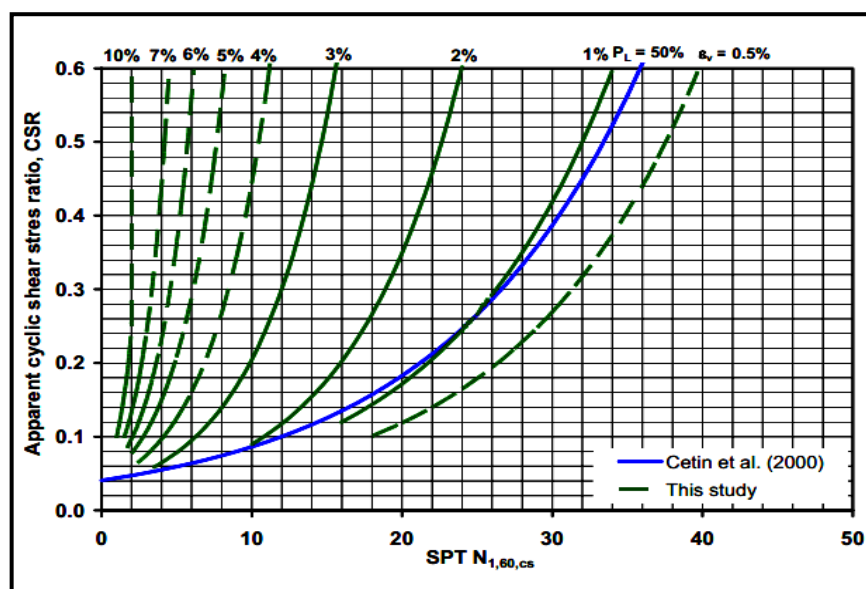


Figure 6 Correlations between CSR, $(N_1)_{60,cs}$ and reconsolidation volumetric strain

Determination of liquefaction induced ground settlement

By using the value of reconsolidation volumetric strain, liquefaction induced ground settlement can be determined. In the evaluation of settlement, computation of field observation is made by Ohsaki (1970) method. In this method, the highest volumetric strain is 10% and it will cause the settlement of 4 in (10.16cm). Depending on this standard, the settlement of individual soil layer can be calculated. The total estimated ground settlement for individual borehole is estimated by adding the settlement of individual soil layers. According to the ground settlement, there is no destruction area where the settlement is 10 cm or less and medium damage area where the settlement are roughly between 10 cm to 20 cm. If the settlement becomes greater than 30 cm, there always occurs considerable destruction on ground surface such as sand spurting, causing fissures and large offsets. The qualitative correspondence between the damage extent and settlements is summarized as shown in Table(3).

Table 3 Relation between damage extent and approximate settlements

Extent of damage	Settlement (cm)	Phenomenon on the ground surface
Light to no damage	0 ~ 10	Minor cracks
Medium damage	10 ~ 30	Small cracks, oozing of sand
Extensive damage	30 ~ 70	Large cracks, spouting of sands, large offsets, lateral movement

Result and Discussion

According to the above procedures (120) representative borehole sites have been performed for ground settlement by earthquake induced liquefaction analysis. The study area is totally covered by alluvial deposits of loosely cemented soil. The most common soil types in these areas are SW, SM, and SC soil types according to the Unified Soil Classification System. The blow count of Standard Penetration Test varies from 2 to 49 within 20 m depth. CL and ML soil type occasionally occurs in some part of downtown area. Groundwater level is high and the soils in these areas are saturated. Moreover, very loose and fine to coarse sand occurs in some part of the downtown area. The extensive damage can occur in these areas. The features of settlement depend on the soil profile and nature of soils composing the deposits. Fig (7) shows the geotechnical properties of borehole at 21st Street, Latha Township. Fig (8) shows subsurface condition of soil at Trader Square, Pebedan Township. Fig (9) shows the geotechnical properties of borehole at proposed Fly Over Project, Kyauktada Township. Fig (10) shows subsurface condition of soil at 48th Street, (10) Ward, Botahtaung Township.

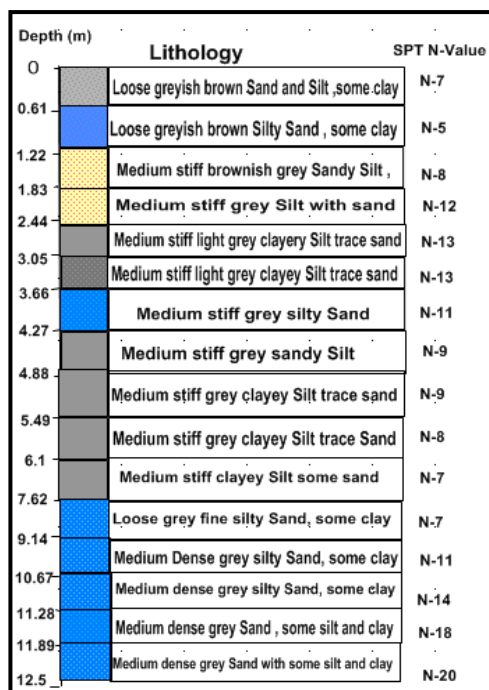


Figure 7 Subsurface soil profile of a site at 21st Street, Latha Township

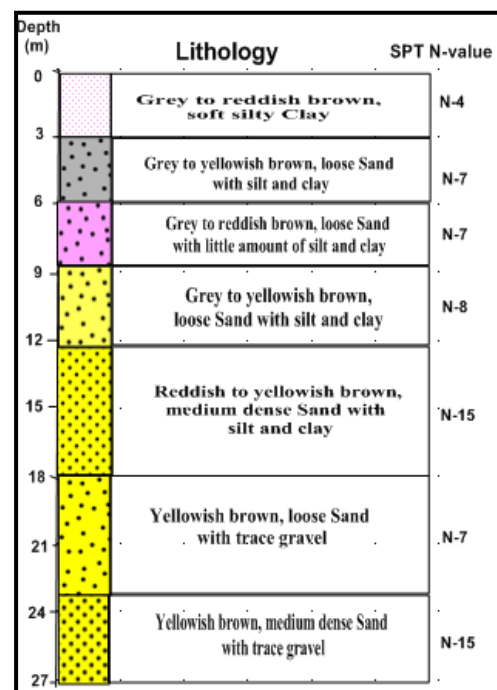


Figure 8 Subsurface soil profile of a site at Trader Square, Pebedan Township

Table 7 Example calculation of liquefaction induced ground settlement in Mya Nanda St. Botahtaung Township

Depth m	γ_{sat} kN/m ³	Soil Type (USCS)	σ' kPa	r_d	CSR	N	$N_{1(60)}$	$N_{1(60)cs}$	$\epsilon_v(\%)$	Settlement	
										(in)	(cm)
1.5	17.5	SM	26.25	0.98	0.13	4	5.90	12.08	2.1	0.84	2.13
3	17.5	SM	52.50	0.96	0.13	3	3.13	8.76	2.8	1.12	2.84
4.5	18.34	SM	77.63	0.95	0.13	3	2.57	8.09	2.9	1.16	2.95
6	18.34	SM	90.42	0.93	0.15	4	3.18	8.82	2.8	1.12	2.84
7.5	20.37	SM	118.44	0.91	0.15	4	2.78	5.96	3.9	1.56	3.96
9	20.37	SM	134.28	0.89	0.16	17	11.09	14.77	1.8	0.72	1.83
10.5	20.37	SM	150.12	0.87	0.16	11	6.79	10.20	2.8	1.12	2.84
12	20.37	SW	165.96	0.86	0.16	27	15.84	19.81	0.8	0.32	0.81
13.5	20.37	SW	181.80	0.84	0.16	20	11.21	14.90	1.8	0.72	1.83
15	20.37	SM	197.64	0.82	0.16	13	6.99	10.42	2.8	1.12	2.84
16.5	20.37	SM	213.48	0.80	0.16	17	8.80	13.50	2	0.80	2.03
18	21.36	SW	247.14	0.78	0.16	25	12.02	17.52	1.8	0.72	1.83
19.5	21.36	SW	264.47	0.77	0.16	16	7.44	12.44	2.3	0.92	2.34
20	21.36	SW	270.24	0.76	0.16	18	8.28	14.19	2	0.80	2.03
Total Settlement										13.04	33.12

Zonal distribution of liquefaction induced ground settlement

Zonal distribution of liquefaction induced ground settlement is presented in the form of contour, based on the ground settlement values by using Surfer software. It shows the level of severity of settlement when the earthquake with the magnitude of $M_w = 7.0$ occurs. Fig (11) shows zonal distribution of liquefaction induced ground settlement.

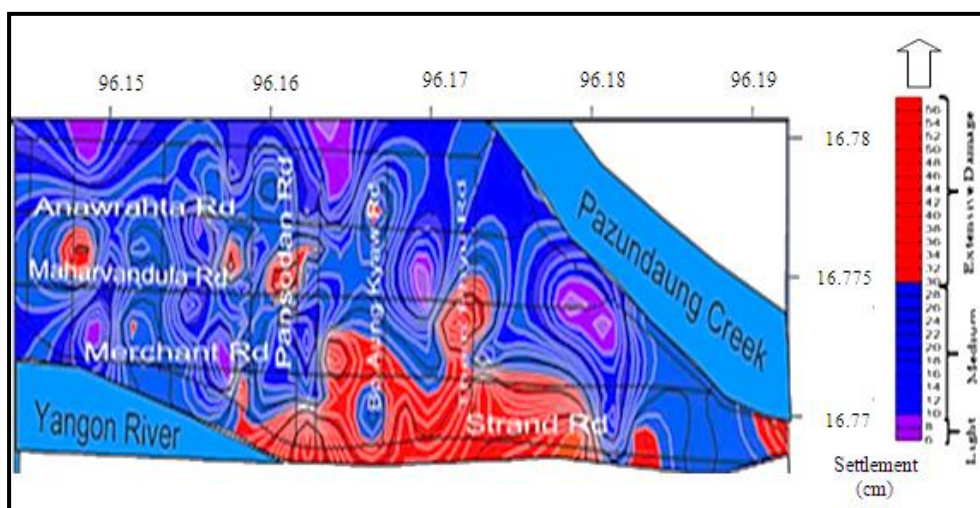


Figure 11 Zonal distribution of liquefaction induced ground settlement when $M_w = 7.0$ earthquake occur

The zonal distribution of estimated ground settlement reveals that light damage may occur in the Ward (2) of Botahtaung Township, General Administrative Department in Kyauktada Township and Ward No.(8) of Botahtaung Township since they have settlement of 6 cm to 10 cm. So, minor cracks may occur due to ground settlement in these areas when an earthquake of $M_w 7.0$ strikes. As shown in Fig (11), most of the downtown area can occur medium settlement since the ground settlement range from 10 cm to 30 cm. Small cracks, oozing

of sand can occur in these area. Extensive damage may be along the Strand Road, lower part of Thein Phyu Road and Bo Aung Kyaw Roads where the ground settlement may be 30 cm to 56 cm. Moreover, some part of Latha, Pebedan and Kyauktada may occur extensive damage. Spouting of sand, large offset and lateral movement of ground will occur in these places when earthquake of M_w 7.0 occur. Therefore, adequate geotechnical investigation and elaborate tests should be carried out and suitable ground improvement methods should be done for multi-storied buildings. It is hoped that the data and results presented herein will contribute to the further development and calibration of increasingly accurate and reliable methods for assessing hazard due to triggering of liquefaction and consequent liquefaction induced ground deformations and displacements.

Acknowledgements

The author is thankful to U Sann Lwin, Rtd Director, Head of Engineering Geology Office (1), for his enthusiasm in sharing knowledge and expertise. I would like to express my heartfelt thanks to Daw Theingi Oo (Suntac Technologies) and Daw Moe Thida (East Yangon University) for their help in collection of borehole data. The author's deepest thanks are due to all persons for their excellent encouragements and supporting in carrying out this research.

References

- Das, B.M. (2007), *Principle of Foundation Engineering*. 6th ed. USA: Nelson, a division of Thomson Canada Limited Press.
- Google Earth. Google Map of the Study Area (2013). < [http:// www.google earth .com](http://www.googleearth.com)>
- Kenji Tokimatsu, A.M.ASCE, and H.Bolton Seed, Hon. M. ASCE. (1986) "Evaluation of Settlements in Sand Due to Earthquakes Shaking". *Journal of Geotechnical Engineering*, Vol.113. No.8, pp.861 - 878.
- Kenji Ishihara and Mitsutoshi Yoshimine (1992) "Evaluation of Settlements in Sand Deposits Following Liquefaction During Earthquakes". *Journal of Soils and Foundation*, Japan, Vol.32. No.1, pp.173-188.
- Maung Thin. (1995). "Some Urban Geological Aspects of Yangon Area," Country Paper: Professor and Head of Geology, University of Yangon.
- Seed, R. B., K. O. Cetin, R. E. S. Moss, A.M.Kammerer, J.Wu, J.M.Pestana and M.F. Riemer (2001) "Recent Advances in Soil Liquefaction Engineering and Seismic Site Response Evaluation". International Conference and Symposium on Recent Advances in Geotechnical Earthquake Engineering and Soil Dynamics. paper SPL-2, San Diego.
- Seed, H.B and Idriss, I.M. (1971) "Simplified Procedure for Evaluating Soil Liquefaction Potential". *Journal for soil mechanics and foundation engineering*, Vol.97.No.9, pp 1249-1274.
- Win Naing (1972) *Hydrogeology of Greater Yangon*. M.Sc Thesis Geology Department, University of Yangon (Unpublished)
- Wu, Jiaer and Seed, Raymond B (2004) "Estimation of Liquefaction Induced Ground Settlement (Case Studies)". Proceedings of Fifth International Conference on Case Histories in Geotechnical Engineering. 6. New York.
- YCDC (Yangon City Development Committee) (2015) < [http:// www.ycdc .gov](http://www.ycdc.gov) .com>

ANALYSIS OF NATURAL ENVIRONMENTAL CHANGES USING REMOTE SENSING AND GEOGRAPHIC INFORMATION SYSTEM (GIS): CASE AREA OF MOEYUNGYI WETLAND WILDLIFE SANCTUARY AND ITS ENVIRONMENT, BAGO REGION IN MYANMAR

Thant Sin¹, Aye Aye Aung²

Abstract

Moeyungyi Wetland Wildlife Sanctuary is located about 6 furlong away from the Yangon-Mandalay old high way, near Pyinpongyi village, Bago and Waw Township, Bago Region. Moeyungyi Wetland WS is a man-made wetland. It was constructed in 1904 and it provides water flow into Bago-Sittaung canal. Many years later, the reservoir changed naturally into wetland, notified as a wildlife Sanctuary in 1988. The maps of the classification of the land use in wetland area are important for natural resource management. The changes of the land use in the natural wetland area have been tested by the accuracy of remote sensing and GIS techniques based on UTM map and Landsat TM satellite data (2006-2019). The maximum likelihood supervised classification technique was applied for land cover classification such as land areas including paddy field and swamp areas, water body area, natural vegetation area consist of shrubby grass. There are many environmental changes year by year. The main water body areas gradually declined during 2006-2015 but water body area sharply enlarged in 2019. Natural Vegetation gradually reduced and shrubby grass areas mainly in wetland decreased during 2006 and 2019 due to deforestation and land use changes which paddy field areas gradually increased duration of 18 years. Over all, not only the original wet land area, but also the whole surrounding area had been transformed into land area by 2019 image analysis. Therefore, the natural ecosystem of wetland can change in the future. If the ecosystem of wetland will be changed, the biodiversity of birds and other species will decrease because the ecosystem of wetland area is not suitable for their habitat.

Keyword: Natural Environmental Changes, Wetland

Introduction

Moeyungyi Wetland Wildlife Sanctuary is one of the 19 wetlands sites in Myanmar (2004, Ministry of Environment, Japan). They designated as a Wildlife Sanctuary with the objective of protecting the seasonal migratory birds and resident birds as well as for conserving the ecosystem of the wetland habitat. People have settled around the wetland as villages in many years ago. There are diverse terrestrial and aquatic animals, birds, insects and natural vegetation in and around the Moeyungyi Wetland Wildlife Sanctuary. The warm wetland habitat attracts various kinds of birds, including the migratory birds from the Arctic Region for wintering, which provides a good indicator of site significance. Moeyungyi Wetland Wildlife Sanctuary is under those flyways and it becomes a crucial sanctuary for both migratory and resident water birds.

Moeyungyi Wetland Wildlife Sanctuary comprises a floodplain and storage reservoir that is important for flood control. Originally, it was constructed in 1904 in the form of a rectangular man-made water storage reservoir by bonding, to provide water to the Bago-Sittaung canal (linking the Bago and Sittaung rivers) for transport of timber by boat. The site now functions as a source of fresh water for downstream areas where rice cultivation takes place. It floods in the

¹ Dr, Lecturer, Department of Geology, Dagon University

² Dr, Professor, Department of Geology, Dagon University

wet season from May to October and from October to March it hosts over 20,000 migratory waterbirds. The local communities use the site for fishing, grazing, duck-rearing and some paddy-growing and there is a small tourist facility to accommodate birdwatchers. Moeyungyi Ramsar site No. is 1431 (Ministry Of Environment Japan, 2004).

Location and Size

The study area including Moeyungyi Wetland WS is located in the southern part of Bago Region, the western and southwestern parts belong to Bago Township and the southern and eastern parts located in Waw Township. It lies between north latitudes $17^{\circ} 26'$ and $17^{\circ} 40'$ and between east longitudes $96^{\circ} 30'$ and $96^{\circ} 44'$. The northern boundary demarcates between the wetland and Daik-Oo Township. It lies immediately the east of Yangon-Mandalay Highway between mile-post 63 and 70. Although the wetland was 16.7 feet deep when the water level rises to the brim, it is 7 feet deep at the time of 2019, February. The frame or the width of the embankment is 8 feet. The wetland covers an area of 40 square miles or 256,000 acres see figure 1.

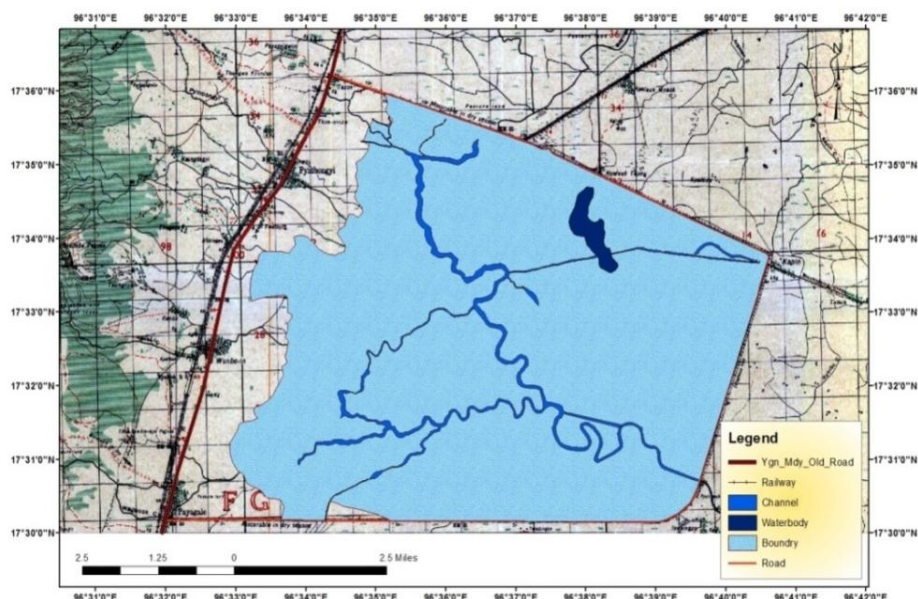


Figure 1 Location Map of Bago Region and Moeyungyi Wetland Wildlife Sanctuary

Aim and Objective

- To study and classify the natural environmental changes especially land use and land cover changes of Moeyungyi Wetland Wildlife Sanctuary and its environment by using remote sensing and GIS approach.
- To investigate and manage the land use planned for natural environment of the Natural Wildlife and its environment.

Material and Methods

Satellite Image Data

The four years of Landsat TM/ETM satellite images which were produced from U.S.Geological survey's (USGS) Earth Explorer website (www.usgs.gov) in Geo tiff file are collected. Four cloud-free Landsat ETM+ and TM data especially 2006, 2011, 2015 and 2019

are collected from USGS and the study area Moeyungyi Wetland Wildlife Sanctuary and its environment is retrieved to analyze land cover and land use changes. These satellite images consist of seven bands for landsat7 and eleven bands for landsat8. And then Universal Transverse Mercator map projection (UTM, Zone 47N) and WGS 84 datum are projected. The details of the collected Landsat satellite images are as shown in Table 1.

Table 1 Characteristics of the Lands at datasets used in the study

Acquisition Date	Sensor	Path/Row	Spatial Resolution of Reflective Bands	Number of Bands	Format
17 February 2006	Landsat 5 TM	132/48	30	7	Geo TIFF
15 February 2011	Landsat 5 TM	132/48	30	7	Geo TIFF
26 February 2015	Landsat 8 OLI	132/48	30	11	Geo TIFF
21 February 2019	Landsat 8 OLI	132/48	30	11	Geo TIFF

Methodology

The study area was studied based on satellite images during 2006 to 2019 by using remote sensing application of unsupervised classification. After that, the field survey was conducted around natural wetland area to confirm the land use and land cover, collected the field data such as the water depth in natural wetland and secondary data of migrated bird and environmental conservation condition. The prime step of this methodology was land use and land cover (LULC) characterization which was done using ENVI 5.1 and ArcGIS 10.1. Land cover maps are classified with five classes; land area including paddy field, water body area, swamp area, plant cultivation area and shrubby grass area by using supervised classification. The depth of wetland basin is measured based on two data sources, the first one is Google Earth Map 2015 and the another one is measured by using Global Positioning System (GPS) and depth sounder which is surveyed during 2019 February.

Previous Works

In 2001, a wetland survey was organized by Ministry of Environment (Japan) for studying the biodiversity and their wetland environments.

In 2012, Dr Win Swe studied geology and economic mineral of Myanmar. He also gathered and combined the valuable geological data of many geologists. And then he published as a journal of the Myanmar Geosciences Society.

In 2014, Biodiversity and Nature Conservation Association (BNCA) and Bago University carried out the biodiversity and socio-economic survey of Moeyungyi Wetland Wildlife Sanctuary.

Topographic Feature and Relief

Generally Moeyungyi Wetland Wildlife Sanctuary lies in a low, flat plain, being part of lower Sittaung valley. However, the land slopes slightly towards the west of study area to the foothill of the Bago Yoma. It is the southern continuation of Daik-U_Pyuntansar plain

characterized by deep water fields. The creeks which drain into the wetland are Sinsu-Phayarlay, U Kaung wathit, Wunbae wetland, Yetarshay and Pyinbongyi which take their sources over the mountain spurs of Bago Yoma See figures 2 and 3.

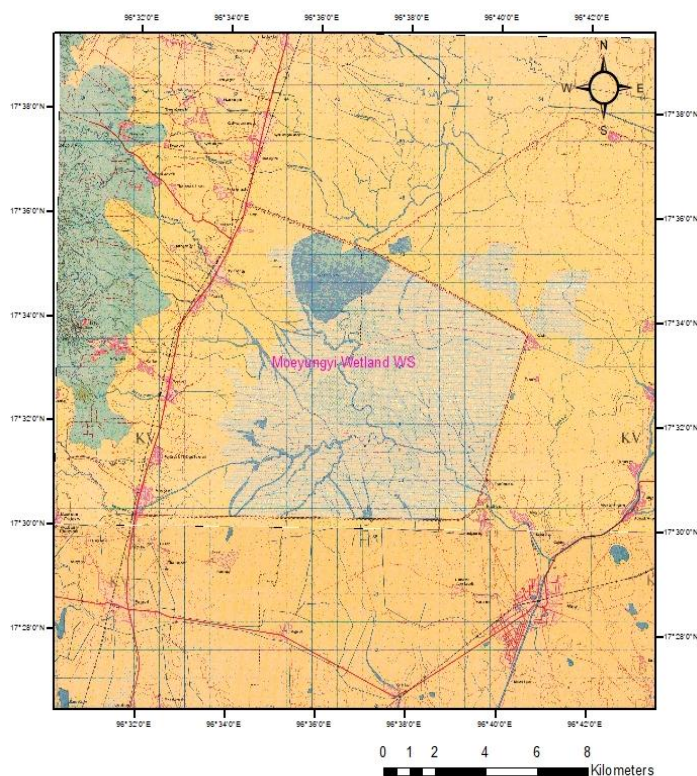


Figure 2 Topography around Moeyungyi Wetland Wildlife Sanctuary

Climate

Moeyungyi Wetland Wildlife Sanctuary falls within the tropics and temperatures fairly high throughout the years with a mean annual temperature of 26.95°C. The mean monthly temperature is highest in April with 30.5°C and lowest in January with 23.72°C. The mean monthly maximum temperature is highest in April with 38°C and the mean monthly minimum temperature is lowest in August with 29.4°C. With an annual rainfall of 3543.05 mm, the study area experiences the Tropical Monsoon climate, characterized by alternate wet and dry season. Moeyungyi Wetland Wildlife Sanctuary serves as a significant link in flying network route of Asian Winter Migratory Birds during the period from December to February. When the water level of the wetland recedes in the dry season, the local inhabitants depend more on catching fish from the wetland.

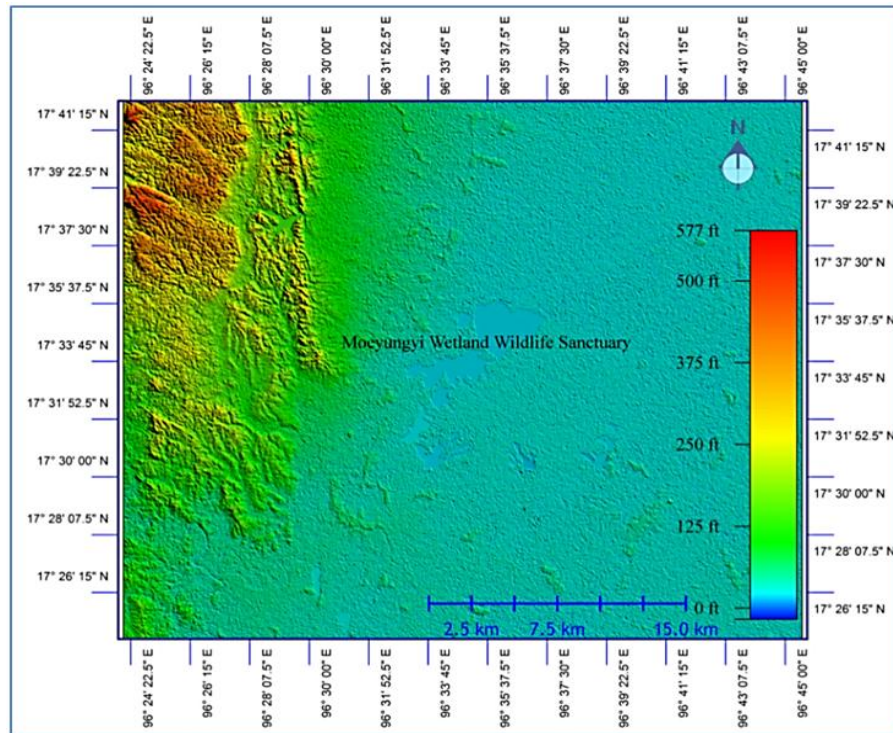


Figure 3 Differential Elevation Map of Moeyungyi Wetland Wildlife Sanctuary

Natural vegetation

The natural vegetation of the study area is more associated with the water body of the wetland, in addition to its low relief and periodical changing of monsoon climate. Therefore, in and near the wetland essentially includes hydrophytes of different species namely reeds, water-hyacinth, water-lily and raw grasses. A certain kind of grasses bear fruits richly in the winter and this is one of the reasons that the wetland can attract more birds in winter. The sacred lotus plants grow in thick groups. Reeds and other hydrophytes serve as favorable habitat for the reproduction processes of the aquatic animals. The natural vegetation of the wetland, to some extent, supports the livelihood of some local inhabitants.

Soils

The dominant soils are original that derived from alluvium and thus meadow grey soils and meadow alluvial soils cover the floor of wetland upon which a substantial amount of sediments is deposited by mountain torrents, causing serious silting. This leads to lowering the depth of the wetland, though it enriches the soil fertility.

General Geology

Bago (Pegu) Region occupies the southernmost on land segment of Central Myanmar Belt. It is bordered on the north by Magway and Mandalay Regions, on the east by Kayin and Mon States, on the south by Yangon and Ayeyarwady Regions, and on the west by Rakhine State. The geology of Bago Region is in fact interesting and is unique because the region embraces the southern segment of Western Ranges (WR), southern segment of Central Myanmar Belt (CMB) and a narrow western part of Eastern Highlands Province (EHP). Geological succession of Bago Region is composed of a mixture of some rock unit of the Western Ranges, the CMB and a few of the EHP. The study area, Moeyungyi Wetland Wildlife Sanctuary is composed mostly of flat alluvial plains.

Geospatial Analysis

In this research, the projected coordinate system is WGS_1984_UTM_Zone_47N. The satellite images were classified for natural environmental changes by using the geospatial analysis of RS and GIS. The land cover changes were studied between the years of 2006 and 2019 images see figures 4-7. The drainage basin of Moeyungyi Wetland Wildlife Sanctuary was analyzed based on differential elevation map. There are four sub-basins. The Moeyungyi Wetland Wildlife Sanctuary is situated at largest sub-basin (1). Most of the first order streams flow into the wetland and then it flows out to the Sittaung River see figure 8. The changes of basin elevation was classified by using the geospatial analysis of two data sources, the Google Earth Map 2015 and field data 2019 see figure 9 and 10. In 2019, the depth of wetland basin is shallower than 2015 because the land use and land cover is more rapid changed during four years.

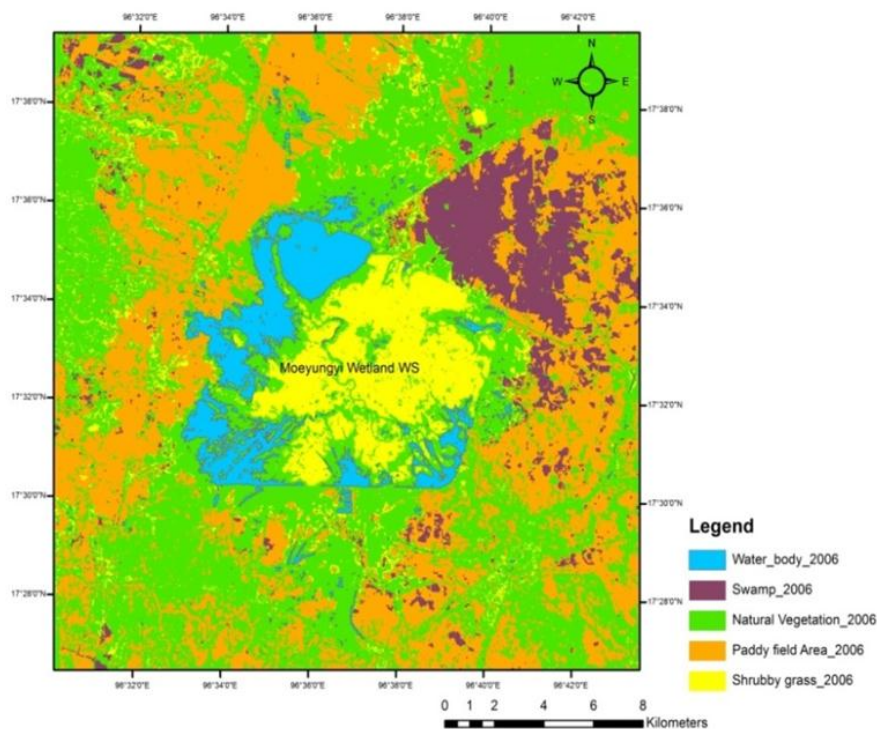


Figure 4 Land Use and Land Cover Classification Map of Moeyungyi Wetland Wildlife Sanctuary of Bago Region in Myanmar: Landsat TM Satellite Data 2006 (132_48N)

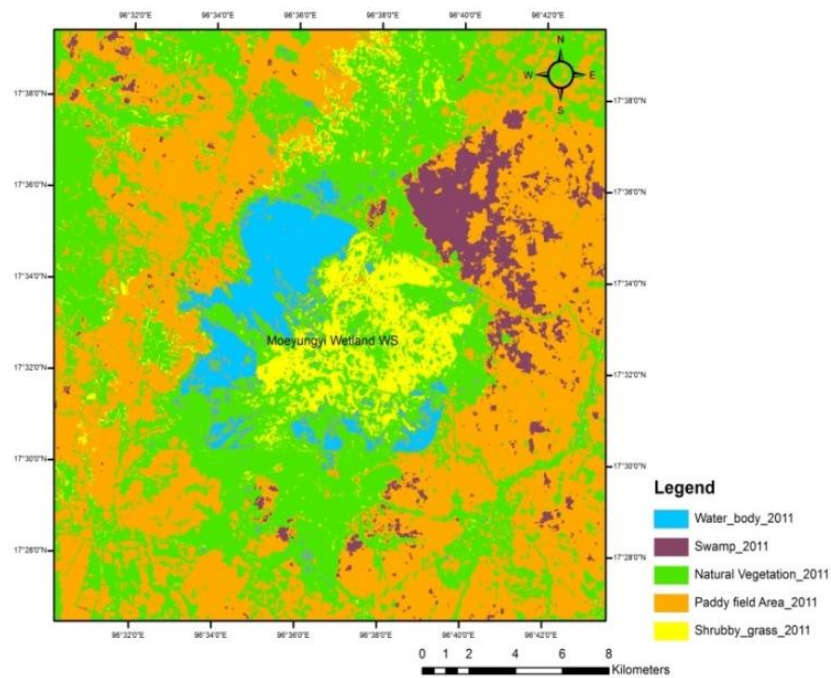


Figure 5 Land Use and Land Cover Classification Map of Moeyungyi Wetland Wildlife Sanctuary of Bago Region in Myanmar: Landsat TM Satellite Data 2011 (132_48N)

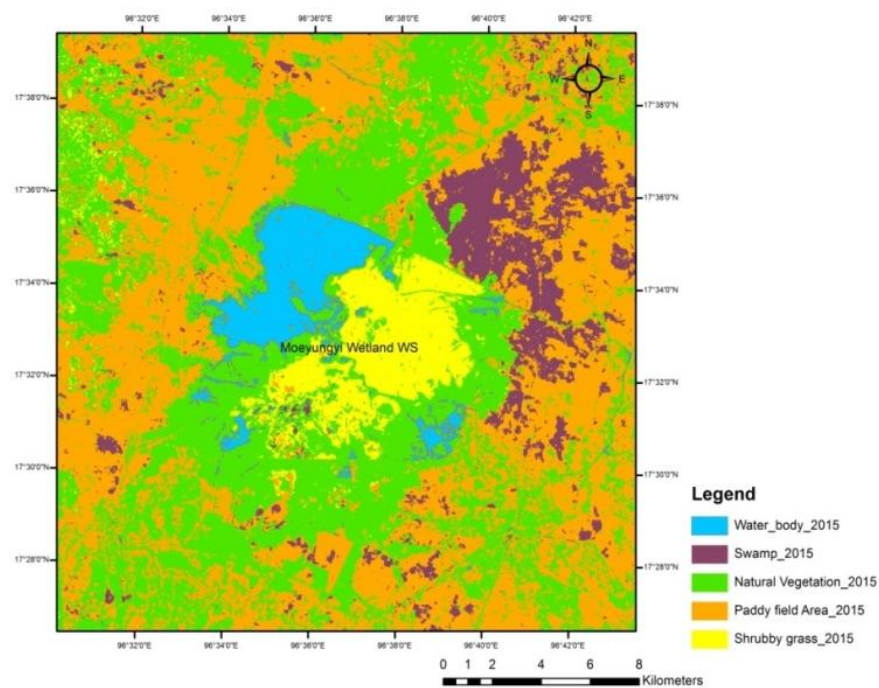


Figure 6 Land Use and Land Cover Classification Map of Moeyungyi Wetland Wildlife Sanctuary of Bago Region in Myanmar: Landsat TM Satellite Data 2015 (132_48N)

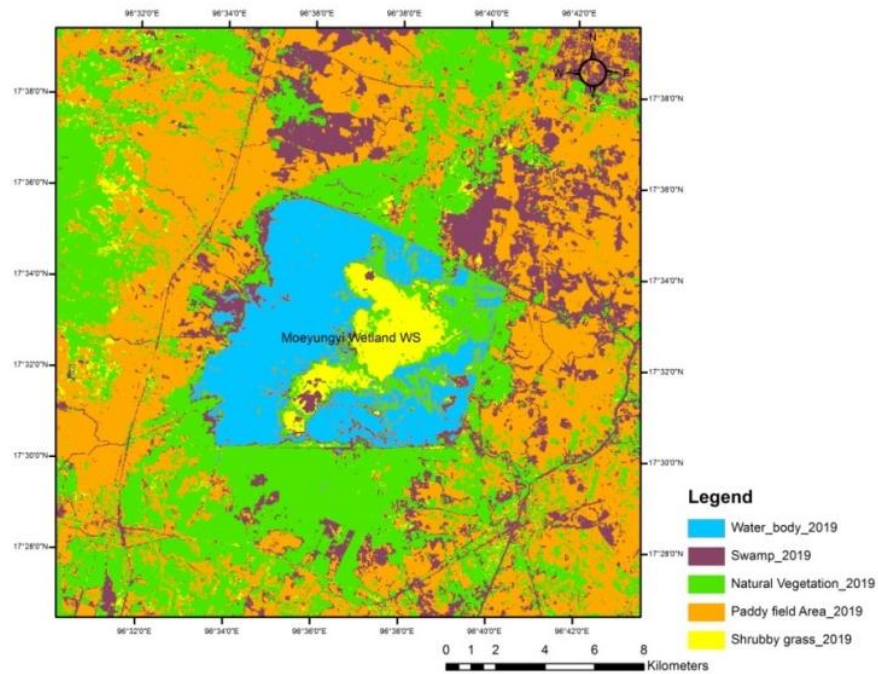


Figure 7 Land Use and Land Cover Classification Map of Moeyungyi Wetland Wildlife Sanctuary of Bago Region in Myanmar: Landsat TM Satellite Data 2019 (132_48N)

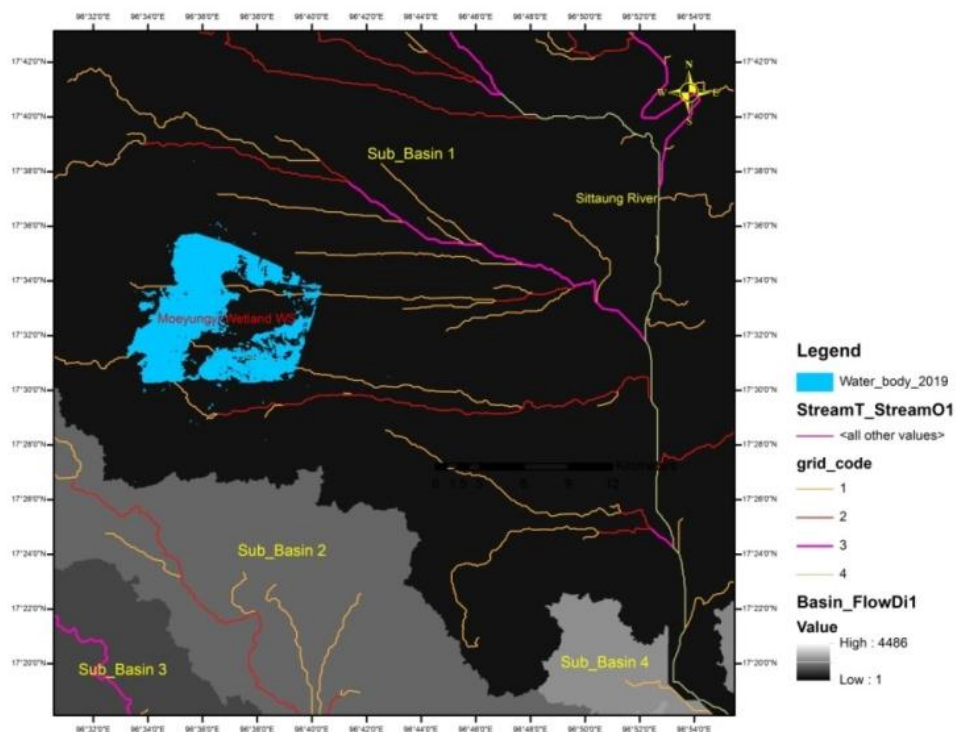


Figure 8 Drainage Basin Analysis Map of Moeyungyi Wetland Wildlife Sanctuary: Data Source from Differential Elevation Model

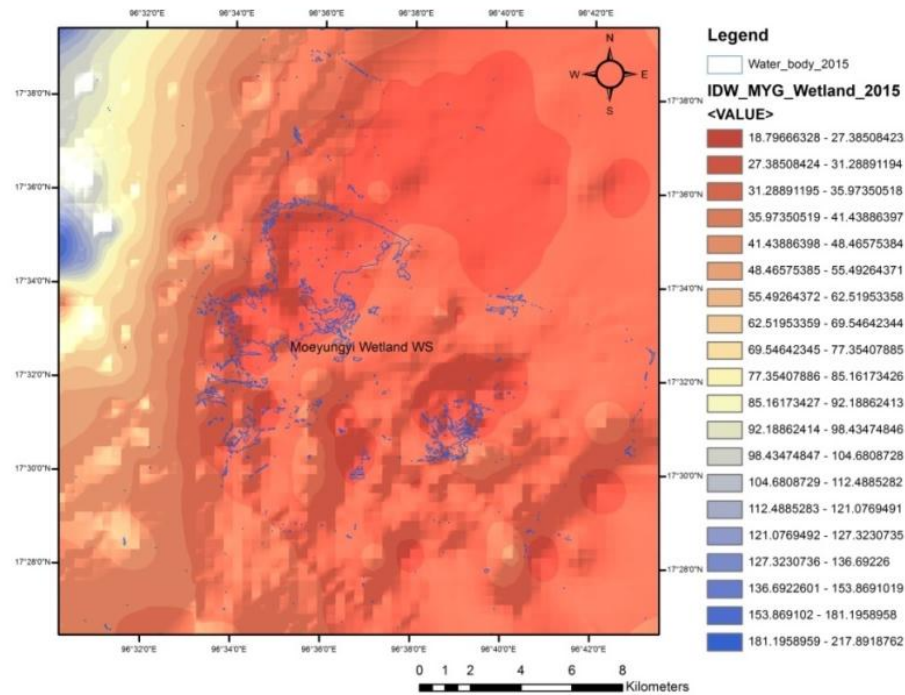


Figure 9 Drainage Basin Analysis Maps of Moeyungyi Wetland Wildlife Sanctuary: Data Source from Google Earth Map 2015

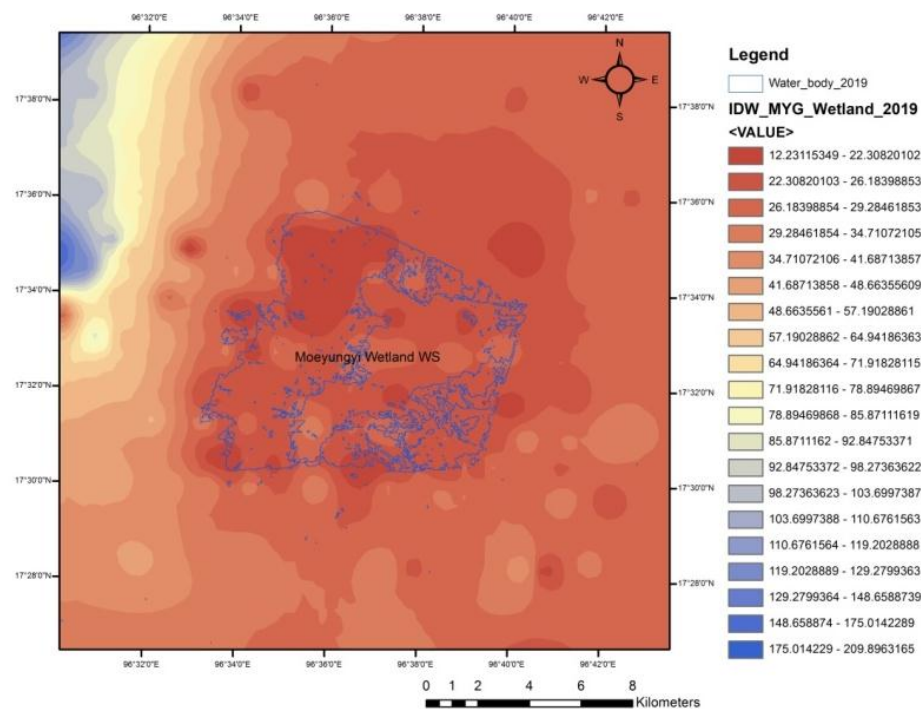


Figure 10 Drainage Basin Analysis Maps of Moeyungyi Wetland Wildlife Sanctuary: Data Source from field data 2019

Results and Discussion

The maps of the classification of the land use in wetland area are important for natural resource management. The changes of the land use in the natural wetland area have been tested by the accuracy of remote sensing and GIS techniques based on UTM map and Landsat TM satellite data (2006-2019). The maximum likelihood supervised classification technique was applied for land cover classification such as land areas including paddy field and swamp areas, water body area, natural vegetation area and shrubby grass.

There are many environmental changes year by year. The main water body areas gradually declined from 31950000m² to 25148700 during 2006-2015 but water body area sharply enlarged to 53869828.5 m² in 2019. Natural cultivation areas gradually reduced from 263204100m² to 195086088 m² and shrubby grass areas mainly in wetland decreased 56643300 m² to 24099446.6m² during 2006 and 2019 due to deforestation and land use changes which paddy field areas gradually increased from 195099300 m² to 229087395 m² duration of 18 years see figure (11).

There are four sub-basins in study area. The Moeyungyi Wetland Wildlife Sanctuary is situated at largest sub-basin (1). Most of the first order streams flow into the wetland and then it flows out to the Sittaung River.

The drainage basin of Moeyungyi Wetland Wildlife Sanctuary is gradually shallower due to the siltation during four years from 2015 to 2019. When the unconsolidated soil from the over cultivated paddy field was much deposited in the wetland, the depth of wetland basin is much shallower. Consequently, the depth of wetland basin declines, the water level gradually rises and it over flows in the wetland area.

Over all, not only the original wet land area, but also the whole surrounding area had been gradually transformed from natural vegetation area to land area by 2019 image analysis. Therefore, the natural ecosystem of wetland can change in the future. If the ecosystem of wetland will be changed, the biodiversity of birds and other species will decrease because the ecosystem of wetland area is not suitable for their habitat.

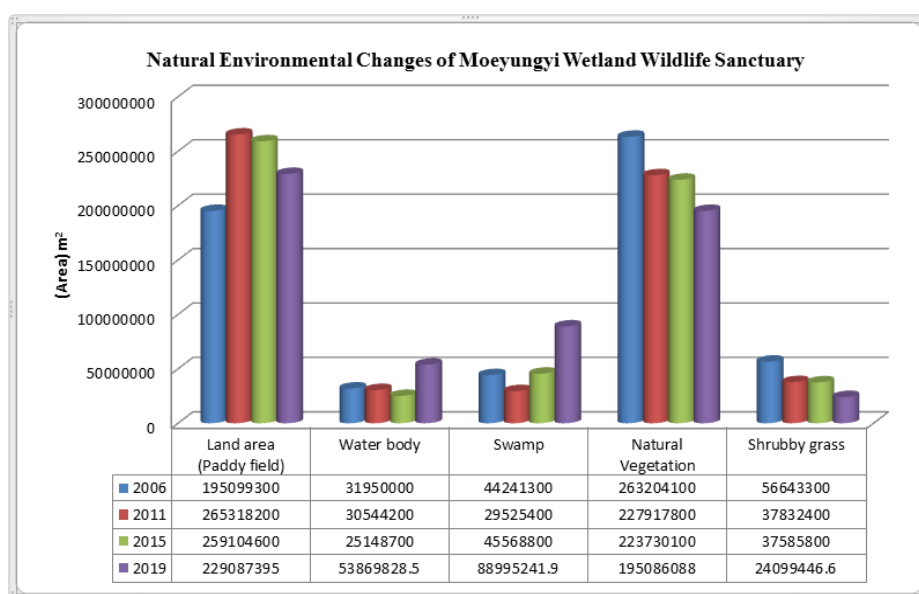


Figure 11 Geospatial analysis of natural environmental changes around the Moeyungyi Wetland Wildlife Sanctuary based on satellite image 132_48N (2006_2011_2015_2019) :land area including paddy field, water body area, swamp area, plant cultivation area and shrubby grass area

Conclusion

This assignment identified that land area including paddy field, water body area, swamp area, natural vegetation area and shrubby grass area were changing year by year with the aid of geospatial analysis. The natural environmental changes maps of Moeyungyi Wetland Wildlife Sanctuary that show the changes of land area including paddy field, water body area, swamp area, natural vegetation area and shrubby grass area are important for the natural resource management. The Remote Sensing and Geographical Informational System technologies can contribute to the land use planning and administration or resources management.

Suggestion

The land use planning is an essential tool for pollution, prevention and controlling of the natural wetland. The changes of the land use refer to the different socioeconomic activities occurring in a particular area and the behavior of the natives has the effect on the environment. The Ministry of Agriculture, Livestock and Irrigation and Ministry of Natural Resources and Environmental Conservation should manage or control the sustainable development and the management of land use in a natural wetland area and protect the water channel to support the agriculture, fishery product, ground water, weather condition, biodiversity system and operational navigable channel of the surrounding regions effectively.

Acknowledgements

I am deeply grateful to Dr Kyi Kyi Maw, Head of Geology Department, Dagon University for permission to carry out the present research paper. I am special thankful to Dr Aye Aye Aung, Professor of Geology Department, Dagon University for her advice and comment on the study work. My special thanks go to Professor Dr Lai Lai Wai, English Department of Dagon University for reading the manuscript. Finally, I wish to thank the Department of Higher Education for financial support.

References

- Win Swe, (2012), Outline Geology and Economic Mineral Occurrences of the Union of Myanmar: journal of Myanmar Geosciences Society, no.1, 97-101
- Biodiversity and Nature Conservation Association (BNCA) and Bago University, (2014), Biodiversity and socio-economic survey of Moeyungyi wetland Wildlife Sanctuary.

HYDROCHEMICAL ANALYSIS AND EVALUATION OF GROUNDWATER QUALITY IN PYAWBWE-NYAUNGYAN- PAYANGAZU AREA, THAZI AND PYAWBWE TOWNSHIPS

Win Khine Tun¹, Aye Thida Mon², Khin Myo Min³

Abstract

Pyawbwe-Nyaungyan-Payangazu area is located in the southeastern part of Dry Zone, between 20° 31' 12" to 20° 45' 54" North latitude and 95° 53' 24" and 96° 14' 24" East Longitude. This area spreads over an area of 995.52 sq. km falling within the semiarid region and frequently facing water scarcity as well as quality problems. The major sources of employment are agriculture, horticulture and animal husbandry, engaging almost 80% of the workforce. On the basis of geological conditions and stratigraphic position, three types of aquifers are recognized in the study area, viz;- alluvial, Irrawaddian and Peguan. In accordance with their morphological characteristics and occurrence, alluvial aquifers are subdivided into those of compound alluvial fans, alluvial unit I and II. Water samples are collected from 140 wells and were subjected to analysis for chemical characteristics. The water samples from the compound alluvial fan aquifer is clustered in $\text{Ca}^{2+}\text{-Mg}^{2+}\text{-Cl}^{-}\text{-SO}_4^{2-}$ dominant section and minor water types identified is $\text{Na}^{+}\text{-K}^{+}\text{-Cl}^{-}\text{-SO}_4^{2-}$ types. Most of the groundwater samples from alluvial unit I are mostly fall in $\text{Na}^{+}\text{-K}^{+}\text{-Cl}^{-}\text{-SO}_4^{2-}$ water types and some are fall in $\text{Ca}^{2+}\text{-Mg}^{2+}\text{-Cl}^{-}\text{-SO}_4^{2-}$ type. In alluvial unit II the groundwater samples fall in $\text{Cl}^{-}\text{-Na}^{+}$ water types and $\text{SO}_4^{2-}\text{-Na}^{+}$ water types. The Irrawaddian aquifer, water are fresh and slightly saline $\text{Na}^{+}\text{-K}^{+}\text{-Cl}^{-}\text{-SO}_4^{2-}$ water type. The groundwater quality of the area is moderately hard to very hard, fresh to slightly alkaline in nature. Most of the water samples were found to be within in WHO guideline value. The suitability of groundwater for irrigation was assessed from (TDS, EC, SAR, MAR, Na% or RSC). Most of the groundwater samples in this area fall in the suitable range for irrigation purpose either from EC and MAR values.

Keywords: Groundwater quality, Chemical characters, Chemical classification, Suitability

Introduction

The Pyawbwe-Nyaungyan-Payangazu area is located in the Pyawbwe and Thazi Townships, and constitutes the eastern margin of dry zone. This study area is bounded by East Longitude 95° 53' 24" and 96° 14' 24" and North Latitude 20° 31' 12" to 20° 45' 54" and refers to one inch to one miles scale topographic map Nos: 93 D/1, 93 D/2, 84 P/13 and 84 P/14. The total coverage area is about 995.52 square kilometer.(see in fig.1)

Description of Aquifers

Based on the geologic and hydrogeologic condition of the Pyawbwe-Nyaungyan-Payangazu Area, five aquifer units can be classified. The present study is emphasized on alluvial aquifer units because most of the tube wells were sunk in these units. Hence, in the study area three major types of aquifer are recognized as follow:

- (I) Alluvial Aquifers
- (II) Irrawaddian Aquifers
- (III) Peguan Aquifers

¹ Dr, Lecturer, Department of Geology, Taungoo University

² Professor, Department of Geology, Taungoo University

³ Associate Professor, Department of Geology, Hinthada University

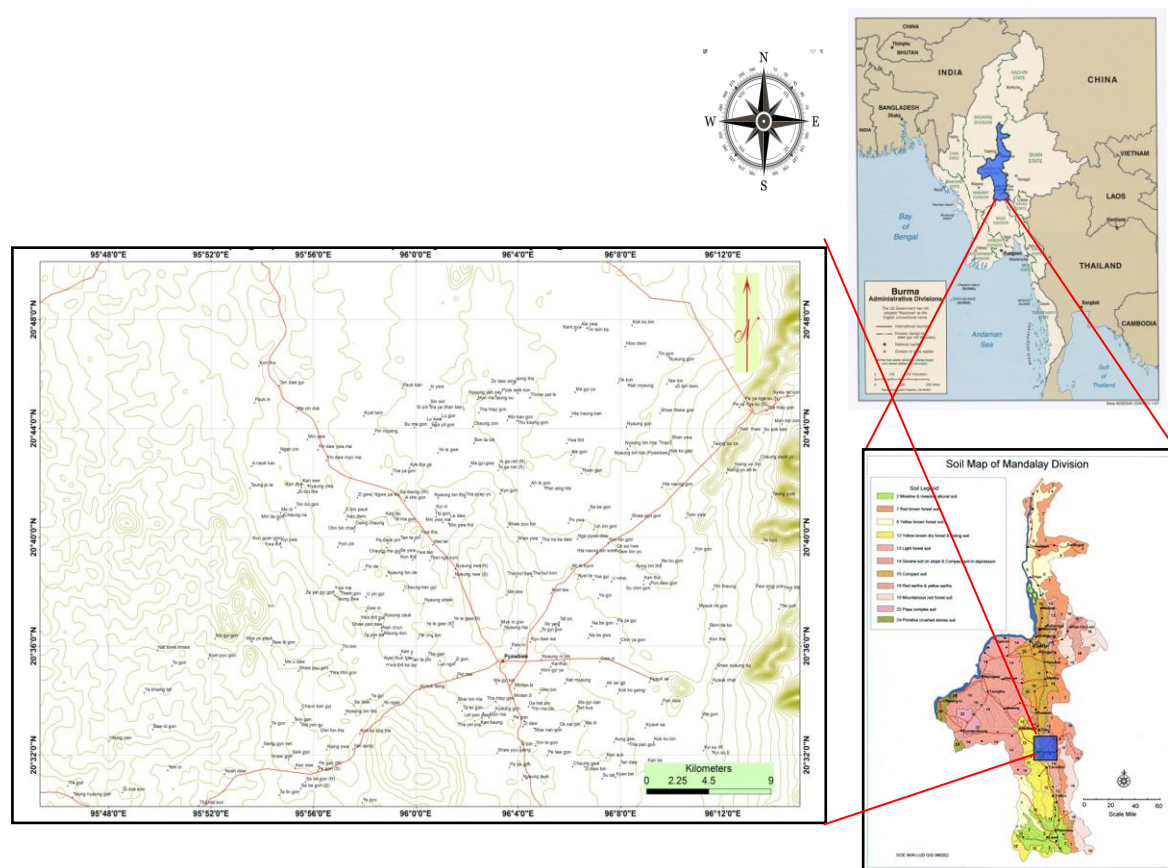


Figure 1 Location map of the study area

Among these, alluvial aquifers and Irrawaddian aquifers are more important groundwater resources for various utilizations especially for agriculture because they contain good quality water of considerable amount and nearly all the cultivated lands are situated on these aquifers. Alluvial aquifers can be sub-divided on the basis of their geomorphology, nature of sediments and their distribution and hydrogeological conditions among the alluvial ones (see in fig.2). They are as follows:

1. Compound alluvial fan Aquifer, (Bajada) (Qal_f)
2. Alluvial aquifer Unit I (between Samon Chaung and Irrawaddian ridges) (Qal₁)
3. Alluvial aquifer Unit II (between Irrawaddian ridges and Bago Yoma) (Qal₂)

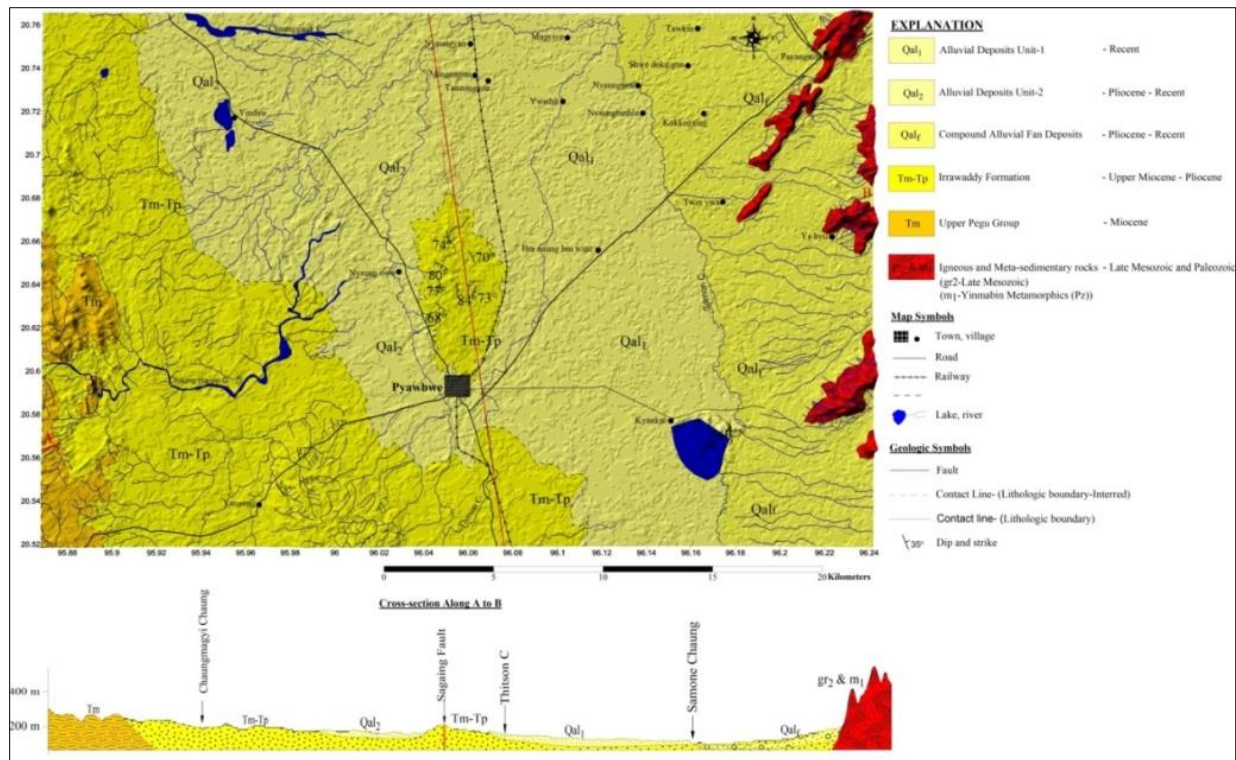


Figure 2 Geological Map of the Pyawbwe-Nyaungyan Payangazu Area

Methodology

Water samples were collected from 140 wells in the study area. These wells are used either for domestic and/or agricultural purposes. The wells were chosen to represent all the aquifers, and on the basis of their geographical location (Fig.3). The aim of such classification is to examine the relationship of the hydrochemistry and hydrochemical facies with the local hydro-environmental factors in each aquifer. Wells in each of these aquifers were defined in a single group. All water samples were analysed for the major ions: Ca^{2+} , Mg^{2+} , Na^{+} , K^{+} , SO_4^{2-} , HCO_3^{-} , Cl^{-} , and CO_3^{-} . Analyses were performed in the laboratories of the Water Resources Utilization Department (WRUD).

Results and Interpretations

Assessment of groundwater quality for domestic and irrigation purposes has been evaluated on the basis of standard guidelines. Different analysis can be used to get the real groundwater condition whether it is suitable for utilization or not.

Chemical Types and Trends of Groundwater

Generally, the chemical composition of groundwater is primarily dependent on the types of chemical reaction as well as the geochemical processes taking place within the groundwater system. The hydrogeochemical characteristics of the major and minor ions with a view to determining the groundwater types and visualizing trends of groundwater chemistry, the Piper trilinear diagrams are used.

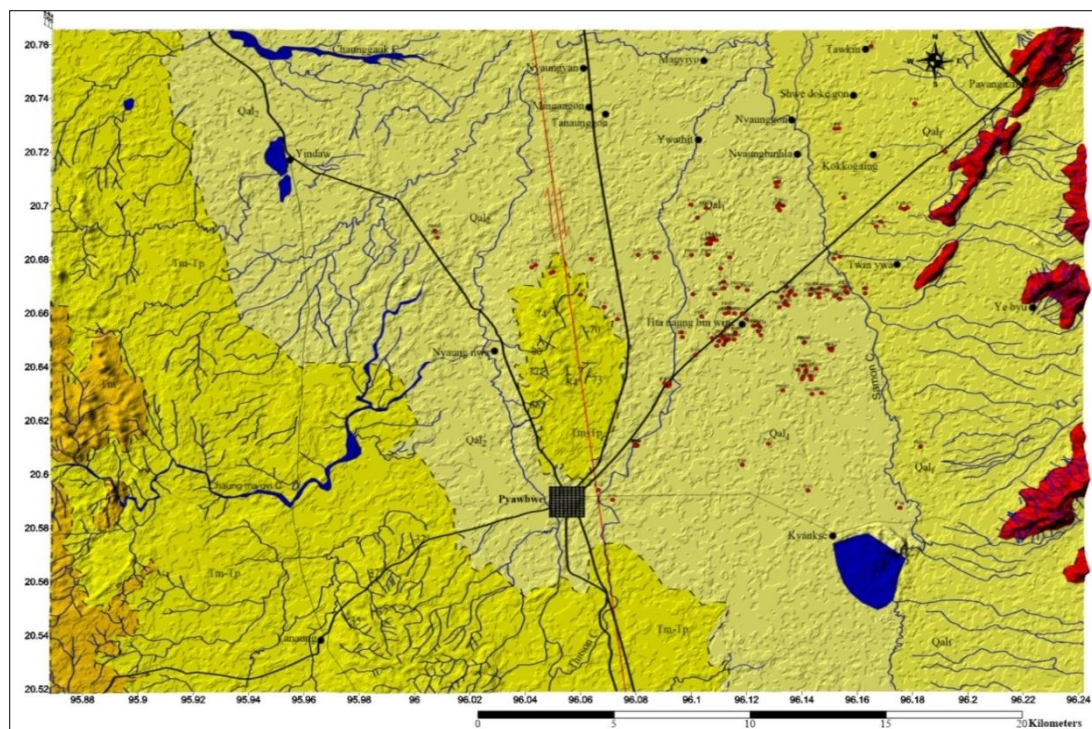


Figure 3 Groundwater sampling location map of Pyawbwe-Nyaungyan-Payangazu Area

Analytical result presents the abundance of these ions in the following order: $\text{Na} > \text{Ca} > \text{Mg} > \text{K} = \text{HCO}_3^- > \text{Cl}^- > \text{SO}_4^{2-}$. Bicarbonate is the dominant anion found in the groundwater of the study area. Its concentration is generally higher than 100 ppm, with mean value of 121 ppm. Chloride is found in considerable amount (25 – 1752 ppm), with mean value of 97 ppm, followed by sulphate (11.52 – 417.6 ppm) with mean value of 71.2 ppm. Sodium dominates the cationic components of the groundwater, with the mean value of 89 ppm, followed by calcium, with mean value of 31.4 ppm. Next to calcium is magnesium with mean value of 15.06 ppm and followed by potassium with mean value of 1.8 ppm.

Classification by Piper Trilinear Diagram

Statistical distribution diagrams such as Piper trilinear, is used to gain better insight into the hydrochemical processes operating in the groundwater system. The Piper trilinear diagram was used for the purpose of characterizing the water types present in the area. It permits the cation and anion compositions of many samples to be represented on a single graph in which major groupings or trends in the data can be discerned visually. Water types are often used in the characterization of waters as a diagnostic tool.

Piper trilinear diagrams are shown in figure (4) and the classification shows that there is a mixture of two types of water with variable concentration of major ions. There are Ca-Mg-Cl-SO_4 type and Na+K-Cl-SO_4 type water. The first type of groundwater mostly found in the eastern part of the study area, especially in compound alluvial fan aquifers. The second groundwater types mostly found in the alluvial unit I, II and Irrawaddian and means that groundwater in the area is mainly made up of mixture of earth alkaline and alkaline metals and predominantly $\text{Cl}^- - \text{SO}_4^{2-}$ water type.

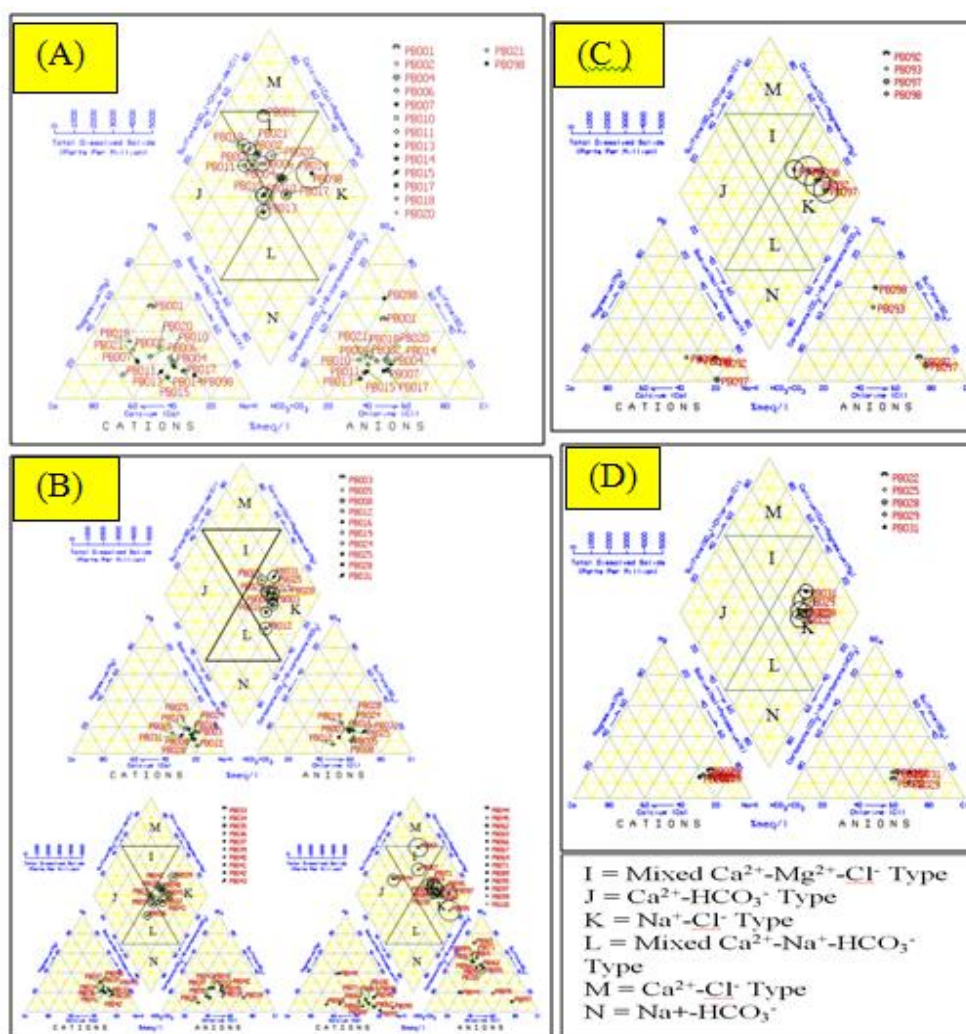


Figure (4) Piper Trilinear Diagram for chemical component of groundwater samples
 (A) Compound alluvial aquifer (B) Alluvial aquifer unit I
 (C) Alluvial aquifer unit II (D) Irrawaddian aquifer

Water Quality for Domestic Purposes

PH is a measure of the intensity of acidity or alkalinity condition of solution. Most of the water samples are slightly alkaline due to present of bicarbonates. The pH values of water samples varied between 6.22 to 9.4. The pH is slightly above the WHO guideline for drinking water which is between 6.5 to 8.5.

The electrical conductivity (E.C.) of groundwater samples range between 400 to 4400 $\mu\text{mho/cm}$. In most of the water samples from the study area, the electrical conductivity does not exceed the WHO standard. Some of the water samples are above the WHO standard of 1500 $\mu\text{mho/cm}$. This is due to high concentration of chloride, sulphate and bicarbonate. From the analysis, the TDS in the area is slightly high (260 -2800 ppm) and some of the water samples are above the WHO guideline of 1000 ppm.

Calcium (Ca^+) content is very common in groundwater of the study area, because they are available in most of the rocks, abundantly and directly related to hardness. Calcium concentration varies between 10.2 to 156.06 ppm and does not exceed the WHO standard. Calcium ion is

commonly present in natural waters and often resulting from the dissolution of calcium-rich rocks; which is evidenced in the study area. It may occur as carbonates and sulphate of calcium, as in limestone and dolomite from the eastern highland.

Magnesium (Mg^{+}) usually occurs in lesser concentration than calcium due to the fact that dissolution of magnesium rich minerals is slow process. Magnesium concentration varies between 1.44 to 89.16 ppm. The water of calcium, together with those of magnesium, are responsible for the hardness of water. If the concentration of calcium and magnesium in drinking water is more than the permissible limit, it causes unpleasant taste to the water.

Sodium concentration more than 50 ppm makes the water salt taste and cause health problems. Sodium concentrations were found in between 14 to 397.15 ppm. In general sodium salts are not actually toxic substance to humans because of the efficiency with which mature kidneys excrete sodium. Most of the water samples, sodium concentrations values were found within the permissible limit (200 ppm) as WHO guideline.

Potassium is slightly less common than sodium in igneous rocks, but more abundant in all the sedimentary rocks. The main source of potassium in groundwater is weathering of potash silicate minerals, potash fertilizers and also due to surface water for irrigation. Potassium varies from 0.00 to 7 ppm.

The value of iron (Fe^{2+}) in the study area range between 0.01 to 3 ppm, and the maximum value was recorded in Twinywa (PB014). WHO guideline indicates a permissible iron value of 0.3 ppm. Most of the water samples are exceeds the WHO limit.

The primary source of bicarbonate (HCO_3^{-}) and carbonate (CO_3^{2-}) ions in groundwater is the dissolved CO_2 in rainwater that on entering in the soil dissolves more CO_2 . The bicarbonate and carbonate are present in natural waters and have been associated with the alkalinity and hardness of water. The major sources of these ions in water include the dissolution of limestone, dolomite chalk, chert, and other carbonate-rich rocks (Todd, 1980). Bicarbonate concentration varied from 32 to 312 ppm. The concentration of these ions ranges between 32 to 312 ppm. WHO recommends a concentration of 200 ppm for potable water supply.

The chloride (Cl^{-}) concentration due to domestic sewage, fertilizers applications and/or leaching from upper soil layers in semi-arid climates. Chloride concentration varies between 25 to 1752 ppm and found few samples exceed the WHO guide line of 250ppm.

Sulphate (SO_4^{2-}) occurs naturally in water due to leaching from gypsum, other common minerals and discharge of domestic sewages tends to increase its concentration. The concentration of sulphate in the study ranges between 11.52 to 417.6 ppm. Sulphate are related to the types of minerals in the soil and bedrock. Sulfer in the form of sulphate is an essential plant nutrient and is considered toxic to plants or animals at lower concentration, but at higher concentrations, it imparts a bitter taste and may cause laxative effects.

Total hardness is an important parameter of water for its use in domestic purpose. Calcium and magnesium are important parameter for total hardness in groundwater. These ions react with soap to form precipitates, and with certain ions present in water to form scale. The acceptable limits for domestic use 75 ppm. Total hardness of groundwater ranged from 53.6 to 601.1 ppm. By the WHO standard, maximum permissible value is 500 ppm. Classification of water was done based on hardness given by Sawyer (1960) and is listed in Table (1). Excess

hardness is undesirable mostly for economic or aesthetic reasons. Most of the samples are moderately hard to very hard water.

Table 1 Hardness Classification of Groundwater (after Sawyer and McCarty, 1960)

Hardness as CaCO ₃	Water Class
0 – 75	Soft
75 – 150	Moderately hard
150 – 300	Hard
Over 300	Very hard

Comparison with WHO Guideline Value for Drinking Water

Groundwater samples compared with the WHO guideline value. Most of the groundwater samples from these aquifers are slightly saline and pH value is high and listed in Table (2), (3), (4) and (5)

Table 2 Alluvial fans groundwater samples compared with the WHO (2011)

Parameter	Range		Mean	WHO (2011)
	Minimum	Maximum		
PH (unit)	6.47	9.4	7.66	6.5 - 8.5
Electrical Conductivity (µmho/cm)	400	1890	885	1500
Sodium (mg/L)	14	318	64	200
Potassium (mg/L)	0.05	6	2.77	----
Calcium (mg/L)	16.23	55.31	31.53	200
Magnesium (mg/L)	6	21.6	12.34	150
Iron (mg/L)	0.01	0.6	0.26	0.3 – 1.0
Chloride (mg/L)	39	125	56.56	250
Sulphate (mg/L)	21.7	307.6	76.1	250
Bicarbonate (mg/L)	70	220	129.37	variable
Carbonate (mg/L)	-	-	-	-
TDS (mg/L)	260	1228.5	744.25	1000
Total Hardness (mg/L)	72	227	149.5	500

Table (3) Alluvial Unit I groundwater samples compared with the WHO (2011)

Parameter	Range		Mean	WHO (2011)
	Minimum	Maximum		
PH (unit)	6.67	9.4	7.54	6.5 - 8.5
Electrical Conductivity (µmhos/cm)	500	1600	843.39	1500
Sodium (mg/L)	43	221.48	85.7	200
Potassium (mg/L)	0.08	7	1.21	----
Calcium (mg/L)	15.4	156.06	32.25	200
Magnesium (mg/L)	1.44	52.8	11.34	150
Iron (mg/L)	0	0.8	0.19	0.3 – 1.0
Chloride (mg/L)	30	259	75.45	250
Sulphate (mg/L)	19.8	386.72	79.43	250
Bicarbonate (mg/L)	70	212	107.94	variable
Carbonate (mg/L)	-	-	-	-
TDS (mg/L)	325	1040	548.2	1000
Total Hardness (mg/L)	58	437	127	500

Table 4 Alluvial Unit II groundwater samples compared with the WHO (2011)

Parameter	Range		Mean	WHO (2011)
	Minimum	Maximum		
PH (unit)	7.9	8.5	8.24	6.5 - 8.5
Electrical Conductivity ($\mu\text{mhos/cm}$)	810	2980	1620	1500
Sodium (mg/L)	109	397	215.5	200
Potassium (mg/L)	-	-	-	----
Calcium (mg/L)	29.65	68.13	50.3	200
Magnesium (mg/L)	15.7	21.6	7.49	150
Iron (mg/L)	-	-	-	0.3 – 1.0
Chloride (mg/L)	57	373	190	250
Sulphate (mg/L)	80.64	307.6	172.94	250
Bicarbonate (mg/L)	118	214	149.5	variable
Carbonate (mg/L)				-
TDS (mg/L)	526.5	1937	1053	1000
Total Hardness (mg/L)	135	243	198	500

Table 5 Irrawaddian groundwater samples compared with the WHO (2011)

Parameter	Range		Mean	WHO (2011)
	Minimum	Maximum		
PH (unit)	6.67	7.76	7.44	6.5 - 8.5
Electrical Conductivity ($\mu\text{mhos/cm}$)	1100	1600	1425	1500
Sodium (mg/L)	69	99	90.3	200
Potassium (mg/L)	0.1	1.0	0.68	----
Calcium (mg/L)	18.02	26.03	22.18	200
Magnesium (mg/L)	12.00	13.84	13.04	150
Iron (mg/L)	0.2	0.3	0.275	0.3 – 1.0
Chloride (mg/L)	134	266	199	250
Sulphate (mg/L)	42.24	76.8	57.62	250
Bicarbonate (mg/L)	146	184	168	variable
Carbonate (mg/L)				-
TDS (mg/L)	715	1040	926.25	1000
Total Hardness (mg/L)	96	122	109	500

Water Quality for Irrigation Purposes

Suitability of irrigation water depends upon many factors including the quality of water, soil type, salt tolerance characteristics of the plants, climate and drainage characteristics of soil. Groundwater always contains small amount of soluble salts dissolved in it. Water chemistry differs depending on the source of water, the degree to which it has been evaporated, the type of rock and mineral it has encountered and the time it has been in contact with reactive minerals. Hence, enough information of groundwater chemistry is very essential to properly evaluated groundwater quality for irrigation purpose. Paddy crops, vegetables and food crops are the common agricultural product of the people in the study area. The area falls under semi-arid region with average rainfall around 800 mm, which is not sufficient for domestic and agriculture purpose. Canal network is strong, but having less output due to less water from the source.

Classification based on chemical indices – Sodium adsorption ratio (SAR), Mg adsorption ratio (MAR), Soluble sodium percentage (SSP or Na %), Residual sodium carbonate (RSC) were calculated. The result was compared with standard parameter in each case for each type of groundwater.

Comparison with standard Guideline Value for Irrigation

In the study area, the assessment of groundwater for irrigation has been evaluated on basis of standard guidelines. Different analysis can be used to get the real groundwater condition whether it is suitable for agriculture or not. Comparisons of different aquifer with standard guidelines are shown in Table (6), (7), (8) and (9).

According to the comparison, most of the water samples are affected by high electrical conductivity, sodium, and magnesium hazards as concerned with irrigation water. In the present study, it is evident that high salinity of groundwater persists at majority of sites. Similarly analytical solution clearly indicates that groundwater in most part of the study area is not suitable for irrigation purpose. It is suggested that suitable measure in terms of enhancement of drainage has be made in area where high salinity is observed for satisfactory crop growth. Artificial recharge and control on extraction of groundwater is the only long term and feasible solution for problem.

Table 6 Alluvial fan groundwater assessment for irrigation purposes

Sr. No.	Well No.	TDS	EC	SAR	MAR	Na%	RSC	Suitability for Irrigation
1	PB001	338	520	0.68	68.65	22.51	2.22	Unsuitable
2	PB002	546	840	0.79	38.89	25.42	1.34	suitable
3	PB004	286	440	1.49	43.43	49.51	0.28	Suitable
4	PB006	715	1100	0.00	39.22	0.04	0.96	Unsuitable
5	PB007	273	420	0.70	32.65	30.78	0.33	Suitable
6	PB010	1040	1600	0.00	45.98	0.23	1.39	Unsuitable
7	PB011	520	800	0.90	19.73	27.63	0.80	Suitable
8	PB013	617.5	950	2.19	26.41	51.19	0.49	Suitable
9	PB014	260	400	1.75	39.43	51.31	0.37	Suitable
10	PB015	585	900	2.02	30.01	46.14	0.22	Suitable
11	PB017	292.5	450	2.30	39.17	57.76	0.04	Suitable
12	PB018	585	900	0.74	43.15	21.46	1.33	Suitable
13	PB020	390	600	1.18	48.43	38.33	0.35	suitable
14	PB021	650	1000	1.08	31.59	31.61	0.45	Unsuitable
15	PB098	877.5	1350	5.45	39.16	64.41	2.24	Unsuitable
16	PB099	1228.5	1890	16.02	35.42	90.28	1.56	Unsuitable

Table 7 Alluvial unit I groundwater assessment for irrigation purposes

Sr. No.	Well No.	TDS	EC	SAR	MAR	Na%	RSC	Sustainability for Irrigation
1	PB003	390	600	3.74	52.50	72.64	0.44	Unsuitable
2	PB005	455	700	2.14	36.10	57.06	0.01	suitable
3	PB008	520	800	4.40	40.79	73.19	0.59	suitable
4	PB012	585	900	5.32	25.60	77.82	1.73	suitable
5	PB016	487.5	750	4.08	41.47	71.90	0.82	suitable
6	PB019	455	700	3.14	51.95	63.46	-0.24	Unsuitable
7	PB024	520	800	4.48	48.46	70.50	-0.14	suitable
8	PB028	585	900	4.31	47.18	69.53	-0.07	suitable
9	PB031	507	780	3.82	38.15	63.82	-0.98	suitable
10	PB033	390	600	3.47	54.32	64.66	-0.06	Unsuitable
11	PB034	390	600	2.40	45.72	54.62	-0.35	suitable
12	PB035	383.5	590	2.46	61.90	50.38	-1.33	Unsuitable
13	PB036	357.5	550	2.82	49.56	57.58	-0.99	suitable
14	PB037	390	600	2.82	50.93	56.25	-1.16	Unsuitable
15	PB039	403	620	3.13	60.55	60.50	-0.70	Unsuitable
16	PB040	390	600	2.73	58.01	55.51	-0.97	Unsuitable
17	PB041	325	500	2.87	49.20	58.77	-0.04	suitable
18	PB042	390	600	2.89	49.51	59.89	-0.71	suitable
19	PB043	390	600	3.83	53.01	66.86	-0.35	Unsuitable
20	PB044	897	1380	1.40	49.67	25.05	-5.27	Unsuitable
21	PB045	390	600	4.02	45.85	67.88	-0.33	suitable
22	PB062	568.75	875	4.36	19.05	72.73	-0.09	suitable
23	PB065	1040	1600	1.78	10.14	29.98	-6.24	Unsuitable
24	PB066	533	820	3.10	15.66	62.66	-0.30	suitable
25	PB067	1001	1540	2.33	13.20	41.71	-2.78	Unsuitable
26	PB069	650	1000	2.90	23.99	56.85	-0.68	Unsuitable
27	PB071	630.5	970	3.42	32.44	62.02	-0.72	suitable
28	PB089	539.5	830	4.47	24.96	67.12	-0.27	suitable
29	PB095	611	940	4.82	47.62	68.08	-0.72	suitable
30	PB097	929.5	1430	8.66	5.25	80.30	-0.45	Unsuitable
31	PB100	890.5	1370	5.33	24.52	64.79	-1.60	Unsuitable

Table 8 Alluvial unit II groundwater assessment for irrigation purposes

Sr. No.	Well No.	TDS	EC	SAR	MAR	Na%	RSC	Sustainability for Irrigation
1	PB090	871	1340	6.26	45.27	72.92	0.64	Unsuitable
2	PB091	1937	2980	11.08	30.05	78.04	1.35	Unsuitable
3	PB093	526.5	810	3.48	34.98	56.12	1.76	suitable
4	PB098	877.5	1350	5.45	39.16	64.41	2.24	Unsuitable

Table 9 Irrawaddian groundwater assessment for irrigation purposes

Sr. No.	Well No.	TDS	EC	SAR	MAR	Na%	RSC	Sustainability for Irrigation
22	PB022	910	1400	4.36	53.3	69.1	0.89	Unsuitable
24	PB025	715	1100	4.01	54.5	66.4	0.30	Unsuitable
26	PB029	1040	1600	4.05	43.5	65.6	0.52	Unsuitable
33	PB038	1040	1600	2.73	46.7	55.3	0.58	Unsuitable

Conclusions

Generally, the groundwater quality of the area is moderately hard to very hard, fresh to slightly alkaline in nature. The major ions in most of the locations were found to be within in WHO guideline for drinking water. Although, some of the water samples exceed the WHO guideline value.

The suitability of groundwater for irrigation was assessed from total dissolved solid (TDS), electrical conductivity (EC), sodium adsorption ratio (SAR), magnesium adsorption ratio (MAR), percentage sodium RSC. Most of the groundwater samples in this area fall in the unsuitable range for irrigation purpose.

In the present study, it is evident that high salinity of groundwater persists at majority of sites. Similarly analytical solution clearly indicates that groundwater in most part of the study area is not suitable for irrigation purpose. It is suggested that suitable measure in terms of enhancement of drainage has be made in area where high salinity is observed for satisfactory crop growth. Artificial recharge and control on extraction of groundwater is the only long term and feasible solution for problem.

Dilution is the only economical way to reduce the salt concentration in irrigation water. Dilution can be done by using nonsaline water add and it mixed with saline water to dilute the salt. Water infiltration problems caused by excess sodium are easier to prevent by continually adding soluble calcium to the irrigated water or soil and by leaching the sodium. Gypsum or other source of calcium (eg., calcium chloride) can be used to treated water. Acid and gypsum reduce the sodium hazard to soil structure posed by high RSC water. Lime residue can be minimized by lowering water pH to below 6.5. Lowering pH is accomplished by injecting acid.

Acknowledgements

The author wishes to express his sincere gratitude to Dr U Thin, Retired Rector for his encouragements, constructive criticisms, careful guidance and critical examination of the author's research works.

The author would like to express his heartfelt appreciation and deep gratitude to Dr Win Naing, Pro-rector of Sittway University, for his close supervision and guidance, numerous suggestions and editing this research paper and for his teaching the first lesson in hydrogeology.

The author is grateful to U Hla Min, Retired Director and U Aung Khine Moe, Assistance Director (Irrigation and Water Utilization Management Department) for permission to use relevant data and providing instruments for this research work.

References

- Aung Kyaw Htoon (1979) *Hydrogeologic nature of Thazi Township and some groundwater supply problem in Thazi*. M.Sc. Thesis Geology Department, Arts and Science University (Unpublished)
- Drury, L.W., Dr. (1986) *An assessment of the hydrogeology and geology in the Dry Zone, Central Burma*. The Agriculture Mechanization Department, Socialist Republic of the Union of Burma and the Australian Development Assistance Bureau.
- Hem. J. D. (1970) *Study and Interpretation of the Chemical Characteristics of the Natural Water*, 2nd ed., U.S Geological Survey Water-Supply Paper, Washington.
- Moe Kyaw (1981) *Hydrogeology of Pyawbwe-Yindaw and Nyaungyan Area*. M.Sc. Thesis Geology Department, Arts and Science University (Unpublished)
- Todd D.K., (1976) *Groundwater Hydrology*, 2nd ed., John Wiley Son, New York.
- Wilcox L. V., (1955). *Classification and use of irrigation water*. U.S. Dept. of Agriculture.